CREEP AND SHRINKAGE OF HIGH PERFORMANCE LIGHTWEIGHT CONCRETE: A MULTI-SCALE INVESTIGATION

A Doctoral Thesis Dissertation
Presented to
The Academic Faculty

by

Mauricio Lopez

In Partial Fulfillment
of the Requirements for the Degree
Doctor of Philosophy in Civil Engineering in the
School of Civil and Environmental Engineering

Georgia Institute of Technology
December 2005

CREEP AND SHRINKAGE OF HIGH PERFORMANCE LIGHTWEIGHT CONCRETE: A MULTI-SCALE INVESTIGATION

Committee Members:

Dr. Kimberly E. Kurtis, Co-advisor
School of Civil and Environmental Engineering
Georgia Institute of Technology

Dr. Lawrence F. Kahn, Co-advisor
School of Civil and Environmental Engineering
Georgia Institute of Technology

Dr. James S. Lai
School of Civil and Environmental Engineering
Georgia Institute of Technology

Dr. Arun M. Gokhale
School of Material and Science Engineering
Georgia Institute of Technology

Dr. Reid W. Castrodale
Director of Engineering
Carolina Stalite Company

Date Approved: November 4, 2005

To Claudia

ACKNOWLEDGEMENTS

Countless people are behind what I am today. First of all, I want to thank God for putting all these wonderful people in my path.

This PhD experience would not have been as amazing as it was without the love and passion for research of my two advisors: Dr Kimberly Kurtis and Dr Lawrence Kahn. To them I owe a truly happy learning experience. To Dr Kahn I thank for his patience and for the excellent example as a researcher, teacher, and person. To Dr Kurtis I thank for her dedication, generosity, and for showing me what excellence is. Dr James Lai spent long hours introducing me into difficult topics. I also appreciate the time and suggestions of Dr Arun Gokhale and Dr Reid Castrodale.

Experimental work always demands many hands to be carried out, and this research was not the exception. I truly thank the time and enthusiasm through long hours of Alan Mullenix, John Barry, Marcus Millard, Julio Cruz, Erik Sweet, and Zach Crumley.

I thank my fellow officemates Adam Slapkus, Scott Canfield, Javier Silva, Brandon Buckberg, Bobby Haines, Brooke Ramage, and Kennan Crane for their patience with me and my coffee, and for those many hours of support and "concrete" reflections. Next, I would like to thank my graduate student friends from CE, Jason McCormick, Leonardo Dueñas, Cesar Asencio, Felix Carreras (†), and Murat Engindeniz, for their patience, positive attitude, and valuable advice.

I have been lucky enough to meet very smart people in the field of concrete to whom I thank for their time and knowledge; they are Nabil El-Ashkar, Nikila Naik, Ben

Mohr, Fred Meyer, and Wonsiri Punurai. Among them, I especially thank Fred Meyer who showed me an outstanding example on how to do good research. I appreciate the effort of Victor Garas and Ron Barbieri who took over my research when it was most needed.

I also owe to my friends, Cristian Escauriaza and Alejandra Valencia the encouragement during these years.

Thank you very much to the CEE staff, especially to Antionette Keith for her kindness and help, Didier Contis for the support with UNIX, Mike Soreson for his time and expertise, and Mahmoud Azari for solving problems at the lab.

The Georgia Department of Transportation sponsored the research reported herein through Georgia DOT research project no. 2041, Task Order no. 02-06. Tindall Corporation constructed all prestressed girders. LaFarge Cement donated the cement, Boral Material Technologies the flyash, Grace Construction Products the silica fume and concrete admixtures, and Augusta Iron and Steel Works helped with the steel cutting. Carolina Stalite Company donated all expanded slate lightweight aggregate and valuable technical advice. The support provided by the sponsors is gratefully acknowledged.

I want to thank to Pontificia Universidad Catolica de Chile, especially its Department of Construction Engineering and Management, and the Chilean Government for believing in me and for their support through these years.

My father gave me his love for new knowledge, my mother her blind confidence in me. To both goes my deeply gratitude for their example and love.

Somehow the word thanks is not enough to recognize the presence and influence of my wife Claudia in my life. She has supported me not only with tremendous love but

also with her intelligence which helped me go through this experience. She is the reason I am here finishing this PhD.

TABLE OF CONTENTS

	Page
ACKNOWLEDGEMENTS	iv
LIST OF TABLES	xvii
LIST OF FIGURES	xxi
LIST OF SYMBOLS AND ABBREVIATIONS	xxxi
SUMMARY	xxxiii
CHAPTER	
Chapter 1 Introduction	1
1.1 Research Need	1
1.2 Research Approach and Scope	1
1.3 Definitions	2
1.4 Dissertation Organization	3
1.5 References	4
Chapter 2 Literature Review	5
2.1 Concrete Performance	6
2.1.1 High Performance Concrete	6
2.1.2 Structural Lightweight Concrete	8
2.1.3 High Performance Lightweight Concrete	10
2.2 Long-Term Deformations in Concrete	12
2.2.1 Shrinkage in Concrete	13
2.2.1.1 Autogenous Shrinkage	13
2.2.1.2 Drying Shrinkage	15
2.2.1.3 Mechanisms	17
2.2.1.4 Factors Influencing Shrinkage	19

2.2.2 Creep in Concrete 25
2.2.2.1 Basic Creep 29
2.2.2.2 Drying Creep 29
2.2.2.3 Creep Mechanisms 30
2.2.2.4 Factors Influencing Creep 36

2.3 Properties of High Performance Lightweight Concrete 45

2.3.1 Microstructure 45
2.3.1.1 Cementitious Matrix Microstructure 45
2.3.1.2 Lightweight Aggregate Microstructure 47
2.3.1.3 Interfacial Transition Zone Microstructure 48
2.3.2 Mechanical Properties 51
2.3.1.1 Compressive Strength 51
2.3.1.2 Modulus of Elasticity 59
2.3.3 Durability 63
2.3.4 Creep and Shrinkage 66
2.3.4.1 Creep of High Performance Concrete 66
2.3.4.2 Creep of Structural Lightweight Concrete 69
2.3.4.3 Creep of High Performance Lightweight Concrete 72
2.3.4.4 Summary of Creep Results 74
2.3.4.5 Shrinkage of High Performance Concrete 76
2.3.4.6 Shrinkage of Structural Lightweight Concrete 78
2.3.4.7 Shrinkage of High Performance Lightweight Concrete 79
2.3.4.8 Summary of Shrinkage Results 82

2.4 Internal Curing in Concrete 85

2.4.1 Need for Curing 85
2.4.2 Curing of High Performance Concrete 86
2.4.3 Internal Curing Philosophy 88
2.4.3.1 Powers' Model 88
2.4.3.2 Internal Curing Principles 90
2.4.3.3 Methods to Incorporate Water in Concrete 91
2.4.4 Effects of Internal Curing 94
2.4.4.1 Effect of Internal Curing on Compressive Strength 94
2.4.4.2 Effect of Internal Curing on Porosity and Permeability 94
2.4.4.3 Effects of Internal Curing on Autogenous Shrinkage 95
2.4.4.4 Effects of Internal Curing on Cracking 97
2.4.4.5 Effects of Internal Curing on Creep 98

2.4.4.6 Summary of Effects of Internal Curing on Concrete Properties 100

2.5 Prestress Losses in Prestressed Members 100

2.5.1 Introduction to Prestress Losses 100
2.5.2 Prestress Losses in Normal Strength Concrete 102
2.5.3 Prestress Losses in High Performance Concrete 102
2.5.4 Prestress Losses in Structural Lightweight Concrete 103
2.5.5 Prestress Losses in High Performance Lightweight Concrete 104

2.6 Assessing Deformations with Image Analysis 105

2.6.1 Digital Image Correlation Technique 105
2.6.2 Digital Image Correlation in Cement-Based Materials 107

2.7 References 108

Chapter 3 Research Program 121

3.1 Research Objectives 121

3.1.1 Assessment of Prestress Losses in High Performance Lightweight Concrete Members 122
3.1.2 Improvement the Fundamental Understanding of Creep and Shrinkage in High Performance Lightweight Concrete 122
3.1.3 Effect of the Constituent Materials and External Conditions on Creep and Shrinkage 122

3.2 Research Methodology 123

3.2.1 Large-scale Approach 123
3.2.2 Medium-scale Approach 124
3.2.3 Small-scale Approach 129

3.3 Experimental Program 133

3.3.1 Large-scale Experimental Program 133
3.3.1.1 Compressive Strength 135
3.3.1.2 Elastic Modulus 136
3.3.1.3 Rupture Modulus 137
3.3.1.4 Rapid Chloride Ion Permeability 137
3.3.1.5 Coefficient of Thermal Expansion Test Procedures 137
3.3.1.6 Creep and Shrinkage 138
3.3.2 Medium-scale Experimental Program 138

3.3.2.1 Compressive Strength 139
3.3.2.2 Elastic Modulus 139
3.3.2.3 Creep Test Procedures 139
3.3.2.4 Shrinkage Test Procedures 141
3.3.3 Small-scale Experimental Program 142
3.3.4 Aggregate Experimental Program 148

3.4 References 149

Chapter 4 Large-scale Study 153

4.1 Introduction 153

4.2 Research Significance 153

4.3 Experimental Results 154

4.3.1 Mixture Design 154
4.3.2 Test Results 155
4.3.2.1 Fresh properties 155
4.3.2.2 Mechanical Properties 156
4.3.2.3 Chloride Permeability 162
4.3.2.4 Coefficient of Thermal Expansion 163
4.3.3 Girder Construction 163
4.3.3.1 Girder Design 163
4.3.3.2 Girder Strains 165

4.4 Prestress Loss Calculations from Design Methods 171

4.5 Comparison of High Performance Lightweight and Normal Weight Concrete 179

4.5.1 Comparison of Mechanical Properties of High Performance Lightweight and Normal Weight Concrete 181
4.5.2 Comparison of Prestress Losses of High Performance Lightweight and Normal weight Concrete 183
4.5.3 Comparison of Creep plus Shrinkage of High Performance Lightweight and Normal Weight Concrete 184

4.6 Conclusions 186

4.7 References 188

Chapter 5 Medium-Scale Study 191

5.1 Introduction 191

5.2 Research Need 192

5.3 Effect of Maturity on Creep 193

5.3.1 Expressions for Maturity and Creep 193
5.3.1.1 Maturity dependence on Temperature 193
5.3.1.2 Creep dependence on Maturity 194
5.3.1.3 Creep Dependency on Compressive Strength 195
5.3.2 Maturity in the Experimental Program 196
5.3.3 Temperature History, Compressive Strength and Creep Results 199
5.3.3.1 Temperature History 199
5.3.3.2 Compressive Strength 205
5.3.3.3 Creep Adjusted by Maturity 210

5.4 Effect of Aggregate on Mechanical Properties, Creep and Shrinkage of High Performance Concrete 223

5.4.1 Two-Phase Models for Concrete. 224
5.4.1.1 Two-phase Model for Concrete Elastic Modulus 224
5.4.1.2 Two-phase Model for Concrete Shrinkage 226
5.4.1.3 Two-phase Model for Concrete Creep 227
5.4.2 Compressive Strength of Concrete vs. Two-Phase Model Estimate 227
5.4.2.1 Compressive Strength of High Performance Matrix 227
5.4.2.2 Compressive Strength of Aggregate 228
5.4.2.3 Compressive Strength of Concrete 229
5.4.3 Modulus of Elasticity 233
5.4.3.1 Elastic Modulus of High Performance Matrix 233
5.4.3.2 Elastic Modulus of Aggregate 233
5.4.3.3 Elastic Modulus of Concrete 234
5.4.4 Shrinkage and Creep Deformations 240
5.4.4.1 Shrinkage and Creep of High Performance Matrix 241
5.4.4.2 Shrinkage of Concrete 242
5.4.4.3 Creep of Concrete 246

5.4.5 Effect of ITZ on High Performance Lightweight and Normal Weight Concrete 251

5.5 Effect of Internally Stored Water on High Performance Lightweight Concrete Properties 253

5.5.1 Compressive Strength 253
5.5.2 Modulus of elasticity 256
5.5.3 Shrinkage Deformations 257
5.5.3.1 Autogenous Shrinkage after Final Set 258
5.5.3.2 Autogenous and Drying Shrinkage Starting at 24 hours 259
5.5.3.3 Total Shrinkage Staring at 24 hours and 28 days 261
5.5.4 Creep Deformations 265
5.5.4.1 Basic and Drying Creep Starting at 24 hours 265
5.5.4.2 Basic and Drying Creep Starting at 28 days 269
5.5.4.3 Total Creep Staring at 24 hours and 28 days 272

5.6 Effect of Pore Connectivity on Drying Creep and Drying Shrinkage 274

5.6.1 Change in Weight 274

5.6.2 Sorptivity 277
5.6.3 Drying Shrinkage Deformations 282
5.6.4 Drying Creep Deformations 284
5.6.5 Long-term drying deformations versus Absorption 286

5.7 Summary 291

5.8 References 294

Chapter 6 Small-Scale Study 301

6.1 Introduction 301

6.2 Research Approach 303

6.3 Image Analysis Procedure 303

6.3.1 Imaging Procedure 303
6.3.2 Pattern Matching Procedure 305
6.3.3 Displacement and Deformation Calculation 306

6.4 Mechanical Properties of Concrete Mixtures 307

6.5 Experimental Validation: Rigid Body Motion 308

6.6 Elastic Deformations 309

6.6.1 Elastic Deformation in Normal Strength Concrete 309
6.6.2 Elastic Deformation in High Performance Concrete 311
6.6.3 Elastic Deformation in High Performance Lightweight Concrete 312

6.7 Creep plus Shrinkage Deformations 313

6.7.1 Creep plus Shrinkage in Normal Strength Concrete 313
6.7.2 Creep plus Shrinkage in HPC 318
6.7.3 Creep plus Shrinkage Deformations in High Performance Lightweight Concrete 322
6.7.4 Comparison of creep plus deformations in Normal Strength Concrete High Performance Concrete and High Performance Lightweight Concrete 325

6.8 Deformations from DIC versus Deformations from DEMEC gauge 327

6.9 Challenges Using This Technique 329

6.10 Summary 330

6.11 References 333

Chapter 7 Multi-Scale Comparison 335

7.1 Introduction 335

7.1.1 Multi-Scale Study 335
7.1.2 Challenges in a Multi-Scale Research 336

7.2 Research Significance 339

7.3 Experimental Results at Different Scales 340

7.3.1 Compressive Strength at Different Scales 343
7.3.2 Elastic Strains at Different Scales 346
7.3.3 Time Dependent Strains at Large and Medium-Scales 348
7.3.4 Time Dependent Strains at Medium and Small-scales 351

7.4 Time Dependent Strains of High Performance Lightweight Concrete versus High Performance Concrete 356

7.5 Conclusions 359

7.6 References 360

Chapter 8 Conclusions and Recommendations 361

8.1 Conclusions 361

8.1.1 Large-Scale Study 361
8.1.2 Medium-Scale Study 362
8.1.2.1 Maturity Effect 362
8.1.2.2 Phase Interaction 363
8.1.2.3 Internal Curing 364
8.1.2.4 Drying Effect 365
8.1.3 Small-Scale Study 366
8.1.4 General 368

8.2 Recommendations for Future Research 369

8.3 Recommendations for Design 371

Appendix A Constituent Properties 373

A.1 Cement 373

A.2 Supplementary Cementing Materials 374

A.3 Aggregates 374

Appendix B Physical and Mechanical Properties of Concrete Mixtures of Large-Scale Study 381

B.1 Density Study 381

B.2 Mechanical Properties 382

B.2.1. Compressive Strength 382
B.2.2. Elastic Modulus 384
B.2.3. Rupture Modulus 385

B.3 Rapid Chloride Permeability 385

Appendix C Prestress Loss Calculations 387

C.1. PCI Method 387

C.2. AASHTO-LRFD Refined Estimate of Time-Dependent Losses 390

C.3. AASHTO-LRFD Approximate Lump Sum Estimate of Time-Dependent Losses 394

C.4. ACI-209 Method 395

C.5. Prestress Loss Computations 398

C.5.1. Prestress Losses in the Girders 398
C.5.2. Prestress Losses with AASHTO-LRFD Refined Method 399
C.5.3. Prestress Losses with AASHTO-LRFD Lump Sum Method 400
C.5.4. Prestress Losses with PCI Method 401
C.5.5. Prestress Losses with ACI-209 Method 403

Appendix D Physical and Mechanical Properties of Concrete Mixtures of Medium-Scale Study 405

D.1. Batching Procedures 405

D.1.1. Constituents Storage and Conditioning 405
D.1.2. Moisture Adjustment for Mixture Designs 406
D.1.3. Mixing Procedure 407

D.2. Fracture Surfaces 407

D.3. Compressive Strength 409

D.4. Elastic Modulus 420

Appendix E Temperature Development 421

E.1 HP Matrix and Cement Matrix 421

E.2 LWW 35-65, NWA 35-65, and STL 35-65 423

E.2 LWW 65-35, NWA 65-35, and STL 65-35 424

Appendix F Creep and shrinkage Results 427

Appendix G Physical and Mechanical Properties of Concrete Mixtures of Small-Scale Study 451

G.1 Compressive Strength 451

G.2 Autogenous Shrinkage 454

G.3 Creep and Shrinkage 457

Appendix H Creep and Drying Shrinkage Models (US Customary Units) 461

H.1 Models for Normal Strength Concrete 461

H.1.1. ACI-209 Method 462
H.1.2. AASHTO-LRFD Method 466
H.1.3. CEB-FIP Method 468
H.1.4. Bažant and Panula's - BP Method 472
H.1.5. Bažant and Baweja's - B3 Method 479
H.1.6. Gardner and Lockman's - GL Method 483
H.1.7. Sakata's - SAK 93 Method 484

H.2 Models for High Strength High Performance Concrete 487

H.2.1 CEB-FIP Method as modified by Yue and Taerwe (1993) 487
H.2.2. Bažant and Panula's - BP Method 488
H.2.3. Sakata's - SAK 01 Method 491
H.2.4. AFREM Method 492
H.2.5. AASHTO-LRFD as modified by Shams and Kahn (2000) 495

Appendix I Creep and Drying Shrinkage Models (S. I. Units) 499

I.1 Models for Normal Strength Concrete 499

I.1.1. ACI-209 Method 499
I.1.2. AASHTO-LRFD Method 502
I.1.3. CEB-FIP Method 504
I.1.4. Bažant and Panula's - BP Method 507
I.1.5. Bažant and Baweja's - B3 Method 514
I.1.6. Gardner and Lockman's - GL Method 518
I.1.7. Sakata's - SAK Method 519

I.2 Models for High Strength Concrete 521

I.2.1. CEB-FIP Method as modified by Yue and Taerwe (1993) 521
I.2.2. Bažant and Panula's - BP Method 522
I.2.3. Sakata's - SAK Method 524
I.2.4. AFREM Method 526
I.2.5. AASHTO-LRFD method as modified by Shams and Kahn (2000) 528

Vita 531

LIST OF TABLES

Page

Table 2.1: Grade of performances characteristics for HPC at the age of 56 days 7

Table 2.2: Summary of compressive strength and density of HPLC in the literature 58

Table 2.3: Elastic modulus of HPLC in the literature 62

Table 2.4: Creep results for HPC, SLC, and HPLC in the literature. 75

Table 2.5: Shrinkage results for HPC, SLC, and HPLC in the literature. 83

Table 3.1: Mixture designs of high performance mixtures with expanded slate in kg/m^3 (lb/yd^3) 127

Table 3.2: Mixture designs of high performance mixtures with granite and steel aggregate in kg/m^3 (lb/yd^3) 128

Table 3.3: Mixture designs of high performance matrix, cement matrix and normal strength normal weight concrete in kg/m^3 (lb/yd^3) 129

Table 3.4: Mixture designs for small-scale study in kg/m^3 (lb/yd^3) 132

Table 4.1: Mixture design of the HPLC in kg/m^3 (lb/yd^3) 154

Table 4.2 Experimental strains of 11.9-m (39-ft) long girders (με) 168

Table 4.3 Comparison between experimental and estimated prestress losses of LWW 55/8 and LWW 69/10 HPLC prestressed girders 172

Table 4.4: Prestress losses of NSC and HPLC elements, expresses as percentage of the initial stress (%) 179

Table 4.5: Mixture design of HLPC and HPC-6 in kg/m3 (lb/yd3) 180

Table 5.1: Mixture nomenclature and characteristics 192

Table 5.2: Properties of aggregates used in HPC mixtures 198

Table 5.3: Equivalent age at of HPC mixtures the time of testing 202

Table 5.4: Specific creep of HPC mixtures after 120 days under loading and drying, in με/MPa (με/psi) 211

Table 5.5: Properties of cementitious matrix and aggregates used in HPC mixtures 224

Table 6.1: Mixture nomenclature and characteristics 304

Table 6.2: Properties of NSC and HPC mixtures under study 309

Table A.1: Chemical Composition and fineness of LaFarge Type III Cement 373

Table A.2: Chemical Composition and fineness of LaFarge Type I Cement 374

Table A.3: Physical Properties of aggregates 376

Table A.4: Mechanical Properties of expanded slate aggregate 378

Table A.5: Elastic modulus of steel bars in tension 379

Table A.6: Elastic modulus of steel bars in tension 380

Table C.1. Loss of prestress ratios for different concretes and time under loading conditions 397

Table D.1. Typical moisture contents in aggregate 406

Table F.1: Creep and shrinkage results for cement matrix in the medium-scale study 428

Table F.2: Creep and shrinkage results for hp matrix in the medium-scale study loading at 24 hours of age 429

Table F.3: Creep and shrinkage results for hp matrix in the medium-scale study loading at 28 days of age 430

Table F.4: Creep and shrinkage results for LWW 65-35-95 in the medium-scale study loaded at 24 hours of age 431

Table F.5: Creep and shrinkage results for LWW 65-35-95 in the medium-scale study loaded at 28 days of age 432

Table F.6: Creep and shrinkage results for LWW 65-35 in the medium-scale study loaded at 24 hours of age 433

Table F.7: Creep and shrinkage results for LWW 65-35 in the medium-scale study loaded at 28 days of age 434

Table F.8: Creep and shrinkage results for LWD 65-35 in the medium-scale study loaded at 24 hours of age 435

Table F.9: Creep and shrinkage results for LWD 65-35 in the medium-scale study loaded at 28 days of age 436

Table F.10: Creep and shrinkage results for NWA 65-35 in the medium-scale study loaded at 24 hours of age 437

Table F.11: Creep and shrinkage results for NWA 65-35 in the medium-scale study loaded at 28 days of age 438

Table F.12: Creep and shrinkage results for STL 65-35 in the medium-scale study loaded at 24 hours of age 439

Table F.13: Creep and shrinkage results for STL 65-35 in the medium-scale study loaded at 28 days of age 440

Table F.14: Creep and shrinkage results for LWW 35-65 in the medium-scale study loaded at 24 hours of age 441

Table F.15: Creep and shrinkage results for LWW 35-65 in the medium-scale study loaded at 28 days of age 442

Table F.16: Creep and shrinkage results for NWA 35-65 in the medium-scale study loaded at 24 hours of age 443

Table F.17: Creep and shrinkage results for NWA 35-65 in the medium-scale study loaded at 28 days of age 444

Table F.18: Creep and shrinkage results for STL 35-65 in the medium-scale study loaded at 24 hours of age 445

Table F.19: Creep and shrinkage results for STL 35-65 in the medium-scale study loaded at 28 days of age 446

Table F.20: Creep and shrinkage results for NSC in the medium-scale study loaded at 28 days of age 447

Table F.21: Creep and shrinkage results for LWW 55/8 in the large-scale study loaded at 24 hours of age 448

Table F.22: Creep and shrinkage results for LWW 69/10 in the large-scale study loaded at 24 hours of age 449

Table G.1: Final setting time 460

This page intentionally left blank

LIST OF FIGURES

Page

Figure 2.1: Various strains in concrete with time 12

Figure 2.2: Water loss versus time from concrete specimens of various sizes under 55% relative humidity 16

Figure 2.3: Representation of cement paste microstructure 17

Figure 2.4: Relationship between shrinkage of concrete and aggregate content 21

Figure 2.5: Effect of water-to-cement ratio and volume of aggregate on shrinkage 23

Figure 2.6: Representation of the three stages of creep 26

Figure 2.7: Instantaneous and creep deformations and recoveries 28

Figure 2.8: Relationship between creep of concrete and aggregate content 38

Figure 2.9: Theoretical and empirical relationship between aggregate elastic modulus and relative creep of concrete for normal weight concrete 40

Figure 2.10: Influence of water-to-cement ratio on creep of concrete 41

Figure 2.11: Comparison of creep of concrete at constant stress-to-strength ratio with and without plasticizers and superplasticizers 44

Figure 2.12: Estimated relationship between water-to-cement ratio and degree of hydration at which capillary continuity is 46

Figure 2.13: Summary of compressive strength and density of HPLC in the literature 59

Figure 2.14: Summary of compressive strength and density of HPLC in the literature 63

Figure 2.15: Relationship between compressive strength of lightweight concrete and one-year specific creep for (a) normally cured concrete and (b) steam-cured concrete 71

Figure 2.16: Specific creep versus time under loading and drying for SLC, HPC, and HPLC for loading and drying beginning at 1 and 28 days of age 74

Figure 2.17: Comparison of Shrinkage of HPC and HPLC 81

Figure 2.18: Shrinkage versus time under loading and drying for SLC, HPC, and HPLC for drying beginning at 1 and 28 days of age 82

Figure 2.19: Effect of moist curing time on strength gain of concrete 86

Figure 2.20 Effect of internal curing on self-desiccation shrinkage in (a) Cement paste and (b) Concrete 96

Figure 2.21: Effect of internal curing on tendency to crack in (a) Mortars, and (b) Concrete 98

Figure 3.1: Factorial design for medium-scale study 125

Figure 3.2: Factorial design for small-scale study 131

Figure 3.3: AASHTO Type II composite girder cross section. 134

Figure 3.4: Modulus of elasticity test 136

Figure 3.5: DEMEC gauge reading during coefficient of thermal expansion test 137

Figure 3.6: Medium-scale creep frames schematic view (left), working principle (center), photograph of the creep frames (right). 140

Figure 3.7: DEMEC reader and calibration bar used for medium-scale creep and shrinkage specimens 141

Figure 3.8: Medium-scale molds for 100 x 380 mm (4 x 15 in) creep specimens (top) and 150 x 300 mm (6 x 12 in) specimens (bottom). 142

Figure 3.9: Small-scale experimental setup working principle 143

Figure 3.10: Small-scale creep frame setup during loading stage. 144

Figure 3.11: Small-scale experimental setup, molds with and without concrete 145

Figure 3.12: Small-scale experimental set up, creep frame and specimens in the stereomicroscope stage (left), image acquisition system (top right), and concrete specimens after cutting and polishing (bottom right). 146

Figure 3.13 length comparator and calibration bar used in autogenous shrinkage 147

Figure 4.1: Density of HPLC under different moisture conditions 156

Figure 4.2: Compressive strength vs. time of LWW 55/8 and LWW 69/10 mixtures for: (a) accelerated and (b) standard curing methods 157

Figure 4.3: 56-day elastic modulus of LWW 55/8 and LWW 69/10 mixtures versus compressive strength 159

Figure 4.4: Rupture modulus of HPLC mixtures versus compressive strength 161

Figure 4.5: Chloride ion permeability of LWW 55/8 and LWW 69/10 mixtures 162

Figure 4.6: Cross section of AASHTO Type II HPLC girder with NSC composite deck 164

Figure 4.7: Vibrating wire strain gage used to measure internal strains in the girders. 165

Figure 4.8: Precast Concrete Plant 166

Figure 4.9: Installation of shear reinforcement during girders construction 166

Figure 4.10: Measuring external strains of the AASHTO Type II precast prestressed HPLC girders 167

Figure 4.11: Experimental strains over time for LWW 55/8 and LWW 69/10 39-ft girders 168

Figure 4.12: Experimental creep and shrinkage and exponential regression for the LWW 55/8 and LWW 69/10 HPLC 39-ft girders (a) linear time scale (b) logarithmic time scale. 170

Figure 4.13: Comparison between experimental and estimated prestress losses from AASHTO-LRFD, PCI, and ACI-209 methods (a) LWW 55/8 HPLC girders, (b) LWW 69/10 HPLC girders 174

Figure 4.14: Predicted-to-measured ratio of prestress losses from AASHTO-LRFD, PCI, and ACI-209 design provision 176

Figure 4.15: Measured prestress losses and the projected prestress losses to a stress level of 60% of the initial concrete strength 178

Figure 4.16: Compressive strength and elastic modulus of LWW 69/10 versus HPC-6 182

Figure 4.17: Predicted-to-measured ratio of prestress losses from AASHTO-LRFD, PCI, and ACI-209 design provisions on AASHTO Type II girders made of LWW 69/10 and HPC-6 184

Figure 4.18: Creep plus shrinkage of LWW 69/10 and HPC-6 mixtures under 27.6-MPa (4000-psi) compressive stress 185

Figure 5.1: Summary of mixtures used in the maturity analysis 197

Figure 5.2: Increase in temperature and maximum temperature reached by HPC mixtures during first 24 hours 200

Figure 5.3: Temperature history of the 65-35 mixtures fabricated under intermediate temperature conditions 201

Figure 5.4: Equivalent and calendar age versus calendar age grouped by type of mixture 204

Figure 5.5: Compressive strength versus calendar age and maturity at testing, (a) HP Matrix, (b) Cement Matrix 206

Figure 5.6: Compressive strength versus calendar age and maturity at testing, (a) LWW 35-65, (b) NWA 35-65, (c) STL 35-65 208

Figure 5.7: Compressive strength versus calendar age and maturity at testing, (a) LWW 65-35, (b) NWA 65-35, (c) STL 65-35 209

Figure 5.8: Relationship between specific creep after 120 days under loading and drying and equivalent age of loading for specimens loaded 24 hours after casting 212

Figure 5.9: Relationship between specific creep after 120 days under loading and drying and equivalent age of loading for specimens loaded 28 days after casting 213

Figure 5.10: Specific creep of Cement Matrix, when loaded at early age, before and after adjustment by maturity and strength 218

Figure 5.11: Specific creep of NWA 65-35, when loaded at early age, before and after adjustment by maturity and strength 218

Figure 5.12: Specific creep of LWW 65-35, when loaded at early age, before and after adjustment by maturity and strength 219

Figure 5.13: Specific creep of LWW 35-65, when loaded 28 days after casting, before and after adjustment by maturity and strength 220

Figure 5.14: Adjusted average specific creep of mixtures after 120 days under loading and drying 222

Figure 5.15: Compressive strength versus age and maturity at testing of HP Matrix 228

Figure 5.16: Compressive strength for HP Matrix, LWW, NWA, and STL mixtures for different age of testing 230

Figure 5.17: Measured compressive strength versus estimated from two-phase model in parallel for LWW, NWA, and STL mixtures 232

Figure 5.18: Elastic modulus of LWW, NWA, and STL aggregate mixtures as a function of coarse aggregate content 235

Figure 5.19: Measured elastic modulus versus estimated from two-phase models for LWW, NWA, and STL aggregate mixtures 236

Figure 5.20: 28-day measured elastic modulus versus Hashin-Shtrikman bounds for LWW, NWA, and STL aggregate mixtures 238

Figure 5.21: Comparison between experimental elastic modulus normalized by density and that estimated using ACI-363 equation versus compressive strength 240

Figure 5.22: Total shrinkage and specific creep of HP Matrix mixtures versus time under loading and drying 241

Figure 5.23: Total Shrinkage of HPC mixtures versus time under drying in logarithm scale 243

Figure 5.24: Comparison between experimental total shrinkage and that estimated using Equation 5.23 for LWW, NWA, and STL mixtures 244

Figure 5.25: Specific Creep of HPC mixtures versus time under drying in logarithm scale 247

Figure 5.26: Comparison between experimental specific creep and that estimated using Equations 5 and 6 (Neville, 1964) for LWW, NWA, and STL mixtures 249

Figure 5.27: Compressive strength of HPC mixtures versus age at testing 254

Figure 5.28: Measured elastic modulus versus estimated using ACI-363 equation 257

Figure 5.29: Change in length versus time after final set for LWW 65-35-95, LWD 65-35-95, and NWA 65-35-95 HPC mixtures 258

Figure 5.30: Autogenous and drying shrinkage between 24 hours and 56 days after casting for LWW 65-35, LWD 65-35, LWW 65-35-95 and NWA 65-35 mixtures 260

Figure 5.31: Total shrinkage for LWW 65-35, LWD 65-35, LWW 65-35-95 and NWA 65-35 mixtures when drying started at the age of 24 hours 262

Figure 5.32: Total shrinkage for LWW 65-35, LWD 65-35, LWW 65-35-95 and NWA 65-35 mixtures when drying started at the age of 28 days 264

Figure 5.33: Creep of HPC mixtures when loaded 24 hours after casting, (a) basic creep, (b) drying creep 266

Figure 5.34: Creep of HPC mixtures when loaded 28 days after casting, (a) basic creep, (b) drying creep 270

Figure 5.35: Total creep for LWW 65-35, LWD 65-35, LWW 65-35-95 and NWA 65-35 mixtures, (a) when testing started at the age of 24 hours, (b) when testing started at the age of 28 days 273

Figure 5.36: Change in weight in unsealed shrinkage specimens for HP Matrix, LWW 65-35, NWA 65-35, and NSC 275

Figure 5.37: Drying and absorption of HP Matrix, LWW 65-35, NWA 65-35, and NSC 278

Figure 5.38: absorption versus square root of time for HP Matrix, LWW 65-35, and NWA 65-35 280

Figure 5.39: Drying shrinkage for HP Matrix, LWW 65-35, NWA 65-35 and NSC mixtures 283

Figure 5.40: Drying creep for HP Matrix, LWW 65-35, NWA 65-35 and NSC mixtures 285

Figure 5.41: One-year relative drying shrinkage versus relative sorptivity 288

Figure 5.42: One-year relative drying creep versus relative sorptivity 290

Figure 6.1: Imaging protocol for the experimental program 307

Figure 6.2: Rigid body motion as seen by DIC at high magnification, (a) ROI before displacement, (b) ROI after displacement, (c) u-displacement field, (d) individual pixel u-displacements 312

Figure 6.3: Elastic deformation at 9.7 MPa (1440 psi) in NSC as seen by DIC in ROI 4 at high magnification, (a) ROI, (b) u-displacement field, (c) deformations in X-direction 313

Figure 6.4: Elastic deformation at 28.4 MPa (4115 psi) in HPC as seen by DIC in ROI 4 at high magnification, (a) ROI, (b) deformations in X-direction 315

Figure 6.5: Elastic deformation in loading direction as seen by DIC in ROI 2 at high magnification, (a) ROI, (b) deformations in X-direction 316

Figure 6.6: Creep plus shrinkage deformation in NSC after one day of loading and drying as seen by DIC in ROI 2 at high magnification, (a) ROI, (b) deformations in X-direction 317

Figure 6.7: Creep plus shrinkage deformation in NSC after 28 days of loading and drying as seen by DIC in ROI 2 at high magnification, (a) ROI, (b) deformations in X-direction 318

Figure 6.8: Creep plus shrinkage deformation in individual pixels of NSC specimen, (a) after 1 day of testing, (b) after 28 days of testing 319

Figure 6.9: Distribution of deformation after one and 28 days under loading and drying 320

Figure 6.10: Creep plus shrinkage deformation in HPC after one day of loading and drying as seen by DIC in ROI 4 at high magnification, (a) ROI, (b) deformations in X-direction 321

Figure 6.11: Creep plus shrinkage deformation in HPC after 28 days of loading and drying as seen by DIC in ROI 4 at high magnification, (a) ROI, (b) deformations in X-direction 323

Figure 6.12: Creep plus shrinkage deformation in pixels of Figure 6.9c after one day under drying and loading 324

Figure 6.13: Creep plus shrinkage deformation in HPLC after one day of loading and drying as seen by DIC in ROI 1 at low magnification, (a) ROI, (b) deformation map 325

Figure 6.14: Creep plus shrinkage deformation in HPLC after 28 days of loading and drying as seen by DIC in ROI 1 at low magnification, (a) ROI, (b) deformation map 326

Figure 6.15: Adjusted creep plus shrinkage deformation maps in after 28 days of testing, (a) NSC, (b) HPC, (c) HPLC 329

Figure 6.16: Total deformation as measured by DEMEC gauge versus average total deformation from DIC 331

Figure 7.1: Small-scale creep specimen cross section and exposed 9.5-mm (0.375-in) MSA 339

Figure 7.2: Mixtures of the multi-scale study 342

Figure 7.3: Compressive strength of HPLC mixtures used on the large, medium and small-scale studies 344

Figure 7.4: Elastic modulus calculated from girders and creep specimens of different sizes 347

Figure 7.5: Creep plus shrinkage under a compressive stress of 9.6 MPa (1385 psi) in the girders and creep specimens of large and medium-scale studies 350

Figure 7.6: Creep plus shrinkage under a compressive stress of 27.6 MPa (4000 psi) in HPLC creep specimens of medium-scale and small-scale studies, (a) mixtures with 12.7-mm (0.5-in) MSA, (b) mixtures with 9.5-mm (0.375-in) MSA 352

Figure 7.7: Creep plus shrinkage in creep specimens of medium-scale and small-scale studies, (a) granite and steel aggregate HPC's under 27.6-MPa (4000-psi) stress, (b) HP Matrix under 27.6-MPa (4000-psi) stress, and NSC under 10.7-MPa (1550-psi) stress 354

Figure 7.8: Creep plus shrinkage in creep specimens under 27.6-MPa (4000-psi) stress of medium-scale and small-scale studies 357

Figure A.1: 19-mm (0.75-in) MSA expanded slate lightweight aggregate 375

Figure A.2: 12-mm (0. 5-in) MSA steel aggregate 375

Figure A.3: Expanded slate prisms 377

Figure A.4: Compressive strength testing of an expanded slate prism 377

Figure D.1: Fracture surface of a STL 65-35 cylinder specimen after testing 407

Figure D.2: Stress concentration induced cracking starting at the ITZ in mixture with steel aggregate. 408

Figure E.1: Temperature history in HP Matrix and Cement Matrix under cold ambient conditions 421

Figure E.2: Temperature history in HP Matrix and Cement Matrix under hot ambient conditions 422

Figure E.3: Temperature history in HP Matrix under intermediate ambient conditions 422

Figure E.4: Temperature history in LWW 35-65, NWA 35-65, and STL 35-65 mixtures under cold ambient conditions 423

Figure E.5: Temperature history in LWW 35-65, NWA 35-65, and STL 35-65 mixtures under hot ambient conditions 423

Figure E.6: Temperature history in LWW 35-65, NWA 35-65, and STL 35-65 mixtures under intermediate ambient conditions 424

Figure E.7: Temperature history in LWW 65-35, NWA 65-35, and STL 65-35 mixtures under cold ambient conditions 424

Figure E.8: Temperature history in LWW 65-35, NWA 65-35, and STL 65-35 mixtures under hot ambient conditions 425

Figure E.9: Temperature history in LWW 65-35, NWA 65-35, and STL 65-35 mixtures under intermediate ambient conditions 425

This page intentionally left blank

LIST OF SYMBOLS AND ABBREVIATIONS

AASHTO	American Association of State Highway and Transportation Officials
ANOVA	analysis of variance
C_2S	dicalcium silicate $(CaO)_2SiO_2$
C_3A	tricalcium aluminate, and it is the cement nomenclature for $(CaO)_3Al2O_3$
C_3S	tricalcium silicate $(CaO)_3SiO_2$
C_4AF	tetracalcium aluminoferrite $(CaO)_3Al_2O_3Fe_2O_3$
CM	cementitious materials
COV	coefficient of variance
C-S-H	calcium silicate hydrates
CTE	coefficient of thermal expansion
DEMEC gauge	detachable mechanical strain gauge
DIC	digital image correlation
Ec	modulus of elasticity of concrete based on 6 x 12 cylinder
E_{ps}	slastic modulus of prestressing steel (ksi)
f_c’	concrete compressive strength at specified time
f_{ci}'	concrete compressive strength at strand release
f_{cds}	stress in concrete at the cgs due to all superimposed dead loads (ksi)
f_r	modulus of rupture of concrete
f_{ps}	stress in prestressed reinforcement at nominal strength of member
f_{pt}	stress in prestressing strand just prior to strand release
f_{pu}	specified tensile strength of prestressed reinforcement

f_{se}	effective prestressing stress after losses
f_{si}	stress in prestressing strand just after strand release
f_{su}	stress in prestressed reinforcement at nominal strength of member
f_y	specified yield strength of non-prestressed reinforcement
HPC	high performance concrete
HPLC	high performance lightweight concrete
HSC	high strength concrete
Ic	moment of inertia of composite girder (girder and deck)
ITZ	interfacial transition zone
Inc	Moment of inertia of girder
LOLAX	low relaxation loss prestressing strand
MSA	maximum size aggregate
NSC	normal weight concrete
NSC	normal strength normal weight concrete
ROI	region of interest
SAP	super absorbent polymer
SCM	supplementary cementing material
SEM	scanning electron microscopy
SLC	structural lightweight concrete
VWSG	vibrating wire strain gauge
W/CM	water to cementitious materials ratio
W/C	water to cement ratio
w_c	density of concret

SUMMARY

High performance lightweight concrete (HPLC) is a material that combines properties of high performance concrete (HPC) and structural lightweight concrete (SLC). It presents not only advantages from its two predecessors but also new characteristics derived from the synergy between a high performance matrix and a porous saturated lightweight aggregate.

HPLC presents an enormous potential for use in precast prestressed bridge girders. First, bridge structures must maintain serviceability for 75 to 100 years which demands high durability. Second, prestressed girders require concrete with high compressive strength to resist large prestressing forces and to provide long span bridges. Finally, precast prestressed girders need to be lightweight so they may be transported and erected efficiently and at a reasonable cost. HPLC exhibits high durability, compressive strengths of 69.0 MPa (10,000 psi) or more, and densities of 1920 kg/m3 (120 lb/ft3) or less. Nevertheless, because HPLC has not been extensively investigated, there is a lack of understanding of its properties which posses as a barrier for future applications.

This multi-scale investigation provided new knowledge and understanding of creep and shrinkage of HPLC by assessing prestress losses in HPLC prestressed members in a large-scale study, by quantifying the effect of the constituent materials and external conditions on creep and shrinkage in a medium-scale study, and by improving the fundamental understanding of creep and shrinkage in a small-scale study. The large-scale and medium-scale studies measured creep and shrinkage in AASHTO Type II prestressed girders and in standard concrete cylinders, respectively, while the small-scale

study measured creep and shrinkage deformations in the paste, aggregate and interface transition zone (ITZ) separately by means of microscopy and image analysis.

Prestress losses in six Type II AASHTO HPLC girders were adequately or conservatively estimated using the AASHTO-LRFD, PCI, and ACI-209 design standards. In particular creep plus shrinkage prestress losses were between two and eight times lower than the long-term losses estimated by the standards. Creep and shrinkage of HPLC after 850 days of testing were 77% of those exhibited by a similar compressive strength normal weight HPC. Prestress losses due to creep and shrinkage in HPLC girders were approximately 50% of those measured in similar HPC girders.

The lower creep and shrinkage exhibited by HPLC was found to be caused by a synergy between the pre-soaked lightweight aggregate and the low water-to-cementitious material ratio matrix. That is, the water contained in the lightweight aggregate enhances hydration by providing internal moist curing. The water in the aggregate also contributes to maintain a high internal relative humidity which reduces autogenous shrinkage which occurs in mixtures with low water-to-cementitious material ratio. This higher internal relative humidity also reduces creep by preventing load-induced water migration. Finally, lightweight aggregate exhibits a better elastic compatibility with the paste than normal weight aggregate. This improved elastic matching and the enhanced hydration are believed to reduce peak deformations at the ITZ which further decreases creep and shrinkage.

CHAPTER 1

INTRODUCTION

1.1 Research Need

Concrete made with lightweight aggregate was probably used about 5000 years in most various applications, and high strength/high performance concrete has been successfully utilized for the last three decades. Both materials have been investigated and many of their special characteristics are already understood.

High performance lightweight concrete (HPLC) possesses not only advantages from each predecessor but also new ones derived from synergy between high performance matrix and lightweight aggregate. HPLC is a novel material that presents new questions and unknowns to concrete technology and concrete design that need to be resolved before it can be used more extensively.

HPLC has not been extensively investigated. Particularly, long-term properties such as creep, shrinkage and prestress losses have not been systematically studied.

The overall purpose of the research was to determine the creep and shrinkage properties of HPLC and to relate this properties to the long term-behavior of precast prestressed bridge girders made using HPLC.

1.2 Research Approach and Scope

This research effort has combined a multi-scale approach designed to contribute to the understanding time-dependent deformations of HPLC. The large-scale portion considered the construction and evaluation of six full-scale HPLC prestressed girders

with an intensive testing of several concrete properties. A medium-scale program considered the study of strength, elastic modulus, creep and shrinkage of ten different mixtures to assess the effect of mixture continents and environmental conditions on HPLC performance. The small-scale study focused on the interaction among the phases of HPLC and used novel techniques to map elastic and time dependent deformations.

There has been no previous research on short and long-term properties of HPLC at these various levels conducted simultaneously. Important information and conclusions can be obtained from each of the single-scale studies, but new insights and further understanding can also be found from combining results at different scales.

1.3 Definitions

High Performance Concrete (HPC): ACI Committee 116 defined HPC as "concrete meeting special combinations of performance and uniformity requirements that cannot always be achieved routinely using conventional constituent materials and normal mixing, placing, and curing practices"[1]. The new report of the American Concrete Institute Committee 363 defined high strength concrete (HSC) as a concrete with a cylinder compressive strength that exceeds 55.2 MPa (8,000 psi) [2].

Structural Lightweight Concrete (SLC): ACI committee 213 defined structural lightweight aggregate concrete as a concrete with an air-dried density at 28 days in the range of 1120 and 1920 kg/m^3 (70 and 120 lb/ft^3) and a compressive strength above17.2 MPa (2500 psi) [3]. The same committee defined high strength lightweight concrete as SLC with a 28-day compressive strength of 41.4 MPa (6000 psi) or greater.

High Performance Lightweight Concrete (HPLC): HPLC is in fact included in the HPC definition since "lightweight" is a special performance; yet, lightweight

aggregate is not a conventional constituent. In this document, HPLC is a combination of HPC and SLC with a compressive strength of 55.2 MPa (8000 psi) or greater.

Shrinkage: is the decrease of hardened concrete volume with time. This is due to changes in the moisture content of the concrete and physico-chemical changes [4]. This includes an autogenous portion that occurs under no moisture loss to the environment and a drying portion that considers moisture loss.

Creep: is the time-dependent increase in strain in hardened concrete subjected to sustained stress [4]. This includes basic creep occurring under no moisture loss to the environment and drying creep which is the additional creep due to moisture loss.

Prestress Losses: is the reduction of tensile stress in prestressing tendons due to shortening of the concrete around the tendons, relaxation of stress within the tendons and external factors which reduce the total initial force before it is applied to concrete [5]. Shortening of concrete is comprised of elastic and time-dependent deformations such as creep and shrinkage.

1.4 Dissertation Organization

This dissertation is comprised of seven additional chapters. It begins with a background review of the research done in the past conducted at each of the three scale levels. Chapter 3 introduces the research objectives and research methodology.

The following chapter focused on the performance evaluation of six prestressed concrete bridge girders. Particularly, Chapter 4 analyzes the prestress losses and compares HPLC performance to a normal weight HPC. This chapter contains the results from the large-scale study.

Chapter 5 presents and analyzes the medium-scale study, and it is comprised of sections on maturity, on the effect of aggregate mechanical properties on elastic and time-dependent deformations of concrete, the influence of water contained in the pre-soaked aggregate on HPLC performance, and the effect of drying on long-term performance of HPLC.

Chapter 6 presents the results from the small-scale study. It discusses the following for HPC and HPLC: on elastic deformation, creep and shrinkage of normal strength and HPC mapped with the aid of microscopy and image analysis techniques; and a comparison of the deformation maps of HPC and HPLC.

Chapter 7 combines the finding of the large, medium, and small-scale studies. Finally, Chapter 8 presents a summary of conclusions given throughout the dissertation and gives recommendations for future research efforts.

In order to facilitate the access to the references, each chapter of the dissertation contains its own reference section.

1.5 References

1. ACI Committee 116, "Cement and Concrete Terminology", in *ACI Manual of Concrete Practice*. American Concrete Institute: Farmington Hills, MI. 2000, p. 116R.1-116R.73.
2. ACI Committee 363, "State-of-the-Art Report on High-Strength Concrete: Chapter 1 - Introduction (Approved)". American Concrete Institute. 2005.
3. ACI Committee 213, "Guide for Structural Lightweight-Aggregate Concrete", in *ACI Manual of Concrete Practice*. American Concrete Institute: Farmington Hills, MI. 2003, p. 38.
4. ACI Committee 209, "Prediction of Creep, Shrinkage, and Temperature Effects in Concrete Structures", in *ACI Manual of Concrete Practice*. American Concrete Institute: Farmington Hills, MI. 1997, p. 209R.1-209R.47.
5. PCI, *PCI Design Handbook, Precast and Prestressed Concrete*. Fifth ed. Chicago: Precast / Prestressed Concrete Institute, 1998.

CHAPTER 2

LITERATURE REVIEW

High performance lightweight concrete (HPLC) can be thought as a combination between high performance concrete (HPC) and structural lightweight aggregate concrete (SLC); for that reason the literature review starts introducing HPC, SLC, and HPLC in Section 2.1.

Section 2.2 is focused on the long-term deformations in concrete; particularly, description, mechanisms, and factors influencing creep and shrinkage. Section 2.3 presents a detailed review on the research carried out in microstructure, mechanical properties and creep and shrinkage of HPLC.

Section 2.4 presents the investigation done in a relatively novel topic in concrete research referred as internal curing. Internal curing deals with the synergy between low water-to-cement ratio cement-based materials and water stored internally within the concrete.

The most of the research presented in Sections 2.2 to 2.4 are related to the more traditional medium-scale portion of this research study. The last two Sections of this chapter are focused on the large-scale and small-scale portions. Specifically, Section 2.5 presents a background review on prestress losses in concrete members with normal strength concrete (NSC), HPC, SLC, and HPLC. Finally, Section 2.6 presents some of the research done using image analysis to assess deformations in cement-based materials, which is the aim of the small-scale study.

2.1 Concrete Performance

2.1.1 High Performance Concrete

ACI Committee 363 [1] defines high strength concrete as concrete with a cylinder compressive strength that exceeds 41.4 MPa (6000 psi), while ACI Committee 116 [2] defines HPC as:

> "concrete meeting special combinations of performance and uniformity requirements that cannot always be achieved routinely using conventional constituent materials and normal mixing, placing, and curing practices. The requirements may involve enhancements of placement, compaction without segregation, long-term mechanical properties, early-age strength, volume stability, or service life in severe environments."

Other definition supported by the Federal Highway Administration (FHWA) [3] went further and stated that HPC can be specified not only by the strength, but by any of the following: freeze-thaw durability, scaling resistance, abrasion resistance, chloride penetration, creep, shrinkage, and modulus of elasticity. Table 2.1 presents a summary of HPC specifications for highways structures. One potential problem of designing HPC to meet a specific performance criterion is that other properties might worse [4]. HPC performance should be considered holistically in order to satisfy the multiple requirements during service life.

From the definitions above it can be concluded that HPC is a broad concept that may include high strength concrete (HSC), but HSC is not necessarily HPC. To avoid confusions it was proposed [5] for HPC the term low water-to-binder ratio concrete because when concrete has a very low water to binder ratio (less than 0.4) not only achieves higher strength, but also typically improves several characteristics, when adequately mixed and cured, such as higher flexural strength, lower permeability, improved abrasion resistance and higher durability.

Table 2.1: Grade of performances characteristics for HPC at the age of 56 days [3]

Property	Grade 1	Grade 2	Grade 3	Grade 4
	limit	limit	limit	limit
Compressive strength 56 days is recommended , MPa (psi)	> 41.4 (6000)	> 55.2 (8000)	> 69.0 (10,000)	> 96.6 (14,000)
Elastic modulus, GPa (ksi)	> 28.0 (4060)	> 40.0 (5800)	> 50.0 (7250)	
Freeze/thaw durability (%)	> 60	> 80		
Chloride permeability (coulombs)	≤ 3000	≤ 2000	≤ 800	
Scaling resistance (visual rating)	4 to 5	2 to 3	0 to 1	
Abrasion resistance (depth of wear, mm (in))	≤ 2.0 (0.08)	≤ 1.0 (0.04)	≤ 0.5 (0.02)	
Shrinkage at 180 days drying, με [1] (mm/mm x 10^{-6}, in/in x 10^{-6})	≤ 800	≤ 600	≤ 400	
Specific creep at 180 days loading, με/MPa (με/psi)	≤ 70 (0.52)	≤ 60 (0.41)	≤ 45 (0.31)	≤ 30 (0.21)

[1] με stands for microstrains in either mm/mm x 10^{-6} or in/in x 10^{-6}

Several authors [1, 5-12] have summarized the advantages of the HPC with low water-to-cement ratio with respect to the normal strength concrete. Some of the most important advantages follow:

- Reduction in member size, resulting in an increase in building rentable space and a decrease in the volume of concrete required
- Decrease in dead load, and reduction in foundation size
- Increase in members spacing as a consequence of the increase of member bearing capacity
- Reduction in axial shortening of compression supporting members and deflection of flexural members
- Improvement in long-term service performance under static, dynamic, and fatigue loading
- Reduction of creep and shrinkage
- Improved durability
- Increased stiffness as a result of a higher modulus of elasticity
- Reduction in cost for a given load capacity

Although HPC presents advantages over conventional concrete, it requires special care during the production process in order to assure its quality. ACI-363 [13] recognized this, and in 1998 prepared the report "Guide to Quality Control and Testing of High-Strength Concrete". Moreover, it was suggested that

> "HPC is not a cheap concrete that can be produced by anyone; on the contrary, it is becoming an engineered, high-tech material." [5]

One problem associated with some HPC is an increase in the autogenous shrinkage with respect to normal strength concrete [5]. A higher autogenous shrinkage can build up stresses, if the member is not free to deform, which can eventually generate cracking. This increase in autogenous shrinkage can be explained based on the creation of strong menisci in small capillaries when the cement particles demand more water. Because normal strength concrete has larger capillaries, the autogenous shrinkage is not an issue. It was pointed out [14] that the self-desiccation and autogenous shrinkage may be increased by the use of low water-to-binder ratios and by addition of silica fume. HPC also presents a lower relaxation and a higher modulus of elasticity which together can lead to a decrease in the concrete extensibility producing cracking. Another disadvantage of HPC is poor fire resistance compared with normal strength concrete [15]. This poor behavior is due to the very low permeability of HPC, which inhibits the egress of steam formed from water at high temperatures in the hydrated cement paste. Cost of HPC per m^3 (yd^3) is approximately between 1.95 and 2.2 times greater than that of NSC.

2.1.2 Structural Lightweight Concrete

Lightweight concrete was used first by the Greeks and the Romans circa 250 B.C., but the main developments of this a material were in the 1920's with the first manufactured lightweight aggregate [16]. ACI-213 [17] defines SLC as structural

concrete made with lightweight aggregate, with an equilibrium density at 28 days in the range of 1120 and 1920 kg/m^3 (70 and 120 lb/ft^3) and a compressive strength above 17.2 MPa (2500 psi).

Several authors [7, 10, 16-23] have studied the advantages of SLC. The most important advantages follow:

- Reduction in structure dead load, which leads to a reduction the foundation size
- Reduction in member size, resulting in an increase in rentable space and a decrease in the volume of concrete required
- Development of a precast technology as a result of self-weight reduction that facilitates the transport and erection of structural members
- Reduction in the seismic forces that are proportional to the mass of the structure
- Increase in thermal insulation
- Increase in fire resistance
- Increase in blast resistance
- Increase in elastic compatibility between aggregate and cement paste which minimizes micro cracking of the interfacial transition zone (ITZ)
- Reduction in susceptibility to temperature-induced microcracking

As occurs with HPC, SLC also has disadvantages when it is compared with ordinary concrete [10, 16, 22, 24-26]. Some of these disadvantages follow:

- Potential reduction of strength at the same cement content and water-to-cement ratio
- Reduction in the modulus of elasticity for the same strength level which is reflected in larger deflections
- Increase in shrinkage and creep for the same strength level

The first is a consequence of a lower aggregate intrinsic strength which controls the concrete strength. The last two are derived from a lower elastic modulus of the aggregate.

Cost of SLC per m^3 (yd^3) is approximately 50% higher than that of a NSC of similar strength.

2.1.3 High Performance Lightweight Concrete

The first use of high strength lightweight concrete was during World War I [27], when an American corporation built lightweight concrete ships with strength of 34.5 MPa (5000 psi). At that time the commercial strength of normal weight concrete (NSC) was only around 13.8 MPa (2000 psi).

Possibly the principal advantage of HPLC is the structural efficiency given by a favorable strength-to-density ratio [26, 27]. HPLC with compressive strength higher than 55.2 MPa (8000 psi) has been obtained using various types of manufactured lightweight aggregate [23, 26, 28-38]. The highest compressive strength HPLC [30] had 99.8 MPa (14,470 psi) at the age of 28 days and 111.7 MPa (16,195 psi) at the age of 90 days. According to Aïtcin [5], strengths in the vicinity of 100 MPa (14,500 psi) represents the upper strength boundary of HPLC.

In a review of five major joint-industry research programs using HPLC [39] it was concluded that lightweight concretes having compressive strength in excess of 50 MPa (7,250 psi) can readily be made using a competent lightweight aggregate. From those results, it was pointed out that the addition of silica fume and superplasticizers in the mixture provide significant benefits. Another author, that developed HPLC with compressive strength of 69 MPa (10,000 psi) and a density of 2000 kg/m^3 (125 lb/ft^3), highlighted that the most promising mixture obtained contained ASTM Type III cement, fly ash and silica fume [35].

It has been suggested that the replacement of normal weight aggregate by lightweight aggregate improves the mechanical properties of the concrete [19]. This improvement is due to enhanced elastic matching between lightweight aggregate and

cementitious matrix (conventional and high strength matrix). The elastic matching reduces the fracture initiation in the ITZ during and prior to loading. However, the use of an ultra-high-strength matrix, with a very high stiffness, produces an elastic mismatch, resulting in fractures in the lightweight aggregate [19].

Although HPLC may reach a modulus of elasticity of 28 GPa (4060 ksi) [29, 31, 36, 37], which is higher than that obtained with commercial normal strength normal weight concrete (NSC), this value is only 80% of that expected from an HPC of the same strength. In fact, some authors [1, 40, 41] have proposed equations for the estimation of the elastic modulus of HPLC that includes a correction factor for densities below 2485 kg/m^3 (155 lb/ft^3).

It was concluded [41] that the high strength and low density of prestressed girders made with HPLC allow reaching span lengths of 47.2 m (155 ft) without overcoming the standard highway maximum weight limit for transportation. A normal weight concrete of similar strength can only reach about 38 m (125 ft) without going above that limit.

Nevertheless, one author [39] concluded that the use of HPLC will not expand unless designers have confidence in their knowledge of its expected properties. Currently the codes do not specifically consider HPLC. Rather, it is considered as an SLC by applying a capacity reduction factor to the formulas commonly used in the design. Such practice might lead to very conservative values, undermining the application of HPLC [39].

Cost of HPLC per m^3 (yd^3) might be between 2.0 and 2.6 times greater than that of a NSC and about 30% higher than that of a HPC of similar strength.

2.2 Long-Term Deformations in Concrete

Concrete as any other civil engineering material presents an instantaneous deformation upon loading. However, it also presents other kinds of deformation because of aging and its hygroscopic nature. Among those are stress and drying induced deformations. Figure 2.1 presents the change of such deformation with time.

As shown in Figure 2.1, total strain in concrete at any given time can be broken into three portions: elastic strain which is the instantaneous response upon loading, shrinkage which is comprised of autogenous and drying shrinkage, and creep which has basic and drying creep portions.

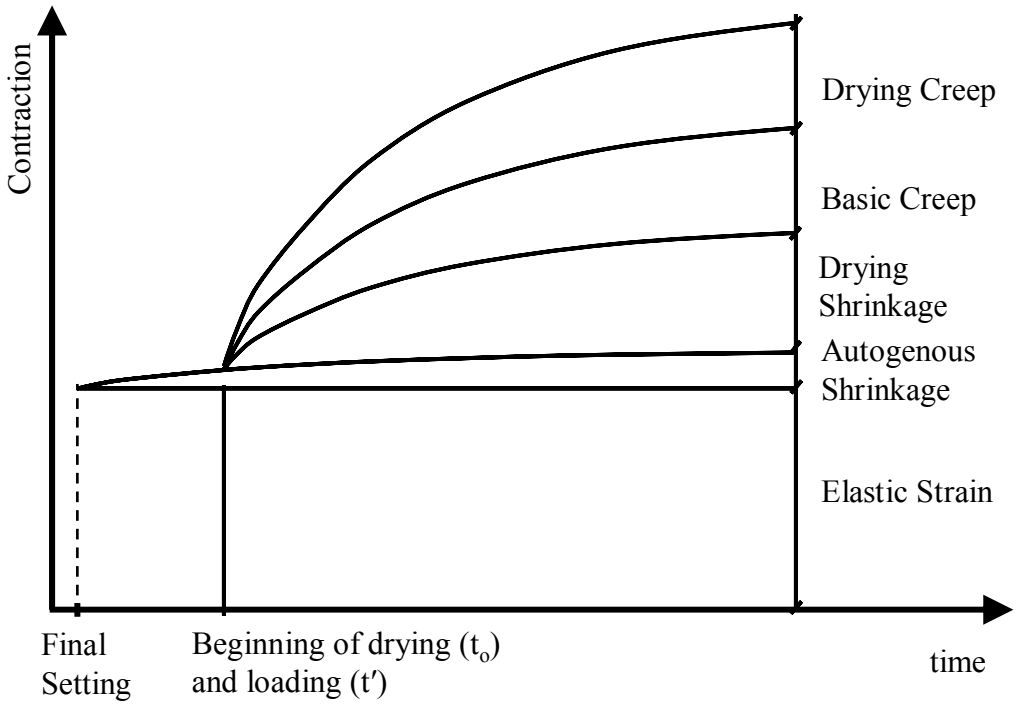

Figure 2.1: Various strains in concrete with time [42]

Creep and shrinkage are usually discussed together because they are influenced by the same factors in similar ways: both are originated in the cement paste, and both

have similar changes with time. Nevertheless, because creep is a stress-dependent strain and shrinkage is not, herein they are analyzed separately.

2.2.1 Shrinkage in Concrete

ACI-116 [2] defines shrinkage as the decrease in length or volume in concrete. Shrinkage has also been defined as a simple phenomenon of contraction of concrete upon loss of water [43]. Behind these simple definitions there are six different types of shrinkage: plastic shrinkage, thermal shrinkage, chemical shrinkage, autogenous (self-desiccation) shrinkage, drying shrinkage, carbonation shrinkage. Thermal shrinkage becomes important during the first days after concrete placement where the heat produced by cement hydration raises the temperature of concrete. During subsequent cooling, concrete experiences thermal shortening that creates tensile stresses in concrete if movement is restrained. Thermal shrinkage stresses can easily overcome the low tensile strength of concrete at early age producing cracking. In addition to thermal shrinkage, only autogenous and drying shrinkage are considered here.

2.2.1.1 Autogenous Shrinkage

Since autogenous shrinkage depends on the concrete mixture design and hydration process and not on the surrounding environment, it is a constitutive property of concrete. For conventional concrete, autogenous shrinkage is relatively small with typical values of 40 με at early ages and 100 to 150 με in the long-term [10, 43, 44]. However, it increases with increasing rate of hydration increases, so cement with higher C_3A (tricalcium aluminate) content, finer cement, the use of some supplementary cementing materials (SCMs), lower water-to-cement ratio, and finer pore structure might increase autogenous shrinkage.

Lynam in 1937 and Davis in 1940 were the first ones in defining and measuring autogenous shrinkage, respectively [45]. Lynam highlighted that autogenous shrinkage was due to neither thermal effect nor loss of moisture to the air. Davis showed with his results that autogenous shrinkage was in the 50-to-100 με range after five years which was very small compared with the concrete thermal and drying deformation at that time.

Nowadays with the use of high-range water reducers, low water-to-cementitious material ratio, higher cement contents, and the use of SCMs, the structure of the paste has drastically changed [45]. This change in microstructure has considerably increased the autogenous shrinkage, making it even greater than thermal and drying shrinkage in some cases. A comparison between the autogenous and drying shrinkage, in concrete mixtures with water-to-cement ratio between 0.17 and 0.40 [46], revealed that the autogenous shrinkage of the 0.40 water-to-cement ratio mixture was 100 με representing the 40% of the total shrinkage (250 με). On the other hand, the autogenous shrinkage of the 0.17 water-to-cement ratio concrete was 700 με which represented the 100% of the total shrinkage. Another study measured autogenous shrinkage in 0.3 water-to-cementitious material ratio cement paste in excess of 3000 με after two weeks [47]. These potentially large volumetric changes occur while concrete has not fully developed its strength. These volumetric changes along with thermal shrinkage might easily crack the concrete [48].

It is usually agreed that chemical shrinkage is a volumetric reduction due to hydration that will not show macroscopic changes after final setting. The autogenous shrinkage, on the other hand, is due to self-desiccation and it manifests after final set.

Le Chatelier in the early 1900s established that the volume of hydration products formed during the hydration of the portland cement is considerably less than the sum of the volume of water and cement. This phenomenon known as Le Chatelier's contraction is the cause of the chemical shrinkage. This volumetric contraction has been found to be between 8 and 12% [49]. Before the cement paste reaches its final set, it is free to move to accommodate such change in volume. However, after final set, the rigid skeleton prevents the further contractions with leads to the creation of pores and the increase in pore size. As further cement reaction occurs and more water is used by the reaction, the internal relative humidity of concrete drops creating capillary stresses that produce shrinkage of concrete. The latter portion is known as autogenous shrinkage or self-desiccation shrinkage [48]. A detail explanation of shrinkage mechanisms is given in Section 2.2.1.3.

2.2.1.2 Drying Shrinkage

Drying shrinkage is the contraction due to moisture migration in concrete [50] and the difference with autogenous shrinkage is that in drying shrinkage the water is not used by the cement reaction, but lost to the environment.

Drying shrinkage is not a constitutive property of concrete because it depends on external characteristics such as member size, shape and the environment.

The main driving force of drying shrinkage is the removal of adsorbed water from the hydrated cement paste [7] . The removal of water in small capillary pores also contributes to shrinkage through tensile hydrostatic forces [43]. Removal of capillary and adsorbed water is increasingly more difficult as water becomes strongly tightened to

the hydrated cement paste. Consequently, the loss of water presents a decreasing rate with time as shown in Figure 2.2.

The CEB-FIP [51] gave values to the final drying shrinkage under 50% relative humidity for a 24.1-MPa (3500-psi) concrete of 645 με. For conventional concrete under standard ambient conditions (23°C / 73.4°F and 50% relative humidity), drying shrinkage, measured in 75 to 150 mm-deep (3 to 6 inch) specimens, generally ranges between 400 and 800 με after two years.

Time under drying is other of the most important factor influencing drying shrinkage. As time under drying increases, more water is withdrawn from capillaries causing larger shrinkage. There is still disagreement on whether the age at the beginning of drying is important or not. The most commonly used empirical models for estimating drying shrinkage considered time under drying as a main variable, but only two of them used age at the beginning of drying [50, 52-57].

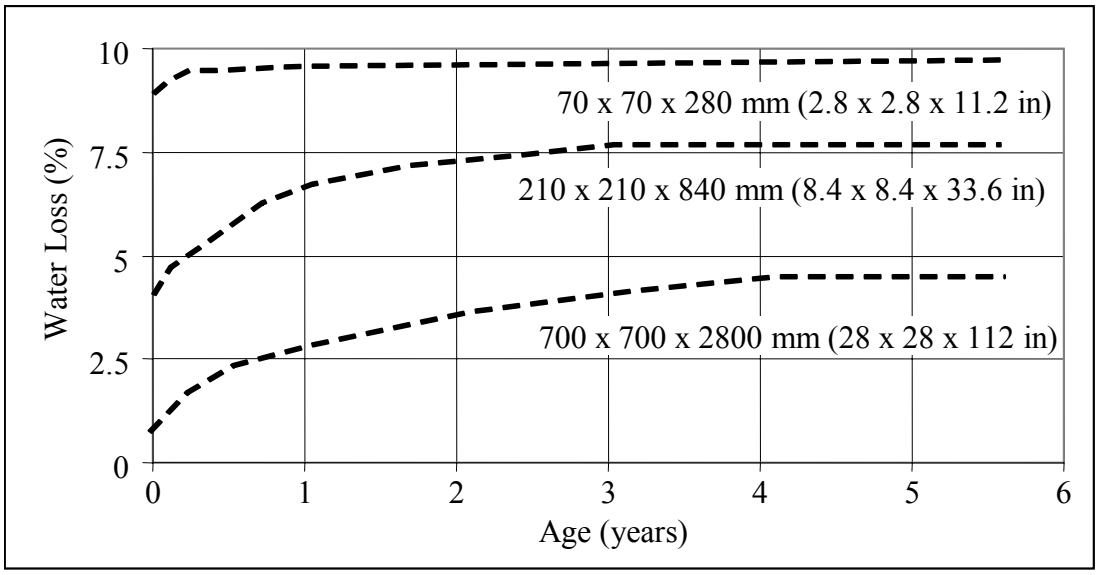

Figure 2.2: Water loss versus time from concrete specimens of various sizes under 55% relative humidity [43]

2.2.1.3 Mechanisms

There are three mechanisms that explain shrinkage of the cement paste as it dries: change in volume by capillary stresses, by disjoining pressure and by surface energy. Even though these three are related to water migration in cement paste, the change in volume of drying concrete is not the same for each due to differences in how tightly the water is bound to the microstructure as shown in Figure 2.3.

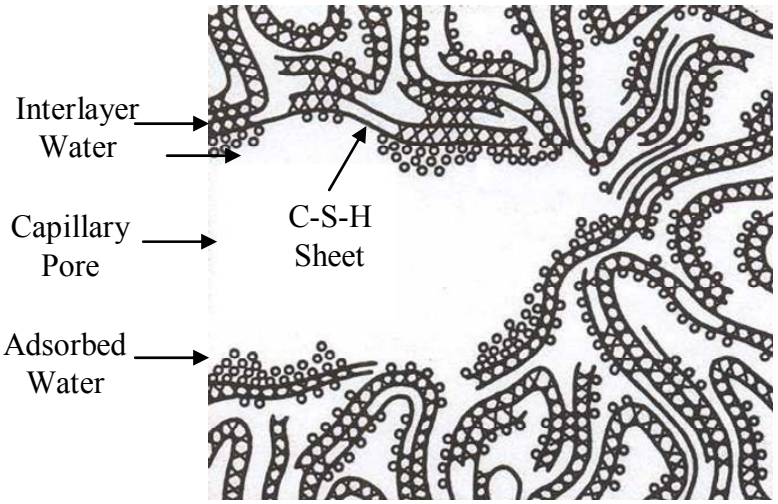

Figure 2.3: Representation of cement paste microstructure [7]

First, there is capillary water which is relatively easy to remove. The drying force required to remove the water from capillaries is inversely proportional to the size of the capillary. Therefore, water is first withdrawn from the void space in the large pores followed by increasingly smaller pores.

Second, adsorbed water which is physically bound to the large surface area present in C-S-H, walls of capillary pores, or surface or other hydration products such as ettringite. This water is more difficult to remove than the capillary water. Third, there is interlayer water, usually bound to two or more C-S-H sheets. The interlayer water is

more difficult to remove because is linked to two or more C-S-H surfaces, and it is only one layer of water molecules [7]. Finally, there is a fourth kind of water not shown in Figure 2.3 called chemically bonded water present in any hydration product. This chemically bonded water is removed only at high temperatures where hydration products decompose.

Researchers agree on three drying shrinkage mechanisms; all of them related to forces initiated by the migration of: (1) water in the capillary pores; (2) adsorbed water; and (3) chemically bounded water. Those mechanisms are:

1. Capillary Stress: When the water is removed from capillary pores, a stress is induced. As the water in the pores is removed, a new liquid-gas (water-air) interface is created. This requires more energy, so the water creates a meniscus (curved surface) in the wall of the pore in order to minimize the water-gas interface surface energy. As a result the water is under capillary tension stress, and the walls of the pore are under compression [8, 58]. The smaller the pore, the higher the capillary stresses meaning that the amount of shrinkage depends on the size of the pores. The shrinkage measured at this level is believed to be caused by the hydrostatic tension in small capillaries [8, 10, 59] because water is removed from large capillaries, little or no shrinkage takes place.

2. Disjoining Pressure: According to RILEM TC69 [59], Powers in 1965 was the first one to notice that below 40% relative humidity, shrinkage of concrete was higher than predicted by the capillary stress theory and concluded that there was another mechanism affecting shrinkage. In fact, if the relative humidity is low enough (drying force is high enough), the water from capillaries is removed, and the C-S-H start to loose their adsorbed water. As shown in Figure 2.3, the adsorbed water can have several layers

of water depending of the relative humidity. As the relative humidity decreases, the thickness of the adsorbed water layer decreases reducing the "disjoining pressure" as described by the Munich model [58]. At this level, the change in volume of unrestrained cement paste is strongly related to the volume of water removed.

3. Surface Energy: When the internal relative humidity gets below 50%, the disjoining pressure disappears, most of the adsorbed water has been removed and the surface free energy of the C-S-H increases causing further contraction. In fact, there is a linear relationship between change in surface energy and change in length proposed by Bangham and Fakhoury in 1931 [58].

Interlayer water can also be removed at room temperature causing a higher volume change than caused by removal of the adsorbed water [8, 59]. However, this change is highly dependent on the C-S-H surface area. At low specific surface microstructure, as the one obtained when high pressure steam curing is used, the observed shrinkage can be 5 to 10 times lower than similar paste cured normally [10].

2.2.1.4 Factors Influencing Shrinkage

Carlson [60] was probably the first to suggest the restraining effect of the aggregate on the shrinkage of concrete. After Carlson, several researchers [61, 62] have recognized the cement matrix as the phase responsible for volumetric changes and the aggregate as an "inert phase" that reduces the overall shrinkage [63]. Nevertheless, some aggregate do shrink on drying, such those from some sedimentary rocks, and would not provide a restraint to cement paste shrinkage [10].

Pickett [62] developed a model of the aggregate restraining effect starting from a sphere of aggregate embedded in a sphere of cement paste . Equations 2.1a and 2.1b

present the expression proposed by Pickett in linear and logarithmic form, respectively. Using Pickett's expression the shrinkage of concrete can be calculated from the shrinkage of the cement paste, relative volume of aggregate, and the mechanical properties of aggregate and paste.

$$S = S_0 \cdot (1 - g)^{\alpha} \tag{2.1a}$$

$$\log\left(\frac{S_0}{S}\right) = \alpha \cdot \log\left(\frac{1}{1-g}\right) \tag{2.1b}$$

where:

S: linear shrinkage of concrete

S_0: linear shrinkage of cementitious matrix

g: volume of aggregate per unit volume of mixture

α: constant representing aggregate restraining effect as shown in Equation 2.2

$$\alpha = \frac{3 \cdot (1 - \mu)}{1 + \mu + 2 \cdot (1 - 2 \cdot \mu_a) \cdot \frac{E_c(t)}{E_a}} \tag{2.2}$$

where:

μ: Poisson's ratio of concrete

μ_a: Poisson's ratio of aggregate

$E_c(t)$: effective modulus of elasticity of concrete (corresponding to sustained load)

E_a: modulus of elasticity of aggregate

This expression was compared to experimental data from four different cement pastes combined with several amounts of three types of normal weight aggregate [62]. The value for α was 1.7 which was within the range between 1.6 and 2.3 reported previously [60] for a gravel and limestone aggregate, respectively.

Figure 2.4 shows some of Picket's experimental [62] results and compares them with Equation 2.1b. Figure 2.4 shows in its X-axis the logarithm of 1/(1-g) which increases as the aggregate content increases. The Y-axis is the logarithm of S_o/S which represents the relative magnitude between the shrinkage in the matrix and the concrete.

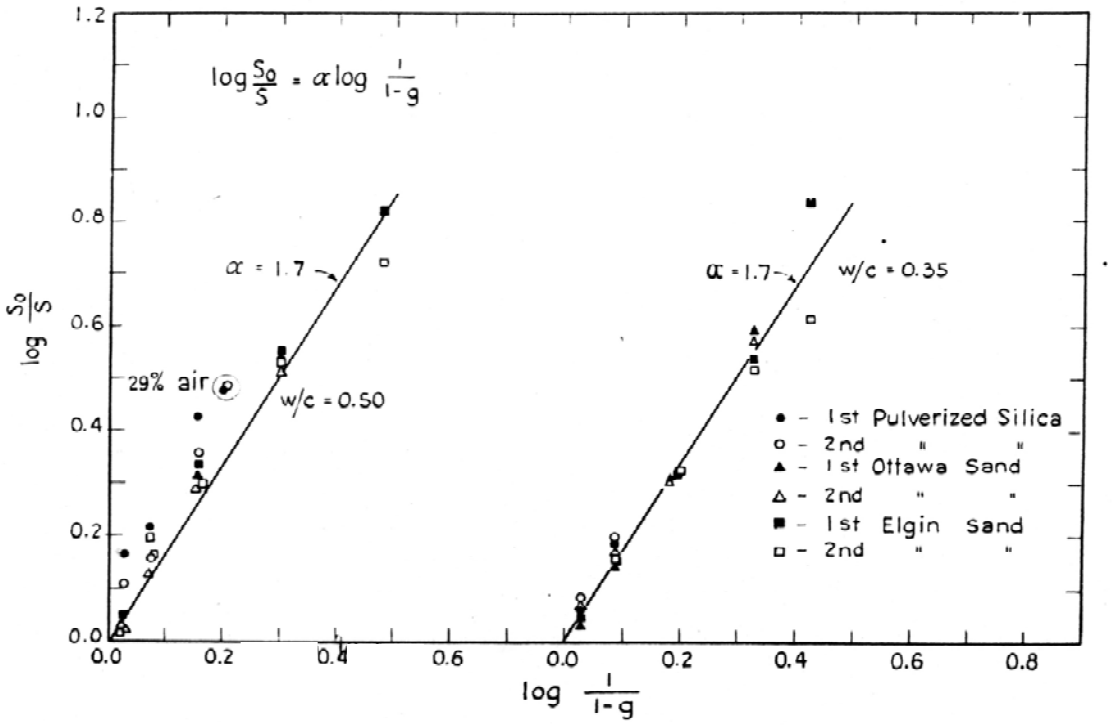

Figure 2.4: Relationship between shrinkage of concrete and aggregate content [62]

As shown in Figure 2.4, the main factor in controlling concrete shrinkage is the aggregate. The slope of the curves represents the α value, which in both cases was 1.7, demonstrating that the restraining effect of the three normal weight aggregates was similar for the two water-to-cement ratios studied.

Based on the Equation 2.2, shrinkage depends not only on the aggregate relative volume but also on aggregate mechanical properties such as stiffness and Poisson's ratio. In addition, the shape of the aggregate and spacing among aggregate particles also play a

role in shrinkage restraining and generation of internal stresses [63]. A larger maximum size of aggregate (MSA) provides a higher restraining effect for shrinkage [8]; in contrast, it was pointed out that this is an indirect effect due to the higher volume of aggregate that is possible to use when a larger MSA is chosen [10].

After aggregate, the second most important factor influencing shrinkage is the water-to-cement ratio. The lower the water-to-cement ratio, the lower the shrinkage experienced by the cementitious matrix. At high water-to-cement ratios autogenous shrinkage decreases, but drying shrinkage increases given an overall increase in shrinkage. On the other hand, at low water-to-cement ratios the autogenous portion increases and the drying one decreases. Because the concrete strength increases too, the overall effect of decreasing water-to-cement ratio is a reduction in total shrinkage.

It is generally agreed that the effect of cement and water contents on drying shrinkage is indirect [7]. Those effect are mainly linked to the fact that they change the total volume of cement paste, and therefore, change the proportion of the aggregate and its retraining effect [7, 10].

Figure 2.5 shows the effect of both water-to-cement ratio and aggregate content on shrinkage of concrete [10]. The X-axis presents the water-to-cement ratio while the Y-axis shows the shrinkage in με. The curves correspond to different aggregate content.

Powers [64] applied the concept of restraining effect to not only to the aggregate but also to the unhydrated cement which acts as filler [7]. This concept becomes important when considering concretes with very low water-to-cement ratio in which not all the cement will hydrate. The unhydrated cement might be the explanation of the great reduction in shrinkage shown in Figure 2.5 when water-to-cement ratio changes from 0.4

to 0.3. This effect is more important as the volume of cement paste increases because there is more unhydrated cement left after hydration.

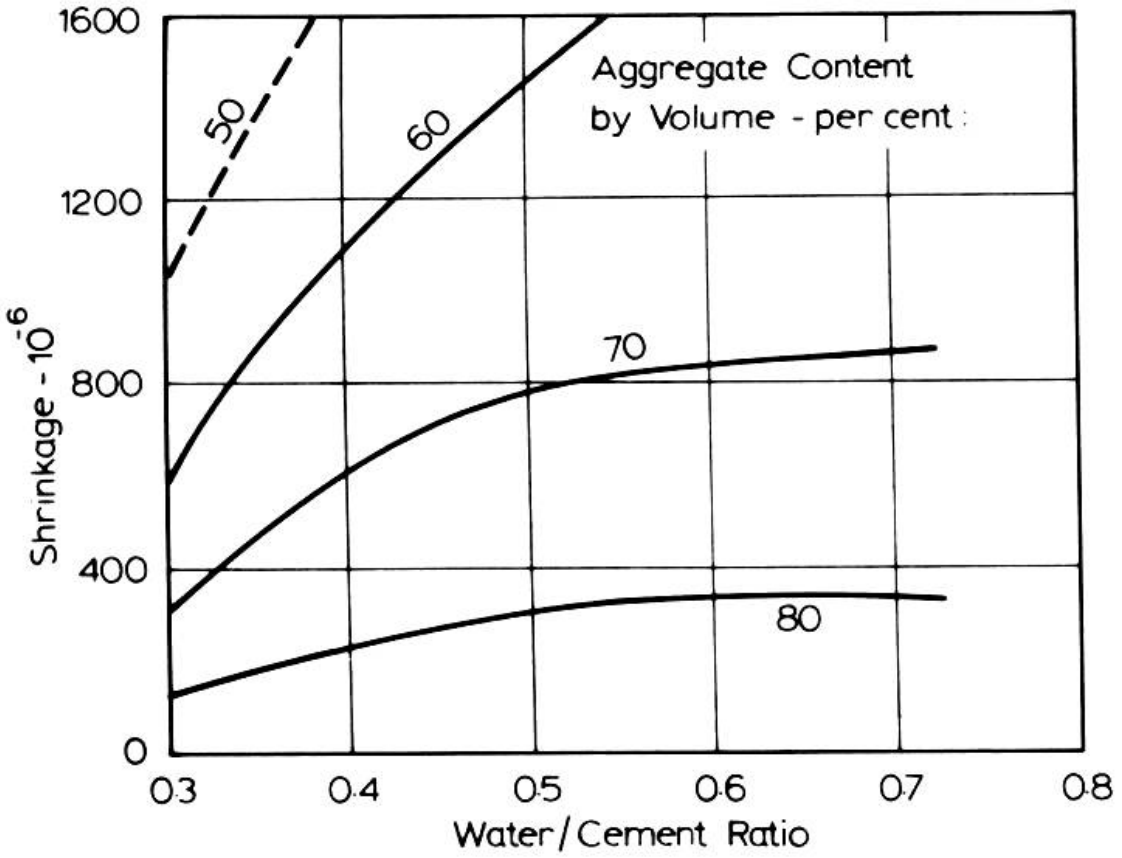

Figure 2.5: Effect of water-to-cement ratio and volume of aggregate on shrinkage [10]

In general, any SCMs that refines the pore structure of the concrete will increase the shrinkage [49]. Nevertheless, others concluded that the influence of SCMs on shrinkage is highly variable and no generalizations can be made [65, 66]. Fly ash, ground granulated blast-furnace slag, and silica fume have different effects at different ages. The first two tend to reduce the water demand for the same workability, so if the content of cementitious materials is maintained, the reduction in the water-to-cementitious material

ratio produces a reduction in drying shrinkage. On the other hand, if the cementitious material content is reduced to keep the water-to-cementitious material ratio constant, the drying shrinkage tends to increase at early ages and remain unchanged at later ages with respect to a similar mixture with only portland cement. This is due to the lower early age compressive strength observed in mixtures with cement replacement by fly ash and slag; consequently, at later ages when the compressive strength of the mixtures with and without those SCMs are similar, drying shrinkage is similar as well. The effects of fly ash and slag also depend on the level of replacement and their chemical composition and fineness [65].

Silica fume produces a slight decrease in drying shrinkage as the level of replacement increases [66]. On the other hand, silica fume refines the pore structure in hardened concrete increasing the capillary stresses produced during self-desiccation. This increase in capillary stresses increases the autogenous shrinkage of the concrete [67]. Nevertheless, this very fine pore structure leads to very low permeability, and consequently slow drying and low values of drying shrinkage [49].

It was reported that mortars with partial replacement of cement by calcareous and siliceous SCMs showed, after one year, four and 23% less shrinkage deformation than that of control specimens with only cement [68].

Finally, it was found that even though increasing amounts of metakaolin or silica fume considerably decreased autogenous shrinkage during the first 24 hours, after 200 days the trends were not clear [69]. The concrete mixtures containing 10 and 15% silica fume showed more autogenous shrinkage than the mixture with no silica fume. Both metakaolin and silica fume considerably reduced the drying shrinkage portion with

replacement levels of only 5%. Higher replacement levels further decreased drying shrinkage to a minor extent. Total shrinkage was consistently decreased as the level of metakaolin replacement increased, while the silica fume mixtures presented a minimum total shrinkage for 5% replacement.

The effect of SCMs on shrinkage depends of multiple factors such as type, chemical composition and fineness of the SCM, replacement level, and overall impact in the mixture design. Thus no general conclusions can be drawn, and every case needs to be addressed specifically.

The effects of chemical admixtures on shrinkage are unclear. While plasticizers can increase shrinkage, their effect varies widely and no significant differences can be found [66, 70]. When the superplasticizers are used to decrease water dosage rather than increase slump, they tend to decrease shrinkage [49]. This reduction might be due to a decrease in the amount of cement paste in concretes with less water and the same amount of cement.

Because shrinkage is the result of water migration within the concrete or from concrete to the environment, curing and storage conditions strongly affect shrinkage. A prolonged moist curing enhances hydration, changes the pore structure, and keeps a high internal relative humidity in the concrete [14, 45]; consequently, shrinkage is decreased with longer curing periods.

2.2.2 Creep in Concrete

Most materials behave elastically or nearly so under small stresses and upon loading immediate elastic (recoverable) strain response is obtained [71]. However, when higher stresses are applied, a slow and continuous increase in strain at a decreasing rate

also occurs in some materials. These are referred to as "viscoelastic materials". Among them, there are different kinds of plastics, wood, natural and synthetic fibers, concrete, and metals. Metals behave viscoelastically only at elevated temperatures.

Creep in materials can be described in terms of three stages as shown in Figure 2.6. The X-axis in Figure 2.6 represents time in linear scale and arbitrary units. The Y-axis represents either creep strain or creep rate in arbitrary units. In the primary stage, creep occurs at a decreasing rate; in the secondary stage, creep is at fairly constant rate; and finally, in the tertiary stage the creep rate accelerates and leads to failure.

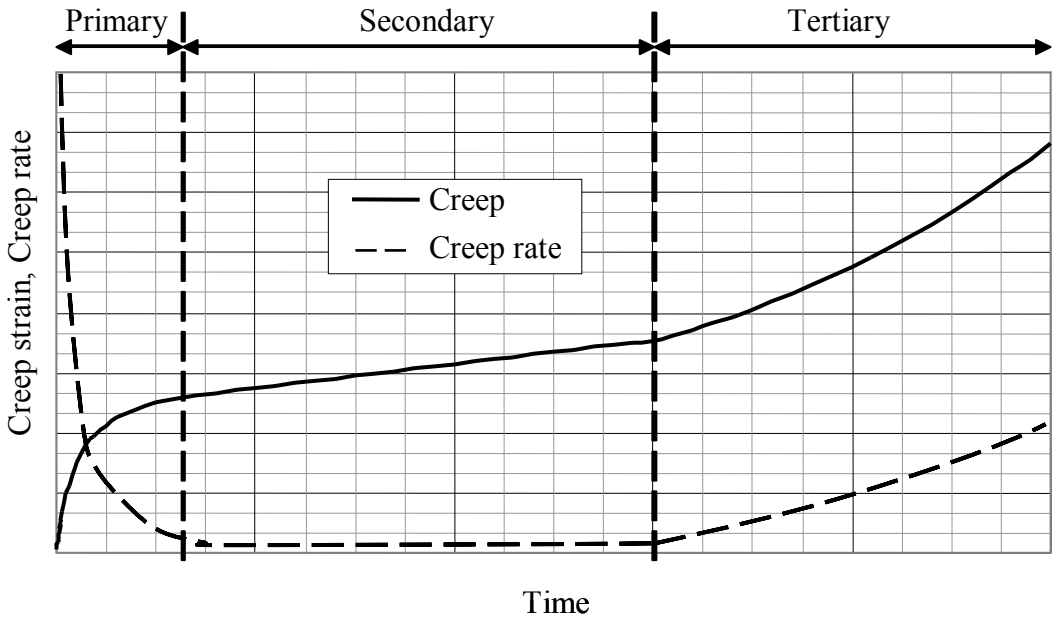

Figure 2.6: Representation of the three stages of creep

For the normal stress level present in concrete, primary and secondary stages cannot be distinguished and tertiary stage does not exist [72]. Based on this, the rate of creep deformation in concrete continuously decreases with time, but it does not reach a limiting state [44].

Two of the earliest research efforts addressing creep of concrete [73, 74] measured time dependent deformations in concrete beams and cylinders as large as the initial elastic deformation. Even though those authors noticed that the creep deformation increased with applied stress, the proportionality between creep and stress was obtained later [75]. Since creep strain is proportional to the applied stress, expressing creep strain in terms of unit stress or in proportion to the elastic strain is convenient. The term specific creep refers to the creep strain divided by the applied stress (με/MPa or με/psi), and the term creep coefficient is the creep strain-to-elastic strain ratio for a given stress.

Specific creep of concretes with compressive strength between 13.8 and 27.6 MPa (2000 and 4000 psi) was reported to be in the wide range between 109 and 267 με/MPa (0.75 and 1.84 με/psi) after 20 years under sustained load [76].

Upon unloading, concrete exhibits an elastic recovery followed by a time-dependent recovery called creep recovery [77]. Both elastic and creep recoveries are less than the initial elastic strain and creep upon loading. Therefore, concrete presents a residual deformation after removing a sustained load as shown in Figure 2.7.

Deformations in materials can be generally classified into two categories: time and recovery. Under time, there are instantaneous and time-dependent deformations while under recovery there are recoverable and irrecoverable deformations. This gives four kinds of deformation:

1. Elastic: an instantaneous and recoverable deformation,
2. Plastic: and instantaneous irrecoverable deformation,
3. Delayed elastic: a time-dependent recoverable deformation, and
4. Viscous: a time-dependent irrecoverable deformation.

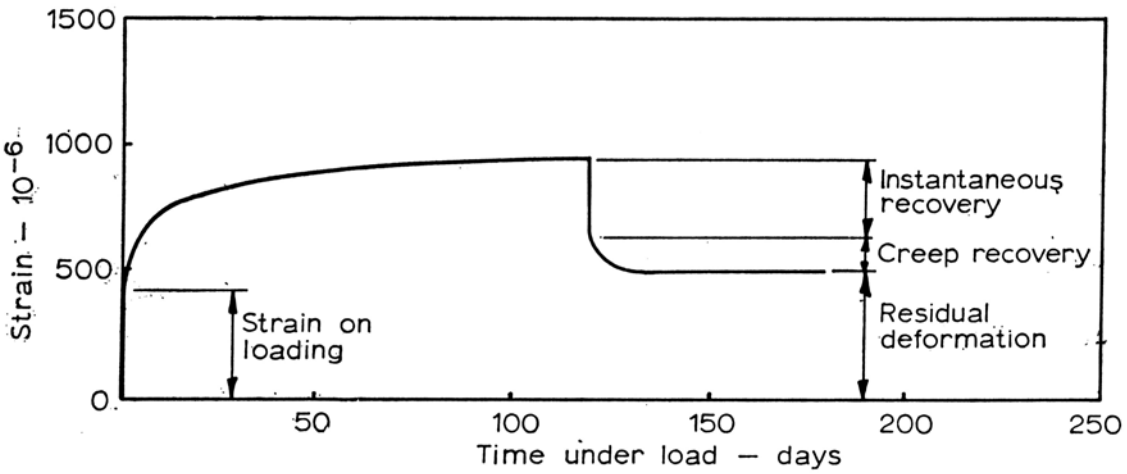

Figure 2.7: Instantaneous and creep deformations and recoveries [77]

The last two forms of deformation are considered to cause creep in concrete. In fact, some authors have associated delayed elasticity and viscous deformation with primary and secondary stages in concrete creep, respectively [77].

Elastic deformation is usually associated with energy stored in the crystals or molecules that is fully recoverable. Plastic deformation occurs when a slip in a plane of maximum shear stress changes positions of crystals, molecules, or atoms have occurred. Slip in plane of maximum stress presents no change in volume and it is not time-dependent [72].

Delayed elasticity is usually a consequence of lack of order in the microstructure; upon loading the microstructure slowly reaccommodates. The energy is not dissipated but stored, so it is fully recoverable. Finally, viscous deformation describes the behavior of fluids and appears only under sustained load. The strain rate is proportional to the applied stress, and there is no recovery upon load removal.

All four kinds of deformation are present in concrete under load, and they are related to the creep mechanisms in concrete explained in Section 2.2.2.3 below.

ACI-209 [50] defines creep in concrete as the time dependent increase in strain in hardened concrete subjected to sustained stress. Several authors [7, 10, 50, 72, 78, 79] have divided creep in concrete into "basic creep", which takes place under conditions of no moisture exchange with the environment, and "drying creep", which is additional creep caused by drying (see Figure 2.1).

2.2.2.1 Basic Creep

Basic creep expressed as strain per unit stress can be conceptualized as a constitutive concrete property since it depends on the material characteristics, but not on member size or ambient conditions. Under normal loading conditions where the loading process is not instantaneous, the so-called "instantaneous strain" is actually comprised of elastic strain and early creep. Therefore, an accurate measure of basic creep is not possible. Moreover, the actual elastic strain decreases with time because the modulus of elasticity increases as the hydration process develops [72, 79]. Consequently, basic creep, defined as the difference between total and elastic strain under no drying conditions, is not easy to measure accurately [10]. Even though there are some inaccuracies in measuring basic creep, for practical purposes it is only important to accurately determine the total strain over time.

2.2.2.2 Drying Creep

Sometimes referred to as the Pickett effect, drying creep not only depends on mixture characteristics, but also on environmental parameters (relative humidity and temperature) and member dimensions. As shown in Figure 2.1, drying creep is the time-dependent deformation of stressed concrete in drying environment, which is in excess of basic creep and drying shrinkage [44]. Therefore, the only way to measure drying creep

is by measuring total strain and by subtracting the elastic strain, basic creep, and shrinkage (autogenous and drying).

Frequently, creep and shrinkage are assumed to be additive which is a convenient simplification, but in reality they are not independent phenomena to which the superposition principle can be applied as the existence of drying creep proves. Again, because they occur simultaneously and from the practical standpoint, the treatment of the two together is convenient and accurate. Drying creep has been referred as one the most difficult aspects of creep [80].

2.2.2.3 Creep Mechanisms

Since creep in concrete was measured for the first time [74], many theories and mechanisms have been proposed over the years. However, two of the most important researchers in the area have recognized that the phenomenon of creep remains uncertain [10, 80]. Among the creep theories proposed in the past, only the most widely accepted are reviewed herein [59, 72, 80, 81].

1. Plastic flow theory: The so called "plastic theories" stated that creep of concrete resulted from some crystalline flow, as occurs in metals beyond the yielding point. Nevertheless, such plastic deformation presents a threshold below which no plastic flow occurs. Concrete and especially neat cement paste present creep at stresses as low as 1% of the ultimate strength [82, 83], so if such a threshold exists in concrete, it is negligible [84]. It was pointed out that plastic deformation is not proportional to the applied stress and is not related to moisture changes as creep in concrete is [85]. Consequently, if plastic flow contributes to creep of concrete, it does it at stresses near to ultimate strength. Other study drew similar conclusions since there was no evidence of

inter-crystalline slip during creep of concrete [84]. Nevertheless, more research concluded that interlayer water within C-S-H structure (see Figure 2.3) can lubricate the maximum shear stress planes facilitating the sliding of crystalline components of the cement paste [72].

2. Viscous flow theory: This theory stated that the cement paste is a fluid with a high viscosity that flows under load [86]. Since concrete also includes aggregate, which typically (i.e., normal weight natural aggregates) do not flow, the load is gradually transmitted from paste to aggregate decreasing the flow rate [72]. Even though this theory explains the absence of a stress threshold for creep to occur, and it represents well the stress dependency of creep, it does not predict any creep recovery as seen in the experimental data [85]. It was suggested that the viscous theory cannot be responsible for all the observed creep because viscous flow requires constant volume, which is not the case in concrete [84].

3. Seepage Theory: This theory stated that creep in concrete is due to seepage of water from the physically adsorbed layers to capillary voids [87]. Applied stress increases vapor pressure of physically adsorbed water, and to restore equilibrium with external conditions, the water is expelled from the C-S-H surface to the capillary pores [81, 84]. As explained in Section 2.2.1.3 of shrinkage mechanisms, a decrease in water content in C-S-H results in volume changes. The cement paste undergoing creep starts to be squeezed out progressively which increases the stress in aggregates and decreases stress in the cement paste. As water is expelled from the C-S-H surface, it becomes increasingly difficult to remove. These two effects produce a decrease in creep rate as observed experimentally.

The seepage theory can explain both basic and drying creep. For instance, under no moisture exchange with the environment, adsorbed water expelled from the C-S-H can migrate to capillary pores or even to aggregate pores [88]. On the other hand, under moisture loss conditions, water evaporates from the air-exposed ends of the capillaries producing tensile stresses that draw further water from the C-S-H surface. This adequately predicts an increase in creep with a decrease in relative humidity. Creep under tension can be explained using the same argument. Tensile stress causes a decrease in vapor pressure transforming capillary free water into adsorbed water. This would restore pressure equilibrium within cement paste microstructure and would cause expansion.

Detractors of this theory stated that if it were true, moisture loss in a specimen under load should be greater than that of a non-loaded companion specimen [85]. The fact that such difference weight loss is normally not present was used oppose the seepage theory. Nevertheless, the loss of adsorbed water can occur with no movement of water to the environment [84]. One possible problem of this theory is that upon unloading, the vapor pressure in the C-S-H surface decreases and adsorbed water should be restored. This implies a total recovery of creep after unloading, which does not happen in concrete [89]. One possible explanation of this inconsistency may be the formation of new bonds in C-S-H that would prevent the total recovery [84]. The applied stress allows contact of the C-S-H sheets creating solid-to-solid attraction forces. Such forces would be large enough in these colloidal structures to prevent total recovery of the creep after unloading.

Some other evidence that supports the main role of water in concrete is that mortar and cement paste with all the evaporable water removed do not undergo creep

[90]. On the other hand, based solely on the seepage theory, tensile creep under water would be increased by water intake from the environment similarly as compressive creep is increased by water loss to the environment. Experimental results show tensile creep under water to be one tenth of tensile creep in air [84].

4. Delayed elasticity: Also referred as viscoelasticity, this theory rested on a two-component model of the cement paste microstructure. The first component is an elastic skeleton comprised of crystalline hydrates while the second component is viscous portion containing the non-crystalline phase with adsorbed water. When such as structure is initially loaded the elastic and viscous component take the load in proportion with their respective stiffness. The viscous phase progressively deforms transferring its portion of the load to the elastic skeleton. The elastic skeleton deforms elastically upon further loading showing a delayed elastic behavior. It was concluded that such mechanism does not offer a satisfactory explanation to the role of moisture exchange in creep [85]. In addition, this mechanism fails to predict irrecoverable creep upon unloading which is the case of creep in concrete as shown in Figure 2.7.

5. Microcracking effect: This mechanism was proposed to explain the non-linearity in the concrete stress-strain relationship by the presence of the ITZ between aggregate and paste [91]. This ITZ is considered, by many, to be the weakest region in concrete [7, 8, 10]. In this region, porosity and density of microcracks tend to be greater than in the bulk paste. It was suggested that creep does not create any new microcracks, but it only propagates those formed at the ITZ during initial loading, drying or thermal shrinkage [79]. Therefore, one explanation of why creep increases under drying conditions (drying creep) might be microcracking initiated by drying shrinkage [92].

Based on this theory it is possible to explain the residual strain upon unloading by the propagation of preexisting microcracks. In addition to the permanent strain in cracks, it is also possible the formation of new bonds in C-S-H [72], in the same way that is presented in the seepage theory. It should be pointed out that at high stresses the role of the microcracking becomes more important. In fact, creep at stresses near to ultimate strength showed that microcracking might be responsible for 10 to 25% of creep [93]. The stress-to-strength ratio constant threshold at which microcracking starts to contribute to creep, and it has been suggested that it increases with compressive stress [89]. One study [94] showed that, under certain heat-curing conditions, there was not significant increase in creep (i.e., no microcracking effect) at stresses equivalent to 70% of the compressive strength, for HPCs with 28-day compressive strength between 56 and 61.3 MPa (8120 and 8890 psi).

In addition to the more widely accepted mechanisms discussed above, some authors have identified additional mechanisms that may cause or influence creep:

6. Solidification Theory: This theory wanted to explain the aging behavior of creep in concrete [95]. The theory stated that the decreasing rate in creep of concrete with time under load is due to the formation of new hydration products inside the micropores of the cement paste. This increasing volume of hydration products is capable of carrying load decreasing the overall stress that causes creep. One deficiency of this theory is that it does not explain the role of water and the increase in creep during drying (drying creep). Another shortcoming acknowledged by the authors is that the increase in hydration product volume would not be significant after one month while that change in creep curves with age is noticeable after several years.

7. Microprestress-solidification Theory: This theory is an extension of the solidification theory above [92]. This theory stated that in addition to the aging effect creep is driven by multiple interatomic bond breaks in overstressed locations. Such an overstress is due to hindered adsorbed water diffusing to the capillary pores. This microdiffusion is proportional to the relative humidity in the capillary pores and accelerates the bond breaking process in the C-S-H. As bonds break, stress decreases at the breaking location, but increases in the vicinity. This creates new overstress location likely to undergo creep. An eventual exhaustion of overstressed sites causes the creep rate to decline. Even though the authors believed the consolidation theory (seepage theory [87]) to be incorrect, their theory can be regarded as a detailed explanation and extension of that theory. Both theories locate the main cause of creep in the movement of water from the C-S-H surface to the capillary pores.

Regardless of the numerous theories on creep and variety research done in creep of concrete, researchers recognized that there are many unknowns.

In 1955 Neville [84] stated:

"… creep of concrete under sustained stress cannot be ascribed to a single cause but to a combination of causes. It is, at the present stage, impossible to tell definitely what proportion of creep is due to each of the influencing factors. Moreover, it is probable that these proportions depend on the conditions to which the concrete is subjected."

In 1964 Ali and Kesler [85] concluded:

"It may be observed that although some of the mechanisms discussed above do offer plausible explanations for certain aspects of observed creep behavior, none of them appear capable of providing a convincing explanation for the great sensitivity of creep to moisture exchange."

In 1970 and 1983, Neville and coworkers [72, 79], after discussing the proposed creep mechanisms, stated:

"A number of theories have been proposed over the years but it is probably justified to say that, as they stand, none is capable of accounting for all the observed facts."

In 1996 Neville [10] suggested:

"Having said all this, we have to admit that the exact mechanisms of creep remain uncertain."

Bažant [80] in 2001 said:

"…despite major successes, the phenomenon of creep and shrinkage is still far from being fully understood, even though it has occupied some of the best minds in the field on cement and concrete research and materials science."

Several authors have concluded that creep is due to more than one mechanism [7, 72, 81, 84, 85]. Researchers generally agreed that aside from microcracking in the ITZ, creep can be understood from viscoelastic (delayed elasticity) deformation in the cement paste and water migration from C-S-H surface to capillary pores. The viscoelastic effect is thought by many as the cause of basic creep and the water migration as the cause of drying creep. In both mechanisms, water possesses a role on creep, but they disagree on the nature of such a role. That is, whether the water movement is a fundamental cause of creep or whether water only modifies the movement of the C-S-H.

2.2.2.4 Factors Influencing Creep

Creep characteristics of any type of concrete are mainly influenced by aggregate-to-cement paste proportion, aggregate characteristics, water and cement content, age at time of loading, type of curing, storage conditions, amount and type of chemical and mineral admixtures, and applied stress-to-strength ratio [10].

It is commonly agreed that, as occurs with shrinkage, the source of creep is the cement paste and the aggregate is an elastic skeleton that retrains creep. Nevertheless,

similarly to shrinkage, results from Kordina [96] where some aggregates showed creep under sustained load has been reported elsewhere [72].

It was suggested that the restraining effect of aggregate on the cement paste deformation is independent of whether the deformation is due to shrinkage or creep [77]. Therefore, the expression proposed for shrinkage [62] is entirely applicable to creep.

Pickett's expression modified by Neville [77] for describing creep is presented in Equation 2.3a (power form) and 2.3b (logarithmic form).

$$c = c_p \cdot (1-g)^{\alpha} \tag{2.3a}$$

$$\log_e(c) = \log_e(c_p) - \alpha \cdot \log_e\left(\frac{1}{1-g}\right) \tag{2.3b}$$

where:

c: creep strain of concrete

c_p: creep strain of cementitious matrix

g: volume of aggregate per unit volume of mixture

α: constant representing aggregate restraining effect as shown in Equation 2.2

Values for "α" measured between 1.2 and 1.7 have been reported, depending on the normal weight aggregate used [7, 61].

Equation 2.3 applies to concretes of constant water-to-cement ratio and loaded to the same stress-to-strength ratio [7]. Figure 2.8 shows the relationship between basic creep after 28 days under load and content of aggregate "g" for concrete made with portland cement, loaded at 14 days to a stress-to-strength ratio of 0.5. Figure 2.8 also compares experimental data and Equation 2.3b. X-axis presents the logarithm of 1/(1-g) which increases as the aggregate content increases. Y-axis shows the logarithm of the creep in concrete (c).

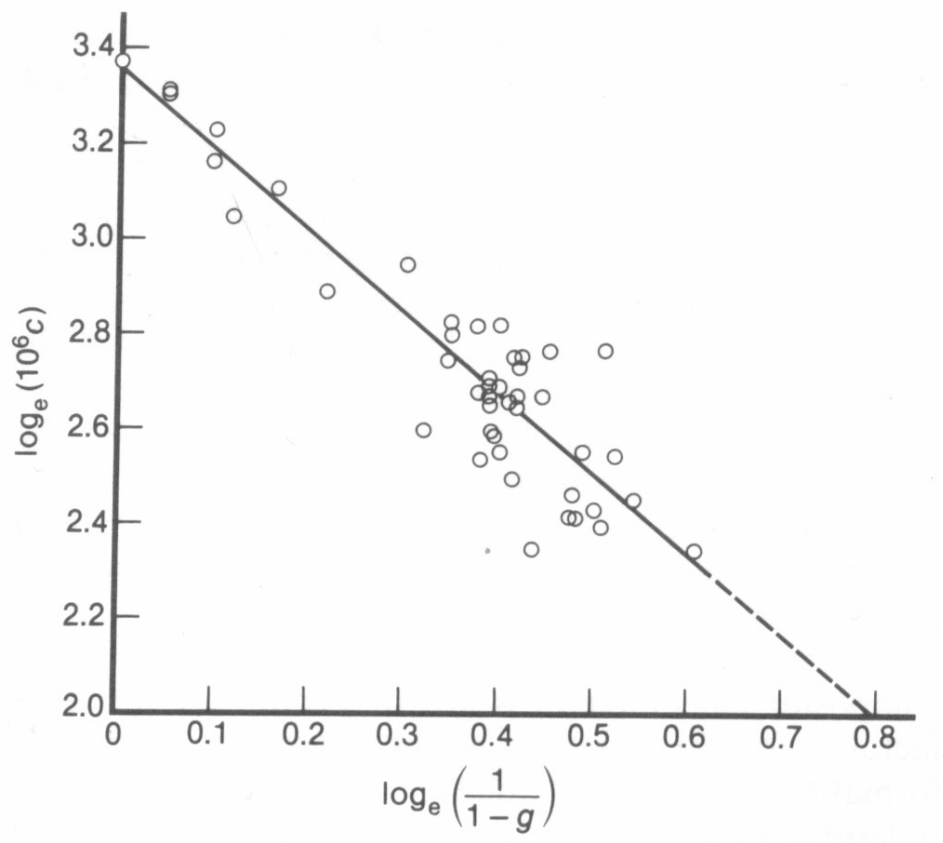

Figure 2.8: Relationship between creep of concrete and aggregate content [79]

From Figure 2.8, it can be concluded that the aggregate content (or cement paste content), explained an important proportion of the variance in creep of concrete, but there is still an unexplained variability around the line in the plot (Equation 2.2b with α=1.71). The variability might be due to "α", which can be conceptualized as the restraining effect of the aggregate. As it can be seen in Equation 2.2, "α" decreases with increasing age of loading and increases with increasing time under load. The latter effect is due to a decrease in $E_c(t)$ with increasing time under load.

Several researchers have investigated the effect of modulus of elasticity of aggregate on creep. Figure 2.9 presents the results from various studies [96-99], where the X- axis is the aggregate elastic modulus and the Y- axis represents the relative creep

which is equal to 1 for an aggregate with an elastic modulus of 69 GPa (10,000 ksi). Equations 2.2 and 2.3 are included in Figure 2.9 for comparative purposes. Poisson's ratio of concrete and aggregate was assumed to be 0.17 and 0.12, respectively. Elastic modulus of concrete was assumed to be 32.7 GPa (4750 ksi). The aggregate content was 73% by volume for some studies [96-98] and 67% for the other [99].

Figure 2.9 shows good general agreement between model and experimental data. It should be noticed that a decrease in aggregate elastic modulus from 80 to 40 GPa (11,600 to 5800 ksi) increased creep by almost a factor of one while an increase from 80 to 120 GPa (11,600 to 17,400 ksi) showed almost no change in creep of concrete.

Considering that most aggregates had an elastic modulus of at least 40 GPa (5800 ksi), it can be concluded that even though the model followed the experimental data tendencies, the latter presented great variability. For instance, there was a quartzite with an elastic modulus of 73 GPa (10,585 ksi) that yielded a relative creep of 1.36 while a granite with a slightly lower elastic modulus of 70 GPa (10,150 ksi) had a creep 40% lower. In fact, the author concluded that creep and shrinkage of concrete are affected by aggregate through a combination of effects like cement paste – aggregate interaction and water demand [99].

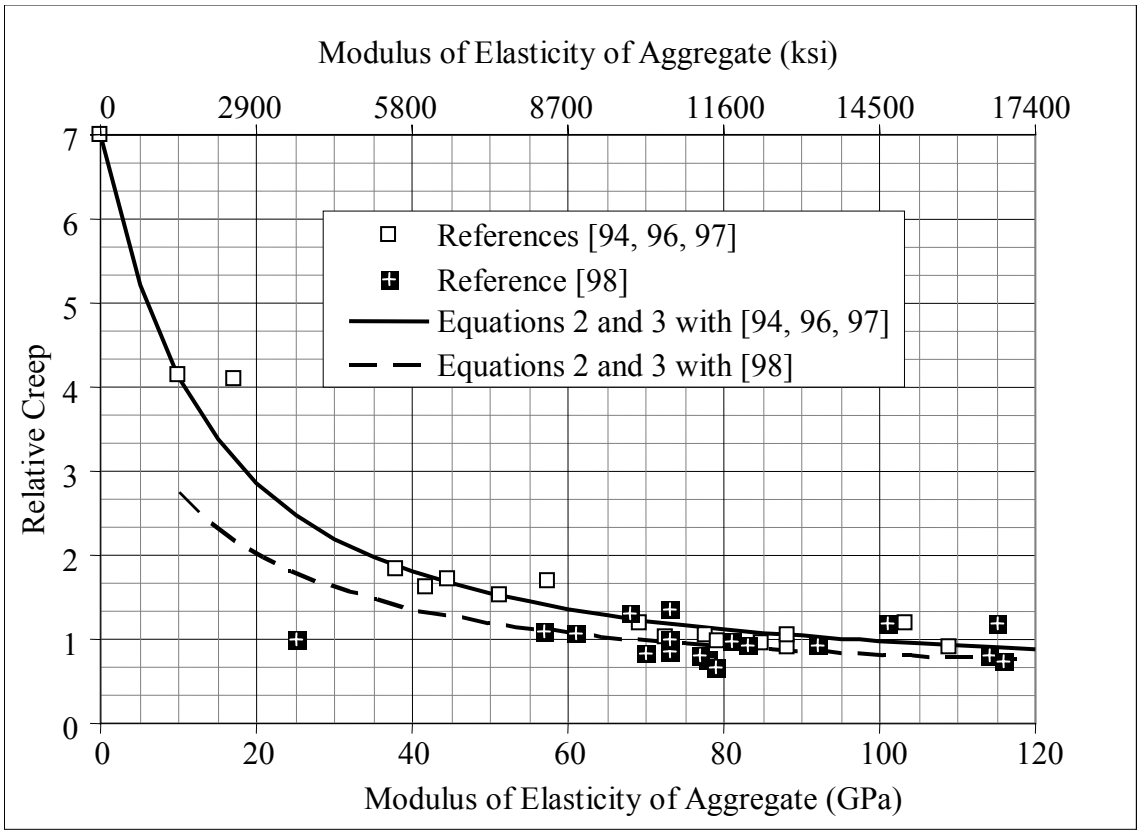

Figure 2.9: Theoretical and empirical relationship between aggregate elastic modulus and relative creep of concrete for normal weight concrete [96-99]

From Figure 2.9 it can be concluded that knowing the amount of aggregate and aggregate elastic modulus is not enough to explain the influence of aggregate in creep of concrete in normal weight concrete. In fact, in interpreting results from previous investigators [76], Mehta and Monteiro [7] explained that the higher degree of microcracking in the ITZ made with non-reactive aggregate like basalt might increase creep, but not affect shrinkage noticeably.

Probably the second most important factor affecting creep is the water-to-cement ratio since it determines the structure and porosity of the cement paste where creep occurs. For a given applied stress creep is inversely proportional to the strength at the time of loading [75], and since water-to-cement ratio is the main factor controlling

strength, lower water-to-cement ratio mixtures present lower creep. It was pointed out that the increase in creep of increasing water-to-cement ratio mixtures might be due to the reduction in strength and increase in permeability [7]. In practice it is difficult to see the influence of water-to-cement ratio in creep because the total volume of cement paste changes if the workability is kept constant. In a summary of the results from various researchers it was shown the influence of water-to-cement ratio in creep [79]. Figure 2.10 shows in the X-axis the water-to-cement ratio and in its Y-axis relative creep expressed as a fraction of creep of a 0.65 water-to-cement ratio concrete. All the creep values were adjusted for the cement paste content in order to make results comparable.

Figure 2.10: Influence of water-to-cement ratio on creep of concrete [79]

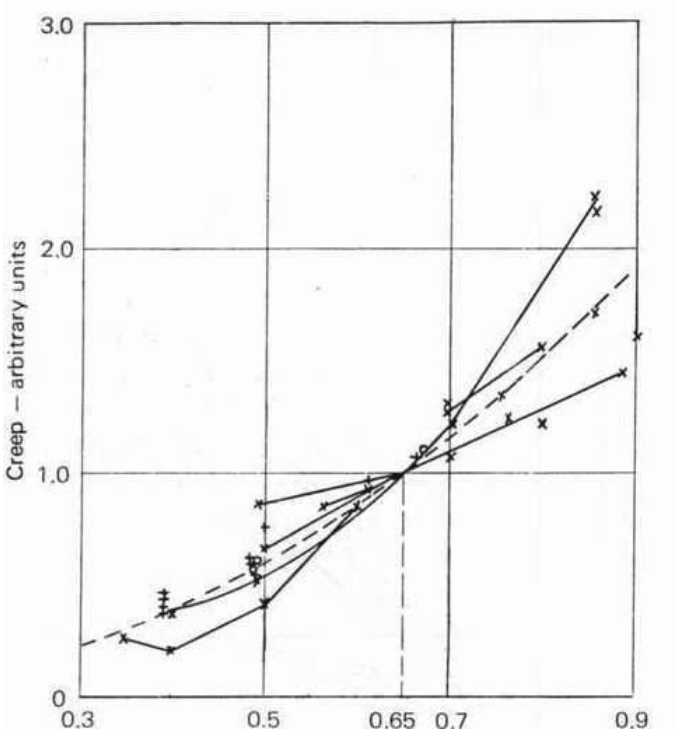

As shown in Figure 2.10, a lower water-to-cement ratio leads to lower creep and also less variability between the maximum and the minimum creep values. It must be remembered that the strength at the time of loading is the critical factor in creep

development, so a lower water-to-cement ratio not only increases the strength but also the rate of strength gain.

The influence of cement itself would not be important other than affecting the strength at the time of loading [7, 75]. The effects of SCMs are directly related with their influence on the cement paste microstructure at the time of loading. The replacement of portland cement by pozzolans increases creep due to the reduction of the strength at the time of loading [79]. The use of pozzolans might delay the rate of strength gain compared with concrete produced with only cement. If the mixtures are loaded at the same age, creep of mixtures using pozzolans with a lower strength might show higher creep. ACI-232 [100, 101] on fly ash and natural pozzolans presented results that show an important decrease in drying creep and in basic creep of concrete with fly ash compared to concretes with only cement when they are loaded at similar strength. This would show that the effect of pozzolans might be through a decrease in concrete water permeability which reduces water migration. A study showed that the general effect of fly ash is to reduce basic creep except for early ages when the fly ash mixture posses lower strength than the concrete with only cement [65]. For total creep, it was concluded that there is a large variability on the results depending on the type of fly ash [66]. In general, concretes containing Class C and Class F fly ash presented more and less creep than their counterparts produced with only cement, respectively.

ACI-233 [102]on ground granulated blast-furnace slag (slag) reported conflicting results on its influence on creep. This might be due to the fact the if slag substitutes cement on equal mass basis the actual volume of paste increases making results difficult to compare. Even though a consistent decrease in long-term basic creep on concrete

containing slag has been measured, the effect of the slag in total creep (basic plus drying creep) might be water-to-cementitious material ratio dependent [66]; i.e., at low water-to-cementitious material ratio increasing amount of slag would reduce creep while for high ones the slag would increase creep.

The use of silica fume increases the compressive strength, so at the same stress level, silica fume concretes exhibits less creep that counterparts with only cement. The ACI-234 [103] on silica fume reported results from the literature that predict either no change in creep or less creep when silica fume replaced a fraction of the cement. It was suggested that creep of silica fume concrete is not higher than that of only cement concrete of similar strength. On the other hand a study [66] showed that basic creep increases with increasing silica fume content if the stress-to-strength ratio is kept constant. In that matter, other investigators [49] reported decrease in basic creep with silica fume contents up to 5%, but an increase for higher replacement levels. Drying creep seemed to be significantly decreased and even stopped with silica fume addition [49]. The strong effect of silica fume on drying creep might be due to a decrease in permeability of the concrete compared to mixtures with no silica fume.

One research work [68] found that the use of SCMs siliceous in nature increased total creep, and calcareous SCMs did not have an effect on creep. On the contrary, others [69] suggested that basic and total creep decreased with increasing amount of metakaolin and silica fume, both siliceous SCMs. The most significant reductions in creep were with 10% of cement replacement; further replacement did not provide considerably improvements.

Figure 2.11 summarizes the effect of the plasticizers and super plasticizers [66, 70]. X-axis and Y-axis show creep of concrete without and with chemical admixtures in με, respectively. Another author also reported increases in creep with superplasticizers, but the effect strongly depended on the type of chemical used in the admixture [49].

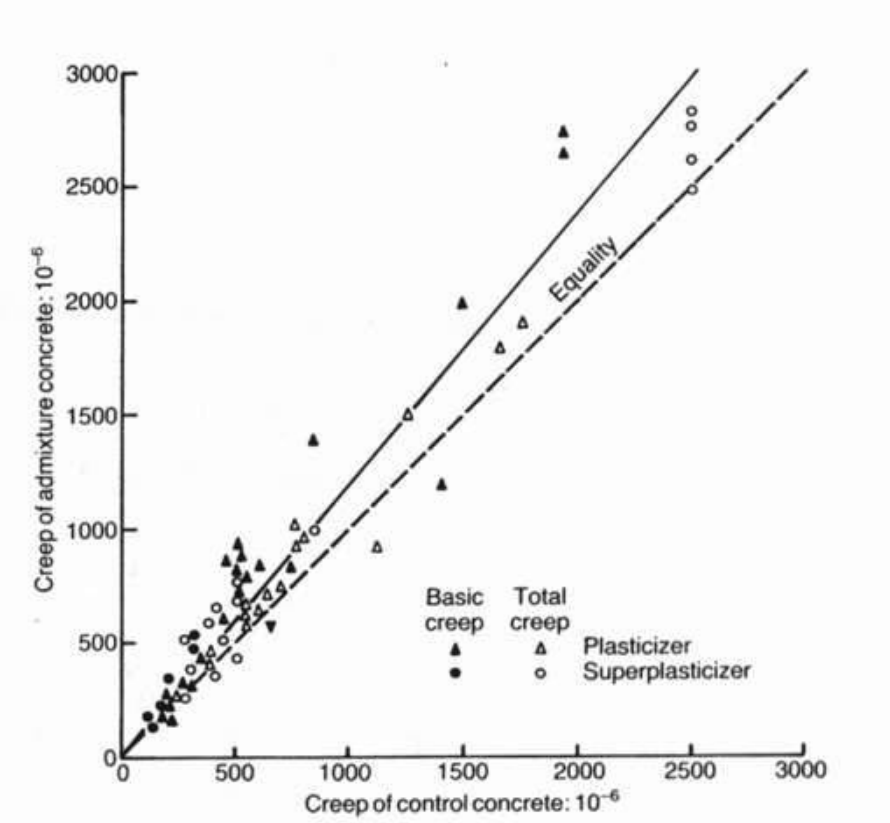

Figure 2.11: Comparison of creep of concrete at constant stress-to-strength ratio with and without plasticizers and superplasticizers [66]

In comparing the effect of various plasticizers and superplasticizers on creep [66, 70], it was concluded that there is in general an increase in creep when using those chemical admixtures, but in some cases the variability was large and no significant differences with plain concrete was found. The average creep increase and standard deviation due to plasticizers and superplasticizers was 120 and 25.2 με, respectively [70].

2.3 Properties of High Performance Lightweight Concrete

When defining HPC, ACI-116 [2] opted for a broad definition to encompass a great variety of special concretes (see Section 2.2.1). HPLC is, therefore, included in the ACI definition of HPC. Nevertheless, ACI-213 [17] requires two characteristics in any SLC: minimum 28-day compressive strength of 17.2 MPa (2500 psi) and equilibrium density between 1120 and 1920 kg/m^3 (70 and 120 lb/ft^3). Therefore, a HPLC must meet both definitions. On the other hand, ACI-213 [17] defines high strength lightweight concrete as a SLC with a 28-day compressive strength in excess of 41.4 MPa (6000 psi) which agrees with that given by ACI-363 [1] for high strength concrete. Committee 363 has currently redefined high strength concrete as concrete with a specified compressive strength of 55.2 MPa (8000 psi) or greater (ACI-363, 2005).

2.3.1 Microstructure

2.3.1.1 Cementitious Matrix Microstructure

HPLC is a material with low water-to-cementitious material ratio. As such, the microstructure of the cementitious matrix possesses low permeability, low porosity, high abrasion resistance, and high compressive strength and elastic modulus.

It was concluded [104] that the capillary pores become discontinuous within the cement paste microstructure once a certain degree of hydration has been attained. That limit depends on the water-to-cement ratio. The lower the water-to-cement ratio, the closer the average distance between the solid particles in the cement paste, and lower the required degree of hydration that creates a discontinuous porosity. Figure 2.12 presents the relationship between water-to-cement ratio (X-axis) and required degree of hydration for a discontinuous porosity (Y-axis).

The authors concluded that above water-to-cement ratio of 0.7, even with full hydration the capillary continuity remains. For mixtures with water-to-cement ratio 0.4 and below, the capillary continuity decreased fairly rapidly after 50% of the cement has hydrated.

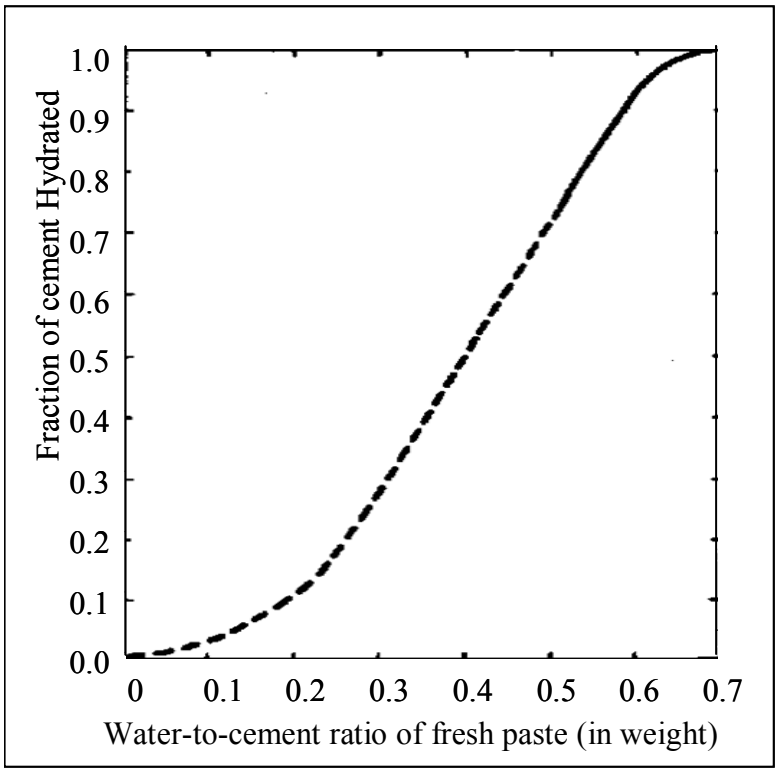

Figure 2.12: Estimated relationship between water-to-cement ratio and degree of hydration at which capillary continuity is [104]

Below a water-to-cement ratio of 0.4 several aspects change. For instance, there is less space for the hydration products to form, so they grow more ordered; moreover, the size of the hydration products decreases, and their compactness greatly increases. Secondly, below a water-to-cementitious material ratio of 0.4, there is not enough water to hydrate all the cement [105, 106] (see Section 2.5.4.1). Thus, the cement grains act as inert filler that improves density.

Most modern HPCs have at least one type of SCM. Many of them use fly ash or ground granulated blast-furnace slag in conjunction with silica fume [107]. These materials promote pozzolanic reactions that transform calcium hydroxide, which does not contribute to strength, to C-S-H which contributes to strength. As unhydrated cement, unreacted silica fume acts as very fine filler that further contributes to form a dense microstructure.

Low water-to-cementitious material ratio mixtures must contain water reducers or high-range water reducers. These chemical admixtures facilitate placing, consolidation and prevent flocculation of cementitious materials. All these contribute to reduce in-homogeneities in the cementitious paste microstructure [5].

Many of these special characteristics are expected to increase under the beneficial effects of internal curing provided by lightweight aggregate (see Section 2.5).

2.3.1.2 Lightweight Aggregate Microstructure

Lightweight aggregates have a cellular pore structure usually developed by heating some types of clays, shales and slates. At high temperatures (1100^{o}C, 2000^{o}F) gases evolve within a pyroplastic mass and expansion occurs. After cooling the expansion is retained and a low density is achieved [16]. Lightweight aggregate contain a uniformly distributed system of pores with sizes between 5 and 300 μm (0.2 and 11.8 mills). The pore system is comprised of interconnected pores or open pores that control absorption and not connected or closed pores [18]. A common way to measure interconnectivity in lightweight aggregate is by the ratio between open and total pores (open plus closed pores); such ration for expanded clay and shale is approximately 46 and 80%, respectively [18]. If two aggregate have a similar dry density and different

absorptions, it can be assumed that they have similar total porosity, but different open porosity. Thus, the interconnectivity of the pore system is higher in the higher-absorption aggregate. Expanded slate usually have a dry density similar to expanded clay and shale, but it has absorption of 6% compared with 10-to-20% of some expanded clays and shales [18, 108]. Consequently, a lower interconnectivity might be expected in the expanded slate aggregate.

Properties like absorption and bonding to the cement paste are strongly determined by the external shell present in some lightweight aggregate [109]. Rotary kiln expanded aggregate forms a vitrified external layer upon rapid cooling which is denser and more impermeable than the rest of the aggregate [109]. In the case of some expanded clays and shales, where the pellets form in the kiln and do not require further crushing, the external shell remains. Expanded slate, on the other hand, is crushed which eliminates the external shell. Agglomerated lightweight aggregate made from fly-ash can be sintered or cold bonded. The former might present an external shell while the latter does not.

2.3.1.3 Interfacial Transition Zone Microstructure

The ITZ was investigated on five high strength lightweight concrete mixtures made with different lightweight aggregates [110]. Four were expanded clay with a dense outer shell and the fifth was sintered fly ash without an outer shell. All the mixtures considered ordinary cement with water-to-cement ratio of 0.3. Scanning electron microscopy and the x-ray dispersion analysis were performed on each sample. It was concluded that high strength lightweight aggregate with a dense outer layer produce an ITZ with the same characteristics as seen in normal weight aggregates. The aggregate

with weaker and more porous external layer produced a denser and more homogenous ITZ with better bonding to the aggregate. The lightweight aggregate was oven-dried before mixing and then soaked in water for ten minutes. Therefore, the more porous aggregate could have absorbed more water which was released later as internal curing water. Other study of the same authors [111] concluded that during mixing cementitious paste penetrated into most of the open pores of the lightweight aggregate. No significant differences were observed between paste penetration into oven-dry or vacuum-saturated lightweight aggregate, so it was suggested that the penetration or interlock depended on the microstructure of the aggregate surface, the size of the cementitious materials and the viscosity of the paste.

There are two points of view regards to the influence of lightweight aggregate moisture in the ITZ [109]. First, a partially saturated lightweight aggregate might give a denser ITZ due to the absorption of water and penetration of cement paste into the aggregate. From this perspective, saturated lightweight aggregate will not take water from the ITZ and thus will develop a more porous microstructure. Second, the water contained in the aggregate can improve the hydration through internal curing. From this perspective, saturated lightweight aggregate leads to an enhance hydration of the ITZ with respect to partially saturated aggregate.

As explained with more detail in Section 2.5, internal curing becomes useful for low water-to-cementitious material ratio mixtures, so the two perspectives presented are not in conflict. For medium to high water-to-cement ratio mixtures (low-to-medium strength) the absorption effect of an unsaturated lightweight aggregate might be

beneficial while in a low water-to-cementitious material ratio mixture (high strength) the water release effect from the saturated aggregate might be beneficial.

One study [112] compared the ITZ of sintered fly ash aggregate with different pozzolanic activity and absorption. In the lowest pozzolanic activity aggregate, almost no rich calcium zone (characteristic of ITZ) was observed outside the aggregate after one and 90 days. Moreover, a 200-μm (0.008-in) thick zone within the aggregate where the lime-to-silica ratio was high was found after 90 days. On the other hand, the heat treated aggregate which had higher pozzolanic activity presented a 50-μm (0.002-in) thick calcium rich ITZ at one day. After 90 days that ITZ was completely eliminated and C-S-H like compounds of about 50 μm (0.002 in) in thickness were detected within the aggregate.

ACI-213 [17] reported the results from Khodrin [113] where an increase in the ITZ microhardness was observed as a consequence of the pozzolanic reaction at the lightweight aggregate surface.

In addition, the lower microcracking at the ITZ afforded by the elastic matching between aggregate and matrix [19] (see Section 2.2.3) can provide a stronger and denser ITZ improving.

Summarizing, the interaction between lightweight aggregate and low water-to-cementitious material ratio paste might occur by three mechanisms: (1) physical mechanisms, such as those attributed enhanced hydration afforded by the water released from a saturated aggregate; (2) mechanical mechanisms, such as by the interlock between matrix and rough and porous aggregate surface and by the reduction of ITZ cracking as a

result of the improved elastic compatibility between aggregate and paste; and (3) chemical mechanism, such as by the pozzolanic activity between aggregate and matrix.

These three mechanisms manifest the synergy between lightweight aggregate and high performance/low water-to-cementitious material ratio matrix present in HPLC.

2.3.2 Mechanical Properties

2.3.1.1 Compressive Strength

The maximum attainable compressive strength in a concrete with lightweight aggregate is ultimately controlled by the compressive strength of aggregate rather than the strength of the matrix. ACI-213 [17] defines the term "strength ceiling" as the maximum tensile and compressive strength attainable with a particular lightweight aggregate and a reasonable amount of cement. In particular, one study found [24, 25] that concrete strength ceiling was proportional to the intrinsic strength of the coarse aggregate. Two kinds of natural pumice and an expanded clay were examined in SLC at four different water-to-cement ratios. For each case, the mixtures with expanded clay yielded the highest compressive strength. Another study [36] using 12.7-mm (0.5-in) MSA expanded slate concluded that water-to-cementitious material ratio below 0.23 did not yield any noticeable increase in strength for their HPLC. Even though the cementitious matrix alone reached a compressive strength of 92.3 MPa (13,380 psi) after 28 days, the mixture with expanded slate had a strength below 79.3 MPa (11,500 psi), and the strength did not change between 3 and 28 days. It was concluded that the strength ceiling of concrete using 12.7-mm (0.5-in) expanded slate was around 79.3 MPa (11,500 psi). The strength ceiling can be increased by a decrease in the MSA. ACI-213 [17] reported increases in compressive strength from 34.5 to 41.4 and 48.3 MPa (5000 to

6100 and 7600 psi) when the aggregate size was reduced from 19 mm to 12.7 and 9.5 mm (0.75 in to 0.5 and 0.375 in), respectively.

Nevertheless, another work [112] concluded that factors like pozzolanic activity or higher absorption can be more important then the aggregate strength itself in defining concrete strength. The mixtures contained sintered fly ash lightweight coarse aggregate which was heat-treated at different temperatures to activate its pozzolanic activity, decreased it water absorption, and increase its strength. Mixtures containing a 19.3-MPa (2800-psi) crushing strength aggregate and lower pozzolanic activity presented similar 90-day compressive strength as mixtures containing a 15-MPa (2175 psi) crushing strength aggregate and higher pozzolanic activity.

The research conducted by Hoff [31, 114, 115] is maybe one of the most comprehensive studies in high strength lightweight concrete. In particular, the performance of two artificial lightweight aggregates in high strength concrete mixtures was compared [31]; one was a 19-mm (0.75-in) MSA pelletized aggregate from Japan and the other a 19-mm (0.75-in) MSA crushed aggregate from USA. The mixture design considered Type I/II portland cement, 10% silica fume, 520 kg/m^3 (880 lb/yd^3) of cementitious materials with a water-to-cementitious material ratio of 0.28. Mixtures with each type of aggregate reached compressive strength at 28 days of 55.2 MPa (8000 psi) or greater with a density of 1877 kg/m^3 (117.2 lb/ft^3); however, the pelletized lightweight aggregate presented 5% higher strength at 28 days for various curing regimes. This Japanese aggregate was used in a new mixture design with a dosage of cementitious materials of 567 kg/m^3 (956 lb/yd^3), 11% of which was silica fume and the same water-to-cementitious material ratio. The new lightweight mixture reached 73.1 MPa (10,600

psi) compressive strength after 14 or more days of moist curing and a density of 1849 kg/m^3 (115.4 lb/ft^3).

Malhotra (1990) used expanded shale as coarse aggregate, normal weight fine aggregate, Type III cement, Class F fly ash and silica fume to develop HPLC. In this mixtures the cementitious materials content ranged from 380 to 615 kg/m^3 (640 to 1040 lb/yd^3) and the water-to-cementitious material ratio from 0.29 to 0.39. The density was between 1900 and 1976 kg/m^3 (118.6 and 123.4 lb/ft^3). MSA was either 19 or 9.5 mm (0.75 or 0.375 in). Twenty-eight-day compressive strength ranged between 50 and 62 MPa (7250 and 9000 psi). One-year compressive strength reached values between 59.7 and 69.3 MPa (8650 and 10,050 psi) with the highest being the mixture with the smaller MSA.

Another research work [37] obtained 91-day compressive strength of 97.6 and 77.2 MPa (14,150 and 11,200 psi) with densities around 2030 kg/m^3 (126.9 lb/ft^3) using two different expanded shales. The cementitious materials considered Type III portland cement and 10% silica fume at 0.27 water-to-cementitious material ratio. The total amount cementitious materials was 500 kg/m^3 (845 lb/yd^3), the MSA was 9.5 mm (0.375 in), and the fine aggregate was entirely normal weight sand. The compressive strength increased to 117.9 MPa (17,100 psi) when the lightweight coarse aggregate was replaced by normal weight granite.

Ninety-day compressive strength between 59.0 and 103.1 MPa (8550 and 14,950 psi) using different types of expanded clay were obtained [23]. Because the testing was performed in cubes instead of cylinders, the authors assumed a 10% reduction in strength when converted to cylinders. According to this, the 90-day cylinder compressive strength

ranged between 53.8 and 92.8 MPa (7795 and 13,455 psi) with a density of 1865 kg/m^3 (116.4 lb/ft^3). The maximum strength was reached by a mixture with water-to-cementitious material ratio of 0.28 and 660 kg/m^3 (1115 lb/yd^3) of cementitious materials. Silica fume was 10% of the total cementitious materials content. About 50% of the aggregate (coarse and fine) was normal weight and the other half was lightweight aggregate.

Another study [38], which also used lightweight aggregate (expanded slate) and normal weight aggregate in both coarse and fine fractions, obtained 16-hour and 28-day compressive strengths of 44 and 50 MPa (6380 and 7250 psi) with a density of 1930 kg/m^3 (120.5 lb/ft^3). The MSA was 19 mm (0.75 in), and the water-to-cementitious material ratio was 0.338 with 447 kg/m^3 (752 lb/yd^3) of cementitious materials (60% pf Type II portland cement and 40% of slag cement).

Another HPLC was developed using expanded slate [33] containing 318 kg/m^3 (536 lb/yd^3) of Type I portland cement, 190 kg/m^3 (323 lb/yd^3) of ground granulated blast-furnace slag, normal weight fine aggregate and 12.7-mm (0.5-in) MSA. The water-to-cementitious material ratio was 0.368, and the 28-day and one-year compressive strength were 49.5 and 57.2 MPa (7180 and 8290 psi), respectively. The density of that HPLC was 1865 kg/m^3 (116.4 lb/ft^3).

Higher compressive strengths were obtained by another study [36, 116, 117] aimed to develop HPLC for prestress girders using expanded slate HPLCs. Two HPLCs were developed; both mixtures had Type III portland cement, fly ash and silica fume, 12.7-mm (0.5-in) expanded slate, and normal weight fine aggregate. Compressive strengths were in the range of 70.7 and 79.0 MPa (10,250 and 11,460 psi) at the age of 28

days and with densities below 1890 kg/m^3 (118 lb/yd^3). The higher strength HPLC had a water-to-cementitious material ratio of 0.23 and 585 kg/m^3 (990 lb/yd^3) of cementitious materials with 15 and 10% of fly ash and silica fume, respectively. The other HPLC had 560 kg/m^3 (945 lb/yd^3) of cementitious materials of which 15 and 2% were fly ash and silica fume, respectively. The water-to-cementitious material ratio was 0.28.

HPLC containing 9.5-mm (0.375-in) MSA expanded Type I/II portland cement and 10% of silica fume totaling 490 kg/m^3 (827 lb/yd^3) of cementitious materials was also developed [28]. The water-to-cementitious material ratio was 0.27, and the 28-day compressive strength slightly higher than 55.2 MPa (8000 psi) with density around 1842 kg/m^3 (115 lb/ft^3). A similar study using 9.5-mm (0.375-in) expanded shale [34] obtained 28-day compressive strengths averaging 93.7 MPa (13,590 psi), but with a higher density 2083 kg/m^3 (130 lb/ft^3) approximately. That HPLC contained 725 kg/m^3 (1225 lb/yd^3) of cementitious materials 10% of which was silica fume and the rest Type I/II portland cement. The water-to-cementitious material ratio was 0.227, and it had 98 kg/m^3 (165 lb/yd^3) of steel fibers.

An HPLC having a 28-day compressive strength in excess of 79.3 MPa (11,500 psi) was developed [26] using 10-mm (0.4-in) expanded clay as lightweight coarse aggregate, 500 kg/m^3 (845 lb/yd^3) of cement and 50 kg/m^3 (84 lb/yd^3) of silica fume. The water-to-cementitious material ratio was 0.3 and the density 1904 kg/m^3 (118.9 lb/ft^3). Another mixture having the same mixture design, but normal weight coarse aggregate instead of expanded clay was considered. That mixture had a 28-day compressive strength of approximately 104.8 MPa (15,200 psi).

One study [29] aimed to develop lightweight concrete with a compressive strength in 60-to-65 MPa (8700-to-9425-psi) range using 525 kg/m^3 (885 lb/yd^3) of cementitious materials (cement plus 8% silica fume), normal weight fine aggregate and 12.7-mm (0.5-in) lightweight aggregate. The mixtures had water-to-cementitious material ratios between 0.30 and 0.32, and used alternatively six sources of lightweight aggregate maintaining all the other constituents the same. Two out of the six lightweight aggregate mixtures reached the minimum average compressive strength of 60 MPa (8700-psi). In fact, those mixtures had a 28-day compressive strength of 63.8 and 67.4 MPa (9245 and 9775 psi). The density in those mixtures were 1907 and 1920 kg/m^3 (119 and 119.9 lb/ft^3), respectively.

Several other authors have successfully developed lightweight concrete mixtures with compressive strength over 41.4 MPa (6000 psi) using expanded clay, natural tuffs, and sintered fly ash [32, 118, 119]. One of those [32] obtained 65 MPa (9425 psi) at 28 days of age with a density of 1890 kg/m^3 (118 lb/ft^3). Their mixtures considered only lightweight sintered fly ash aggregate in the coarse and fine fractions. The total cementitious material content was about 785 kg/m^3 (1325 lb/yd^3), including the fly ash used to replace the fines in the aggregate. The amounts of Type I cement and silica fume were 550 and 55 kg/m^3 (925 and 93 lb/yd^3), respectively, and the water-to-cementitious material ratio was 0.224.

A summary [30] of the most recent experimental results of HPLC made out of expanded slate included results from four different projects were presented: a bridge in Norway, a bridge in California, an study carried out by Carolina Stalite Company

(expanded slate manufacturer), and the work done in HPLC prestressed girders mentioned above [36, 116].

In the bridge project in Norway, a compressive strength of 71.9 MPa (10,425 psi) was obtained after 28 days using only 455 kg/m^3 (768 lb/yd^3) of cementitious materials (5% silica fume) and water-to-cementitious material ratio of 0.38. The density of the mixtures was in the vicinity of 2000 kg/m^3 (125 lb/ft^3) which is higher than the limit of 1920 kg/m^3 (120 lb/ft^3) proposed by ACI-213 [17], the higher density is probably related to lower quantities of lightweight aggregate (12.7-mm (0.5-in) expanded slate) which also explains the high strength obtained with relatively low cementitious material content.

In the research conducted by Carolina Stalite Company, 28-day compressive strength between 75.8 and 99.8 MPa (10,990 and 14,470 psi) were reached for 0.25 water-to-cementitious material ratio mixtures depending on the MSA of the expanded slate. The highest values were obtained for the 9.5-mm (0.375-in) lightweight aggregate mixture with 735 kg/m^3 (1240 lb/yd^3) of cement. After 90 days, that mixture had 111.7 MPa (16,200 psi) in compressive strength, the highest reported herein, with a density of 1905 kg/m^3 (119 lb/ft^3).

Table 2.2 presents a summary of the HPLC mixtures including their compressive strength, density of the type of aggregate. Figure 2.13 presents the compressive strength (Y-axis) versus density (X-axis) of all HPLC mixtures. The maximum density as suggested by ACI-213[17] and the minimum compressive strength as recommended by ACI-363 in 1997 and 2005 [1, 120] are also included in Figure 2.13.

The highest strengths reached by HPLC are in the vicinity of 100 MPa (14,500 psi). Those levels have been reached with expanded clay, shale and slate. Most of them

used lightweight coarse aggregate and normal weight fine aggregate. The exceptions are two studies [23, 38] that considered lightweight and normal weight aggregate in both coarse and fine fractions. In general the highest strengths were obtained using 9.5-mm (0.375-in) MSA. When MSA was 12.7 mm (0.5 in) the compressive strength were in the order of 70 to 75 MPa (10,150 to 10,875 psi).

Table 2.2: Summary of compressive strength and density of HPLC in the literature

Source	compressive strength MPa (psi) / (days)	Density kg/m3 (lb/ft3)	Aggregate type / MSA mm (in)
[35]	60-70 (8700-10,150)/ 365	1900-1976 (118.6-123.4)	exp. shale / 19 (0.75)
[37]	97.6 (14,152)/ 90	2030 (126.9)	exp. shale / 9.5 (0.375)
[28]	55.2 (8000)/ 28	1842 (115)	exp. shale / 9.5 (0.375)
[34]	93.7 (13,585)/ 28	2083 (130)	exp. shale / 9.5 (0.375)
[31]	58.7(8520)/28	1878 (117.2)	exp. slate / 19 (0.75)
	73.1 (10,600)/ 28	1849 (115.4)	exp. shale / 19 (0.75)
[32]	65 (9425)/ 28	1890 (118)	sintered fly ash
[23]	92.8 (13,460) / 90	1865 (116.4)	coarse and fine exp. clay and normal weight
[29]	63.8 & 67.4 (9250 & 9775)/ 28	1914 (119.4)	exp. clay / 12.7 (0.5)
[26]	79.3 (11,500)	1904 (118.9)	exp. clay / 10 (0.4)
[33]	49.5 (7180)/ 28	1938 (121)	exp. slate / 12.7 (0.5)
[38]	50 (7250)/ 28	1930 (120.5)	exp. slate / 19 (0.75)
[36]	79.0 (11,460) / 28	1874 (117)	exp. slate / 12.7 (0.5)
[30]	71.9 (10,425)/ 28	1932 (123)	exp. slate / 12.7 (0.5)
	99.8 (14,470)/ 28 111.7 (16,195)/ 90	1905 (119)	exp. slate / 9.5 (0.375)

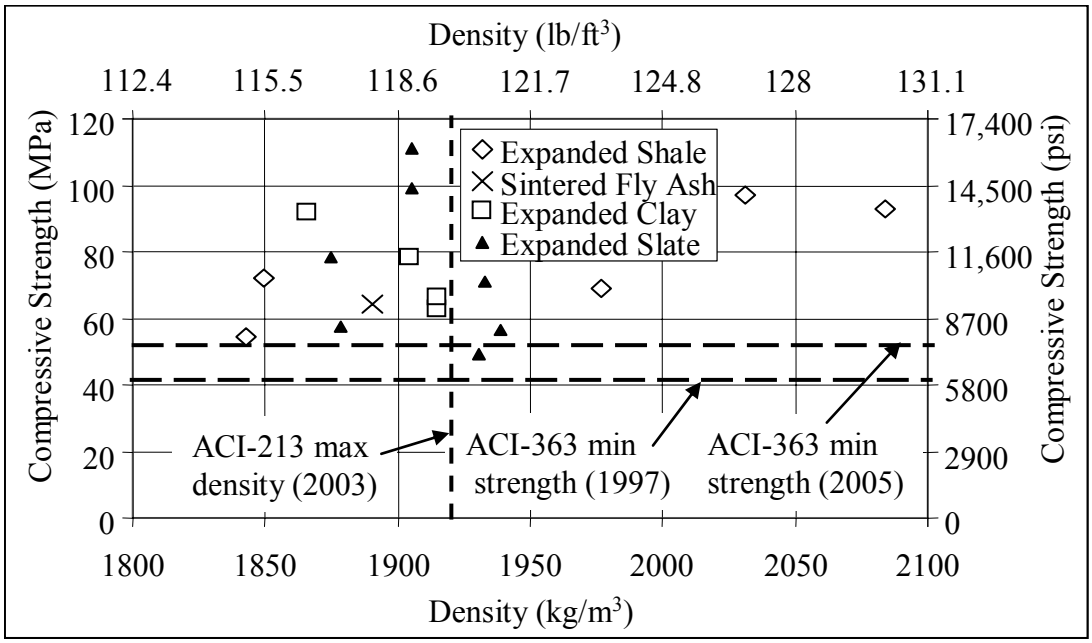

Figure 2.13: Summary of compressive strength and density of HPLC in the literature

Among the HPLCs that met the maximum density proposed by ACI-213 [17] and the minimum strength proposed by ACI-363 [1, 120], the highest strengths were obtained with densities between 1850 and 1920 kg/m^3 (115 and 120 lb/ft^3).

2.3.1.2 Modulus of Elasticity

Most of the studies on HPLC mentioned in the previous section also reported values of elastic modulus. For instance, one study [31] reported values for elastic modulus 28.3 GPa (4100 ksi) at 28 days which is the value estimated for a 35.7-MPa (5175 psi) normal weight concrete using the Equation proposed by ACI-318 [121] for NSC.

Another study [35] obtained 28-day elastic moduli in the range of 25 and 26 GPa (3625 and 3770 ksi) for all the different mixture designs examined. These results show

that the modulus of elasticity was greatly affected by the aggregate which was the only constant in the mixtures.

Other investigator [37] observed that the moduli of elasticity of their two HPLCs were between 25.9 and 29.0 GPa (3750 and 4200 ksi) were lower than the values predicted by ACI-318 [121] equation considering the actual density of the concrete. Twenty-eight-day moduli of elasticity obtained for a HPLC produced with expanded clay [23], ranged between 17.8 and 25.9 GPa (2580 and 3760 ksi). These results were not only overestimated by the ACI-318 [121] equation but also considerably lower than other HPLCs with similar strength. One reason for this lower elastic modulus might be the use of an lightweight fine aggregate which does not affect strength severely, but reduces elastic modulus.

Others [33, 38] reported elastic moduli at the age of 28 days in the range 20 and 24.7 GPa (2900 and 3600 ksi) when using expanded slate lightweight aggregate. A somewhat higher 56-day elastic modulus of 29.7 GPa (4300 ksi) was obtained [36] also using expanded slate. Other research on HPLC with expanded slate [30] reported elastic moduli ranging from 25.4 and 31.9 GPa (3690 to 4630 ksi) for the project in Norway and study by Carolina Stalite Company, respectively.

Using sintered fly ash lightweight aggregate one study [32] obtained an elastic modulus of 24 GPa (3480 ksi) for a 65-MPa (9425 psi) compressive strength mixtures. Another research work [29] obtained 28-day elastic modulus of 27.9 and 25.5 GPa (4050 and 3700 ksi) for the two mixtures having compressive strength of 63.8 and 67.4 MPa (9245 and 9775 psi), respectively. Both experimental values of elastic modulus were lower than that estimated using ACI-318 [121] equation. This overestimate has been also

seen with normal weight HPC as well, there overestimated of 33% have been reported [26].

In fact, an extensive investigation [12] in normal weight HPC concluded that the ACI-318 [121] equation overestimated modulus of elasticity for concretes with compressive strength over 41.4 MPa (6000 psi), and proposed a new equation that better represents modulus of elasticity of high strength concrete. Later, that equation was extended for high strength lightweight concrete [40]. This is the current expression considered by ACI-363 [13] to estimate elastic modulus of high strength concrete of various densities, and it is shown in Equations 2.4a and 2.4b in international and customary units, respectively.

$$E_c = \left(3.32 \cdot \sqrt{f_c'} + 6.9\right) \cdot \left(\frac{w_c}{2325}\right)^{1.5} \quad (2.4a)$$

$$E_c = \left(40 \cdot \sqrt{f_c'} + 1000\right) \cdot \left(\frac{w_c}{145}\right)^{1.5} \quad (2.4b)$$

where:

E_c: elastic modulus in GPa (ksi)

f_c': compressive strength in MPa (psi)

w_c: concrete density in kg/m^3 (lb/ft^3)

Table 2.3 summarizes the elastic modulus of HPLCs found in the literature. Table 2.3 also includes the elastic modulus as predicted by Equation 2.4 [1] and description of the type of lightweight aggregate used. The compressive strength and density used for the estimated were taken from Table 2.2.

Table 2.3: Elastic modulus of HPLC in the literature

Source	28-day elastic modulus GPa (ksi)	Estimate Equation 2.4 [1]	Aggregate type / MSA mm (in)
[35]	25-26 (3625-3770)	not available	exp. shale / 19 (0.75)
[37]	29 (4205)		exp. shale / 9.5 (0.375)
[31]	24.3 (3520)	23.5 (3410)	exp. slate / 19 (0.75)
	28.3 (4100)	25.0 3625)	exp. shale / 19 (0.75)
[32]	24 (3480)	24.7 (3580)	sintered fly ash
[23]	17.8 – 25.9 (2580 – 3755)	not available	coarse and fine exp. clay and normal weight
[29]	27.9 & 25.5 (4045 & 3700)	25.0-25.5 (3625-3700)	exp. clay / 12.7 (0.5)
[26]	24 (3480)	27.0 (3915)	exp. clay / 10 (0.4)
[33]	24.7 (3580)	24.4 (3540)	exp. slate / 12.7 (0.5)
[38]	20 (2900)	23.0 (3335)	exp. slate / 19 (0.75)
[36]	29.7 (4305) at 56 days	26.3 (3815)	exp. slate / 12.7 (0.5)
[30]	25.4 (3685)	26.6 (3855)	exp. slate / 12.7 (0.5)
	31.4 (4555)	29.7 (4305)	exp. slate / 9.5 (0.375)

Most of the experimental elastic moduli were between 24 and 28 GPa (3480 and 4060 ksi). The HPLCs with the lowest two elastic moduli [23, 38] were the only ones that contained lightweight and normal weight aggregate in both coarse and fine fractions. From Table 2.3 it can be concluded that the use of normal weight fine aggregate yielded higher elastic modulus.

Figure 2.14 present a comparison between the experimental elastic modulus (X-axis) and that estimated using Equation 2.4 [1] (Y-axis). The solid diagonal line represents the equivalence between measured and estimate values. Overestimates are shown above the equivalence line and underestimates below. The dashed diagonal lines represent the 10% error in the estimate.

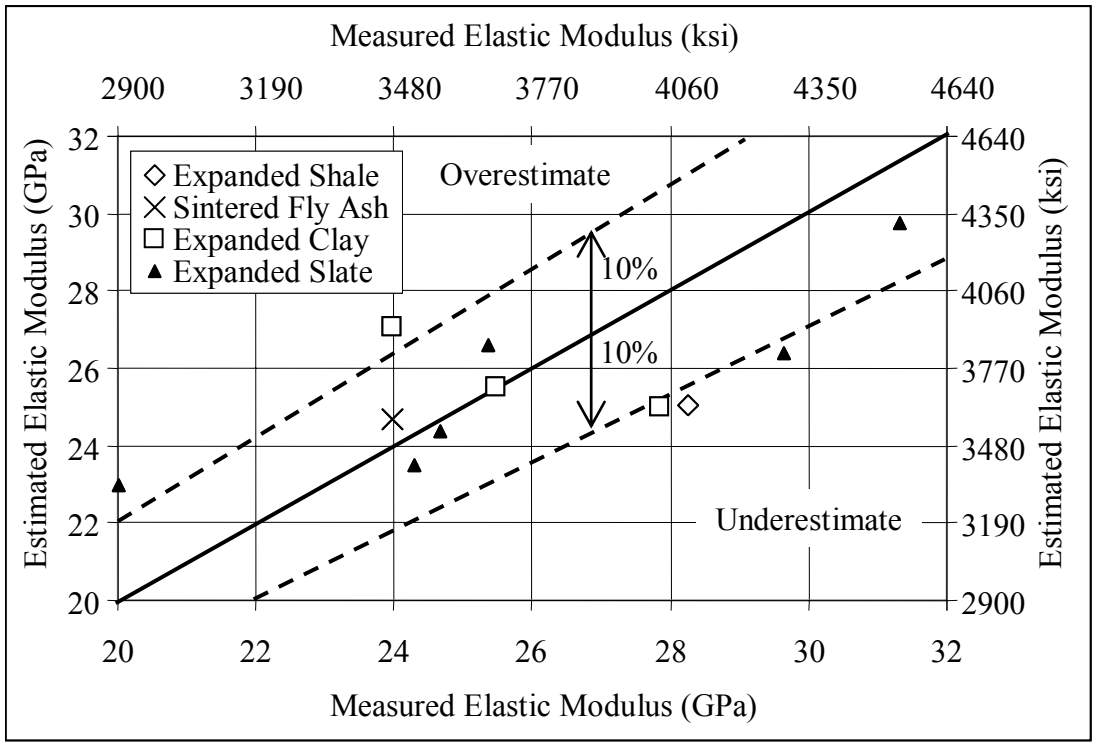

Figure 2.14: Summary of compressive strength and density of HPLC in the literature

With the expectation of two cases [26, 38], all the other HPLCs were underestimate in more than 10% or estimated within 10% of error. In general the highest strength and elastic modulus were obtained using 9.5-mm (0.375-in) MSA.

HPLCs with elastic modulus similar or higher than 28 GPa (4060 ksi) were obtained with expanded shale and expanded slate [29, 30, 36].

2.3.3 Durability

A key factor to ensure the durability of concrete is limiting the permeability. Concrete transport properties are governed by the three main phases in concrete, the cementitious matrix, aggregate and ITZ. It was pointed out that ITZ causes concrete and mortar to have a higher permeability than the cement paste [7]. The same authors

showed results of permeability in normal weight rocks comparable to those in a poor paste (0.71 water-to-cement ratio).

Water permeability, chloride penetration, electrical resistivity, and chloride permeability was measured on HPLC produced with five different lightweight coarse aggregate [122]. It was concluded that permeability of the concrete was governed by the matrix porosity rather than the lightweight aggregate because the more porous lightweight aggregate did not increase the HPLC permeability compared to a less porous normal weight aggregate. The authors attributed this to an improved ITZ as occurs with normal strength lightweight concrete (see Section 2.3.1). Permeability decreased as cement content increased, but no further improvement was observed when cement content increased above 500 kg/m^3 (845 lb/yd^3) probably due to thermal cracking originated by large thermal gradients. This might be relevant due to the relatively high cementitious materials contents in HPLC.

One study [123, 124] measured water permeability coefficients one order of magnitude lower in 0.55 water-to-cement ratio lightweight aggregate concrete compared to its normal weight counterpart. However, for water-to-cement ratio of 0.35 there was no significant difference between mixtures with lightweight and normal weight aggregate. This was also true for the 0.35 water-to-cementitious material ratio mixtures using 10% silica fume. It can be concluded that in low water-to-cement ratio mixtures where the ITZ might not be present [5, 125], the beneficial effect of lightweight aggregate were not noticeable. The mixtures considered the expanded clay partially saturated at the time of mixing, so little or no internal curing was provided by the aggregate. No significant differences due to the use of lightweight or normal weight

aggregate were found in chloride ion penetration and chloride permeability regardless of the water-to-cement ratio of the mixtures.

A study of chloride diffusion [126] found that 0.3 and 0.4 water-to-cement ratio expanded slate HPLC had chloride ion permeability after one year, measured according to ASTM C1202, of 162 and 202 coulombs, respectively which are both classified as very low permeability. Those mixtures had 350 and 450 kg/m^3 (590 and 760 lb/yd^3) of blended cement (90% cement and 10% silica fume). When 25, 40 and 56% by weight of the cement was replaced by Class F fly ash in the 0.3 water-to-cementitious material ratio mixture, the one-year chloride permeability further decreased to 63, 44, and 28 coulombs, respectively. The latter being a synergy between internal curing and high amounts of fly ash.

According to ACI-213 [17], although there is a potential alkali-silica reaction between the cement and amorphous silica in the lightweight aggregate, the laboratory and field experiences have not recorded reactive deleterious expansion. One study found no appreciable differences in expansion due to alkali-silica reaction between SLCs produced with either an inert or reactive normal weight sand [127]. Both showed an expansion below 200 με after one year, which is below the 400 με generally accepted as maximum in ASTM C 1293 [128]. This might be due to the lightweight aggregate capacity of accommodate the volume change [17].

Research done for accelerated freezing-and-thawing testing and in deterioration in the presence of deicing salts, have found similar performance between SLC and normal lightweight concrete [17].

2.3.4 Creep and Shrinkage

There are two opposing arguments that can be examined in assessing creep and shrinkage of HPLC. First, HPLC has a low water-to-cementitious material ratio, so the long-term deformations such as creep and shrinkage should be greatly reduced [5, 49]. On the other hand, the use of a comparatively low stiffness aggregate will reduce the aggregate restraining effect on the creep and shrinkage of the cementitious matrix, so the overall long-term deformations may increase [77]. These two competing effects make the estimate of creep and shrinkage difficult in HPLC. Because creep and shrinkage of HPLC are intimately related to those in HPC and SLC, this Section starts with those type of concrete first.

2.3.4.1 Creep of High Performance Concrete

It was concluded that creep deformation after a several years in NSC was normally two to four times the elastic deformation (creep coefficient 2 x to 4 x). In contrast, the creep coefficient of HPC was somewhere in the range between 1.8 to 2.4 [129]. The authors stated that NSC and HPC are affected by the same parameters in similar ways. The main factors responsible for lower creep of HPC are low water-to-cementitious materials ratio and silica fume addition. The same authors also concluded that the main difference between creep in NSC and HPC was given by the significantly lower drying creep observed in HPC.

Many times HPC is produced with Type III cement or finer cement and SCMs in order to obtain high early strength derived from a faster cement hydration. An extensive experimental program [130] on high strength concrete varied type of cement (Type I and III) with silica fume and/or fly ash cement replacement. It was found that, as occurs with

normal strength concrete, the higher the compressive strength, the lower the specific creep.

It is known that cement hydration is also affected by temperature. Faster cement hydration due to the use of high volumes of cementitious materials, low water-to-cementitious material ratio, finer or Type III cements can lead to important increment in temperature during the first hours after casting. This rise in temperature might accelerate the hydration of the cementitious materials, further generating more heat and early hydration. As a result, there is an increase in maturity of concrete at the same age which would lead to a reduction in creep. Contrarily, other study [130] on creep of HPC, made with either Type I, Type III cement or different combinations between cements and SCMs, reported reduced specific creep of HPC when cured under lower temperatures. The authors concluded that high temperature curing had a negative effect on creep.

As mentioned above, permeability of HPC is usually much lower than NSC. Some authors [129, 131] related low permeability of HPC with low creep. The relationship between permeability and creep can be explained based on creep mechanisms. Some creep mechanisms involve water transport; thus, a lower permeability would reduce water migration within the concrete and from the concrete to the environment. As a consequence, low permeability concrete would lose less water more slowly which would decrease drying creep.

Under drying conditions non-silica fume HPC presented 30 to 50% less creep than NSC [131], but under non-drying condition the differences was only between 10 and 25%. It was suggested that larger differences under drying conditions based on the reduced water content and low permeability of HPC.

It has been reported that the use of silica fume can reduce total creep (basic plus drying creep) between 30 and 50% with respect to non-silica fume mixtures [132, 133]. This improvement was found to be lower when the specimens remained sealed (i.e., only basic creep portion was considered) [134]. This suggests that the reduction in creep of HPC due to silica fume is in the drying creep portion rather than basic creep.

Normal weight HPC can present total specific creep in a wide range. For instance, it was found to be between 24.7 and 33.4 με/MPa (0.17 and 0.23 με/psi) after 1000 days under testing in HPCs with 28-day compressive strengths in the 81 and 85 MPa (11,750 and 12,360 psi) range [135]. Another study [136] reported specific creep values up to 48 με/MPa (0.33 με/psi) after only 100 days under load when loaded at the age of 24 hours. Those mixtures had a 28-day compressive strength around 122 MPa (17,690 psi). Under early age loading conditions, 100-day specific creep from 33 to 68 με/MPa (0.23 to 0.47 με/psi) was obtained [117] for two HPC with 56-day compressive strength between 80 and 94 MPa (11,620 and 13,630 psi). Those mixtures reached 46 and 83 με/MPa (0.32 and 0.57 με/psi) after 550 days under load.

Values of one-year total specific creep of HPC loaded at 28 days of age were reported in the range of 15 to 65 με/MPa (0.1 to 0.45 με/psi) with most of them in the 20-to-40 με/MPa (0.138 to 0.275 με/psi) range [49]. Under similar testing conditions other study [136] obtained specific creep of 22 με/MPa (0.15 με/psi) after only 100 days under loading.

There is agreement that HPC presents lower specific creep than NSC. This has been attributed to the lower permeability afforded by the low water-to-cement ratio and

the use of SCM. Nevertheless, as occurs with NSC, there are many factor influencing creep that need to be considered, so no generalizations about creep values can be made.

2.3.4.2 Creep of Structural Lightweight Concrete

Creep of concrete can be expressed in terms of the creep of cement paste, relative aggregate volume in the mixture, and the aggregate restraining effect. The aggregate restraining effect depends on the aggregate modulus of elasticity. A soft aggregate (low modulus of elasticity) would impose less restraint to cement paste movements, so creep is expected to increase. The elastic modulus of lightweight aggregate usually ranges between 4.8 and 20.0 GPa (700 and 2900 ksi) [17, 137, 138] while that of normal weight aggregate ranges between 40 and 120 GPa (5800 and 17,500 ksi) [10, 99]. Hence, creep in lightweight aggregate concrete is expected to be greater than creep of normal concrete.

SLC with a compressive strength of 34.5 MPa (5000 psi) loaded at the age of 7 days has shown after 2 years under load specific creep as high as 170 με/MPa (1.17 με/psi) and as low as 105 με/MPa (0.72 με/psi) for expanded clay and shale coarse aggregate, respectively [139]. Those mixtures had cement in the range of 315 and 400 kg/m^3 (527 and 677 lb/yd^3) of cement and a water-to-cement ratio around 0.6 and normal weight fine aggregate. A similar strength normal weight concrete tested in the same study showed specific creep of 123 με/MPa (0.85 με/psi) after two year under load. It was concluded that although most of the SLC mixtures presented more creep than NSC, such behavior cannot be generalized because even 15% less creep than NSC.

Two fly ash based lightweight aggregate HPLC presented creep of 50 and 100 με/MPa (0.35 and 0.69 με/psi) after 200 days under load when loaded at 28 days [140]. One of the lightweight aggregates was produced by sintering and the other by lower

temperature treating (autoclaved). Given that the mixture designs were similar, the authors attributed the large difference in creep of concrete to the lower elastic modulus and probable creep presented by the autoclaved lightweight aggregate. Contrarily, it was stated that lightweight aggregate, as normal weight natural aggregate, are not likely to creep under sustained stress [10].

Some research has shown that the creep rate of normal weight NSC and SLC might vary differently [22]. For instance, SLC might present a lower one-year creep than that of normal weight NSC of similar strength, but at later ages the higher creep rate of lightweight aggregate concrete gives a higher ultimate creep value. The authors pointed out that as strength increased, the reduction in creep shown the SLC was somewhat larger than the reduction in NSC. Results from other investigators showed that SLC having compressive strengths of 41.4 MPa (6000 psi) and higher might have comparable ultimate specific creep than their normal weight counterparts [22]. For instance, a one-year creep was between 64 and 76 με/MPa (0.44 and 0.525 με/psi) for a SLC compressive strength of 48.3 MPa (7000 psi) loaded at 28 days. For comparison, the same authors presented results of a similar strength normal weight concrete of 65 με/MPa (0.45 με/psi).

These results agree with the general relationship between compressive strength and creep of SLC given by ACI-213 [17] where the difference between lightweight and normal weight concrete consistently decreases as compressive strength increases. Figure 2.15 present such relationship for normally cured concrete (part a) and steam-cured concrete (part b). The X-axis presents the compressive strength in MPa and ksi and the Y-axis has the specific creep after one year under load.

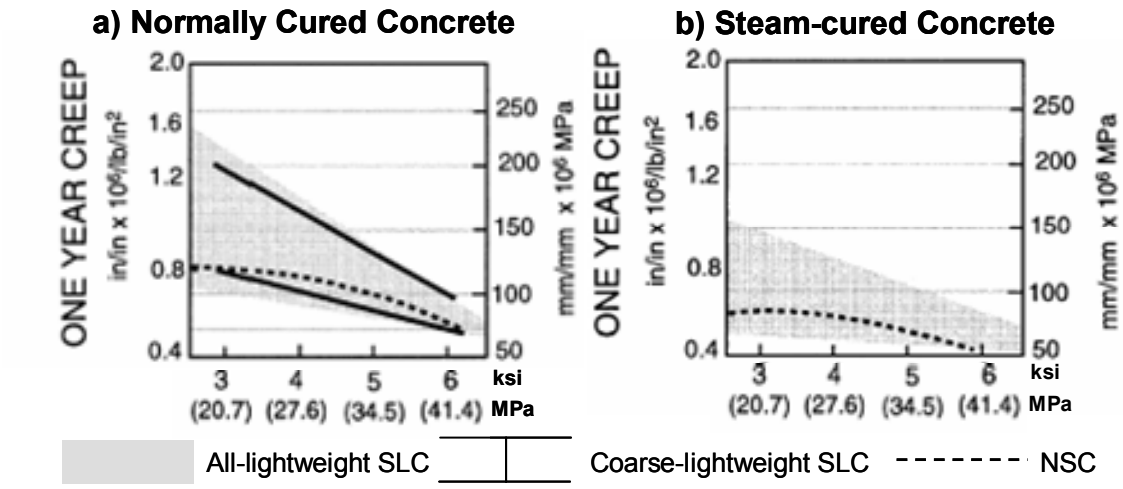

Figure 2.15: Relationship between compressive strength of lightweight concrete and one-year specific creep for (a) normally cured concrete and (b) steam-cured concrete [17]

Figure 2.15 shows three kinds of concrete "all-lightweight" with coarse and fine lightweight aggregate, coarse lightweight and normal weight fine aggregate, and a reference normal weight concrete. On average, lightweight concrete exhibits a higher creep than normal weight concrete. Nevertheless, there are some individual lightweight concretes that present a lower creep than the normal weight concrete.

A study in creep [141] investigated the effect of nine different lightweight aggregate in SLC with compressive strength of 20.7 and 34.5 MPa (3000 and 5000-psi). One-year creep from 147 and 254 με/MPa (1.02 to 1.75 με/psi) were reported for the 20.7 MPa (3000 psi) mixtures when loaded at the age of seven days; The 34.5 MPa (5000 psi) mixtures, on the other hand, had specific creep between 121 and 213 με/MPa (0.83 and 1.47 με/psi) under the same conditions. The lowest creep results were consistently obtained when using expanded shale and expanded slate aggregate.

Another study [142] that used concrete that might be considered in the limit between SLC and HPLC. Even thought 28-day compressive strength was not reported,

the 7-day compressive strengths were between 34 and 36 MPa (4950 and 5220 psi) which was higher than the typical strengths used at that time (late 1950's). When loaded at the age of 24 hours his mixtures had a creep after 400 days under load between 145 and 170 με/MPa (1 and 1.17 με/psi) which on average represented the 81% of creep showed by a similar strength normal weight aggregate under the same testing conditions.

Creep in SLC is on average higher than that of NSC with a similar strength. This has been attributed to the lower elastic modulus of lightweight aggregate in comparison to normal weight aggregates. This would reduce the restraint imposed by the aggregate to the creep occurring in the paste. Nevertheless, there are many cases where creep in SLC is lower than that of its normal weight concrete counterparts, and as the compressive strength increases, there were more of these cases. This might be showing a synergy between a higher strength paste and the use of lightweight aggregate; nevertheless, that might be also caused by the usually higher cement contents and lower water-to-cement ratio used in SLC as compared to a NSC of similar strength.

2.3.4.3 Creep of High Performance Lightweight Concrete

There are only few studies on creep of HPLC which makes difficult to draw any conclusions about HPLC creep performance. Moreover, the age at loading was not the same among those studies which makes them not comparable.

A creep study of HPLC [143], that considered only lightweight aggregate in the coarse and fine fractions, used either fast hardening blast furnace cement or a fast hardening portland cement mixed with fly ash, and silica fume. The two mixtures with lower creep had 28-day cube compressive strength of 53.5 and 47.6 MPa (7760 and 6900 psi) with 374 and 308 kg/m^3 (630 and 520 lb/yd^3) of cementitious materials (blast

furnace cement and 10% of silica fume), respectively; the corresponding water-to-cementitious material ratio were 0.305 and 0.390. The specimens were loaded at the age of 28 days, and after 200 days under load they had a similar specific creep of 58 με/MPa (0.4 με/psi). A normal weight HPC of similar mixture design was also tested; it had a 28-day compressive strength equivalent to 140% and a 200-day specific creep equivalent to 43% of that observed in the stronger HPLC.

Two HPLCs containing fly ash, silica fume and expanded shale coarse lightweight aggregate were tested for creep at the age of one year and remained under load for an additional year. The HPLCs presented one-year creep of 27 and 40 με/MPa (0.19 and 0.275 με/psi) with a compressive strength at time of loading of 60 and 70 MPa (8700 and 10,150 psi), respectively [35]. The lower creep of these HPLCs compared to previous ones [143] might be in part explained by differences in compressive strength and age at the time of loading.

Creep of HPLC made with expanded slate has been investigated by three research efforts. One study [33] conducted creep tests on a HPLC loaded at the age of 28 days with a compressive strength of 49.5 MPa (7180 psi). The creep coefficient after one year under load was 42 με/MPa (0.29 με/psi) which was 72% of that presented for a similar strength HPLC that contained only lightweight aggregate [143]. Other study loaded its HPLC mixture at 24 hours of age [38]. A specific creep in the order of 75 με/MPa (0.52 με/psi) was reported after 250 days under load. The HPLC mixture had a 28-day compressive strength of 50 MPa (7250 psi) and used lightweight and normal weight aggregate in both coarse and fine fractions.

Finally, 620-day specific creep of 75 and 45 με/MPa (0.52 and 0.31 με/psi) was reported [117] for two HPLC mixtures having a 24-hour compressive strength (time of loading) of 52 and 66 MPa (7540 and 9570 psi), respectively. After 250 day under load, those mixtures had a specific creep equivalent to 89 and 52% of the value measured in the previous study [38]. It was concluded that the lower creep HPLC had specific creep equivalent to 57% of the creep measured on a HPC mixture of similar strength and cement paste content.

2.3.4.4 Summary of Creep Results

Figure 2.16 and Table 2.4 present a summary of the creep results shown in Sections 2.3.4.1 – 3. Figure 2.16 presents only the specific creep of those mixtures loaded either at 1 days or 28 days (Y-axis) versus the time under loading and drying (X-axis).

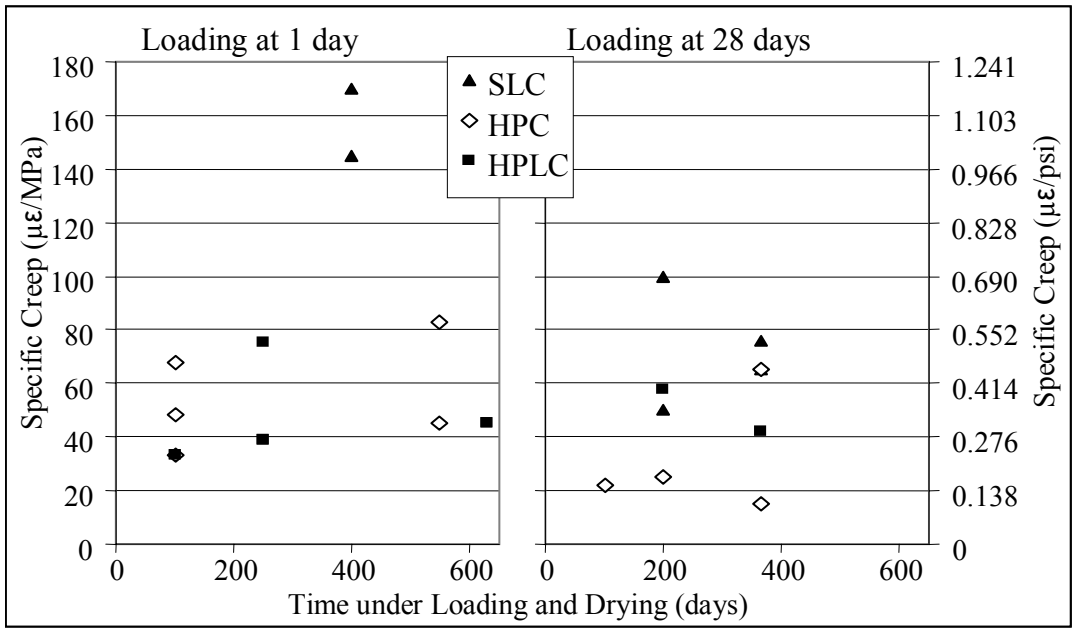

Figure 2.16: Specific creep versus time under loading and drying for SLC, HPC, and HPLC for loading and drying beginning at 1 and 28 days of age

Table 2.4 is organized by the age of concrete at loading, and it contains 28-day compressive strength and specific creep measured for each mixture.

Table 2.4: Creep results for HPC, SLC, and HPLC in the literature.

Age at loading - days	28-day compressive strength MPa (psi)	time under load - days	Specific creep - με/MPa (με/psi)	Type	Source
1	122 (17,690)	100	48 (0.33)	HPC	[136]
1	80/94 [1] (11,600 / 13,360)	550	83/45 (0.57-031)	HPC	[117]
		100	68/33 (0.47-0.23)		
1	35 [2] (5365)	400	145-170 (1-1.17)	SLC	[142]
1	35 [2] (5365)	400	193 (1.33)	NSC	
1	50 (7250)	250	75 (0.52)	HPLC	[38]
1	68.5/75.4 [1] (9950/10,950)	100	60/33(0.41-0.23)	HPLC	[117]
		250	67/39 (0.46-0.27)		
		630	75/45 (0.52-0.31)		
7	83 (12,035)	1000	25-33 (0.17-0.23)	HPC	[135]
7	34.5 (5000)	700	105-173 (0.72-1.19)	SLC	[139]
7	34.5 (5000)	700	123 (0.85)	NSC	
7	20 (2900)	365	140-250 (0.97-1.72)	SLC	[141]
7	34.5 (5000)	365	120-215 (0.82-1.49)	SLC	[141]
28	70 (10,150) and up	365	15-65 (0.1-0.45)	HPC	[49]
28	122 (17,690)	100	22 (0.15)	HPC	[136]
28	38/30 (5510/4350)	200	50/100 (0.34-0.69)	SLC	[140]
28	48.3 (7000)	365	64-76 (0.44-0.52)	SLC	[22]
28	48.3 (7000)	365	65 (0.45)	NSC	
28	50 (7250)	200	58 (0.4)	HPLC	[143]
28	70 (10,150)	200	25 (0.17)	HPC	
28	50 (7250)	365	42 (0.29)	HPLC	[33]
365	50 (7250) and up	365	27-40 (0.19-0.28)	HPLC	[35]

[1]: 56-day compressive strength

[2]: 7-day compressive strength

From Table 2.4 and Figure 2.16 it can be concluded that creep at early ages of SLC and HPLC concrete is either similar or lower than that of the normal weight counterparts at similar strength. When loaded at the age of 28 days, creep of normal weight concrete is on average lower than that of lightweight concrete at comparable strengths. However, there are specific lightweight concrete mixtures with less creep than their normal weight counterparts. The comparatively higher creep measured by two study [38, 143] might be due to the use of lightweight aggregate in the coarse and fine aggregate fractions. This is known to yield higher creep and shrinkage in SLC [139].

As with other properties in HPLC, creep depends on particular properties of the aggregate. Among these properties there are not only mechanical properties of the aggregate but also physical properties like pozzolanic reactivity, roughness and porosity of the aggregate surface. Thus, creep might be also affected by some physical properties of the aggregate. The internal curing provided by the aggregate might also play an important role in reducing creep. More research is needed in order to further understand the role of aggregate in creep.

However, there is a lack of systematic research comparing creep of HPLC and HPC with similar mixture designs. This would allow isolation of the effect of lightweight aggregate on creep. Moreover, systematic research needs to address creep on concrete loaded at early ages and at later ages as well.

2.3.4.5 Shrinkage of High Performance Concrete

It had been suggested [5] that at very low water-to-cement ratios, as the ones used in HPC, autogenous shrinkage can be as high as 700 με. Nevertheless, somewhat lower values have been reported by several researchers. For instance, two HPCs with

compressive strengths of 80 and 100 MPa (11,600 and 14,500 psi) presented an autogenous shrinkage of 200 and 230 με [129] after 24 hours of mixing. In contrast, the drying shrinkage portion of both HPCs was only 120 με during the first four weeks of drying and increased to 350 με after 220 days of drying. For the higher strength mixture, the autogenous shrinkage was approximately 50% of the total shrinkage. This results agree with those from another study [46] that measured autogenous shrinkage as 50 and 40% of the total shrinkage for concretes with water-to-cement ratio of 0.3 and 0.4, respectively.

Drying shrinkage of 400 με was obtained [131] on a 63-MPa (9135-psi) compressive strength HPC mixture after 90 days of drying. Similar results were obtained for an HPC with compressive strength in the vicinity of 83 MPa (12,035 psi) [135] where 400 με of drying shrinkage after 100 days of drying were reported. HPC with strengths in the 80-to-120 MPa (11,600-to-17,400 psi) range showed 3-year drying shrinkage, after 28 days of moist curing, between 500 and 750 με [132].

There is very little information concerning drying shrinkage of HPC because most studies do not include sealed specimens, so the measured total shrinkage cannot be divided into autogenous and drying portions. However, from the little data available it can be concluded that drying shrinkage was reduced when the water-to-cementitious material ratio was reduced. In contrast, higher autogenous shrinkage was found as the water-to-cementitious material ratio decreased, so the sum remained roughly constant [49].

2.3.4.6 Shrinkage of Structural Lightweight Concrete

An extensive investigation on drying shrinkage [139] considered 47 SLCs using seven different lightweight aggregates. Two-year drying shrinkage values for 20.7-MPa (3000-psi) compressive strength SLC were between 475 and 780 με depending on the lightweight aggregate considered. Under the same conditions, a similar strength normal weight concrete had shrinkage of 540 με. The study also examined 34.5-MPa (5000-psi) compressive strength SLCs which presented drying shrinkage between 560 and 980 με after 2 years of drying. The corresponding value for a similar strength normal weight concrete was 610 με. Rotary kiln expanded shale showed the least shrinkage regardless the strength of concrete. The drying of all the testing started at the age of 7 days, so it might be assumed that the autogenous shrinkage included in the two-year shrinkage was not important.

The increase in drying shrinkage with strength is also reported by ACI -213 [17]. This might be due to the increase in cement paste content associated with higher strengths. That committee gave a range for one year drying shrinkage between 450 and 850 με for a 17.2 MPa (2500 psi) compressive strength SLC and 600 to 1000 με for their 41.4 MPa (6000 psi) counterparts. The increase in shrinkage with compressive strength might be also due to an increase of the autogenous shrinkage portion as higher strength usually implies lower water-to-cement ratio. Unfortunately, most of the research done in shrinkage of SLC reported only total shrinkage since it did not include measurement on sealed specimens.

Drying shrinkage of SLC is determined by the same factors as normal weight concrete [20]. However, the SLC has some characteristics that would make those factors

have a different impact on drying shrinkage: (1) it usually requires a higher cement content than normal weight concrete for a given compressive strength which increases the relative volume of cement paste; (2) stiffness of lightweight aggregate is lower than normal weight aggregate, so lightweight aggregate allows more movement of the cement paste; and (3) SLC has a higher water retention capacity which slows down the drying process and delays the dimensional stabilization.

Among the different lightweight aggregate available for concrete, it was pointed out that drying shrinkage of expanded slate lightweight concrete was lower than most of lightweight concretes [22].

Shrinkage in SLC tends to be higher than that of a similar strength NSC; however, the results are greatly affected by the type of lightweight aggregate used. SLC made with expanded shales and expanded slates have shown lower shrinkage than those made with other lightweight aggregates or even with normal weight aggregate. The increase in shrinkage of SLC with increasing strength suggests that HPLC, which usually have high strength too, might present even higher shrinkage values.

2.3.4.7 Shrinkage of High Performance Lightweight Concrete

Section 2.5.5.3 on effects of internal curing in autogenous shrinkage reviews the results and conclusions of research done in HPC using lightweight aggregate. Summarizing, the water released by pre-soaked lightweight aggregate after final setting helps to maintain a high internal relative humidity and prevent self-desiccation which prevents or reduces autogenous shrinkage.

As occurs with creep, there are only a few articles regarding shrinkage of HPLC. In addition, autogenous and drying shrinkage are usually not reported separately, but as overall shrinkage.

It was found that compared with HPC, HPLC had a lower shrinkage rate, but a higher ultimate value [143]. According to the authors, the lower rate was caused by the presence of water in the aggregate which delays drying. Shrinkage of two HPLCs produced with lightweight aggregate in coarse and fine aggregate fractions was measured for 90 days after one day or one week of moist curing. Ninety-day shrinkage for the 45 and 60 MPa (6525 and 8700 psi) compressive strength HPLCs was 180 and 380 με, respectively. When shrinkage measurements started after one day, the 90-day shrinkage increased to 300 and 800 με for the same mixtures, respectively. The latter results might have included an important portion of autogenous shrinkage. Other study [27] also observed that shrinkage of HPLC lagged behind at early ages, but one-year shrinkage was approximately 14% higher than the HPC counterpart.

One study [33] measured shrinkage on two lightweight concrete mixtures made with expanded slate after a 28-day curing period. The two mixtures were a SLC and a HPLC with 28-day compressive strengths of 27.6 and 55.2 MPa (4000 and 8000 psi), respectively. One-year shrinkage of 390 and 310 με were reported for the SLC and HPLC. This decrease in one-year shrinkage with increase in compressive strength opposes the trend seen for SLC.

After only 7 days of curing prior to drying, HPLCs having 28-day compressive strength ranging from 50 to 69 MPa (7,250 to 10,000 psi) presented a 450-day shrinkage in the range 518 to 667 με [29]. Other study [26] reported a similar one-year and

ultimate shrinkage of 500 με for an HPLC with Type III cement and fly ash. That mixture had a 28-day compressive strength of 80 MPa (11,600 psi) and the drying started after only one day of curing.

Figure 2.17 presents the results from an investigation that compared shrinkage of HPC and HPLC with drying starting at different ages [37]. The X-axis shows time o drying and the Y-axis shrinkage in με.

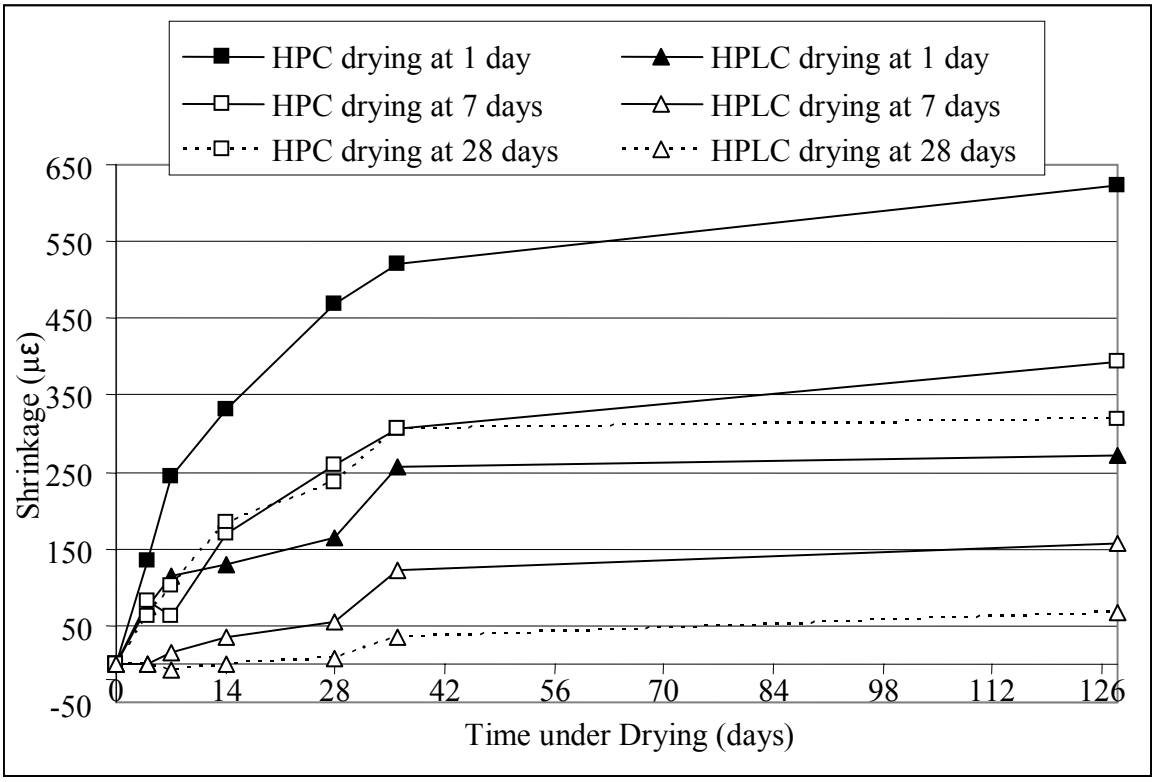

Figure 2.17: Comparison of Shrinkage of HPC and HPLC [37]

The HPC and HPLC were produced using the same mixture design but the coarse aggregate was glacial gravel for the HPC and expanded shale for the HPLC. Shrinkage data when drying started at one day includes autogenous and drying shrinkage while the shrinkage after 28 days of curing is mostly drying shrinkage. From Figure 2.17 it can be seen that HPLC had 128-day shrinkage between 271 and 68 με depending on the start of

drying. The HPC had shrinkage between 623 and 318 με for the different ages at the start of drying. Thus, HPLC experienced shrinkage equivalent to 40% of that measured on HPC regardless of the age at the beginning of drying.

2.3.4.8 Summary of Shrinkage Results

Table 2.5 and Figure 2.18 present a summary of the shrinkage results shown in Sections 2.3.4.5 – 7 above. Data in Table 2.5 is organized by the age of concrete at the beginning of drying, and it also includes total shrinkage, and compressive strength of the mixtures. Figure 2.18 shows shrinkage in με (Y-axis) versus time under drying (X-axis) grouped by age at the beginning of drying.

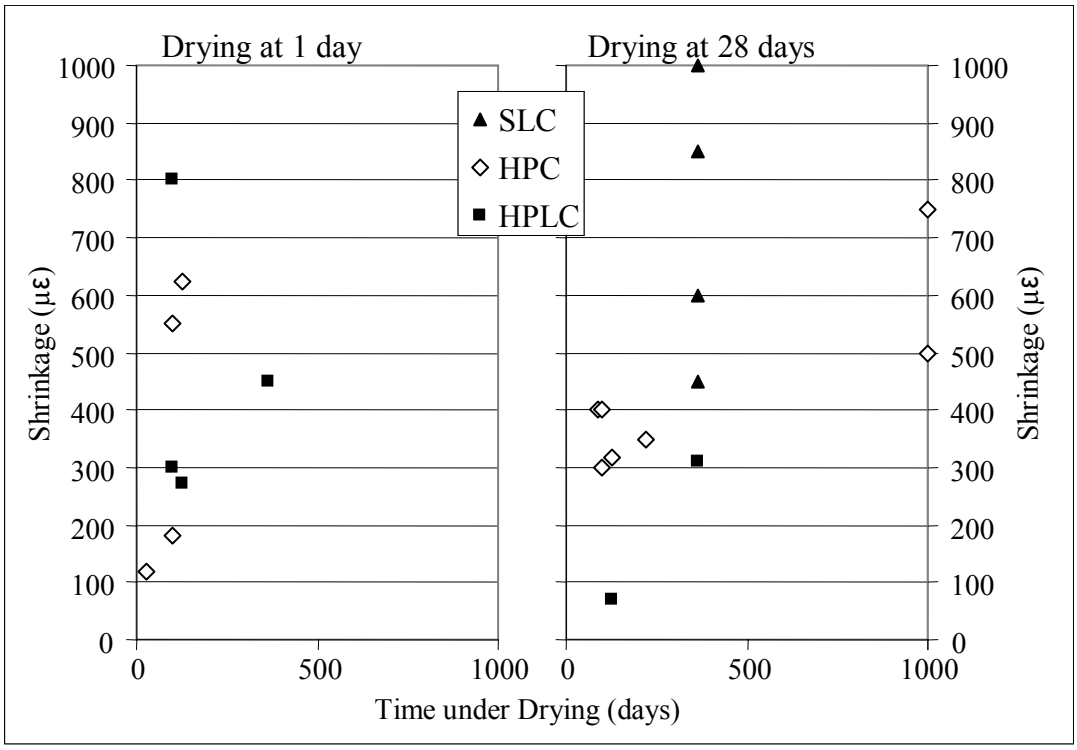

Figure 2.18: Shrinkage versus time under loading and drying for SLC, HPC, and HPLC for drying beginning at 1 and 28 days of age

Table 2.5: Shrinkage results for HPC, SLC, and HPLC in the literature.

Age at drying - days	28-day compressive strength MPa (psi)	time under drying - days	Shrinkage - με	Type	Source
0	80 and 100 (11,600 and 14,500)	1	200 and 230	HPC	[129]
1		28	120	HPC	
1	45 – 60 (6525 – 8700)	100	300 - 800	HPLC	[143]
1	60 – 90 (8700 – 13,050)	100	180 - 550	HPC	
1	80 (11,600)	365	450	HPLC	[26]
1	90.5 (13,120)	128	271	HPLC	[37]
1	96.7 (14,020)	128	623	HPC	
7	20.7 (3000)	700	475 - 780	SLC	[139]
7	20.7 (3000)	700	540	NSC	
7	34.5 (5000)	700	560-980	SLC	
7	34.5 (5000)	700	610	NSC	
7	45 – 60 (6525 – 8700	100	180 - 380	HPLC	[143]
7	60 – 90 (8700 – 13,050)	100	150 - 450	HPC	
7	50 – 69 (7525 – 10,000)	450	518 - 667	HPLC	[29]
28	17.2 (2500)	365	450-850	SLC	[17]
28	41.4 (6000)	365	600-1000	SLC	
28	100 (14,500)	220	350	HPC	[129]
	63 (9135)	90	400	HPC	[131]
28	80 – 120 (11,600 – 17,400)	1000	500 - 750	HPC	[132]
28	83 (12,035)	100	300 - 400	HPC	[135]
28	55 (8000)	365	310	HPLC	[33]
28	90.5 (13,120)	128	68	HPLC	[37]
28	96.7 (14,020)	128	318	HPC	

It can be assumed that when drying started at early ages shrinkage measurements included autogenous and drying shrinkage. At those ages, HPLC and HPC presented similar average shrinkage; however Figure 2.18 shows a wide range in the results. Some HPLC showed lower shrinkage than that of HPC of similar strength or even higher strength. The only exception [143] was a HPLC with 800 με of shrinkage after only 100

days of drying. That particular mixture considered lightweight aggregate in both coarse and fine aggregate which is not typical in HPLC and leads to higher shrinkage [139]; in addition, the lightweight aggregate, pre-soaked for 10 minutes prior to mixing, might have absorbed water from the paste increasing shrinkage.

When drying starts at 7 or 28 days of age, there are researchers that obtained opposite results comparing shrinkage of HPLC and HPC. Nevertheless, is might be stated that HPLC has a lower shrinkage than the normal weight counterpart when the strengths are comparable.

HPLC exhibited lower shrinkage than SLC which indicates that the trend of increase in shrinkage with increasing strength seen for SLC is not followed by HPLC. Thus, it can be concluded that HPLC presents some synergy between lightweight aggregate and high performance paste which makes its shrinkage lower than that of its two predecessors (SLC and HPC).

The lower shrinkage exhibited by HPLC might the caused by the water stored within the lightweight aggregate when it is pre-soaked before mixing. This can decrease or eliminate the autogenous shrinkage as explained in Section 2.4.4.3 yielding to a lower ultimate total shrinkage. However, some researchers have concluded that the low shrinkage shown by HPLC with respect to HPC is temporary, and in the long-term HPLC might present the higher shrinkage. More research is needed in order to know if the beneficial effects of the presoaked lightweight aggregate are permanent or temporary.

2.4 Internal Curing in Concrete

Low water-to-cementitious material ratio concretes are difficult to cure due to their high impermeability [5]. It has been suggested that the water contained in pre-soaked lightweight aggregate can help to provide an internal curing [14] to such mixtures. This Section introduces internal curing and summarizes the research that has been done in this area.

2.4.1 Need for Curing

Curing was defined as all the procedures that promote the hydration of cement [7]. Those include control of time, temperature and humidity immediately after placement. The curing is required not only to reach the specified strength but also to reach the best of all concrete properties. It was concluded that moisture supply assures the hydration of the cementing materials, reduces porosity and maximizes the mechanical properties and durability [8].

The mixing water in conventional concrete is usually more than required for complete hydration. Nevertheless, the losses of water to the environment can undermine hydration [6]. Figure 2.19, contains the results [144] which empirically demonstrates the effect of curing water in the strength gain of concrete.

It was demonstrated that hydration stops if the relative humidity within capillary pores drops below 80% [145]. This implies that if there is enough water added initially and the ambient relative humidity is above 80% the supply of external water would not be necessary. Nevertheless, it was pointed out that in reality there is always water migration from the concrete to the environment due to wind, and temperature difference, among others [10].

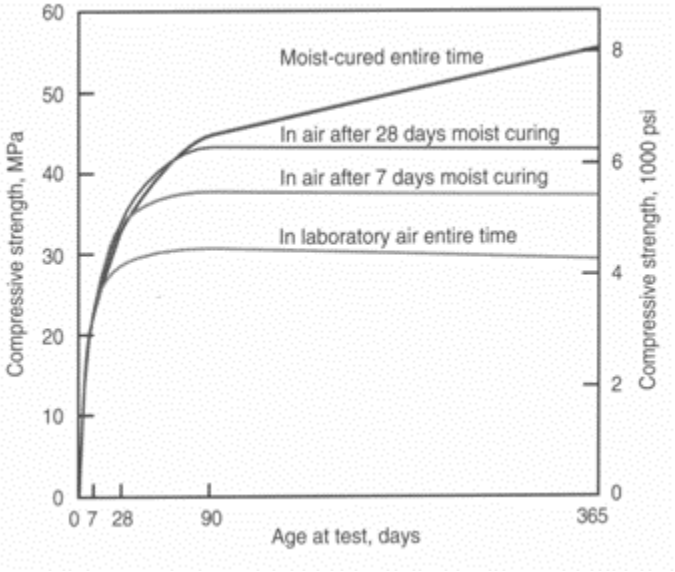

Figure 2.19: Effect of moist curing time on strength gain of concrete [144]

2.4.2 Curing of High Performance Concrete

In developing a HPC there are variations with respect to conventional portland cement-water-aggregate systems. New materials like fly ash, ground granulated blast-furnace slag, silica fume, natural pozzolans, water reducers/plasticizers, high-range water reducers/superplasticizers, fibers, and artificial aggregates, among others are commonly used [6-8, 10].

One of the main factors that allowed the manufacturing of high strength / high performance concrete is the development of high range water reducers [5]. With them, it is possible use a very low water-to-cementitious material ratio (less than 0.35) which gives a great improvement to the compressive strength, elastic modulus, flexure strength, impermeability and abrasion resistance. This kind of concrete, so different from the

conventional concrete, has produced a new scenario with respect to the role and need of curing.

Fly ash, ground granulated blast-furnace slag, natural pozzolans, and silica fume are only a part of the SCMs for concrete [100-103]. Most of them include silica that present a pozzolanic reaction with the calcium hydroxide and water to produce secondary or pozzolanic C-S-H. With the exception of very finely divided reactive silica or silicates (e.g., silica fume), the reaction between calcium hydroxide and silica is rather slow, so the strength gain rate is usually slower than concrete with 100% portland cement. Curing in this kind of system should last longer, so it is assured that the "secondary" reactions take place [146, 147]. Silica fume, on the other hand, produces porosity refinement and presents a relatively high chemical shrinkage during hydration. Both effects promote self-desiccation and require water to be mitigated [45, 146].

Additionally, concrete with water-to-cementitious materials ratio lower than 0.35 possibly do not contain enough water to hydrate all the cementitious materials they have. Thus, even with no water loss to the environment, it would not be feasible to reach 100% hydration.

HPC usually has low permeability which makes penetration of curing water difficult. This means that external water might not penetrate to the unhydrated grains and formation of new hydration products might be limited even with good curing practices [5].

There are conflicting results with respect to curing of HPC [107]. Some authors obtained 28-day compressive strength 10% lower when the curing period was reduced from 28 to only 7 days [12]. On the other hand, some results have suggested that the

moisture and temperature conditions after 7-day moist curing do not affect the 28-day strength significantly [148]. The latter might be due to the permeability of this kind of concrete which might be low enough after 7 days of moist curing that no further water in or out of the concrete. In fact, ACI-213[13] on high strength concrete stated:

> "Many acceptable methods for curing are available, as discussed in ACI-318. However, high-strength concretes are extremely dense and impermeable. Therefore, appropriate curing methods for various structural elements should be selected in advance."

Conflicting results about curing needs of HPC has been also reported previously [43] where some authors recommended following the same curing practices that are used for conventional concrete, and others that suggested that curing is not required for HPC. Nevertheless, it was concluded [5] that in HPC the curing is even more important that in conventional concrete. In such concretes, curing must start at very early ages to prevent the self-desiccation. After final set has occurred, the hydration develops within the "rigid skeleton" decreasing the relative humidity within the pores. This, called self-desiccation, may start at very early ages if not enough water is provided (see Section 2.2.1.1 on autogenous shrinkage).

2.4.3 Internal Curing Philosophy

Internal curing is a relatively new concept that involves the introduction of a curing agent into the concrete mixture [149]. When the curing agent acts as an internal water reservoir that releases water when needed, it is referred as internal water curing [150].

2.4.3.1 Powers' Model

Powers and co-workers ([104-106, 145] developed a group of empirical equations to model the different phases in a system of portland cement and water. The model

considers five parts: (1) unhydrated cement, (2) hydration products, (3) porosity within hydration products, (4) capillary water, and (5) gel water (adsorbed water). The volume occupied by each of these depends on the degree of hydration of the cement. For instance, for 0% hydration, only water and unhydrated cement exist in the proportion of the water-to-cement ratio. For 100% hydration, the unhydrated cement volume is zero while the hydration product volume is assumed to be 0.68 cm^3 per gram of cement (1.18 in^3 per once of cement). The porosity in the hydration products and capillaries is given by the water-to-cement ratio.

The hydration products formation can be carried out only when there is enough space for growth, and there is enough water for hydration [8]. The available space for new hydration products decreases as hydration proceeds. Eventually, this can constrain further hydration. Based on Powers' equations, in a system with a water-to-cement ratio below 0.36, there will be no complete hydration even if external water is supplied. Based on slightly different assumptions, others [7, 151] have concluded that the minimum water-to-cement ratio that still provides space for reach a theoretical full hydration is approximately 0.30. Nevertheless, such a low water-to-cement ratio will require additional external water to provide full hydration.

In a closed system with enough space for hydration and with no loss of water to the environment, the water-to-cement ratio needs to be above 0.42 to reach the theoretical 100% hydration [48].

Consequently, any system with a water-to-cement ratio between 0.30 and 0.42 requires additional water to reach the 100% hydration. Likewise, mixtures with water-to-cement ratio below 0.36 require an additional source of water to reach their maximum

degree of hydration. In reality, there is loss of water to the environment, so even more water is required to reach the maximum attainable degree of hydration.

Even though Powers' equations were developed for hydration of portland cement, its flexibility allow for extension to pozzolanic reactions such as the silica fume reaction [48]. Thus, the conclusions regarding water needs hold for more complex systems such as portland cement, water and SCMs.

Recently, several investigators [5, 152, 153] have proposed the use of water-to-cementitious material ratio below 0.30 which have exhibited increase in compressive strength, impermeability and reduction in long-term deformations even though complete hydration is not theoretically reached.

2.4.3.2 Internal Curing Principles

Given the importance of curing water and the difficulty of supplying such water into HPC, the idea of providing water from inside the concrete becomes attractive [154].

From Powers' equations it is clear that porosity decreases as water-to-cement ratio decreases. On the other hand, the same model shows that for very low water-to-cement ratio mixtures there can be not enough water to hydrate the cement. Thus, during mixing the amount of water needs to be as low as possible, but later water is needed to assure hydration [14, 48]

The main principle of internal curing is to incorporate water which is not readily available at the beginning (low water-to-cement ratio), but is released later when it is required for hydration.

It was pointed out that internal curing must be applied homogenously because it is not enough to have water within concrete, but it has to be available everywhere [14].

Most of the unhydrated cement grains have to be close of the internal water reservoir because the effective travel distance might be very short. Water displacements from the reservoir up to 4 mm (0.16 in) in mixtures with water-to-cement ratio of 0.3 have been traced [155]. Nevertheless, it was concluded that the water migration within concrete depends on the permeability which decreases as hydration proceeds, the water-to-cement ratio, and the use of silica fume or other SCMs. Considering this, the traveling distance can be as low as 0.1 mm (0.004 in) [14].

As previously discussed, as hydration proceeds, a capillary pore system is created. The pore radii and relative humidity decrease as more hydration products are formed increasing the capillary tension forces. Eventually, the increased capillary forces are great enough to take water from the internal curing reservoir [154, 156]. As more hydration is allowed by the internal curing water, pores become finer and the suction forces higher assuring further water intake. This process stops if the water in the reservoir has been used, if 100% hydration has been reached, or if the permeability is too low for allowing water to reach the unhydrated cement grains.

2.4.3.3 Methods to Incorporate Water in Concrete

Philleo [157] has been indicated as the first in suggesting internal curing using lightweight aggregate in 1991 [14]. Since then, several authors have investigated the use of lightweight aggregate as internal curing reservoir [14, 154-156, 158-162]. These authors have explored the use of natural and artificial lightweight aggregate, fine and coarse lightweight aggregate, and the partial or total replacement of normal weight aggregate by lightweight aggregate. In these studies, the effectiveness of internal curing using lightweight aggregate has been demonstrated. Due to their porous structure,

lightweight aggregates can absorb, after 24 hours of immersion, between 5 and 25% of their weight in water [16]. The amount of internally incorporated water depends on the absorption and the amount of lightweight aggregate in the mixture. It can normally reach 59 kg of water per cubic meter (100 lb per cubic yard) of concrete [156], but it can be as high as 190 kg of water per cubic meter (320 lb per cubic yard) of concrete [163].

It was concluded that because water moves spontaneously to lower energy levels [163]; i.e., from larger to smaller pores, pores in the aggregate smaller than 0.1 μm (0.004 mills) do not contribute to internal curing. It was also suggested that not all lightweight aggregates are the same, and its efficiency in regards to internal curing depends on the pore structure [162]. Their results indicated that expanded clay lightweight aggregate possesses a relatively coarse pore structure and loses most of its water at 97.4% relative humidity while expanded slate holds water down to 70% relative humidity. The latter implies that the very fine pore structure of the expanded slate would be less efficient for internal curing and that higher contents of it are needed to achieve the same level of internal curing than that of expanded clay.

One work [164] showed that the water transfer from pumice to the cement paste occurs mostly during the first 24 hours. Also, about the 50% of the water remained in the aggregate, and it was not used to support hydration. This finding might indicate that the pumice used to produce the mixtures, had two well defines pore sizes: A large one that gave up water relatively easily and a very fine pore system that did not release its water.

One of the inherent disadvantages of replacing normal weight aggregate by lightweight aggregate is the potential reduction in compressive strength and modulus of elasticity in the concrete [5, 16, 17]. Superabsorbent polymers (SAP) became a more

efficient, but more costly, alternative to lightweight aggregate for incorporating water in concrete [47, 48, 149]

There is a great variety of SAP, some can absorb up to 5000 times their weight in water. Most of them, with absorption capacities of 50 times their weight, are used by the diaper industry and are readily available. These polymers are added to the mixture as dry powder. The average size in dry condition is between 0.1 and 0.25 mm (0.004 and 0.01 in) which can increase up to three times in saturated condition [47]. Once the SAP has given up water to the paste, it leaves porosity similar to that of an air entrainment agent [47]. The main advantage of this polymers compared to lightweight aggregate is that their much higher absorption allows for reduction in the dosage for incorporate the same total water. SAP might segregate due to its low density compared to the other constituents [47]. Another problem SAP can present is an increase in the effective water-to-cement ratio if their absorption capacity is diminished by the other constituents. This might be the reason behind the 19% decrease in strength showed by some mixtures with SAP [47].

A comparison of the effectiveness of internal curing when using fine lightweight aggregate and SAP [165] showed that in those particular proportions (20% of fine aggregate being lightweight and 0.04% weight of cement for SAP), both provided adequate internal curing.

Other methods of internal curing are the use of natural and organic compounds of high absorption. Pulp fibers such as those used for paper manufacturing can provide internal curing at the same time that they improve the tensile strength and ductility of concrete [166]. Diatomaceous earth, comprised of skeletons of single cell algae,

possesses high absorption. One problem is the higher water demand for a given workability due to the angularity size and porosity of the particles [163].

2.4.4 Effects of Internal Curing

The effects of internal curing come from the increase in the degree of hydration of the cementitious materials. This increase enhances mechanical properties, decreases permeability, and reduces shrinkage of concrete.

2.4.4.1 Effect of Internal Curing on Compressive Strength

Internal curing was investigated in mixture with water-to-cementitious material ratio of 0.3 and 10% by weight of the cement was replaced by silica fume [154]. Twenty-five % of the fine aggregate was replaced by saturated lightweight aggregate to apply internal curing. After one year the difference in strength between sealed and continuously external cured specimens was only 3% which demonstrated the gain in strength due to external curing was not significant if an adequate internal curing was provided.

One investigation [165] showed that the use of lightweight aggregate or SAP reduced the compressive strength of mortars at 7 days by 20 and 8%, respectively[165]. However, at the age of 28 days the two types of internally cured specimens had a similar compressive strength of 72.4 MPa (10,500 psi) which was 19% higher than the mortar with no internal curing.

2.4.4.2 Effect of Internal Curing on Porosity and Permeability

Internal curing has showed an important decrease in average pore size, between 180 and 365 days, in sealed samples with lightweight aggregate [154]. This demonstrates an increase in the degree of hydration without external curing.

Chloride permeability of different mixtures of HPC with and without pre-soaked lightweight aggregate was investigated for over three years [126]. At the age of 28 days the main differences among mixtures was given by the water-to-cementitious material ratio, and there were not significant differences between the lightweight and normal weight aggregate mixtures. However, after one and three years the lightweight aggregate mixtures showed lower permeability than that of their normal weight aggregate counterparts. The difference in performance was explained with the internal curing supplied by the lightweight aggregate.

2.4.4.3 Effects of Internal Curing on Autogenous Shrinkage

One of the most important benefits from using internal curing is the reduction or elimination of self-desiccation and the shrinkage associated with it. Several authors have investigated the use of internal curing for reducing autogenous shrinkage [14, 47, 158, 160, 161]. All concluded that the mixtures with lightweight aggregate or SAP had considerably less autogenous shrinkage than that of their counterparts with no internal curing. Figure 2.20 presents autogenous shrinkage as measured in sealed specimens produced with cement paste [47] and concrete[158]. The X-axis in Figures 2.20a and 2.20b present time, and self-desiccation shrinkage is shown in the Y-axis.

Cement pastes in Figure 2.20a had a water-to-cementitious material ratio of 0.3 with 80% white portland cement and 20% silica fume and considered two dosages of SAP: 0.3 and 0.6% by weight of cement. Concrete mixtures in Figure 2.20b had a water-to-cementitious material ratio of 0.33 with 10% of silica fume by weight and either normal weight aggregate, expanded clay lightweight aggregate in air-dry condition, or

expanded clay in saturated condition. When air-dry condition was used, the water dosage was adjusted accordingly.

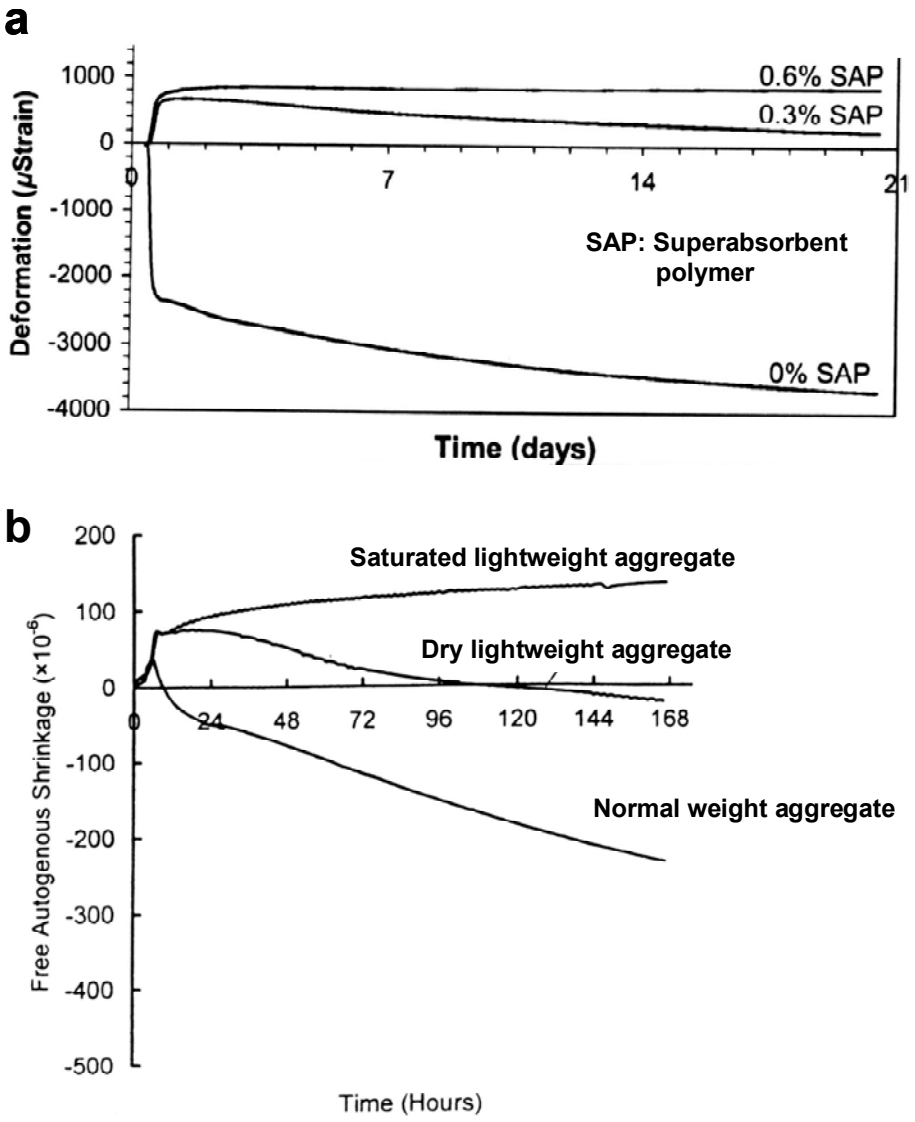

Figure 2.20 Effect of internal curing on self-desiccation shrinkage in (a) Cement paste [47] and (b) Concrete [158]

Some of the mixtures in Figure 2.20 not only did not present shrinkage but also expanded. This might be due to disjoining pressure provided by the water once released from the internal curing source. The expansion can act as "reservoir" of deformations

when the concrete undergoes drying shrinkage and creep. Those time dependent deformations would have to be larger than the expansion in order to be noticeable.

2.4.4.4 Effects of Internal Curing on Cracking

. Figure 2.21a shows results of restrained shrinkage tests carried out in mortars with and without internal curing [47]. Time under testing is shown in X-axis and built up stress in Y axis. The mortars had a water-to-cementitious material ratio of 0.3, and 60% of the volume was quartz sand. As shown in Figure 2.21a, the specimen without internal curing cracked after 3.5 days with a tensile stress equivalent to 1.5 MPa (218 psi). The specimens with the higher dosage of SAP did not crack after 20 days and the tensile stress was only 0.1 MPa (14 psi).

Figure 2.21b presents the results of similar testing performed in 0.33 water-to-cementitious material ratio concrete mixtures with either normal weight aggregate, air-dry expanded clay, or saturated expanded clay [158]. The mixture with normal weight aggregate, and therefore, without internal curing, cracked after 6 days at a tensile stress of 3 MPa (435 psi). None of the mixtures with lightweight aggregate failed during the 7-day monitoring period. The mixtures with air-dried and saturated lightweight aggregate developed a tensile stress of 0.7 MPa (100 psi) and a compressive stress of 0.14 MPa (20 psi), respectively. These values are still far from the cracking stress of the specimen without internal curing.

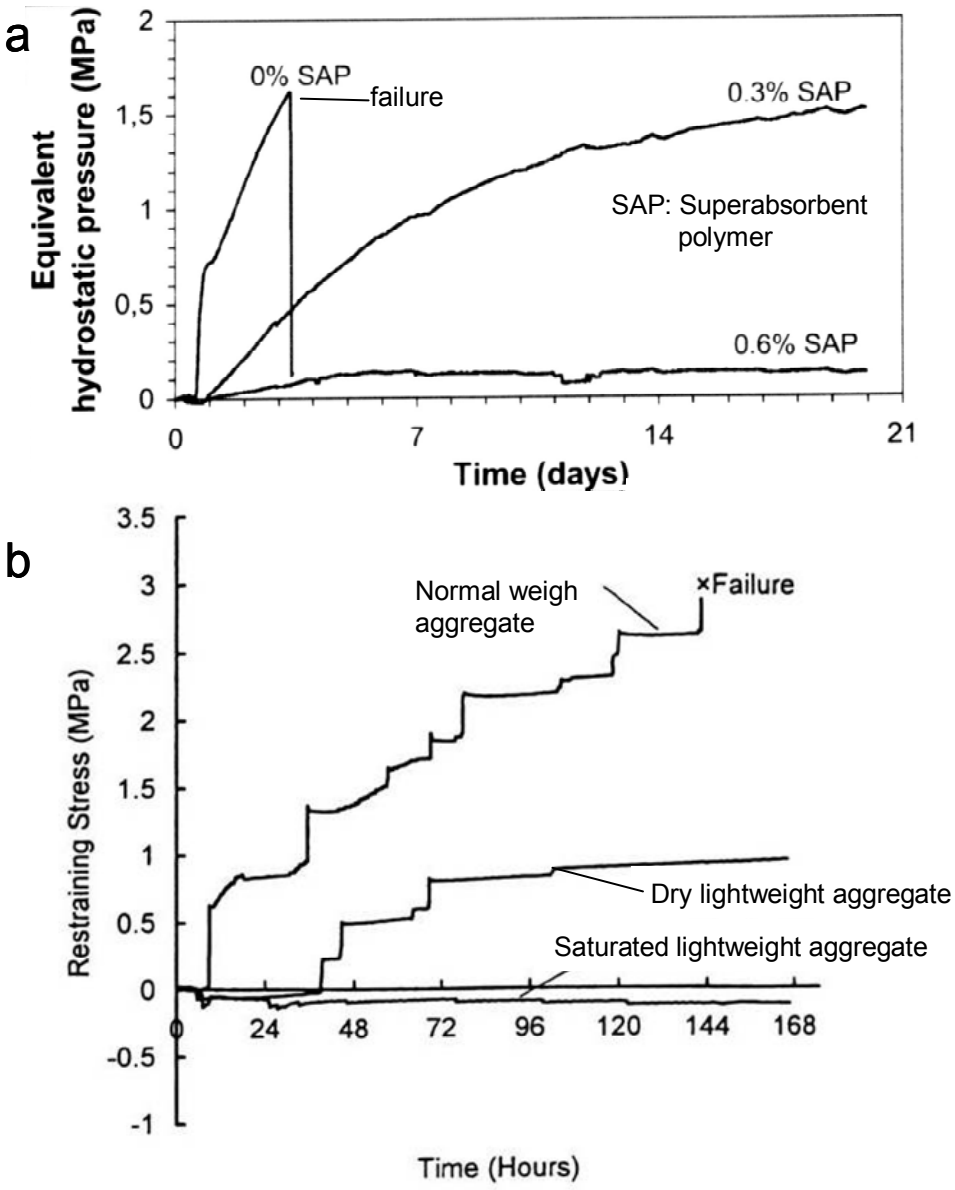

Figure 2.21: Effect of internal curing on tendency to crack in (a) Mortars [47], and (b) Concrete [158]

2.4.4.5 Effects of Internal Curing on Creep

There has been some research on creep of SLC and little research on creep of HPLC (see Section 2.3.4). Nevertheless, there has been no systematic research in the effects of internal curing on creep performance of concrete.

From the research conducted in creep and internal curing the following can be concluded:

a) Internal curing increases compressive strength of concrete. Thus, it can be expected that a higher strength concrete will have lower creep.

b) Internal curing increases the internal relative humidity of concrete. Several of the proposed creep mechanisms state that creep is caused by water migration within the concrete and from concrete to the environment. If a higher internal relative humidity is maintained, a reduction in creep can be expected. Depending on the creep mechanisms, the reduction will be in the drying creep portion or in both drying and basic creep portions.

c) Internal curing decreases permeability of concrete. A reduced permeability reduces water loss from concrete to the environment which reduces drying creep portion.

d) Internal curing enhances the degree of hydration. An increase in the hydration reduces the amount of unhydrated cement in the concrete. As stated above, unhydrated cement contributes to the aggregate restraining effect on creep and shrinkage. Thus, an increase in creep might be expected due to the relative reduction in inert stable phase and relative increase in the cement paste.

e) Internal curing is provided by various systems. Whatever system is used, porosity is expected to increase after water has been released. For instance, porosity in the aggregate (lightweight aggregate) or porosity left by SAP after releasing water.

2.4.4.6 Summary of Effects of Internal Curing on Concrete Properties

Internal curing has proved to be an effective mean of improving performance of HPC. Extensive research in this area has demonstrated that internal curing can improve the following:

1. hydration of cementitious materials in mixtures of low water-to-cementitious material ratio
2. increase in compressive strength
3. decrease in porosity and permeability of the cementitious matrix
4. reduction of autogenous shrinkage
5. reduction of cracking under restrained shrinkage

Even though there are no studies considering the effect of internal curing on creep, it is concluded that improvements in compressive strength, increases in internal relative humidity, and decreases in permeability might reduce creep of concrete. Nevertheless, an increase in hydration might reduce the aggregate restraining effect, thus, increasing creep. More research is needed to understand how internal curing affects creep.

2.5 Prestress Losses in Prestressed Members

2.5.1 Introduction to Prestress Losses

The prestressing force in a prestressed concrete member continuously decreases with time [167]. The Precast Prestressed Concrete Institute (PCI) Committee on Prestress Losses, identified the factors influencing prestress losses as friction in post-tensioning operations, movement of the prestressing steel at the end anchorage, elastic shortening at transfer, effect due to connection of the prestressed member with other structural member, and time dependent losses due to steel relaxation and creep and shrinkage of the concrete [168]. The same committee pointed out that the accurate

determination of stress losses in prestressed members is an extremely complicated problem because the effect of one factor is continuously being altered by changes in stress due to other factors. In describing the loss of prestress, ACI-209 [50] stated, "Prestress losses due to steel relaxation and concrete creep and shrinkage are inter-dependent and also time dependent."

In the same way, it was pointed out that in the actual structure, several losses are occurring simultaneously and are affecting each other in an interdependent manner [169]. Another study [170] concluded that, in real members, there is an important decline of prestress losses resulting from the continuous reduction of concrete compressive stress at the level of prestressing reinforcement. This conclusion suggests that the results of creep measured on concrete cylinder specimens in the laboratory would overestimate the creep prestress losses in an actual prestressed member. This was strongly supported by experimental results [171] that measured total prestress losses in girders of about 21.3% of the initial stress while the computed values from experimental cylinder creep was 33.8%.

The contribution of each loss factor to the total losses depends on the following: the structural design, material properties (concrete and steel), prestressing method (pretensioned or post-tensioned), concrete age at stressing, and the method of prestress computation [172].

A study [173] investigated the potential drop in prestress due to thermal expansion mismatch between concrete and steel reinforcement during the accelerated curing. The results, obtained from actual members and specimens, indicated a nearly full recovery of the thermal stress loss in the strand.

2.5.2 Prestress Losses in Normal Strength Concrete

It was suggested that for normal strength concrete, deformations due to creep and shrinkage in concrete are several times the elastic deformation [174]. In a numerical example [175], the initial and long-term strains were estimated for a NSC subjected to 6.2-MPa (900-psi) compressive stress. The instantaneous elastic, shrinkage and creep strains after one year were estimated as 250, 500 and 750 με, respectively. Those multiplied by the elastic modulus of the prestressing steel were 49.1, 98.3, and 147.4 MPa (7125, 14,250, and 21,375 psi), respectively. Thus, the time-dependent losses; i.e., creep and shrinkage losses, can be 5 times the initial elastic losses.

Partial loss of prestress in a prestressed concrete member is affected by friction (only post-tensioned members), anchorage seating, elastic shortening, shrinkage of concrete, creep of concrete, and relaxation of prestressing steel. Friction, anchorage seating and elastic shortening are usually grouped as initial or instantaneous losses, and shrinkage, creep and steel relaxation are grouped as long-term or time dependent losses. According to the Precast/Prestressed Concrete Institute - PCI [172], total loss of prestress in typical members will range from about 172 and 345 MPa (25,000 to 50,000 psi) for normal strength concrete.

Some references reported values of prestress losses due to creep and shrinkage of NSC [169] within the range between 15.5 and 17.5 percent of the initial stress when concrete was stressed to 60% of its initial strength.

2.5.3 Prestress Losses in High Performance Concrete

HPC usually has higher modulus of elasticity, a lower creep and a similar or lower shrinkage than a normal strength concrete (see Sections 2.2.1 and 2.3.4).

Therefore, it is expected to obtain lower losses due to elastic shortening, reduced losses due to creep losses, similar or lower losses due to shrinkage, and higher losses due to steel relaxation. The expected increase in steel relaxation losses is a consequence of a higher stress in the prestressing steel due to a decrease in losses associated with concrete. Total losses in HPC are expected to be less than NSC.

One study [176, 177] measured prestress losses due to long-term strains; i.e., creep and shrinkage, in HPC girders in the order of 2.5% of the initial stress after 18 months. Those losses projected to 40 years were about 7.4% of the initial stress. The short term elastic losses were 8.9% of the initial stress which was 75% of the strand ultimate strength. Another investigation [178] of normal weight HPC with design strength of 69 MPa (10,000 psi) obtained creep plus shrinkage losses between 7 and 14%.

A National Cooperative Highway Research Program – NCHRP project [179], after their analysis of creep of HPC from Nebraska, New Hampshire, Texas, and Washington, concluded that one year creep of the 12 HPC mixtures was considerably lower than those predicted by the design methods. In addition, elastic and long-term strains were measured in seven girders for more than one year. Long-term strains projected at ultimate were on average 76% of the elastic strains, but values ranged between 50% and 110% of the elastic strains. The AASHTO refined and AASHTO Lump-sum methods for estimating prestress losses overestimated total prestress loses in the girders by 57% and 41%, respectively.

2.5.4 Prestress Losses in Structural Lightweight Concrete

Properties of SLC may vary in a wide range, so the prestress losses can also be expected to vary. In general SLC presents a lower modulus of elasticity than a normal

weight concrete of similar strength. It also has a higher ultimate creep and ultimate shrinkage than the normal weight counterparts. Therefore, elastic shortening, and final creep and shrinkage losses are expected to be greater in SLC. Steel relaxation losses, however, are going to decrease due to the increase in the other losses. In a previous report, ACI-213 [180] concluded that combined loss of prestress in a SLC member is about 110 to 115% of the total losses for normal weight concrete when both are cured normally. If they are steam-cured, prestress losses in SLC are expected to be 124% of the losses in normal weight concrete. Total prestress losses of SLC members with normal weight fine aggregate were found to be between 207 to 379 MPa (30,000 to 55,000 psi) [172] which was about 15% higher than the range given for normal weight concrete.

In an early study of prestress losses of lightweight and normal weight concrete [181], it was concluded that SLC of high quality can be used in prestressed structures because prestress losses due to creep and shrinkage would not be materially larger than those obtained with normal weight concrete of equivalent strength. Prestress losses due to creep and shrinkage were 24 and 22% for lightweight and normal weight concrete, respectively. It was also suggested that the accelerated curing reduced prestress losses from 24 to 19% for SLC and from 22 to 15% for normal weight concrete members.

2.5.5 Prestress Losses in High Performance Lightweight Concrete

To the authors' knowledge, there is no previous research on prestress losses of HPLC; however, from the material properties some conclusions can be drawn. Elastic shortening losses are expected to be similar or less than NSC but more than HPC. Creep and shrinkage losses would be similar to the one of HPC. Steel relaxation losses would tend to be higher than losses in NSC because the previous losses are lower.

2.6 Assessing Deformations with Image Analysis

One criticism to traditional methods for measuring deformations in concrete is that they give global or averaged deformations. While the "bulk" characterization has been useful for designing purposes, it does not provide enough information to understand deformations mechanisms. Some research efforts have been conducted in order to measure deformations at the phase level (i.e., matrix or paste fraction, aggregate and interfacial transition zone) with the use of image analysis. This section presents some of the techniques used for image analysis and some of the applications in cement-based materials.

2.6.1 Digital Image Correlation Technique

Digital image correlation (DIC), as any other deformation measuring technique, provides quantitative information about global or bulk deformations in concrete. However, unlike more traditional techniques, it is a full-field measuring system that provides information about local deformations and variation of deformations on a sample surface. This feature becomes important when measuring deformations in heterogeneous materials that might present non-uniform deformation fields.

DIC is a two-dimensional deformation measuring technique that performs pattern recognition between two images. If the two images correspond to the same region of interest (ROI) at different states of deformation, the pattern recognition provides the coordinates of a certain feature on each of the images. Once the coordinates are known in both states of deformation, the displacements in vertical and horizontal directions can be computed. Deformations in the region of interest are represented by the difference in

displacements between two features. This difference implies a change in the relative distance of the features; i.e., deformation.

The pattern matching is performed by computing the level of resemblance between sub-regions from each of the images. If the level of resemblance is higher than a certain threshold, the two sub-regions are said to be the same feature and the difference between their coordinates are displacements. The resolution of the deformations is given by the magnification of the images; i.e., the actual size of the pixels in the image.

There are different ways to compute the level of resemblance, but the most widely used are based on gray-scale level of the image. The grays in a black and white image are represented by an integer positive number. Zero represents black and the maximum represents white. The wider the range between black and white levels, the more levels a system can represent. The most used system is the 8-bit gray-scale which has 2^8 levels of grays: zero being black and 255 being white.

A sub-region within an 8-bit image (image-1) is comprised of a two-dimensional array of numbers between zero and 255. This particular array can be located in another image (image-2) by a trial and error process. The mathematical difference between the array from image-1 and a candidate array from the image-2 is calculated. If the difference is too large; i.e., the threshold is not passed, the searching continues with other candidate array from image-2. If the threshold is passed the two arrays are said to be the same feature and the coordinates of each are recorded [182].

This technique is usually known as “computer vision”, and its fundamentals were developed in the early 70’s [183-185].

2.6.2 Digital Image Correlation in Cement-Based Materials

It has been demonstrated that DIC provides new and useful information on deformation in heterogeneous materials. The research carried out in cement-based materials has demonstrated that DIC can be applied to cement paste, mortar and concrete.

Image analysis have been used to measure deformations in concrete specimens under monotonically increasing mechanical stresses [186-188], and to assess the strain field in concrete under environmental stress [189-191].

It was found that axial and lateral displacements in concrete under compression load are non-uniform even at early stages in the loading process [188]. This is a consequence of the heterogeneity of concrete where cement paste and aggregate have different elastic properties.

One limitation of measuring deformations at the surface, is that concrete is a three-dimensional structure that deforms accordingly. For that reason, two studies compared the information obtained using DIC and x-ray microtomography in mortar and concrete under compression [186, 187]. X-ray microtomography produces three-dimensional maps of concrete, so deformation inside the specimens can be measured. Even though strong correspondence between the information provided by the two techniques was found, it was concluded that the use of both techniques yielded the best results because each provided inherently different information. DIC is able to visualize strain at early stages, but once cracking has reached a certain level it cannot perform an adequate matching.

The work performed at Northwestern University [189-193] have shown that the use of digital images from an environmental scanning electron microscope can give

information about drying shrinkage of cement-based materials. In those research works a mathematical procedure was developed to measure not only displacements but also strains. With the aid of a mathematical procedure to measure not only displacements but also strains, it was concluded that strains measured at small-scale have similar trends that those measured by more traditional techniques in larger specimens. It was also concluded that shrinkage is the net result of expanding and contracting regions within the microstructure.

DIC has been used in cement-based materials for measuring elastic deformation, cracking and drying shrinkage. However, creep has not been studied using DIC. Preliminary results [182] suggested that the creep strain field in HPLC is non-uniform and changes with time.

2.7 References

1. ACI Committee 363, "State-of-the-Art Report on High-Strength Concrete", in *ACI Manual of Concrete Practice*. American Concrete Institute: Farmington Hills, MI. 1997, p. 55.
2. ACI Committee 116, "Cement and Concrete Terminology", in *ACI Manual of Concrete Practice*. American Concrete Institute: Farmington Hills, MI. 2000, p. 116R.1-116R.73.
3. Goodspeed, C.H., S. Vanikar, and R.A. Cook, "High-performance concrete defined for highway structures". *Concrete International*, 18(2): 1996. p. 62-67.
4. Mehta, P.K., "Advancements in Concrete Technology". *Concrete International*, 21(6): 1999. p. 69-76.
5. Aïtcin, P.-C., *High-performance concrete*. London; New York: E. & F.N. Spon, 1998, xxxii, 591.
6. Kosmatka, S.H., B. Kerkhoff, and W.C. Panarese, *Design and control of concrete mixtures*. 14th ed: Portland Cement Association, 2002.
7. Mehta, P.K. and P.J.M. Monteiro, *Concrete : microstructure, properties, and materials*. 2nd ed: McGraw-Hill, 1993.
8. Mindess, S., J.F. Young, and D. Darwin, *Concrete*. 2nd ed: Prentice Hall, 2003.
9. Nawy, E.G., *Fundamentals of high-performance concrete*. 2nd ed: John Wiley, 2001.
10. Neville, A.M., *Properties of concrete*. 4th and final ed: J. Wiley, 1996.

11. Carrasquillo, P.M. and R.L. Carrasquillo, "Evaluation of the Use of Current Concrete Practice in the Production of High-Strength Concrete". *ACI Materials Journal*, 85(1): 1988. p. 49-54.
12. Carrasquillo, R.L., A.H. Nilson, and F.O. Slate, "Properties of High-Strength Concrete Subject to Short-Term Loads". *Journal of the American Concrete Institute*, 78(3): 1981. p. 171-178.
13. ACI Committee 363, "Guide to Quality Control and Testing of High-Strength Concrete", in *ACI Manual of Concrete Practice*. American Concrete Institute: Farmington Hills, MI. 1998, p. 18.
14. Bentz, D.P. and K.A. Snyder, "Protected paste volume in concrete - Extension to internal curing using saturated lightweight fine aggregate". *Cement and Concrete Research*, 29(11): 1999. p. 1863-1867.
15. Gjørv, O.E., "Durability", in *High Performance Concrete: Properties and Applications*, S.P. Shah and S.H. Ahmad, Editors. McGraw-Hill: New York. 1994, p. 139-160.
16. Holm, T.A. and T.W. Bremner, *State-of-the-Art Report on High-Strength, High-Durability Structural Low-Density Concrete for Applications in Severe Marine Environments*, in *Innovations for Navigation Projects Research Program*. US Army Corps of Engineers. Engineer Research and Development Center, Structures Laboratory: Vicksburg, MS. 2000.
17. ACI Committee 213, "Guide for Structural Lightweight-Aggregate Concrete", in *ACI Manual of Concrete Practice*. American Concrete Institute: Farmington Hills, MI. 2003, p. 38.
18. Chandra, S. and L. Berntsson, *Lightweight aggregate concrete : science, technology, and applications*: Noyes Publications/William Andrew Pub., 2003.
19. Bremner, T.W. and T.A. Holm, "Elastic Compatibility and the Behavior of Concrete". *Journal of the American Concrete Institute*, 83(2): 1986. p. 244-250.
20. Holm, T.A., *Lightweight Concrete and Aggregates, Standard Technical Publication STP 169C*. Philadelphia, PA: American Society for Testing and Materials, 1995.
21. Speck, J.F. and R.G. Burg. "Low-Density High-Performance Concrete". in *High Performance Concrete Research to Practice*. Chicago, IL: American Concrete Institute, 1999.p. 121-131.
22. Short, A. and W. Kinniburgh, *Lightweight concrete*: C. R. Books; Wiley, 1963.
23. Zhang, M.H. and O.E. Gjørv, "Mechanical-Properties of High-Strength Lightweight Concrete". *ACI Materials Journal*, 88(3): 1991. p. 240-247.
24. Videla, C. and M. Lopez, "Effect of lightweight aggregate intrinsic strength on lightweight concrete compressive strength and modulus of elasticity". *Materiales De Construccion*, 52(265): 2002. p. 23-37.
25. Videla, C. and M. Lopez, "Mixture proportioning methodology for structural sand-lightweight concrete". *ACI Materials Journal*, 97(3): 2000. p. 281-289.
26. Curcio, F., et al. "High-Performance Lightweight Concrete for the Precast Prestressed Concrete Industry". in *Fourth CANMET/ACI/JCI International Symposium on Advances in Concrete Technology, SP-179*. Tokushima, Japan: American Concrete Institute, 1998.p. 389-404.

27. Holm, T.A. and T.W. Bremner, "High Strength Lightweight Aggregate Concrete", in *High Performance Concrete: Properties and Applications*, S.P. Shah and S.H. Ahmad, Editors. McGraw-Hill: New York, NY. 1994, p. 341-374.
28. Berner, D.E., "High Ductility, High Strength Lightweight Aggregate Concrete", in *Structural Lightweight Aggregate Concrete Performance SP-136*, T.A. Holm, and Vaysburd, A.M., Editor. American Concrete Institute: Detroit. 1992, p. 319-343.
29. Bilodeau, A., et al. "Mechanical Properties, Durability and Fire Resistance of High Strength Lightweight Concrete". in *International Symposium on Structural Lightweight Aggregate Concrete*. Sandefjord. Norway, 1995.p. 432-443.
30. Harmon, K.S. "Recent Research on the Mechanical Properties of High Performance Lightweight Concrete". in *Theodore Bremner Symposium on High-Performance Lightweight Concrete*. Tessaloniki, Greece, 2003.p. 131-150.
31. Hoff, G.C., "High Strength Lightweight Aggregate Concrete for Arctic Applications - Part 2", in *Structural Lightweight Aggregate Concrete Performance SP-136*, T.A. Holm, and Vaysburd, A.M., Editor. American Concrete Institute: Detroit. 1992, p. 67-173.
32. Kayali, O., M.N. Haque, and B. Zhu, "Some characteristics of high strength fiber reinforced lightweight aggregate concrete". *Cement and Concrete Composites*, 25(2): 2003. p. 207-213.
33. Leming, M.L., *Creep and Shrinkage of Lightweight Concrete*. Department of Civil Engineering, North Carolina State University: Raleigh, NC. 1990.
34. Luther, M.D., "Lightweight Microsilica (Silica Fume) Concrete in USA", in *Structural Lightweight Aggregate Concrete Performance SP-136*, T.A. Holm, and Vaysburd, A.M., Editor. American Concrete Institute: Detroit. 1992, p. 273-293.
35. Malhotra, V.M. "Properties of High-Strength Lightweight Concrete Incorporating Fly Ash and Silica Fume". in *High-Strength Concrete. Second International Symposium, SP-121*. Berkeley, California: American Concrete Institute, 1990.p. 645-666.
36. Meyer, K.F., B.S. Buchberg, and L.F. Kahn. "Development of High Strength Lightweight Concrete Mix Designs: A Practical Approach". in *49th Annual PCI Convention & Exhibition, the 3rd PCI/FHWA International Symposium on High Performance Concrete, and the National Bridge Conference.* Orlando, Florida: Precast / Prestressed Concrete Institute, 2003.
37. Nilsen, A.U. and P.C. Aïtcin, "Properties of High-strength Concrete Containing Light-, Normal- and Heavy-weight Aggregate". *Cement Concrete and Aggregates*, 14(1): 1992. p. 8-12.
38. Vincent, E.C., *Compressive Creep of Lightweight, High Strength Concrete Mixture*, in *Civil Engineering*. Virginia Polytechnic Institute and State University: Blacksburg. 2003, p. 137.
39. Hoff, G.C. "High-Strength Lightweight Concrete - Current Status and Future Needs". in *High-Strength Concrete. Second International Symposium*. Berkeley, California: American Concrete Institute, 1990.p. 619-644.
40. Slate, F.O., A.H. Nilson, and S. Martinez, "Mechanical Properties of High-Strength Lightweight Concrete." *Journal of The American Concrete Institute*, 83(4): 1986. p. 606-613.

41. Meyer, K.F. and L.F. Kahn, "Lightweight concrete reduces weight and increases span length of pretensioned concrete bridge girders". *PCI Journal*, 47(1): 2002. p. 68-75.
42. ACI Committee 209, "Report on Factors Affecting Shrinkage and Creep of Hardened Concrete", in *ACI Manual of Concrete Practice*. American Concrete Institute: Farmington Hills, MI. 2005, p. 12.
43. Aïtcin, P.-C., A.M. Neville, and P. Acker, "Integrated view of shrinkage deformation". *Concrete International*, 19(9): 1997. p. 35-41.
44. Carreira, D.J. and R.G. Burg. "Testing for Concrete Creep and Shrinkage". in *The Adam Neville Symposium: Creep and Shrinkage - Structural Design Effects SP-194*. Atlanta: American Concrete Institute, 2000.p. 381-420.
45. Jensen, O.M. and P.F. Hansen, "Autogenous deformation and RH-change in perspective". *Cement and Concrete Research*, 31(12): 2001. p. 1859-1865.
46. Tazawa, E. and S. Miyazawa, "Experimental-Study on Mechanism of Autogenous Shrinkage of Concrete". *Cement and Concrete Research*, 25(8): 1995. p. 1633-1638.
47. Jensen, O.M. and P.F. Hansen, "Water-entrained cement-based materials II. Experimental observations". *Cement and Concrete Research*, 32(6): 2002. p. 973-978.
48. Jensen, O.M. and P.F. Hansen, "Water-entrained cement-based materials I. Principles and theoretical background". *Cement and Concrete Research*, 31(4): 2001. p. 647-654.
49. de Larrard, F., P. Acker, and R. Le Roy, "Shrinkage, Creep and Thermal Properties", in *High Performance Concrete: Properties and Applications*, S.P. Shah and S.H. Ahmad, Editors. McGraw-Hill: New York, NY. 1994, p. 65-114.
50. ACI Committee 209, "Prediction of Creep, Shrinkage, and Temperature Effects in Concrete Structures", in *ACI Manual of Concrete Practice*. American Concrete Institute: Farmington Hills, MI. 1997, p. 209R.1-209R.47.
51. Comite Euro-Internacional du Beton (CEB) and Federation Internationale de la Precontrainte (FIP), *CEB Code Final Draft Section 3 Materials prEN 1992-1*. 2001, p. 25-31.
52. Comite Euro-Internacional du Beton (CEB) and Federation Internationale de la Precontrainte (FIP), *Evaluation of the Time Dependent Behavior of Concrete*. Lancaster: The Construction Press, 1990.
53. AASHTO-LRFD, *AASHTO LRFD Bridge Design Specifications*. Third Edition ed. Washington: American Association of State Highway and Transportation Officials, 2004.
54. Bažant, Z.P. and S. Baweja, "Creep and Shrinkage Prediction Model for Analysis and Design of Concrete Structures - Model B3, RILEM Draft Recommendation". *Materials and Structures*, 28: 1995. p. 357-365.
55. Gardner, N.J. and M.J. Lockman, "Design provisions for drying shrinkage and creep of normal-strength concrete". *ACI Materials Journal*, 98(2): 2001. p. 159-167.
56. Sakata, K. "Prediction of Creep and Shrinkage, Creep and Shrinkage of Concrete,". in *Fifth International RILEM Symposium*. Barcelona, Spain: RILEM, 1993.p. 649-654.

57. Sakata, K., et al. "Prediction Equations of Creep and Drying Shrinkage for Wide-Ranged Strength Concrete". in *Creep Shrinkage and Durability Mechanics of Concrete and Other Quasi-Brittle Materials*. Cambridge, Massachusetts, United States: Elsevier, 2001.p. 753-758.
58. Wittmann, F.H. "Creep and Shrinkage Mechanisms". in *Creep and Shrinkage in Concrete Structures*. Lausanne, Switzerland: John Wiley & Sons, 1982.p. 129-161.
59. RILEM TC69 Subcommittee 1, "Physical Mechanisms and their Mathematical Descriptions", in *Mathematical Modeling of Creep and Shrinkage of Concrete*, Z.P. Bažant, Editor. John Wiley & Sons: New York. 1988.
60. Carlson, R.W., "Drying Shrinkage of Large Concrete Members". *ACI Journal*, 33: 1937. p. 337-336.
61. L'Hermite, R. "Volume Changes of Concrete". in *Fourth International Symposium on the Chemistry of Cement*. Washington, D.C.: National Bureau of Standards, 1960.p. 659-702.
62. Pickett, G., "Effect of aggregate on shrinkage of concrete and hypothesis concerning shrinkage". *American Concrete Institute -- Journal*, 27(5): 1956. p. 581-590.
63. Moon, J.-H., et al. "Autogenous Shrinkage, Residual Stresses, and Cracking in Cementitious Composites: The Influence of Internal and External Restraint". in *Self-Desiccation and Its Importance in Concrete Technology*. Gaithersburg, Maryland, USA: Lund University Lund Institute of Technology, 2005.p. 1-20.
64. Powers, T.C., *Rev. Mater. Construct (Paris)*, (545): 1961. p. 79-85.
65. Brooks, J.J. and A.M. Neville. "Creep and Shrinkage of Concrete as Affected by Admixtures and Cement Replacement Materials". in *Creep and Shrinkage of Concrete: Effect of Materials and Environment SP-135*. San Diego, California: American Concrete Institute, 1992.p. 19-36.
66. Brooks, J.J. "Elasticity, Creep, and Shrinkage of Concretes Containing Admixtures". in *The Adam Neville Symposium: Creep and Shrinkage - Structural Design Effects SP194*. Atlanta: American Concrete Institute, 2000.p. 283-360.
67. de Larrard, F. "Creep and Shrinkage of High Strength Field Concretes". in *High Strength Concrete, Second International Symposium SP121*. Berkeley, CA: American Concrete Institute, 1990.p. 577-598.
68. Belaribi, N., G. Pons, and B. Perrin, "Delayed behaviour of concrete: Influence of additions and aggregate characteristics in relation to moisture variations". *Cement and Concrete Research*, 27(9): 1997. p. 1429-1438.
69. Brooks, J.J. and M.A. Megat Johari. "Long-term Deformations of High-Strength Concrete Containing Silica Fume and Metakaolin". in *5th CANMET/ACI International Conference on Recent Advances in Concrete Technology SP 200*. Singapore: American Concrete Institute, 2001.p. 97-111.
70. Brooks, J.J., "Influence of mix proportions, plasticizers and superplasticizers on creep and drying shrinkage of concrete". *Magazine of Concrete Research*, 41(148): 1989. p. 145-153.
71. Findley, W.N., J.S. Lai, and K. Onaran, *Creep and relaxation of nonlinear viscoelastic materials : with an introduction to linear viscoelasticity*: Dover, 1989.

72. Neville, A.M., W.H. Dilger, and J.J. Brooks, *Creep of plain and structural concrete*: Construction Press, 1983.
73. Fuller, A.H. and C.C. Moore, "Time Tests of Concrete". *ACI Journal*, 12: 1916. p. 302.
74. Hatt, W.K., "Effect of Time Element in Loading Concrete". *ASTM Proceedings*: 1907. p. 421.
75. Neville, A.M., "Role of cement in creep of mortar". *Journal of the American Concrete Institute*, 30(9): 1959. p. 963-984.
76. Troxell, G.E., J.M. Raphael, and R.E. Davis. "Long-term Creep and Shrinkage Tests of Plain and Reinforced Concrete". in *Cement and Concrete*. Los Angeles: ASTM Proceedings, 1958.p. 1101-1120.
77. Neville, A.M., "Creep of concrete as function of its cement paste content". *Magazine of Concrete Research*, 16(46): 1964. p. 21-30.
78. Bažant, Z.P., ed. *Mathematical Modeling of Creep and Shrinkage of Concrete*. Wiley Series in Numerical Methods in Engineering. John Wiley and Sons: New York. 1988, 459.
79. Neville, A.M. and W.H. Dilger, *Creep of concrete: plain, reinforced, and prestressed*. Amsterdam, New York,: North-Holland Pub. Co., American Elsevier, 1970, xix, 622.
80. Bažant, Z.P., "Prediction of concrete creep and shrinkage: past, present and future". *Nuclear Engineering and Design*, 203(1): 2001. p. 27-38.
81. ACI Committee 209. "Effect of Concrete Constituent, Environment, and Stress on the Creep and Shrinkage of Concrete". in *Designing for Effects of Creep, Shrinkage, and Temperature in Concrete Structures SP 27*. Farmington Hills, MI: American Concrete Institute, 1971.p. 1-42.
82. Jensen, R.S. and F.E. Richart, "Short-Time Creep Test of Concrete in Compression". *ASTM Proceedings*, 38: 1938. p. 410-417.
83. Vogt, F., *On the Flow and Extensibility of Concrete*. Stockolm, 1935, 24.
84. Neville, A.M., "Theories of Creep in Concrete". *ACI Journal*, 52: 1955. p. 47-60.
85. Ali, I. and C.E. Kesler. "Mechanisms of creep in concrete". in *American Concrete Institute -- Symposium on Creep of Concrete, 1964*: American Concrete Institute, Detroit, MI, United States, 1964.p. 35-63.
86. Thomas, F.G. "Creep of Concrete under Load". London: International Association of Testing Materials, 1937.p. 292-294.
87. Lyman, C.G., *Growth and Movement in Portland Cement Concrete*. London: Oxford University Press, 1934, 139.
88. Davis, R.E., H.E. Davis, and J.S. Hamilton, "Plastic flow of concrete under sustained stress". *American Society for Testing Materials -- Proceedings*, 34(Part 11): 1934. p. 354-386.
89. Han, N., *Time dependent behaviour of high strength concrete*. 1996.
90. Glucklich, J., "Creep Mechanisms in Cement Mortar". *ACI Journal*, 59: 1962. p. 923-948.
91. Hsu, T.T.C., *Inelastic Behavior T-Loading*. Cornell University: Ithaca. 1956, p. 6.
92. Bažant, Z.P., et al., "Microprestress-solidification theory for concrete creep .1. Aging and drying effects". *Journal of Engineering Mechanics-ASCE*, 123(11): 1997. p. 1188-1194.

93. Meyers, B.L., *Time Dependent Strains and Microcracking of Plain Concrete*. Cornell University: Ithaca. 1967, p. 86.
94. Staquet, S. and B. Espion. "Effects of Heat Treatment on Creep Functions of HPC Loaded at Very Early Age". in *Advances in Cement and Concrete*. Copper Mountain, Colorado: Engineering Conferences International, 2003.p. 471-479.
95. Bažant, Z.P. and S. Prasannan, "Solidification Theory for Concrete Creep .1. Formulation". *Journal of Engineering Mechanics-ASCE*, 115(8): 1989. p. 1691-1703.
96. Kordina, K., "Experiments on the Influence of the Mineralogical Character of Aggregates on Creep of Concrete". *RILEM Bulletin*, 6: 1960. p. 7-22.
97. Browne, R.D. and R. Blundell, "The Behavior of Concrete in Prestressed Concrete Pressure Vessels". *First International Conference on Structural Mechanics in Reactor Technology. Nuclear Engineering and Design*, 20(2): 1972. p. 429-475.
98. Counto, U.J., "Effect of elastic modulus of aggregate on elastic modulus, creep and creep recovery of concrete". *Magazine of Concrete Research*, 16(48): 1964. p. 129-138.
99. Alexander, M.G., "Aggregate and the deformation properties of concrete". *ACI Materials Journal*, 93(6): 1996. p. 569-77.
100. ACI Committee 232, "Use of Fly Ash in Concrete", in *ACI Manual of Concrete Practice*. American Concrete Institute: Farmington Hills, MI. 1996.
101. ACI Committee 232, "Use of Raw or Processed Natural Pozzolans in Concrete", in *ACI Manual of Concrete Practice*. American Concrete Institute: Farmington Hills, MI. 2000.
102. ACI Committee 233, "Ground Granulated Blast-Furnace Slag as a Cementitious Constituent in Concrete", in *ACI Manual of Concrete Practice*. American Concrete Institute: Farmington Hills, MI. 1995.
103. ACI Committee 234, "Guide for the Use of Silica Fume in Concrete", in *ACI Manual of Concrete Practice*. American Concrete Institute: Farmington Hills, MI. 1996.
104. Powers, T.C., L.E. Copeland, and H.M. Mann, *Capillary Continuity or Discontinuity in Cement Pastes*. Bulletin 110, Portland Cement Association: Skokie. 1959, p. 1-12.
105. Powers, T.C., *Physical Properties of Cement Paste*. Bulletin 154, Portland Cement Association: Skokie. 1960, p. 577-613.
106. Powers, T.C. and T.L. Brownyard, *Studies on the Physical Properties of Hardened Cement Paste*. Bulletin 22, Portland Cement Association: Skokie. 1948.
107. Mindess, S., "Material Selection, Proportioning and Quality Control", in *High Performance Concrete: Properties and Applications*, S.P. Shah and S.H. Ahmad, Editors. McGraw-Hill: New York, NY. 1994, p. 1-26.
108. Harmon, K.S. "Physical Characteristics of Rotary Kiln Expanded Slate Lightweight Aggregate". in *Second International Symposium on Structural Lightweight Aggregate Concrete.* Norway: Norwegian Concrete Association, 2000.p. 11.

109. Katz, A., A. Bentur, and K.O. Kjellsen, "Normal and High Strength Concretes with Lightweight Aggregates", in *RILEM Report 20: Engineering and Transport Properties of the Interfacial Transition Zone in Cementitious Composites*, M.G. Alexander, Arliguie, G., Ballivy, G., Bentur, A., and Marchand, J., Editor. RILEM Publications S.A.R.L.: Cachan Cedex, France. 1999, p. 71-88.
110. Zhang, M.H. and O.E. Gjørv, "Microstructure of the Interfacial Zone between Lightweight Aggregate and Cement Paste". *Cement and Concrete Research*, 20(4): 1990. p. 610-618.
111. Zhang, M.H. and O.E. Gjørv, "Penetration of Cement Paste into Lightweight Aggregate". *Cement and Concrete Research*, 22(1): 1992. p. 47-55.
112. Wasserman, R. and A. Bentur, "Interfacial interactions in lightweight aggregate concretes and their influence on the concrete strength". *Cement & Concrete Composites*, 18(1): 1996. p. 67-76.
113. Khokrin, *The Durability of Lightweight Concrete Structural Members (in Russian)*: Kuibyshev, USSR. 1973, p. 114.
114. Hoff, G.C., "High Strength Lightweight Aggregate Concrete for Arctic Applications - Part 3", in *Structural Lightweight Aggregate Concrete Performance SP-136*, T.A. Holm, and Vaysburd, A.M., Editor. American Concrete Institute: Detroit. 1992, p. 175-245.
115. Hoff, G.C., "High Strength Lightweight Aggregate Concrete for Arctic Applications - Part 1", in *Structural Lightweight Aggregate Concrete Performance SP-136*, T.A. Holm, and Vaysburd, A.M., Editor. American Concrete Institute: Detroit. 1992, p. 1-65.
116. Meyer, K.F. and L.F. Kahn. "Transfer and Development Length of 0.6-inch. Strand in High Strength Lightweight Concrete". in *High Performance Structural Lightweight Concrete. SP-218*. Phoenix, AZ: American Concrete Institute, 2002.p. 9-28.
117. Lopez, M., L.F. Kahn, and K.E. Kurtis, "Creep and shrinkage of high-performance lightweight concrete". *ACI Materials Journal*, 101(5): 2004. p. 391-399.
118. Rossignolo, J.A., M.V.C. Agnesini, and J.A. Morais, "Properties of high-performance LWAC for precast structures with Brazilian lightweight aggregates". *Cement and Concrete Composites*, 25(1): 2003. p. 77-82.
119. Smadi, M. and E. Migdady, "Properties of high strength tuff lightweight aggregate concrete". *Cement & Concrete Composites*, 13(2): 1991. p. 129-135.
120. ACI Committee 363, "State-of-the-Art Report on High-Strength Concrete: Chapter 1 - Introduction (Approved)". American Concrete Institute. 2005.
121. ACI Committee 318, *Building Code Requirements for Structural Concrete (ACI318-02), and Commentary (ACI 318R-02)*. Farmington Hills, MI: American Concrete Institute, 2002.
122. Zhang, M.H. and O.E. Gjørv, "Permeability of High-Strength Lightweight Concrete". *ACI Materials Journal*, 88(5): 1991. p. 463-469.
123. Chia, K.S. and M.H. Zhang, "Water Permeability and Chloride Penetration of High-Strength Lightweight Aggregate Concrete". *Cement and Concrete Research*, 32: 2002. p. 639-645.

124. Chia, K.S. and M.H. Zhang. "A Comparative Study of Water Permeability and Chloride Penetration in Lightweight and Normalweight Aggregate Concrete". in *Theodore Bremner Symposium on High-Performance Lightweight Concrete*. Tessaloniki, Greece, 2003.p. 31-44.
125. Mindess, S. and S. Diamond, "SEM Investigations of Fracture Surfaces Using Stereo Pairs .2. Fracture Surfaces of Rock-Cement Paste Composite Specimens". *Cement and Concrete Research*, 22(4): 1992. p. 678-688.
126. Thomas, M.D.A. "Chloride Diffusion in High-Performance Lightweight Aggregate Concrete". in *Theodore Bremner Symposium on High-Performance Lightweight Concrete*. Tessaloniki, Greece, 2003.p. 77-93.
127. Boyd, S.R., T.A. Holm, and T.W. Bremner. "Performance of Structural Lightweight Concrete Made with a Potentially Reactive Natural Sand". in *Theodore Bremner Symposium on High-Performance Lightweight Concrete*. Tessaloniki, Greece, 2003.p. 65-75.
128. ASTM C 1293, *Standard Test Method for Determination of Length Change of Concrete Due to Alkali-Silica Reaction*. West Conshohocken, PA: American Society for Testing and Materials, 2005.
129. Dilger, W.H. and C. Wang. "Creep and Shrinkage of High-Performance Concrete". in *The Adam Neville Symposium: Creep and Shrinkage - Structural Design Effects, SP-194*. Atlanta: American Concrete Institute, 2000.p. 361-379.
130. Mokhtarzadeh, A. and C.E. French, *Mechanical Properties of High Strength Concrete*. Center of Transportation Research, University of Minnesota. 1998, p. 595.
131. Ngab, A.S., A.H. Nilson, and F.O. Slate, "Shrinkage and Creep of High-Strength Concrete". *Journal of the American Concrete Institute*, 78(4): 1981. p. 255-261.
132. Burg, R.G. and B.W. Ost, *Engineering Properties of Commercially Available High Strength Concrete (Including Three-year Data)*. Research and Development Bulletin RD104 Portland Cement Association. 1994.
133. Wolsiefer, J., "Ultra High-Strength Field Pleaceable Concrete with Silica Fume Admixture". *Concrete International*, 6(4): 1984. p. 25-31.
134. Buil, M. and P. Acker, "Creep of a Silica Fume Concrete". *Cement and Concrete Research*, 15(3): 1985. p. 463-466.
135. Huo, X.M.S., N. Al-Omaishi, and M.K. Tadros, "Creep, shrinkage, and modulus of elasticity of high-performance concrete". *ACI Materials Journal*, 98(6): 2001. p. 440-449.
136. Yang, Y., et al. "Experimental Investigation on Shrinkage and Creep of High Strength Concrete at Early Ages". in *Fourth CANMET / ACI / JCI International Symposium on Advances in Concrete Technology, SP-179*. Tokushima, Japan: American Concrete Institute, 1998.p. 201-215.
137. Nilsen, A.U., P.J.M. Monteiro, and O.E. Gjørv, "Estimation of the Elastic-Moduli of Lightweight Aggregate". *Cement and Concrete Research*, 25(2): 1995. p. 276-280.
138. Yang, C.C., "Approximate elastic moduli of lightweight aggregate". *Cement and Concrete Research*, 27(7): 1997. p. 1021-1030.

139. Pfeifer, D.W., "Sand replacement in structural lightweight concrete -- Creep and shrinkage studies". *Journal of the American Concrete Institute*, 65(2): 1968. p. 131-140.
140. van der Wegen, G.J.L. and J.M. Bijen, "Properties of Concrete made with Three Types of Artificial PFA Coarse Aggregate". *The International Journal of Cement Composites and Lightweight Concrete*, 7(3): 1985. p. 159-167.
141. Shideler, J.J., "Lightweight-aggregate concrete for structural use". *Journal of the American Concrete Institute*, 29(4): 1957. p. 299-328.
142. Rogers, G.L. "On the Creep and Shrinkage Characteristics of Solite Concretes". in *World Conference on Prestressed Concrete*. San Francisco, CA, 1957.
143. Berra, M. and G. Ferrada. "Normalweight and Total-Lightweight High-Strength Concretes: A Comparative Experimental Study". in *High-Strength Concrete. Second International Symposium*. Berkeley, California: American Concrete Institute, 1990.p. 701-733.
144. Gonnerman, H.F. and E.C. Shuman, *Flexure and Tension Tests of Plain Concrete*. Report of the Director of Research Series 171, 209, and 210, Portland Cement Association. 1928, p. 143-163.
145. Powers, T.C., *A Discussion of Cement Hydration in Relation to the Curing of Concrete*. Bulletin 25, Portland Cement Association: Skokie. 1947, p. 178-188.
146. Ayers, M.E. and M.S. Khan. "Overview of Fly Ash and Silica Fume Concretes: The Need for Rational Curing Standards". in *Concrete Technology: Past, Present, and Future, Proceedings of V. Mohan Malhotra Symposium*: American Concrete Institute, 1993.p. 605-617.
147. Malhotra, V.M. and P.K. Mehta, *High-Performance, High-Volume Fly Ash Concrete: Materials, Mixture Proportions, Properties, Construction Practice, and Case Histories*. 2nd ed. Ottawa: Supplementary Cementing Materials for Sustainable Development Inc., 2005.
148. Peterman, M.B. and R.L. Carrasquillo, *Production of High Strength Concrete*. Park Ridge: Noyes, 1986.
149. Kovler, K. and O.M. Jensen, "Novel Techniques for Concrete Curing - New Methods for low w/cm mixtures". *Concrete International*, 27(9): 2005. p. 39-42.
150. RILEM TC 196-ICC, *Internal Curing of Concrete (Draft)*. 2005.
151. Hansen, T.C., "Physical Structure of Hardened Cement Paste. A Classical Approach". *Materials and Structures*, 19(114): 1986. p. 423-430.
152. Richard, P. and M.H. Cheyrezy. "Reactive Powder Concretes with High Ductility and 200-800 MPa Compressive Strength". in *Concrete Technology. Past, Present, and Future, SP-144*: American Concrete Institute, 1994.p. 508-518.
153. Richard, P. and M. Cheyrezy, "Composition of Reactive Powder Concretes". *Cement and Concrete Research*, 25(7): 1995. p. 1501-1511.
154. Weber, S. and H.W. Reinhardt, "A new generation of high performance concrete: Concrete with autogenous curing". *Advanced Cement Based Materials*, 6(2): 1997. p. 59-68.
155. Lura, P., D.P. Benz, and D.A. Lange. "Measurements of Water Transport from Saturated Pumice Aggregates to Hardening Cement Paste." in *Advances in Cement and Concrete*. Copper Mountain, Colorado: Engineering Conferences International, 2003.p. 89-99.

156. Holm, T.A., O.S. Ooi, and T.W. Bremner. "Moisture Dynamics in Lightweight Aggregate and Concrete". in *Theodore Bremner Symposium on High-Performance Lightweight Concrete*. Tessaloniki, Greece, 2003.p. 167-184.
157. Philleo, R. "Concrete Science and Reality". in *Materials Science of Concrete II*. Westerville, OH: American Ceramic Society, 1991.p. 1-8.
158. Bentur, A., S. Igarashi, and K. Kovler, "Prevention of autogenous shrinkage in high-strength concrete by internal curing using wet lightweight aggregates". *Cement and Concrete Research*, 31(11): 2001. p. 1587-1591.
159. Hoff, G.C. "Internal Curing of Concrete using Lightweight Aggregate". in *Theodore Bremner Symposium on High-Performance Lightweight Concrete*. Tessaloniki, Greece, 2003.p. 185-203.
160. Kohno, K., et al., "Effects of artificial lightweight aggregate on autogenous shrinkage of concrete". *Cement and Concrete Research*, 29(4): 1999. p. 611-614.
161. Zhutovsky, S., K. Kovler, and A. Bentur, "Efficiency of lightweight aggregates for internal curing of high strength concrete to eliminate autogenous shrinkage". *Materials and Structures*, 35(246): 2002. p. 97-101.
162. Hammer, T.A., Ø. Bjøntegaard, and E.J. Sellevelod. "Internal Curing - Role of Absorbed Water in Aggregates". in *High Performance Structural Lightweight Concrete. SP-218*. Phoenix, AZ: American Concrete Institute, 2002.p. 131-142.
163. Jensen, O.M. and P. Lura. "Techniques for Internal Curing of Concrete". in *Advances in Cement and Concrete*. Copper Mountain, Colorado: Engineering Conferences International, 2003.p. 67-78.
164. Cano Barrita, F.d.J., T.W. Bremner, and B.J. Balcom. "Use of Magnetic Ressonance Imaging to Study Internal Moist Curing in Concrete Containing Saturated Lightweight Aggregate". in *High Performance Structural Lightweight Concrete. SP-218*. Phoenix, AZ: American Concrete Institute, 2002.p. 155-175.
165. Geiker, M.R., D.P. Bentz, and O.M. Jensen. "Mitigating Autogenous Shrinkage by Internal Curing". in *High Performance Structural Lightweight Concrete. SP-218*. Phoenix, AZ: American Concrete Institute, 2002.p. 143-154.
166. Mohr, B.J., et al. "Examination of Wood-derived Powders and Fibers for Internal Curing of Cement-based Materials". in *Self-Desiccation and Its Importance in Concrete Technology*. Gaithersburg, Maryland, USA: Lund University Lund Institute of Technology, 2005.p. 229-244.
167. Zia, P., et al., "Estimating Prestress Losses." *Concrete International*, 1(6): 1979. p. 32-38.
168. PCI-Committee on Prestress Losses, "Recommendations for Estimating Prestress Losses". *PCI Journal*, 28(4): 1975. p. 43-75.
169. Podolny, W.J., "Understanding the Losses in Prestressing". *PCI Journal*, 14(5): 1969. p. 43-53.
170. Tadros, M.K., A. Ghali, and W.H. Dilger, "Time-Dependent Prestress Loss and Deflection in Prestressed Concrete Members". *PCI Journal*, 20(3): 1975. p. 86-98.
171. Shing, P.B., et al., "Strand development and transfer length tests on high performance concrete box girders". *PCI Journal*, 45(5): 2000. p. 96-+.
172. PCI, *PCI Design Handbook, Precast and Prestressed Concrete*. Fifth ed. Chicago: Precast / Prestressed Concrete Institute, 1998.

173. Huang, T., "Study of Prestress Losses Conducted by Lehigh University". *PCI Journal*, 27(5): 1982. p. 48-61.
174. Bandyopadhyay, T.K. and B. Sengupta, "Determining Time-Dependent Losses of Prestress with Due Consideration of Aging Coefficient and Percentage of Steel". *Journal of the American Concrete Institute*, 83(2): 1986. p. 236-243.
175. Nawy, E.G., *Prestressed concrete : a fundamental approach*. 4th ed. Prentice-Hall International Series in Civil Engineering and Engineering Mechanics. Upper Saddle River, NJ: Prentice Hall, 2003, xx, 939.
176. Roller, J.J., et al., "Performance of Prestressed High Strength Concrete Bridge Girders". *PCI Journal*, 38(3): 1993. p. 35-45.
177. Roller, J.J., et al., "Long-term performance of prestressed, pretensioned high strength concrete bridge girders". *PCI Journal*, 40(6): 1995. p. 48-59.
178. Stanton, J.F., P. Barr, and M.O. Eberhard. "Behavior of High-Strength High-Performance Concrete Bridge Girders". in *High-Performance Concrete: Research to Practice*. Chicago, IL, 1999.p. 71-89.
179. Tadros, M., et al., *NCHRP Report 496: Prestressed Losses in Pretensioned High-Strength Concrete Bridge Girders*. Transportation Research Board: Washington D.C. 2003, p. 63 pp.
180. ACI Committee 213, "Guide for Structural Lightweight Aggregate Concrete", in *ACI Manual of Concrete Practice*. American Concrete Institute: Farmington Hills, MI. 1999, p. 213R.1-231R.27.
181. Hansen , J.A., "Prestress Loss as Affected by Type of Curing". *Prestressed Concrete Institute Journal*, 9(4): 1964. p. 69-94.
182. Lopez, M., K.E. Kurtis, and L.F. Kahn. "Creep Strain Distribution and Deformation Mechanisms of High Performance Lightweight Concrete". in *Advances in Cement and Concrete*. Copper Mountain, Colorado: Engineering Conferences International, 2003.p. 423-428.
183. Barnea, D.I. and H.F. Silverman, "A class of algorithms for fast digital image registration". *IEEE Transactions on Computers*, C-21(2): 1972. p. 179-86.
184. Vanderbrug, G.J. and A. Rosenfeld, "2-Stage Template Matching". *IEEE Transactions on Computers*, 26(4): 1977. p. 384-393.
185. Rosenfeld, A. and G.J. Vanderbrug, "Coarse-Fine Template Matching". *IEEE Transactions on Systems Man and Cybernetics*, 7(2): 1977. p. 104-107.
186. Lawler, J.S., D.T. Keane, and S.P. Shah, "Measuring three-dimensional damage in concrete under compression". *ACI Materials Journal*, 98(6): 2001. p. 465-475.
187. Lawler, J.S., D.T. Keane, and S.P. Shah. "Measuring Three-Dimensional Damage of Mortar in Compression with X-ray Microtomography and Digital Image Correlation". in *High-Performance Concrete: Research to Practice*. Chicago, IL, 1999.p. 187-202.
188. Choi, S. and S.P. Shah, "Measurement of Deformations on Concrete Subjected to Compression Using Image Correlation". *Experimental Mechanics*, 37(3): 1997. p. 307-313.
189. Neubauer, C.M. and H.M. Jennings, "The use of digital images to determine deformation throughout a microstructure - Part II - Application to cement paste". *Journal of Materials Science*, 35(22): 2000. p. 5751-5765.

190. Neubauer, C.M., H.M. Jennings, and E.J. Garboczi, "Mapping drying shrinkage deformations in cement-based materials". *Cement and Concrete Research*, 27(10): 1997. p. 1603-1612.
191. Neubauer, C.M., et al., "Drying shrinkage of cement paste as measured in an environmental scanning electron microscope and comparison with microstructural models". *Journal of Materials Science*, 32(24): 1997. p. 6415-6427.
192. Neubauer, C.M., E.J. Garboczi, and H.M. Jennings, "The use of digital images to determine deformation throughout a microstructure - Part I - Deformation mapping technique". *Journal of Materials Science*, 35(22): 2000. p. 5741-5749.
193. Xi, Y., T.B. Bergstrom, and H.M. Jennings, "Image Intensity Matching Technique: Application to the Environmental Scanning Electron Microscope". *Computational Material Science*, 2: 1994. p. 249-260.

CHAPTER 3

RESEARCH PROGRAM

3.1 Research Objectives

High performance lightweight concrete (HPLC) is a relative new material that combines properties of high performance concrete (HPC) and structural lightweight concrete (SLC). It presents not only advantages from its two predecessors but also new characteristics derived from the synergy between them. Enhanced hydration, reduction or elimination of self-desiccation, and improved interfacial transition zone are some of these new advantages.

However, as it is new material HPLC has not been extensively investigated. Particularly, long-term properties such as creep, shrinkage and prestress losses have not been systematically studied.

For effective use of HPLC in precast prestressed bridge girders, the long-term losses of prestressing must be well understood. In order to predict such prestress losses creep and shrinkage of the HPLC material must be understood and be predictable. Therefore, this multi-scale investigation has three main objectives:

- To assess prestress losses in high performance lightweight concrete members
- To improve the fundamental understanding of creep and shrinkage in high performance lightweight concrete
- To characterize and quantify the effect of the constituent materials and external conditions on creep and shrinkage

The following sections discuss each objective.

3.1.1 Assessment of Prestress Losses in High Performance Lightweight Concrete Members

A major concern when using concrete in structural members is the time-dependent deformation due to creep and shrinkage. This is especially true in the case of prestressed members. An important application of creep and shrinkage results is the estimate of prestress losses. Findings from the aforementioned research objectives will be used to assess prestress losses in HPLC.

3.1.2 Improvement the Fundamental Understanding of Creep and Shrinkage in High Performance Lightweight Concrete

A multi-scale approach was used to characterize creep at three different scales: (a) large-scale approach in full-size prestressed girders to measure creep and shrinkage under service conditions; (b) medium-scale approach which is the traditional creep and shrinkage testing in 150 x 300 mm (6 x 12 in) concrete cylinder specimens; and (c) small-scale approach in order to obtain information of creep and shrinkage of the different phases within concrete and how they interact.

3.1.3 Effect of the Constituent Materials and External Conditions on Creep and Shrinkage

HPLC is a material that may include portland cement, supplementary cementing materials (e.g., fly ash, silica fume, and slag), chemical admixtures, water, lightweight or normal weight coarse aggregate, lightweight or normal weight fine aggregate. HPLC presents densities in the 1840 to 1920 kg/m^3 (115 to 120 lb/ft^3) range with compressive strength between 50 and 110 MPa (7250 and 15,950 psi). It is well-known that the

amount and properties of the constituent materials affect creep behavior of concrete. In addition, HPLC is an aging and hygroscopic material; so its creep behavior is affected by its temperature-time history and ambient humidity.

This research proposes a systematic experimental program to isolate the effect of some of the constituent materials, temperature-time conditions and drying conditions.

3.2 Research Methodology

3.2.1 Large-scale Approach

Many have concluded that results from standard testing do not represent actual field conditions very well. Large structural elements in the field present a time-temperature history different from the smaller cylindrical specimens. In addition, the drying of large elements is less severe that those in the laboratory. This is because the volume-to-exposed surface ratio is larger in the former case, so water migration is slowed; and secondly, because the relative humidity of the actual environment is on average higher than those in the laboratory. Finally, a third difference is that in prestressed members, creep does not occur at constant stress. Rather it happened at a decreasing stress due to the prestress losses. This makes creep measured in the laboratory usually higher than that recorded in full-scale prestressed members.

This large-scale study built six AASHTO Type II prestressed bridge girders using alternatively two HPLCs. One was a 55.2-MPa (8000-psi) 56-day compressive strength HPLC identified as LWW 55/8 for its lightweight pre-soaked aggregate (LWW) and the design compressive strength in MPa and ksi (55/8). The other was a 69-MPa (10,000-psi) 56-day compressive strength identified as LWW 69/10. These are the same mixtures and girders used for transfer and development tests [1]. Elastic strains during strand

prestressing force transfer and long-term strains were measured on each girder. This information was used to calculate prestress losses due in girders made using HPLC.

3.2.2 Medium-scale Approach

The medium-scale approach is the more traditional research to measure time-dependent deformations in concrete. It consisted of measuring change in length in cylindrical specimens under sustained load and constant ambient conditions of temperature and relative humidity. Among these, there are companion specimens which undergo the same ambient conditions, but are not loaded. The specimens under load undergo creep and shrinkage, and the companion specimens undergo only shrinkage. This conventional approach allows comparison with results from other investigators.

The design of experiment for the medium-scale portion was based on the LWW 69/10 of the large-scale portion [2, 3], a 69-MPa (10,000-psi) 56-day compressive strength HPLC which coarse aggregate was 12.7-mm (0. 5-in) maximum size aggregate (MSA) pre-soaked expanded slate lightweight aggregate.

The first mixture considered was termed high performance matrix (HP Matrix); it was the same mixture design used in LWW 69/10, but without coarse aggregate, so all other constituents were increased proportionally by volume to occupy the coarse aggregate volume. HP Matrix used cementitious materials, water, chemical admixtures and normal weight siliceous sand. Eight other mixtures were studied, one termed LWW 65-35 which was the same as LWW 69/10 and seven alternative modifications to LWW 65-35 (see numbers in Figure 3.1):

1. LWW 65-35-95: Same as LWW 65-35, but with 9.5-mm (0.375-in) MSA lightweight aggregate

2. LWW 35-65: Same as LWW 65-35, but with half of the volume of expanded slate aggregate
3. LWD 65-35: Same as LWW 65-35, but with air-dried lightweight aggregate instead of pre-soaked
4. NWA 65-35: Like LWW 65-36, but with full replacement. by volume, of expanded slate lightweight aggregate by normal weight granite coarse aggregate
5. NWA 35-65: Same as NWA 65-35, but with half of the volume of granite
6. STL 65-35: Like LWW 65-36, but with full replacement, by volume, of expanded slate lightweight aggregate by 12.7-mm (0.5-in) A36 steel cubes
7. STL 35-65: Same as STL 65-35, but with half of the volume of steel cubes

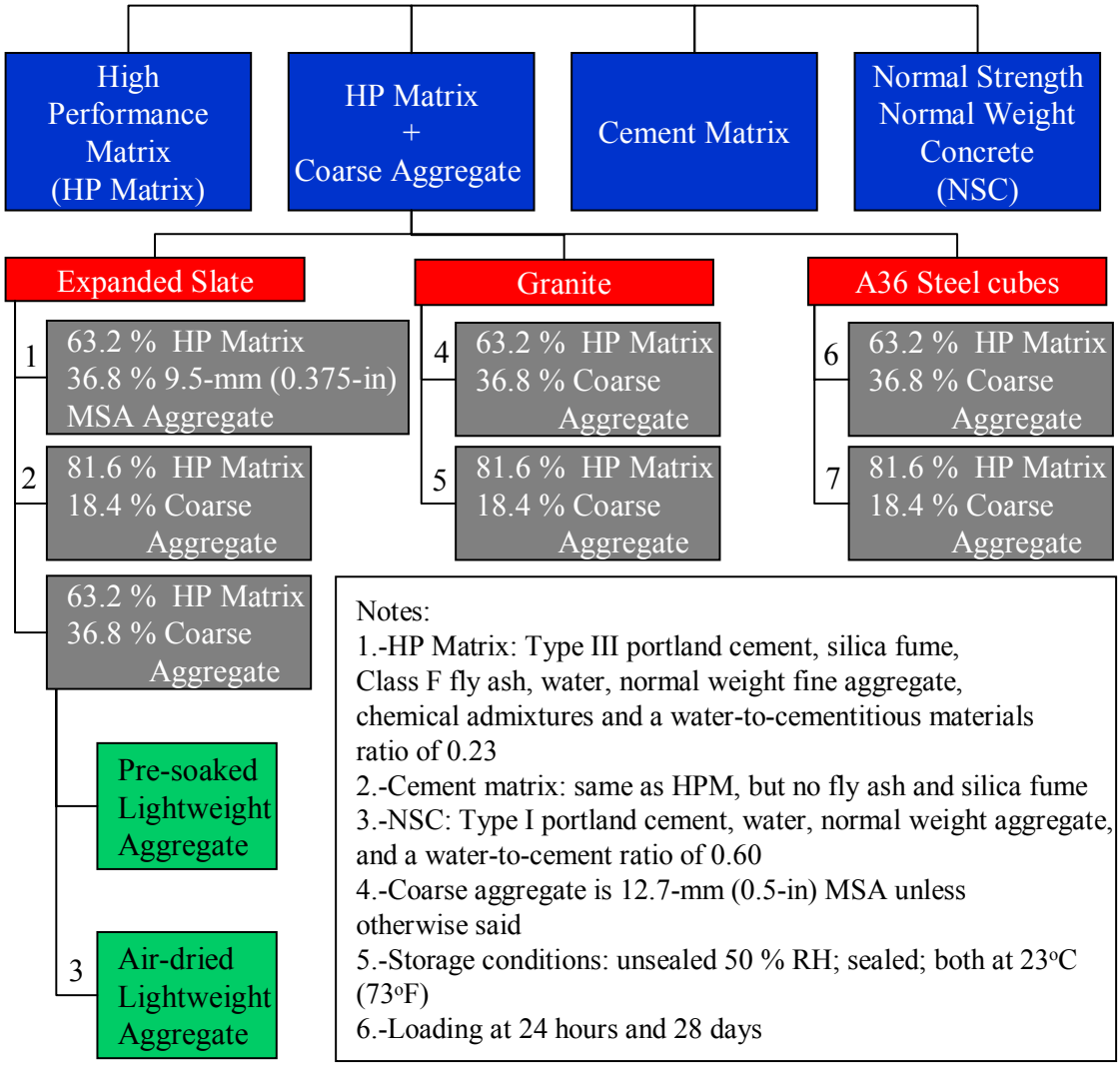

Figure 3.1: Factorial design for medium-scale study

The first variation (i.e., the HPLC with 9.5-mm (0.375-in) MSA), was intended to match the mixture design used in the small-scale study described in the next section. Modifications No. 2, 4, 5, 6, and 7 were expected to provide information about the effects of the type and relative amount of coarse aggregate in the short and long-term performance of the mixture. The steel aggregate constituted a homogeneous material and had well-known mechanical and physical properties; additionally, it does not present creep at room temperature. Finally, the third variation was the same mixture design as the original LWW 65-35 mixture, but the lightweight aggregate was air-dried instead of pre-soaked at the time of mixing. Additional water was added at the time of mixing to account for the absorption by the air-dried aggregate. This mixture was not expected to store as much water as the original HPLC. This comparison was meant to provide information about the beneficial effects of internally stored water on the short and long-term performance of the mixture.

Two additional mixtures were studied; one of them, identified as Cement Matrix, had the same mixture proportions that the HP Matrix, but supplementary cementing materials (i.e., silica fume and fly ash) were replaced by more Type III cement by weight. Finally, a normal strength normal weight concrete (NSC) was studied to have a comparison between high performance cement based materials and conventional concrete. The mix design was the same as used in a 20-year research program [4].

Table 3.1 presents the mixture design of the four HPLC, and Table 3.2 gives the mixture design of the HPC mixtures made with granite or steel aggregate. Table 3.3 present the mixture designs of the remaining three mixtures (i.e., HP Matrix, Cement Matrix, and NSC).

Table 3.1: Mixture designs of high performance mixtures with expanded slate in kg/m^3 (lb/yd^3)

	LWW 65-35	LWW 65-35-95	LWW 35-65	LWD 65-35
Type III Cement	442 (745)	442 (745)	574 (967)	442 (745)
Type I cement				
Silica fume	59 (100)	59 (100)	82 (139)	59 (100)
Class F fly ash	89 (150)	89 (150)	116 (196)	89 (150)
Water	128 (215)	135 (228)	180 (300)	177 (298)
Normal weight fine aggregate	612 (1032)	612 (1032)	796 (1342)	612 (1032)
coarse aggregate [1]	pre-soaked[2] expanded slate 576 (972)	pre-soaked[2] expanded slate 613 (1033)	pre-soaked[2] expanded slate 285 (480)	air-dried [3] expanded slate 530 (894)
WRDA 35 [4]	2.7 (4.6)	2.7 (4.6)	3.6 (61)	2.7 (4.6)
Adva Flow [5]	5.9 (9.9)	5.9 (9.9)	7.7 (13)	5.9 (9.9)
Daravair 1000 [6]	0.3 (0.5)	0.3 (0.5)	0.4 (0.6)	0.3 (0.5)
water/cementitious ratio	0.230	0.230	0.230	0.230
Cement paste content (%)	39	39	50	39
Coarse/fine ratio by volume	1.5	1.5	0.58	1.5
Theoretical density kg/m^3(lb/ft^3)	1920 (119.9)	1959 (122.3)	2046 (127.7)	1920 (119.9)

[1]: MSA was 12.7 mm (0.5 in) except for LWW 65-35-95 which used 9.5-mm (0.375-in) MSA

[2]: pre-soaked lightweight aggregate was water-sprayed with sprinklers in the aggregate bins for 24 hours after which the sprinklers were shut off and water was allowed to drain for 24 additional hours. This prevented a moisture gradient throughout the aggregate bins while still maintaining moisture content at SSD condition.

[3]: air-dried lightweight aggregate was allowed to dry at 50% relative humidity for five days prior to mixing.

[4]: Water reducer (0.45% of cementitious materials by weight)

[5]: high range water reducer (1.0% of cementitious materials by weight)

[6]: Air entrainer agent (0.05% of cementitious materials by weight).

Table 3.2: Mixture designs of high performance mixtures with granite and steel aggregate in kg/m^3 (lb/yd^3)

	NWA 65-35	NWA 35-65	STL 65-35	STL 35-65
Type III Cement	442 (745)	574 (967)	442 (745)	574 (967)
Type I cement				
Silica fume	59 (100)	82 (139)	59 (100)	82 (139)
Class F fly ash	89 (150)	116 (196)	89 (150)	116 (196)
Water	135 (228)	178 (300)	135 (228)	178 (300)
Normal weight fine aggregate	611 (1030)	796 (1342)	611 (1030)	796 (1342)
12.7 mm (0.5 in) maximum size coarse aggregate	normal weight granite 987 (1664)	normal weight granite 494 (832)	A36 steel cubes 2891 (4872)	A36 steel cubes 1441 (2429)
WRDA 35 [3]	2.7 (4.6)	3.6 (61)	2.7 (4.6)	3.6 (61)
Adva Flow [4]	5.9 (9.9)	7.7 (13)	5.9 (9.9)	7.7 (13)
Daravair 1000 [5]	0.3 (0.5)	0.4 (0.6)	0.3 (0.5)	0.4 (0.6)
water/cementitious ratio	0.230	0.230	0.230	0.230
Cement paste content (%)	39	50	39	50
Coarse/fine ratio by volume	1.5	0.58	1.5	0.58
Theoretical density kg/m^3(lb/ft^3)	2400 (149.8)	2254 (140.7)	4372 (272.9)	2254 (140.7)

[1]: High performance matrix

[2]: normal strength normal weight concrete

[3]: Water reducer (0.45% of cementitious materials by weight)

[4]: high range water reducer (1.0% of cementitious materials by weight)

[5]: Air entrainer agent (0.05% of cementitious materials by weight).

Table 3.3: Mixture designs of high performance matrix, cement matrix and normal strength normal weight concrete in kg/m^3 (lb/yd^3)

	HP Matrix[1]	Cement Matrix	NSC[2]
Type III Cement	712 (1200)	1001 (1689)	
Type I cement			319 (537)
Silica fume	96 (162)		
Class F fly ash	144 (242)		
Water	222 (374)	234 (394)	188 (317)
Normal weight fine aggregate	985 (1660)	985 (1660)	845 (1424)
12.7 mm (0.5 in) maximum size coarse aggregate	none	none	normal weight granite 963 (1623)
WRDA 35 [3]	4.4 (7.5)	4.7 (7.9)	
Adva Flow [4]	9.5 (16.0)	10 (16.8)	
Daravair 1000 [5]	0.5 (0.8)	0.5 (0.8)	
water/cementitious ratio	0.230	0.230	0.604
Cement paste content (%)	60.8	60.8	29
Coarse/fine ratio by volume	NA	NA	1.07
Theoretical density kg/m^3(lb/ft^3)	2243 (140.2)	2241 (139.9)	2355 (147.0)

[1]: High performance matrix

[2]: normal strength normal weight concrete

[3]: Water reducer (0.45% of cementitious materials by weight)

[4]: high range water reducer (1.0% of cementitious materials by weight)

[5]: Air entrainer agent (0.05% of cementitious materials by weight)

3.2.3 Small-scale Approach

Standard creep and shrinkage testing in concrete [5] measured overall or "bulk" deformation within a gauge length. Such a measurement averages the deformation occurring on the cement paste, aggregate and transition zone and does not provide information of deformation distribution among those different phases. This knowledge is

necessary in order to achieve a more complete understanding of the mechanisms of creep and shrinkage in HPLC.

This research includes the development, use, and validation of a novel creep and shrinkage testing methodology. This new methodology combines civil engineering testing, microscopy, and image analysis to measure time dependant deformations in the composite material and to differentiate the contributions of the individual components to the overall creep.

The factorial design for the small-scale study (Figure 3.2) considered some of the same mixtures used in the medium-scale, but the MSA was reduced to 9.5 mm (0.375 in) to be used in small-scale specimens designed for microscopy.

Figure 3.2 presents the factorial design for the small-scale study and Table 3.4 presents the mixture designs.

The first mixture was HP Matrix which did not required to be modified since it did not used coarse aggregate. Other four HPC mixtures and one normal strength concrete were considered (see Figure 3.2):

1. LWW 65-35-95: Same as LWW 65-35-95 used in medium-scale study
2. LWD 65-35-95: Same as LWD 65-35 used in medium-scale study, but with 9.5-mm (0.375-in) MSA lightweight aggregate
3. NWA 65-35-95: Same as NWA 65-35 used in medium-scale study, but with 9.5-mm (0.375-in) MSA granite coarse aggregate
4. STL 65-35-95: Same as STL 65-35 used in medium-scale study, but with 9.5-mm (0.375-in) MSA steel cubes
5. NSC-95: Same as NSC used in medium-scale study, but with 9.5-mm (0.375-in) MSA steel cubes

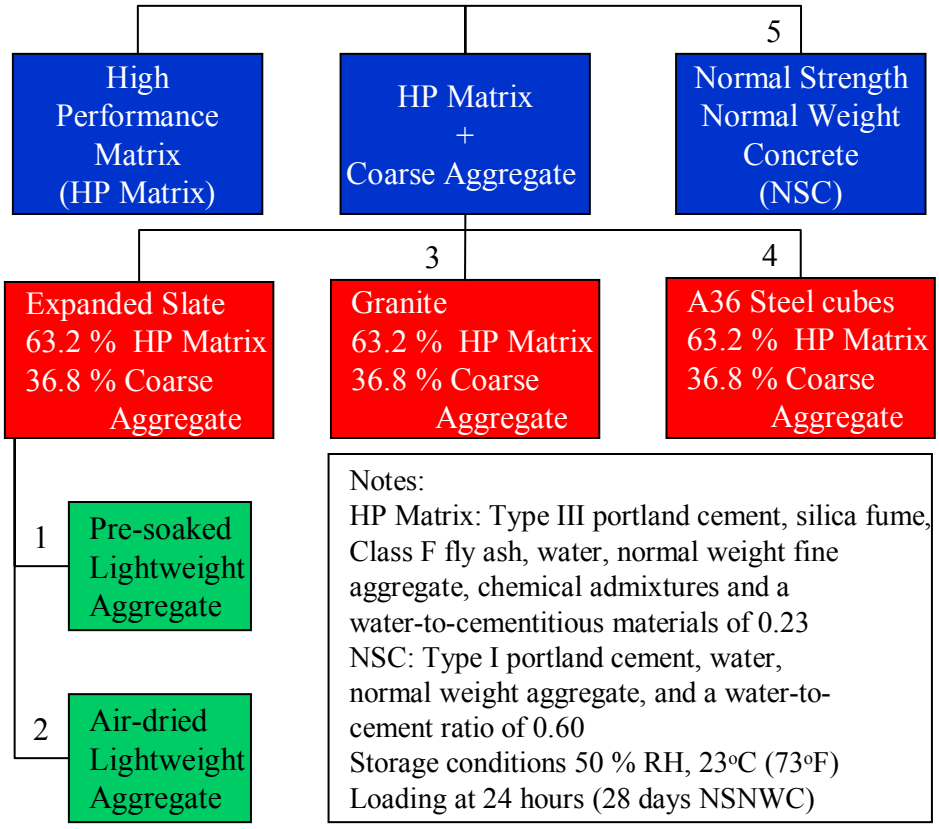

Figure 3.2: Factorial design for small-scale study

As for the medium-scale study, NWA and STL versions of the high performance concrete mixture were expected to provide information about the effect of the type of coarse aggregate in the short and long-term performance of the mixture. The LWD HPC was meant to represent the case of HPLC with no water stored within the lightweight aggregate. Finally, the NSC-95 was intended to provide a reference of conventional concrete.

Table 3.4: Mixture designs for small-scale study in kg/m^3 (lb/yd^3)

	HP Matrix	LWW 65-35-95	LWD 65-35-95	NWA 65-35-95	STL 65-35-95	NSC-95
Type III Cement	712 (1200)	442 (745)	442 (745)	442 (745)	442 (745)	
Type I cement						319 (537)
Silica fume	96 (162)	59 (100)	59 (100)	59 (100)	59 (100)	
Class F fly ash	144 (242)	89 (150)	89 (150)	89 (150)	89 (150)	
Water	222 (374)	135 (228)	173 (291)	135 (228)	135 (228)	188 (317)
Normal weight fine aggregate	985 (1661)	612 (1032)	612 (1032)	611 (1030)	611 (1030)	845 (1424)
9.5 mm (0.375 in) maximum size coarse aggregate		expanded slate pre-soaked 613 (1033)	expanded slate air-dried 576 (971)	normal weight granite 987 (1664)	steel cubes 2891 (4872)	normal weight granite 963 (1623)
WRDA 35 [1]	4.4 (7.5)	2.7 (4.6)	2.7 (4.6)	2.7 (4.6)	2.7 (4.6)	
Adva Flow [2]	9.5 (16.0)	5.9 (9.9)	5.9 (9.9)	5.9 (9.9)	5.9 (9.9)	
Daravair 1000 [3]	0.5 (0.8)	0.3 (0.5)	0.3 (0.5)	0.3 (0.5)	0.3 (0.5)	
water/ cementitious ratio	0.23	0.23	0.23	0.23	0.23	0.60
Cement paste content (%)	60.8	39	39	39	39	29
Coarse/fine ratio by volume		1.5	1.5	1.5	1.5	1.07
Theoretical density kg/m^3(lb/ft^3)	2243 (140.2)	1959 (122.3)	1959 (122.3)	2400 (149.8)	4372 (272.9)	2355 (147)

[1]: Water reducer (0.45% of cementitious materials by weight)

[2]: high range water reducer (1.0% of cementitious materials by weight)

[3]: Air entrainer agent (0.05% of cementitious materials by weight)

3.3 Experimental Program

3.3.1 Large-scale Experimental Program

The large-scale investigation of prestress losses and long-term behavior of high performance lightweight concrete was part of an overall study to develop high performance lightweight concrete mixtures for design strengths of 55.2 and 69 MPa (8000 and 10,000 psi) with densities below 1920 kg/m^3 (120 lb/ft^3). After developing the mixtures, the aim of the research was to study the flexural and shear strength plus the prestressing strand transfer and development lengths of precast prestressed bridge girders constructed with such high performance lightweight concrete. Details of the mixture design development and the tests results for transfer and development length are presented in previous reports [1, 2, 6, 7].

Three AASHTO Type II girders, two 11.9-m (39-ft) long, and one 13.1-m (43-ft) long were cast from each HPLC mixture for a total of 6 girders [6]. Each girder was reinforced with ten 15-mm (0.6-in.) diameter, 1860 MPa (270 ksi), 7-wire, low relaxation strands. Eight of them were located in the bottom flange and two in the top flange as shown in Figure 3.3. The girders were designed to test the shear capacity plus the transfer and development length of the 15-mm (0.6-in) strand and to compare with results of normal weight high performance concrete Type II girders studied previously [8]. The stress level in the concrete at the center of gravity of the strands was about 18% of the initial strength (f_{ci}') which is lower than the typical stress level in actual bridge girders. The strands were stressed to 75 percent of the ultimate strength (1400 MPa, 202.5 ksi). Shear reinforcement was No. 4 (12.7 mm / 0.5 in) Grade 60 bars (yield strength 428 MPa, 62 ksi).

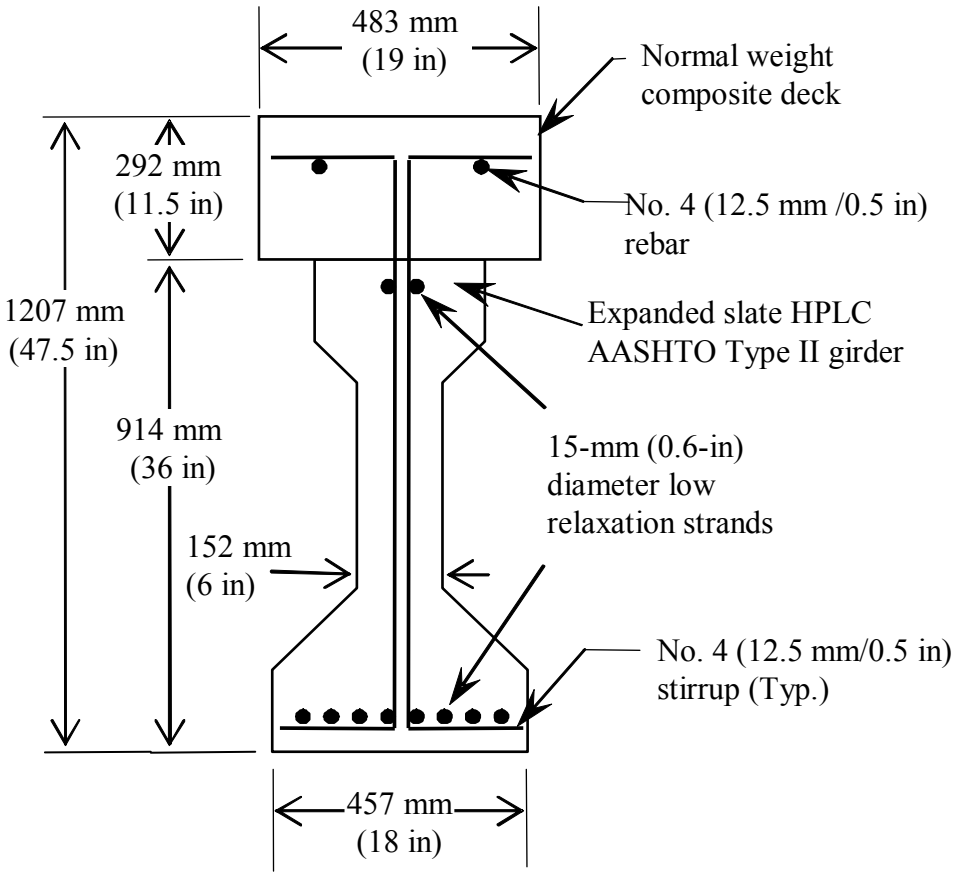

Figure 3.3: AASHTO Type II composite girder cross section.

Five batches of concrete were required for the two 11.9-m (39-ft) long girders while three batches were used to cast each 13.1-m (43-ft) long girders. All girders were cast at the Tindall Corporation precast concrete plant in Jonesboro, Georgia. After the concrete was placed, the girders were screeded, the top surface raked, and covered by insulating tarps until cut-down the next day. A normal weight composite deck was cast atop each girder approximately 2 months after the girders were constructed (see Figure 3.12). The deck was 292-mm (11.5-in) thick and 483-mm (19-in) wide, and the average 56-day compressive strength of the deck was 37.1 MPa (5380 psi). External DEMEC

gauge readers and internal vibrating wire strain gauges (VWSG) were used to measure long-term deformations at the girder midspan.

A complete characterization of HPLC mixtures properties was considered. Specimens for compressive strength, elastic modulus, rupture modulus, and chloride permeability were cast during the girder construction. In addition, creep, shrinkage, and coefficient of thermal expansion (CTE) specimens were also cast. CTE was required to separate thermal and load-related deformations in the girders since the readings from the VWSG contained both kinds of deformations.

The specimens were either standard-cure or accelerated-cured. The standard curing followed the recommendations of ASTM C 192 [9] while the accelerated curing used insulated cure boxes for the first 24 hours in order to maintain the heat generated during the hydration and to match the temperature within the AASHTO Type II girders. This curing system, based on procedure C from ASTM C 684 [10], was found to adequately simulate the condition within a precast prestressed concrete member as measured using thermocouples in both the cylinders and in the precast girders. The insulated cureboxes were preferred over the match-curing for their relative low cost and because it is easy to apply to many specimens of different shapes and dimensions.

3.3.1.1 Compressive Strength

Compressive strength was determined by testing 100 x 200-mm (4 x 8-in) cylinders according to ASTM C 39 [11]. All compressive testing was performed in a SATEC MKIII 800 RD 3,558,580 kN (800 kip) capacity compression testing machine. Hard rubber pads seated in steel end caps were used to provide an adequate distribution of the load according to ASTM C 1231 [12]. Prior to testing the cylinders ends were

ground to provide a smooth surface. A minimum of three specimens were tested from each batch for each measurement. Both standard-cure and accelerated-cured specimens were tested at the age of 24 hours, 7, 28, 56, and 365 days.

3.3.1.2 Elastic Modulus

The chord modulus of elasticity was measured using 150 x 300-mm (6 x 12-in) cylinders loaded in compression according to ASTM C 469 [13]. The tests were run in an SATEC Balwin 400 BTE 1,779,300 kN (400 kip) universal testing machine. Steel caps and rubber pads were used at the ends as suggested in ASTM C 1231 [12]. Figure 3.4 shows the elastic modulus test.

Figure 3.4: Modulus of elasticity test

Three standard-cure specimens and three accelerated-cured specimens from each mixture were tested at the age of 24 hours and 56 days.

3.3.1.3 Rupture Modulus

Rupture modulus was measured on 100 x 100 x 350-mm (4 x 4 x 14-in) beams according to ASTM C 78 [14]. Each measurement considered both three accelerated-cured and three standard-cure specimens tested at 24 hours and 56 days of age.

3.3.1.4 Rapid Chloride Ion Permeability

Chloride ion permeability was measured according ASTM C 1202 [15] on four accelerated-cured specimens for each HPLC mixture at the age of 56 days.

3.3.1.5 Coefficient of Thermal Expansion Test Procedures

Figure 3.5 shows the specimen and measurement procedure. Three accelerated-cured specimens were tested at the age of 56 days for each of the HPLC mixtures.

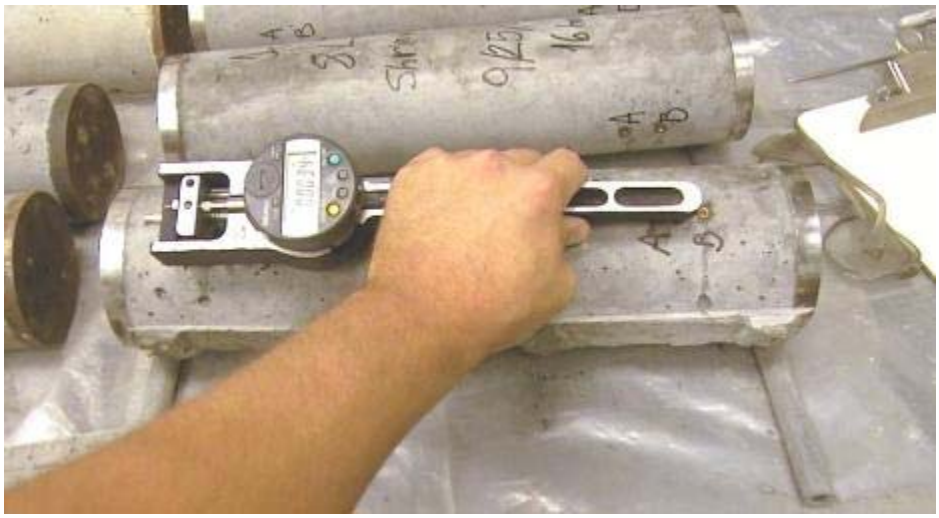

Figure 3.5: DEMEC gauge reading during coefficient of thermal expansion test

The coefficient of thermal expansion was determined by testing 100 x 380 mm (4 x 15 in) cylinders following the guidelines of the Army Corps of Engineers Specification CRD-C39 [16]. Specimens were immersed in water, heated up to 60 ^{o}C (140 ^{o}F) and then cooled down to 4 ^{o}C (40 ^{o}F). The immersion of the specimens maintained a relative

humidity of 100%. The difference between the DEMEC gauge readings in hot and cold conditions was the thermal expansion of concrete for a gradient of 56 ^{o}C (100 ^{o}F).

3.3.1.6 Creep and Shrinkage

Creep was measured on twelve 100 x 380 mm (4 x 15 in) cylinders under sustained load from each HPLC mixture according to ASTM C 512 [5] specifications. Four additional non-loaded companion specimens were used to measure shrinkage. The procedures used are described in Sections 3.3.2.3 and 3.3.2.4 of the medium-scale study. Only accelerated-cured specimens were used for creep and shrinkage testing and they remained unsealed for the duration of the test, so the creep and shrinkage strains included their autogenous and drying shrinkage and their basic and drying creep portions.

Creep and shrinkage were measured in both AASHTO Type II girders and 100 x 380 mm (4 x 15 in) cylinders which allowed for comparisons between them.

3.3.2 Medium-scale Experimental Program

All concrete specimens were taken from mixtures produced according to standard procedures [9]. Mixing and testing of all specimens was done at the Georgia Tech Structural Engineering Laboratory. All specimens were cured and removed from their forms as required. The following tests were performed: (a) compressive strength, (b) modulus of elasticity, (c) creep and shrinkage, and (d) coefficient of thermal expansion.

In order to increase the statistical significance of the experimental results, all mixtures from Tables 3.2 and 3.3 were cast in the laboratory on three occasions called "Stage 1", "Stage 2" and "Stage 3". Two batches of each mixture were cast during each stage, and specimens for mechanical properties, creep, and shrinkage were obtained. All

the specimens were accelerated-cured for 24 hours and then either tested or stored in a fog room until tested.

3.3.2.1 Compressive Strength

The same procedures described in Section 3.3.1.1, used for the large-scale study, were used to measure compressive strength in the medium-scale study. Specimens from Stage 1 were tested at the age of 24 hours, 7, 28, 56, and 365 days while specimens from Stage 2 and Stage 3 were tested only at 24 hours and 28 days.

3.3.2.2 Elastic Modulus

Elastic modulus was measured on two specimens from each mixture at the age of 24 hours and two at 28 days. All the specimens came from batches from Stage 1. The test procedures are described in Section 3.3.1.2.

3.3.2.3 Creep Test Procedures

Creep was determined by testing both 150 x 300 mm (6 x 12 in) and 100 x 380 mm (4-in. x 15 in) cylinders according the ASTM C 512 guidelines[5]. Creep testing started either after 24 hours or 28 days after casting. Figure 3.6 shows a schematic of the creep frames with the working principle and a picture of the creep frames for 150 x 300 mm (6 x 12 in) and 100 x 380 mm (4 x 15 in) specimens.

There were three differences with respect to the ASTM procedure. The first difference was that the diameter of some of the cylinders was smaller than the standard from ASTM because the bearing capacity of some creep frames used was not enough for applying the required stress to 150 x 300 mm (6 x 12 in) cylinders. The other two deviations were the age of loading of some specimens (24 hours instead of 2 days or greater) and the use of an accelerated curing regime as explained earlier. The latter

changes were adopted in order to more closely match the actual conditions of typical precast prestressed bridge girders and specifically, to match companion HPLC pretensioned girders from the large-scale experimental program which were stressed at very early ages.

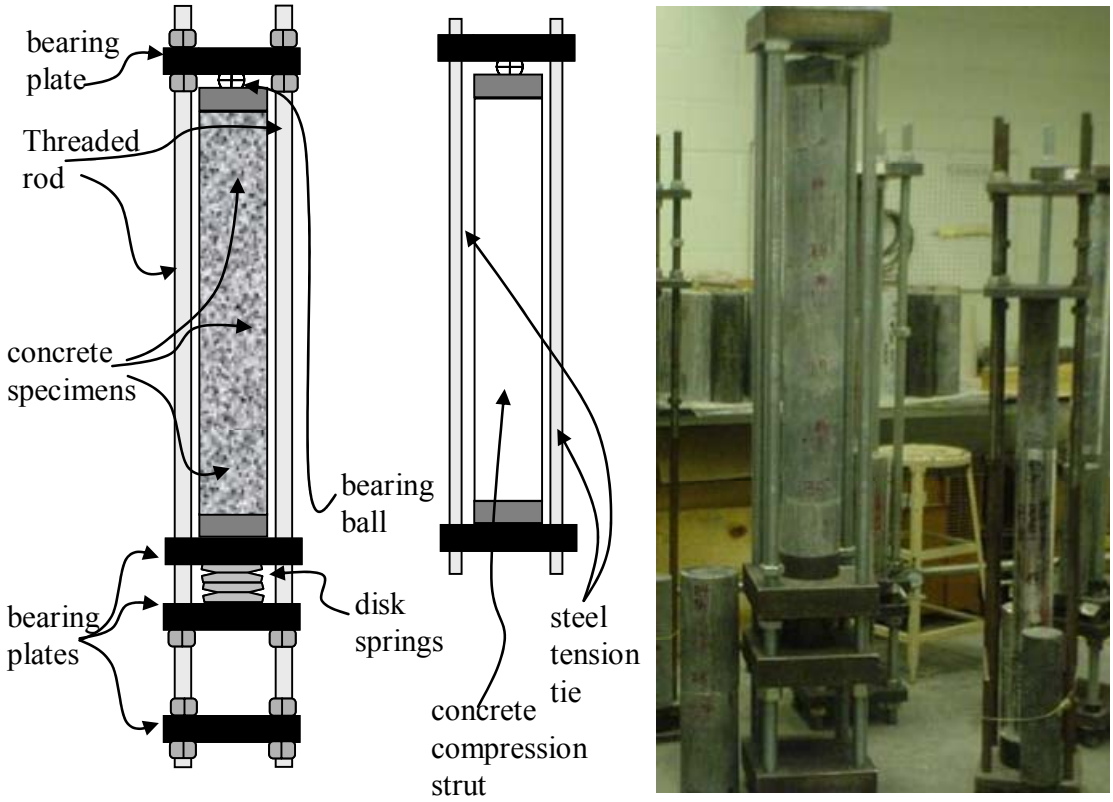

Figure 3.6: Medium-scale creep frames schematic view (left), working principle (center), photograph of the creep frames (right).

After the initial curing, the specimens from the two batches were demolded and either prepared for testing or placed in the fog room for 28-day testing. Among the specimens for 24-hour testing, some were sealed with two layers of aluminum tape to prevent moisture interchange between the specimen and the environment. Later on, sealed and unsealed specimens were placed in the environmentally controlled room at 50

± 3% relative humidity and 23± 2°C (73 ± 3°F) where the creep and shrinkage testing was conducted.

The cylinders were instrumented with four sets of steel inserts located diametrically opposite on the surface of the specimen. Each set was a 254-mm (10-in) long gauge line for measuring deformation with a detachable mechanical gauge (DEMEC gauge) shown in Figure 3.7.

Figure 3.7: DEMEC reader and calibration bar used for medium-scale creep and shrinkage specimens

Steel inserts were bolted to the wall of the cylindrical forms, as shown in Figure 3.8, and after final set of the concrete (4 to 6 hours), the screws holding them were removed allowing specimens to expand freely during curing.

3.3.2.4 Shrinkage Test Procedures

Shrinkage specimens were identical to the creep specimens described in the previous section. They were made following the same procedures as creep specimens, but they remained non-loaded for the time of testing. Figure 3.6 shows some shrinkage specimens placed next to the creep frames.

Figure 3.8: Medium-scale molds for 100 x 380 mm (4 x 15 in) creep specimens (top) and 150 x 300 mm (6 x 12 in) specimens (bottom).

3.3.3 Small-scale Experimental Program

This novel experimental setup consists of reduced size, permanently loaded creep specimen that can be observed and imaged in situ overtime. Image analysis, by digital image correlation (DIC), can be performed in order to analyze deformations in the different phases under sustained loading. The creep testing setup is shown in reality in Figure 3.9-top and schematically in Figures 3.9-bottom. The setup is an unbonded post-tensioned system, where an internal rod is under tension, and the prismatic concrete specimen is under compression. The setup follows the guidelines provided in ASTM C 512 [5], but it uses 38 x 38 x 127 mm (1.5 x 1.5 x 5 in) prismatic specimens instead of 150 x 300 mm (6 x12 in) cylindrical specimens. The prismatic shape is required to provide a flat surface which yields an undistorted image with an adequate depth of field.

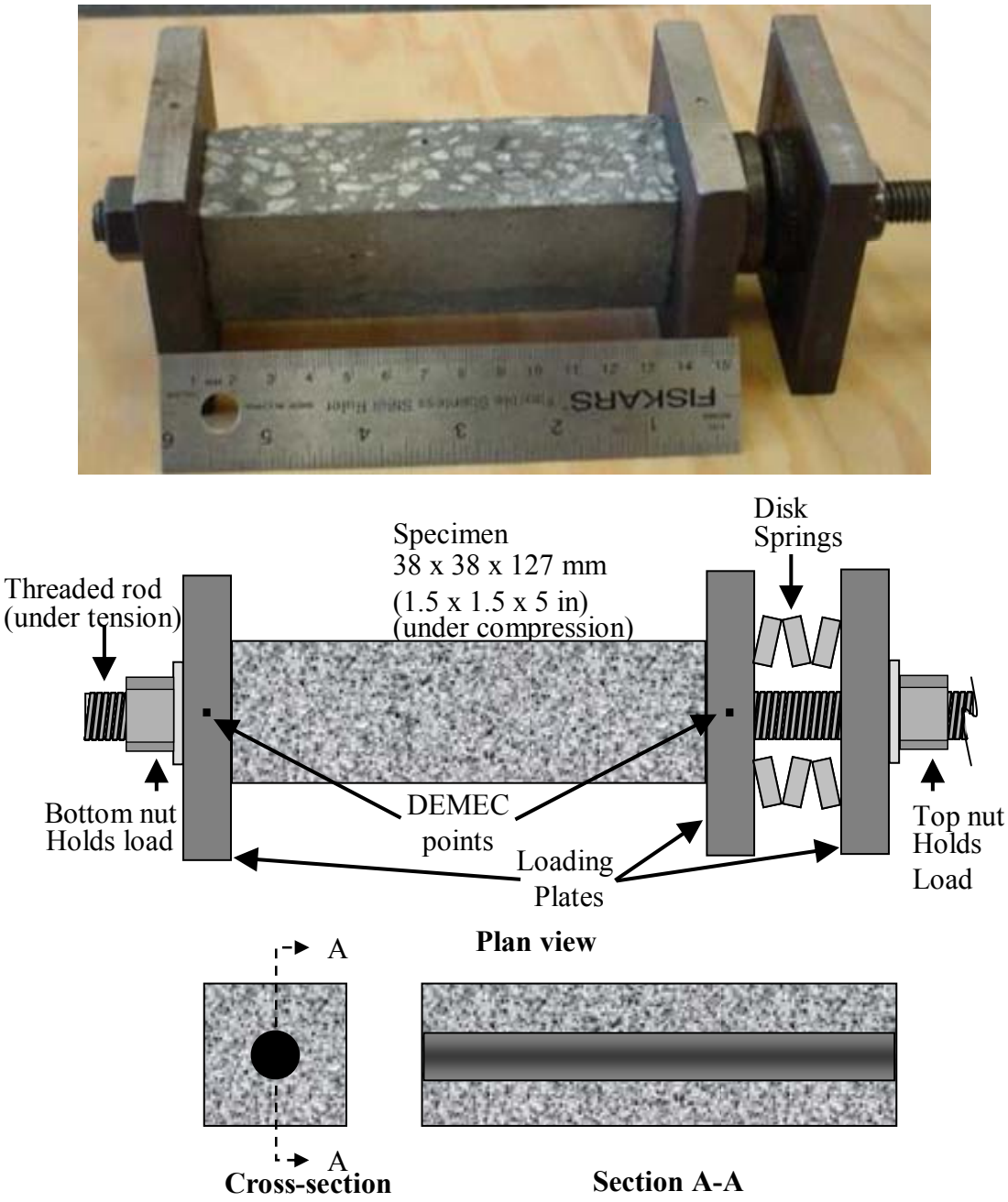

Figure 3.9: Small-scale experimental setup working principle

The specimen has a 12.7-mm (0.5-in) center hole that allows a 12.7-mm (0.5-in) tension rod to go through with no contact or bonding. The test setup requires the use of

companion specimens without any load to measure the environmental stresses (drying shrinkage and thermal strains) as recommended by ASTM C 512.

Figure 3.10 shows the loading system used for the small-scale setup: from left to right are the creep frame and specimen, the loading transfer plate, center hole hydraulic jack, and a full-bridge load cell. The loading transfer plate was used to transmit the load from the jack to the top loading plate of the creep frame. A manual pump was used pressurize the cylinder. The load is read from the load cell strain indicator box (not shown). Once the desired load was reached, the load transfer plate allowed the access for a wrench to tighten the top nut. After it has been tightened, the jack and load cell were removed; the top nut maintains the load in the frame.

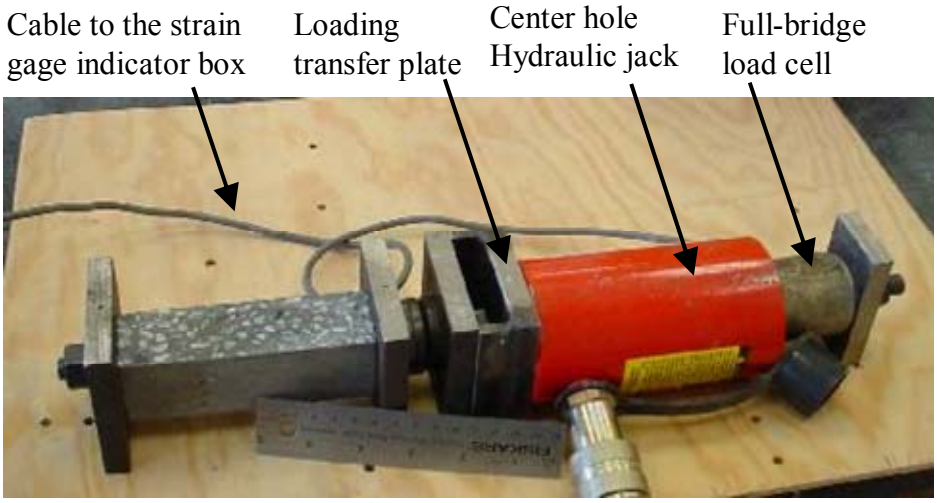

Figure 3.10: Small-scale creep frame setup during loading stage.

The compressive load applied onto top loading plate was transmitted to the loading plate in the middle through the disk springs (see Figure 3.9). That second loading plate applied the load to the specimens which finally transmitted the load to the bottom loading plate and bottom nut. The frame allowed for measurements with a detachable

mechanical (DEMEC) gauge. Once the top nut was tightened, the threaded rod stayed under tension while the rest of the frame and concrete specimen remained under compression. It was a self-equilibrating system where the disk springs maintained the load when the specimen underwent creep and shrinkage. The frames were reloaded periodically, as shown in Figure 3.10, to assure that the specimen stays under constant load.

Figure 3.11 presents pictures of the molds with and without concrete. Those molds, which were coated with an oil-based release agent, formed two specimens simultaneously. After demolding, the two specimens were separated with a concrete saw. The sawn surfaces were then polished using a silicon carbide (SiC) 120, 240, 360, and 600 grits in order to obtain a suitable surface for imaging.

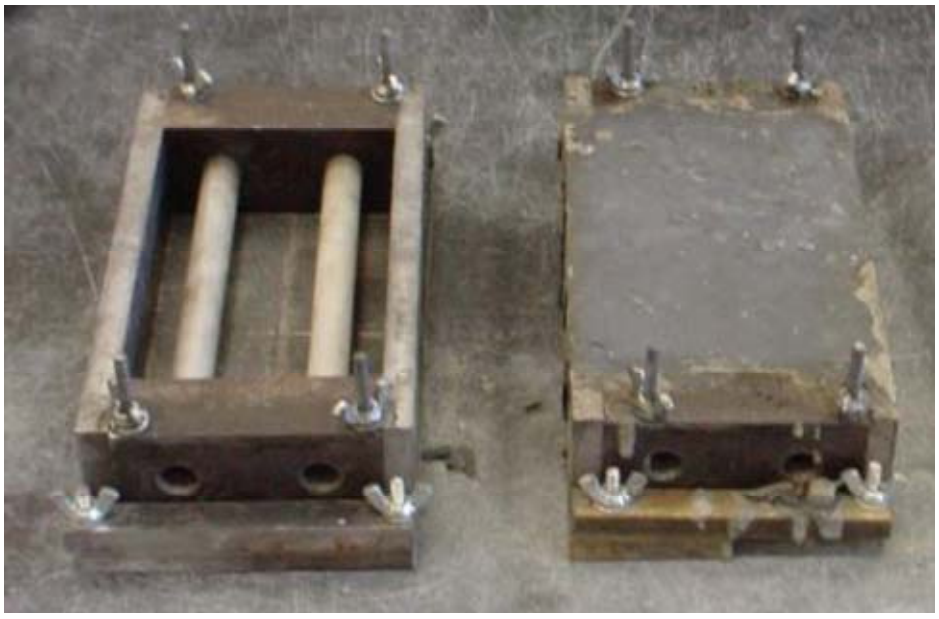

Figure 3.11: Small-scale experimental setup, molds with and without concrete

Figure 3.12 shows, on the left, the small-scale creep frame in the stereomicroscope indexible stage while an image is being acquired. Figure 3.12 also shows the image acquisition system comprised by the stereomicroscope, digital camera, computer, software and monitor (top right). Finally, some samples after cutting and polishing are also shown (bottom right).

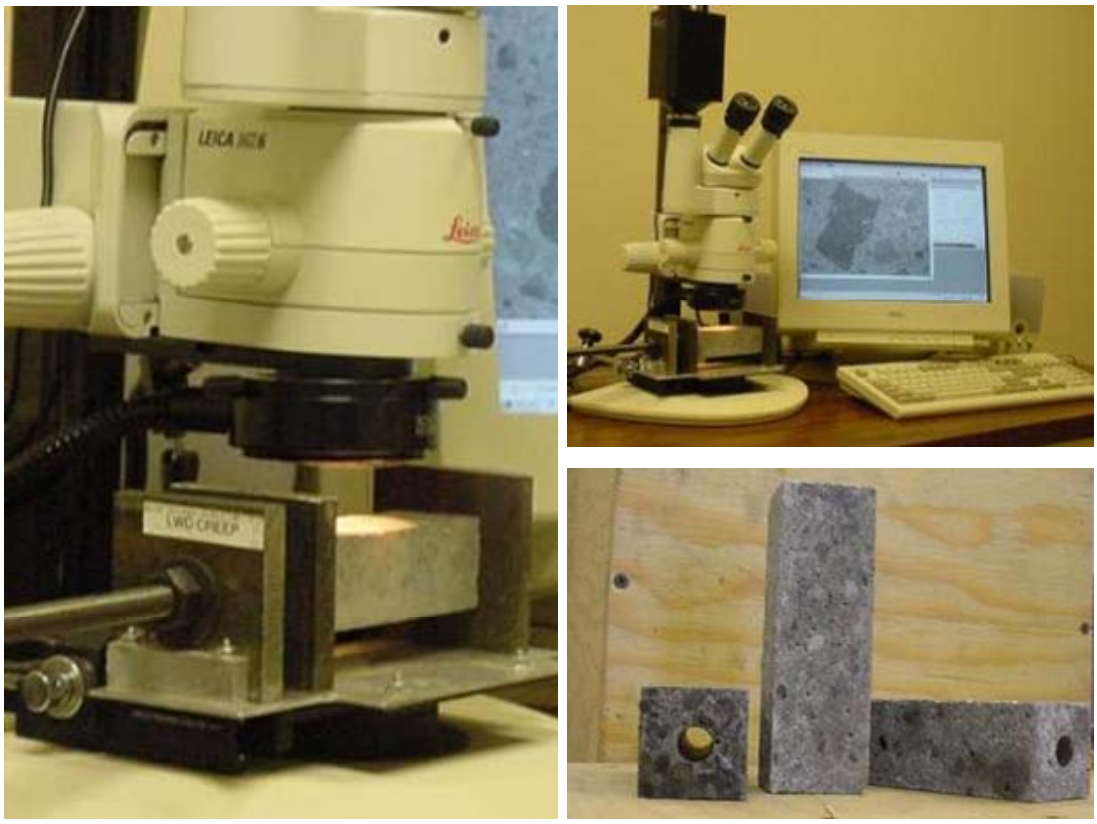

Figure 3.12: Small-scale experimental set up, creep frame and specimens in the stereomicroscope stage (left), image acquisition system (top right), and concrete specimens after cutting and polishing (bottom right).

Images and DEMEC reading were taken with five minutes before and after loading. More DEMEC readings and images were taken after one, seven, 28, and 120 days under loading and drying. The companion specimens were installed in a similar frame without any load, and DEMEC reading and images were obtained in the same

fashion as that of the creep specimens. Figure 3.7 presents a picture of the DEMEC reader and the calibration bar used in this study.

Data acquired from the loaded specimens included elastic, creep and shrinkage deformations. The elastic portion was captured between the measurements before and immediately after loading. In order to separate the creep and shrinkage portions, the data from the loaded and non-loaded specimens was needed. The non-loaded specimens underwent only shrinkage while the loaded ones underwent both creep and shrinkage. Creep and shrinkage portions obtained with DEMEC gauge were separated by subtracting shrinkage (obtained in the non-loaded specimens) from the creep plus shrinkage (obtained in the loaded specimens).

Autogenous shrinkage was also measured in all concrete mixtures with the exception of the normal strength normal weight concrete. The procedure was performed as recommended by Jensen and Hansen [17]. Figure 3.13 shows the length comparator and one of the specimens used in this investigation.

Figure 3.13 length comparator and calibration bar used in autogenous shrinkage

Concrete, taken from the same batch used for casting the prismatic creep and shrinkage specimens, was placed in three corrugated plastic tubular molds. Those molds

were designed to not impose any restraints to shortening caused by self-desiccation. Setting time was monitored in a concrete sample following the guidelines of ASTM C 191 [18]. After final set was reached, an initial length measurement was taken for each specimen. Length measurements after one, four, 12 and 24 hours, 2, 4, 7, 14, 28, 56, 112, and 120 days followed the initial reading.

Compressive strength was measured on three 50-mm (2-in) cubes according to ASTM C 109 [19] and two 38 x 38 x 127 mm (1.5 x 1.5 x 5 in) prismatic specimens. The cubes allowed for comparison with results from previous research, and the prisms provided the strength of the non-standard creep specimens. Both creep and shrinkage specimens were placed in the small-scale frames, but only the creep specimen was loaded to 40% of the ultimate load as measured on the prisms tested in compression.

Small-scale creep and shrinkage prismatic specimens along with compressive cube specimens underwent an accelerated curing using insulated cureboxes for the first 24 hours as explained for the large-scale and medium-scale studies.

3.3.4 Aggregate Experimental Program

Three types of coarse aggregate and one fine aggregate were used in this investigation. The coarse aggregates were: expanded slate lightweight aggregate, gneissic granite, A36 carbon steel 248 MPa (36,000 psi) yield strength. The fine aggregate was siliceous normal weight natural sand. The coarse steel aggregate for the small-scale study was obtained from 6.35-mm (0.25-in) square steel bars cut every 6.35 mm (0.25 in), and the coarse aggregate for the medium-scale study came from 12.7-mm (0.5-in) square steel bars cut every 12.7 mm (0.5 in).

The physical and mechanical characterization of the aggregate considered:

- Relative density and absorption of fine aggregate according to ASTM C 128 [20]
- Relative density and absorption of coarse aggregate according to ASTM C 127 [21]
- Sieve analysis of coarse and fine aggregate according to ASTM C 136 [22]
- Modulus of elasticity of steel bars in tension
- Tensile yielding strength of steel bars
- Modulus of elasticity of expanded slate prisms in compression
- Compressive strength of expanded slate prisms
- Relative density and absorption of expanded slate prisms according to ASTM C 127 [21]

The slate was expanded in a rotary kiln process which gives large pieces of expanded slate particles called clinker. Most of clinker particles have a maximum length of 100 mm (4 in). After the kiln expansion and subsequent cooling, the clinker was crushed to produce three coarse aggregate fractions: 19 to 5 mm, 12.7 to 5 mm, and 9.5 to 5 mm (0.75 to 0.2 in, 0.5 to 0.2 in, 0.375 to 0.2 in) and a lightweight fine aggregate in the range 5 to 0.15 mm (0.2 to 0.006 in. For testing mechanical properties of expanded slate, prisms having dimensions between 0.5 and 1 in were cut from expanded slate clinker.

3.4 References

1. Meyer, K.F. and L.F. Kahn. "Transfer and Development Length of 0.6-inch. Strand in High Strength Lightweight Concrete". in *High Performance Structural Lightweight Concrete. SP-218*. Phoenix, AZ: American Concrete Institute, 2002.p. 9-28.
2. Meyer, K.F., B.S. Buchberg, and L.F. Kahn. "Development of High Strength Lightweight Concrete Mix Designs: A Practical Approach". in *49th Annual PCI Convention & Exhibition, the 3rd PCI/FHWA International Symposium on High Performance Concrete, and the National Bridge Conference.* Orlando, Florida: Precast / Prestressed Concrete Institute, 2003.
3. Lopez, M., L.F. Kahn, and K.E. Kurtis, "Creep and shrinkage of high-performance lightweight concrete". *ACI Materials Journal*, 101(5): 2004. p. 391-399.
4. Troxell, G.E., J.M. Raphael, and R.E. Davis. "Long-term Creep and Shrinkage Tests of Plain and Reinforced Concrete". in *Cement and Concrete*. Los Angeles: ASTM Proceedings, 1958.p. 1101-1120.

5. ASTM C 512, *Standard Test Method for Creep of Concrete in Compression*. West Conshohocken, PA: American Society for Testing and Materials, 1992.
6. Meyer, K.F., *Transfer and development length of 0.6-inch diameter prestressing strand in high strength lightweight concrete*. 2002.
7. Buchberg, B.S., *Investigation of mix design and properties of high-strength/high-performance lightweight concrete*. 2002.
8. Kahn, L.F., J.C. Dill, and C.G. Reutlinger, "Transfer and development length of 15-mm strand in high performance concrete girders". *Journal of Structural Engineering-Asce*, 128(7): 2002. p. 913-921.
9. ASTM C 192, *Standard Practice for Making and Curing Concrete Test Specimens in the Laboratory*. West Conshohocken, PA: American Society for Testing and Materials, 2002.
10. ASTM C 684, *Standard Test Method for Making, Accelerated Curing, and Testing Concrete Compression Test Specimens*. West Conshohocken, PA: American Society for Testing and Materials, 1999.
11. ASTM C 39, *Standard Test Method for Compressive Strength of Cylindrical Concrete Specimens*. West Conshohocken, PA: American Society for Testing and Materials, 2004.
12. ASTM C 1231, *Standard Practice for Use of Unbonded Caps in Determination of Compressive Strength of Hardened Concrete Cylinders*. West Conshohocken, PA: American Society for Testing and Materials, 2000.
13. ASTM C 469, *Standard Test Method for Static Modulus of Elasticity and Poisson's Ratio of Concrete in Compression*. West Conshohocken, PA: American Society for Testing and Materials, 2002.
14. ASTM C 78, *Standard Test Method for Flexural Strength of Concrete (Using Simple Beam with Third-Point Loading)*. West Conshohocken, PA: American Society for Testing and Materials, 2002.
15. ASTM C 1202, *Standard Test Method for Electrical Indication of Concrete's Ability to Resist Chloride Ion Penetration*. West Conshohocken, PA: American Society for Testing and Materials, 1997.
16. CRD C 39, *Test Method for Coefficient of Linear Thermal Expansion of Concrete*: U.S. Army Corps of Engineers, Handbook of Concrete and Cement, 1981.
17. Jensen, O.M. and P.F. Hansen, "A Dilatometer for Measuring Autogenous Deformation in Hardening Portland-Cement Paste". *Materials and Structures*, 28(181): 1995. p. 406-409.
18. ASTM C 191, *Standard Test Method for Time of Setting of Hydraulic Cement by Vicat Needle*. West Conshohocken, PA: American Society for Testing and Materials, 2004.
19. ASTM C 109, *Standard Test Method for Compressive Strength of Hydraulic Cement Mortars (Using 2-in or [50-mm] Cube Specimens)*. West Conshohocken, PA: American Society for Testing and Materials, 2002.
20. ASTM C 128, *Standard Test Method for Density, Relative Density (Specific Gravity), and Absorption of Fine Aggregate*. West Conshohocken, PA: American Society for Testing and Materials, 2004.

21. ASTM C 127, *Standard Test Method for Density, Relative Density (Specific Gravity), and Absorption of Coarse Aggregate*. West Conshohocken, PA: American Society for Testing and Materials, 2004.
22. ASTM C 136, *Standard Test Method for Sieve Analysis of Fine and Coarse Aggregate*. West Conshohocken, PA: American Society for Testing and Materials, 2005.

This page intentionally left blank

CHAPTER 4

LARGE-SCALE STUDY

4.1 Introduction

The aim of the large-scale study was the implementation of high performance lightweight concrete (HPLC) in the field for construction and the testing of full-scale prestressed girders. Two HPLC mixtures were considered. These are LWW 69/10, which had a 56-day design compressive strength of 69 MPa (10,000 psi) and corresponds to LWW 65-35 mixture from the medium-scale study, and LWW 55/8 with a 56-day design compressive strength of 55.2 MPa (8000 psi). Both had approximately the same volume of natural siliceous sand and pre-soaked expanded slate coarse aggregate, but the water-to-cementitious material ratio and proportion of cementitious materials varied.

4.2 Research Significance

HPLC with compressive strength in the range 55.2 to 69 MPa (8000 to 10,000 psi) is a novel material. There have been multiple research efforts in developing HPLC with locally available materials, but there have not been previous university research on field production and performance of full-scale bridge girders. This research assesses the applicability of the current design methods to girder design using HPLC.

4.3 Experimental Results

4.3.1 Mixture Design

The mixture designs were obtained from a parametric study that optimized the mixture proportions to obtain the specified compressive strengths with a density under 1920 kg/m^3 (120 lb/yd^3) [1-3]. Table 4.1 presents the mixtures design for the two HPLC mixtures used in the large-scale study. Appendix A presents the properties of the cementitious materials and aggregates used in the mixture designs.

Table 4.1: Mixture design of the HPLC in kg/m^3 (lb/yd^3)

Materials / Characteristics	LWW 55/8	LWW 69/10
Type III Cement	465 (783)	442 (745)
Silica fume	11 (19)	59 (100)
Class F fly ash	84 (142)	89 (150)
Water	159 (268)	135 (228)
Natural siliceous sand	606 (1022)	611 (1030)
12.7 mm (0.5 in) maximum size aggregate	562 (947)	571 (963)
WRDA 35 (water reducer)	2.1 (3.5)	2.7 (4.6)
Adva Flow (high range water reducer)	1.8 (3.0)	5.9 (9.9)
Daravair 1000 (air entraining agent)	0.3 (0.5)	0.3 (0.5)
water/cementitious ratio	0.28	0.23
cement paste content (% by volume)	39	39
coarse/fine ratio by volume	1.5	1.5
theoretical air content (% by volume)	3.5	3.5
theoretical density kg/m^3(lb/ft^3)	1903 (118.8)	1918 (119.7)

The main difference between the HPLC mixtures was in the cementitious materials contents and water dosages. LWW 55/8 had 30 kg/m^3 (50 lb/yd^3) less of total cementitious materials and 24 kg/m^3 (40 lb/yd^3) more of water than LWW 69/10. Consequently, the water-to-cementitious material ratio was increased from 0.23 to 0.28.

Among cementitious materials, LWW 55/8 had 48 kg/m^3 (81 lb/yd^3) less of silica fume that was in part compensated by 23 kg/m^3 (39 lb/yd^3) more of Type III portland cement.

4.3.2 Test Results

4.3.2.1 Fresh properties

Slump [4], density [5], and air content [6] were measured in all field batches. From the workability results, LWW 55/8 slump might be classified as 165 ± 38 mm (6.5 ± 1.5 in) and LWW 69/10 as 100 ± 13 mm (4.0 ± 0.5 in). The air content, on the other hand, averaged 4.5% for LWW 55/8 and 3.3% for LWW 69/10. The temperature of concrete during placing was 29.5 ^{o}C (85 ^{o}F).

Plastic density of HPLC varied from 1825 to 1955 kg/m^3 (114 to 122 lb/ft^3) with most of the values slightly lower than 1920 kg/m^3 (120 lb/ft^3). LWW 55/8 averaged a density of 1875 kg/m^3 (117 lb/ft^3) while LWW 69/10 an average density of 1905 kg/m^3 (119 lb/ft^3). These values represent 78 and 79% of the weight of an HPC of 2400 kg/m^3 (150 lb/ft^3)

ACI-213 [7] proposed the "air-dry" condition as a standard for measuring hardened lightweight concrete density. Figure 4.1 presents measured plastic, air-dry and oven-dry density for each HPLC mixture and of one normal weight HPC of standard density of 2400 kg/m^3 (150 lb/ft^3). Tables with the results are shown in Appendix B. The oven-dry condition was obtained by drying 100 x 200 mm (4 x 8 in) cylinders at 105 ^{o}C (221 ^{o}F) until constant mass as measured with a 0.1 g (0.0002 lb) precision balance. The change in density between plastic and dry conditions was small. Equilibrium air-dry density was 0.3% lower than plastic density regardless the mixture. Likewise, oven-dry density was about 1% lower than plastic density.

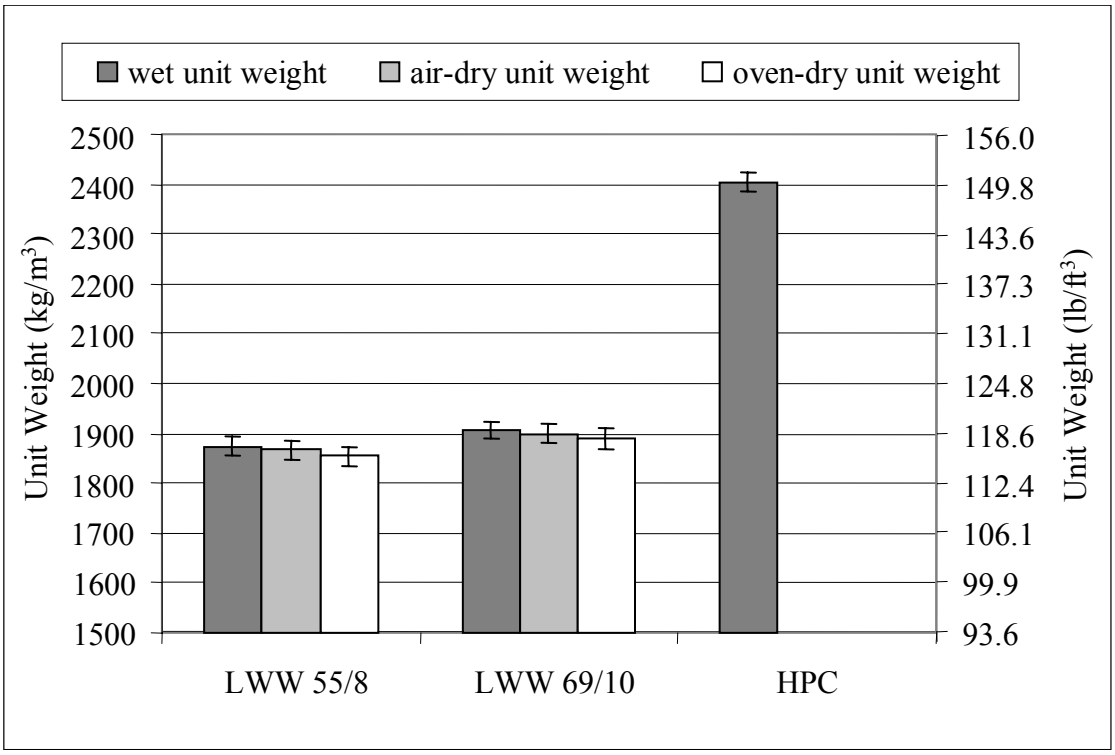

Figure 4.1: Density of HPLC under different moisture conditions

The small variation in weight with air-dry or oven-dry condition was expected because these two low water-to-cementitious material ratio mixtures are expected to exhibit very low water permeability which makes the water migration difficult [8], even thought the pre-soaked aggregate might have contained additional 40 kg/m^3 (67.5 lb/ft^3) of absorbed water.

4.3.2.2 Mechanical Properties

The following properties were tested on each HPLC mixture. Compressive strength was determined on 100 x 200 mm (4 x 8 in) cylinders according to ASTM C 39 [9]. A minimum of four specimens were tested for each data point at 24 hours, 7, 28, 56 and more than 365 days after casting. Elastic modulus was determined on 150 x 300 mm (6 x 12 in) cylinders according to ASTM C 469 [10] using four cylinders for each age at

24 hours and 56 days after casting. Modulus of rupture was also tested on 100 x 100 x 355 mm (4 x 4 x 14 in) prisms following ASTM C 78 guidelines [11].

Specimens used for testing mechanical properties were cured in two different ways: standard curing in a fog room and 22.8 ^{o}C (73^{o}F) according to ASTM C 192 [12] and accelerated curing that simulated the condition within a precast prestressed member [13]. The average compressive strength and individual results obtained for LWW 55/8 and LWW 69/10 are shown in Figure 4.2. Detailed results are presented in Section B.2 of Appendix B. The X-axis presents the age at testing in logarithmic scale, and the Y-axis gives the compressive strength in MPa (psi). Figure 4.2a shows the results for the accelerated-cured specimens, and Figure 4.2b shows the compressive strength measured on the standard-cured specimens.

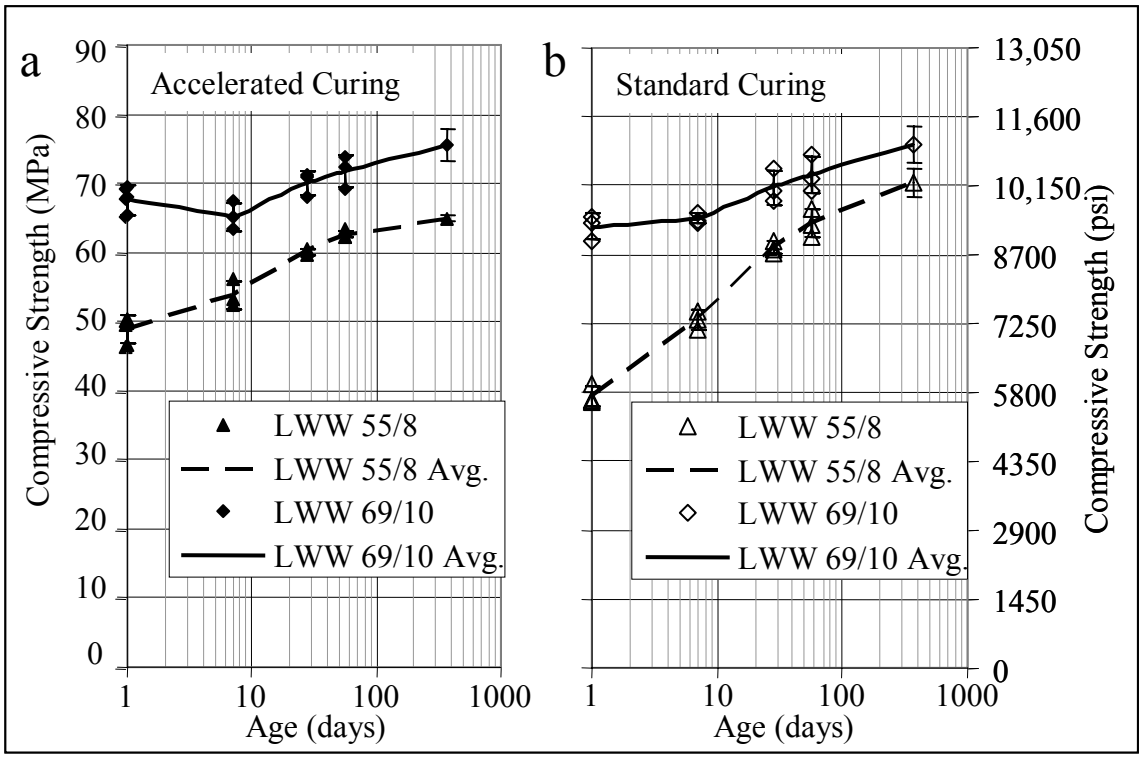

Figure 4.2: Compressive strength vs. time of LWW 55/8 and LWW 69/10 mixtures for: (a) accelerated and (b) standard curing methods

From the accelerated-cured data, LWW 55/8 satisfied the specified strength after the age of 28 days. At 56 days, it reached 62.1 MPa (9000 psi) , and after one year the compressive strength was 65 MPa (9420 psi). At early ages, accelerated-cured specimens had a compressive strength 23.7% than the standard-cured specimens. However, that difference was only 6.7% after 7 days and -1.4% at 28 days. That is, after 28 days the two regimens presented approximately the same strength. Standard cured specimens kept a higher strength gain than the accelerated-cured ones, and after one year, standard-cured specimens from LWW 55/8 had 70.5 MPa (10,230 psi) which was 8% higher than accelerated-cured ones.

LWW 69/10 accelerated-cured specimens had an average 24-hour compressive strength of 67.6 MPa (9810 psi) very close to the 56-day specified strength. After 56 days, those specimens had a compressive strength of 71.8 MPa (10,420 psi), and after one year the strength of LWW 69/10 was 75.9 MPa (11,000 psi). The differences between accelerated-cured and standard-cure specimens were less than that obtained for the LWW 55/8 mixture. At the age of 1 day, accelerated-cured specimens had a compressive strength 5.5% higher than that of standard-cure specimens, but at the age of 7, 28, 56 days, and one year, the differences was less than 1%.

It was expected that the elastic modulus (E_c) of the HPLC would be lower than HPC with the same mixture design, but made with normal weight coarse aggregate, because the lightweight aggregate has lower stiffness [14]. ACI-363 [15], proposed equation 4.1 for estimating the elastic modulus of high strength concrete based on its compressive strength and density. Equation 4.1a and 4.1b presents the same expression in international and customary units, respectively.

$$E_c = \left(3.32 \cdot \sqrt{f_c'} + 6.9\right) \cdot \left(\frac{w_c}{2325}\right)^{1.5} \quad (4.1a)$$

$$E_c = \left(40 \cdot \sqrt{f_c'} + 1000\right) \cdot \left(\frac{w_c}{145}\right)^{1.5} \quad (4.1b)$$

where:

E_c: elastic modulus in GPa (ksi)

f_c': compressive strength in MPa (psi)

w_c: concrete density in kg/m^3 (lb/ft^3)

Figure 4.3 presents the average 56-day elastic modulus for each of the mixtures grouped by the type of curing used versus the 56-day compressive strength. Detailed experimental results are reported in Appendix B, Section B.2.

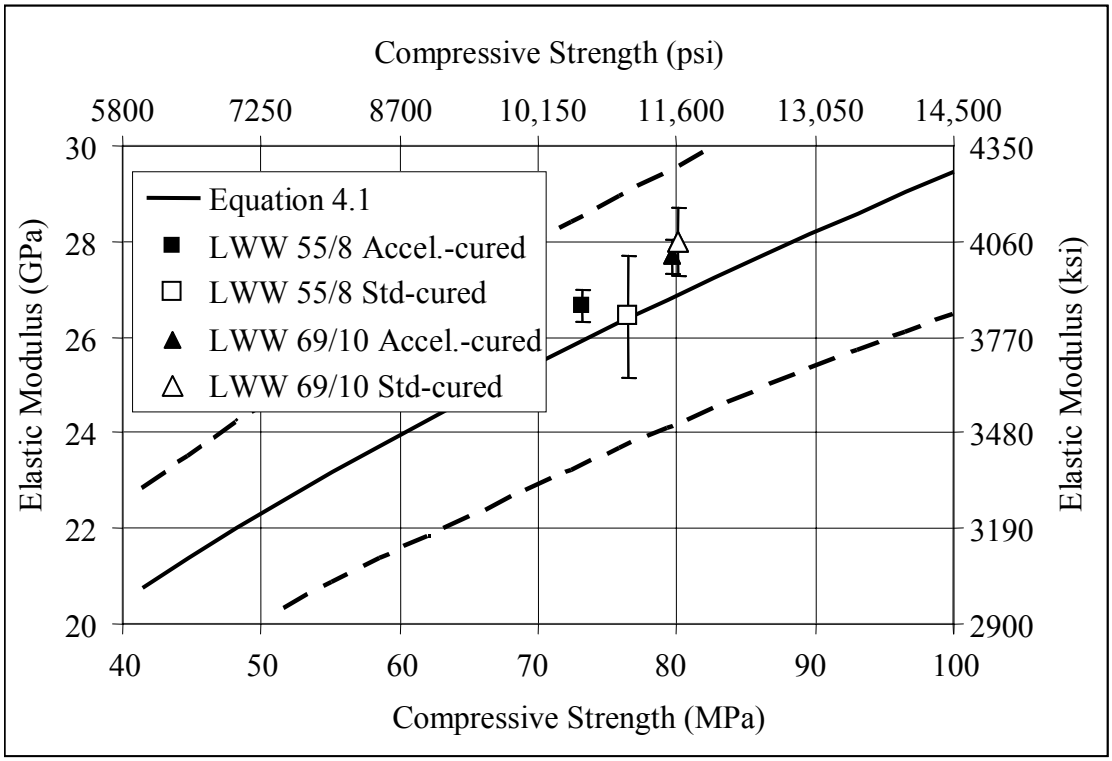

Figure 4.3: 56-day elastic modulus of LWW 55/8 and LWW 69/10 mixtures versus compressive strength

Figure 4.3 also present the elastic modulus estimated using equation 4.1 as a solid line and the ±10% variation around the estimate in dashed lines [15].

LWW 55/8 had a 56-day elastic modulus between 24.8 and 28.3 GPa (3590 and 4100 ksi) which was higher than the range of 27.0 and 28.5 GPa (9320 and 4130 ksi) obtained fro LWW 69/10.

At the age of 56 days, the differences in the elastic modulus between the two curing methods were small and ranged from 1 to 2%. This indicates that, as seen with compressive strength, the temperature history during the first 24 hours does not have an important effect on the 56-day elastic modulus.

When analyzing the estimates using Equation 4.1 (solid line in Figure 4.3), it can be seen that it slightly underestimated some of the values by approximately 5%. This might be due to the use of a comparatively high strength lightweight aggregate while Equation 4 was developed to estimate elastic modulus of high strength concrete made with various kinds of aggregate.

Average 56-day Poisson's ratio was 0.190 with 90% of the results in the range 0.188 and 0.192. These values were within the range reported previously for normal weight HPC [16].

Rupture modulus (f_r) was measured at the age of 56 days on 100 x 100 x 350-mm (4 x 4 x 14-in) beams under 4-point bending [11]. The accelerated-cured specimens presented 5-10% higher 56-day rupture modulus than standard-cured specimens. There were no significant differences between the rupture modulus of the LWW 55/8 and LWW 69/10 mixtures. ACI-318 [17] proposed equation 4.2 to estimate rupture modulus

of concrete in function of its compressive strength. Equation 4.a and 4.2b presents the same expression in international and customary units, respectively.

$$f_r = \lambda \cdot 0.623 \cdot \sqrt{f_c'} \quad (4.2a)$$

$$f_r = \lambda \cdot 7.5 \cdot \sqrt{f_c'} \quad (4.2b)$$

where:

f_r: rupture modulus in MPa (psi)

f_c': compressive strength in MPa (psi)

λ; reduction factor: 0.85 for sand-lightweight concrete (concrete with lightweight coarse aggregate and normal weight fine aggregate); 1.0 for normal weight concrete

Figure 4.4 shows rupture modulus (Y-axis) versus compressive strength (X-axis) grouped by type of mixture and curing.

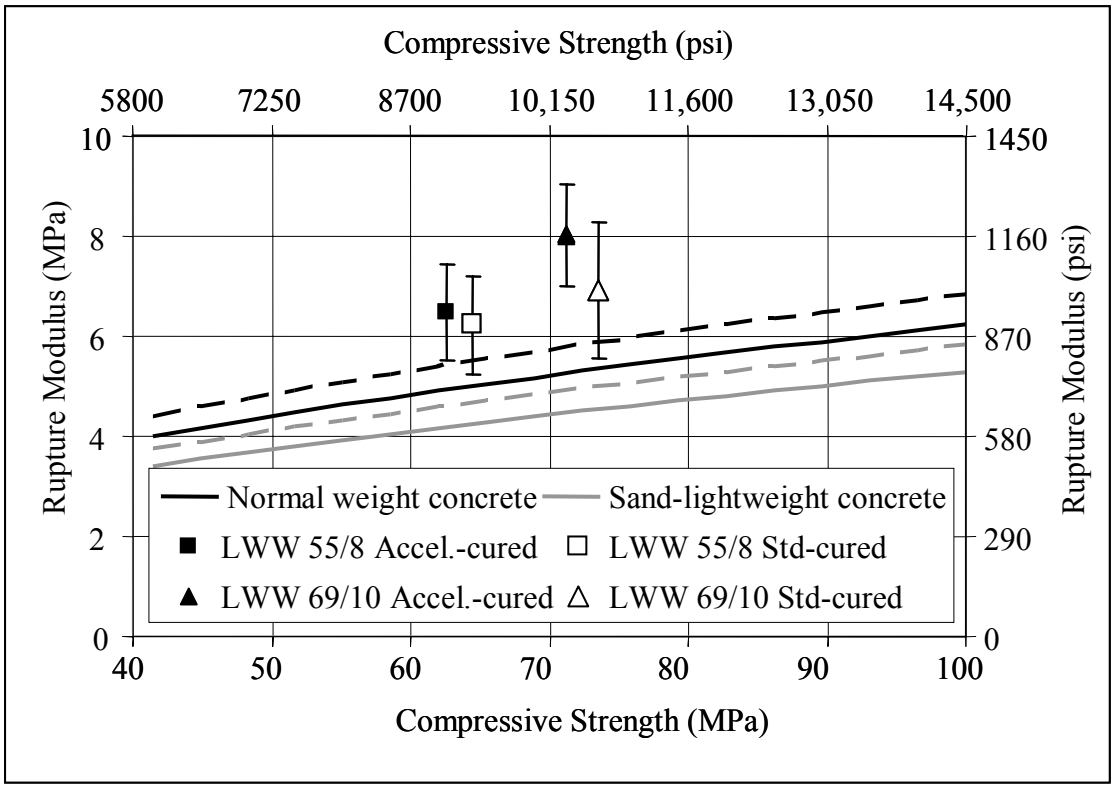

Figure 4.4: Rupture modulus of HPLC mixtures versus compressive strength

In Figure 4.4 the values predicted with equation 4.2 are also shown. The solid black line are for λ=1.0 (normal weight concrete) and the solid gray line for λ=0.85 (sand-lightweight concrete). The black and gray dashed lines represent a 10% overestimate for normal weight and sand-lightweight concrete, respectively.

Experimental values were on average 45% higher than predicted with Equation 4.2 and λ=0.85, and 25% higher than the values estimated with equation 4.2 and λ=1.0. It was concluded that equation 4.2 with λ=1.0 is conservative for predicting modulus of rupture of HPLC.

4.3.2.3 Chloride Permeability

Rapid chloride ion permeability was tested at the age of 56 days on 100 x 50 mm (4 x 2 in) cylinders according to ASTM 1202 [18]. Four accelerated-cured specimens were tested from each HPLC. The results are presented in Figure 4.5 and in Appendix B.

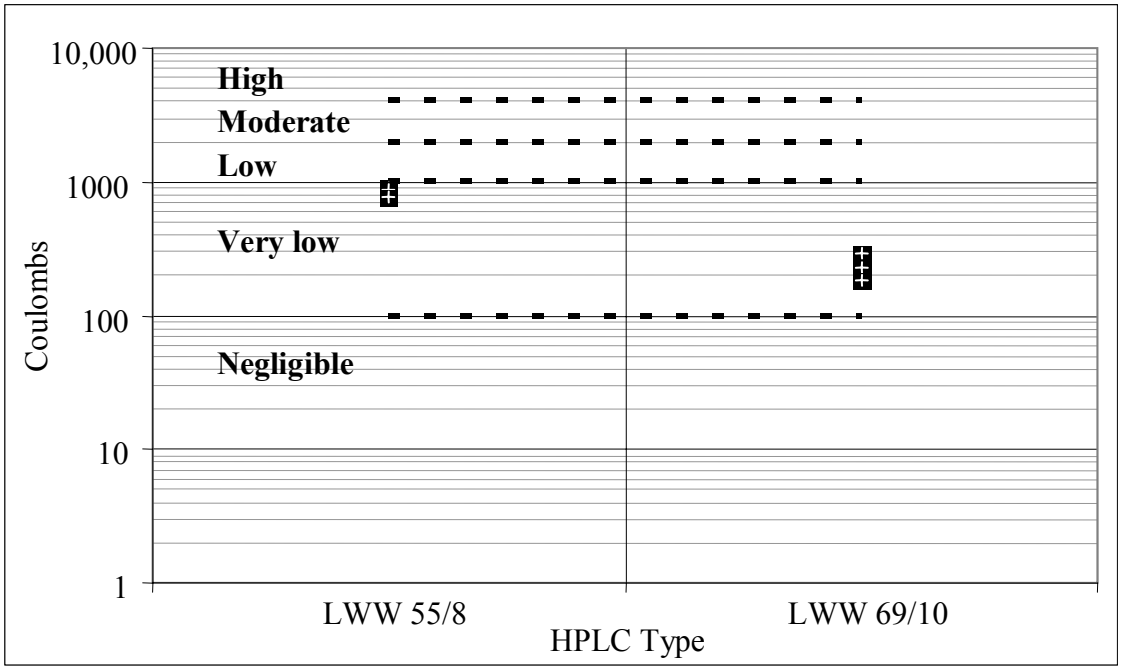

Figure 4.5: Chloride ion permeability of LWW 55/8 and LWW 69/10 mixtures

All HPLC mixtures had chloride ion permeability below 1000 coulombs, classified as "very low" by ASTM C 1202. The LWW 55/8 results were in the range 615 - 900 coulombs while the LWW 69/10 presented results within the range of 180 - 350 coulombs. These values are within in the range obtained previously for HPLCs of similar strengths [19, 20] and similar to those reported for normal weight HPC [16].

4.3.2.4 Coefficient of Thermal Expansion

Coefficient of thermal expansion (CTE) was measured at the age of 56 days using accelerated-cured specimens tested at 100% of relative humidity [21]. LWW 55/8 and LWW 69/10 CTE were close to one another with all values in the range between 9.25 and 9.58 με/^{o}C (5.14 and 5.32 με/^{o}F). All HPLC CTE results were lower than the 11 με/^{o}C (6.0 με/^{o}F) commonly used for concrete [22].

4.3.3 Girder Construction

Three AASHTO Type II girders, two 11.9-m (39-ft) long, and one 13.1-m (43-ft) long were cast from each HPLC mixture for a total of 6 girders [23]. Five batches of concrete were required for two 39-ft (11.9-m) long girders while three batches were used to cast the 43-ft (13.1-m) long girders.

4.3.3.1 Girder Design

Figure 4.6 shows the cross section of the AASHTO Type II girders and the NSC deck. Each girder was reinforced with ten 15-mm (0.6-in) diameter, 1860 MPa (270 ksi), 7-wire, low relaxation strands. Eight were located in the bottom flange and two in the top flange. The stress level in the concrete at the center of gravity of the strands was about 18% of the initial strength (f_{ci}') which is lower than the typical stress level in actual bridge girders. The strands were stressed to 75% of the ultimate strength (1400 MPa,

202.5 ksi). After the concrete was placed, the girders were screeded, the top surface raked and covered by tarps until cut-down the next day.

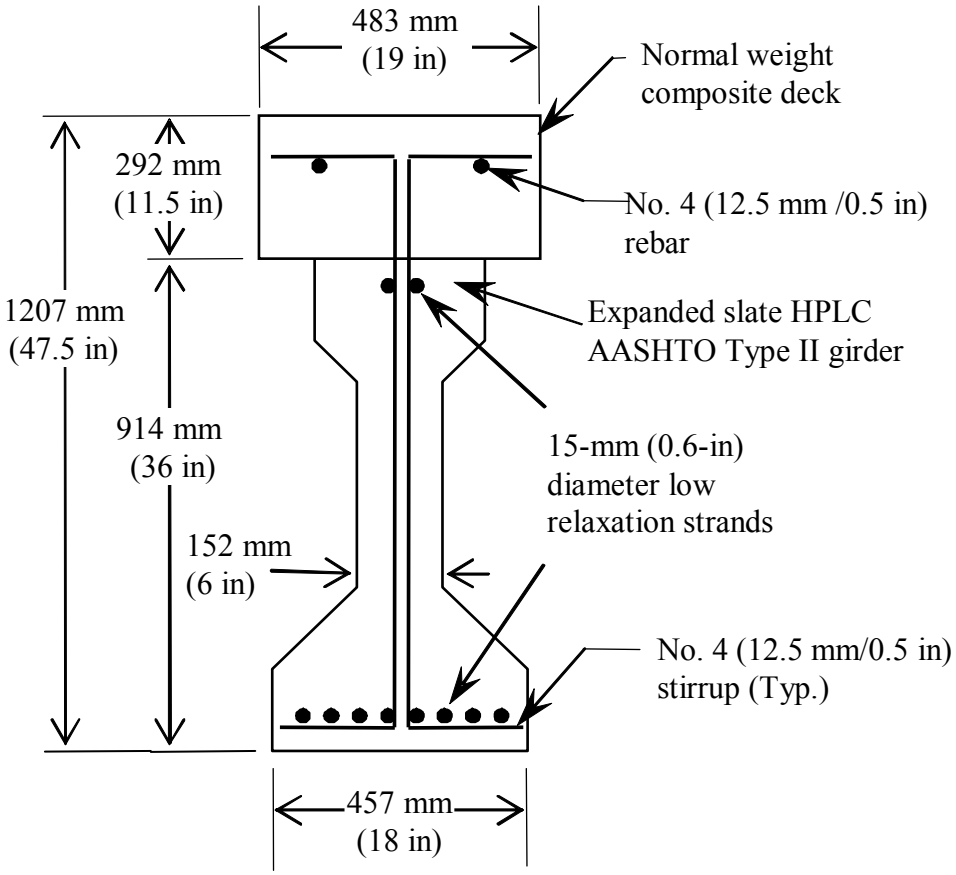

Figure 4.6: Cross section of AASHTO Type II HPLC girder with NSC composite deck

A normal weight normal strength concrete (NSC) composite deck was cast atop each girder approximately 2 months after the girders were constructed. The deck was 292 mm (11.5-in) thick and 483-mm (19-in) wide, and the average 56-day compressive strength of the deck was 37.1 MPa (5380 psi).

Internal vibrating wire strain gauges (VWSG) were used to measure long-term deformations in the girders. The 152-mm (6-in) long VWSG were placed at the center of

gravity of the strands at the midspan of each girder. Figure 4.7 shows the embedded VWSG used to measure strains at the center of gravity of the strands.

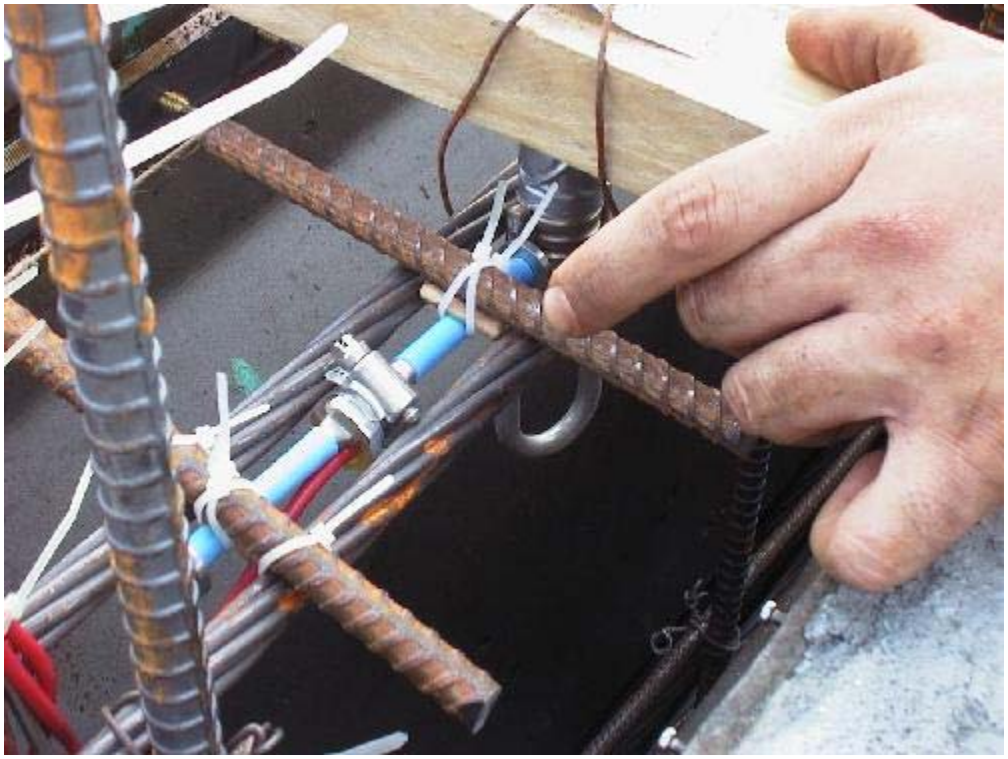

Figure 4.7: Vibrating wire strain gage used to measure internal strains in the girders.

4.3.3.2 Girder Strains

Figures 4.8 and 4.9 show the AASHTO Type II girders while being cast at the precast plant. Figure 4.10 shows the six prestressed girders at the Georgia Tech Structures and Materials Laboratory before the deck placement.

Strain measurements started before prestressing force transfer and finished four to five months later when the girders were tested for flexure and shear strength. The temperature of the girders varied from 33.2^{o}C (91.8^{o}F) before strand release to 20^{o}C (68^{o} F) four months later.

Figure 4.8: Precast Concrete Plant

Figure 4.9: Installation of shear reinforcement during girders construction

The readings from the vibrating wire strain gauges were corrected for temperature changes in order to obtain "load related" strains. Even though coefficient of thermal

expansion (CTE) of concrete varies with age, only the 56-day CTE was available to perform the temperature corrections. Actual prestressing force losses were computed from experimental strains of concrete. The experimental data did not include steel relaxation losses which were calculated using experimental concrete strains and the AASHTO-LRFD refined method expression (See equation C.11, Appendix C). Experimental strains were projected to ultimate condition, as explained below, in order to compare with the predicted calculated losses.

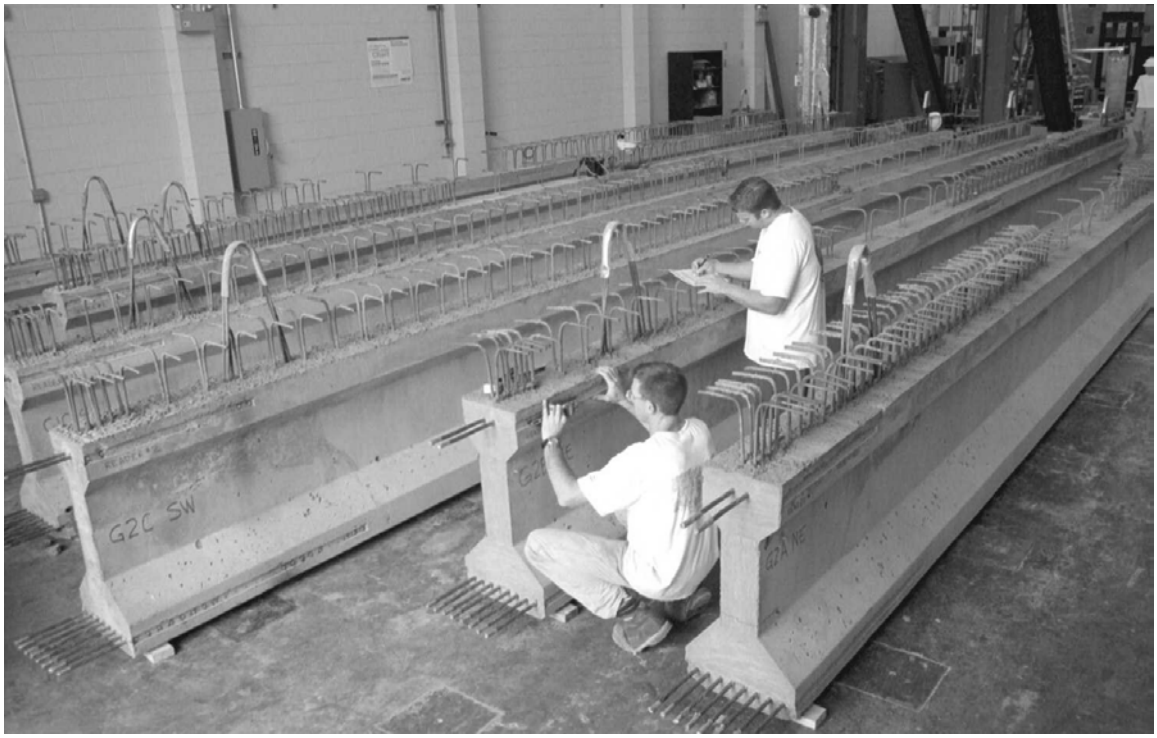

Figure 4.10: Measuring external strains of the AASHTO Type II precast prestressed HPLC girders

Table 4.2 and Figure 4.11 present the mid-length strain data obtained from the 11.9-m (39-ft) long girders. The X-axis in Figure 4.11 presents time after strand release, while the Y-axis gives the total concrete strain at the level of the center of gravity of the strands in με.

Table 4.2 Experimental strains of 11.9-m (39-ft) long girders (με)

	LWW 55/8			LWW 69/10	
Time	Girder G1A	Girder G1B	Time	Girder G2A	Girder G2B
Before Release	0	0	Before Release	0	0
After Release	-583	-609	After Release	-426	-417
2 days	-661	-695	1 day	-475	-471
3 days	-696	-731	3 days	-482	-479
7 days	-768	-811	7 days	-506	-496
14 days	-822	-870	14 days	-506	-506
106 days	-865		125 days	-531	
113 days		-945	140 days		-520

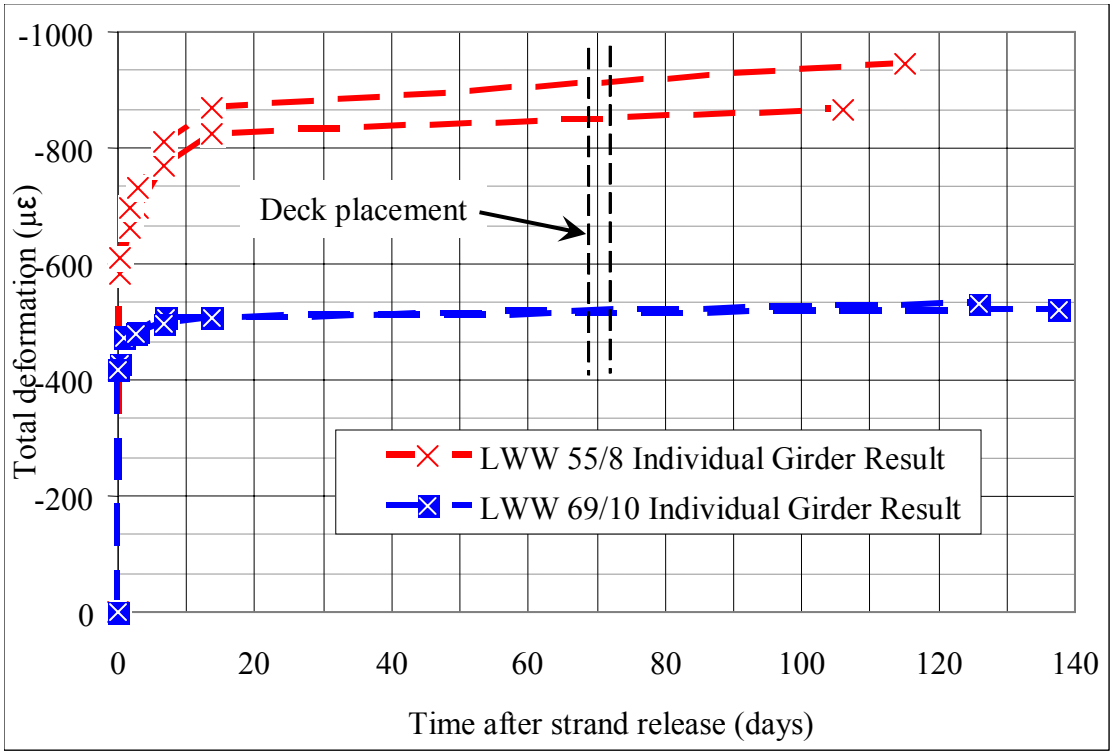

Figure 4.11: Experimental strains over time for LWW 55/8 and LWW 69/10 39-ft girders

Elastic strain of the LWW 55/8 girders was about -600 με while total strain after an average 110 days was approximately -900 με. The LWW 69/10 girders, on the other

hand, had an elastic strain of -420 με and total strain after an average 130 days of -525 με.

Creep and shrinkage strains of the girders were computed as the difference between total strain and initial elastic strain. After approximately 110 days, creep and shrinkage strains were -309 με for the LWW 55/8 girders, and after 130 days they were -104 με for the LWW 69/10 girders. Figure 4.12 presents creep and shrinkage strains for individual girders and the exponential regression obtained for each. Figure 4.12(a) presents the data in a linear time scale until the time of the last measurement, and Figure 4.12(b) presents the data in a logarithmic time scale projected until 10,000 days (27.4 years).

After 100 days under loading and drying combined, creep and shrinkage of the LWW 55/8 and LWW 69/10 girders were approximately -300 and -100 με, respectively. Various regression lines were tested against the experimental data in order to obtain the least sum of square errors. The exponential regression was the better fit for the experimental trends of both HPLC mixtures. The regression predicted that, after 100 days, creep plus shrinkage was not going to increase significantly. Based on the regressions shown in Figure 4.12b, the creep plus shrinkage strains at ultimate would be -309 and -104 με for the LWW 55/8 and LWW 69/10 girders, respectively.

Such low long-term deformations were not unexpected since HPC concrete mixtures show, in general, less creep and less shrinkage than NSC. Many have concluded that HPC exhibits less creep and less shrinkage than NSC [22, 24-28]. Some of them have suggested that such reduction is due to the considerably lower drying shrinkage and drying creep that HPC exhibits because of its low permeability.

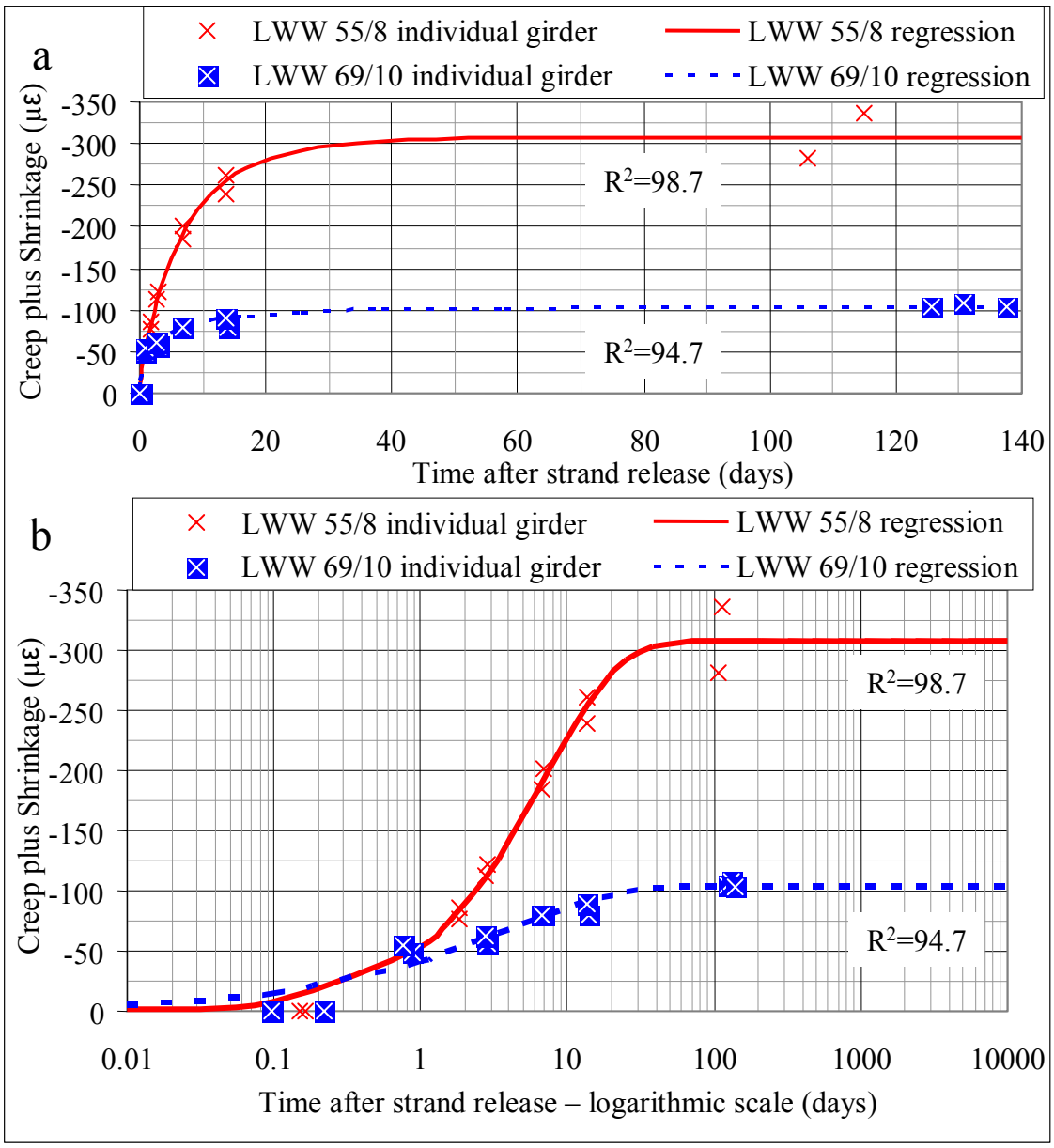

Figure 4.12: Experimental creep and shrinkage and exponential regression for the LWW 55/8 and LWW 69/10 HPLC 39-ft girders (a) linear time scale (b) logarithmic time scale.

Another reason to conclude that drying creep and shrinkage could have been very small, or practically non-existent in these girders, is the fact that the volume of concrete relative to its exposed area was relatively high (100 mm or 3.57 in) which drastically

reduces drying. Finally, HPLC girders were exposed to ambient relative humidity between 50 and 95% during the time of testing. This high ambient relative humidity together with the possibly low internal relative humidity and low water-to-cement ratio mixtures [29] could have reduced the moisture gradient, and therefore, the drying.

4.4 Prestress Loss Calculations from Design Methods

Prestress loss calculation methods can be classified into two groups: (1) final prestress loss estimate and (2) time-step estimate which can be used to obtain losses at any time. Among the most commonly used design methods, there are three methods for estimating final prestress losses: Precast/Prestressed Concrete Institute Method [30], refined estimate and approximate lump sum estimate, both given by the American Association of State Highway and Transportation Officials [31]. For losses at any time, American Concrete Institute Committee 209 [32] proposed a prestress loss estimate method based on creep and shrinkage estimates. The computation procedures of each design method are outlined in the Appendix C.

Even though anchorage seating losses can be an important portion of the total prestress losses, they were not considered here because such losses are related to the manufacturing process rather than material properties.

Prestress losses for AASHTO Type II girders were computed by using the methods proposed by design methods [30-32]. Section C.5, Appendix C presents details of the prestress loss calculations. Table 4.3 presents a comparison among the four models and the average actual losses for the HPLC prestressed girders made with either LWW 55/8 or LWW 69/10. Details of the calculations are given in Appendix C.

Table 4.3 Comparison between experimental and estimated prestress losses of LWW 55/8 and LWW 69/10 HPLC prestressed girders

LWW 55/8	Measured Projected			AASHTO refined			AASHTO Lump sum			PCI			ACI 209		
	MPa	ksi	%	MPa	ksi	%	MPa	ksi	%	MPa	ksi	%	MPa	ksi	%
Initial Stress	1400	202.5	100.0	1400	202.5	100.0	1400	202.5	100.0	1400	202.5	100.0	1400	202.5	100.0
Elastic Shortening	-117	-17.0	-8.4	-77	-11.1	-5.5	-72	-10.4	-5.2	-72	-10.5	-5.2	-83	-12.0	-5.9
Creep	not measured separately			-113	-16.2	-8.1	not estimated separately			-97	-14.1	-7.0	-102	-14.8	-7.3
Shrinkage				-45	-6.5	-3.2				-35	-5.1	-2.5	-78	-11.3	-5.6
CR+SH	-60	-8.8	-4.3	-158	-22.7	-11.3				-132	-19.2	-9.5	-180	-26.1	-12.9
Relaxation[1]	-23	-3.4	-1.7	-23	-3.3	-1.6				-26	-3.8	-1.9	-39	-5.6	-2.8
Total Time-dependent	-84	-12.2	-6.0	180	-26.0	-12.9	-167	-22.3	-12.0	-158	-23.0	-11.3	-219	-31.7	-15.7
Total Losses	-201	-29.2	-14.4	-257	-37.1	-18.4	-239	-32.8	-17.1	-231	-33.5	-16.5	-301	-43.7	-21.6
LWW 69/10	Measured			AASHTO refined			AASHTO Lump sum			PCI			ACI 209		
	MPa	ksi	%	MPa	ksi	%	MPa	ksi	%	MPa	ksi	%	MPa	ksi	%
Initial Stress	1400	202.5	100.0	1400	202.5	100.0	1400	202.5	100.0	1400	202.5	100.0	1400	202.5	100.0
Elastic Shortening	-83	-12.0	-5.9	-70	-10.0	-5.0	-67	-9.8	-4.8	-62	-9.0	-4.4	-75	-10.9	-5.4
Creep	not measured separately			-111	-15.9	-7.9	not estimated separately			-90	-13.0	-6.4	-88	-12.7	-6.3
Shrinkage				-45	-6.5	-3.2				-35	-5.1	-2.5	-78	-11.2	-5.6
CR+SH	-20	-3.0	-1.5	-156	-22.4	-11.2				-125	-18.1	-8.9	-165	-24.0	-11.8
Relaxation[1]	-30	-4.4	-2.2	-23	-3.5	-1.7				-27	-3.9	-1.9	-39	-5.6	-2.8
Total Time-dependent	-50	-7.3	-3.6	-179	-25.9	-12.8	-162	-23.5	-11.6	-152	-22.2	-10.8	-204	-29.6	-14.6
Total Losses	-134	-19.4	-9.6	-249	-35.9	-17.8	-229	-31.3	-16.4	-214	-31.0	-15.3	-280	-40.5	-20.0

[1]: Relaxation was determinate with equation from AASHTO refined method and experimental ES, CR and SH.

The PCI and the two AASHTO models estimated final prestress losses while ACI-209 model estimates losses at any time after prestressing. For comparison purposes, ACI-209 estimates were computed for 10,000 days (27.4 years) after prestressing assuming that as the final state of losses. Actual losses were computed from experimental strains of concrete at the center of gravity of the strands. The AASHTO lump sum model gave a single time-dependent loss estimate, so comparison of creep, shrinkage and relaxation was not possible for that model.

The experimental data, on the other hand, included only losses associated with concrete: elastic shortening (ES), creep (CR) and shrinkage (SH). Steel relaxation was not measured. Rather the "experimental" relaxation was computed using the AASHTO-LRFD refined technique, considering the measured elastic, creep and shrinkage losses.

Experimental strains were projected to ultimate condition for comparison with the estimates from the design methods as shown in Figure 4.12.

Figure 4.13 (a) and (b) shows a comparison of estimated prestress losses with experimental prestress losses, for the LWW 55/8 and LWW 69/10 AASHTO Type II girders. Figure 4.13 presents elastic, creep plus shrinkage, steel relaxation, and total time-dependent and total losses.

Experimental projected "total losses" for LWW 55/8 girders were 201 MPa (29.2 ksi), which represented 14.4% of the initial applied stress in the strands. The AASHTO-LRFD refined and ACI-209 methods estimated total losses by -257 and 301 MPa (-37.3 and 43.7 ksi), respectively. Thus, AASHTO-LRFD method overestimated losses by 28% while ACI-209 overestimated losses by 50%. The estimates of the AASHTO-LRFD lump sum and PCI methods overestimated total losses by 19 and 15%, respectively.

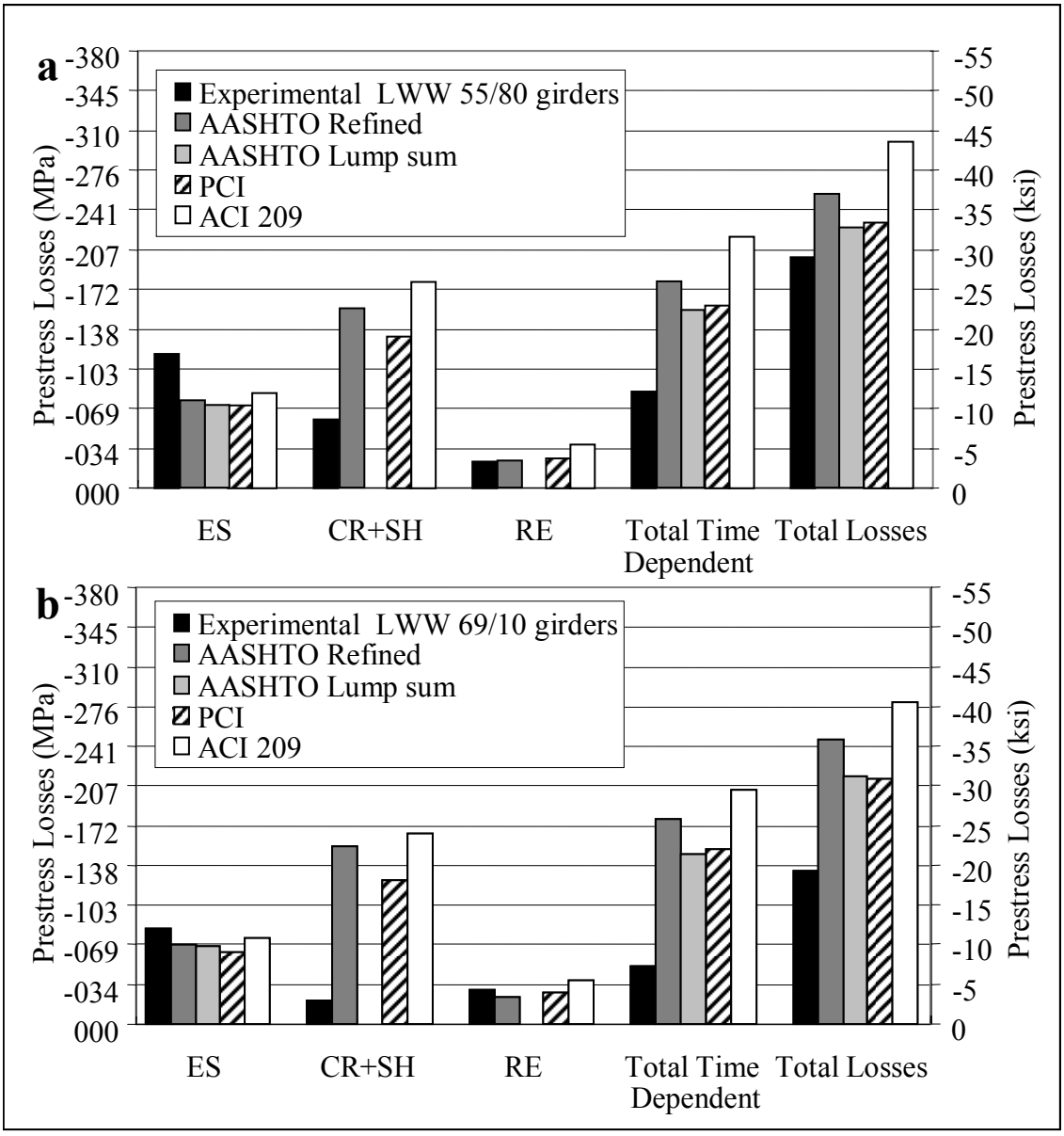

Figure 4.13: Comparison between experimental and estimated prestress losses from AASHTO-LRFD, PCI, and ACI-209 methods (a) LWW 55/8 HPLC girders, (b) LWW 69/10 HPLC girders

The errors in the prestress loss estimates with respect to the experimental losses expressed as percentage of the experimental losses were: 28, 50, 19, and 15%, for the

AASHTO-LRFD refined, ACI-209, AASHTO-LRFD lump sum and PCI techniques, respectively. Therefore, the four design methods overestimated prestress losses of the girders made with LWW 55/8.

The experimental projected prestress losses in the LWW 69/10 girders were 134 MPa (19.4 ksi) which represented 9.6% of the initial stress in the strands. Total losses in the LWW 69/10 girders were equivalent to 67% of those measured in the LWW 55/8 girders.

The four methods shown in Figure 4.13b overestimated the projected, measured losses for the LWW 69/10 girders. The AASHTO-LRFD refined method and ACI-209 greatly overestimated total losses by 86 and 109%. The AASHTO-LRFD lump sum and PCI methods, on the other hand, overestimated losses by 71 and 60%.

Figure 4.14 shows the predicted-to-measured ratio. Losses are grouped in elastic shortening, creep and shrinkage, total time dependent and total losses. Overestimates appear as a predicted-to-measured ratio greater than one and the underestimates as lower than one.

The fact that all methods underestimated elastic shortening was probably a consequence of the strand release operations. The strain reading after prestress transfer was taken approximately one hour after the initial reading. Therefore, the difference between readings included not only instantaneous elastic strain, but also early creep plus autogenous and drying shrinkage.

The AASHTO-LRFD refined, PCI and ACI methods greatly overestimated creep and shrinkage losses. The closest estimate was almost 120% higher than experimental data and the farthest, more than 700% higher. The same argument used to explain the

underestimate of elastic shortening can be used to explain part of the overestimate of creep and shrinkage, i.e., the first measurement after transfer probably included some creep and shrinkage which makes experimental creep and shrinkage seem lower. Nevertheless, as explained above, previous research has shown that high strength concrete had considerably less creep and shrinkage than NSC [26, 28, 33].

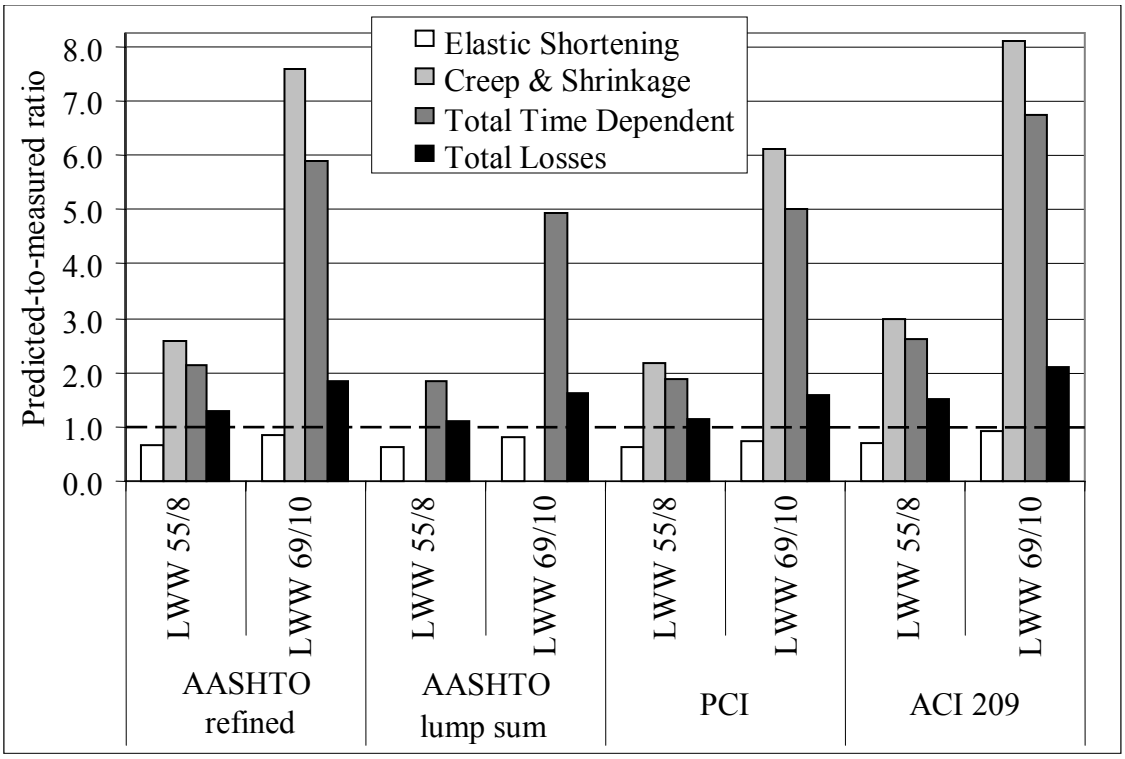

Figure 4.14: Predicted-to-measured ratio of prestress losses from AASHTO-LRFD, PCI, and ACI-209 design provision

All four methods overestimated total time-dependent losses in the two types of HPLC mixtures, meaning that they are conservative in considering those losses.

Within time-dependent losses, differences between estimates were due primarily to shrinkage losses. For LWW 55/8, the PCI method estimated shrinkage losses to be 35 MPa (5.1 ksi) which represents 2.5% of the initial stress, while the ACI-209 method estimated it to be 78 MPa (11.3 ksi) which is 5.6% of the initial stress.

The total measured prestress losses due to creep and shrinkage in the LWW 69/10 girders were 20 MPa (3 ksi) for the stress level in the girders of 17% of the initial concrete strength. They needed to be projected to a stress level of 60% of the initial concrete strength for being compared against results from previous investigations [34-36].

Elastic shortening, creep losses, and steel relaxation are load dependent prestress losses while shrinkage losses depend only on the ambient relative humidity and the dimensions of the element. In order to project the experimental losses to a stress in the concrete equivalent to 60% of the initial strength, it was required to separate creep from shrinkage deformation to adjust only the creep portion. By assuming the creep and shrinkage in the girders had the same behavior as that of standard cylinders tested according to ASTM C 512 [37], they could be separated, and the stress adjustment could be applied. Figure 4.15 shows the average measured prestress losses and the projected losses to a stress level of 60% of the initial concrete strength.

An early publication on prestress losses [36] showed reference values of prestress losses in elements made with concrete having 24.1 and 31.0 MPa (3500 and 4500 psi) compressive strength at the moment of strand release. Table 4.4 summarizes some of the data reported there [36] and obtained herein.

Creep plus shrinkage losses in the NSC mixtures were approximately 16% of the initial stress. Those losses in the HPLC mixtures totaled about one third of those from NSC. Elastic shortening of the HPLC mixtures was roughly double those reported for NSC. The difference was not due to a lower elastic modulus of HPLC because those were between 24.6 and 27.0 GPa (3570 and 3910 ksi) compared to the 23.5-to-26.7 GPa

(3410-to-3870 ksi) range reported for NSC. The larger elastic shortening losses in HPLC were in part due to due to the higher stress level applied to the HPLC girders. As shown in Table 4.4, the applied stress in the HPLC girders was 60% of the initial compressive stress compared to the 48% of the initial strength used in the NSC girders. Overall, losses due to concrete strains were slightly lower for HPLC mixtures even though those girders carried considerably higher compressive stress.

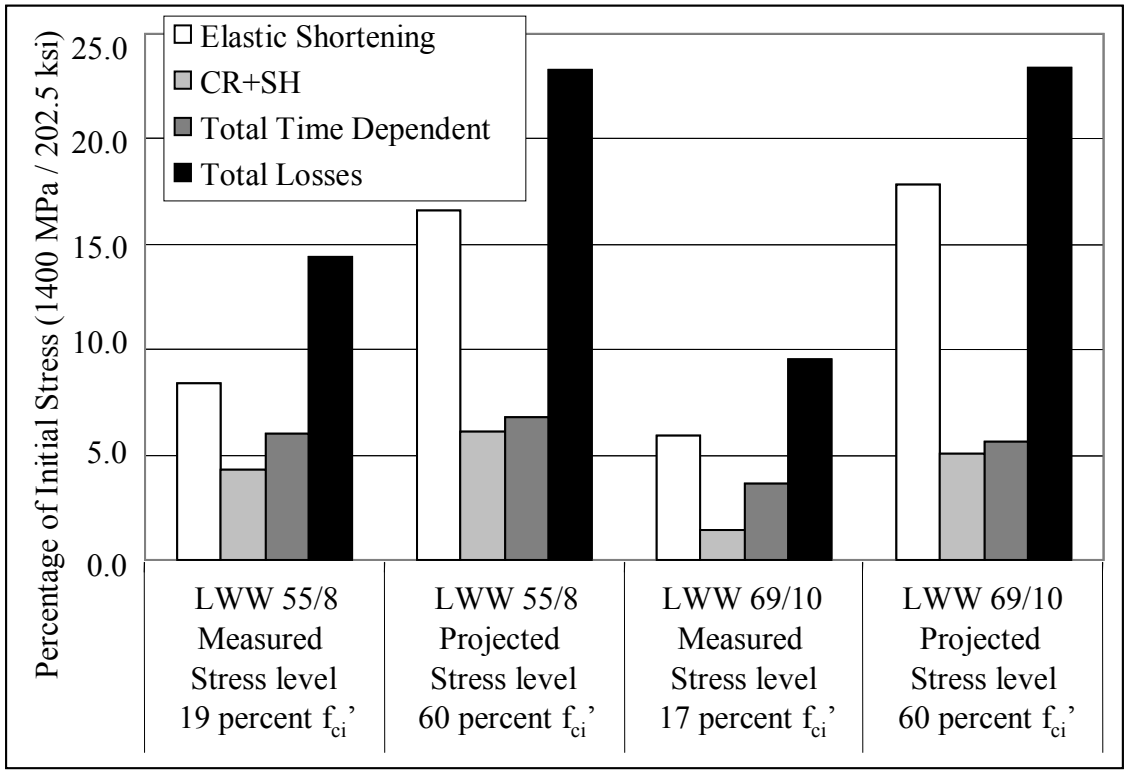

Figure 4.15: Measured prestress losses and the projected prestress losses to a stress level of 60% of the initial concrete strength

Projected to a stress level of 60%, prestress losses in the LWW 69/10 girders would be 71 MPa (10.3 ksi) which is 5.1% of the initial stress in the steel reinforcement. That 5.1% due to long-term strains was slightly lower than the value of 7.4% obtained previously [35] for a normal weight HPC of similar strength.

Table 4.4: Prestress losses of NSC and HPLC elements, expresses as percentage of the initial stress (%)

Concrete type	NSC	NSC	HPLC LWW 55/8	HPLC LWW 69/10
Concrete strength at release, MPa (psi)	24.1 (3500)	31.0 (4500)	48.9 (7090)	57.3 (8310)
Applied stress [1], MPa (psi)	11.6 (1680)	14.9 (2160)	29.0 (4200)	34.1 (4950)
Applied stress divided by concrete strength at release	0.48	0.48	0.60	0.60
Elastic shortening (%)	7.4	8.4	16.6	17.8
Creep plus shrinkage (%)	15.7	17.1	6.1	5.1
Total losses due to concrete strains [2] (%)	23.1	25.5	22.7	22.9
Area of strands, mm^2 (in^2)	1386 (2.149)	1783 (2.763)	3920 (6.076)	4620 (7.161)
Applied Prestressing Force, MPa (ksi)	2800 (406)	3600 (522)	7920 (1148)	9335 (1355)

[1]: stress at the center of gravity of the strands

[2]: elastic shortening, creep and shrinkage

Another study [34] on prestress losses of normal weight HPC with design strength of 69 MPa (10,000 psi) obtained creep plus shrinkage losses between 7 and 14% of the initial applied stress. Thus, prestress losses measured on LWW 69/10 were similar to the lowest values reported previously. That same study obtained elastic shortening losses in the range between 5 and 14%, so the elastic shortening of LWW 69/10 girders were larger than the highest values by 3%. Overall, elastic shortening, creep and shrinkage losses reported herein were within the range of 12.5 and 28.6% obtained previously [34].

4.5 Comparison of High Performance Lightweight and Normal Weight Concrete

Another research program conducted at the Georgia Institute of Technology considered the development and characterization of a normal weight HPC made with locally available materials from Georgia. After the material was developed, full size

prestressed bridge girders were tested and a four span 107.5-m (353-ft) long HPC bridge was constructed over Interstate I-75 [23, 38].

This section presents a comparison between mechanical properties, creep plus shrinkage and prestress losses of the LWW 69/10 mixture and those from a normal weight HPC called HPC-6 of equivalent mechanical properties from the HPC bridge. LWW 69/10 and HPC-6 mixture designs are shown in Table 4.5. Experimental results are presented in detail in Appendix B.

Table 4.5: Mixture design of HLPC and HPC-6 in kg/m^3 (lb/yd^3)

	LWW 69/10	HPC-6
Type III Cement	442 (745)	
Type I cement		479 (807)
Silica fume	59 (100)	44(75)
Class F fly ash	89 (150)	61 (102)
Water	135 (228)	154 (260)
Normal weight fine aggregate	611 (1030)	582 (981)
Coarse aggregate	571 (963) [1]	1080 (1820) [2]
Water reducer	2.7 (4.6)	1.6 (2.7)
High-range water reducer	5.9 (9.9)	5.6 (9.4)
Air entrainer	0.3 (0.5)	0.3 (0.5)
water/cementitious ratio	0.230	0.264
Cement paste content (%)	38.7	38.4
Slump, mm (in)	100 (4)	115 (4.6)
Air Content (%)	3.3	4.2
Theoretical densitykg/m^3(lb/ft^3)	1905 (119)	2355 (147)

[1]: 12.7-mm (05.-in) MSA pre-soaked expanded slate; [2]: 19-mm (0.75-in) granite

HPC-6 was also a 69-MPa (10,000-psi) compressive strength HPC, but of a different mixture design. The main differences were the use of Type I portland cement instead of Type III and the coarse aggregate which was pre-soaked expanded slate for LWW 69/10 and granite for HPC-6. The two mixtures were very comparable since they

had similar water-to-cementitious material ratio, and they both used class F fly ash and silica fume. They had virtually the same cement paste content which considered all constituents but aggregate. The total cementitious materials content were 590 kg/m^3 (995 lb/yd^3) for LWW 69/10 and 584 kg/m^3 (985 lb/yd^3) for HPC-6.

4.5.1 Comparison of Mechanical Properties of High Performance Lightweight and Normal Weight Concrete

Similar testing programs were considered in both projects, so age at testing, curing procedures, testing machines were all the same, and direct comparison of the properties could be made.

Figure 4.16 compare compressive strength and elastic modulus measured on specimens under accelerated curing at the age of 24 hours. It also shows the corresponding compressive strength and modulus at the age of 56 days with standard curing. Figure 4.16 presents both compressive strength in MPa (psi) and elastic modulus in GPa (ksi), and X-axis showed the property and type of mixture.

The 24-hour compressive strength of the lightweight mixture was 7% higher than that of HPC-6. This difference was possibly caused by the differences in cement type. LWW 69/10 used high early strength cement while HPC-6 used an ordinary portland cement. At the age of 56 days, HPC-6 had 30% higher compressive strength. LWW 69/10 56-day compressive strength averaged 71.1 MPa (10,310 psi) while HPC-6 averaged 93.9 MPa (13,620 psi). This large difference was due to the strength ceiling imposed by the lightweight aggregate on the compressive strength of concrete [2, 14, 39].

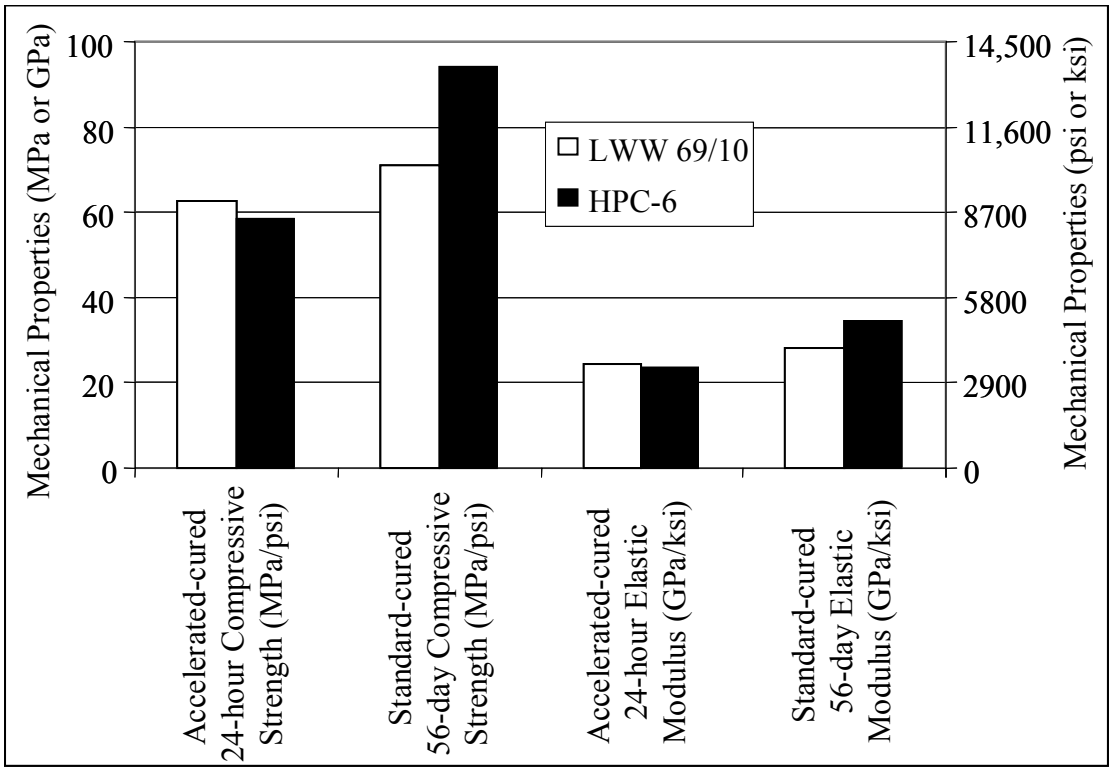

Figure 4.16: Compressive strength and elastic modulus of LWW 69/10 versus HPC-6

Surprisingly, elastic modulus at the age of 24 hours was very similar in the two mixtures (within 5%) which indicated than at such an early age, the elastic modulus may be mainly function of the cement paste properties rather than the aggregate. After 56 days, elastic modulus of HPC-6 was 22% higher than that of LWW 69/10. This difference in stiffness clearly indicated the influence of the lightweight aggregate.

It was concluded that mechanical properties at very early age were mainly determined by the cementitious matrix rather than the aggregate. The two mixtures had similar 24-hour compressive strength and elastic modulus, so time-dependent strain from the girders and creep testing were comparable.

4.5.2 Comparison of Prestress Losses of High Performance Lightweight and Normal weight Concrete

The HPC bridge was constructed using 30 AASHTO Type IV prestressed girders and 22 AASHTO Type II girders. Two of each girder type were instrumented in a similar fashion as those used in the large-scale study of HPLC as described in Section 4.3.3.1.

Elastic and creep plus shrinkage strains in the girders were monitored for a period of 1195 days (3.27 years) which was used to extrapolate time-dependent deformation to ultimate condition. Prestress losses were calculated and the same comparison was made against design methods. Figure 4.17 compares the predicted-to-measured ratio obtained by each of the methods on the AASHTO Type II girders made with LWW 69/10 and HPC-6.

As shown by Figure 4.17, all the methods conservatively estimated total prestress losses of both mixtures. Total losses were overestimated by a greater amount in the case of HPC-6 girders. Elastic shortening losses were underestimated for LWW 69/10, but closely predicted for HPC-6 girders. This might indicate that the similar elastic modulus of those mixtures, tested according standard procedures [10], could have not accurately represented the actual properties of the girders.

Large predicted-to-measured ratio of creep plus shrinkage losses was obtained. Such ratios were in the range between 6.1 and 8.1 for LWW 69/10 girders and between 2.5 and 4.3 for the HPC-6 girders. Thus, the same methods applied to same type of girders made with two similar mechanical properties concrete mixtures presented very different performance in assessing creep plus shrinkage prestress losses. This suggested

than the unusual overestimates obtained by the methods in the LWW 69/10 girders was not only caused by the high strength but also by particular properties of the pre-soaked expanded slate HPLC.

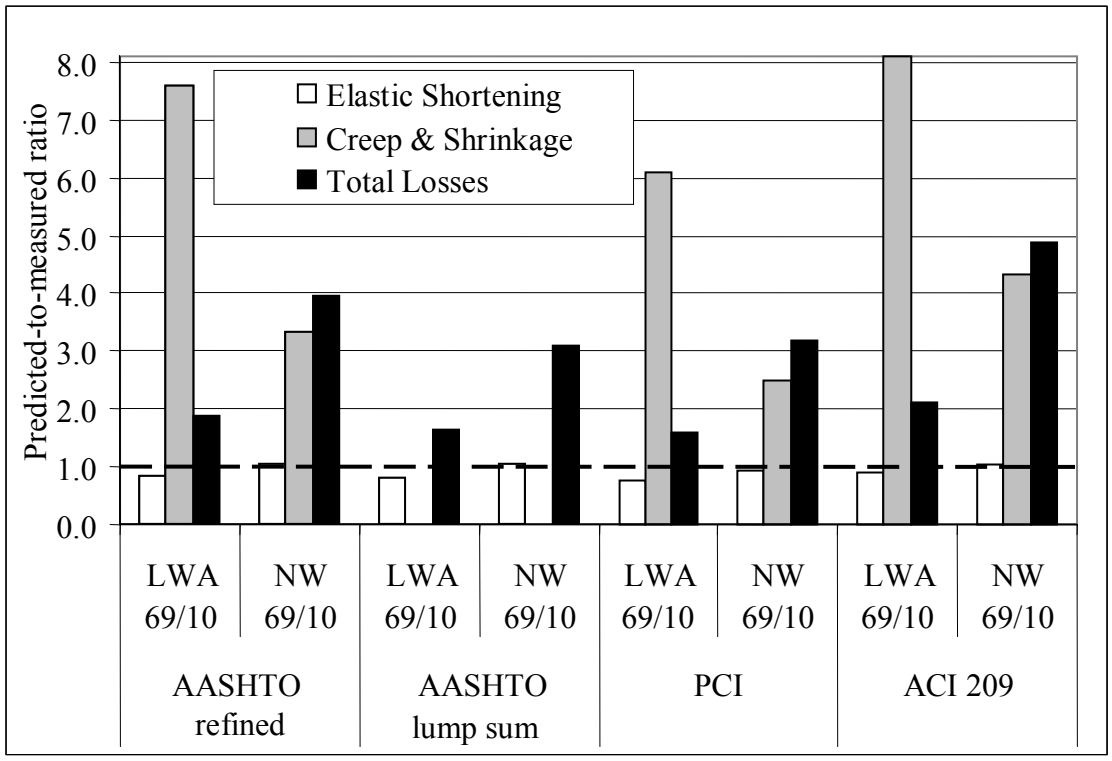

Figure 4.17: Predicted-to-measured ratio of prestress losses from AASHTO-LRFD, PCI, and ACI-209 design provisions on AASHTO Type II girders made of LWW 69/10 and HPC-6

4.5.3 Comparison of Creep plus Shrinkage of High Performance Lightweight and Normal Weight Concrete

Creep and shrinkage were measured on specimens cast at the same time as the girders. Loading and drying started at the age of 24 hours and followed the guidelines of ASTM C 512 [37]. The size of the cylinder specimens was 100 x 380 mm (4 x 15 in) which is smaller than the ASTM recommendation because the load capacity of the creep frames was not enough to load 150 x 300 mm (6 x 12 in) to a stress of 40% of the

compressive strength. Twelve creep specimens from the two mixtures remained under load for at least 850 days. Figure 4.18 presents comparison of average creep plus shrinkage measured on LWW 69/10 and HPC-6 under a stress of 27.6 MPa (4000 psi).

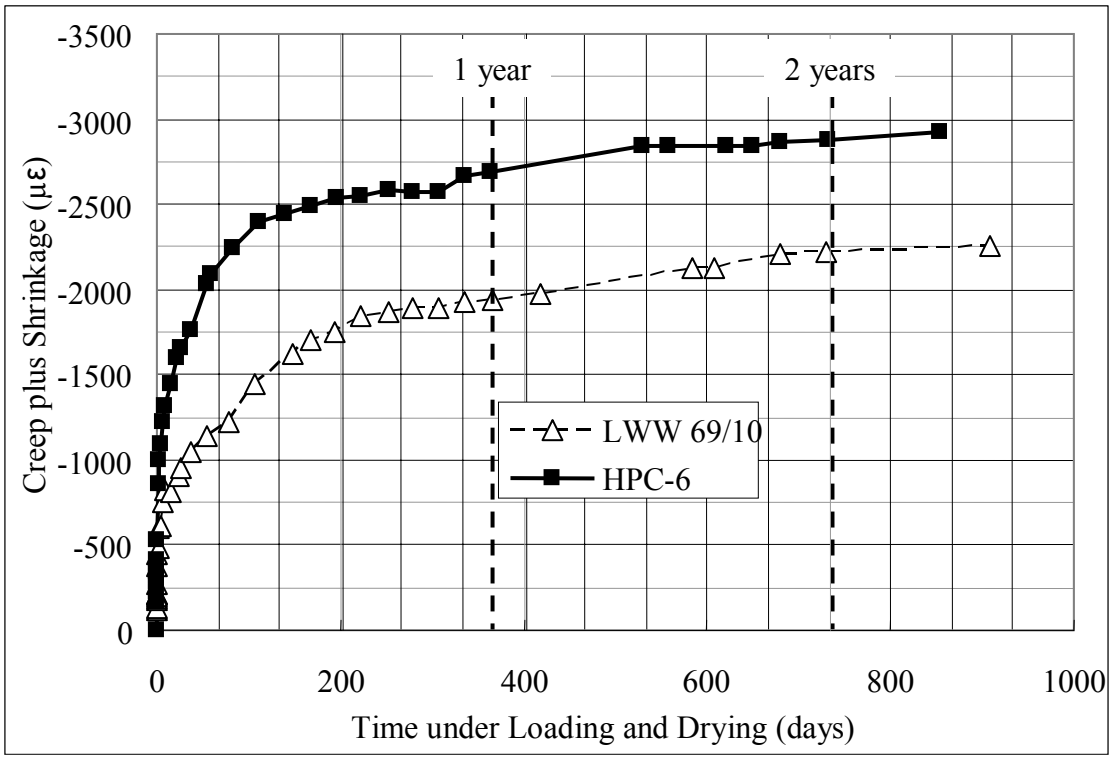

Figure 4.18: Creep plus shrinkage of LWW 69/10 and HPC-6 mixtures under 27.6-MPa (4000-psi) compressive stress

Creep plus shrinkage results confirmed the finding from the prestress losses comparison. LWW 69/10 had considerably less creep plus shrinkage deformations than HPC-6. The difference started at times as early as 24 hours under loading and drying. After one day of testing, creep plus shrinkage strain of LWW 69/10 was -444 με while HPC-6 strain was -533 με. After one week the difference increased from 89 to 473 με. The strain difference between mixtures kept increasing up to one year when it stabilized around 685 με. After 855 days under load, LWW 69/10 creep plus shrinkage was about 77% of that measured on HPC-6.

Therefore the greater overestimate in time-dependent prestress losses in the LWW 69/10 girders was a direct cause of the lower creep plus shrinkage presented by that mixture.

LWW 69/10 had a similar 24-hour compressive strength but a 33% lower 56-day strength than HPC-6. Even though the large compressive strength difference, LWW 69/10 had a considerably lower creep plus shrinkage deformations monitored during 855 days.

It was concluded that besides compressive strength, other factors, possibly related to the water contained in the pre-soaked lightweight aggregate, reduced the long-term deformations in the LWW 69/10 mixture.

4.6 Conclusions

This study investigated prestress losses, creep and shrinkage of six pretensioned girders made with expanded slate HPLC. The two concretes examined here LWW 55/8 and LWW 69/10 HPLC had 56-day strengths of 64.5 and 73.0 MPa (9350 and 10,580 psi), and densities of 1855 and 1890 kg/m^3 (116 and 118 lb/ft^3), respectively.

Elastic modulus of HPLC was about 5% higher than that predicted using ACI-363 [15] equation (Equation 4.1) based on compressive strength and density. Rupture modulus of HPLC was 30% higher than that estimated using ACI-318 [17] (Equation 4.2). Chloride permeability at 56 days was classified as very low according to ASTM C 1202 [18].

Final prestress losses were estimated using AASHTO refined, AASHTO lump sum, PCI, and ACI-209 methods. All these methods overestimated the total prestress losses in LWW 69/10 and LWW 55/8 AASHTO Type II prestressed girders made with

expanded slate HPLC. Thus, based on these observations, it might be concluded that these methods are conservative for estimating total prestress losses of expanded slate HPLC girders.

Compared to NSC, HPLC had roughly one-third of the creep plus shrinkage losses. Overall, HPLC had slightly lower prestress losses than NSC for an applied stress between 2.2 and 3.3 times greater than that applied to NSC. Prestress losses of HPLC girders where within the range reported for normal weight HPC of similar characteristics.

Based on these results, it is proposed that both the AASHTO-LRFD refined and ACI-209 methods may be used conservatively for predicting prestress losses in girders made of expanded slate high performance lightweight concrete. However, further research on the influence of mixture design on long-term performance of HPLC for prestressed concrete is recommended.

Long-term performance of the LWW 69/10 mixture was compared to that of a normal weight HPC (named HPC-6) made with similar constituents and of comparable 24-hour compressive strength. LWW 69/10 had creep plus shrinkage strains equivalent to the 77% of those measured on HPC-6 over a period of 855 days.

Design methods overestimated prestress losses due to creep plus shrinkage by more on AASHTO Type II girders made with LWW 69/10 than with HPC-6. Thus, the good time-dependent performance exhibit by HPLC was not only due to the high strength but also by particularities of the pre-soaked expanded slate HPLC.

It was concluded that time-dependent testing, according ASTM [37], adequately represented the difference in performance between LWW 69/10 and HPC-6 seen in the Type II girders.

The prestress losses and conclusions with regard to the design methods reported herein are in agreement to those obtained by the National Cooperative Highway Research Program – NCHRP, for high strength concrete girders [40]. That program did not include HPLC girders, but the constituents, compressive strengths, strand diameter, and experimental methods were comparable to those used herein.

4.7 References

1. Meyer, K.F., *Transfer and development length of 0.6-inch diameter prestressing strand in high strength lightweight concrete*. 2002.
2. Meyer, K.F., B.S. Buchberg, and L.F. Kahn. "Development of High Strength Lightweight Concrete Mix Designs: A Practical Approach". in *49th Annual PCI Convention & Exhibition, the 3rd PCI/FHWA International Symposium on High Performance Concrete, and the National Bridge Conference.* Orlando, Florida: Precast / Prestressed Concrete Institute, 2003.
3. Buchberg, B.S., *Investigation of mix design and properties of high-strength/high-performance lightweight concrete*. 2002.
4. ASTM C 143, *Standard Test Method for Slump of Hydraulic Cement Concrete*. West Conshohocken, PA: American Society for Testing and Materials, 2005.
5. ASTM C 138, *Standard Test Method for Density (Unit Weight), Yield, and Air Content (Gravimetric) of Concrete*. West Conshohocken, PA: American Society for Testing and Materials, 2001.
6. ASTM C 173, *Standard Test Method for Air Content of Freshly Mixed Concrete by the Volumetric Method*. West Conshohocken, PA: American Society for Testing and Materials, 2001.
7. ACI Committee 213, "Guide for Structural Lightweight Aggregate Concrete", in *ACI Manual of Concrete Practice*. American Concrete Institute: Farmington Hills, MI. 1987, p. 213R.1-231R.27.
8. Gjørv, O.E., "Durability", in *High Performance Concrete: Properties and Applications*, S.P. Shah and S.H. Ahmad, Editors. McGraw-Hill: New York. 1994, p. 139-160.
9. ASTM C 39, *Standard Test Method for Compressive Strength of Cylindrical Concrete Specimens*. West Conshohocken, PA: American Society for Testing and Materials, 2004.
10. ASTM C 469, *Standard Test Method for Static Modulus of Elasticity and Poisson's Ratio of Concrete in Compression*. West Conshohocken, PA: American Society for Testing and Materials, 2002.
11. ASTM C 78, *Standard Test Method for Flexural Strength of Concrete (Using Simple Beam with Third-Point Loading)*. West Conshohocken, PA: American Society for Testing and Materials, 2002.

12. ASTM C 192, *Standard Practice for Making and Curing Concrete Test Specimens in the Laboratory*. West Conshohocken, PA: American Society for Testing and Materials, 2002.
13. ASTM C 684, *Standard Test Method for Making, Accelerated Curing, and Testing Concrete Compression Test Specimens*. West Conshohocken, PA: American Society for Testing and Materials, 1999.
14. ACI Committee 213, "Guide for Structural Lightweight-Aggregate Concrete", in *ACI Manual of Concrete Practice*. American Concrete Institute: Farmington Hills, MI. 2003, p. 38.
15. ACI Committee 363, "State-of-the-Art Report on High-Strength Concrete", in *ACI Manual of Concrete Practice*. American Concrete Institute: Farmington Hills, MI. 1997, p. 55.
16. Aïtcin, P.-C., *High-performance concrete*. London; New York: E. & F.N. Spon, 1998, xxxii, 591.
17. ACI Committee 318, *Building Code Requirements for Structural Concrete (ACI318-02), and Commentary (ACI 318R-02)*. Farmington Hills, MI: American Concrete Institute, 2002.
18. ASTM C 1202, *Standard Test Method for Electrical Indication of Concrete's Ability to Resist Chloride Ion Penetration*. West Conshohocken, PA: American Society for Testing and Materials, 1997.
19. Zhang, M.H. and O.E. Gjørv, "Permeability of High-Strength Lightweight Concrete". *ACI Materials Journal*, 88(5): 1991. p. 463-469.
20. Holm, T.A. and T.W. Bremner, "High Strength Lightweight Aggregate Concrete", in *High Performance Concrete: Properties and Applications*, S.P. Shah and S.H. Ahmad, Editors. McGraw-Hill: New York, NY. 1994, p. 341-374.
21. CRD C 39, *Test Method for Coefficient of Linear Thermal Expansion of Concrete*: U.S. Army Corps of Engineers, Handbook of Concrete and Cement, 1981.
22. Neville, A.M., *Properties of concrete*. 4th and final ed: J. Wiley, 1996.
23. Lopez, M. and L.F. Kahn, *Evaluation of Georgia's High Performance Concrete Bridge - Time Dependent Behavior*. Structural Engineering, Mechanics and Materials, School of Civil and Environmental Engineering, Georgia Institute of Technology: Atlanta. 2004, p. 265.
24. Kosmatka, S.H., B. Kerkhoff, and W.C. Panarese, *Design and control of concrete mixtures*. 14th ed: Portland Cement Association, 2002.
25. Mindess, S., J.F. Young, and D. Darwin, *Concrete*. 2nd ed: Prentice Hall, 2003.
26. Ngab, A.S., A.H. Nilson, and F.O. Slate, "Shrinkage and Creep of High-Strength Concrete". *Journal of the American Concrete Institute*, 78(4): 1981. p. 255-261.
27. Buil, M. and P. Acker, "Creep of a Silica Fume Concrete". *Cement and Concrete Research*, 15(3): 1985. p. 463-466.
28. Dilger, W.H. and C. Wang. "Creep and Shrinkage of High-Performance Concrete". in *The Adam Neville Symposium: Creep and Shrinkage - Structural Design Effects, SP-194*. Atlanta: American Concrete Institute, 2000.p. 361-379.
29. Jensen, O.M. and P.F. Hansen, "Autogenous deformation and RH-change in perspective". *Cement and Concrete Research*, 31(12): 2001. p. 1859-1865.

30. PCI, *PCI Design Handbook, Precast and Prestressed Concrete*. Fifth ed. Chicago: Precast / Prestressed Concrete Institute, 1998.
31. AASHTO, *AASHTO LRFD Bridge Design Specifications*. 3rd Edition ed. Washington: American Association of State Highway and Transportation Officials, 2004.
32. ACI Committee 209, "Prediction of Creep, Shrinkage, and Temperature Effects in Concrete Structures", in *ACI Manual of Concrete Practice*. American Concrete Institute: Farmington Hills, MI. 1997, p. 209R.1-209R.47.
33. de Larrand, F., P. Acker, and R. Le Roy, "Shrinkage Creep and Thermal Properties", in *High Performance Concrete: Properties and Applications*, S.P. Shah and S.H. Ahmad, Editors. McGraw-Hill: New York, NY. 1994, p. 65-114.
34. Stanton, J.F., P. Barr, and M.O. Eberhard. "Behavior of High-Strength High-Performance Concrete Bridge Girders". in *High-Performance Concrete: Research to Practice*. Chicago, IL, 1999.p. 71-89.
35. Roller, J.J., et al., "Long-term performance of prestressed, pretensioned high strength concrete bridge girders". *PCI Journal*, 40(6): 1995. p. 48-59.
36. Podolny, W.J., "Understanding the Losses in Prestressing". *PCI Journal*, 14(5): 1969. p. 43-53.
37. ASTM C 512, *Standard Test Method for Creep of Concrete in Compression*. West Conshohocken, PA: American Society for Testing and Materials, 1992.
38. Slapkus, A., *Evaluation of Georgia's high performance concrete bridge*. 2002.
39. Videla, C. and M. Lopez, "Mixture proportioning methodology for structural sand-lightweight concrete". *ACI Materials Journal*, 97(3): 2000. p. 281-289.
40. Tadros, M., et al., *NCHRP Report 496: Prestressed Losses in Pretensioned High-Strength Concrete Bridge Girders*. Transportation Research Board: Washington D.C. 2003, p. 63 pp.

CHAPTER 5

MEDIUM-SCALE STUDY

5.1 Introduction

The aim of the medium-scale study was to characterize and quantify the effect of the constituent materials and external conditions on creep and shrinkage of high performance lightweight concrete (HPLC). The experimental program, presented in Section 3.3.2, consisted on mixing and testing of ten high performance concrete (HPC) mixtures under various ambient conditions. All the mixtures designs were based on the LWW 69/10 HPLC mixture. In addition, one normal strength concrete (NSC) mixture was included to compare against HPC mixtures.

This chapter presents an analysis of the mechanical properties and time-dependent deformations obtained in the medium-scale study. Results and analysis are grouped in four sections. The first section presents an analysis of the effect of maturity on creep of HPCs where an adjustment procedure was defined. Such adjustment allowed for comparison of creep among mixtures with different maturity at the time of loading. The second section analyzes the influence of properties and amount of coarse aggregate in the mechanical properties, creep and shrinkage of the HPC mixtures under study. The third section analyzes the influence of using pre-soaked lightweight aggregate on the short- and long-term performance of HPLC. Finally, the fourth section analyzes the effect of pore interconnectivity on drying shrinkage and drying creep of HPC. Detailed experimental results and batching procedures are given in Appendix D.

Table 5.1 presents a summary of the eleven mixtures, nomenclature and their main characteristics.

Table 5.1: Mixture nomenclature and characteristics

Mixture ID	Description	Phases of interest (% by volume)
LWW 65-35	HPLC	12.7-mm (0.5-in) MSA pre-soaked expanded slate at 36.8% and HP Matrix at 63.2%
LWW 35-65	high paste content HPLC	12.7-mm (0.5-in) MSA pre-soaked expanded slate at 18.4% and HP Matrix at 81.6%
NWA 65-35	normal weight HPC	12.7-mm (0.5-in) MSA granite at 36.8% and HP Matrix at 63.2%
NWA 35-65	high paste content normal weight HPC	12.7-mm (0.5-in) MSA granite at 18.4% and HP Matrix at 81.6%
STL 65-35	steel aggregate HPC	12.7-mm (0.5-in) MSA steel cubes at 36.8% and HP Matrix at 63.2%
STL 35-65	high paste content steel aggregate HPC	12.7-mm (0.5-in) MSA steel cubes at 18.4% and HP Matrix at 81.6%
LWD 65-35	HPLC with air-dried lightweight aggregate	12.7-mm (0.5-in) MSA air-dried expanded slate at 36.8% and HP Matrix at 63.2%
LWW 65-35-95	HPLC with reduced MSA	9.5-mm (0.375-in) MSA pre-soaked expanded slate at 36.8% and HP Matrix at 63.2%
HP Matrix	high performance matrix used in all mixtures above	2.36-mm (#8 sieve) siliceous sand at 39.2% and cementitious paste at 60.8%
Cement Matrix	similar to HP Matrix, but without SCMs	2.36-mm (#8 sieve) siliceous sand at 39.2% and cement paste at 60.8%
NSC	normal weight normal strength concrete	19.0-mm (0.75-in) MSA granite at 35.9%, siliceous sand at 33.6% and cement paste at 30.5%

.

5.2 Research Need

HPLC is a novel material that has enormous potential for being used in concrete construction. Nevertheless, there is still lack of understanding on his long-term properties mainly because it has not been extensively investigated.

This investigation does not only present new data on creep and shrinkage of HPLC but also contributes to the understanding on the factors driving such time-dependent deformations.

5.3 Effect of Maturity on Creep

5.3.1 Expressions for Maturity and Creep

5.3.1.1 Maturity dependence on Temperature

It was pointed out [1] that higher curing temperatures not only accelerate strength gain but also lower the maximum attainable strength in the long-term (limiting strength).

A common way to express maturity is by the equivalent age concept. Equivalent age is defined as the age at a constant standard temperature that results in the same relative strength that actual temperature conditions produce. Equation 5.1 shows equivalent age when using Arrhenius dependency on temperature [1]:

$$t_e = \sum_i \exp\left\{\frac{-E}{R \cdot \left(\frac{1}{T(\Delta t_i)} - \frac{1}{T_s}\right)}\right\} \Delta t_i \qquad (5.1)$$

where

t_e: equivalent age (days)

E: apparent activation energy

R: gas constant, 8.3145 J/ g mol/ ^oK (1.9859 Btu/ lb mol/ ^oR)

$T(\Delta t_i)$: temperature during the interval Δt_i (^oK)

Δt_i: period of time at temperature T

T_s: standard temperature

HPC typically contains high volumes of cementitious materials, low water-to-cementitious material ratio, and finer (rapid hardening) cements. All those characteristics are well known to accelerate cement hydration. Fast hydration can lead to significant increase in temperature during the first hours after casting. Moreover, rise in temperature accelerates the hydration of the cementitious materials, thus generating more heat. As a result, this self-feeding reaction yields to an increase in the equivalent age (maturity) of HPC.

Among the models for creep, only CEB-FIP [2, 3] explicitly provides expressions to incorporate the temperature history at the time of loading.

$$t_e = t_{0,T} \cdot \left(\frac{9}{2 + t_{0,T}^{1.2}} + 1 \right)^{\alpha} \geq 0.5 \qquad (5.2)$$

$$t_{0,T} = \sum_i \exp\left\{ \frac{-4000}{273 + T(\Delta t_i)} - 13.65 \right\} \Delta t_i \qquad (5.3)$$

where

t_e: equivalent age (days) to be used in Equations 5.4 to 5.7.

$t_{0,T}$: temperature adjusted age (days)

T: temperature during the interval Δt_i (^oC)

Δt_i: period of time at temperature T (days)

α: parameter depending on the type of cement (-1 for slowly hardening cement, 0 for normal and rapid hardening cement, and 1 for rapid hardening high strength cement).

5.3.1.2 Creep dependence on Maturity

The decrease in creep as age of loading increased was identified by some of the first studies of creep [4]. Several of the most used empirical models for creep include age

of loading among their input variables. They commonly included it as a multiplier to the ultimate creep value. The following expressions have been proposed to account for the influence of age of loading on creep:

ACI-209 [5]

$$F'(t') = \begin{cases} \dfrac{1.25}{t'^{0.118}} \ for\ moist\ curing \\ \dfrac{1.13}{t'^{0.094}} \ for\ steam\ curing \end{cases} \quad (5.4)$$

AASHTO-LRFD [6]

$$F'(t') = \frac{1}{t'^{0.118}} \ for\ moist\ curing \quad (5.5)$$

CEB-FIP [3]

$$F'(t') = \frac{1}{0.1 + t'^{0.20}} \quad (5.6)$$

Sakata, 1993 [7]

$$F'(t') = \frac{1}{\left[\ln(t')\right]^{0.67}} \quad (5.7)$$

where

F′(t′): age-of-concrete-at-loading multiplier

t′: age of concrete at loading (days)

5.3.1.3 Creep Dependency on Compressive Strength

For a given applied stress creep is inversely proportional to the strength at the time of loading [8]. Since water-to-cement ratio is the main factor controlling strength, lower water-to-cement ratio mixtures present lower creep. Therefore, empirical models for creep considered either the strength of concrete at the age of loading or the water-to-

cement ratio of the mixture. The following expressions have been proposed to account for the influence of strength on creep:

AASHTO-LRFD [6]

$$F''(f_c') = \frac{1}{0.67 + \frac{f_c'}{62.07}} \text{ with fc': in MPa} \quad (5.8a)$$

$$F''(f_c') = \frac{1}{0.67 + \frac{f_c'}{9}} \text{ with fc': in ksi} \quad (5.8b)$$

CEB-FIP [3]

$$F''(f_c') = \frac{16.8}{\sqrt{f_c'}} \text{ with fc': in MPa} \quad (5.9a)$$

$$F''(f_c') = \frac{6.398}{\sqrt{f_c'}} \text{ with fc': in ksi} \quad (5.9b)$$

NCHRP [9]

$$F''(f_c') = \frac{34.483}{6.897 + f_c'} \text{ with fc': in MPa} \quad (5.10a)$$

$$F''(f_c') = \frac{5}{1 + f_c'} \text{ with fc': in ksi} \quad (5.10b)$$

where

F″(f_c'): strength-of-concrete multiplier

f_c': compressive strength of concrete

5.3.2 Maturity in the Experimental Program

Eight mixtures were considered for this analysis. Two of them were HP Matrix and Cement Matrix which contained approximately 1000 kg/m^3 (1686 lb/yd^3) of cementitious materials and generated high heat of hydration and therefore high

temperature rises during the first 24 hours. Those two mixtures also contained 39.2% by volume of fine aggregate. The other mixtures were produced with either 63.2% HP Matrix-36.8% coarse aggregate by volume (LWW 65-35, NWA 65-35, STL 65-35) or 81.6% HP Matrix-18.4% coarse aggregate (LWW 35-65, NWA 35-65, STL 35-65). Each combination had approximately 590 and 771 kg/m^3 (995 and 1300 lb/yd^3) of cementitious materials respectively, so they generated different amounts of heat of hydration. Details on the mixture design are provided in Section 3.2.2. Figure 5.1 present a summary of the mixtures used for the maturity analysis and Table 5.2 presents the main properties of the aggregates used in this study.

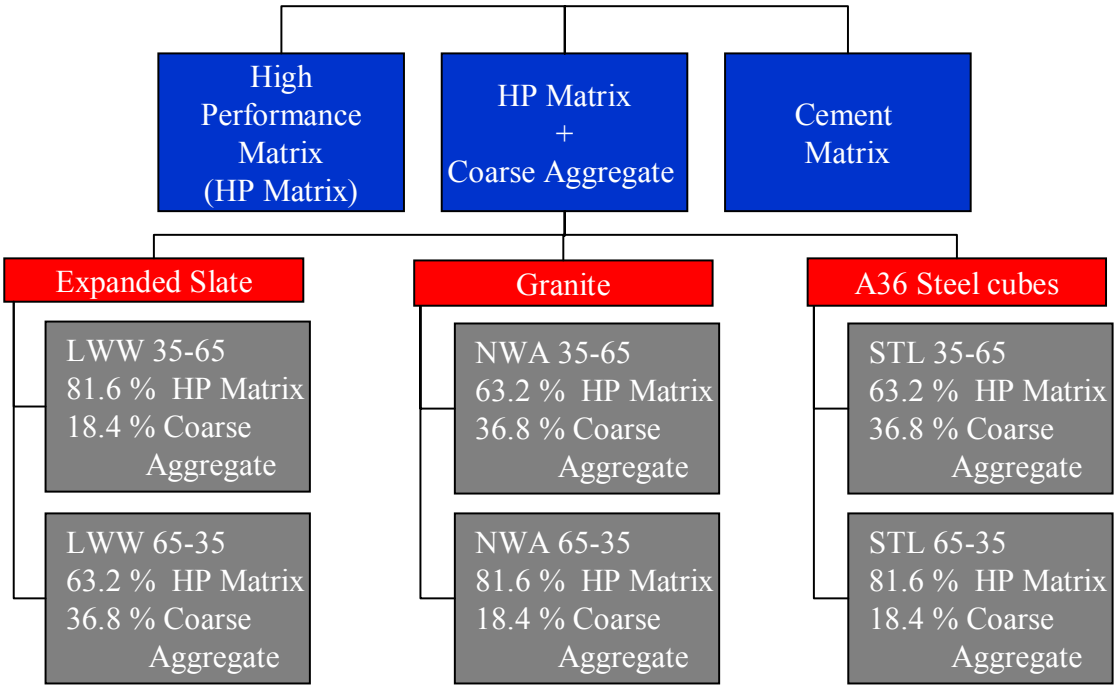

Figure 5.1: Summary of mixtures used in the maturity analysis

Each coarse aggregate had different heat absorption capacities, so mixtures with the same volume of cementitious materials yielded different temperature histories; therefore, they had different maturities at the time of testing.

Table 5.2: Properties of aggregates used in HPC mixtures

	Fine Aggregate	Lightweight aggregate	Normal weight aggregate	Heavy weight aggregate
Description	Siliceous Natural Sand	Rotary Kiln Expanded Slate	Granite	A 36 steel cubes
Maximum size aggregate	2.36 mm (#8 sieve)	12.7 mm (0.5 in)	12.7 mm (0.5 in)	12.7 mm (0.5 in)
Heat Capacity, J /g / ^{o}C (BTU /lb /^{o}F)	0.795 [1] (0.190)	1.10 [2] (0.262)	0.795 [1] (0.190)	0.498 [1] (0.119)
Density kg/m^3(lb/ft^3)	2650 (165.2)	1150 (96.8)	2680 (167.4)	7850 (490.1)
Heat Capacity x Density, J /m^3 / ^{o}C (BTU/ft^3/^{o}F) [1]	2.11 x 10^6 (31.4)	1.27 x 10^6 (25.5)	2.13 x 10^6 (31.8)	3.91 x 10^6 (58.3)
24-hour absorption %	0.1	6 to 8	0.1	0.0
Fineness modulus (FM)	3.15	6.93	7.6	8.0

[1] From tables [10]

[2] assuming 56% of solids (with heat capacity of granite), 38% of porosity filled with air (with heat capacity of air) and 6% of porosity filled with water (with heat capacity of water)

Among the properties shown in Table 5.2, the heat capacity and density are of special interest for the temperature development. Table 5.2 also presents the heat capacity multiplied by density which gives the amount of heat required to raise the temperature of 1 m^3 (1 ft^3) of the aggregate by 1^{o}C (1.8^{o}F). It should be noticed that steel aggregate will require 2.28 times more heat than an equal volume of pre-soaked expanded slate in order to increase its temperature by 1^{o}C (1.8^{o}F). Thus, if the heat

source remains constant (i.e., same volume cementitious materials), it can be concluded that the HPC with steel aggregate will reach considerably lower temperatures during hydration than those reached by the HPC with lightweight aggregate.

All the mixtures were fabricated on three occasions (Stage 1, 2 and 3) each under different ambient conditions (cold, hot and medium). Two batches of each mixture were cast at each stage; and specimens for compressive strength, creep, and shrinkage were obtained. Creep and shrinkage were measured for 120 days under loading and drying.

All specimens were accelerated-cured for 24 hours by placing them in insulated cureboxes in order to maintain the heat generated during the hydration to increase the maturity of the specimens at the time of testing. This curing system, based on procedure C from ASTM C 684 [11], was found to adequately simulate the condition within a precast prestressed concrete member as measured using thermocouples in both the cylinders and in the precast girders. The accelerated-cured applied after mixing in cold, intermediate and hot ambient conditions yielded to a diverse range of maturities of a given mixture tested at a given calendar age.

5.3.3 Temperature History, Compressive Strength and Creep Results

5.3.3.1 Temperature History

Figure 5.2 presents the increase in temperature and maximum temperature reached by each mixture during the first 24 hours after casting. Stage 1, Stage 3 and Stage 2 represent cold, intermediate, and high casting temperatures with average ambient temperatures around 20, 26, and 30 ^{o}C (68, 78.8, and 83 ^{o}F), respectively. Detail experimental data is given in Appendix E.

Figure 5.2 shows that in most cases the highest maximum temperatures were obtained in Stage 2 and the lowest in Stage 1 which were the hot and cold cases, respectively. The dark bars demonstrate that the higher maximum temperatures reached in Stage 2 were due to increase in temperature during hydration rather than just differences in initial ambient temperature. Therefore, the hydration and heat generation rate were affected by the initial ambient temperature, and hydration generated large differences in temperature history within each type of HPC.

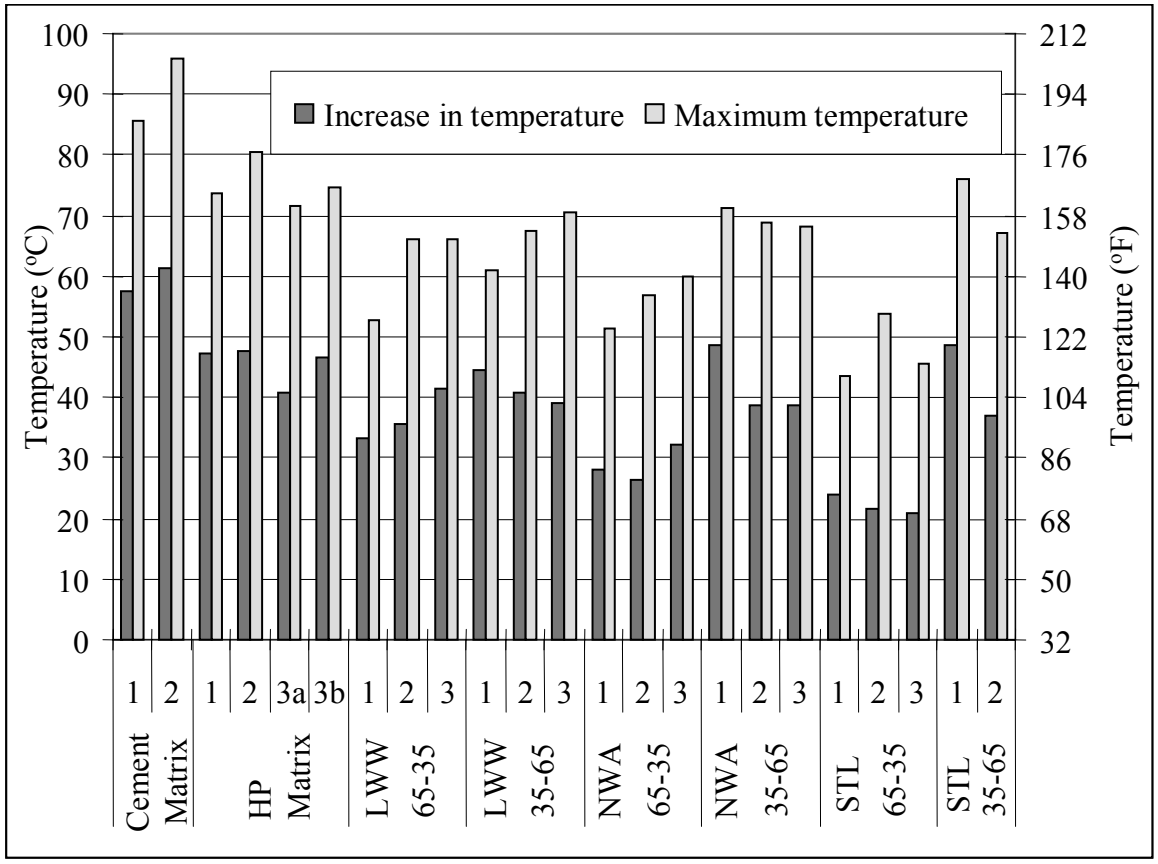

Figure 5.2: Increase in temperature and maximum temperature reached by HPC mixtures during first 24 hours

When comparing different types of HPC, it can be seen that there is a direct relationship between amount of cementitious materials added and temperature

development. Cement Matrix presented the highest temperatures followed by HP matrix, 35-65 mixtures and 65-35 mixtures, independently from the stage considered.

As anticipated, the mixtures with expanded slate (LWW), granite (NWA) and steel aggregate (STL) presented different temperature histories. This was caused by the dissimilar heat capacity of each mixture shown in Table 5.2. For example, if the cementitious materials generated 100,000 J (94.78 BTU) under adiabatic conditions. The resulting increase in temperature of the LWW 65-35, NWA 65-35, and STL 65-35 mixtures would be 33.2, 31.1 and 19 ^{o}C (91.8, 88.0, and 67.5 ^{o}F) even though the three of them had the same amount of cementitious materials. This was supported by the experimental results that shown similar trend in temperature rise.

Figure 5.3 presents the temperature history of the LWW 65-35, NWA 65-35, and STL 65-35 mixtures made during stage 3 (intermediate temperature conditions).

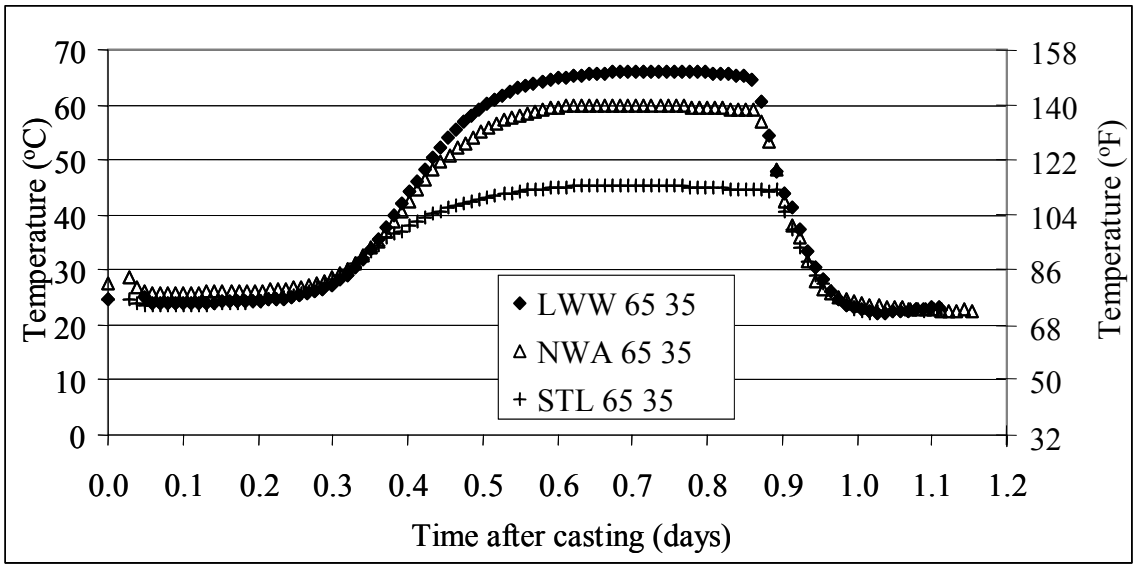

Figure 5.3: Temperature history of the 65-35 mixtures fabricated under intermediate temperature conditions

Figure 5.3 shows that when using lightweight aggregate, the heat generated by the cementitious reaction causes higher temperatures within the first 24 hours. The heavier the aggregate, and therefore, the higher the mass included in the mixture, the lower the temperature profile during the first 24 hours. This means that those mixtures with lightweight aggregate will have a higher maturity at the time of testing than those made with granite or steel. Table 5.3 presents the equivalent age as calculated from the temperature history of each mixture and stage using Equations 5.2 and 5.3 and assuming rapid hardening cement (Type III).

Table 5.3: Equivalent age at of HPC mixtures the time of testing

Mixture and stage		Equivalent age (days)	
		24 hours	28 days
Cement Matrix	1	6.35	36.91
	2	8.57	39.09
HP matrix	1	5.12	35.59
	2	6.95	37.61
	3a	4.65	35.16
	3b	4.81	35.38
LWW 65-35	1	2.19	32.65
	2	4.72	35.38
	3	3.63	34.17
LWW 35-65	1	2.67	33.15
	2	3.99	34.59
	3	3.98	34.53
NWA 65-35	1	2.05	32.58
	2	3.51	34.50
	3	3.23	33.74
NWA 35-65	1	3.11	33.84
	2	4.94	35.59
	3	4.57	35.14
STL 65-35	1	1.79	32.18
	2	3.33	33.91
	3	2.24	32.21
STL 35-65	1	3.38	33.73
	2	4.81	35.44

Setting time was not measured in this medium-scale study, but results from the small-scale study (see Section G.4, Appendix G) revealed showed no direct relationship between generated heat and setting. Therefore, considering setting time in the equivalent age computations would not change the comparisons and conclusions obtained in this chapter.

Equivalent age was computed after 24 hours and 28 days after casting. The temperature between 24 hours and 28 days was taken as 22.8 ^{o}C (73^{o}F) which was the average temperature in the fog room. Figure 5.4 presents the average equivalent age grouped by mixture in the Y-axis versus the calendar age in the X-axis. The diagonal dashed line represents the equivalence between equivalent and calendar day which would occur if the samples remain at 20.0^{o}C (68.1^{o}F) all the time.

Twenty four hours after casting, the equivalent ages ranged between 1.79 for STL 65-35 to 8.57 days for Cement Matrix.

Figure 5.4 shows that all mixtures had equivalent ages at least one day greater than calendar age.

The average equivalent ages were 3.33, 3.87, and 5.10 days for the cold, intermediate, and hot mixing temperature conditions. The average equivalent age grouped by type of mixture was 3.51, 2.93, and 2.45 days for LWW 65-35, NWA 65-35, STL 65-35, respectively, and 3.55, 4.20, and 4.09 days for LWW 35-65, NWA 35-65, and STL 35-65, respectively.

The difference in maturity at early ages was proportionally larger than that obtained after 28 days because the temperature history after demolding was the same for all mixtures and stages.

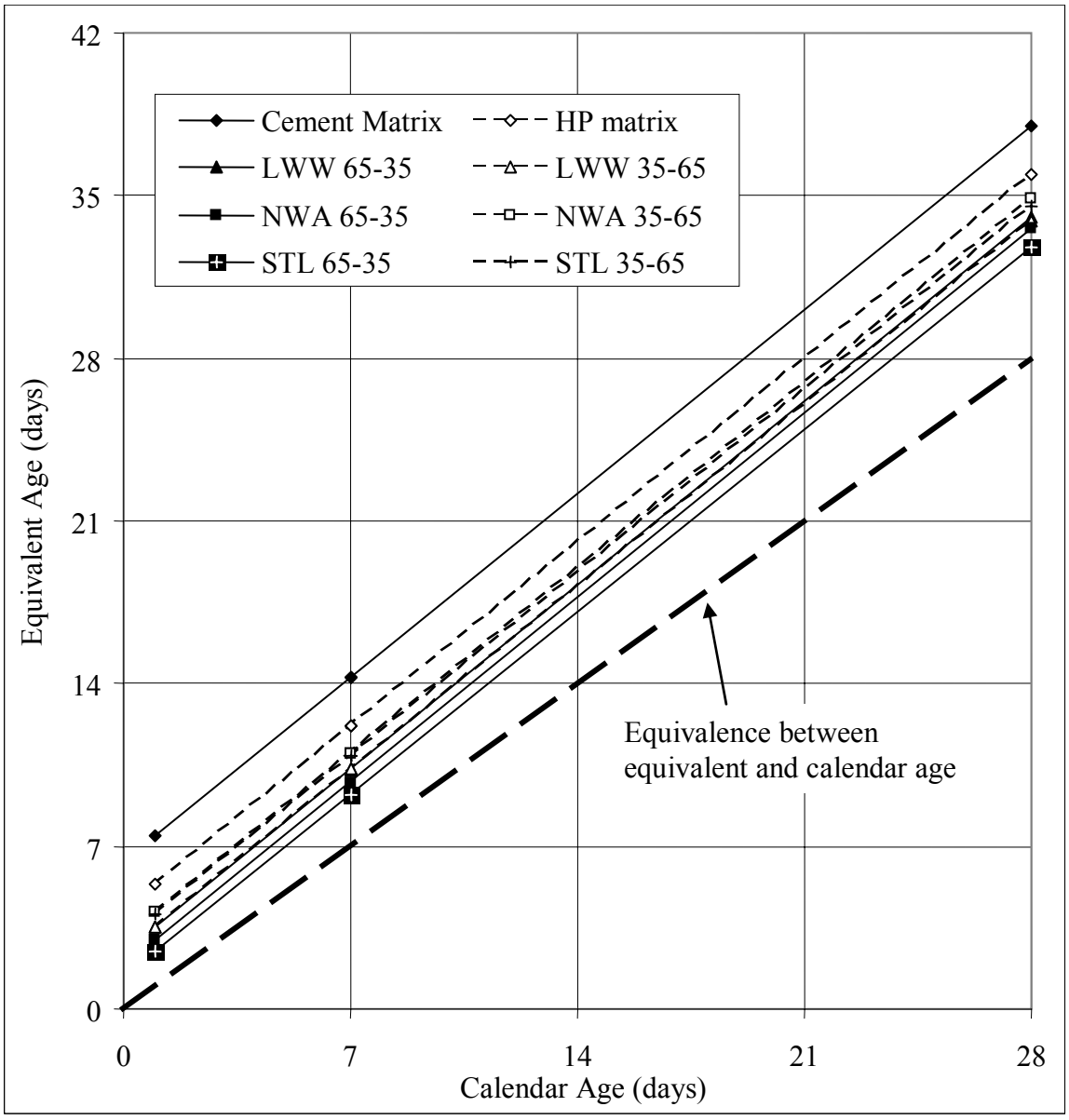

Figure 5.4: Equivalent and calendar age versus calendar age grouped by type of mixture

5.3.3.2 Compressive Strength

Figure 5.5 presents the compressive strength results of HP Matrix and Cement Matrix. The gray bars present results grouped by calendar age while the white bars give the results in terms of maturity in days.

The average standard deviation decreased from 6.1 to 4.0 MPa (880 to 580 psi) when maturity is used instead of calendar age. This was expected because when compressive strength is analyzed versus calendar age, data from batches with very different temperature history are considered the same. That difference is taken into account when using maturity instead of calendar age and the variability decreases.

Similar conclusions can be drawn from the compressive strength results from the Cement Matrix. Its standard deviation decreased from 4.7 to 3.5 MPa (680 to 510 psi).

Compressive strength 24 hours after casting was 95.7 and 113.2 MPa (13,875 and 16,420 psi), for HP Matrix and Cement Matrix, respectively. After 56 days, those same mixtures had a compressive strength of 109.3 and 122.3 MPa (15,845 and 17,735 psi), respectively. Thus, the difference between the compressive strength decreased from 17.5 MPa (2535 psi) at one day to 13.0 MPa (1885 psi) at 56 days. After one year, the compressive strength of Cement Matrix was only 4.8 MPa (695 psi) higher than that of HP Matrix which represents 3.8% of difference. The different rate of strength gain was a consequence of the use of 15% by weight of Class F fly ash in HP Matrix which reacts slower than Type III cement.

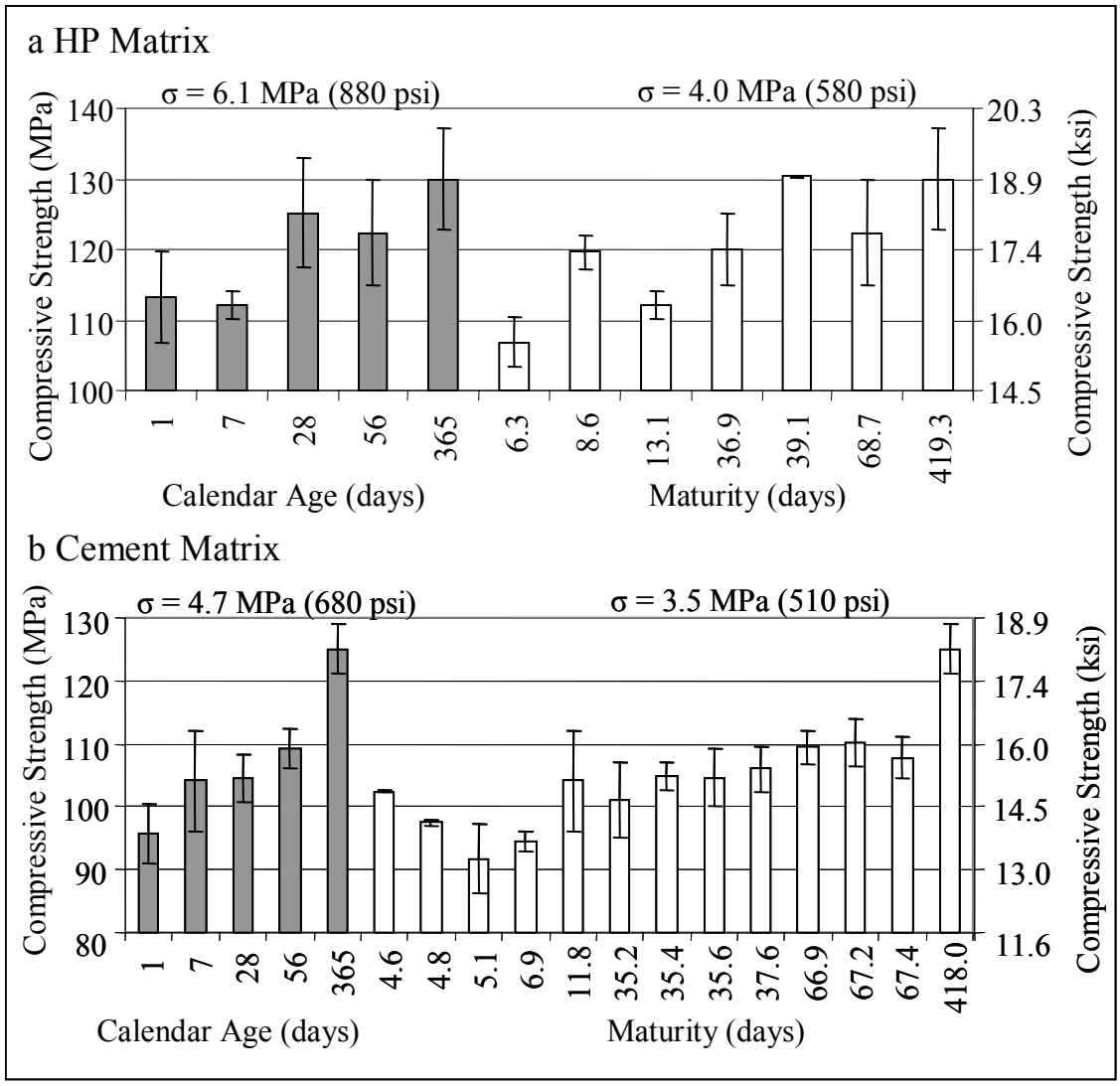

Figure 5.5: Compressive strength versus calendar age and maturity at testing, (a) HP Matrix, (b) Cement Matrix

Figure 5.6 presents compressive strength (Y –axis) versus both calendar age (gray bars) and maturity (white bars) for the three 35-65 mixtures. Part (a), (b), and (c) correspond to expanded slate (LWW), granite (NWA), and steel (STL), respectively.

Standard deviation of compressive strength for LWW 35-65 decreased from 7.5 to 4.4 MPa (1090 to 640 psi) when using maturity instead of calendar age; that is, a 41% reduction in variability due to temperature history. The compressive strength standard

deviation decreased 47 and 43% for the NWA 35-65 and STL 35-65 HPC respectively. The three 35-65 HPC mixtures decreased its standard deviation by more than the HP Matrix and Cement Matrix which presented a 34 and 25% decrease, respectively.

Average compressive strength after 24 hours was 80.1, 96.1, and 58.3 MPa (11,615, 13,930, and 8450 psi) for LWW, NWA and STL mixtures while HP Matrix had 95.7 MPa (13,875 psi). After one year, compressive strength of the LWW, NWA and STL mixtures was 95.0, 120.9, and 78.5 MPa (13,770, 17,540, and 11,385 psi), respectively.

Figure 5.7 presents the same type of comparison shown in Figures 5.5 and 5.6 for the 65-35 HPCs made with expanded slate (6a), granite (6b) and steel aggregate (6c).

As concluded for the others HPCs, the use of maturity decreased the compressive strength variability importantly for the 65-35 mixtures. For instance, NWA 65-35 and STL 65-35 reduced their standard deviation by 42 and 48% when including time temperature history in the analysis. LWW 65-35, on the other hand showed only a 5% reduction due to an already low initial standard deviation.

LWW 65-35 had an average compressive strength after one day and one year of casting of 73.5 and 87.5 MPa (10,655 and 12,690 psi). NWA 65-35 compressive strength after one day and one year was 90.5 and 122.2 MPa (13,130 and 17,715 psi), respectively. Finally, STL 65-35 had average compressive strength of 56.2 MPa (8150 psi) after one day which increased to 71.9 MPa (10,410 psi) after year. Considering all eight mixtures the standard deviation decreased from an average of 5.6 MPa (810 psi) to 3.5 MPa (510 psi) totaling a 37.5% reduction when maturity is used.

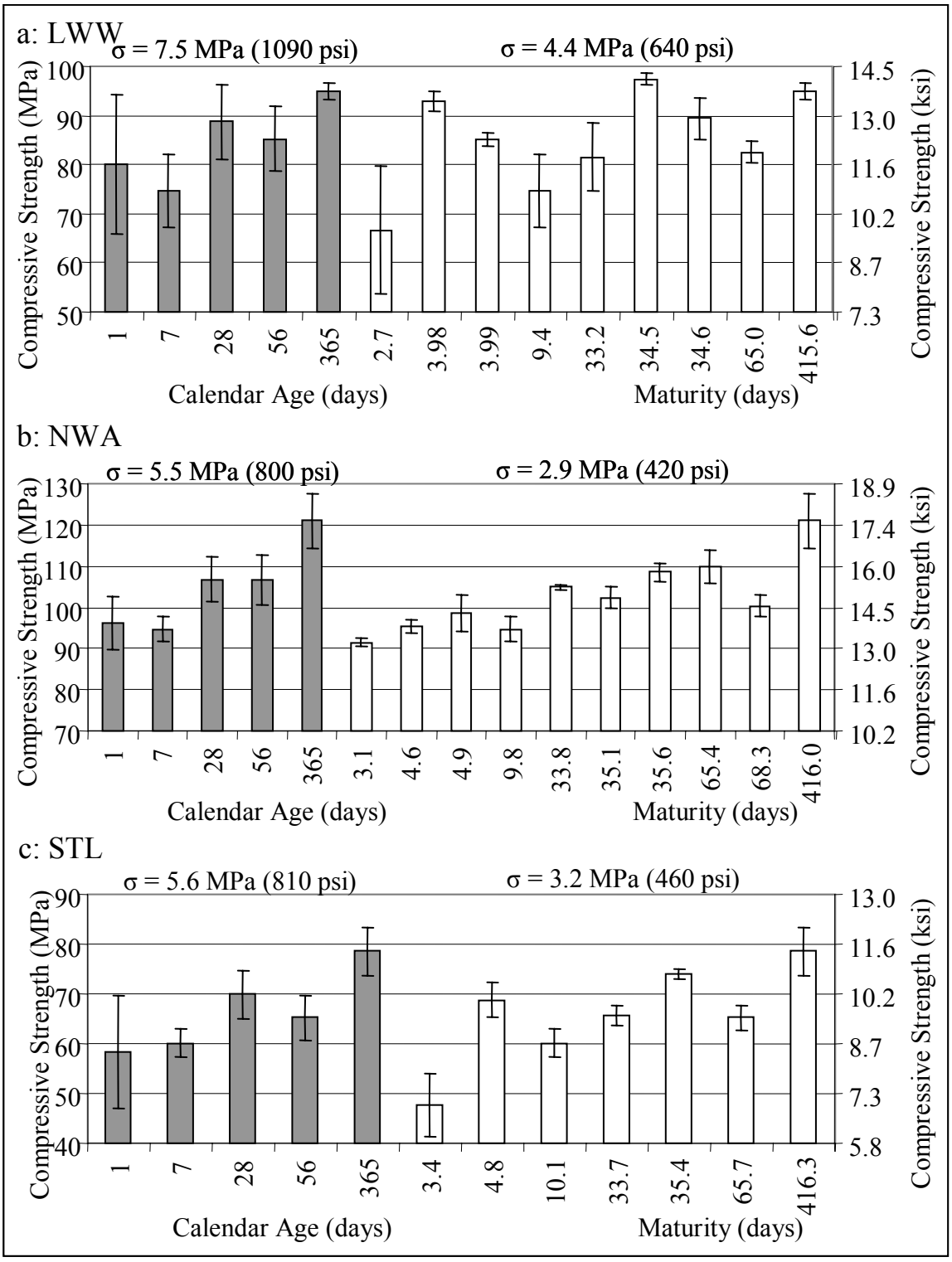

Figure 5.6: Compressive strength versus calendar age and maturity at testing, (a) LWW 35-65, (b) NWA 35-65, (c) STL 35-65

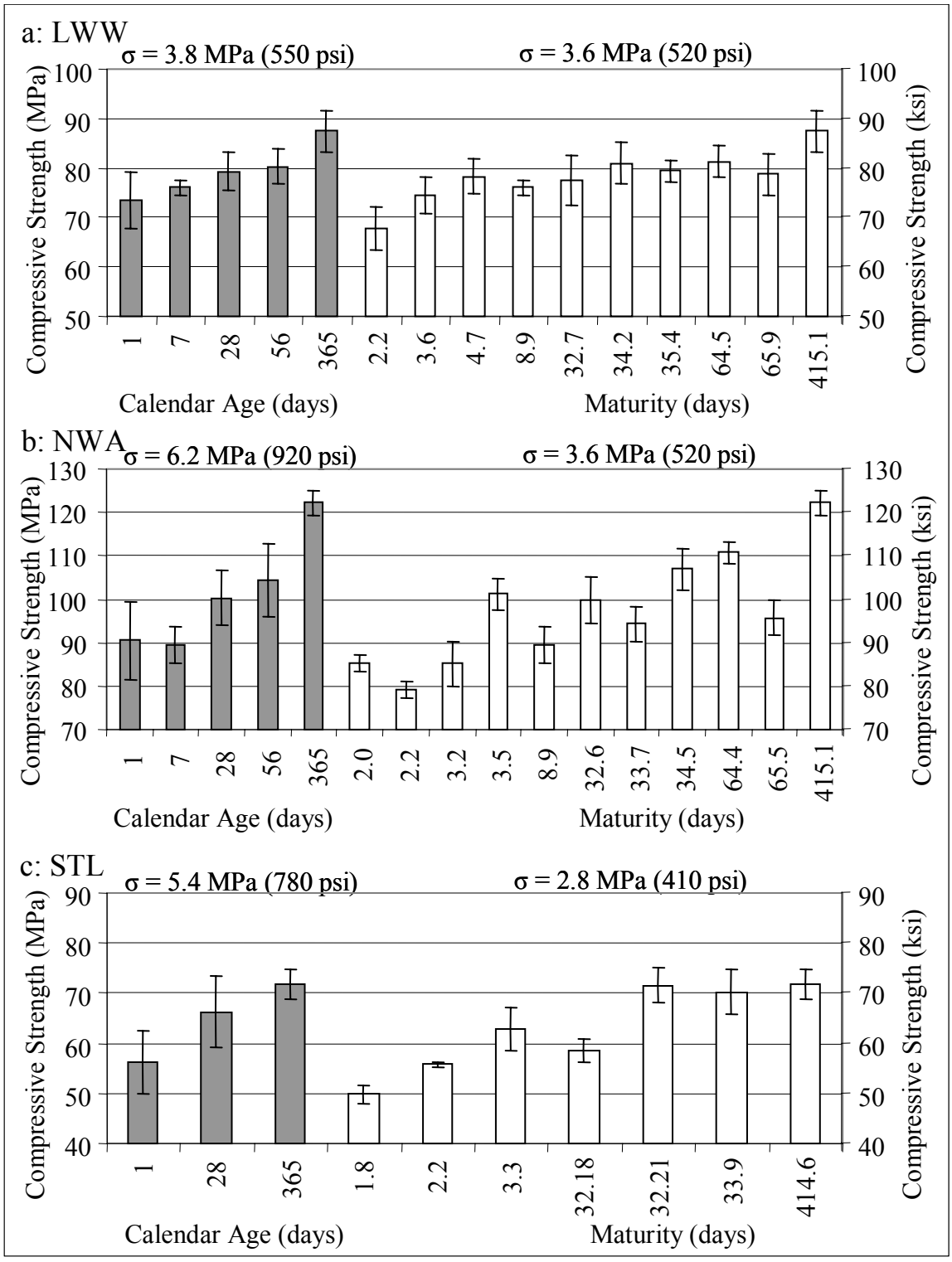

Figure 5.7: Compressive strength versus calendar age and maturity at testing, (a) LWW 65-35, (b) NWA 65-35, (c) STL 65-35

In addition, an analysis of variance (ANOVA) was also performed. Since there were two batches per stage in most of the mixtures, the ANOVA was used to compare the variability between batches (without differences in maturity) with the variability among stages. ANOVA revealed that in six out of the eight mixtures, the variance among stages was more significant difference than that between batches. Moreover, in most of the mixtures equivalent age explained proportionally more variance of strength than calendar age alone.

5.3.3.3 Creep Adjusted by Maturity

To analyze the effect of maturity at the time of loading in creep, 120-day specific creep separated by stage is shown in Table 5.4. The results are grouped by testing condition: loaded 24 hours and 28 days after casting. The average specific creep for all stages of a mixture is also included.

Table 5.4 shows significant variation in creep between stages for any given HPC mixture. For instance, Cement Matrix had a lower average specific creep than that of HP Matrix; nevertheless, the HP Matrix had the lowest value when considering each stage separately.

The coefficient of variation of creep between two specimens from the same batch was 4% or lower and between two specimens from different batches (from the same stage) was 9% or lower, so the experimental error for mixing and testing was acceptable according to the ASTM requirements [12]. Contrarily, the large variance among stages indicates the existence of another factor, besides experimental variability, that is affecting creep.

Table 5.4: Specific creep of HPC mixtures after 120 days under loading and drying, in με/MPa (με/psi)

Mixture and stage		Calendar age at loading			
		24 hours		28 days	
		με/MPa	με/psi	με/MPa	με/psi
Cement Matrix	1	25.5	0.176		
	2	20.4	0.141		
	Avg.	23.0	0.159		
HP matrix	1	17.8	0.123	23.1	0.159
	2	21.0	0.145	15.2	0.105
	3b	31.0	0.214		
	Avg.	23.3	0.161	19.1	0.132
LWW 65-35	1	22.3	0.154	15.5	0.107
	2	18.0	0.124	11.2	0.077
	3	15.2	0.105		
	Avg.	18.5	0.128	13.3	0.092
LWW 35-65	1	28.3	0.195	17.1	0.118
	2	22.0	0.152	14.2	0.098
	3	18.9	0.13		
	Avg.	23.1	0.159	15.7	0.108
NWA 65-35	1	26.0	0.179	11.6	0.08
	2	15.8	0.109	13.9	0.096
	3	17.3	0.119		
	Avg.	19.7	0.136	12.8	0.088
NWA 35-65	1	37.6	0.259	15.7	0.108
	2	13.9	0.096	14.2	0.098
	3	12.5	0.086		
	Avg.	21.3	0.147	14.9	0.103
STL 65-35	1	27.7	0.191	14.8	0.102
	2	14.4	0.099	8.7	0.06
	3	25.4	0.175		
	Avg.	22.5	0.155	11.7	0.081
STL 35-65	1	24.5	0.169	25.5	0.176
	2	19.1	0.132	14.9	0.103
	Avg.	21.8	0.151	20.2	0.140

Figure 5.8 presents the relationship between 120-day specific creep and the maturity at the time of loading, when the specimens were loaded 24 hours after casting. The X-axis present maturity as obtained using Equations 5.2 and 5.3, and Y-axis shows specific creep after 120 days under loading and drying.

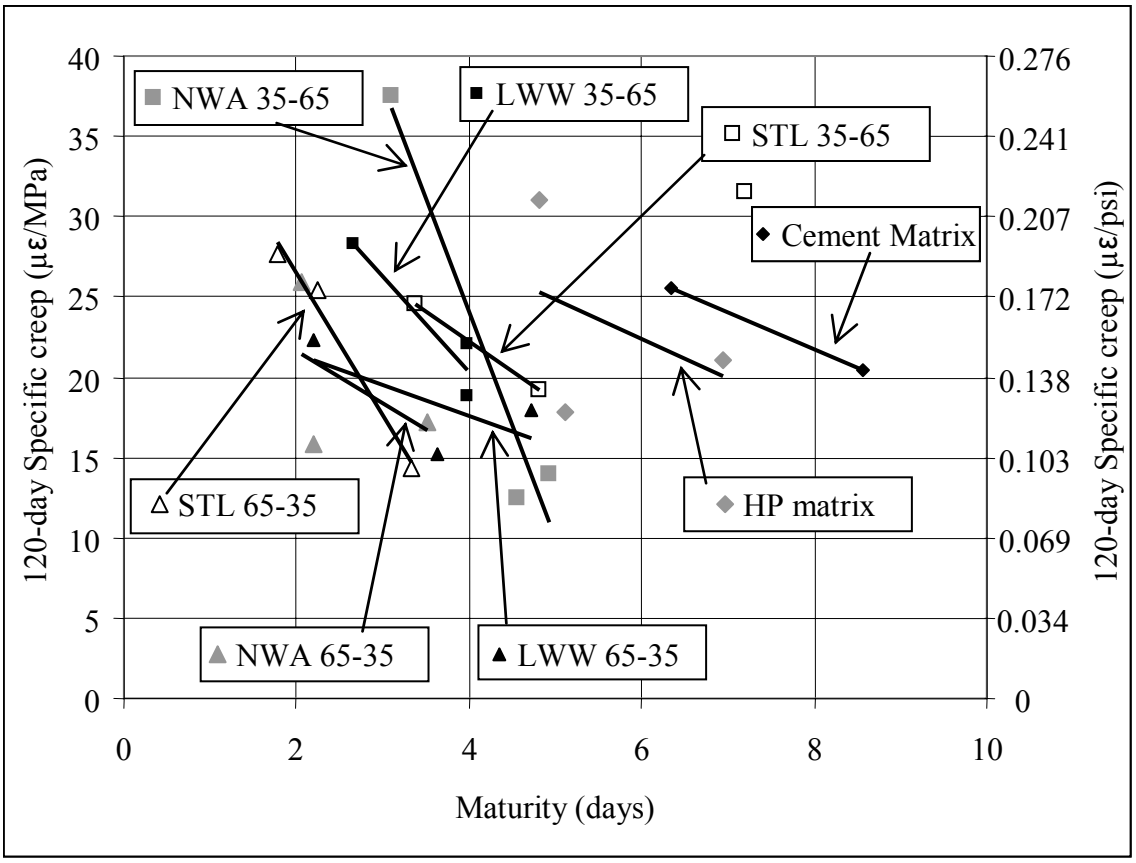

Figure 5.8: Relationship between specific creep after 120 days under loading and drying and equivalent age of loading for specimens loaded 24 hours after casting

Linear regression lines were included in Figure 5.8 in order to represent the interaction between the two variables for each of the eight mixtures. It should be noticed that all mixtures presented negative slope in the regression lines meaning that creep decreased when maturity increased. With the exception of NWA 35-65, which presented the most pronounced slope, all mixtures had slopes between -2 and -9 με/MPa (-0.014 and -0.062 με/psi) per maturity day. The average slope was -5.81 με/MPa (-0.04 με/psi) per maturity day. This decrease represents approximately 20 to 30% of the 120-day specific creep per each additional day of maturity before loading.

Figure 5.9 presents the relationship between maturity at loading and 120-day specific creep when specimens were loaded 28 days after casting.

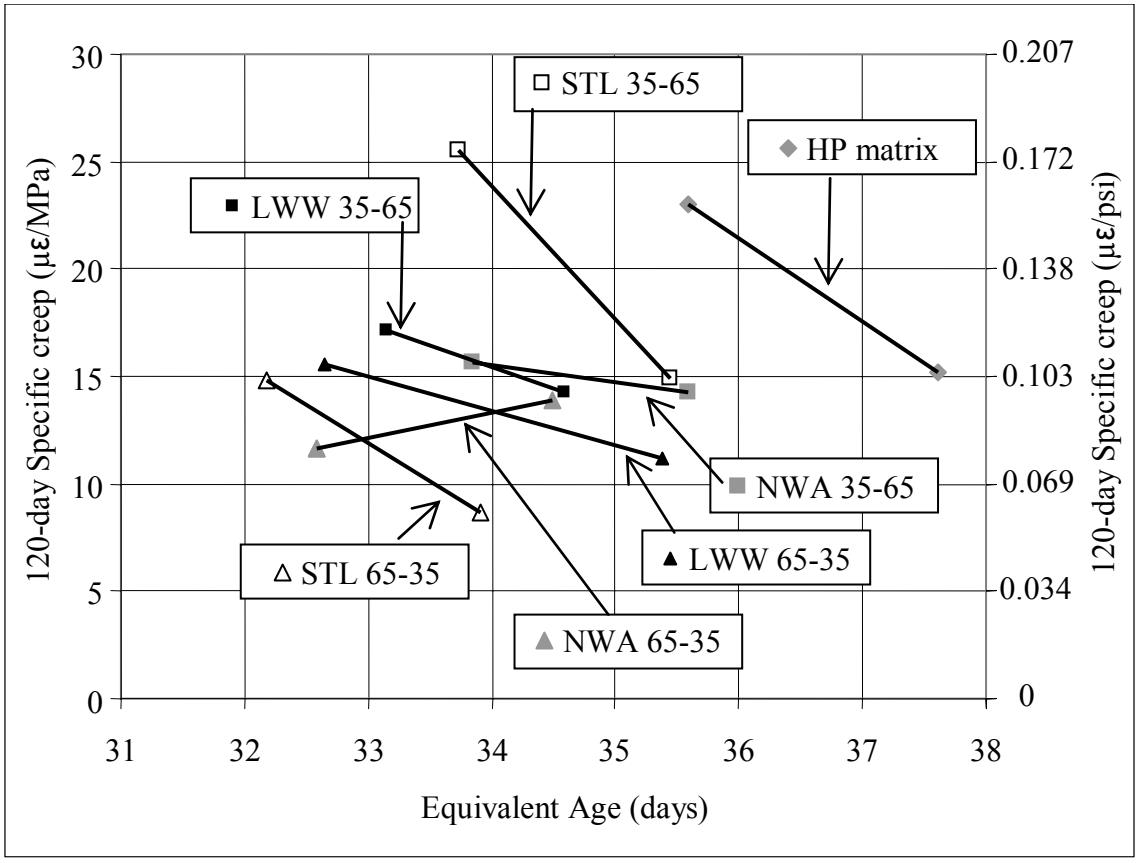

Figure 5.9: Relationship between specific creep after 120 days under loading and drying and equivalent age of loading for specimens loaded 28 days after casting

Figure 5.9 shows the same tendency seen for early age loading. That is, for each HPC mixture, 120-day specific creep decreased as the maturity at loading increased. With the only exception of NWA 65-35, all mixtures presented an inversely proportional relationship between specific creep and maturity. The average slope was -2.40 με/MPa (-0.017 με/psi) per maturity day meaning that 120-day specific creep decreased about that amount for each additional maturity day. This average slope represented only 41% of

that obtained at early age loading (Figure 5.8). The decrease in the slope absolute value denotes less sensitivity of creep to maturity as time at start of testing increased.

This strong relationship between creep and maturity implied that the average specific creep presented in Table 5.4 were not comparable because the maturity of each mixture at the time of loading varied importantly. Mixtures with more cementitious materials had higher equivalent ages at the time of testing as shown in Figure 5.4. Also, mixture with lower weight aggregate also had higher maturity than their counterparts at the time of testing as shown in Figure 5.3.

Therefore, the creep data of each mixture needs to be adjusted to a standard maturity at the time of loading in order to be comparable. Consequently, the next step in the analysis was to test the expressions proposed in the literature against the experimental data which included a variety of maturities and compressive strength for each of the eight HPC mixtures.

Since maturity affects compressive strength and creep, but compressive strength also affects creep, the analysis considered both, the expressions between maturity at loading and creep (Equations 5.4 to 5.7), and the expressions relating compressive strength and creep (Equations 5.8 to 5.10). All those relationships were compared against the experimental data to obtain the most accurate for these HPC. The performance of any particular adjustment was tested against the following criterion: after adjustment, the coefficient of variance (COV) of creep considering specimens from different stages must be similar to the COV obtained between specimens from two batches of the same stage.

The adjustment procedure consisted on multiplying the experimental creep of a given stage by the quotient between the expressions evaluated with an average maturity

and average strength (considering all three stages) and the same expressions evaluated with the maturity and strength of the particular stage. This quotient between "expressions at average" and "expressions at particular stage" represents the factor for adjusting creep from a particular stage conditions to average conditions; for example:

Let Equation 5.11 and 5.12 be any of the creep-maturity and creep-strength expressions shown previously:

$$F'(t') \tag{5.11}$$

$$F''(f_c') \tag{5.12}$$

where

F′(t′): age-of-concrete-at-loading multiplier (Equations 5.4 to 5.7)

t′: maturity of concrete at loading (days)

F″(f_c'): strength-of-concrete multiplier (Equations 5.8 to 5.10)

f_c': compressive strength of concrete

The average maturity and average compressive strength of a given mixture would be:

$$t'_{avg} = \sum_{j}^{n} \frac{t_j'}{n} \tag{5.13}$$

$$f'_{c\,avg.} = \sum_{j}^{n} \frac{f_c'_j}{n} \tag{5.14}$$

t_j': maturity of stage j at loading

$f_c'_j$: compressive strength of stage j

n: number of stages

The adjusted creep values for stage j (either at early age loading or late loading) would be:

$$creep_{ADJ} = creep_j \cdot \frac{F'(t'_{avg})}{F'(t_j')} \cdot \frac{F''(f'_{c\,avg.})}{F''(f'_{c\,j})} \quad (5.15)$$

where

$creep_{ADJ}$: adjusted creep

$creep_j$: as-measured creep from stage j (j = 1, 2, 3)

$F'(t'_{avg})$: age-of-concrete-at-loading multiplier evaluated with average maturity

$F'(t_j')$: age-of-concrete-at-loading multiplier evaluated with maturity of stage j

$F''(f_c'_{avg.})$: strength-of-concrete multiplier evaluated with average compressive strength

$F''(f_c'_j)$: strength-of-concrete multiplier evaluated with compressive strength of stage j

All adjustments and combination of adjustments were considered and the was calculated for every combination. Among the alternatives for adjustment (Equations 5.4 through 5.10), the following two were found to yield the lower COV considering all eight mixtures and loading times of 24 hours and 28 calendar days after casting.

Equivalent age at loading adjustment (based on Equation 5.7 [7])

$$F'(t') = \frac{1}{[\ln(t')]} \quad (5.16)$$

where

$F'(t')$: age-of-concrete-at-loading multiplier

t': maturity of concrete at loading (days)

Therefore, creep of HPC was found to be inversely proportional to the natural logarithm of its equivalent age at the time of loading.

Compressive strength adjustment [9]

$$F''(f_c') = \frac{34.483}{6.897 + f_c'} \text{ with } f_c' \text{: in MPa} \quad (5.10a)$$

$$F''(f_c') = \frac{5}{1 + f_c'} \text{ with } f_c' \text{: in ksi} \quad (5.10b)$$

where

F″(f_c'): strength-of-concrete multiplier

f_c': compressive strength of concrete at 28 days

Thus, creep of HPC was found to be inversely proportional to 28-day compressive strength.

Figures 5.10, 5.11 and 5.12 present creep before and after adjustment for Cement Matrix, NWA 65-35 and LWW 65-35, respectively when load was applied 24 hours after casting. The X-axis shows time under loading and drying, and the Y-axis is specific creep. The plot on the left presents "as measured" creep while the one on the right shows creep after adjustment using Equations 5.15, 5.16 and 5.10. The curves correspond to individual specimens from particular stages (stage 1, 2, or 3) and batches (B1 or B2).

Since creep data were adjusted to an average equivalent age and strength, the average creep considering all stages did not change considerably for any given mixture. Creep values from lower-strength / lower-maturity stages were reduced while creep values from higher-strength / higher maturity stages were increased.

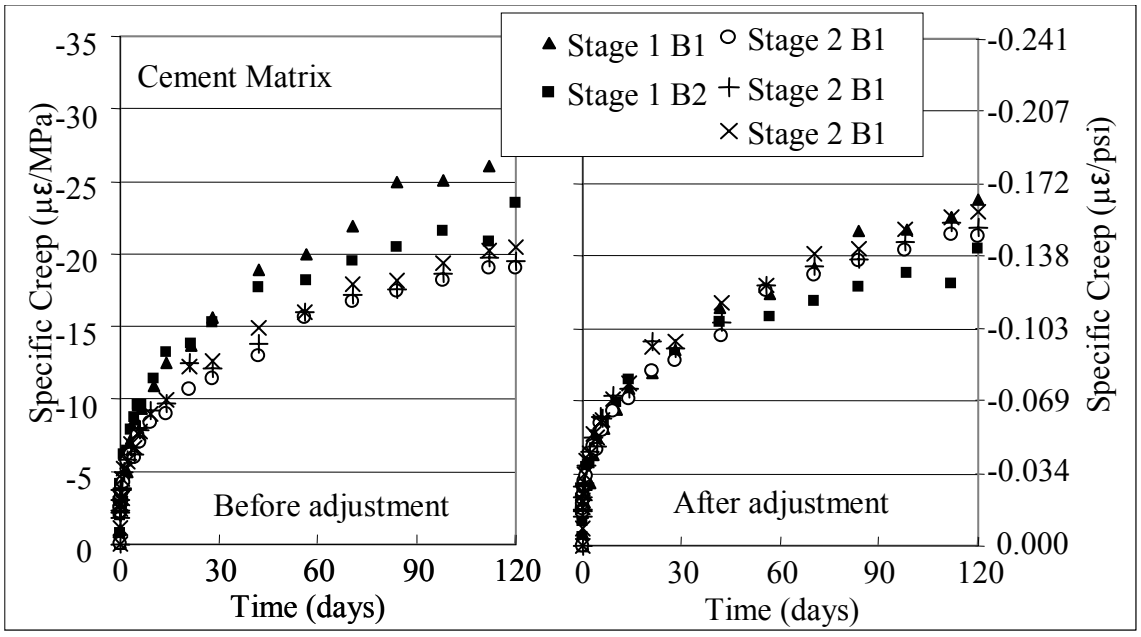

Figure 5.10: Specific creep of Cement Matrix, when loaded at early age, before and after adjustment by maturity and strength

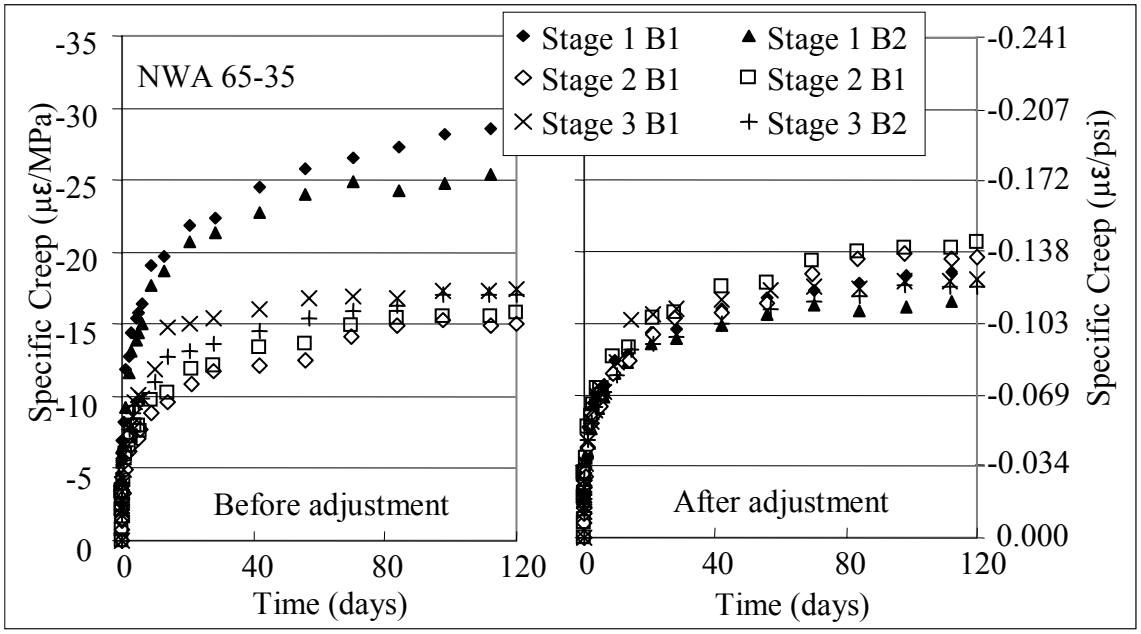

Figure 5.11: Specific creep of NWA 65-35, when loaded at early age, before and after adjustment by maturity and strength

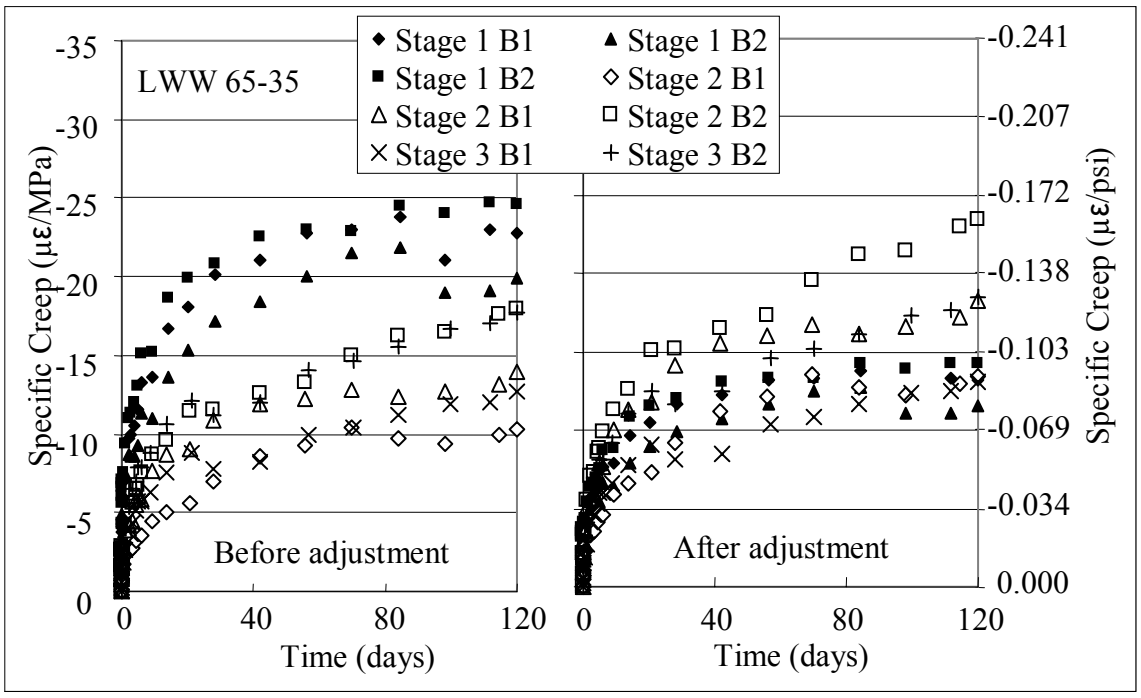

Figure 5.12: Specific creep of LWW 65-35, when loaded at early age, before and after adjustment by maturity and strength

Figures 5.10 and 5.11 present a great improvement due to the adjustment procedure. Variability among stages was reduced to similar level than that between batches of the same stage. In both cases, creep data from Stage 1 (cold) was reduced and from Stage 2 (hot) and Stage 3 (intermediate) was increased. Figure 5.12 also shows good improvement in variability for the LWW 65-35 mixture; nevertheless, the adjustment seemed to be more than required because Stage 1 went from having the highest creep before adjustment to one of the lower creep after adjustment. Stage 2, which had intermediate creep before adjustment, presented the highest creep after adjustment. The range between maximum and minimum 120-day creep decreased little after adjustment for LWW 65-35 loaded 24 hours after casting. Nevertheless, the

adjustment decreased variability importantly between 0 and 80 days under loading and drying.

Figure 5.13 shows the creep adjustment applied to LWW 35-65 when loaded 28 calendar days after casting. Again, the plot on the left shows specific creep as measured before adjustment and the plot on the right after adjustment. Time under loading and drying is shown on the X-axis.

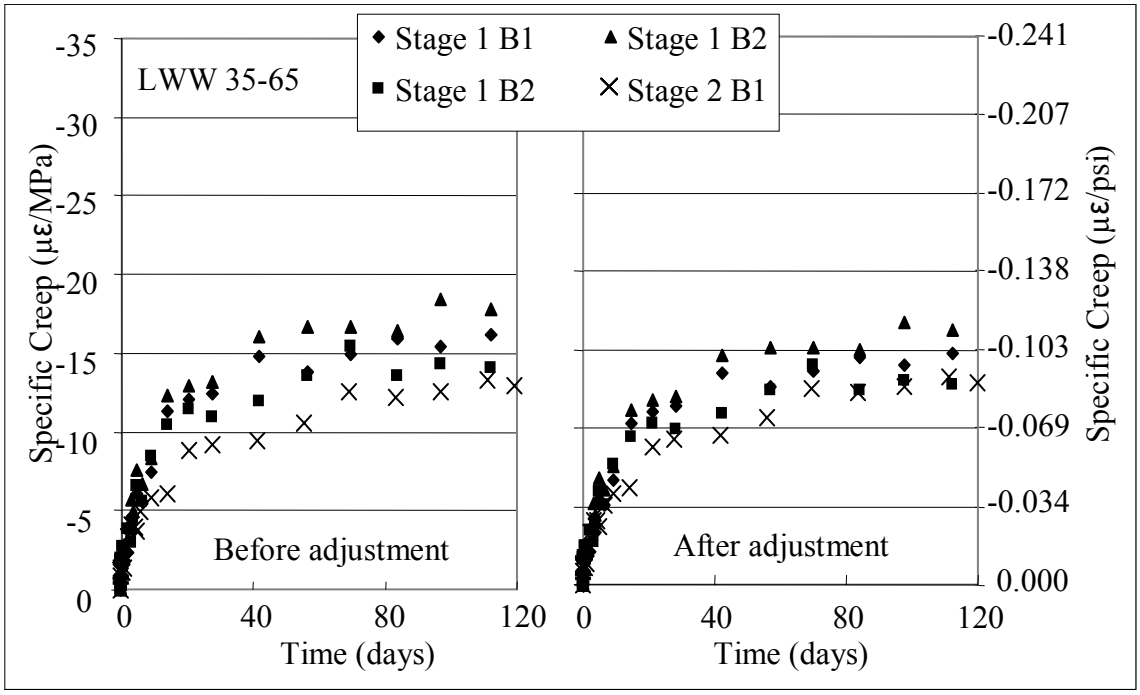

Figure 5.13: Specific creep of LWW 35-65, when loaded 28 days after casting, before and after adjustment by maturity and strength

Figure 5.13 shows the beneficial effect of adjusting creep for maturity and compressive strength. As seen for early age of loading, creep of Stage 2 , which had the greater maturity and compressive strength at the time of loading, was lower than that of Stage 1. Even though differences between stages were not as large as those seen in Figures 5.10, 5.11, and 5.12, the proposed adjustment reduced variability of creep when loaded after 28 calendar days after casting.

Once the best expressions to adjust creep of HPC were determined, the creep data in Table 5.4 was adjusted to a unique maturity at the time of loading in order to establish comparisons among creep measured on the eight HPC mixtures. Creep was not adjusted by compressive strength because that was considered to be an inherent difference between HPC mixtures.

Figure 5.14 presents the maturity-adjusted average specific creep after 120 day under loading and drying. Creep data from testing at 24 hours after casting was adjusted to a maturity of 4.2 days which was the average maturity of loading considering all mixtures and stages. Likewise, creep from testing at 28 calendar days after casting was adjusted to an equivalent age of 34.8 days. Data shown in Figure 5.14 is entirely comparable since it was adjusted for the differences in maturity at the time of loading.

As expected, Cement Matrix and HP Matrix presented the two highest creep values because they had the lowest amount of aggregate (only fine aggregate) and the highest volume of cementitious paste. HP Matrix presented 15% less creep than Cement Matrix due to the use of silica fume and fly ash. This agrees with the results reported previously [13, 14].

For all cases, 120-day specific creep decreased when the time of loading increased from 24 hours to 28 calendar days after casting.

Creep of the 35-65 mixtures, which considered 18.4% of coarse aggregate by volume, was on average 72% of that measured on HP Matrix with no coarse aggregate. Similarly, creep of the 65-35 mixtures, which had 36.8% of coarse aggregate by volume, was 50% of that measured on HP Matrix. This proportional reduction on creep with

increasing aggregate volume strongly agrees with the aggregate restraining effect which predicts creep reduction with an increase in aggregate volume [15].

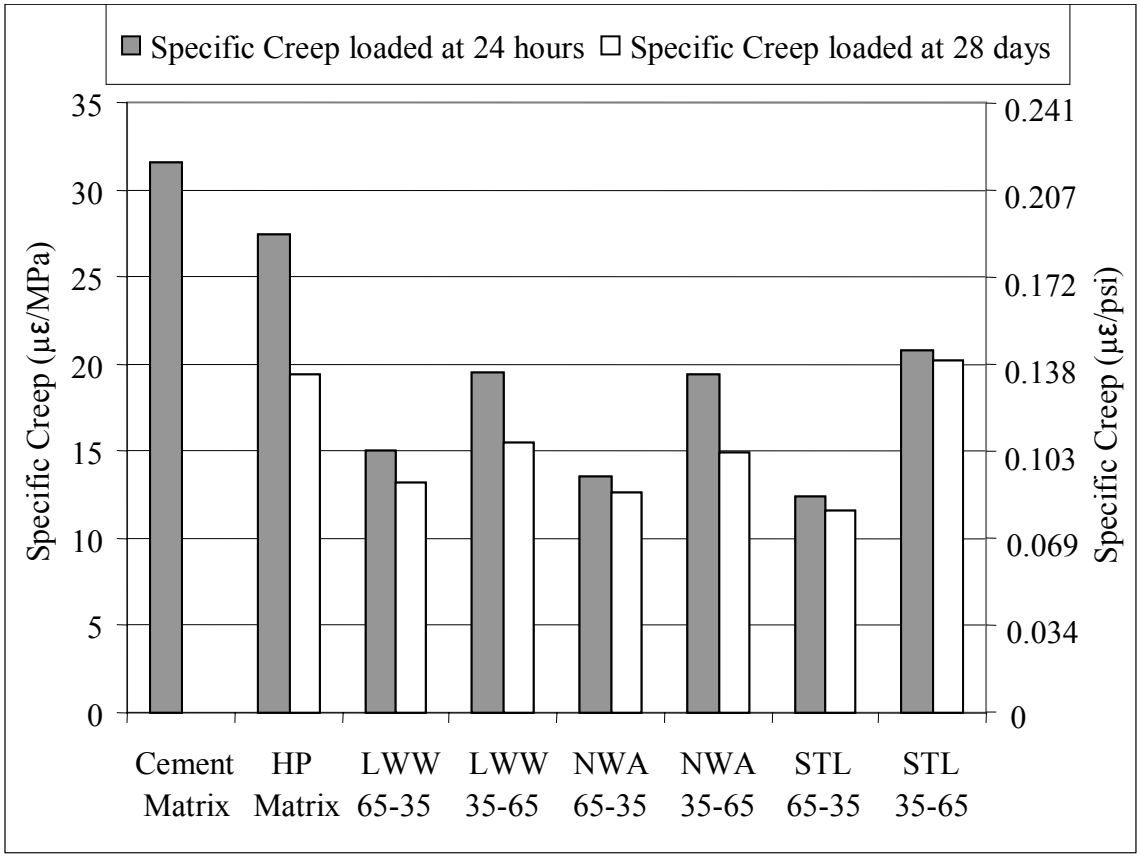

Figure 5.14: Adjusted average specific creep of mixtures after 120 days under loading and drying

On the other hand, comparison of creep among LWW, NWA and STL showed no significant changes even though the stiffness of the aggregates were very different. This result shows that aggregate restraining effect model could not adequately predict such behavior.

It was believed that the low stiffness of the expanded slate was counteracted by the beneficial effect afforded by the internally stored water in the presoaked aggregate

[16-18] and/or by improvement in the interfacial transition zone (ITZ) [19, 20] between lightweight concrete and paste.

It should be noticed that the adjustment for maturity at the time of loading was very useful to establish comparisons between mixtures with different cementitious material contents. Those mixtures presented considerably different maturities due to heat of hydration that needed to be considered. On the other hand, such adjustment might have hidden inherent differences between mixtures; for instance, LWW 65-35 and STL 65-35 had an average maturity of 3.51 and 2.45 days after 24 hours, even though they used the same amount of cementitious materials. As shown in Figures 5.2, 5.3, and 5.4, the lower the weight of the aggregate, the higher the temperature rise and maturity. Thus, LWW mixtures presented an intrinsic advantage over NWA and STL mixtures that is not shown in Figure 5.14.

5.4 Effect of Aggregate on Mechanical Properties, Creep and Shrinkage of High Performance Concrete

The experimental program allowed for comparison of various properties of HP Matrix and those of mixtures produced with different proportions of such HP Matrix and LWW, NWA, and STL aggregates. The aggregate effect on compressive strength, elastic modulus, creep and shrinkage was assessed by comparing the measured properties with the estimate using HP Matrix properties, aggregate. properties, and two-phase models.

Table 5.5 presents the properties of the two phases used in this study: HP matrix and coarse aggregate.

Table 5.5: Properties of cementitious matrix and aggregates used in HPC mixtures

	HP Matrix	Lightweight aggregate	Normal weight aggregate	Heavy weight aggregate
Description	0.23 water-to-cementitious material ratio with 10% silica fume, 15% fly ash and 39% of siliceous sand	Rotary Kiln Expanded Crushed Slate	Crushed Granite	A 36 steel cubes
Maximum size aggregate	NA	12.7 mm (0.5 in)	12.7 mm (0.5 in)	12.7 mm (0.5 in)
Density $kg/m^3(lb/ft^3)$	2243 (140.2)	1150 (96.8)	2680 (167.4)	7850 (490.1)
Compressive strength MPa (psi)	95.7 (13,875) [1] 104.5 (15,160)[2]	22.2 (3220)[3]	181 (26,245)[5]	> 282.8 (41,000)[7]
Elastic modulus GPa (ksi)	36.2 (5255)[1] 38.4 (5560)[2]	8.4 (1210)[4] 16.8 (2440)[4]	70 (10,150)[6] 79 (11,455)[6] 77 (11,165)[6]	212.8 (30,855)[7]
Shape	NA	crushed and angular	crushed and angular	cubic
Absorption	NA	6 to 8%	0.1%	0.0%
Texture	NA	very rough with open pores	rough	smooth
Fineness Modulus		6.3	6.9	7.0

1: Tested at 24 hours; 2: tested at 28 days; 3: tested on expanded slate prisms; 4: [21]; 5: [22]; 6:[23]; 75: tested on 12.7-mm (0.5-in) square bars.

5.4.1 Two-Phase Models for Concrete.

5.4.1.1 Two-phase Model for Concrete Elastic Modulus

Several models have been proposed for concrete elastic modulus. They mainly differ in the assumptions about matrix – aggregate arrangement. Voigt's model assumed a parallel arrangement of the phases with uniform strain. A series arrangement with uniform stress between phases was used by Reuss in developing his model. Hirsch

combined the parallel and series arrangements in one model trying to better represent concrete behavior [24]. Other models were proposed by Hansen and Counto where they assumed either spherical or prismatic aggregate particle embedded in cement matrix [25]. Mori-Sanaka model modeled mathematically soft inclusions in a matrix [26]. The models equations follow:

Voigt's Model

$$E_c = E_M \cdot (1-g) + E_A \cdot g \tag{5.17}$$

Hansen Model for Poisson's ratio of aggregate and matrix of 0.2

$$E_c = \left[\frac{(1-g)\cdot E_M + (1+g)\cdot E_A}{(1+g)\cdot E_M + (1-g)\cdot E_A} \right] \cdot E_M \tag{5.18}$$

Counto's Model

$$E_c = \left[\frac{1-\sqrt{g}}{E_M} + \frac{1}{\left(\frac{1-\sqrt{g}}{\sqrt{g}} \right) \cdot E_M + E_A} \right]^{-1} \tag{5.19}$$

Mori-Sanaka's model

$$E_c = \frac{9 \cdot K_C \cdot G_C}{3 \cdot K_C + G_C} \tag{5.20}$$

$$K = \frac{(1-g)}{\frac{1}{K_M - K_A} + \frac{3 \cdot g}{3 \cdot K_A + 4 \cdot G_A}} \tag{5.21}$$

$$G = \frac{(1-g)}{\frac{1}{G_M - G_A} + \frac{6 \cdot (K_A + 2 \cdot G_A) \cdot g}{5 \cdot G_A \cdot (3 \cdot K_A + 4 \cdot G_A)}} \tag{5.22}$$

where:

g: volume of aggregate per unit volume of mixture

E_C, E_M, E_A: modulus of elasticity of concrete, matrix, and aggregate, respectively

K_C, K_M, K_A: bulk modulus of concrete, matrix, and aggregate, respectively

G_C, G_M, G_A: shear modulus of concrete, matrix, and aggregate, respectively

5.4.1.2 Two-phase Model for Concrete Shrinkage

Pickett developed a model of the aggregate restraining effect starting from a sphere of aggregate embedded in a sphere of cement paste [27]. Equation 5.23 presents the expression proposed by Pickett in logarithmic form. Using Pickett's expression the shrinkage of concrete can be calculated from the shrinkage of the cement paste, relative volume of aggregate, and the mechanical properties of aggregate and paste. In this expression aggregate is assumed not to present shrinkage.

$$\ln(S_C) = \ln(S_M) - \alpha \cdot \ln\left(\frac{1}{1-g}\right) \tag{5.23}$$

where:

S_C: linear shrinkage of concrete

S_M: linear shrinkage of cementitious matrix

g: volume of aggregate per unit volume of mixture

α: constant representing aggregate restraining effect as shown in empirical Equation 5.24

$$\alpha = \frac{3 \cdot (1-\mu_C)}{1+\mu_C + 2 \cdot (1-2 \cdot \mu_A) \cdot \frac{E_C(t)}{E_A}} \tag{5.24}$$

where:

μ_c: Poisson's ratio of concrete

μ_A: Poisson's ratio of aggregate

$E_C(t)$: effective modulus of elasticity of concrete (after a time period of sustained load)

E_A: modulus of elasticity of aggregate

"α" decreases with increasing age of loading and increases with increasing time under load. Both effects due to change in concrete elastic modulus.

5.4.1.3 Two-phase Model for Concrete Creep

It was concluded that the restraining effect of aggregate on deformation is independent of whether the deformation is due to shrinkage or creep [15]. Therefore, Equation 7.23 is entirely applicable to creep [27]. Equation 5.23 as modified for creep [15] in logarithmic form is shown in Equation 5.25:

$$\ln(c_C) = \ln(c_M) - \alpha \cdot \ln\left(\frac{1}{1-g}\right) \qquad (5.25)$$

where

c_C: creep of concrete

c_M: creep of cementitious matrix

g: volume of aggregate per unit volume of mixture

α: constant representing aggregate restraining effect as shown in Equation 5.24

Values for "α" measured between 1.2 and 1.7 have been reported previously [24, 28], depending on the type of normal weight aggregate used.

5.4.2 Compressive Strength of Concrete vs. Two-Phase Model Estimate

5.4.2.1 Compressive Strength of High Performance Matrix

Figure 5.15 presents the compressive strength (on Y-axis in MPa / ksi) versus age of testing and maturity of testing in logarithmic scale (X-axis) of HP Matrix. Compressive strength after 24 hours of casting was 95.7 MPa (13,875 psi). After 56 and

365 days of moist curing, compressive strength increased to 109.3 and 125.1 MPa (15,845 and 18,140 psi), respectively.

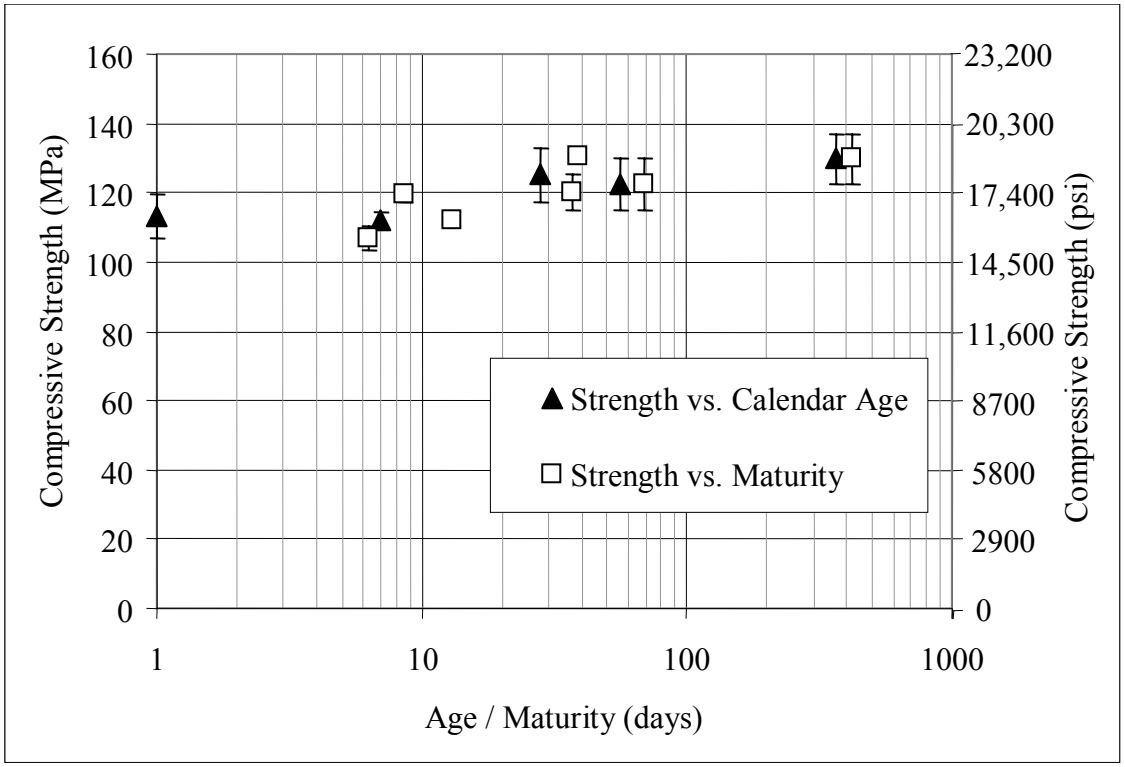

Figure 5.15: Compressive strength versus age and maturity at testing of HP Matrix

5.4.2.2 Compressive Strength of Aggregate

The average compressive strength as measured on the expanded slate prisms was 22.2 MPa (3220 psi) with wide range in results between 9.8 and 45.0 MPa (1420 and 6525 psi). Detailed results are given in Appendix A, Section A.3. It is believed that these values might have underestimated the actual compressive strength of the 12.7-mm (0.5-in) aggregate particles because some of the prism showed cracks before testing. The test specimens were obtained from relatively large pieces (100 mm / 4 in) of clinker that cracked upon cooling as seen by ultrasonic pulse velocity tests (see Appendix A, Section

A.3). The lightweight aggregate is obtained from crushing those large particles, thus reducing or eliminating cracks.

The strength of the lightweight aggregate was believed to limit the strength of the concrete mixtures because the aggregate strength was lower than that measured on HP Matrix.

Granite was not tested in compression due to the difficulty of making test specimens from the small aggregate particles. Elastic modulus for granite from North America ranges between 114 and 257 MPa (16,600 and 37,300 psi) with an average value of 181 MPa (26,245 psi) [22].

The average yield stress of the steel bars was higher than expected 282 MPa (41,000 psi), which was higher than HP Matrix strength.

5.4.2.3 Compressive Strength of Concrete

Figure 5.16 presents the compressive strength (Y –axis) for each of the seven HPC mixtures at the age of 1, 28 and 365 days.

A first comparison among mixtures reveals that NWA mixtures exhibited higher strength than that of LWW and STL mixtures for all ages. LWW 35-65 had higher strength than STL 35-65 for any age as well.

NWA 35-65 presented similar compressive strength as HP Matrix. Contrarily, the LWW 35-65 and STL 35-65 decreased the compressive strength by roughly 20 and 40 MPa (2900 and 5800 psi), respectively independently of age.

LWW 35-65 mixture had lower strength gain between one and 365 days than the other 35-65 mixtures. This lack of strength increase indicates the influence of the aggregate intrinsic strength on the compressive strength of the concrete. This

phenomenon is called strength ceiling [29-31]. LWW 35-65 strength was governed by the expanded slate intrinsic strength rather than ITZ as the mixtures with granite and steel which showed similar strength gain with time as the ITZ got stronger.

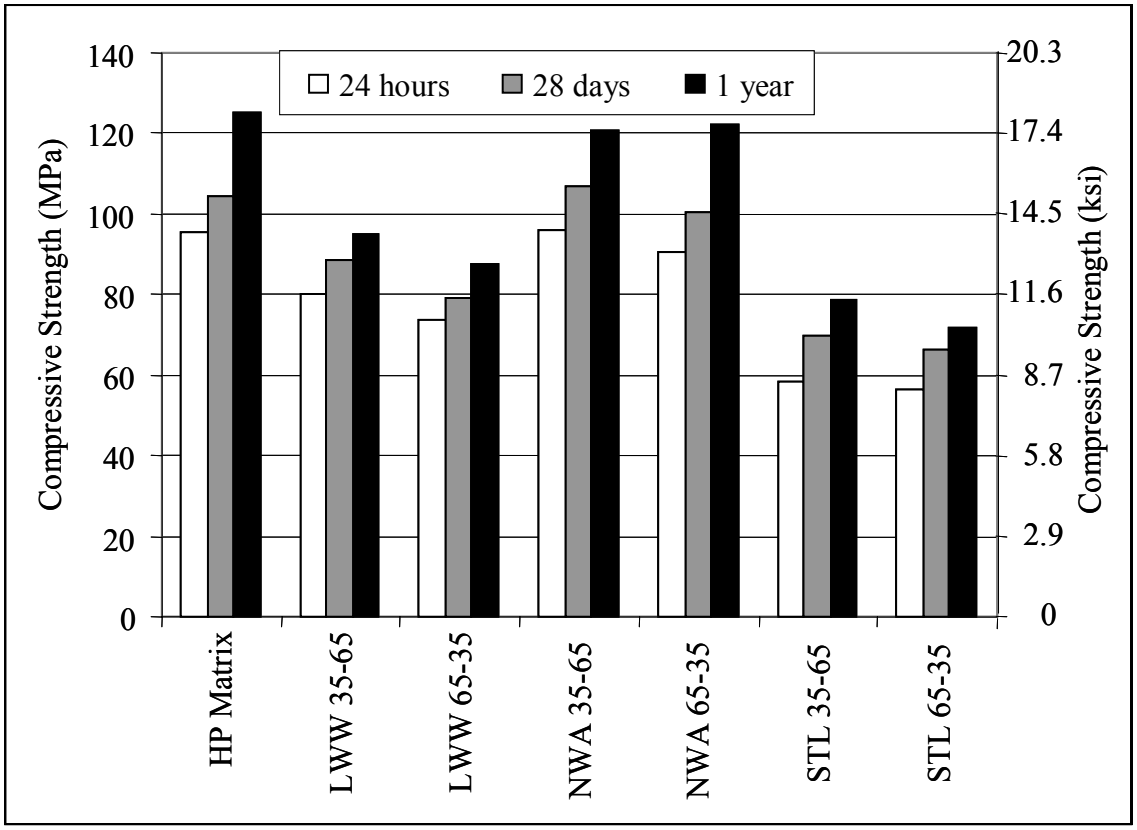

Figure 5.16: Compressive strength for HP Matrix, LWW, NWA, and STL mixtures for different age of testing

The 35-65 mixtures presented average compressive strength after 24 hours of 80.1, 96.1, and 58.3 MPa (11,615, 13,930, and 8450 psi) for LWW, NWA and STL, respectively while HP Matrix had 95.7 MPa (13,875 psi). It is believed that the great decrease in strength when using steel aggregate was given by a weak bond at early ages between steel aggregate and cementitious matrix. After one year, compressive strength of the LWW, NWA and STL mixtures was 95.0, 120.9, and 78.5 MPa (13,770, 17,540, and 11,385 psi), respectively.

The 65-35 mixtures had 36.8% of coarse aggregate, twice the amount considered in the 35-65 mixtures. Results followed similar tendency as mixtures with less coarse aggregate. It is believed that this was a consequence of the lower compressive strength of the lightweight aggregate that imposed a strength ceiling on the concrete mixture. Consequently, a higher amount of lightweight aggregate further lowered the strength ceiling. LWW 65-35 had an average compressive strength after one day and one year of casting of 73.5 and 87.5 MPa (10,655 and 12,690 psi), respectively. NWA 65-35 compressive strength after one day and one year was 90.5 and 122.2 MPa (13,130 and 17,715 psi), which were approximately 10 MPa (1450 psi) less than HP Matrix

Finally, STL 65-35 had average compressive strength of 56.2 and 71.9 MPa (8150 and 10,410 psi) after one day 365 days, respectively. The reduction in compressive strength experienced by the STL mixtures was not attributed to the aggregate itself, as in the case of expanded slate, because the steel yield stress was twice HP Matrix strength. The strength reduction factor was situated in cracking and debonding at the ITZ after careful examination of the tested cylinders.

Figure 5.17 shows a comparison between compressive strength as measured in cylinder specimens and as estimated using a two-phase model with the aggregate and matrix in parallel. From that model compressive strength can be calculated as the sum of the strength of each phase multiplied by its relative volume. This simple model neglects ITZ effect on strength. X-axis of Figure 5.17 presents the measured strength and the Y-axis the estimated strength. The diagonal solid line represents where estimated and measured strengths are the same. The 10% difference between estimated and measured is shown by the dashed lines.

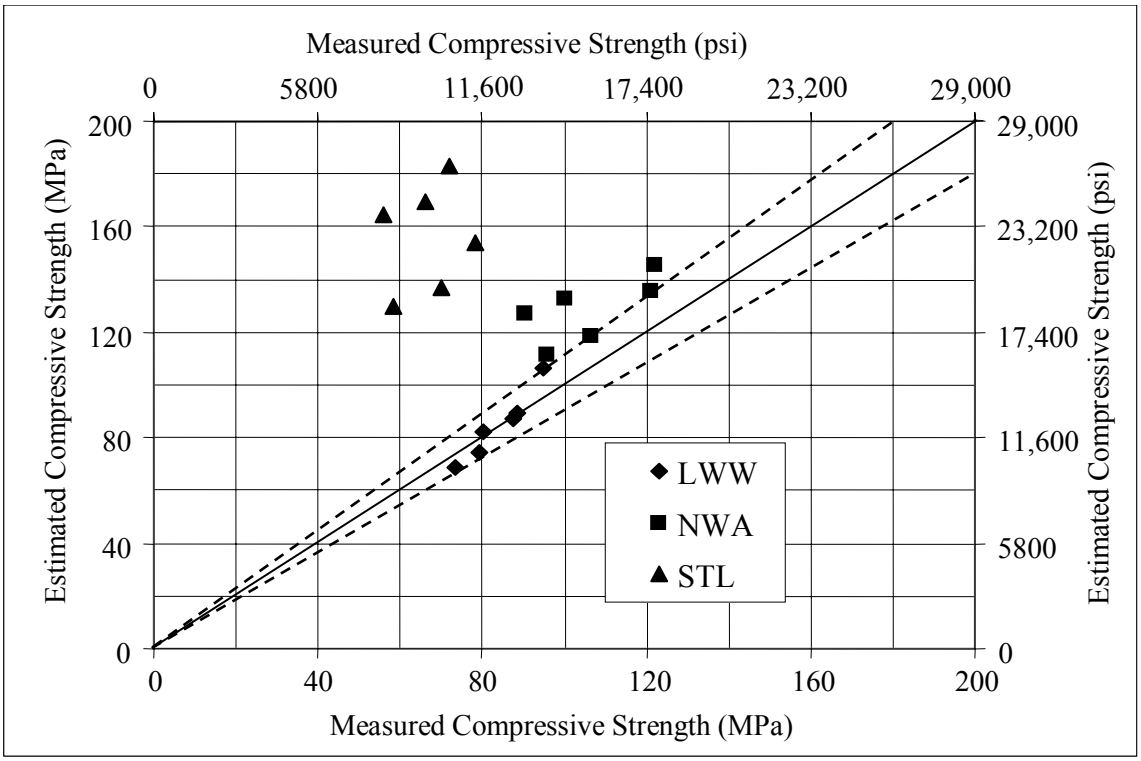

Figure 5.17: Measured compressive strength versus estimated from two-phase model in parallel for LWW, NWA, and STL mixtures

Figure 5.17 corroborates most of the conclusions stated before. STL mixtures presented a compressive strength of approximately 50% of the estimated strength. This highlights the level of error when using a model that neglects the role of ITZ on compressive strength. HPC mixtures with granite (NWA) and expanded slate (LWW) showed better agreement between measured and estimated strength. Among those, LWW mixtures showed values close to the estimate possibly indicating that ITZ does not limit the strength in high performance lightweight concrete. This is in agreement with previous results [19, 20] which showed that lightweight aggregate improved the ITZ of high performance lightweight concrete.

The fact that the model overestimated compressive strength of the granite mixtures does not necessarily indicate effect of ITZ but that granite aggregate could have had a lower compressive strength than assumed.

5.4.3 Modulus of Elasticity

5.4.3.1 Elastic Modulus of High Performance Matrix

Elastic modulus of the HP Matrix is shown in Table 5.5. After 24 hours, HP Matrix elastic modulus was 36.2 GPa (5255 ksi) which was predicted by the ACI-363 [32] expression within 1% accuracy for the two specimens tested. At the age of 28 days, the average elastic modulus was 38.1 GPa (5560 ksi) which was estimated within 5% by that same expression.

ACI-363 expression was proposed for high strength concrete after it was concluded that the ACI 318 [33] equation overestimated elastic modulus of such kind of concrete.

5.4.3.2 Elastic Modulus of Aggregate

The expanded slate (LWW) yielded an elastic modulus between 0.3 and 9.0.GPa (44 and 1,305 ksi) with an average of 2.7 GPa (392 ksi). These values were much lower than the 8.4-to-16.8 range reported by other researchers for expanded slate [21]. It is believed that the elastic modulus of the 12.7-mm (0.5-in) aggregate particles was higher than that measured in the prismatic specimens because the former contain less cracks. Section A.3 of Appendix A presents details of results and experimental procedure.

Granite (NWA) was assumed to have an elastic modulus between 70 and 79 GPa (10,150 and 11,455 ksi) as reported by other study [23].

Steel bars had an elastic modulus in tension of 212.8 GPa (30,855 psi) with maximum and minimum of 201 and 224.5 GPa (29,130 and 32,550 ksi), respectively.

Expanded slate had en elastic modulus around 7% of that measured on HP Matrix, and granite and steel moduli were 200% and 570% higher than that of the HP Matrix. Therefore, the slate was expected to reduce the stiffness of concrete while granite and steel were expected to increase it.

5.4.3.3 Elastic Modulus of Concrete

Figure 5.18 presents the elastic modulus of all six HPC mixtures at the age of 24 hours and 28 days. Average elastic modulus is on the Y-axis and percentage of coarse aggregate is on the X-axis. From left to right, Figure 5 shows results from LWW, NWA and STL aggregate mixtures, respectively.

As expected, the inclusion of lightweight aggregate decreased the elastic modulus of concrete with respect to HP Matrix (shown as 0% aggregate). The slope seemed to be similar for the 24-hour and 28-days cases when going from 0 to 36.8% coarse aggregate.

NWA mixtures also presented a decrease in elastic modulus as volume of coarse aggregate increased. The opposite was expected since granite elastic modulus was about the double than that of HP Matrix. This can be evidence of presence of ITZ which was weaker than either the HP Matrix or granite.

STL mixtures presented a dual behavior depending on the amount of steel aggregate considered. When 18.4% by volume was added, elastic modulus dropped at both 24 hours and 28 days. When further steel aggregate was considered, the elastic modulus increased to values 25 to 35% higher than that of the HP Matrix alone. The decrease in stiffness is believed to be caused by the weak ITZ that also affected strength.

On the other hand, the increase in stiffness experienced by STL 65-35 is believed to have been caused by the high stiffness of the steel cubes which in those larger amounts formed a rigid skeleton.

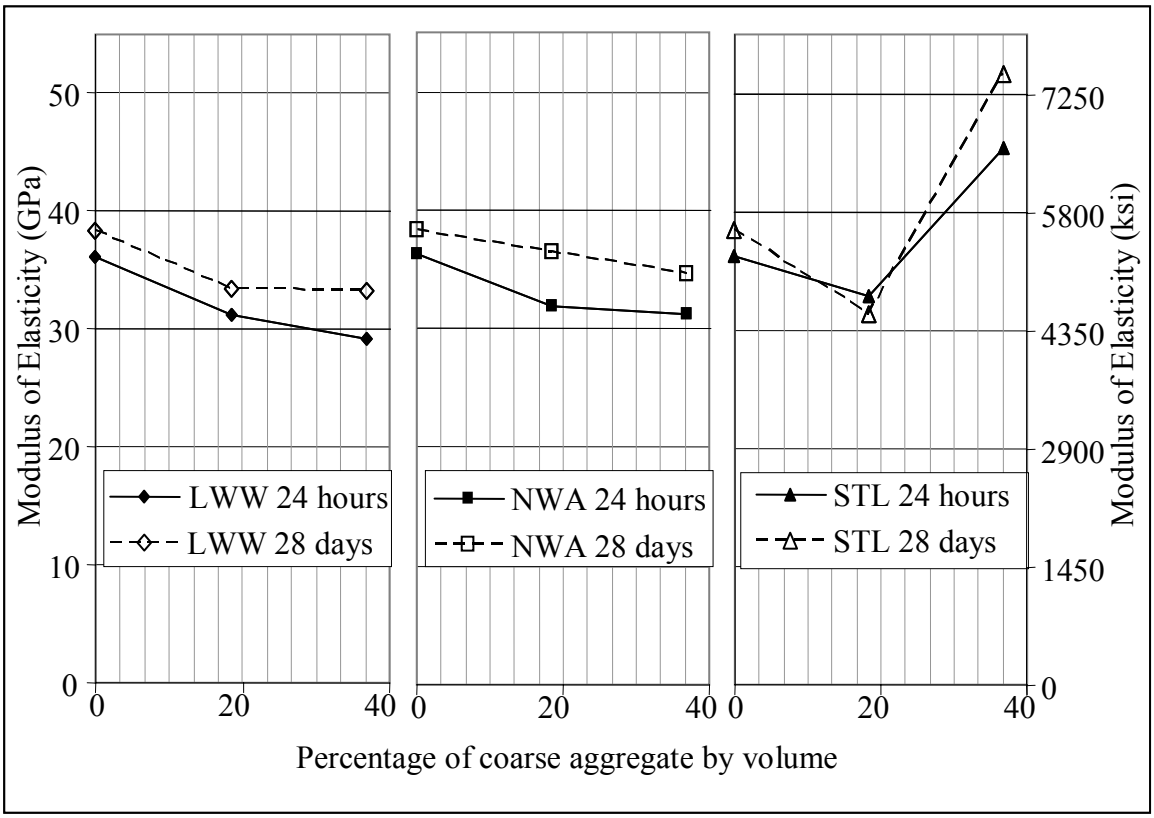

Figure 5.18: Elastic modulus of LWW, NWA, and STL aggregate mixtures as a function of coarse aggregate content

Several mechanistic models have been proposed to estimate concrete elastic modulus based on elastic modulus of the matrix and of the aggregate. Among those two-phase models, four were considered herein: Voigt's model (parallel model), Hansen's model (embedded aggregate sphere), Counto's model (embedded aggregate prisms) [25], and Mori-Tanaka model when the aggregates are softer than the cement paste [26].

Models using the expanded slate elastic modulus underestimated the concrete elastic modulus by as much as 55%. Nevertheless, when 16.8 GPa (2440 ksi) from Table

5.5 was used, all four models estimated the elastic modulus of the LWW mixtures within 15%. Among those, Voigt's model was with 9%.

Figure 5.19 shows a comparison between measured and estimated elastic modulus for all HPC mixtures and testing at the age of 24 hours and 28 days. X-axis shows measured values and Y-axis the estimated values. The diagonal solid line represents the equivalence between the two axes, and the dashed lines the 10% error. Mori-Tanaka model was applied only to LWW mixtures because it assumed aggregate softer than the matrix.

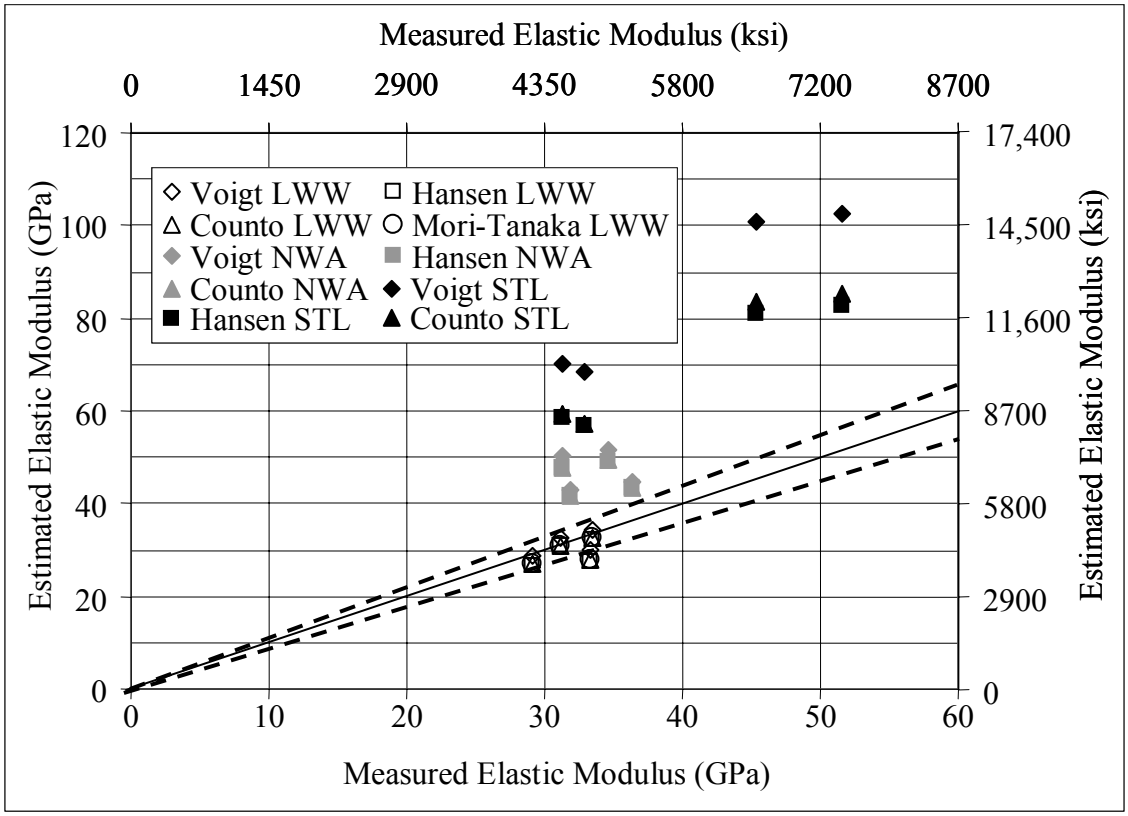

Figure 5.19: Measured elastic modulus versus estimated from two-phase models for LWW, NWA, and STL aggregate mixtures

The models performed reasonably well for HPC made with expanded slate, and in general they overestimated elastic modulus for granite and STL mixtures elastic modulus.

For granite HPC, the four models yielded similar results, and the overestimates were between 18% and 55% of the measured modulus. This overestimate might be due to an actual granite elastic modulus lower than assumed. STL mixtures presented the greatest deviations from the estimated values.

For LWW mixtures, Mori-Tanaka model gave the better results, but Hansen's and Counto's models performed comparatively better than Voigt's indicating that aggregate and matrix do not deform uniformly.

The good performance of the models in estimating LWW mixtures elastic modulus led to the conclusion that assuming an elastic modulus for expanded of 16.8 GPa (2440 ksi) was better than using the experimental values found from the prism test.

In addition the Hashin-Shtrikman bounds were applied to each HPC mixture using the aggregate and HP Matrix modulus of elasticity, and HP Matrix, expanded slate, granite and steel Poisson's ratios of -0.17, -0.12, -0.12, and -0.31, respectively. If the experimental concrete elastic modulus is out of the Hashin-Shtrikman bounds [34], it is said that such concrete is not a two-phase material.

Figure 5.20 presents the elastic moduli obtained at the age of 28 days in gray. Lower and upper bound given by Hashin-Shtrikman's expression are shown in the black and white bars.

As seen in Figure 5.20, the two NWA mixtures and STL 35-65 had a 28-day elastic modulus below the lower Hashin-Shtrikman bound. This means that the two-phase approach did not capture the experimental behavior of those mixtures and the mode should include ITZ as a third phase [34]. Elastic modulus of both LWW mixtures were between the bounds indicating that they behaved as two-phase materials. These findings

supported the conclusion obtained from Voigt's, Hansen's, Counto's and Mori-Tanaka's models.

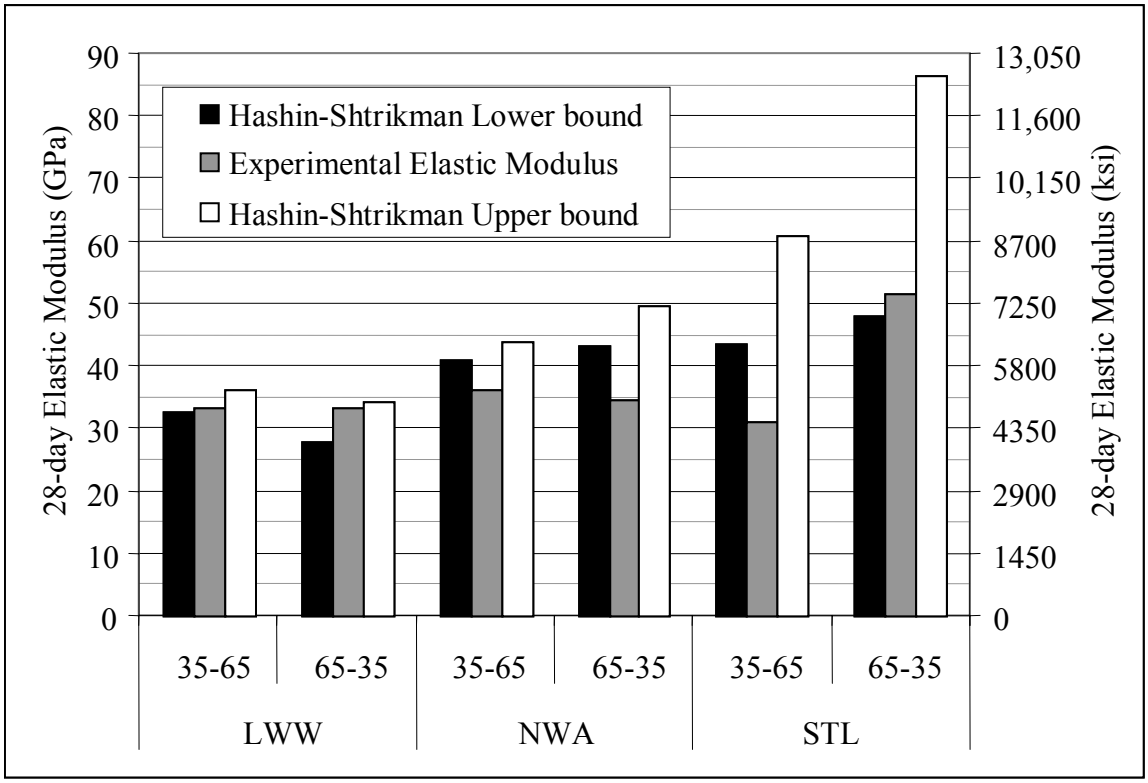

Figure 5.20: 28-day measured elastic modulus versus Hashin-Shtrikman bounds for LWW, NWA, and STL aggregate mixtures

Even though the STL 65-35 had an elastic modulus between bound which normally would indicate that it could be modeled as a two phase material, this opposed the poor performance of the two-phase models shown in Figure 6, where estimates were about the double that the experimental results. It is concluded that STL mixtures cannot be adequately modeled as a two-phase material.

Figure 5.21 present a comparison between the experimental elastic modulus and the values obtained using ACI-363 [32] equation based on compressive strength and density of the concrete. The X-axis gives the compressive strength, and the Y-axis

presents the elastic modulus normalized by density as shown in Equation 5.26, so ACI-363 equation depends only on the compressive strength as shown in Equation 5.27a and 5.27b in international and customary units, respectively.

$$E_{CN} = \frac{Ec}{\left(\frac{w_C}{a}\right)^{1.5}} \tag{5.26}$$

$$E_{CN} = \left(3.32 \cdot \sqrt{f_c'} + 6.9\right) \tag{5.27a}$$

$$E_{CN} = \left(40 \cdot \sqrt{f_c'} + 1000\right) \tag{5.27b}$$

where:

E_{CN}: elastic modulus normalized by density in GPa or ksi

E_C: elastic modulus in GPa or ksi

w_C: density on concrete in kg/m^3 or lb/ft^3

a: constant 2325 kg/m^3 (145 lb/ft^3)

f_c': compressive strength in MPa or psi

The solid line in Figure 5.21 represents the normalized elastic modulus as estimated with Equation 11, and the dashed lines give the ±10% error.

As mentioned before, the ACI-363 estimate for HP Matrix was very close to the actual values. Such good agreement was not the case of the mixtures with coarse aggregate. Even though the elastic modulus of HP Matrix was adequately estimated by Equation 5.27, the stiffness of each HPC containing lightweight aggregate was underestimated by 9% or more. Elastic modulus of HPC with granite was consistently lower than that predicted by the Equation 5.27. The 24-hour and 28-day elastic moduli were overestimated by approximately 19 and 13%, respectively, regardless of the amount of granite in the mixtures.

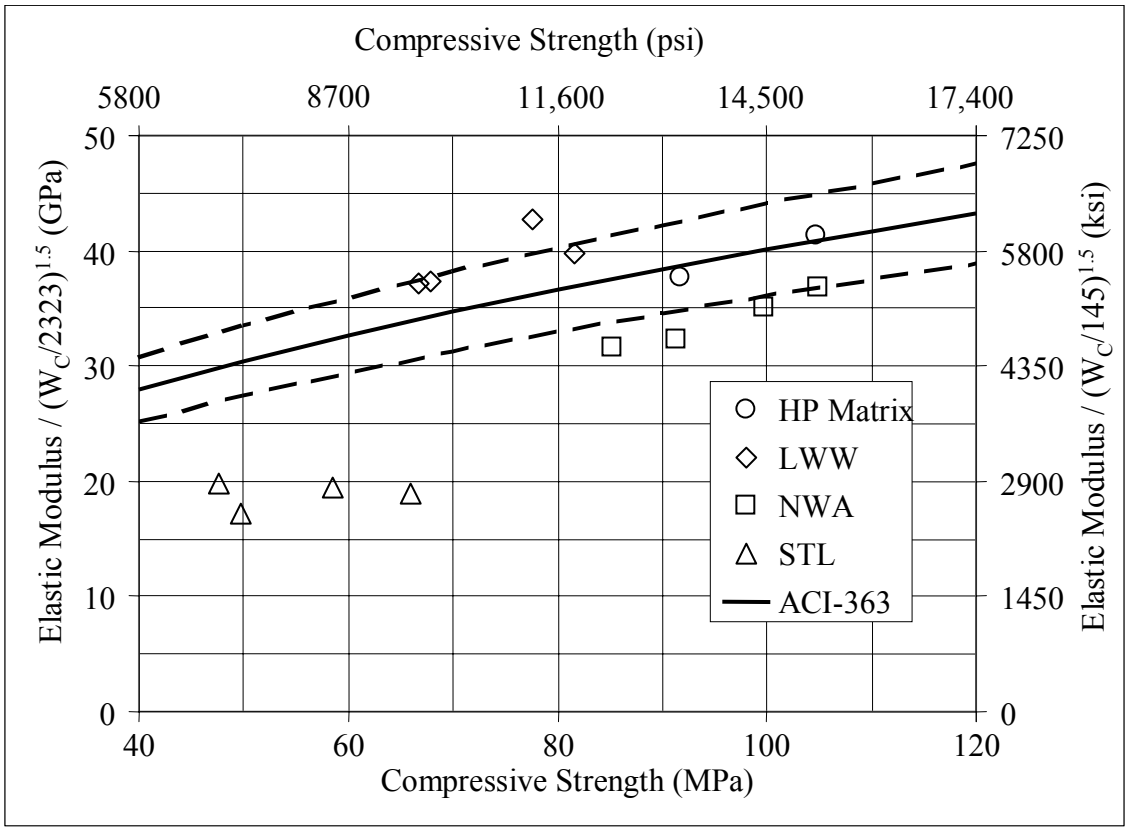

Figure 5.21: Comparison between experimental elastic modulus normalized by density and that estimated using ACI-363 equation versus compressive strength

Equation 5.27 greatly overestimated the elastic modulus of STL mixtures. The equation yielded values between 50 and 80% higher that those measured experimentally. This was probably due to the weak ITZ as pointed out earlier. It should be noted that HPC made with STL is not in the scope of the ACI-363, so the observed deviation was somehow expected.

5.4.4 Shrinkage and Creep Deformations

Creep was measured on at least ten specimens under loading and drying and shrinkage on at least seven specimens under drying. Loading and drying started either 24

hours or 28 days after casting, and it was performed on HP matrix and on the six HPC mixtures. Shrinkage measurement were carried out for one year while creep measurement for at least 223 days.

5.4.4.1 Shrinkage and Creep of High Performance Matrix

Figure 5.22 presents, from left to right, shrinkage and specific creep of HP Matrix versus time under loading and drying. Shrinkage after one year of drying was around 400 με independently of the time at which drying started. This was unexpected because autogenous shrinkage was supposed to be considerable when testing started as early ages.

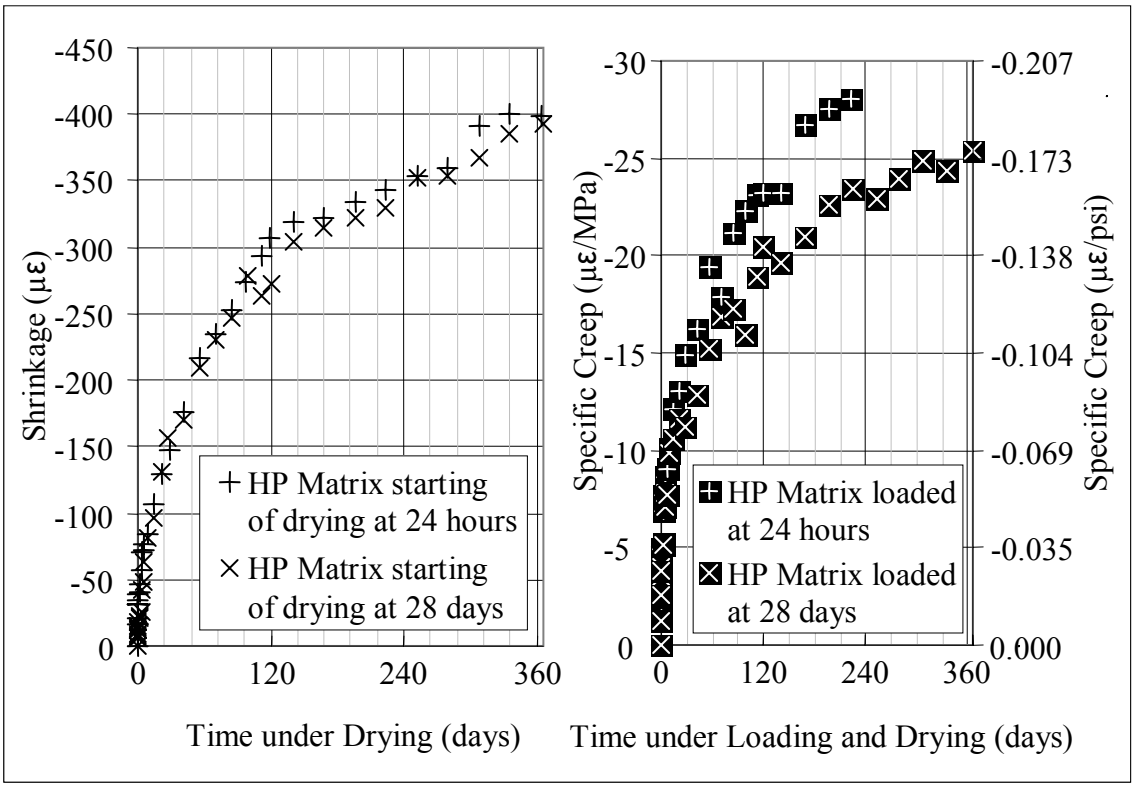

Figure 5.22: Total shrinkage and specific creep of HP Matrix mixtures versus time under loading and drying

One possible explanation is that most of the autogenous shrinkage already had occurred when measurement started. The specimens reached temperatures between 75

and 80 ^{o}C (167 and 176 ^{o}F) within the first 24 hours which gave equivalent maturity as those obtained in specimens 5-to-7 days old under standard curing conditions. In fact, autogenous shrinkage as measured on three sealed companion shrinkage specimens between 24 hours and 28 days ranged between 15 and 30 με after 28 days.

Specific creep was greater in cylinders loaded 24 hours than in those loaded 28 days after casting. After 223 days under loading and drying, specific creep was 28.0 and 23.5 με/MPa (0.183 and 0.162 με/psi) for loading age of 24 and 28 days, respectively.

5.4.4.2 Shrinkage of Concrete

Drying started either after 24 hours or 28 days. When drying started as early as 24 hours, specimens underwent not only drying shrinkage but autogenous shrinkage as well. Figure 5.23 shows the total shrinkage obtained when drying started at the age of 24 hours for all six HPC mixtures. X-axis presents time under drying in logarithmic scale while Y-axis shrinkage in με.

Among the 35-65 mixtures, STL concrete presented the lowest shrinkage for any time under drying greater than 10 days. NWA 35-65 and LWW 35-65 presented very similar total shrinkage at all times under drying. In fact, the difference between shrinkage of those two mixtures was within the 10-με resolution of the DEMEC gauge. The shrinkage rate of NWA 35-65 and LWW 35-65 after one year under drying was also similar indicating that they are likely to continue being the same in the long-term. Shrinkage rate of the STL mixture was lower than those of its expanded slate and granite counterparts which means that the difference in shrinkage will continue to increase as drying goes on.

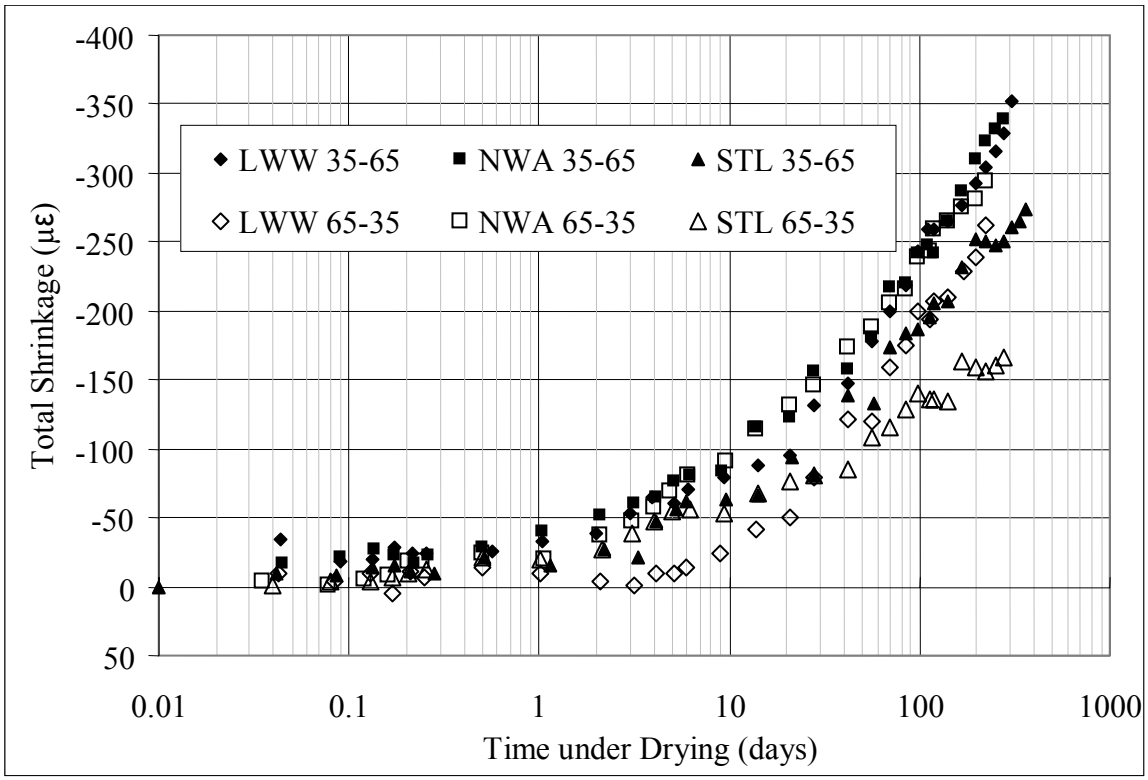

Figure 5.23: Total Shrinkage of HPC mixtures versus time under drying in logarithm scale

Shrinkage decreased when more coarse aggregate was added to the mixtures as seen when comparing 35-65 and 65-35 mixtures in Figure 5.23. STL mixture again presented the lowest shrinkage, followed by LWW 65-35 and NWA 65-35. From Figure 5.23 it can be seen that LWW 65-35 had lower shrinkage than NWA 65-35 with the former being lower. Nevertheless, The difference between the two decreased in the 56-to-224 day period indicating that the HPC made with lightweight aggregate might have had a higher shrinkage rate than that of HPC made with granite; however, the differences were less than 40 με.

When drying started at the age of 28 days, the conclusions were similar. STL mixtures presented less shrinkage than its expanded slate and granite counterparts. NWA

and LWW presented small differences between them regardless of the volume of coarse aggregate considered.

Figure 5.24 presents a comparison between experimental shrinkage and that estimated using the Pickett's two-phase model [27] as presented in Equation 5.23. Shrinkage of HP Matrix, aggregate elastic modulus, and aggregate volume were the main variables considered in the estimates. Figure 5.24 shows, from left to right, the comparison for LWW, NWA, and STL, respectively. Solid diagonal lines show when estimate and measured shrinkage were the same, and dashed diagonal lines give the 10% difference between estimate and experimental shrinkage.

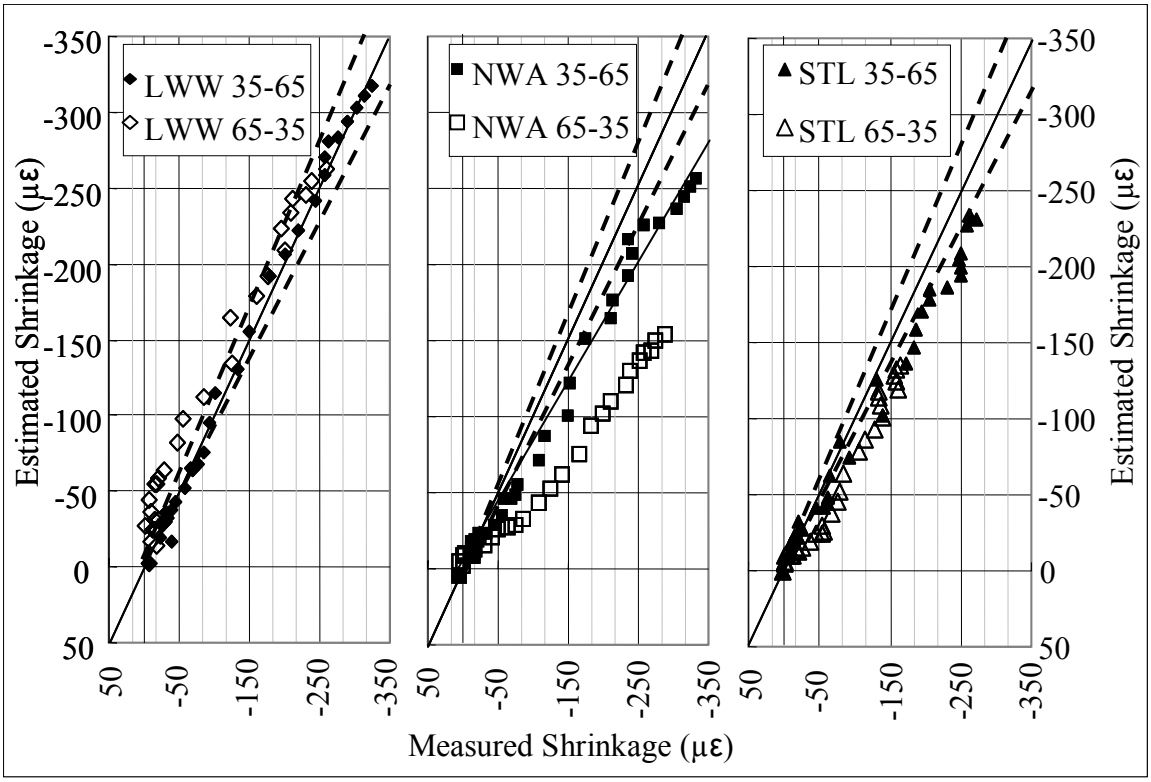

Figure 5.24: Comparison between experimental total shrinkage and that estimated using Equation 5.23 [27] for LWW, NWA, and STL mixtures

Mixtures with expanded slate presented good agreement between measured and estimated shrinkage. The model either adequately estimated or overestimated shrinkage of LWW mixtures. Shrinkage occurring during the first days of drying, denoted as lower shrinkage strains, was in general overestimated by 50 με or more. As drying continued, the agreement between model and experimental results increased with most cases falling within the 10% error (dashed lines). The greater shrinkage overestimate of LWW 65-35 mixture at the beginning of drying might indicate that expanded slate HPC dried slower than the HP Matrix.

Estimated shrinkage for STL mixtures also presented good agreement with experimental results. Unlike LWW mixtures, shrinkage of STL mixtures was predominantly underestimated by the model. The error of the model was between 10 and 20% for shrinkage strains higher than 100 με.

Pickett's model generally underestimated shrinkage of NWA mixtures. The underestimate was more noticeable for NWA 65-35 for which the estimated was 50% of the measured shrinkage in some cases. The greater the amount of coarse aggregate, the larger was the underestimate. If it is assumed that the elastic modulus of 74.5 GPa (10,800 ksi) selected for granite of was too high, a new elastic modulus can be assumed to improve the estimate. Nevertheless, such value would need to be 27.6 GPa (4000 ksi) to obtain an estimate as good as seen for LWW and STL mixtures. Clearly such a value is too low compared to the ranges presented for granite [23] or any other normal weight aggregate. It was concluded that the underestimate for NWA mixtures cannot be explained solely based on the granite elastic modulus. Increased cracking in the ITZ as shrinkage of the paste occurs might be one possible explanation to the poor performance

exhibited for NWA mixtures. This increased cracking will decreased the aggregate restraining effect which would also explain the progressive increase in error as shrinkage developed. A similar argument was used to explain the higher creep observed in concrete made with basalt aggregate [24].

5.4.4.3 Creep of Concrete

As described in Section 5.3, differences in maturity at the time of loading affected creep exhibited by the concrete mixtures. Accordingly, creep results for different stages within a particular mixture were adjusted to an average maturity of that mixture at loading.

The average specific creep for each HPC mixture, as measure on specimens under loading and drying, is presented in Figure 5.25. The plot to the left shows the 35-65 mixtures and the one to the right has the 65-35 mixtures. Time under loafing and drying is presented in X-axis while specific creep is given in με/MPa (με/psi) in the Y-axis.

Specific creep after one year varied little among the three 35-65 mixtures. After 280 days of creep testing, LWW 35-65 and STL 35-65 had virtually the same creep of -25.7 and -25.5 με/MPa (-0.177 and -0.176 με/psi), respectively which shown that the mechanical properties of the aggregate do not fully explain the aggregate restraining effect on creep. This represented an average difference of 5 με which is less than the resolution of the DEMEC gauge. NWA 35-65 closely followed the previous two with specific creep of -23.3 με/MPa (-0.161 με/psi). There were no significant differences between creep rates of those three mixtures. Using a logarithmic scale for time under testing, the 35-65 mixtures showed approximately two creep rates: one between zero and

seven days and a higher one between seven and 300 days of approximately 9.5 με/MPa (0.066 με/psi) per decade. Dash lines in Figure 5.25 illustrate the two rates of creep.

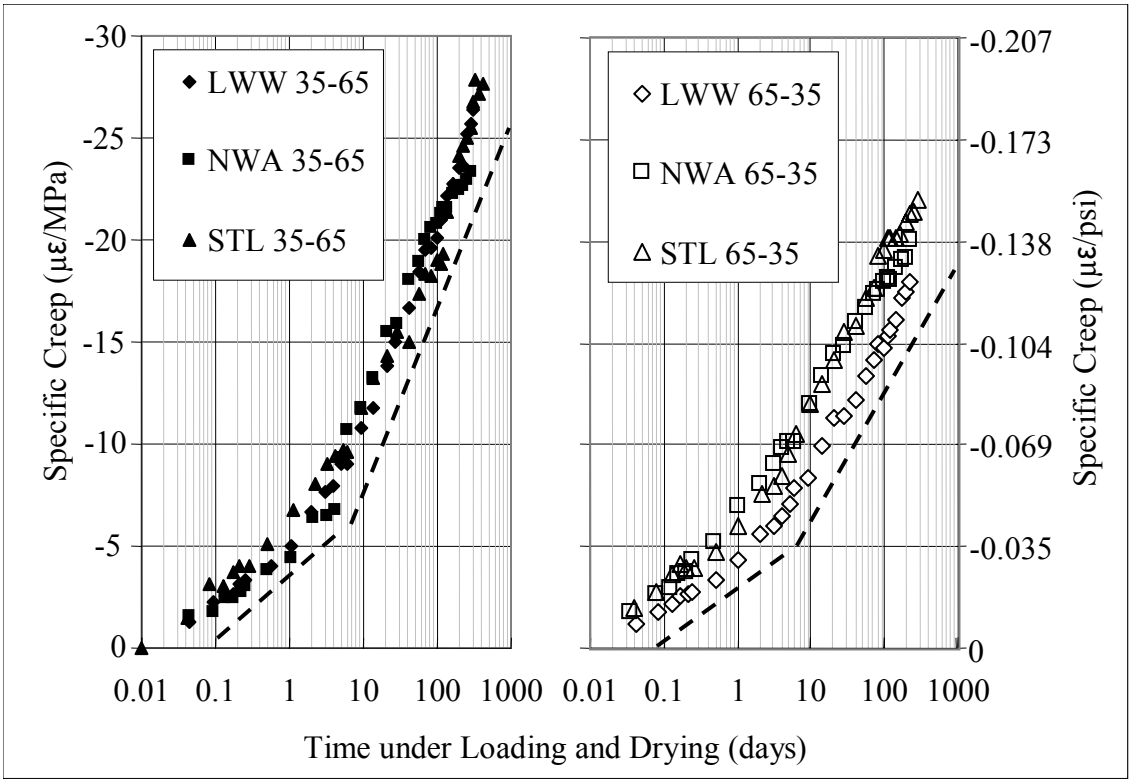

Figure 5.25: Specific Creep of HPC mixtures versus time under drying in logarithm scale

Creep of the 65-35 mixtures with more coarse aggregate was significantly lower than that of the 35-65 mixtures. After 280 days under loading and drying, STL 65-35, NWA 65-35, and LWW 65-35 had specific creep values of 21.8, 20.0 and 18.0 με/MPa (-0.150, -0.138, and -0.124 με/psi), respectively. The difference between the steel and LWW mixtures multiplied by the applied stress was approximately 105 με which is well above the instrument resolution.

The 65-35 mixtures also presented two distinct creep rates as illustrated in Figure 5.25 by the dash lines. Creep rate between 7 and 280 days was approximately 6.2 με/MPa (0.043 με/psi) per decade which was two thirds of that obtained for the 35-65

mixtures. Thus, the higher amount of coarse aggregate not only lowered creep, but also the creep rate.

Figure 5.26 presents a comparison between measured specific creep and that predicted using the two-phase model shown in Equation 5.25. The data considered correspond to the specimens loaded 24 hours after casting. Due to the large difference in cementitious materials content among HP Matrix and the mixtures with coarse aggregate, the maturities at the time of loading were quite different. HP Matrix, 35-65 mixtures and 65-35 mixtures had a maturity close to that obtained after 5.6, 3.9, and 2.9 days under standard curing conditions, respectively. In order to obtain comparable creep between HP Matrix and mixtures with coarse aggregate, the former was adjusted to represent creep when maturity of loading was either 2.9 days for the 65-35 mixtures or 3.9 days for the 35-65 mixtures.

Figure 5.26 presents from left to right the measured (X-axis) versus predicted (Y-axis) creep of the LWW, NWA, and STL mixtures. The equivalence between measured and predicted is given by the solid diagonal lines while dashed lines represent the 10% deviation from equivalence.

Figure 5.26 shows that the two phase creep model overestimated creep of both LWW mixtures for any time under loading and drying as shown by all data points in the top left portion of the plot. In most cases the measured creep was lower than that estimated by more than 10%. For instance, the highest three data points of LWW 35-65 creep were overestimated by 30%. Experimental creep of LWW 65-35 was on average 55% of the predicted value which indicated that the aggregate stiffness alone did not represent adequately the aggregate reduction effect on creep of the matrix phase. The

overestimate more than doubled when coarse aggregate volume increased, which clearly demonstrated that the model did not describe well the effect of expanded slate on creep.

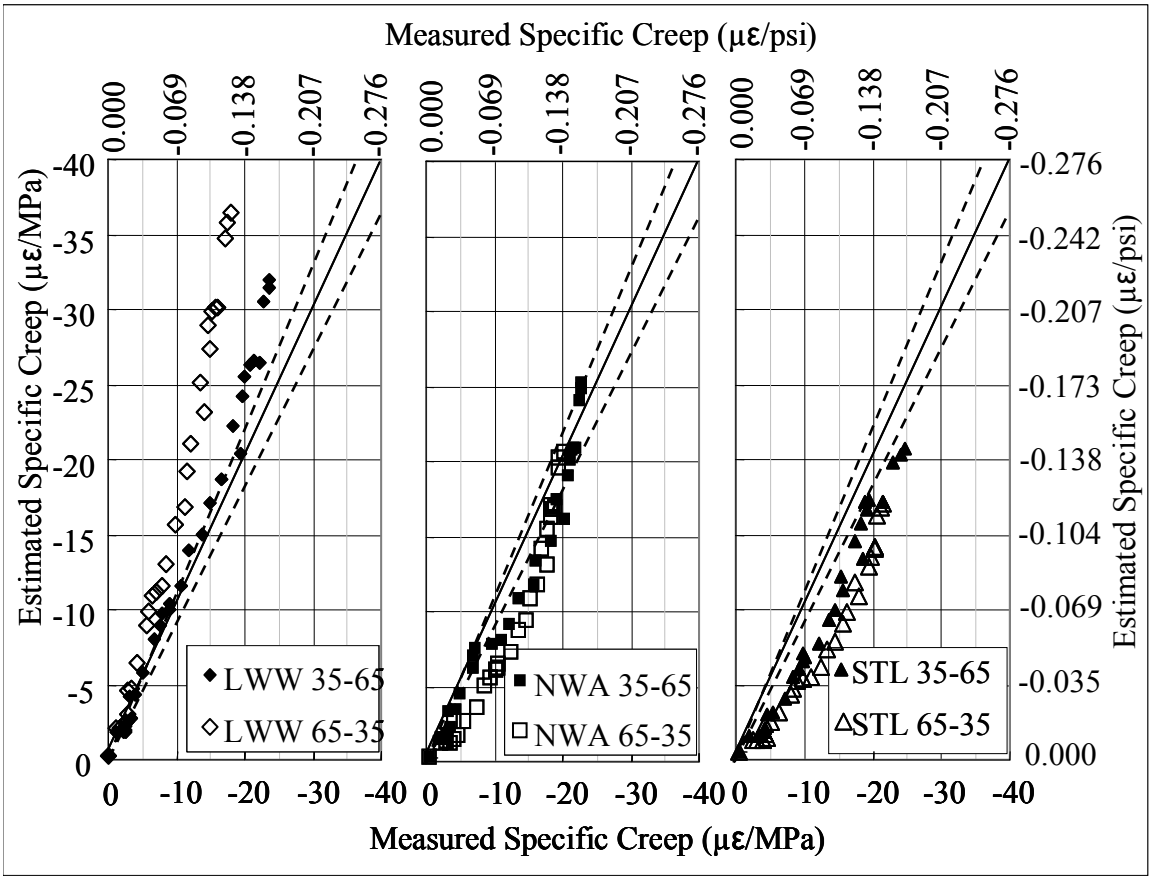

Figure 5.26: Comparison between experimental specific creep and that estimated using Equations 5 and 6 (Neville, 1964) for LWW, NWA, and STL mixtures

NWA mixtures presented good agreement between measured an estimated creep. The two-phase creep models tended to underestimate creep at the beginning; i.e., creep lower than -15 με/MPa (-0.104 με/psi). Nevertheless, most of estimates were within 20% of error which is considered acceptable. It was concluded that the two-phase model adequately represented creep of the granite HPC mixtures regardless of the amount of coarse aggregate considered.

Creep of STL mixtures generally was larger than predicted from the model. Although differences between the two STL mixtures were not large, it seemed that the model under predicted creep of STL 65-35 mixture by more than it did for STL 35-65. As concluded for the two-phase models for compressive strength and elastic modulus, the ITZ between matrix and STL seemed to affect creep and to cause a higher value than expected.

In summary, two-phase models adequately estimated shrinkage of LWW, STL and NWA 35-65 mixtures. NWA 65-35 presented more shrinkage than expected which could not be attributed solely to inaccuracies in the granite elastic modulus.

The two-phase creep model gave fairly good estimates of STL 35-65 and NWA mixtures, but considerably overestimated creep of HPC with expanded slate. Higher lightweight aggregate amounts somehow worsened the model performance. This was not the case of the shrinkage model which implies that the chosen elastic modulus for expanded slate was appropriate.

Similar conclusions were obtained from creep and shrinkage specimens tested at the age of 28 days. In general, compared to creep results with loading age of 24 hours, the measured creep for STL mixtures, when testing started at 28 days, was closer to the estimated by the model indicating a stronger ITZ between steel and matrix at 28 days compared to the 24 hour case. Creep of LWW mixtures was still overestimated by the model.

The comparatively low creep presented by expanded slate HPC is believed to be a consequence of the internal curing provided by the pre-soaked lightweight aggregate which improved hydration and reduced autogenous shrinkage. Internal curing has proven

to increase strength, degree of hydration, and reduce autogenous shrinkage [17, 18, 35-37]. Some of those authors did not only observe reduction in autogenous shrinkage but also expansion in sealed specimens as the hydration continued. This expansion might work as creep and drying shrinkage strain "reservoir" because those strains will need to be larger than the initial expansion in order to be measurable.

5.4.5 Effect of ITZ on High Performance Lightweight and Normal Weight Concrete

Since compressive strength of the LWW and NWA mixtures was adequately estimated by some of the two-phase models, it was concluded that ITZ did not limit the strength in those mixtures. These results empirically demonstrate previous observations with scanning electron microscopy (SEM) [38] on low water-to-cementitious material ratio mixtures containing silica fume where no obvious indication of ITZ on normal weight HPC was found. These results also corroborate the results of previous work on HPLC [21, 39, 40] where the improved elastic compatibility between paste and lightweight aggregate have led to the conclusion that HPLC does not possess a strength limiting ITZ.

On the contrary, the STL mixtures presented a compressive strength about 45% of that estimated by the two phase models indicating the great influence of the ITZ. Visual examination of the fracture surface (see Figure D.1, Appendix D) revealed poor bonding between HP Matrix and the steel aggregate. In addition the steel aggregate might have acted as a hard inclusion in a relatively less stiff matrix producing stress concentrations in the ITZ where the load is transmitted from matrix to aggregate. Figure D.1 (Appendix D) presents an image showing cracking of the matrix starting in the ITZ due to stress concentration.

Similar conclusions can be drawn from the elastic modulus, where the estimates with of the two-phase models were in good agreement with the experimental results for the LWW mixtures. This agreement supports the hypothesis of the enhanced elastic matching between lightweight aggregate and matrix [21]. The mixtures with granite and steel aggregate, which present larger differences in stiffness with the cement matrix, had experimental elastic moduli lower than that estimated by the two-phase models. The overestimate given by the models increased as the aggregate stiffness and the aggregate volume increased showing that the lack of strain compatibility between the HP Matrix and the aggregate decreased the experimental concrete elastic modulus. These results might be explained by microcracking at the ITZ which might have decreased the elastic modulus of the mixtures with stiffer aggregates.

Pickett [27] and Neville [15] conceived that aggregate with higher elastic moduli would restraint creep and shrinkage. The experimental results did not show a good correlation between aggregate elastic moduli and restraint of creep and shrinkage. Creep and shrinkage estimates using the aggregate restraining effect as a function of the aggregate mechanical properties presented, in general, poor agreement with the experimental data. Creep and shrinkage of the LWW mixtures was in general lower than the model estimates meaning that the mechanical properties alone do not provide enough information to explain the lightweight aggregate's restraining effect on creep and shrinkage, as discussed in Section 5.5.

STL mixtures presented higher creep and shrinkage than the model estimates showing that the high stiffness of the steel did not provide more restraint to the paste creep and shrinkage than the expanded slate or the granite. It is believed that the poor

bonding between HP Matrix and steel aggregate greatly decreased the steel aggregate's restraining effect on creep and shrinkage. In this case, the relatively weak ITZ was not able to restrain the time-dependent deformations in the paste.

5.5 Effect of Internally Stored Water on High Performance Lightweight Concrete Properties

Internally stored water has proven to effectively increase strength, decrease porosity and permeability, and substantially decrease autogenous shrinkage and early age cracking. This section examines the effect of the internally stored water in the creep and shrinkage of three HPLCs (LWW 65-35, LWW 65-35-95, and LWD 65-35) and the HPC produced with granite (NWA 65-35).

LWW mixtures, which considered pre-soaked lightweight aggregate, were expected to present marked effects of the internally stored water on their properties. LWD 65-35 that used air-dried lightweight aggregate represent a HPLC with the same mixture design as LWW, but with less internally stored water. Finally, NWA 65-35 mixture provides a comparison of normal weight HPC with no internally stored water.

5.5.1 Compressive Strength

Figure 5.27 present the average compressive strength results of the four HPC mixtures. Y-axis presents the strength in MPa (psi) and X-axis the age at testing in days. Figure 5.27 also includes logarithmic regression lines for each HPC mixtures obtained by minimizing the sum of the square error.

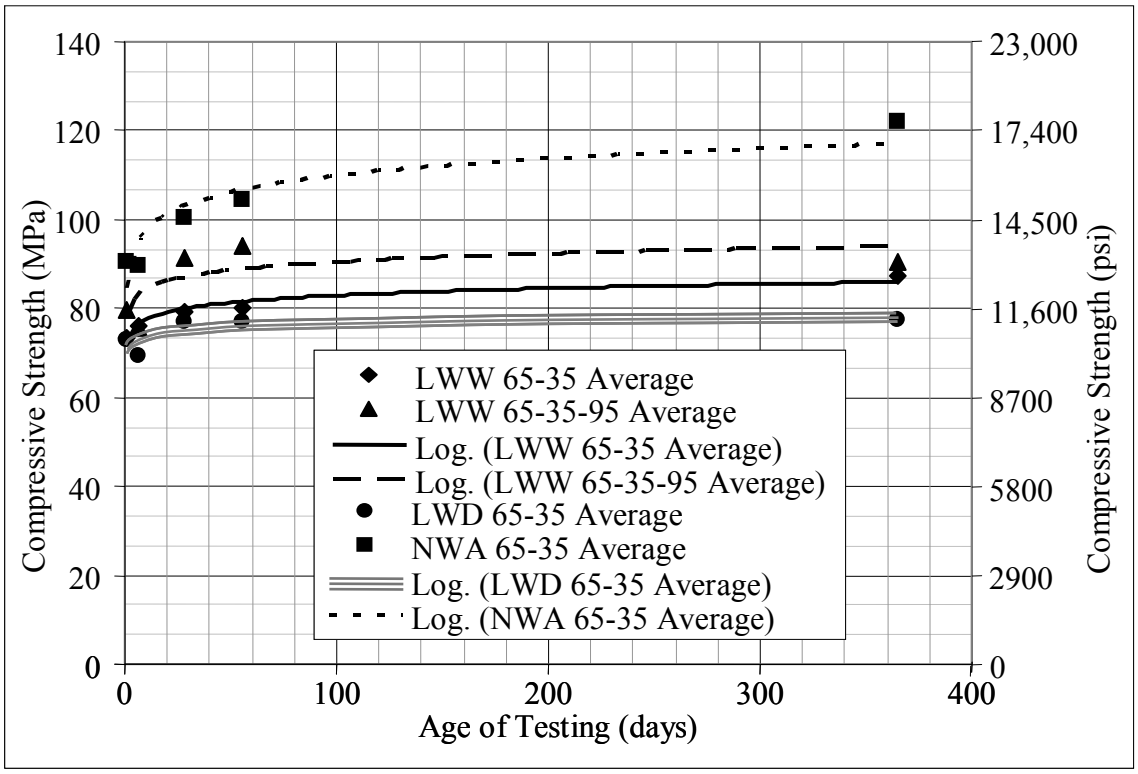

Figure 5.27: Compressive strength of HPC mixtures versus age at testing

LWW 65-35 had an average 24-hour compressive strength of 73.5 MPa (10,657 psi) which reached 80.2 and 87.5 MPa (11,635 and 12,690 psi) after 56 days and one year, respectively. Thus, LWW 65-35 increased its strength with respect to 24-hour strength by 9% after 56 days and by 19% after one year. LWD 65-35 on the other hand, had a 24-hour compressive strength of 72.8 MPa (10,550 psi) which was virtually the same as its LWW 65-35 counterpart. The latter would prove that the two mixtures had an equivalent water-to-cementitious material ratio with yielded to similar early age strength. LWD 65-35 reached a compressive strength of 77.0 and 77.5 MPa (11,160 and 11,245 psi) at the ages of 56 days and one year, respectively. Those values represented only 5.8% and 6.5% increase with respect to the 24-hour strength.

Thus, LWD 65-35 gain less strength over one year than LWW 65-35 mixture. In fact, LWW 65-35 continuously increased the difference in compressive strength over its LWD 65-35 counterpart. After 1, 28, 56, and 365 days, LWW 65-35 overcame LWD 65-35 strength by 1.0, 3.2, 4.2, and 12.9%, respectively. From the logarithmic regressions, it can be said that the strength gain of LWW 65-35 and LWD 65-35 were 5.3 and 2.6 MPa (770 and 380 psi) per decade, respectively.

Since the two mixtures had the same mixture design and similar strength after 24 hours, it is believed that the difference showed at later ages were due to internal curing. The water contained in the pre-soaked lightweight aggregate increased the degree of hydration transforming unhydrated cement into C-S-H capable of increasing strength. The external curing provided was not able to reach the unhydrated cement probably due to the low permeability of the mixtures.

LWW 65-35-95 presented higher strength than LWW 65-35 at any age of testing. After 24 hours and one year, LWW 65-35-95 had presented compressive strength of 79.5 and 90.6 MPa (11,530 and 13,135 psi), respectively. This was expected because compressive strength of high strength lightweight concrete is governed by the intrinsic strength of the aggregate. This strength ceiling was been reported by many to rise as the maximum size aggregate decreases [29, 39]. The strength gain of LWW 65-35-95 was 6.2 MPa (900 psi) per decade which was 17% higher than the gain registered for LWW 65-35.

Finally, NWA 65-35 was a 24-hour compressive strength of 90.5 MPa (13,130 psi) which was 23% higher than that of LWW 65-35. Thus, the higher intrinsic strength of granite allowed NWA 65-35 mixtures for attaining higher strength than expanded slate

mixtures using the same water-to-cementitious material ratio and dosage of cementitious materials. NWA 65-35 mixture compressive strength reached 104.3 and 122.2 MPa (15,130 and 17,715 psi) after 56 and 365 days, respectively. Thus, NWA 65-35 had a 35% increase in strength between 24 hours and 365 days. The strength gain was 12.6 MPa (1835 psi) per decade which was considerably higher than any of the HPC with lightweight aggregate. This difference is due to the fact the NWA 65-35 strength was not limited by the aggregate intrinsic strength as LWW 65-35, LWD 65-35, and LWW 65-35-95 were.

5.5.2 Modulus of elasticity

Experimental elastic moduli at the age of 24 hours and 28 days were compared against the values estimated using ACI-363 equation [32]. This expression estimates high strength concrete elastic modulus based on its compressive strength and density. Figure 5.28 presents a comparison between measured elastic modulus in X-axis and estimated values in Y-axis. Figure 5.28 also includes a solid diagonal line representing the equivalence between measured and estimated values. Below that line there was an underestimate of measured values, and above it, the equation overestimated elastic modulus. The two dashed diagonal lines represent 10% deviation from equivalence.

At the age of 24 hours, all three lightweight HPC had a similar elastic modulus in the 28.1-to-29.1 GPa (4075-to-4220 ksi) range. NWA 65-35 elastic modulus at the same age was 31.2 GPa (4525 ksi) which was approximately 9.5% higher than any of its lightweight counterparts. After 28 days, lightweight HPC mixtures increased their elastic moduli to 31.2-to-33.3 GPa (4525-to-48-30 ksi) range. LWW 65-35 elastic modulus increased more than LWD 65-35 which is believed to be a consequence of curing

provided by the internally stored water. NWA 65-35 presented a 28-day elastic modulus of 34.7 GPa (5030 ksi) which was only 4% higher than that of LWW 65-35.

As shown in Figure 5.28, ACI-363 equation underestimated elastic modulus of lightweight HPC by 7% at 24 hours and 15% at the age of 28 days. Contrarily, ACI-363 equation overestimated the elastic modulus of granite HPC by roughly 15% regardless of the age.

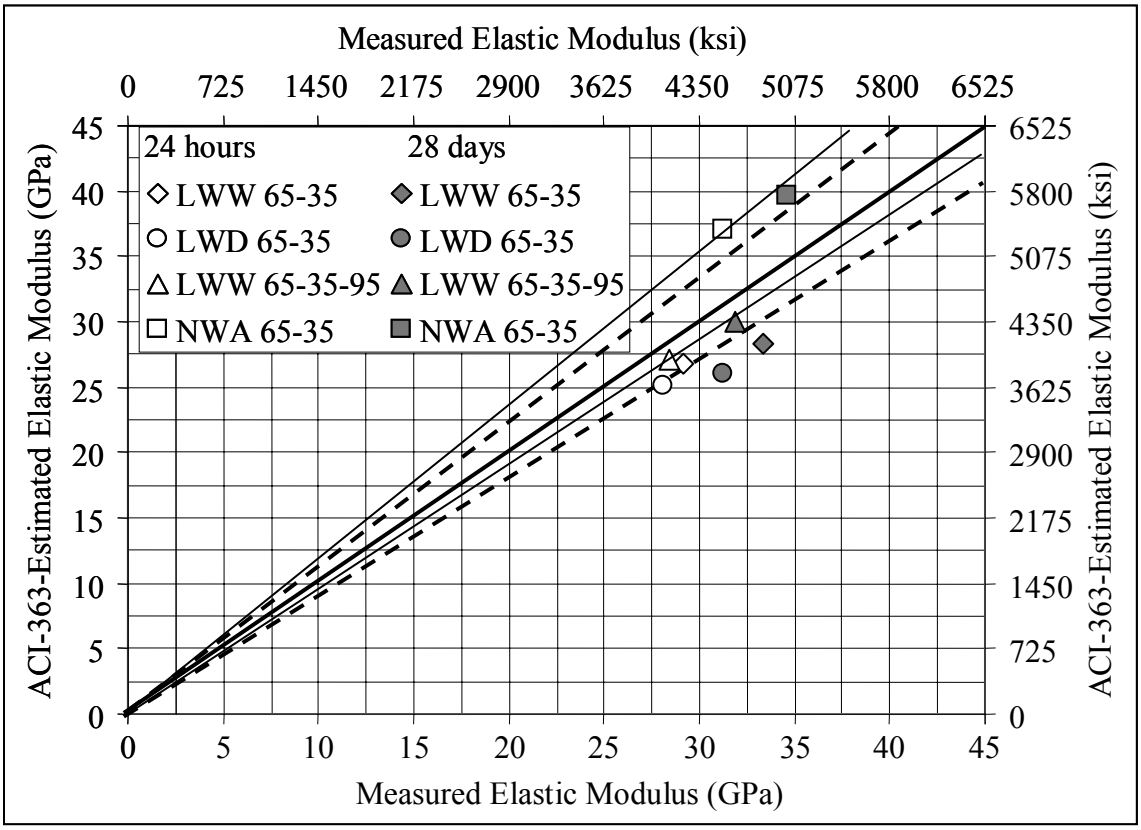

Figure 5.28: Measured elastic modulus versus estimated using ACI-363 equation

5.5.3 Shrinkage Deformations

Shrinkage was measured on ten 100 x 380 mm (4 x 15 in) cylinder specimens and four 150 x 300 mm (6 x 12 in) cylinder specimens for each HPC mixture. Autogenous

shrinkage was measured in the half of 100 x 380 mm (4 x 15 in) cylinder specimens and total shrinkage in the rest of them.

5.5.3.1 Autogenous Shrinkage after Final Set

Three LWW 65-35-95 specimens were fabricated for autogenous shrinkage measurements. In addition, three more specimens made of LWD 65-35 and NWA 65-35, but with MSA of 9.5 mm (0.375 in) instead of 12.7-mm (0.5 in) were fabricated. Those were named LWD 65-35-95 and NWA 65-35-95, respectively. Measurements started after final set and extended for 56 days. Figure 5.29 presents the change in length (Y-axis) versus time after final set (X-axis) in logarithmic scale.

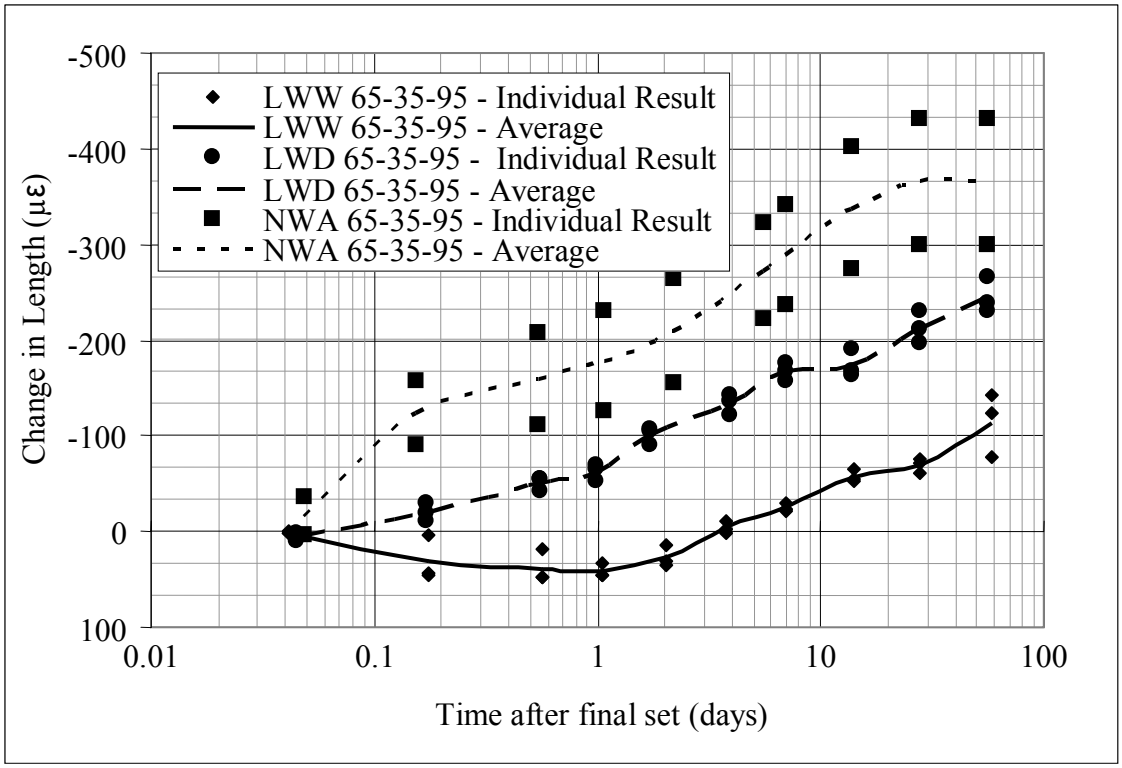

Figure 5.29: Change in length versus time after final set for LWW 65-35-95, LWD 65-35-95, and NWA 65-35-95 HPC mixtures

After 56 days, LWW 65-35-95, LWD 65-35-95 and NWA 65-35-95 mixtures showed an autogenous shrinkage of -114. -245 and -365 με, respectively. Since they

have the same mixture design and were batched and tested under the same conditions, the difference in performance can be attributed to the coarse aggregate used in each of them. LWW 65-35-95 with pre-soaked lightweight aggregate not only showed the least autogenous shrinkage but also presented expansion during the first 2 days. This is believed to be caused by the water stored in the pre-soaked lightweight aggregate that prevented self desiccation and the associated autogenous shrinkage. LWD 65-35-95 that contained less water in the aggregate presented more than twice the autogenous shrinkage after 56 days. It did not present any expansion during the first 48 hours which would demonstrate the internal curing was not as efficient as in LWW 65-35-95.

Finally, NWA 65-35-95 presented the highest shrinkage at any time. After 56 days, it had an autogenous shrinkage three times of that measured in LWW 65-35-95. These results followed similar trends than reported on previous studies [18].

5.5.3.2 Autogenous and Drying Shrinkage Starting at 24 hours

Autogenous shrinkage measurements started at the age of 24 hours and until the age of 56 days which was considered enough for the most of the autogenous shrinkage to occur. The average change in weight in that period was less than 0.02% of the initial weight of the specimens, so it could be neglected. Since change in weight reflected almost no moisture loss, it was concluded that change in length measured on the sealed specimens was only autogenous shrinkage.

Autogenous measurement started 24 hours after casting, so an important portion of it had already occurred. Moreover, the specimens had maturities close to those obtained in specimens with standard curing after 3-to-4 days.

Figure 5.30a and 5.30b present the autogenous shrinkage and drying shrinkage portions, respectively measured on the four HPC mixtures between 24 hours and 56 days after casting. Drying shrinkage was computed by subtracting autogenous shrinkage from total shrinkage measured on unsealed specimens. X-axis presents the time under testing and the Y-axis shrinkage in με.

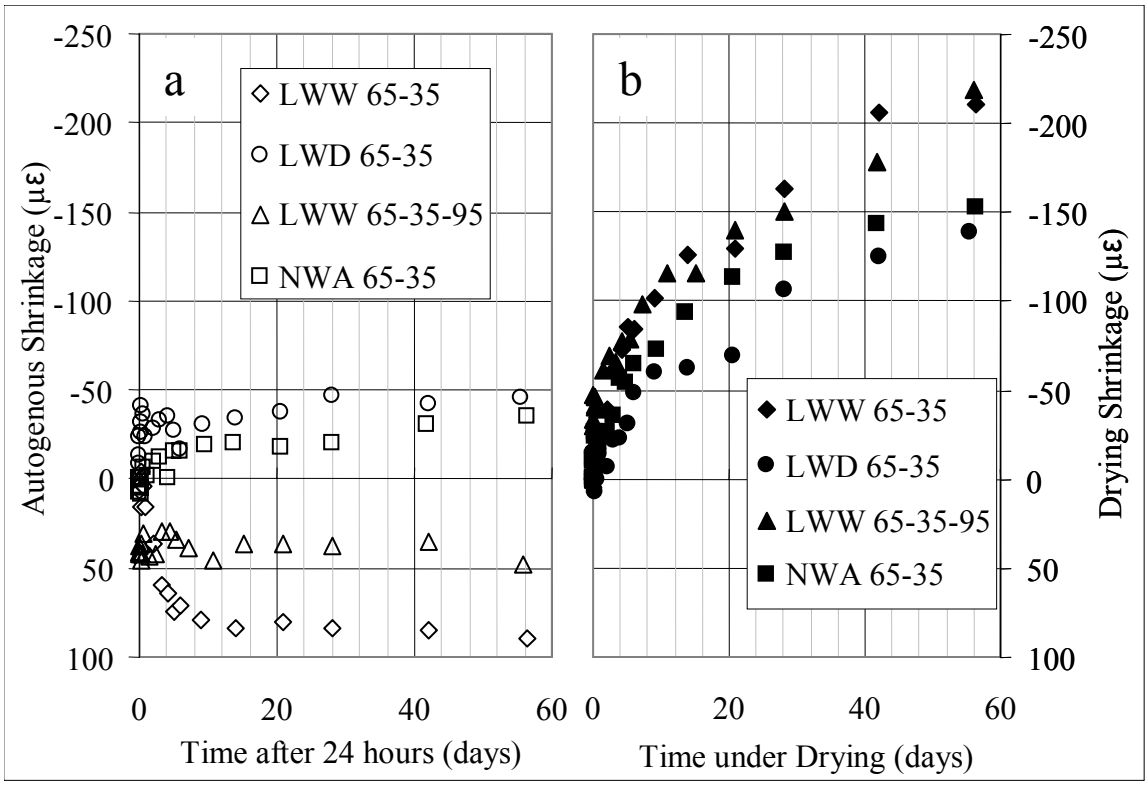

Figure 5.30: Autogenous and drying shrinkage between 24 hours and 56 days after casting for LWW 65-35, LWD 65-35, LWW 65-35-95 and NWA 65-35 mixtures

Autogenous shrinkage after 24 hours was clearly different for the pre-soaked lightweight aggregate mixtures than for the air-dried lightweight and normal weight aggregate mixtures. After 56 days, LWW 65-35 and LWW 65-35-95 presented expansion of 47 and 90 με, respectively while LWD 65-35 and NWA 65-35 had contractions of -35 and -45 με, respectively. The effect of the water stored in the pre-

soaked lightweight aggregate not only reduced autogenous shrinkage after initial curing period but caused expansion. Similar expansion has been reported by other investigators using pre-soaked lightweight aggregate [18, 41]. One of those presented similar expansion in magnitude for a lightweight HPC of similar strength. made using expanded clay.

When the aggregate was air-dried before mixing, it did not reduced autogenous shrinkage as compared to NWA 65-35 HPC. It was concluded that LWD 65-35 did not have enough stored water to significantly change autogenous shrinkage.

Drying shrinkage presented somehow opposite results than autogenous shrinkage. NWA 65-35 had a drying shrinkage lower than that of LWW 65-35 and LWW 65-35-95 mixtures by approximately 50 με. Lower drying shrinkage in NWA 65-35 was expected since the normal weight aggregate had a higher stiffness and therefore imposed more restraint to the cementitious paste shrinkage [27]. The comparatively lower drying shrinkage exhibited by LWD 65-35 mixture was unexpected since the aggregate restraining effect was similar to its pre-soaked counterparts.

5.5.3.3 Total Shrinkage Staring at 24 hours and 28 days

Total shrinkage was measured on specimens from every stage for a period of at least one year, and it included autogenous and drying shrinkage. Figure 5.31 presents total shrinkage in its Y-axis versus time under testing in its X-axis when measurements started 24 hour after casting.

There were no large differences in total shrinkage among the HPC mixtures after one year of measurements. One-year shrinkage averaged -302 and -314 με for LWW 65-35 and LWW 65-35-95, respectively. LWD 65-35 and NWA 65-35 mixtures had a total

shrinkage of -333 and -330 με, respectively after one year. Since the resolution of DEMEC gauge was 10 με, it can be concluded that the two pre-soaked lightweight aggregate mixtures had the same one-year shrinkage. LWW 65-35 mixture had lower shrinkage than its two counterparts: LWD 65-35 and NWA 65-35 mixtures.

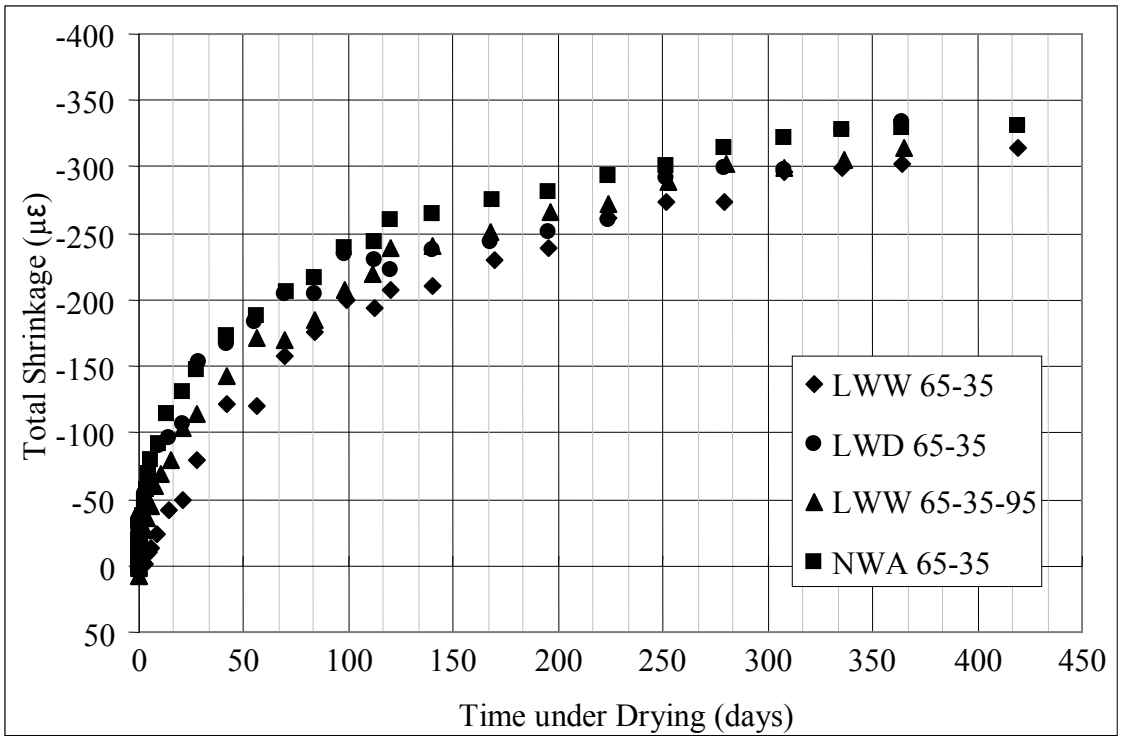

Figure 5.31: Total shrinkage for LWW 65-35, LWD 65-35, LWW 65-35-95 and NWA 65-35 mixtures when drying started at the age of 24 hours

The rate of shrinkage seemed to be different. After 21 days under drying, total shrinkage of LWW 65-35 was approximately 100 με lower than that of NWA 65-35 mixture. The difference decreased to 50 and 30 με after 100 and 365 days of drying. This might be due to the higher drying shrinkage component showed by LWW 65-35 compared to NWA 65-35. Thus, as time under drying increases LWW 65-35 total shrinkage came closer to NWA 65-35 values. Similar finding were reported by other

studies where lightweight HPC showed lower shrinkage, but higher shrinkage rate than normal weight HPC [42-44].

Shrinkage of lightweight HPC made with different lightweight aggregate with drying starting at one day has been reported [42, 45, 46]. Those studies obtained values between -300 and -800 με after 100 days HPC with for sintered fly ash, one-year shrinkage of 450 με for expanded clay HPC, and 270 με after 128 days for expanded slate HPC. LWW 65-35 mixture had shrinkage of -200, -210, and -300 με after 100, 120, and 365 days. Therefore, LWW 65-35 had considerably less shrinkage than that of HPC made with sintered fly ash and less shrinkage than HPC made with expanded clay and shale.

Total shrinkage was also measured on specimens after 28 days of moist curing. It was expected that after 28 days total shrinkage corresponded mostly to drying shrinkage because the small autogenous shrinkage at that age. Figure 5.32 shows total shrinkage for the mixtures under study. X-axis presents time under drying while Y-axis has shrinkage in με.

One-year shrinkage of LWW 65-35 and NWA 65-35 mixtures was -265 and -305 με respectively. Those values were roughly 30 με lower than its counterparts when drying started after 24 hours. It was believed that drying shrinkage did not change much between the two ages of staring of drying, so the 30 με difference might have been due to autogenous shrinkage. According to four out of the six most used empirical models for shrinkage, age at the beginning of drying is not an important variable in estimating drying shrinkage [2, 5, 47-50].

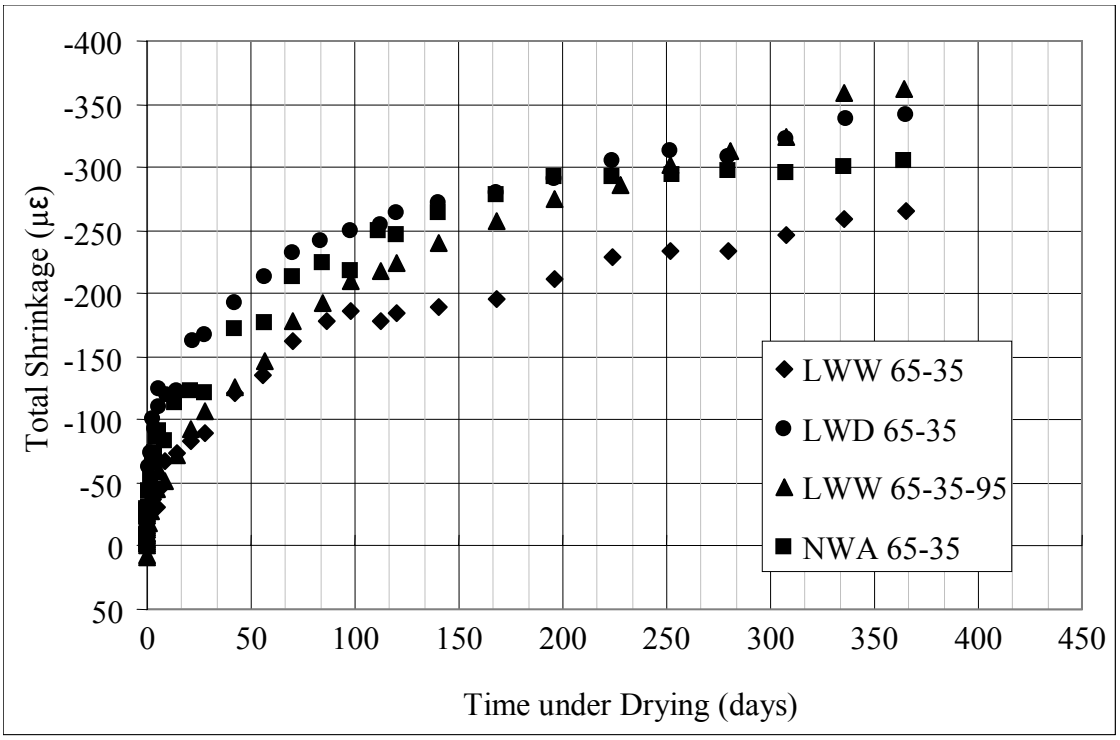

Figure 5.32: Total shrinkage for LWW 65-35, LWD 65-35, LWW 65-35-95 and NWA 65-35 mixtures when drying started at the age of 28 days

LWW 65-35-95 and LWD 65-35 presented one-year total shrinkage of -362 and -341 με, respectively. The former value was unexpectedly high since it was 50 με higher than the one-year shrinkage when drying started at only 24 hours. LWD 65-35 presented virtually the same one-year shrinkage than that obtained when drying started at early age.

When comparing LWW 65-35 and NWA 65-35 shrinkage rates, it seems that the former presented considerably lower rate during the first 10 days which yielded to less shrinkage. Between 10 and 200 days they had a similar rate, but NWA 65-35 showed an important decrease in shrinkage rate after 200 days which lowered the difference with respect to LWW 65-35.

A similar study of HPC made with expanded slate [51] reported one-year shrinkage of -310 με which was higher than the -264 με obtained for LWW 65-35. That

mixture had a 28-day compressive strength equivalent to 72% of that obtained in LWW 65-35 which might explain the differences in shrinkage. Other study on shrinkage of HPC made with expanded shale HPC obtained -68 με after 128 days of drying [45]. That was considerably lower than that of LWW 65-35 at the same time of drying. Those authors reported 90-day compressive strength of 97.6 MPa (14,150 psi) which was considerably higher than the one-year strength obtained with LWW 65-35.

Since shrinkage of LWW 65-35 mixture was lesser than that of lightweight HPC with lower strength and greater than that of a mixture with higher strength, it was concluded that it was in agreement with previous research.

5.5.4 Creep Deformations

Total creep was measured on ten 100 x 380-mm (4 x 15-in) and six 150 x 300-mm (6 x 12-in) cylinder unsealed specimens under loading and drying on each of the mixtures. Basic creep was measured on six 100 x 380-mm (4 x 15-in) cylinder sealed specimens under loading. During the first two stages, specimens were loaded for 120 days, and during the third stage they remained under loading for at least 225 days.

Total creep was calculated by subtracting total shrinkage from the strain measured on the specimens under loading and drying. Basic creep was obtained from the difference between sealed specimens under loading and sealed specimens without load. Drying creep was obtained by subtracting basic creep from total creep.

5.5.4.1 Basic and Drying Creep Starting at 24 hours

Figures 5.33a and 5.33b present basic and drying creep, respectively versus time for the mixtures under study. Time under testing is shown in the X-axis while creep expressed as specific creep is shown in the Y-axis in με/MPa (με/psi).

Figure 5.33 clearly shows the basic creep was much higher than drying creep for any mixture and time under loading. For instance, after 225 days under load, basic creep of LWW 65-35, LWD 65-35, and NWA 65-35 were 6.3, 5.2, and 12.8 times the drying creep portion. This agrees with the conclusion that the better creep performance of HPC is due to a reduction in the drying creep portion [52].

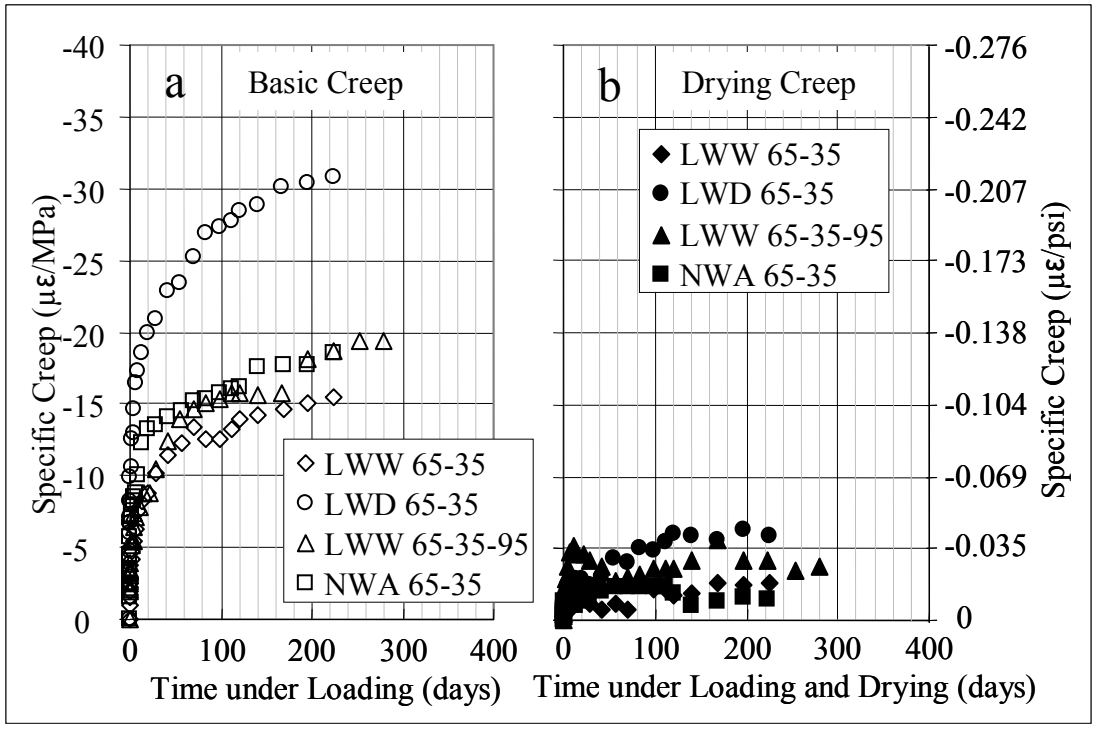

Figure 5.33: Creep of HPC mixtures when loaded 24 hours after casting, (a) basic creep, (b) drying creep

Since the drying shrinkage portion was comparatively low, it was suggested that total creep of these HPC mixtures would not vary considerably with the size of the specimens.

LWW 65-35 mixture had lower creep than LWD 65-35 in both basic and drying creep portions. LWW 65-35 had a 225-day basic creep of -15.5 με/MPa (-0.107 με/psi)

while LWD 65-35 double that with -30.9 με/MPa (0.213 με/psi). Drying creep after 225 days was -2.5 and -5.9 με/MPa (-0.017 and .041 με/psi). It was concluded that the water stored within the pre-soaked lightweight aggregate reduced basic creep by approximately 50%.

It is believed that internally stored water might have reduced creep by three mechanisms:

(a) Enhanced hydration: the internally stored water could have prolonged internal curing improving hydration [53-55]. The cementitious paste microstructure could have become denser, stronger and better able to resist creep;

(b) Expansion of microstructure: as occurs with concrete immersed in water, cementitious paste could have taken water from the pre-soaked aggregate causing swelling. Creep would have needed to be greater than swelling in order to be measurable. Expansion was seen in sealed specimens with pre-soaked lightweight aggregate, and other authors have also reported expansion in specimens with pre-soaked lightweight aggregate and SAP and [17, 18].

(c) Water seepage blockage: internally stored water could have kept internal relative humidity high [56] which could have reduced or prevented water migration from C-S-H surface caused by sustained loading.

There is no agreement on the mechanisms that cause creep in concrete [4, 22, 57-60]. Researchers generally agreed that aside from microcracking in the interface zone, creep can be understood from viscoelastic deformation in the cement paste and water seepage of water under stress from C-S-H surface to capillary pores. The viscoelastic effect is thought by many as the cause of basic creep and the water seepage as the cause

of drying creep. Nevertheless, some authors stated that seepage theory can explain both basic and drying creep. They argued that under no moisture exchange with the environment, adsorbed water expelled from the C-S-H can move to capillary pores or even to aggregate pores [61].

The latter would explain differences between creep of LWW 65-35 and LWD 65-35 mixtures. Air-dried lightweight aggregate had empty pores that would have facilitated water seepage from C-S-H. On the other hand, pre-soaked lightweight aggregate could have kept capillary pores near to saturation leaving no place for seepage to go.

NWA 65-35 presented 225-day basic and drying creep of 18.6 and 1.5 με/MPa (0.128 and 0.010 με/psi), respectively. The basic creep portion was 3.0 με/MPa (0.021 με/psi) higher than that of LWW 65-35 mixture and the drying portion was 1.0 με/MPa (0.007 με/psi) lower than that of LWW 65-35. Thus, total creep of LWW 65-35 and NWA 65-35 mixtures was 18.0 and 20.0 με/MPa (0.124 and 0.138 με/psi), respectively after 225 days under load. This 10% difference was in despite of the fact that NWA 65-35 that a 24-hour compressive strength 23% higher than that of LWW 65-35 mixture.

The latter is thought to be caused by the fact the strength and creep of concrete do not depend on the same factors and to the same extent. It is well known that the use of a lightweight and porous aggregate with lower intrinsic strength reduces the compressive strength of concrete. Nevertheless, the use of pre-soaked lightweight aggregate might reduce creep though enhanced hydration, expansion and water seepage blockage.

It should be noticed that basic creep of NWA 65-35 was bounded by that of LWW 65-35 and LWD 65-35 mixtures. Without pre-soaking, LWD 65-35 mixture had higher creep than its NWA 65-35 counterpart. This obeyed the concept of the aggregate

restraining effect on creep [15] where a lower stiffness aggregate would yield to higher creep all other variable being the same. Nevertheless, when lightweight aggregate was pre-soaked, creep of LWW 65-35 was lower than that of NWA 65-35 mixture showing the importance of the water to creep development.

LWW 65-35-95 had less basic and drying creep than the LWD 65-35 mixture which again can be explained by the use of pre-soaked lightweight aggregate. Nevertheless, LWW 65-35-95 had more basic creep than LWW 65-35 and about the same basic creep than that of NWA 65-35. Thus, the use of 9.5-mm (0.375-in) MSA lightweight aggregate instead of 12.7 mm (0.5 in) reduced the effectiveness of water storing on the reduction of creep.

It is believed that the average pore size of the 9.5-mm (0.375-in) MSA lightweight aggregate could have been smaller than that of the 12.7-mm (0.5-in) MSA aggregate. The latter being a consequence of the crushing process to reduce the size of aggregate. The efficiency of the internal curing have been found to be related to the pore size and pore structure [62, 63] , so finer pores will hold water reducing the amount of free water able interact with cementitious paste.

5.5.4.2 Basic and Drying Creep Starting at 28 days

Total and basic creep of HPC mixtures when loaded at the age of 28 days were measured during stage 1 for 120 days and during stage 2 for one year. Figure 5.34a presents basic creep in the Y-axis versus time under load in the X-axis. Figure 5.34b shows drying creep in the same fashion as basic creep.

As seen for creep at early age loading, the basic creep was much larger than drying creep at all times under testing for all mixtures. The main difference with the 24-hour testing was that here the difference was even larger. For LWW 65-35, LWW 65-35-95 and NWA 65-35 one-year basic creep was about 13 times larger than its drying creep counterpart.

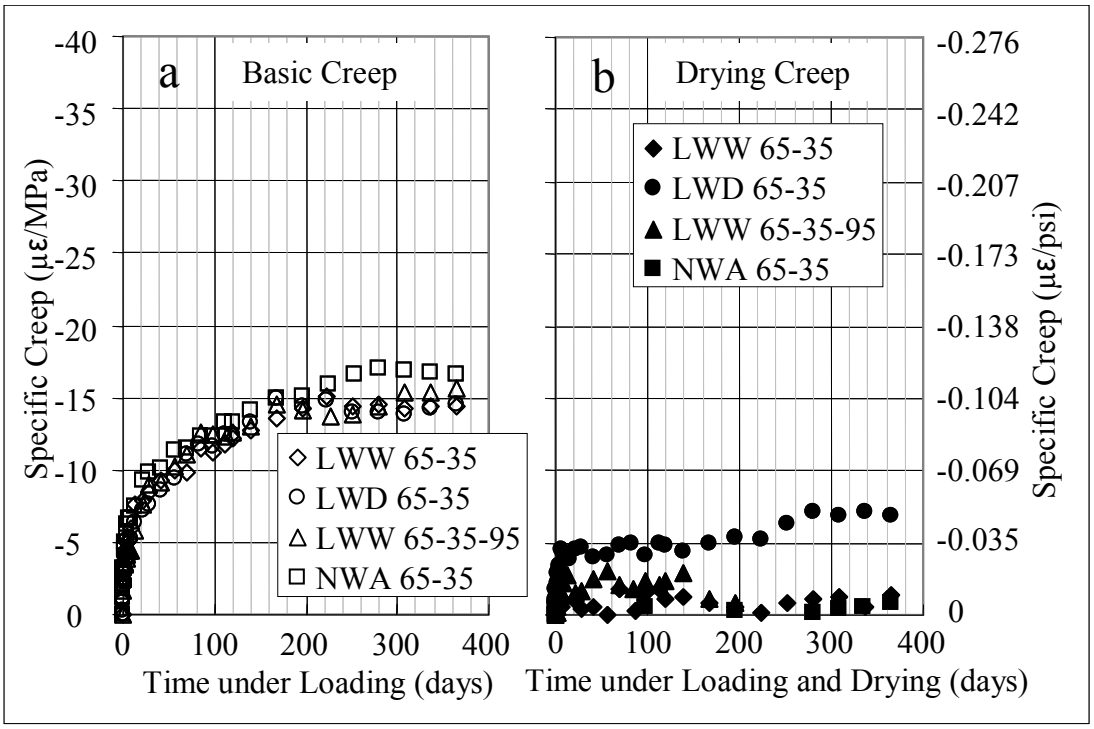

Figure 5.34: Creep of HPC mixtures when loaded 28 days after casting, (a) basic creep, (b) drying creep

Basic creep of all four mixtures decreased with respect to the one measured with loading at early age. Decrease in creep with increasing age at loading had been documented by many researchers and also incorporated in the empirical models for estimating creep [2, 5, 47-50]. It is believed that such improvement in creep performance

with increasing loading age is, as occurs with compressive strength, caused by an increase in the degree of hydration of the cementitious paste.

One-year basic creep was -14.4, -14.5, -15.7, and -16.8 με/MPa (0.099, 0.100, 0.108, and 0.115 με/psi) for LWW 65-35, LWD 65-35, LWW 65-35-95, and NWA 65-35, respectively.

The least amount of improvement between early age loading and 28-day loading was shown by LWW 65-35 which only decreased drying creep by 8%. This is believed to be a consequence of the curing afforded by internally stored water; i.e., LWW 65-35 already had good curing when loaded at 24 hours compared to the other three HPC mixtures. Therefore, after 28 days in the fog room the improvement is not as high as that obtained in the other mixtures.

In the opposite case, LWD 65-35 which did not have a good internal curing registered a great decrease in basic creep after 27 days in the fog room.

Drying creep portions were only -1.5 and 0.7 με/MPa (0.010, and 0.005 με/psi), for LWW 65-35 and NWA 65-35, respectively. These values multiplied by a service load of 40 MPa (5800 psi) were in the range 20-to-40 με range which is extremely low compared to shrinkage and basic creep portions.

One-year drying creep of LWD 65-35 mixture was 7.0 με/MPa (0.048 με/psi) which was comparatively large compared to its counterparts. This was unexpectedly high, and might have been caused by a comparatively higher water permeability of those specimens. The latter would explain not only the higher drying creep but also the great improvement in basic creep. If water permeability in those specimens was actually higher, water during the moist storage period could have provided a better curing

improving the basic creep performance of the sealed specimens, but facilitating drying of the unsealed specimens at the same time. The latter constitutes only a hypothesis since permeability was not measured in this study.

5.5.4.3 Total Creep Staring at 24 hours and 28 days

In addition to the 100 x 380-mm (4 x 15-in) cylinder specimens, total creep was also measured on standard 150 x 300-mm (6 x 12-in) cylinders. Since statistical analysis revealed not consistent differences in total creep between the two sized specimens, the values obtained from them were averaged together.

Total creep as measured for the 24-hour and 28-day loading is shown in Figure 5.35a and 5.35b, respectively. Time under loading and drying is presented un the X-axis and specific creep in με/MPa (με/psi) in the Y-axis.

When creep testing started at the age of 24 hours, LWW 65-35 mixture presented the lowest total creep for any time under load between zero and 225 days. When the aggregate was not pre-soaked (LWD 65-35 mixture), total creep increased by 69%. NWA 65-35 mixture had lower creep than LWD 65-35, but higher creep than LWW 65-35 for all the period under testing. LWW 65-35-95 presented great improvements in creep performance compared to LWD 65-35, but it sill had higher creep than NWA 65-35 mixture.

There is a clear difference in creep rate between LWW 65-35 and NWA 65-35 mixtures. Creep rate of the latter seemed to have decreased faster than that of LWW 65-35. This means that if the current creep rates persist, creep of LWW 65-35 could be larger than that of NWA 65-35.

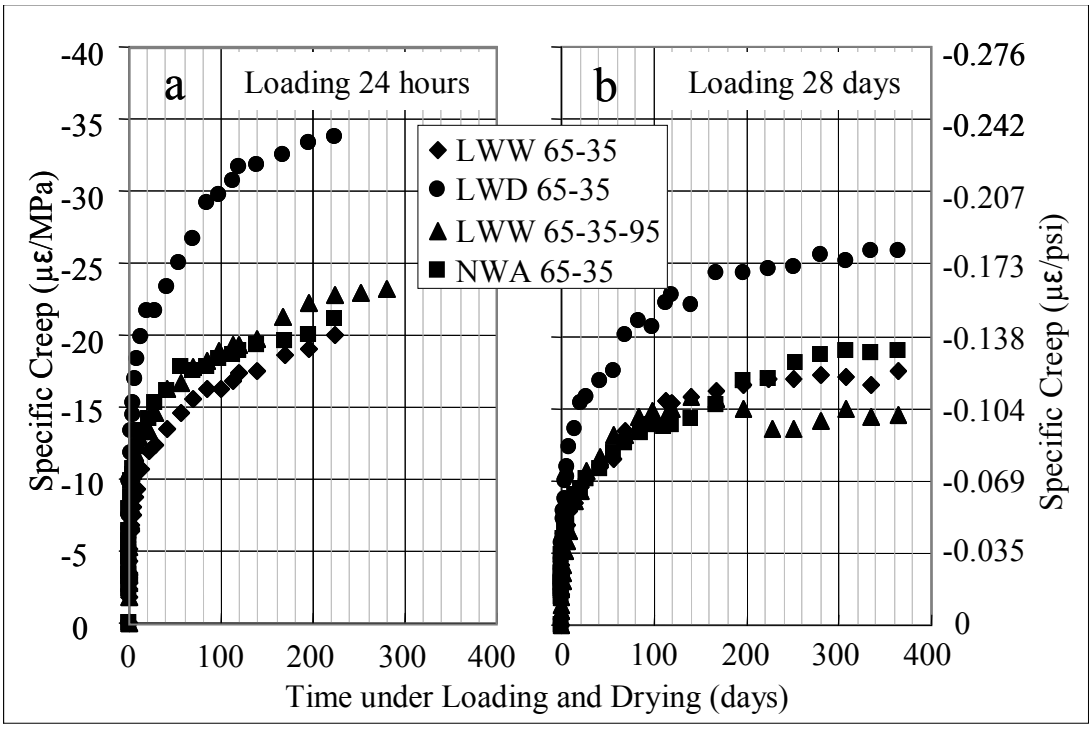

Figure 5.35: Total creep for LWW 65-35, LWD 65-35, LWW 65-35-95 and NWA 65-35 mixtures, (a) when testing started at the age of 24 hours, (b) when testing started at the age of 28 days

The results reported herein confirmed the conclusions obtained in an earlier creep study with loading at 24 hours [64].

When testing started at the age of 28 days, the favorable curing conditions inside the fog room helped to decrease creep of all four HPC mixtures. Nevertheless, the improvement was more noticeable in those mixtures with poor curing such as LWD 65-35 and NWA 65-35. LWW 65-35 improved comparatively less than its counterparts.

Creep of LWW 65-35 loaded at 28 days of age was considerably lower than that reported by other authors in lower strength lightweight HPC [42, 51]. To the authors' knowledge, there is no previous investigation on creep of lightweight HPC loaded at 28 days with similar strength than those reported herein. The one-year creep obtained for LWW 65-35, LWD 65-35, LWW 65-35-95, and NWA 65-35 mixtures are within the

range reported for HPC with compressive strength of 70 MPa (10,150 psi) and higher [65].

5.6 Effect of Pore Connectivity on Drying Creep and Drying Shrinkage

Great impermeability has been pointed out by many to be responsible of the reduction in creep and shrinkage observed in HPC. This section explores the relationship between concrete volumetric changes due to drying and pore connectivity measured by absorption. Four mixtures are considered in this section: LWW 65-35, NWA 65-35 and HP Matrix, which had low water-to-cementitious material ratio, and NSC mixture.

5.6.1 Change in Weight

Sealed and unsealed shrinkage specimens were weighted on every length measurement. As the sealed specimens had a change in weight of less than 3 g (0.007 lb) or 0.05% during the one-year testing period, it was concluded that the method of sealing was effective in preventing moisture loss. The change in mass of the unsealed specimens was between 0.43 and 2.88% during one year that was assumed to be entirely due to water loss.

Figures 5.36 presents average change in weight measured on specimens from the four mixtures under study (Y-axis) versus time under drying (X-axis). Particularly, Figure 5.36a presents the change expressed as percentage of the initial weight.

Since the initial weight of the specimens varied widely between 6150 and 7790 g (13.6 and 17.2 lb) due to its different densities (see Table 5.2), Figure 5.36b presents the change in weight expressed as a percentage of the water contained in the specimens at the beginning of drying. Initial water in the specimens was calculated from the mixture

design and specimen volume, and any change in weight during the 28-day storage period in the fog room was neglected. This non-standard way to express moisture loss was believed to best describe the drying phenomenon in this study.

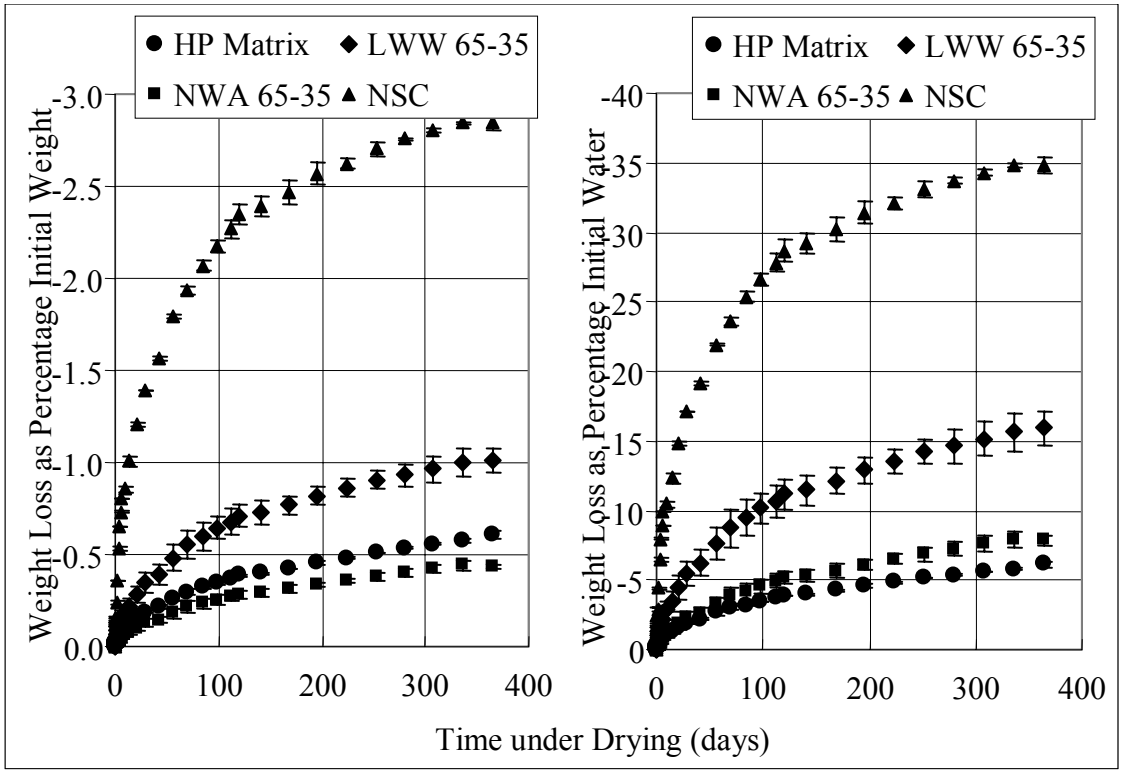

Figure 5.36: Change in weight in unsealed shrinkage specimens for HP Matrix, LWW 65-35, NWA 65-35, and NSC

Figure 5.36a shows that after one year moisture loss represented 2.9, 1.0, 0.4 and 0.6% of the initial weight for NSC, LWW 65-35, NWA 65-35, and HP Matrix, respectively. This means the moisture loss in NSC was approximately three times greater than in LWW 65-35 and almost six times greater than in NWA 65-35 or HP Matrix. This large difference is presumably due to the lower water-to-cementitious material ratio, use of silica fume and the lower permeability of the HPC mixtures.

Among HPCs, LWW 65-35 showed 1.6 and 2.5 times more weight loss than HP Matrix and NWA 65-35, respectively; however, HP Matrix had initially 64% more

mixing water than LWW 65-35 or NWA 65-35, and LWW 65-35 had a density close to 82% any of the other two HPCs. This suggested that even though variations in mass loss represented well the differences between HPCs and NSC, it did not fully reflect the water binding capacity within HPCs. That is, the fact that HP Matrix lost more weight than NWA 65-35 does not mean necessarily that it had higher permeability or lower capillary forces.

An analysis of Figure 5.36b reveals that NSC lost 35% of its initial water during the one-year drying period. This was still considerably greater than water loss of 16, 8, and 6% measured in LWW 65-35, NWA 65-35, and HP Matrix, respectively.

The LWW 65-35 HPLC exhibited a moisture loss which was double that of its NWA 65-35 counterpart. Even though those to mixture had 135 kg/m^3 (228 lb/yd^3) of mixing water, the pre-soaked lightweight aggregate could have contributed an additional 40 kg/m^3 (67.4 lb/yd^3) of water that was also lost during 50% relative humidity exposure. Several authors [18, 35-37, 66] have demonstrated that the water contained in the pre-soaked lightweight aggregate can prevent self-desiccation, which can occur in HPC, particularly in the presence of silica fume. Thus, the pre-soaked lightweight aggregate might have produced higher internal relative humidity in the LWW 65-35 HPLC than HP Matrix or NWA 65-35 HPCs, which in turn increases the moisture gradient with the environment and likely resulted in faster rate of moisture loss observed in Figure 5.36.

Relative water loss, shown in Figure 5.36b, clearly shows that the HP Matrix was the mixture that showed the least drying closely followed by NWA 65-35. Those two mixtures lost only 6 and 8% of it initial water content. This is believed to be caused by three factors. First, low interconnectivity of their capillary porosity in these HPC

mixtures impeded moisture migration from inside. Secondly, the fine pore structure developed within such low water-to-cementitious material ratio resulted in greater binding of moisture in the pore system (larger capillary forces). And finally, due to the low water-to-cementitious material ratio and the use of 10% of silica fume, self-desiccation could have been considerably. This reduced internal relative humidity, so the moisture gradient; i.e., the drying driving force, decreased.

5.6.2 Sorptivity

Figure 5.37a presents mass loss during oven-drying at 105 ^{o}C (222 ^{o}F) for each type of mixture under study. Its X-axis shows time of drying in days and the Y-axis the average mass loss, of four specimens, expressed as percentage of its initial weight.

All mixtures reached the constant weight condition between 48 and 72 hours where the change in weight was less than 0.5%.

The oven-drying curves showed smaller differences between HPC mixtures and NSC than the air-drying ones in Figure 5.36. NSC lost approximately twice the water than LWW 65-35 or HP Matrix and 3 times more than that of NWA 65-35 HPC. The shape of the drying curves versus time was also different with respect to those obtained in air-drying. NSC lost on average 6% of its weight during the first 48 hours and only 0.06% between 48 and 72 hours of drying. HPC mixtures presented a much slower rate of drying, although, the lost in weight between 48 and 72 hours was comparatively larger than in NSC. The small differences in drying among HP Matrix, LWW 65-35, and NWA 65-35 were likely due to differences in the initial water contents. HP Matrix considered more mixing water than LWW 65-35 or NWA 65-35, and LWW 65-35 had additional

water absorbed by the pre-soaked aggregate. Thus HP Matrix and LWW 65-35 lost more water than NWA 65-35.

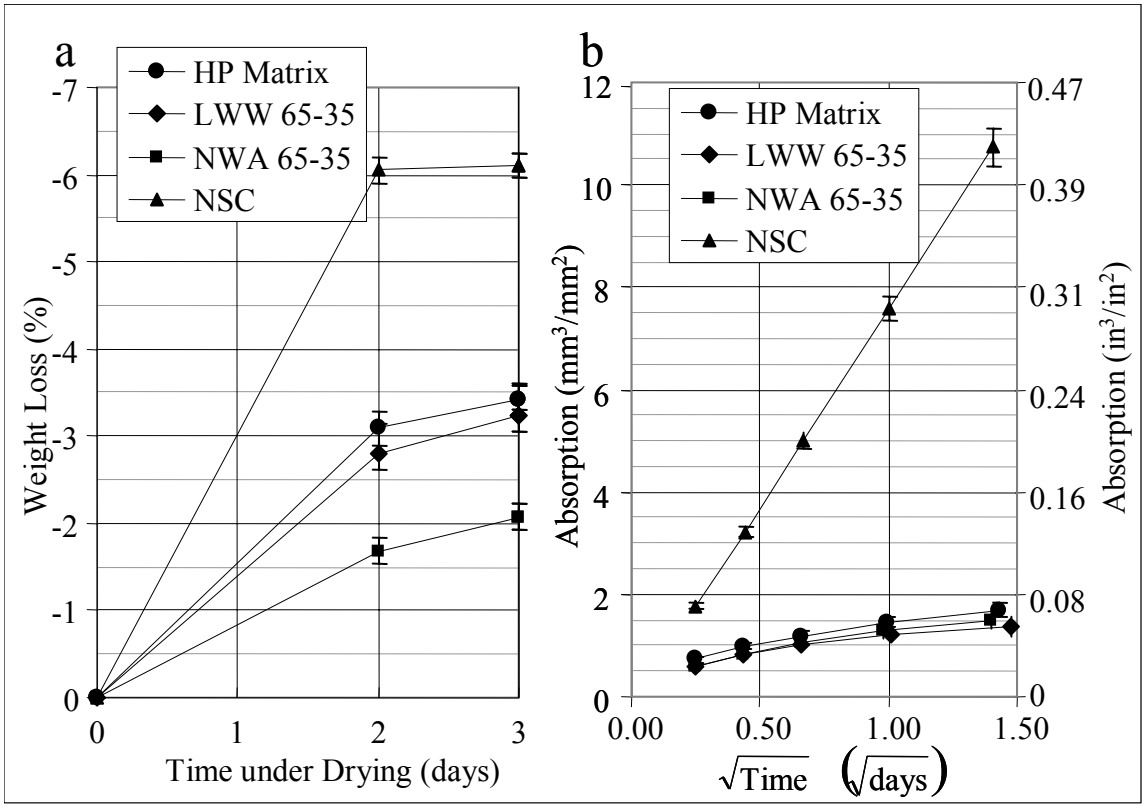

Figure 5.37: Drying and absorption of HP Matrix, LWW 65-35, NWA 65-35, and NSC

After drying, the samples were immersed in water as explained previously. Change in mass by absorption was recorded for 16 days to meet the guidelines by RILEM [67], although, further analysis revealed that the change in absorption rate (nick point) occurred after eight days for NSC and only after two days for the HPC mixtures.

Figure 5.37b presents average absorption versus square root of time during the first two days of testing. Absorption was expressed as the volume of absorbed water divided by the exposed area; that is, the average penetration depth of water into the specimens expressed in units of length (mm^3/mm^2 or mm / in^3/in^2 or in).

Average penetration rate of NSC after two days (1.41 days^{05}) of testing was 10.7 mm (0.42 in) while the HPC mixtures were between 1.4 and 1.6 mm (0.05 and 0.06 in). That is, penetration depth in HPCs was about 14% of that seen in NSC which is more than the relative differences seen between HPCs and NSC in the drying curves. It should be noticed that the three HPCs behaved very similarly and most of the individual results overlapped. Thus, when they initially had the same moisture state (via oven dry), the absorption depended only on the capillary pore size and interconnectivity which were expected to be similar in those mixtures.

Sorptivity of NSC was 7.75 mm^3/mm^2/day$^{0.5}$ (0.305 in^3/in^2/day$^{0.5}$). Values in the range between 6.4 and 7.5 mm^3/mm^2/day$^{0.5}$ (0.18 and 0.30 in^3/in^2/day$^{0.5}$), have been reported in the past for NSC of similar characteristics tested at the age of 28 days [68, 69].

After 16 days, NSC specimens absorbed an average of 96.7 g (0.21 lb) of water which represented an average penetration of 21.21 mm (0.835 in).

Figure 5.38 presents the absorption curves obtained for HP Matrix, LWW 65-35 and NWA 65-35 mixtures. They are the same showed in Figure 5.37b, but without NSC results, to better allow for comparisons of the HPC results.

As seen in Figure 5.38, the absorption curves of the three HPCs are very similar and individual values overlap. Nevertheless, an analysis of variance (ANOVA) revealed significant differences between LWW 65-35 and HP Matrix and between NWA 65-35 and HP Matrix.

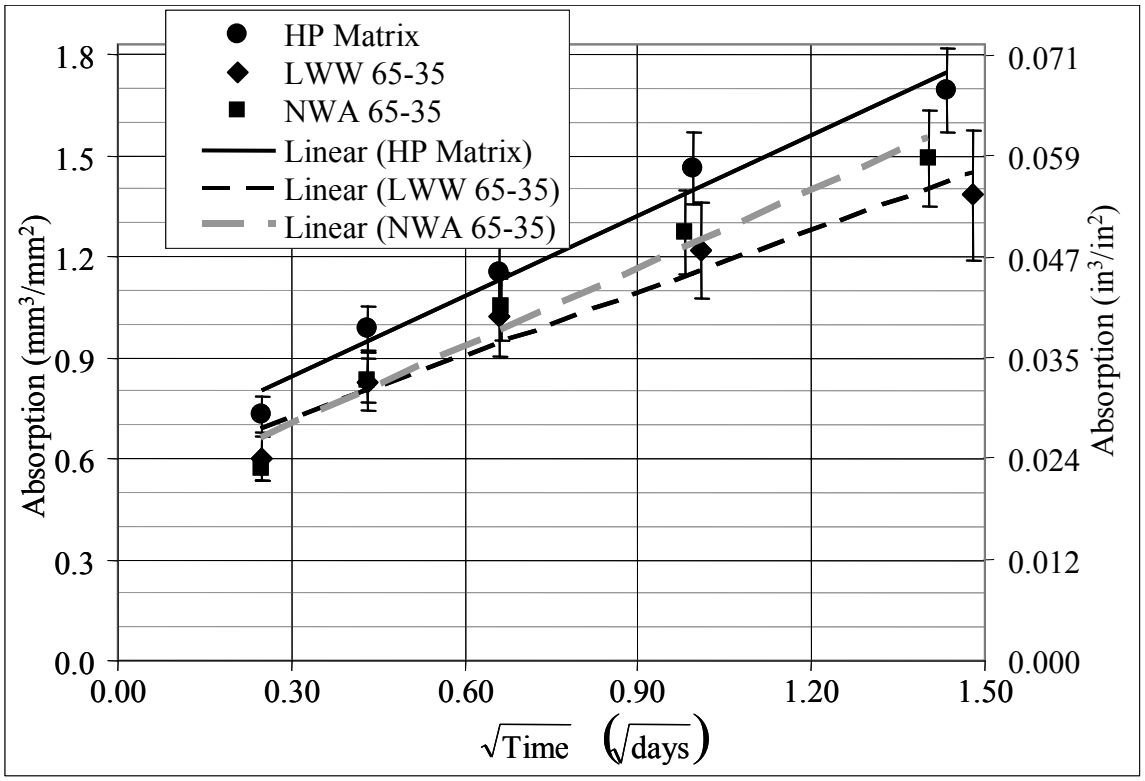

Figure 5.38: absorption versus square root of time for HP Matrix, LWW 65-35, and NWA 65-35

The relatively higher absorption of HP Matrix, which was unexpected, might have been related to the temperature history of the specimens as HP Matrix specimens reached higher temperatures during the 24-hour insulated-curing than LWW 65-35 or NWA 65-35 due to higher content of cementitious materials. This could have produced cracking with the consequent increase in absorption. The two HPC mixtures with coarse aggregate showed very similar average absorption versus time. In fact, ANOVA showed no significant differences between LWW 65-35 and NWA 65-35 mixtures. Therefore, the use of a porous aggregate did not affect water capillary absorption significantly as measured by this procedure.

Nevertheless, when looking at the trends shown in Figure 5.38, it seems that the absorption of NWA 65-35 develops faster than LWW 65-35. In fact, Sorptivities of LWW 65-35 and NWA 65-35 were 0.615 and 0.736 $mm^3/mm^2/day^{0.5}$ (0.024 and 0.029 $in^3/in^2/day^{0.5}$), respectively while sorptivity of HP Matrix resulted in 0.801 $mm^3/mm^2/day^{0.5}$ (0.032 $in^3/in^2/day^{0.5}$). The three HPCs presented an average sorptivity of 0.717 $mm^3/mm^2/day^{0.5}$ (0.028 $in^3/in^2/day^{0.5}$) which is precisely one order of magnitude lower than that of NSC. One study reported that a HPC mixture with water-to-cementitious material ratio of 0.4 and 5% of silica fume had a sorptivity of 2.6 $mm^3/mm^2/day^{0.5}$ (0.102 $in^3/in^2/day^{0.5}$) [69]. The lower values obtained herein are in agreement since they had 10% of silica fume and water-to-cementitious material ratio of 0.23 which are both expected to further decrease sorptivity as concluded by the same study [69].

LWW 65-35 HPLC presented the lowest sorptivity in despite of using a more porous aggregate. Similar conclusions have been obtained when comparing water permeability and chloride permeability of a low water-to-cementitious material ratio HPC with lightweight aggregate and a similar HPC with normal weight aggregate [55, 70].

It should be noticed that the absorption curves of the three HPCs did not present a strong linear development with the square root of time as absorption of NSC (see Figure 5.37b), their rates rather continuously decreased with time. Thus, somehow assumption of linear relationship between during the first two days (nick point after 2 days), could have affected the results. When sorptivity was calculated using more data points the results did not vary importantly and LWW 65-35 and HP Matrix continued presenting the lowest and highest sorptivities, respectively. It was concluded that the selection of the

nick point, which was in agreement with previous research [68, 69, 71], adequately represented the absorption characteristics of HPCs under study.

The use of silica fume and low a water-to-cementitious material ratio could have had two potentially competing effects on sorptivity. First, both are expected to decrease the interconnectivity of the pore system, limiting absorption and slowing the rate of water intake. Second, they are expected to refine the pores increasing the capillary suction. From these results, it seemed that the decrease in interconnectivity of the pore system governed since the absorption values for each of the HPCs were lower by an order of magnitude than those of NSC.

5.6.3 Drying Shrinkage Deformations

Drying shrinkage was obtained from the measured total shrinkage by subtracting autogenous shrinkage component. For NSC, it was assumed that total and drying shrinkage were equivalent because of the small autogenous shrinkage expected in a 0.60 water-to-cement ratio concrete after 28 days. Figure 5.39 shows drying shrinkage for the mixtures under study. X-axis presents time under drying while Y-axis has shrinkage in με.

As expected, NSC had one-year shrinkage of -560 με which was higher than any of the HPC mixtures. This was somewhat lower than the -650 με obtained in the past [72], for this mixture design also with granite coarse aggregate. One potential difference might be the greater fineness and greater proportion of fast reacting tricalcium silicate (C_3S) in modern Type I portland cement.

Drying shrinkage for the three HPC mixtures were similar and ranged between -210 and -220 με after one year of drying. Those differences were lower than the resolution of the DEMEC gauge, so there were not significant.

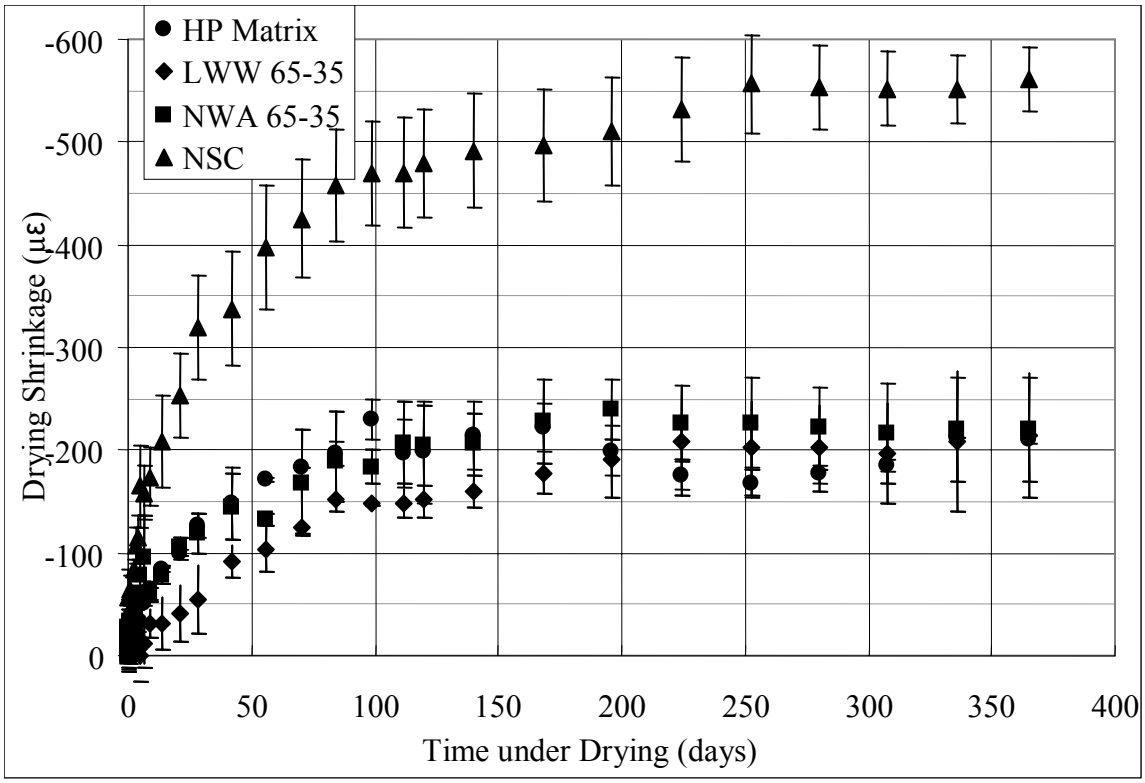

Figure 5.39: Drying shrinkage for HP Matrix, LWW 65-35, NWA 65-35 and NSC mixtures

Shrinkage of NSC agreed very well with the hyperbolic relationship with time proposed by the ACI-209 model [5], where 50% of the ultimate shrinkage is reached after 35 days of drying. The ultimate shrinkage value extrapolated from the experimental data and ACI-209 equation was -567 με.

The HPC Matrix, LWW 65-35, and NWA 65-35 mixtures also showed a hyperbolic change with time, but they occurred at different rates. For instance, the HP

Matrix and NWA 65-35 seemed to have reached 50% of their ultimate values after only 20 days, while the LWW 65-35 attained this after 84 days of drying. Assuming that the hyperbolic change with time was adequate for the HPCs, the ultimate shrinkage values obtained by extrapolating experimental data with ACI-209 equation were -245, -211, and -260 με for the HP Matrix, LWW 65-35, and NWA 65-35, respectively.

Some similarities were apparent when comparing trends in the data for absorption (Figure 5.37b) and drying shrinkage (Figure 5.39). For instance, the NSC exhibited the highest 2-day absorption and sorptivity and also had the highest drying shrinkage. The three HPC mixtures had relatively similar absorption characteristics and virtually the same one-year drying shrinkage.

Larger relative differences between NSC and the three HPC mixtures were apparent in the sorptivity, as compared to differences in drying shrinkage. Although encouraging as this suggests that sorptivity might be a good predictor for deformation, this was, however, expected. Sorptivity will be most influenced by the pore system while drying shrinkage will be also influenced by additional factors including relative humidity, and the relative volume and properties of the aggregate.

5.6.4 Drying Creep Deformations

Drying creep as calculated from the total creep by subtracting the basic creep portion is shown in Figure 5.40. Creep strain divided by applied stress (specific creep) is presented in the Y-axis while time under loading and drying is shown in X-axis.

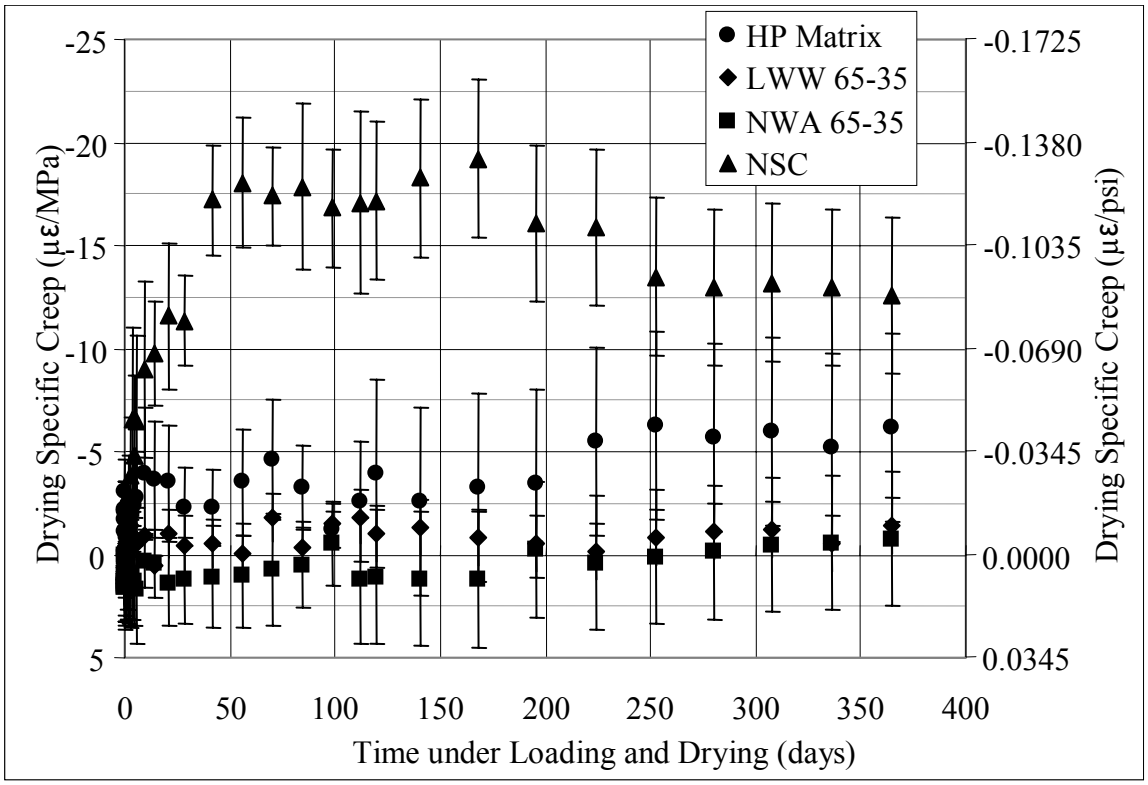

Figure 5.40: Drying creep for HP Matrix, LWW 65-35, NWA 65-35 and NSC mixtures

As seen if all other properties, large differences are observed between NSC and the three HPC mixtures. Drying creep of NSC reached a value in the vicinity of -17 με/MPa (-0.117 με/psi) after 50 days, and then decreased to -13 με/MPa (-0.090 με/psi) which changed little after 250 days. This unexpected reduction in drying creep might likely reflect experimental error. It should be noticed that drying creep was calculated from data from three different types of specimens: unsealed non-loaded, unsealed under loading, and sealed under loading. Any variability among the several specimens from each of these three sources could affect overall trend in drying creep. Upon examination of the three data sets, it was concluded that the drying creep of NSC asymptotes rather than decreased. This means that the creep seen after 200 days was mainly due to basic creep.

The LWW 65-35 and the NWA 65-35 HPCs showed almost no drying creep with values varying between ± 1.2 με/MPa (± 0.008 με/psi) during the one-year period. Those values multiplied by an applied service stress of 27.6 MPa (4000 psi) would yield to creep strains up to -28 με which is small compared to the -220 με of drying shrinkage.

The HP Matrix also showed little drying creep with values between -2.6 and -6.1 με/MPa (-0.018 and -0.042 με/psi). As was concluded for NSC, drying creep of HP Matrix seemed to reach an asymptote after 200 days of loading and drying.

When comparing Figures 5.37b and 5.40, some similarities between drying creep and absorption of the mixtures is concluded. The more interconnected the pore system in NSC, which also affected absorption behavior seems to facilitate the occurrence of drying creep.

Drying creep of NSC was on average 3.6, 28.1, and 20.5 times larger than that of HP Matrix, LWW 65-35, and NWA 65-35, respectively.

5.6.5 Long-term drying deformations versus Absorption

Figure 5.41 presents a comparison between sorptivity (X-axis) and one-year drying shrinkage (in Y-axis) as measured in the NSC and the three HPCs. All data was expressed relative to that obtained for NSC. That is, the one-year shrinkage and sorptivity of each mixture was divided by that of the NSC, so the relative change in sorptivity can be directly related with changes in drying shrinkage. In the plot each mixtures appears as one data point; for instance, the NSC shows in the top right portion of the plot, as its sorptivity and one-year drying shrinkage were divided by themselves, similarly, the three HPC mixtures appear with values toward to the bottom left of the plot since they present lower shrinkage and lower sorptivity than NSC. The diagonal dashed

line represents the equivalence between reduction in sorptivity and reduction in one-year shrinkage. Finally, Figure 5.41 also presents a detailed area of the three HPCs to better establish comparison among them.

Figure 5.41 shows good agreement between the two variables when comparing the NSC and with any of the HPC mixtures. The use of low water-to-cementitious material ratio and the use of silica fume produced a 90% reduction in sorptivity and, at the same time, yielded a 60% decrease in one-year drying shrinkage regardless of the king of the mixture.

The slope of the regression line, showed a solid line in the plot, was 0.68 meaning that for each one percent reduction in sorptivity, drying shrinkage was reduced a 0.68%. When comparing the three HPC (see detailed area) it can be seen that LWW 65-35 and NWA 65-35 HPCs followed the same trend described previously as they appear to be parallel to the solid line. This means that the further decrease in sorptivity showed by LWW 65-35 with respect to NWA 65-35 was accompanied by a relative decrease in average drying shrinkage of approximately 68%. It might be reminded that the variability in the one-year shrinkage was important and the differences between the three HPCs were not significant. The detailed are also shows that the HP Matrix did not follow the trend because had higher sorptivity than the HPCs with coarse aggregate, but less average drying shrinkage after one year. As mentioned previously, the sorptivity of the HP Matrix could have been exaggerated due to potential cracking in the ITZ during the insulated curing.

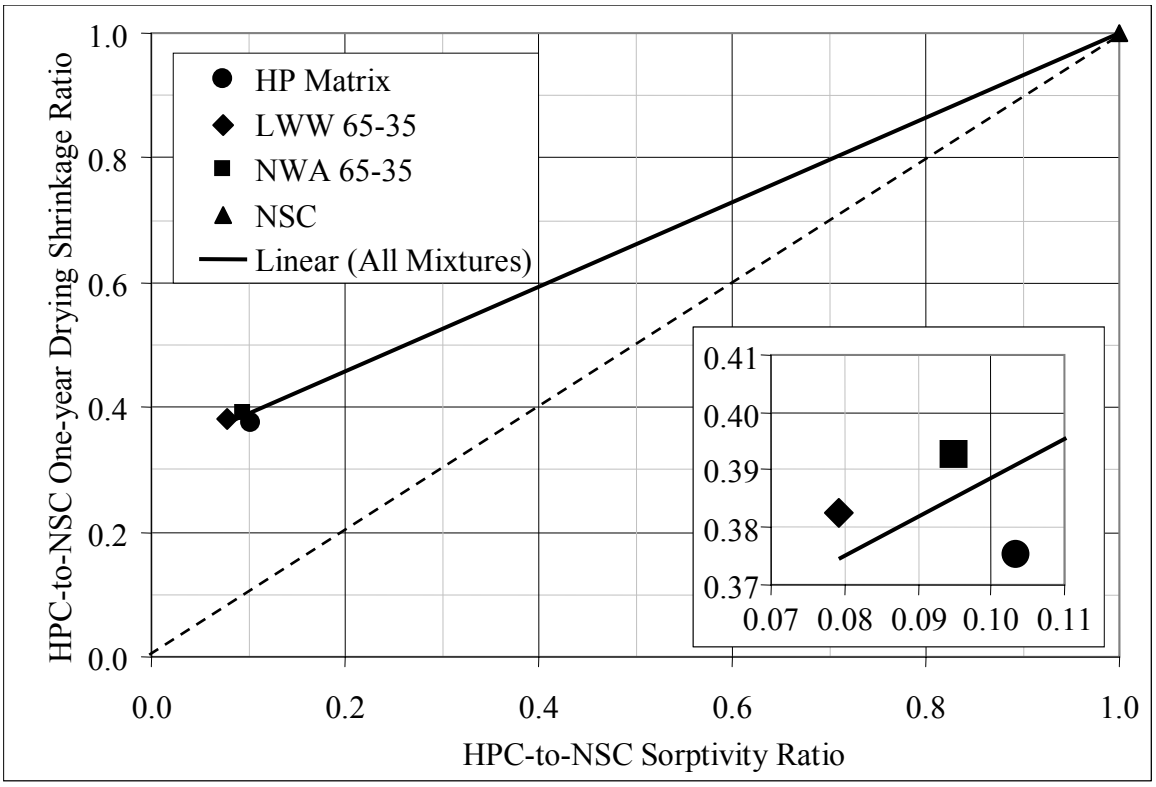

Figure 5.41: One-year relative drying shrinkage versus relative sorptivity

Sorptivity of the LWW 65-35 and NWA 65-35 HPCs were similar even though LWW 65-35 used a more porous lightweight aggregate that could have affected the microstructure facilitating water loss and drying. One-year drying shrinkage of LWW 65-35 HPLC was, on average, also lower than that of the NWA 65-35 HPC, although, the LWW 65-35 HPLC used a lightweight coarse aggregate. That mixture could have shown higher drying shrinkage as the lower stiffness aggregate is believed to impose less restraint to the paste deformation. The use of lightweight aggregate did not affect the sorptivity or drying shrinkage of the LWW 65-35 HPLC negatively, if any contributed to decrease drying shrinkage and sorptivity as shown in Figure 5.41 by the lower relative values of the LWW 65-35 mixture. The water stored in the pre-soaked aggregate is believed to contribute to the comparatively good performance shown by LWW 65-35

mixture by enhancing hydration of the cementitious materials [35, 37] and further reducing interconnectivity in the pore system and indirectly reducing both sorptivity and drying shrinkage.

Figure 5.42 presents a comparison between absorption (X-axis) and one-year drying creep for the mixtures under study. Data in Figure 5.42 is shown, as explained for Figure 5.41, relative to that measured in the NSC mixture. Again, NSC is represented by one data point with coordinated equal to the unity and HPCs mixtures with coordinates below unity since they had lower sorptivity and lower drying creep than NSC. The diagonal dashed line corresponds to equivalence between relative change in sorptivity and drying creep.

As shown in Figure 5.42, drying creep also was greatly reduced by using silica fume and by lowering the water-to-cementitious material ratio from 0.60 to 0.23; at the same time, sorptivity was also decreased. One clear difference of drying creep compared with respect to drying shrinkage is that HP Matrix and the other two HPCs showed very different effect in creep and sorptivity.

There was a one-to-one relationship between drying creep of NSC and those from LWW 65-35 and NWA 65-35 HPCs as shown by the position of the data points with respect to the equivalence dashed line. The reduction of approximately 90% in sorptivity had similar reduction in drying creep. The HP Matrix presented one-year drying creep about 5 times greater than LWW 65-35 or NWA 65-35, but its sorptivity was only 30% higher than that of LWW 65-35 mixture and 8% higher than the sorptivity measured in NWA 65-35 HPC. This was in despite of the fact that HP Matrix sorptivity might have been overestimated, and should have been even lower. It was believed the potential

reduction in drying creep afforded by the decrease in pore interconnectivity of the HP Matrix has been offset by the lack of coarse aggregate which does not deform as much as the paste and which typically restrains the creep occurring in the paste [15].

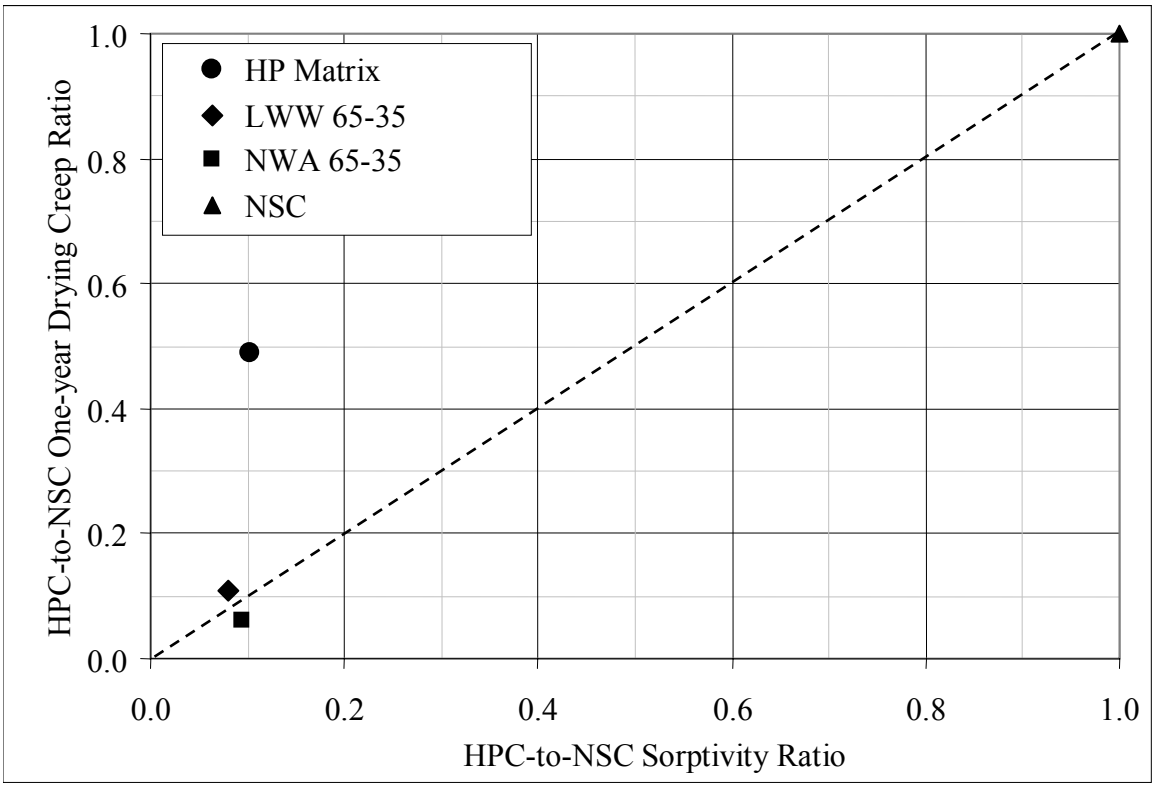

Figure 5.42: One-year relative drying creep versus relative sorptivity

LWW 65-35 and NWA 65-35 mixtures showed no significant differences in drying creep even though the former used a comparatively lower stiffness aggregate which imposes less restraint to the creep occurring in the paste. As it was argued before, the water stored within the pre-soaked lightweight aggregate could have contributed to the formation of a less inter-connected pore system, making water migration through the microstructure more difficult. Water migration, is believed by many to be a fundamental cause of creep [4, 24].

5.7 Summary

From temperature history it was concluded that for the same amount of cementitious materials, LWW mixtures experienced a higher increase in temperature leading to higher maturity at the time of testing than NWA and STL mixtures.

The experimental results obtained herein pointed out the great influence of maturity on creep, especially when loaded 24 hours after casting. It was concluded that creep of concrete was inversely proportional to the natural logarithm of maturity at the time of loading. This relationship was based on that proposed by the Sakata Model [7]. The effect of compressive strength on creep was found to be inversely proportional to the 28-day compressive strength as suggested previously [9].

From the adjusted creep, it was concluded that replacement of cement by silica fume and fly ash reduced 120-day creep by 15%. The addition of 18.4 and 36.8% of coarse aggregate by volume reduced creep by 28 and 50% respectively.

Compressive strength of the expanded slate and granite HPC mixtures was adequately estimated by a weighted average of HP Matrix and coarse aggregate compressive strength. STL mixtures presented a compressive strength considerably lower than the estimate. It was concluded that ITZ did not limit the strength of expanded slate and granite mixture, but it determined the strength of the STL mixtures.

Elastic modulus of the expanded slate HPC was in agreement with the estimated values using two-phase models proposed by three different researchers [24-26]. Granite and STL mixtures deviated from estimates by 25 and 45%, respectively. ITZ in the STL mixtures was believed to limit its elastic modulus. ACI-363 [32] equation for elastic modulus underestimated some of the values measured in expanded slate HPC. It

overestimated granite and steel aggregate HPC elastic modulus by 15% and by more than 50%, respectively.

From the experimental data it was concluded that the expanded slate HPLC can be considered as a two-phase material because the ITZ did not affect its compressive strength and elastic modulus; thus, compressive strength and elastic modulus of HPLC can be adequately estimated by two-phase models.

The two-phase model proposed for shrinkage of concrete [27] and the aggregate restraining effect presented good agreement with experimental data. This suggested the aggregate restraining effect on shrinkage was well represented by its mechanical properties.

Neville's two-phase model for creep of concrete [15] deviated from the experimental values. Creep of expanded slate HPLC was considerably lower than predicted meaning that the restraining effect of expanded slate on creep cannot be modeled based solely on the aggregate mechanical properties. Creep of the STL mixtures was higher than expected showing a weak ITZ. Creep of granite HPC was adequately estimated by the two-phase model. The two-phase creep model was derived using normal weight aggregate which explained in part the comparatively better results obtained on the granite HPC.

LWW 65-35 presented practically the same 24-hour compressive strength, but considerably higher 56-day and one-year strength than that of LWD 65-35. It is believed that the water stored in the pre-soaked lightweight aggregate improved the hydration yielding to a better strength gain.

Basic creep was on average 8 times larger than drying creep when creep testing started at the age of 24 hours. That proportion increased to 13 times when testing started at the age of 28 days. It was concluded that the size of the specimens played a little role on creep because drying creep portion was comparatively low. This was confirmed by comparing total creep obtained on 100 x 380-mm (4 x 15-in) and 150 x 300-mm (6 x 12-in) cylinder specimens. The latter might imply that results from creep testing performed in standard specimens can be used in estimating creep of full-scale concrete members without a large error.

When tested at the age of 24 hours, statistical analysis revealed that autogenous shrinkage, total shrinkage, basic creep, and total creep of LWD 65-35 mixture were higher than those of LWW 65-35 with a confidence level of 95%. This difference was believed to be caused by hydration enhancement and expansion in LWW 65-35 due to curing provided by the internally stored water. It was also proposed that the internally stored water could have inhibited the water migration from the C-S-H surface caused by sustained load by equilibrating the relative humidity through the microstructure.

The statistical comparison also suggested, with 95% confidence, that LWW 65-35 HPLC had lower autogenous shrinkage, total shrinkage, basic creep, and total creep than NWA 65-35 HPC. Thus, the reduction in creep afforded by the pre-soaked lightweight aggregate could have counteracted the lower restraining effect imposed by a lower stiffness lightweight aggregate.

The differences between NSC and HPC which might be responsible for the reduction in drying shrinkage and drying creep associated with HPC, were well represented by the measured sorptivity.

Drying shrinkage, which is primary driven by moisture migration, was also found to be mainly affected by changes in the pore structure, when comparing HPC and NSC. The HPC mixtures with their reduced porosity and pore interconnectivity, exhibited decrease in drying shrinkage proportional to the decrease in its sorptivity. Drying creep changed in the same proportion as sorptivity suggesting that the interconnectivity of the pore system largely influenced the extent of the drying creep.

The use of a more porous aggregate, as the expanded slate, did not increase the sorptivity of the LWW 65-35 HPLC. It was believed that the water stored within the pre-soaked lightweight aggregate enhanced hydration and further reduced interconnectivity of the capillary porosity. The same effect was believed to reduce water migration and water loss reducing drying shrinkage and drying creep of the LWW 65-35 HPLC and offsetting the possible increase in time-dependent deformations due to the lower stiffness of the lightweight aggregate.

5.8 References

1. Carino, N.J., "The Maturity Method: Theory and Applications". *Cement, Concrete and Aggregates*, 6(2): 1984. p. 61-73.
2. Comite Euro-Internacional du Beton (CEB) and Federation Internationale de la Precontrainte (FIP), *Evaluation of the Time Dependent Behavior of Concrete*. Lancaster: The Construction Press, 1990.
3. Comite Euro-Internacional du Beton (CEB) and Federation Internationale de la Precontrainte (FIP), *CEB Code Final Draft Section 3 Materials prEN 1992-1*. 2001, p. 25-31.
4. Neville, A.M. and W.H. Dilger, *Creep of concrete: plain, reinforced, and prestressed*. Amsterdam, New York,: North-Holland Pub. Co., American Elsevier, 1970, xix, 622.
5. ACI Committee 209, "Prediction of Creep, Shrinkage, and Temperature Effects in Concrete Structures", in *ACI Manual of Concrete Practice*. American Concrete Institute: Farmington Hills, MI. 1997, p. 209R.1-209R.47.
6. AASHTO-LRFD, *AASHTO LRFD Bridge Design Specifications*. Third Edition ed. Washington: American Association of State Highway and Transportation Officials, 2004.

7. Sakata, K. "Prediction of Creep and Shrinkage, Creep and Shrinkage of Concrete,". in *Fifth International RILEM Symposium*. Barcelona, Spain: RILEM, 1993.p. 649-654.
8. Neville, A.M., "Role of cement in creep of mortar". *Journal of the American Concrete Institute*, 30(9): 1959. p. 963-984.
9. Tadros, M., et al., *NCHRP Report 496: Prestressed Losses in Pretensioned High-Strength Concrete Bridge Girders*. Transportation Research Board: Washington D.C. 2003, p. 63 pp.
10. Harrell II, E.M. and J.V. Herod, *Linear Methods of Applied Mathematics*, in *Website:http://www.mathphysics.com/pde/kvalues.html*. June 2005.
11. ASTM C 684, *Standard Test Method for Making, Accelerated Curing, and Testing Concrete Compression Test Specimens*. West Conshohocken, PA: American Society for Testing and Materials, 1999.
12. ASTM C 512, *Standard Test Method for Creep of Concrete in Compression*. West Conshohocken, PA: American Society for Testing and Materials, 1992.
13. Burg, R.G. and B.W. Ost, *Engineering Properties of Commercially Available High Strength Concrete (Including Three-year Data)*. Research and Development Bulletin RD104 Portland Cement Association. 1994.
14. Wolsiefer, J., "Ultra High-Strength Field Pleaceable Concrete with Silica Fume Admixture". *Concrete International*, 6(4): 1984. p. 25-31.
15. Neville, A.M., "Creep of concrete as function of its cement paste content". *Magazine of Concrete Research*, 16(46): 1964. p. 21-30.
16. Lopez, M., L.F. Kahn, and K.E. Kurtis, "Internal Curing in High Performance Concretes - a New Paradigm (in Spanish)". *Revista Ingenieria de Construccion*, 20(2): 2005. p. 117-126.
17. Jensen, O.M. and P.F. Hansen, "Water-entrained cement-based materials II. Experimental observations". *Cement and Concrete Research*, 32(6): 2002. p. 973-978.
18. Bentur, A., S. Igarashi, and K. Kovler, "Prevention of autogenous shrinkage in high-strength concrete by internal curing using wet lightweight aggregates". *Cement and Concrete Research*, 31(11): 2001. p. 1587-1591.
19. Zhang, M.H. and O.E. Gjørv, "Microstructure of the Interfacial Zone between Lightweight Aggregate and Cement Paste". *Cement and Concrete Research*, 20(4): 1990. p. 610-618.
20. Zhang, M.H. and O.E. Gjørv, "Penetration of Cement Paste into Lightweight Aggregate". *Cement and Concrete Research*, 22(1): 1992. p. 47-55.
21. Bremner, T.W. and T.A. Holm, "Elastic Compatibility and the Behavior of Concrete". *Journal of the American Concrete Institute*, 83(2): 1986. p. 244-250.
22. Neville, A.M., *Properties of concrete*. 4th and final ed: J. Wiley, 1996.
23. Alexander, M.G., "Aggregate and the deformation properties of concrete". *ACI Materials Journal*, 93(6): 1996. p. 569-77.
24. Mehta, P.K. and P.J.M. Monteiro, *Concrete : microstructure, properties, and materials*. 2nd ed: McGraw-Hill, 1993.
25. Counto, U.J., "Effect of elastic modulus of aggregate on elastic modulus, creep and creep recovery of concrete". *Magazine of Concrete Research*, 16(48): 1964. p. 129-138.

26. Nilsen, A.U., P.J.M. Monteiro, and O.E. Gjørv, "Estimation of the Elastic-Moduli of Lightweight Aggregate". *Cement and Concrete Research*, 25(2): 1995. p. 276-280.
27. Pickett, G., "Effect of aggregate on shrinkage of concrete and hypothesis concerning shrinkage". *American Concrete Institute -- Journal*, 27(5): 1956. p. 581-590.
28. L'Hermite, R. in *Fourth International Symposium in Chemistry of Cements*. Washington, D.C.: National Bureau of Standards, 1962.p. 659-694.
29. ACI Committee 213, "Guide for Structural Lightweight-Aggregate Concrete", in *ACI Manual of Concrete Practice*. American Concrete Institute: Farmington Hills, MI. 2003, p. 38.
30. Meyer, K.F., B.S. Buchberg, and L.F. Kahn. "Development of High Strength Lightweight Concrete Mix Designs: A Practical Approach". in *49th Annual PCI Convention & Exhibition, the 3rd PCI/FHWA International Symposium on High Performance Concrete, and the National Bridge Conference.* Orlando, Florida: Precast / Prestressed Concrete Institute, 2003.
31. Videla, C. and M. Lopez, "Mixture proportioning methodology for structural sand-lightweight concrete". *ACI Materials Journal*, 97(3): 2000. p. 281-289.
32. ACI Committee 363, "State-of-the-Art Report on High-Strength Concrete", in *ACI Manual of Concrete Practice*. American Concrete Institute: Farmington Hills, MI. 1997, p. 55.
33. ACI Committee 318, *Building Code Requirements for Structural Concrete (ACI318-02), and Commentary (ACI 318R-02)*. Farmington Hills, MI: American Concrete Institute, 2002.
34. Nilsen, A.U. and P.J. Monteiro, "Concrete: a three phase material". *Cement and Concrete Research*, 23(1): 1993. p. 147-151.
35. Bentz, D.P. and K.A. Snyder, "Protected paste volume in concrete - Extension to internal curing using saturated lightweight fine aggregate". *Cement and Concrete Research*, 29(11): 1999. p. 1863-1867.
36. Lura, P., D.P. Benz, and D.A. Lange. "Measurements of Water Transport from Saturated Pumice Aggregates to Hardening Cement Paste." in *Advances in Cement and Concrete*. Copper Mountain, Colorado: Engineering Conferences International, 2003.p. 89-99.
37. Zhutovsky, S., K. Kovler, and A. Bentur, "Efficiency of lightweight aggregates for internal curing of high strength concrete to eliminate autogenous shrinkage". *Materials and Structures*, 35(246): 2002. p. 97-101.
38. Mindess, S. and S. Diamond, "SEM Investigations of Fracture Surfaces Using Stereo Pairs .2. Fracture Surfaces of Rock-Cement Paste Composite Specimens". *Cement and Concrete Research*, 22(4): 1992. p. 678-688.
39. Holm, T.A. and T.W. Bremner, *State-of-the-Art Report on High-Strength, High-Durability Structural Low-Density Concrete for Applications in Severe Marine Environments*, in *Innovations for Navigation Projects Research Program*. US Army Corps of Engineers. Engineer Research and Development Center, Structures Laboratory: Vicksburg, MS. 2000.

40. Holm, T.A., *Lightweight Concrete and Aggregates, Standard Technical Publication STP 169C*. Philadelphia, PA: American Society for Testing and Materials, 1995.
41. Lura, P., K. van Breugel, and I. Maruyama. "Autogenous and drying shrinkage of high strength lightweight aggregate concrete at early ages -The effect of specimen size". in *RILEM International Conference on Early Age Cracking in Cementitious System (EAC'01)*. Hifa, 2001.p. 337-344.
42. Berra, M. and G. Ferrada. "Normalweight and Total-Lightweight High-Strength Concretes: A Comparative Experimental Study". in *High-Strength Concrete. Second International Symposium*. Berkeley, California: American Concrete Institute, 1990.p. 701-733.
43. Holm, T.A. and T.W. Bremner, "High Strength Lightweight Aggregate Concrete", in *High Performance Concrete: Properties and Applications*, S.P. Shah and S.H. Ahmad, Editors. McGraw-Hill: New York, NY. 1994, p. 341-374.
44. Zhang, M.H., L. Li, and P. Paramasivum, "Shrinkage of High-Strength Lightweight Aggregate Concrete Exposed to Dry Environment". *ACI Materials Journal*, 102(2): 2005. p. 86-92.
45. Nilsen, A.U. and P.C. Aïtcin, "Properties of High-strength Concrete Containing Light-, Normal- and Heavy-weight Aggregate". *Cement Concrete and Aggregates*, 14(1): 1992. p. 8-12.
46. Curcio, F., et al. "High-Performance Lightweight Concrete for the Precast Prestressed Concrete Industry". in *Fourth CANMET/ACI/JCI International Symposium on Advances in Concrete Technology, SP-179*. Tokushima, Japan: American Concrete Institute, 1998.p. 389-404.
47. AASHTO-LRFD, *AASHTO LRFD Bridge Design Specifications*. Washington: American Association of State Highway and Transportation Officials, 1998.
48. Bažant, Z.P. and S. Baweja, "Creep and Shrinkage Prediction Model for Analysis and Design of Concrete Structures - Model B3, RILEM Draft Recommendation". *Materials and Structures*, 28: 1995. p. 357-365.
49. Gardner, N.J. and M.J. Lockman, "Design provisions for drying shrinkage and creep of normal-strength concrete". *ACI Materials Journal*, 98(2): 2001. p. 159-167.
50. Sakata, K., et al. "Prediction Equations of Creep and Drying Shrinkage for Wide-Ranged Strength Concrete". in *Creep Shrinkage and Durability Mechanics of Concrete and Other Quasi-Brittle Materials*. Cambridge, Massachusetts, United States: Elsevier, 2001.p. 753-758.
51. Leming, M.L., *Creep and Shrinkage of Lightweight Concrete*. Department of Civil Engineering, North Carolina State University: Raleigh, NC. 1990.
52. Dilger, W.H. and C. Wang. "Creep and Shrinkage of High-Performance Concrete". in *The Adam Neville Symposium: Creep and Shrinkage - Structural Design Effects, SP-194*. Atlanta: American Concrete Institute, 2000.p. 361-379.
53. Geiker, M.R., D.P. Bentz, and O.M. Jensen. "Mitigating Autogenous Shrinkage by Internal Curing". in *High Performance Structural Lightweight Concrete. SP-218*. Phoenix, AZ: American Concrete Institute, 2002.p. 143-154.

54. Weber, S. and H.W. Reinhardt, "A new generation of high performance concrete: Concrete with autogenous curing". *Advanced Cement Based Materials*, 6(2): 1997. p. 59-68.
55. Thomas, M.D.A. "Chloride Diffusion in High-Performance Lightweight Aggregate Concrete". in *Theodore Bremner Symposium on High-Performance Lightweight Concrete*. Tessaloniki, Greece, 2003.p. 77-93.
56. Jensen, O.M. and P.F. Hansen, "Autogenous deformation and RH-change in perspective". *Cement and Concrete Research*, 31(12): 2001. p. 1859-1865.
57. Neville, A.M., "Theories of Creep in Concrete". *ACI Journal*, 52: 1955. p. 47-60.
58. Ali, I. and C.E. Kesler. "Mechanisms of creep in concrete". in *American Concrete Institute -- Symposium on Creep of Concrete, 1964*: American Concrete Institute, Detroit, MI, United States, 1964.p. 35-63.
59. Neville, A.M., W.H. Dilger, and J.J. Brooks, *Creep of plain and structural concrete*: Construction Press, 1983.
60. Bažant, Z.P., "Prediction of concrete creep and shrinkage: past, present and future". *Nuclear Engineering and Design*, 203(1): 2001. p. 27-38.
61. Davis, R.E., H.E. Davis, and J.S. Hamilton, "Plastic flow of concrete under sustained stress". *American Society for Testing Materials -- Proceedings*, 34(Part 11): 1934. p. 354-386.
62. Jensen, O.M. and P. Lura. "Techniques for Internal Curing of Concrete". in *Advances in Cement and Concrete*. Copper Mountain, Colorado: Engineering Conferences International, 2003.p. 67-78.
63. Hammer, T.A., Ø. Bjøntegaard, and E.J. Sellevelod. "Internal Curing - Role of Absorbed Water in Aggregates". in *High Performance Structural Lightweight Concrete. SP-218*. Phoenix, AZ: American Concrete Institute, 2002.p. 131-142.
64. Lopez, M., L.F. Kahn, and K.E. Kurtis, "Creep and shrinkage of high-performance lightweight concrete". *ACI Materials Journal*, 101(5): 2004. p. 391-399.
65. de Larrand, F., P. Acker, and R. Le Roy, "Shrinkage Creep and Thermal Properties", in *High Performance Concrete: Properties and Applications*, S.P. Shah and S.H. Ahmad, Editors. McGraw-Hill: New York, NY. 1994, p. 65-114.
66. Bentz, D.P. and K.K. Hansen, "Preliminary observations of water movement in cement pastes during curing using X-ray absorption". *Cement and Concrete Research*, 30(7): 2000. p. 1157-1168.
67. RILEM TC 6-PAN, "Testing Methods for Natural and Artificial Stones". *Materials and Structures*, 5: 1972. p. 231-245.
68. Martys, N.S. and C.F. Ferraris, "Capillary transport in mortars and concrete". *Cement and Concrete Research*, 27(5): 1997. p. 747-760.
69. Gjørv, O.E. "Important Test Methods for Evaluation of Reinforced Concrete Durability". in *Concrete Technology: Past, Present, and Future*: American Concrete Institute, 1993.p. 545-574.
70. Zhang, M.H. and O.E. Gjørv, "Permeability of High-Strength Lightweight Concrete". *ACI Materials Journal*, 88(5): 1991. p. 463-469.
71. Ho, D.W.S. and R.K. Lewis, "The Water Sorptivity of Concretes: The Influence of Constituents under Continuous Curing". *Durability of Building Materials*, 4: 1987. p. 241-252.

72. Troxell, G.E., J.M. Raphael, and R.E. Davis. "Long-term Creep and Shrinkage Tests of Plain and Reinforced Concrete". in *Cement and Concrete*. Los Angeles: ASTM Proceedings, 1958.p. 1101-1120.

This page intentionally left blank

CHAPTER 6

SMALL-SCALE STUDY

6.1 Introduction

Research in civil engineering has traditionally studied creep and shrinkage from the perspective given by large-scale and medium-scale studies. Those approaches measure creep and shrinkage in a bulk sense where deformations in the different phases (i.e., paste, aggregate and interfacial transition zone - ITZ) are grouped together giving an overall result.

A novel test method that combined traditional creep and shrinkage testing principles with microscopy and image analysis was developed during the small-scale study. This test method was applied to several of the mixtures used in the medium-scale study, with the only difference that the coarse aggregate MSA was reduced from 12.7 to 9.5 mm (0.5 to 0.375 in). The experimental program, presented in Section 3.3.3, consisted of measuring deformations by means of DIC on six different concrete mixtures under loading and drying. Table 6.1 presents a summary of the six mixtures, nomenclature and their main characteristics.

This chapter is organized in five main parts, Sections 6.2 and 6.3 present the research approach used in the small-scale study and the testing and analysis procedure followed to obtain deformation maps by applying DIC. Section 6.4 presents the compressive strength of the concrete mixtures studied here, and Section 6.5 assesses the accuracy of the system by comparing the DIC output with rigid body motion. Sections 6.6 and 6.7 present the deformation maps obtained for elastic and creep plus shrinkage

deformations respectively. The results in Sections 6.6 and 6.7 referred only to NSC-95, NWA 66-35-95 and LWW 65-35-95, so they are referred as NSC, HPC, and HPLC, respectively. Section 6.8 presents a comparison between deformation results from DIC with deformations as measured with a DEMEC gauge.

Section 6.9 describes some challenges encountered during this study which did not allowed an adequate image analysis for LWD 65-35-95, STL 65-35-95, and HP Matrix mixtures. The same difficulties prevented the algorithm to obtain meaningful results for the images after 120 days under load. Finally, Section 6.10 presents a summary of conclusions.

Table 6.1: Mixture nomenclature and characteristics

Mixture ID	Description	Phases of interest (% by volume)
LWW 65-35-95	HPLC with reduced MSA	pre-soaked expanded slate at 36.8% and HP Matrix at 63.2%
LWD 65-35-95 [1]	HPLC with air-dried lightweight aggregate and reduced MSA	air-dried expanded slate at 36.8% and HP Matrix at 63.2%
NWA 65-35-95	normal weight HPC with reduced MSA	granite at 36.8% and HP Matrix at 63.2%
STL 65-35-95 [1]	steel aggregate HPC with reduced MSA	steel cubes at 36.8% and HP Matrix at 63.2%
HP Matrix [1]	high performance matrix used in all mixtures above	2.36-mm (#8 sieve) siliceous sand at 39.2% and cementitious paste at 60.8%
NSC-95	normal weight normal strength concrete with reduced MSA	granite at 35.9%, siliceous sand at 33.6% and cement paste at 30.5%

.1: Results were not included for the reasons given in Section 6.9.

6.2 Research Approach

In this research, image analysis, performed by digital image correlation (DIC), was used to map elastic and time-dependent deformations in the composite and to assess relative deformations in the different phases, while the material remained under sustained load and drying. A new experimental setup was developed to cast, load, and image the surface of concrete specimens, and a commercially available software package was adapted to perform the analysis. The goal of this study was to compare creep and shrinkage in HPLC, HPC, and NSC to determine how the distribution of deformation varies between those. This will contribute to understand the causes of the lower creep plus shrinkage shown by HPLC and HPC with respect to NSC and the causes behind the low creep plus shrinkage of HPLC when compared to HPC.

6.3 Image Analysis Procedure

6.3.1 Imaging Procedure

Four regions of interest (ROI) were selected on each specimen and they were imaged using two levels of magnification. In the lower level of magnification one pixel represented 5.92 μm (2.3×10^{-4} in) which roughly corresponded to 12.6 X (12.6 times magnification) when using the eyepieces instead of the digital camera. In the higher level of magnification one pixel represented 1.08 μm (4.2×10^{-5} in) and it was equivalent to 80 times as seen through the eyepieces. ROIs at high magnification were selected in order to image aggregate, paste, and ITZ. The two levels of magnification corresponded to the maximum and minimum attainable with the microscope configuration, and were used to compare deformation maps at different magnifications.

The digital camera had a 2-megapixel resolution yielding images of 1600 x 1200 pixels. Thus, each ROI was either an image of 0.673 cm^2 / 7104 μm x 9472 μm (0.104 in^2 / 0.280 in x 0.373 in) at low magnification or an image of 0.02 cm^2 / 1296 μm x 1512 μm (0.003 in^2 / 0.051 in x 0.060 in) at high magnification. Figure 6.1 shows a schematic of the specimen surface, the ROIs and the images at the two magnification levels and the coordinate system. In order to minimize boundary effects from the loading plates, All ROIs were located more than 38 mm (1.5 in) away from the ends.

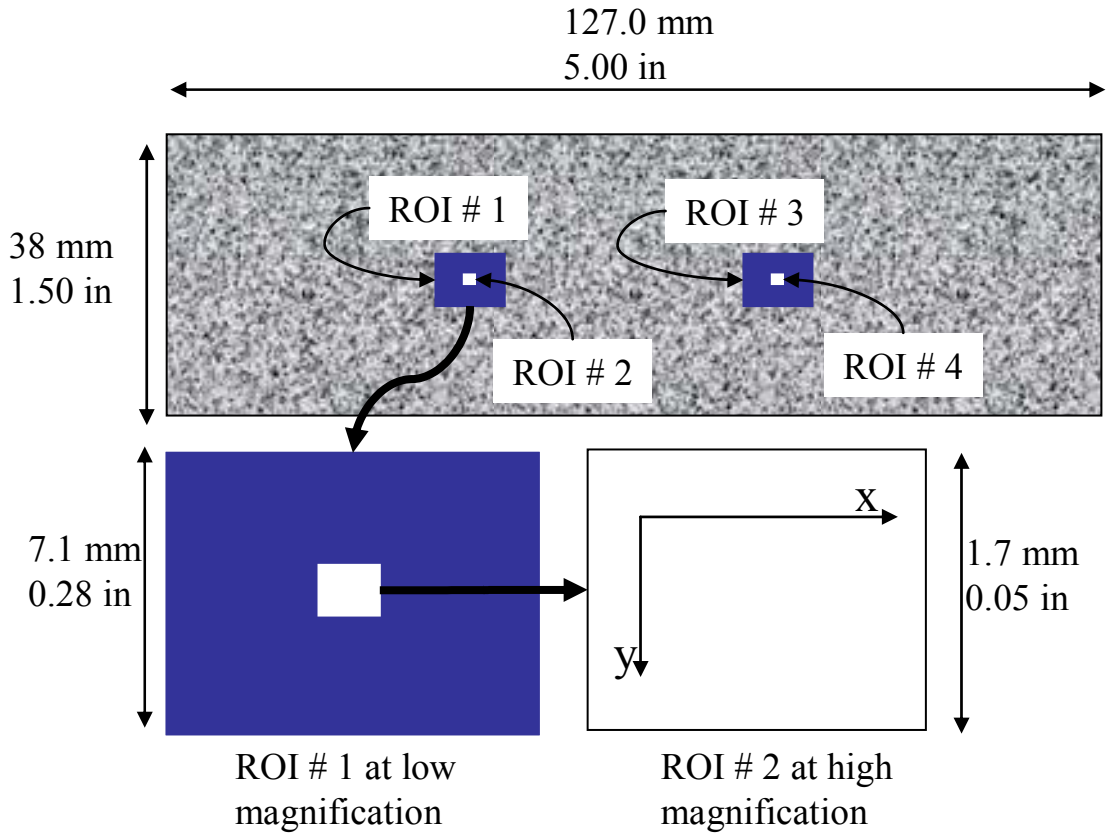

Figure 6.1: Imaging protocol for the experimental program

6.3.2 Pattern Matching Procedure

Once the images were acquired, the DIC procedure was applied to different image pairs from the same ROI to perform the matching. Commercially available software with pattern recognition capabilities was used (Matrox Inspector Version 4.1). Each pair of images had a "reference image" (REF) and a "deformed image" (DEF). A c-code was written in order to iteratively run the pattern recognition feature of the software throughout the images. The algorithm, initially applied to the pixel (100, 100) from top and left edges, had the following four steps:

- In REF: it selected a 65 x 65 pixel area with the pixel of interest at its center. This sub-region was called reference window
- In output file: it recorded the coordinates of the pixel of interest in REF
- In DEF: it located pixel of interest and its neighbors (reference window)
- In output file: it recorded the coordinates of the pixel of interest in DEF

After recording the coordinates of the pixel in REF and DEF, the algorithm moved to the following pixel, located 15 pixels apart, and repeated the cycle until completed the ROI. In order to fit the reference window and to allow for some shift between images, the matching did not consider a 100-pixel edge, so the actual matching area had 1400 x 1000 pixels instead of 1600 x 1200 pixels as the original image.

The pattern matching / recognition procedure is a trial-and-error algorithm that performs a numeric comparison between the reference window from REF and a candidate sub-region from DEF. A "similarity score" is obtained which is compared against a threshold value. If the score is lower than the threshold, a new candidate is evaluated. If the score overcomes the threshold, the matching is complete. One difficulty of using a threshold values is that images always contain some level of noise (e.g., variation in lightning, variation in focus, variation of the specimen surface). This noise lowers the

scores of the candidate regions, so high thresholds might lead to rejection of the correct match and even lead to obtaining unmatched pixels. On the other hand, a low threshold value may lead the acceptance a good candidate, even though it is not the correct match. Consequently, the output file from the pattern matching procedure may contain unmatched pixels that need to be reassessed and wrong matches that need to be filtered out, as described in the next section.

6.3.3 Displacement and Deformation Calculation

The output file from the matching stage was further processed to compute displacements and deformations. This post-process was automatically carried out by another c-code. There were three stages in the post-processing procedure: (1) displacement computation, (2) displacement filtering, and (3) deformation computation.

Displacements were calculated in X and Y directions and received the name of u- and v-displacements, respectively (see Figure 3 for coordinate reference system). The u-displacements were calculated as the difference between the X-coordinates of the same pixel from DEF and REF. Likewise, v-displacements were the difference between Y-coordinates of a pixel on each of the images. Whenever an unpaired pixel was found, the displacement was assumed to be a very large number, so that could be filtered in the next stage.

The filtering stage aimed to eliminate the incorrect matches and to fill in the unmatched pixels. Chauvenet's criterion is a commonly used statistical technique that allows for discrimination of outliers in a data set [1]. It computes the average and variance of a data set and then the deviation of any particular data point from the average. If the deviation is higher than a particular threshold, the data point is said to be an outlier.

For this case the data set was comprised of a pixel and its eight nearest neighbors. If that pixel was an outlier according to Chauvenet's criterion, its value was replaced by the average of its eight neighbors. Because the displacements of the unpaired pixels were very high, they were automatically classified as outliers.

After the displacements were filtered, the deformations were computed as the relative displacement between two pixels. Thus, the difference in u- and v-displacements between two pixels was called deformation in X- and Y-direction, respectively.

6.4 Mechanical Properties of Concrete Mixtures

Creep and shrinkage testing began at the age of 28 days for NSC-95 and 24 hours for NWA 65-35-95 and LWW 65-35-95. Table 6.2 presents the compressive strength as measured on three 50-mm (2-in) cubes and three 38 x 38 x 125-mm (1.5 x 1.5 x 5-in) prisms. Since the following sections deal only with NSC-95, NWA 66-35-95 and LWW 65-35-95, they are referred as NSC, HPC, and HPLC, respectively.

Table 6.2: Properties of NSC and HPC mixtures under study

Compressive strength, MPa (psi)	NSC	HPC	HPLC
Cube	24.5 (3550)	77.0 (11,165)	64.8 (9400)
Prism	21.1 (3065)	67.8 (9835)	45.2 (6552)
Applied load to creep specimens	9.7 (1410)	28.4 (4115)	21.0 (3040)

Cube compressive strength was higher than that of the prism by 16 to 43% which was believed to be caused by the larger height-to-width ratio of the prism specimens. The creep specimens were loaded to a stress of approximately 40% of the compressive strength shown by the prisms as shown in Table 6.2.

6.5 Experimental Validation: Rigid Body Motion

Before using DIC system to measure deformations, data was collected during rigid body motion and analyzed to assess the variability and possible error induced by the pattern matching algorithm.

Two images of the same ROI were obtained, as shown in Figures 6.2a and 6.2b, before and after displacing the specimen by 0.06 mm (2.3×10^{-3} in) by shifting the mobile indexible stage to the right. The horizontal displacements (u-displacements) obtained by DIC are shown in Figure 6.2c and the individual values in 6.2d. Such a displacement represented 8.4 and 46.3 pixels at low (12.6 x) and high (80x) magnification, respectively.

From the u-displacements (Figures 5c and 5d) it can be seen that all pixels displacements were between 61.84 and 62.74 pixels. The average u-displacement was 62.4 pixels which corresponds to 0.067 mm (0.0027 in). The variation between maximum and minimum values was only 0.9 pixels or less than one μm (0.00004 in). That measured displacement was 0.067 mm (2.6×10^{-3} in) instead of the actual 0.060 mm (2.3×10^{-3} in) displacement suggests the presence of some error, likely due to inaccuracies in the stage movement and possibly human error. Nevertheless, these variations will not affect measured deformations using DIC because these are calculated as relative differences in displacements.

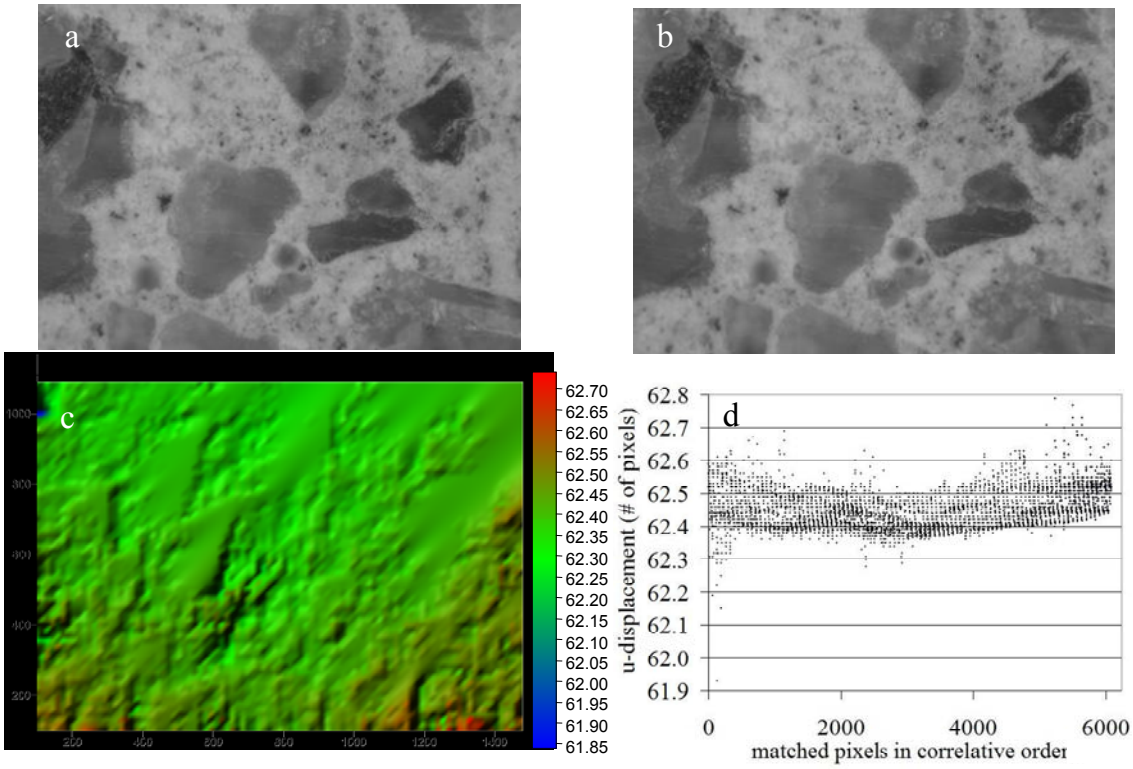

Figure 6.2: Rigid body motion as seen by DIC at high magnification, (a) ROI before displacement, (b) ROI after displacement, (c) u-displacement field, (d) individual pixel u-displacements

6.6 Elastic Deformations

6.6.1 Elastic Deformation in Normal Strength Concrete

The NSC specimen was loaded at the age of 28 days with an effective applied stress of 9.7 MPa (1410 psi) which corresponded to 46% of the ultimate strength. Images were obtained in the four ROIs before and after the application of load, for image analysis. Figure 6.3 shows some representative results obtained by performing DIC in the loading direction (X-direction). Figure 6.3a shows ROI 4 at high magnification, and Figure 6.3b presents the displacement field which includes not only deformations but also

some unavoidable rigid body motion while the deformations alone are shown in Figure 6.3c.

From Figure 6.3c it can be seen that the displacements decrease from left to right which means, according to the coordinate system selected, that these are getting closer to one another (i.e., they are under compression). The average deformations in X-direction obtained in ROI 1, 2, 3, and 4 were -660, -266, -655, and -655 με, respectively. Thus, deformation in X-direction gave results which consistently indicated a compression field.

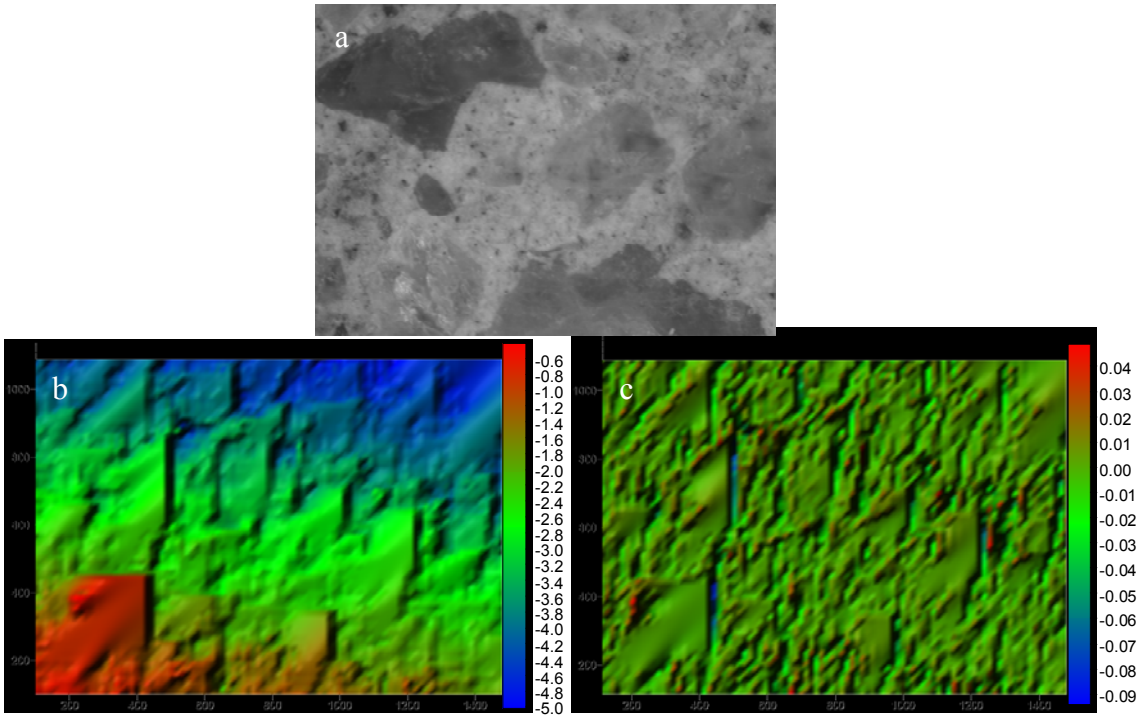

Figure 6.3: Elastic deformation at 9.7 MPa (1440 psi) in NSC as seen by DIC in ROI 4 at high magnification, (a) ROI, (b) u-displacement field, (c) deformations in X-direction

The average deformation in Y-direction for ROI 1 averaged +126 με which yields a Poisson's ratio of 0.19. ROI 2 presented an average elastic deformation equivalent to 40% of that measured in any of the other three ROIs. This difference might be due to the fact that DIC was applied to an area equivalent to only 0.04% of the total specimen area

in the case of ROI 2. Thus, important deviations throughout the specimen surface might be expected. For instance, the ROI 4 shown in Figure 6.3c included four relatively large pieces of aggregate which higher stiffness might reduce deformation locally. However, the objective with this research approach was to examine variations in the displacement field with structure, and that information can only be gained through this kind of approach.

The deformation map in Figure 6.3c, shows an non-uniform deformation field as a consequence of a heterogeneous microstructure of NSC as concluded by a previous research effort [2]. In addition, stiffness was expected to vary widely between cement paste and aggregate which might have contributed to the non-uniformity seen in the deformation map.

6.6.2 Elastic Deformation in High Performance Concrete

The HPC specimen was loaded 24 hours after casting with an applied stress of 28.4 MPa (4115 psi) corresponding to 42% of the compressive strength measured on companion prismatic specimens, and it was. Images, before and after loading, were taken at four ROIs. Figure 6.4 shows the results obtained using DIC in the loading direction (X-direction). Part (a) shows the actual region of interest (ROI 4) at high magnification and part (b) presents the deformation map.

The average elastic deformations from DIC in ROI 2 and ROI 4 (in Figure 6.4) were -1480 and -1533 με, respectively. Similarities are clearly evident between the deformation map (Figure 6.4b) and the actual ROI (Figure 6.4a). An aggregate particle at the center of the ROI gave lower and less heterogeneous elastic strain than the surrounding paste. At the top-left side of the deformation map there were two other zones

with lower and more uniform deformation which correspond to two other aggregate particles as seen in ROI. The lower part of the map presented more deformation as it is more paste-rich zone. From the deformation it can be concluded that there was more deformation located at the cementitious matrix than it was at the aggregate particles. This might be due to the dissimilar elastic properties of aggregate and cement paste.

This elastic mismatch could have induced microcracking at the ITZ as the arrows in Figure 6.4b highlight.

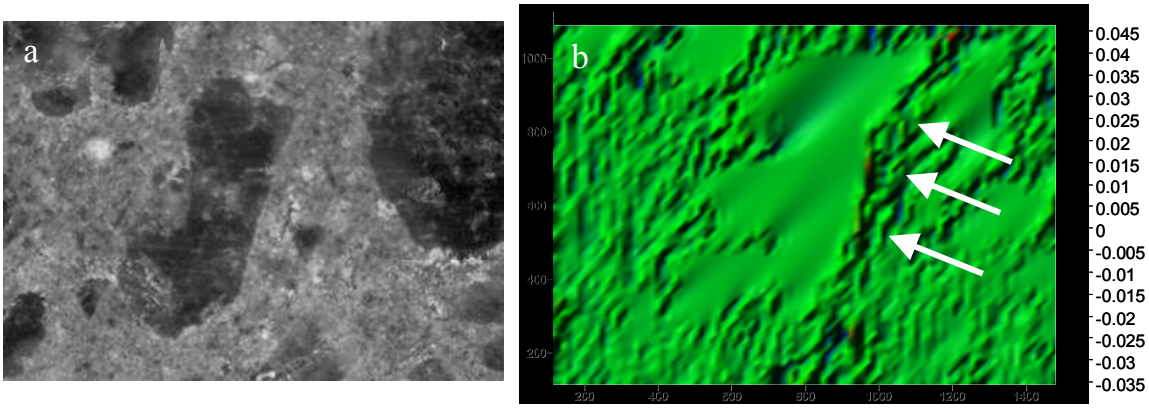

Figure 6.4: Elastic deformation at 28.4 MPa (4115 psi) in HPC as seen by DIC in ROI 4 at high magnification, (a) ROI, (b) deformations in X-direction

6.6.3 Elastic Deformation in High Performance Lightweight Concrete

HPLC specimen was loaded at the age of 24 hours with an applied stress of 21.0 MPa (3040 psi) which corresponded to 46.5% of the compressive strength at that age. Figure 6.5a and 6.5b show the ROI and the corresponding deformation map, respectively.

The average deformation for ROI 2 was -557 με while the averages obtained for the other three ROIs were -680, -604 and -622 με. The axial deformation map shows non-uniform elastic deformations across the ROI as HPLC is not a homogeneous material. However, one important difference in the deformation map from HPLC

compared with those from NSC and HPC is that in HPLC coarse lightweight aggregate and cement paste seemed to deform together. There were not clear distinctions between deformations in the paste and the aggregate, and the HPLC deformation map did not show high deformations regions at the ITZ.

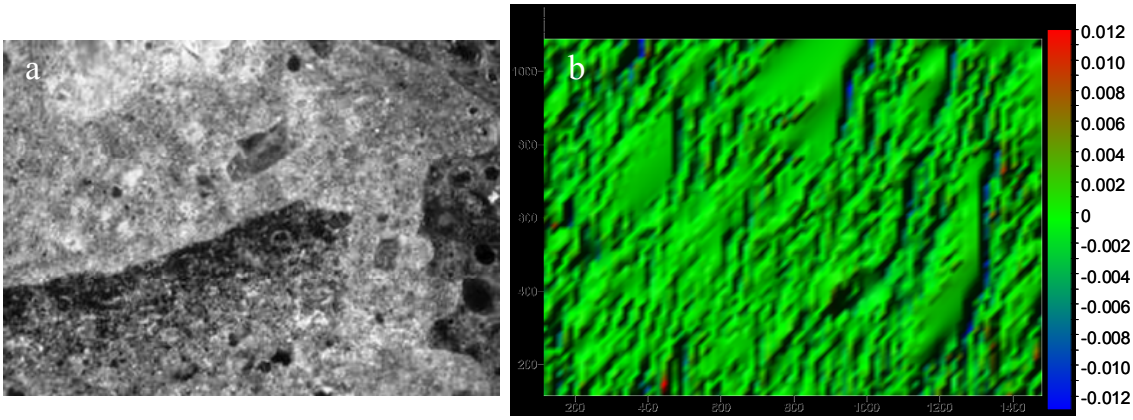

Figure 6.5: Elastic deformation in loading direction as seen by DIC in ROI 2 at high magnification, (a) ROI, (b) deformations in X-direction

It was concluded that an elastic mismatch between cement paste and granite used in NSC and HPC could have induced microcracking at ITZ. The improved elastic matching afforded by the use of lightweight aggregate was postulated previously [3] based on the mechanical properties of the two phases, but this is the first time that experimental evidence shows such deformation compatibility especially in opposition to the mismatch found between normal weight aggregate and cement paste.

6.7 Creep plus Shrinkage Deformations

6.7.1 Creep plus Shrinkage in Normal Strength Concrete

The loaded NSC specimen was imaged again after one, seven, 28 and 120 days under loading and drying. For these analyses the REF used was the image immediately

after loading to eliminate elastic effects. Figure 6.6 shows a representative deformation map (Part b) obtained after one day under sustained load in ROI 2 at high magnification (Part a).

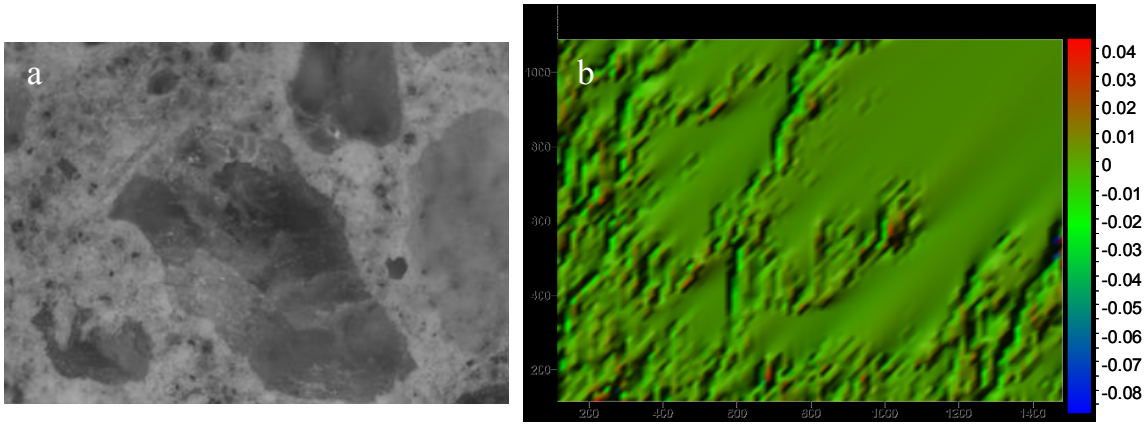

Figure 6.6: Creep plus shrinkage deformation in NSC after one day of loading and drying as seen by DIC in ROI 2 at high magnification, (a) ROI, (b) deformations in X-direction

As seen for the elastic deformation case, the displacements (not shown) shown decreased from left to right indicating a compression field which average resulted in -290 με. Figure 6.6b clearly shows a heterogeneous deformation field where the top-right region, which contains more aggregate, is smoother and presents less compressive deformation. In fact, it presents some areas undergoing tensile deformation.

Figure 6.7 presents the deformation maps obtained for creep plus shrinkage in the NSC specimen after 28 days under drying and loading. Part (a) presents the ROI and part (b) the computed deformations.

Figure 6.7b show similar features as Figures 6.6b, as they represent deformation fields of the same ROI. The main difference is the magnitude of deformations. As expected, after 28 days undergoing creep and shrinkage the average deformation as seen by DIC increased to -1389 με. Time-dependent deformations were not uniform and

greatly varied around the average. The bottom-left corner of the ROI appears to concentrate most of the compressive deformations and the higher variability.

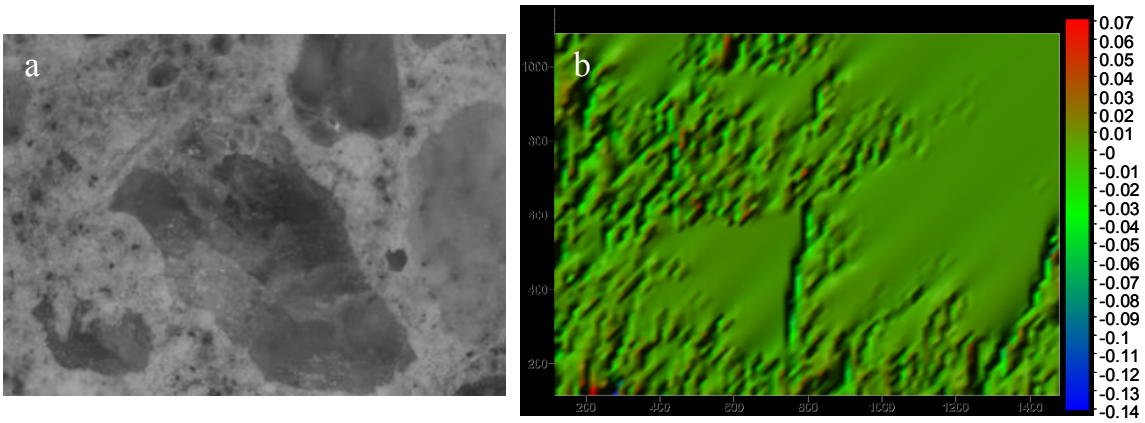

Figure 6.7: Creep plus shrinkage deformation in NSC after 28 days of loading and drying as seen by DIC in ROI 2 at high magnification, (a) ROI, (b) deformations in X-direction

Deformation maps after 1 and 28 days show that more deformation was traced in the paste-rich zones. This would prove the commonly held understanding that in NSC time-dependent deformations occur primary in the cement paste while the aggregate, being the stable phase, helps to restrain those deformations. It should be noticed that such difference between phases was not observed in Figure 6.3 for the elastic deformations indicating that elastic deformation had a different nature. Elastic deformations presented high variability due to its heterogeneity, but they did not show large differences between aggregate and paste-rich regions that Figures 6.6 and 6.7 show.

In order to visualize the heterogeneity of the creep plus shrinkage deformations, Figure 6.8 presents deformations calculated for the individual pixels from the deformation maps in Figures 6.6b and 6.7b. The X-axis presents the matched pixels in a correlative order (starting from the pixel at the top-left corner of the ROI and finishing with the pixel at the bottom-right corner of the ROI), and the Y-axis shows the

deformation of each pixel in με. Two plots are presented in Figure 6.8; part (a) shows creep plus shrinkage in the NSC after 1 day while part (b) after 28 days.

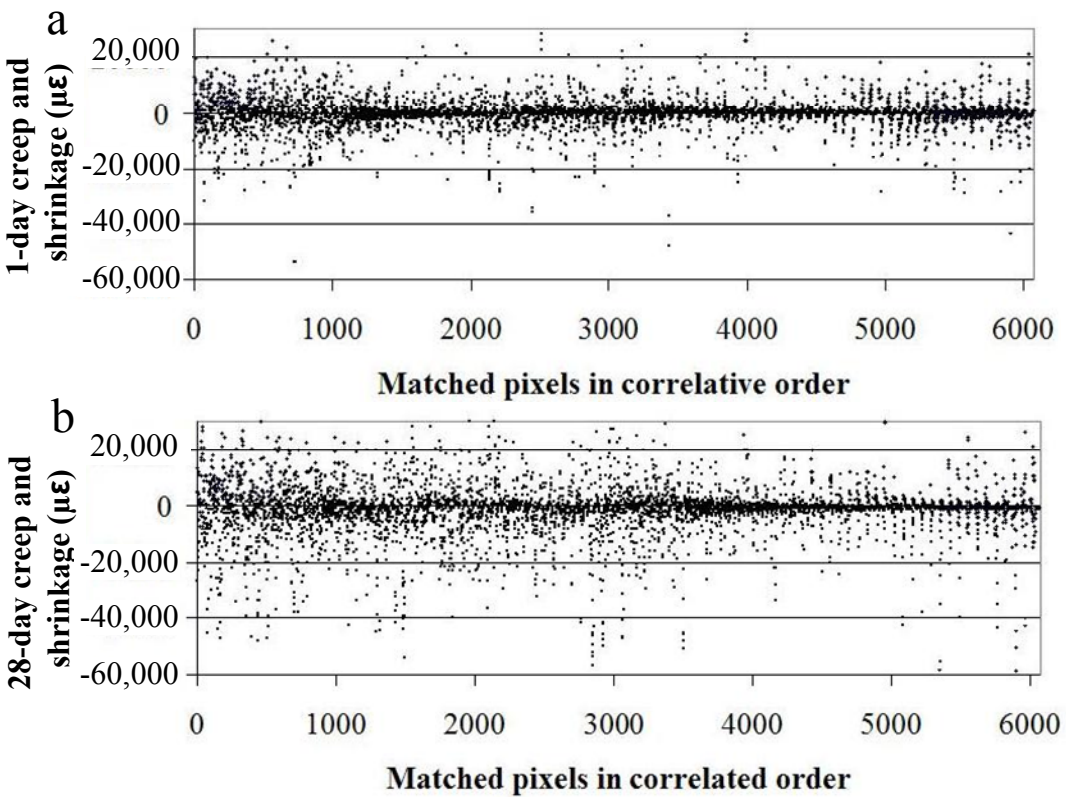

Figure 6.8: Creep plus shrinkage deformation in individual pixels of NSC specimen, (a) after 1 day of testing, (b) after 28 days of testing

Figure 6.8 presents great variability including with some deformation values in tension. Although tensile regions were not expected in this research, the presence of compressive and tensile regions has also been reported for drying shrinkage of cement paste [4]. Figure 6.8a shows that deformation can be as high as 1 and 2% (10,000 and 20,000 με) in both compressive and tensile directions. Nevertheless, most of the deformations fell within a much narrower range; for example the 72.2% of the matched pixels presented deformations between 3000 and -3000 με after one day of testing

(Figure 6.8a), and 70.0% of the pixels had deformations falling between 5000 and -5000 με after 28 days of testing.

Figure 6.9 shows the percentage of pixels showing high tensile deformation (more than 1500 με), intermediate deformation, (between 1500 and -1500 με), and high compressive deformations (less than -1500 με) for one and 28 days of testing.

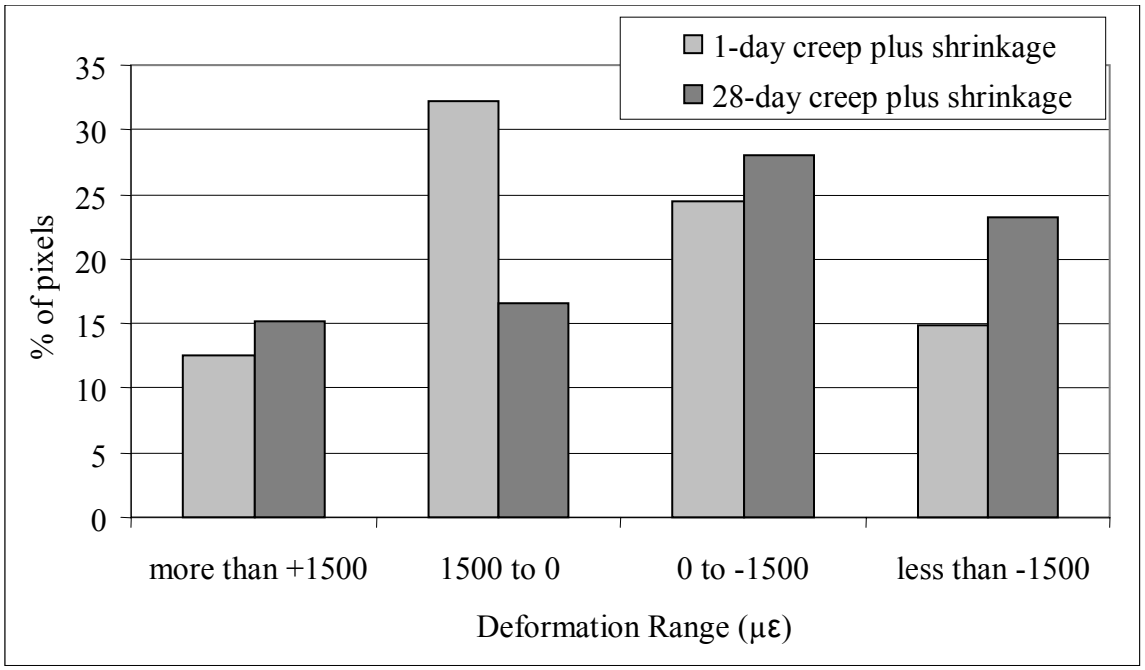

Figure 6.9: Distribution of deformation after one and 28 days under loading and drying

Figure 6.9 clearly shows how distribution of deformation changed between one and 28 days of testing. Percentage of pixels showing deformations in the intermediate range (between 1500 and -1500 με) decreased from 57.6% after one day to 45.2% after 28 days. This decrease shown in the intermediate range was compensated by increases in the percentage of pixels with high deformations. However, the pixels showing high compressive deformations increased by 15.5% while those showing high tensile deformation increased by only 8.3%. Consequently average creep plus shrinkage

deformation became more negative as shown by the averages of -290 and -1389 με after one and 28 days if testing, respectively.

It can be concluded that not only the average deformation increased when time under loading and drying increase but also the standard deviation experienced an increment from 5575 to 9566 με. This evidences the dissimilar behavior between aggregate and paste; i.e., as NSC underwent more creep and shrinkage, the paste presented larger differences in deformation with respect to the aggregate which increased the standard deviation.

6.7.2 Creep plus Shrinkage in HPC

For the time-dependent deformations, the images obtained immediately after loading were used as REF. DIC was applied to compare REF with images obtained after one, seven, 28 and 120 days under load while stored at 50% relative humidity. Figure 6.10 the examined ROI (part a), and the axial deformation map (part b).

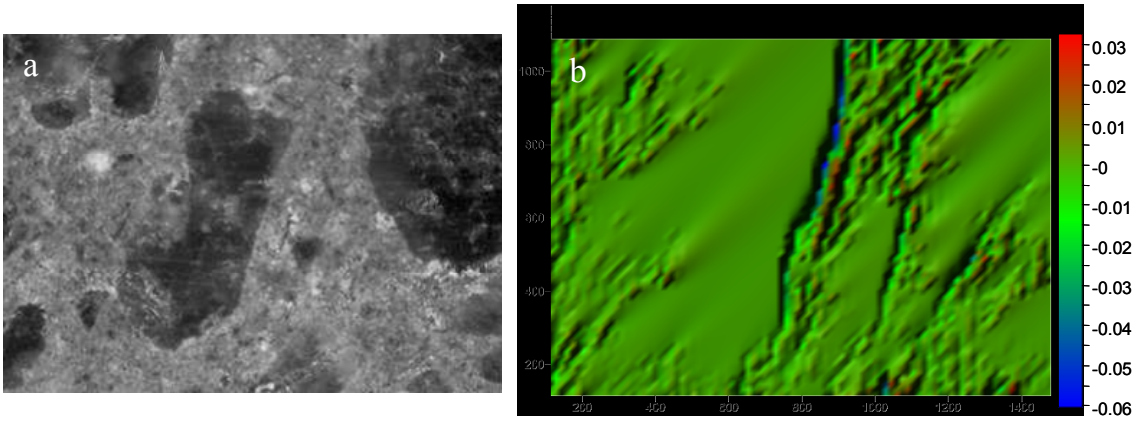

Figure 6.10: Creep plus shrinkage deformation in HPC after one day of loading and drying as seen by DIC in ROI 4 at high magnification, (a) ROI, (b) deformations in X-direction

The average deformation calculated from the deformation map in Figure 6.10b was -266 με. Figure 6.10b clearly shows a heterogeneous deformation field where the center and top-right corner of the image, which contains aggregate particles, appears "smoother" and presents less compressive deformation than the cement fraction.

Two differences between the creep plus shrinkage and the elastic deformation maps were apparent. These differences are that the near-aggregate paste showed some evidence of the restraining effect of the aggregate and the likely indication of cracking, initiated at the ITZ while undergoing creep and shrinkage. Figures 6.4 and 6.10 are images of the same ROI, mapping elastic and creep plus shrinkage deformation, respectively. First, the "smoother" area at the center of Figure 6.10b seems to be larger than that of Figure 6.4b. In Figure 6.10b the lower deformation region encompasses not only the aggregate, but some cementitious matrix around it as well. This might be due to the influence of the aggregate restraining effect on cement paste creep and shrinkage as postulated by Pickett [5] and Neville [6]. The cement paste surrounding the aggregate is not as free to deform as paste farther from the aggregate. The second difference was the presence of a high-deformation line across the map at the right-hand edge of the aggregate particle at the center of ROI in Figure 6.10b. Such a high-deformation line might indicate cracking probably initiated along the ITZ. It should be pointed out that the high deformation zone represents deformations in addition to those obtained after elastic deformation (see Figure 6.4b) because the image obtained after elastic deformation was used as REF when assessing creep and shrinkage by DIC.

The sample examined in Figures 6.4 and 6.10 remained under sustained load at 50% relative humidity; Figure 6.11 presents the deformation map obtained for creep plus

shrinkage for the same ROI on than HPC specimen after 28 days under drying and loading.

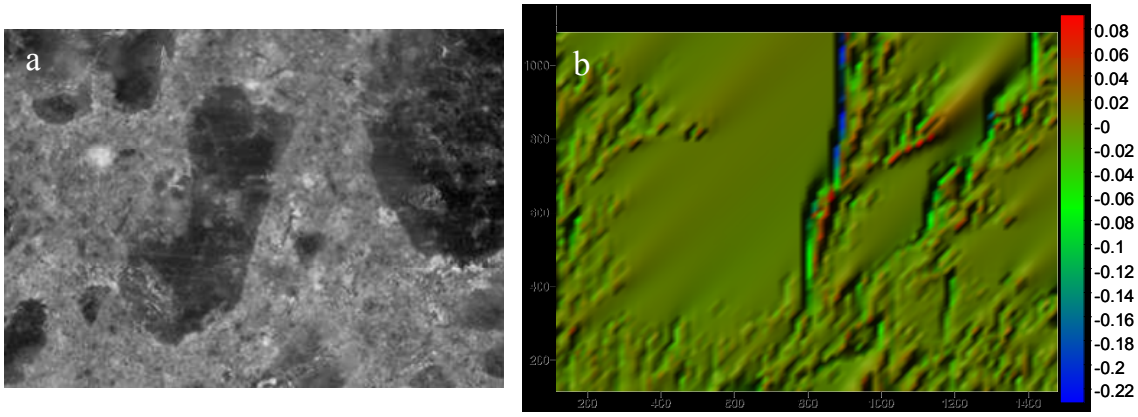

Figure 6.11: Creep plus shrinkage deformation in HPC after 28 days of loading and drying as seen by DIC in ROI 4 at high magnification, (a) ROI, (b) deformations in X-direction

U-displacements and deformations after one (Figure 6.10) and 28 days (Figure 6.11) under loading and drying showed similar features, as they represent deformation fields of the same ROI. As expected, the average deformation from DIC increased, with deformations of -266 με at one day to -1136 με at 28 days. As it was seen for NSC (Figures 6.6 and 6.7), time-dependent deformations in HPC were non-uniform and greatly varied around the average value. At the bottom part of ROI where there was a paste-rich region, the deformation map shows higher and more heterogeneous deformation. In general, deformations were greater in the region with less aggregate. Time dependent deformations increased with respect to those shown in Figure 6.10b. In particular, deformations along ITZ also showed an increase between 1 and 28 days of testing.

Figure 6.12a present creep and shrinkage deformations calculated for individual pixels from ROI 4 in the HPC specimen after 1 day of testing (from deformation map in

Figure 6.10b). Likewise, Figure 6.12b shows the creep and shrinkage deformation of the matched pixels after 28 days of testing (from deformation map in Figure 6.11b). The X-axis presents the pixels ordered from the top-left corner to the bottom-right corner of the

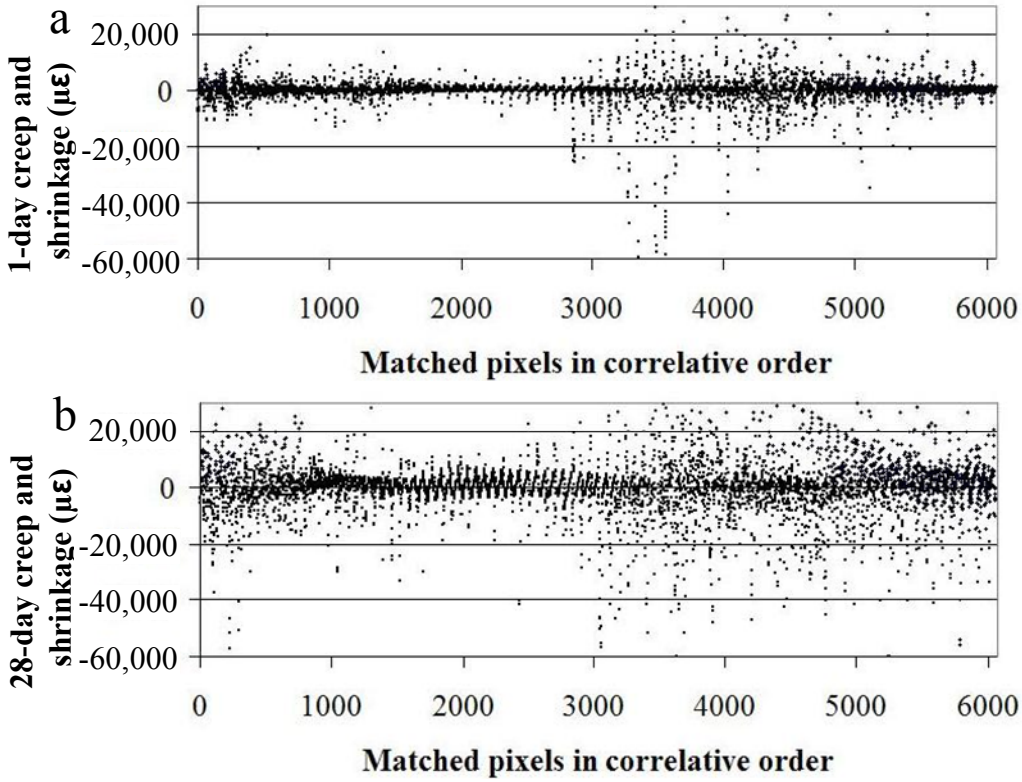

ROI, and the Y-axis the shows corresponding deformation in με.

Figure 6.12: Creep plus shrinkage deformation in pixels of Figure 6.9c after one day under drying and loading

As shown by the comparison between Figures 6.12a and 6.12b, as time under loading and drying increased, the number of pixels in compression also increased. There was an increment not only of the average deformation from -266 to -1163 με but also an increase of the standard deviation by a factor of 3.5 times. The increase in standard deviation might prove that creep and shrinkage are phenomena occurring primary in the

paste. Thus, overtime the difference between deformations located in the paste and the aggregate became larger; i.e., variability increased.

Despite the large variability, 71.8% of the pixels presented deformation between +2000 and -2000 με after one day under testing, and 67.2% of the pixels deformed between +5500 and -5500 με after 28 days.

6.7.3 Creep plus Shrinkage Deformations in High Performance Lightweight Concrete

Figure 6.13 presents the deformation maps obtained after one and 28 days under load in ROI 1 at low magnification. Parts (a) and (b) show the actual ROI and computed deformation map for one day, respectively.

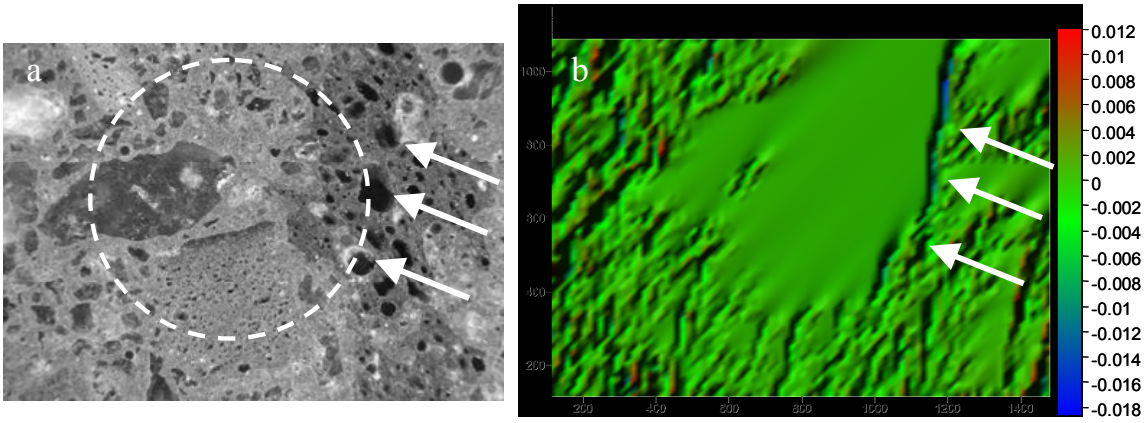

Figure 6.13: Creep plus shrinkage deformation in HPLC after one day of loading and drying as seen by DIC in ROI 1 at low magnification, (a) ROI, (b) deformation map

The average deformation obtained from the deformation map in Figure 6.13b was -179 με. That deformation map shows non-uniform time-dependent deformation in HPLC. Even though the average deformation was always negative (compression) for the four ROIs examined, the deformation map presents both tensile and compressive regions. The 69.1% of the pixels deformed between +1000 and -1000 με. Unlike elastic

deformation in HPLC, where aggregate and paste deformed together, the creep and shrinkage map shows differences in deformation between aggregate and paste. For instance, the center-top region, that includes some aggregate particles (see dashed circle in Figure 6.13a), showed less and "smother" creep plus shrinkage than the surrounding paste-rich regions. There was a high deformation area to the right of the "smooth" region that seemed to go vertically through the lightweight aggregate. That high deformation might have been caused by the uncommon large pores presented by that aggregate particle (see arrows in Figure 6.13a).

The deformation map obtained for ROI 1 in the HPLC specimens after 28 days of loading and drying is shown in Figure 6.14.

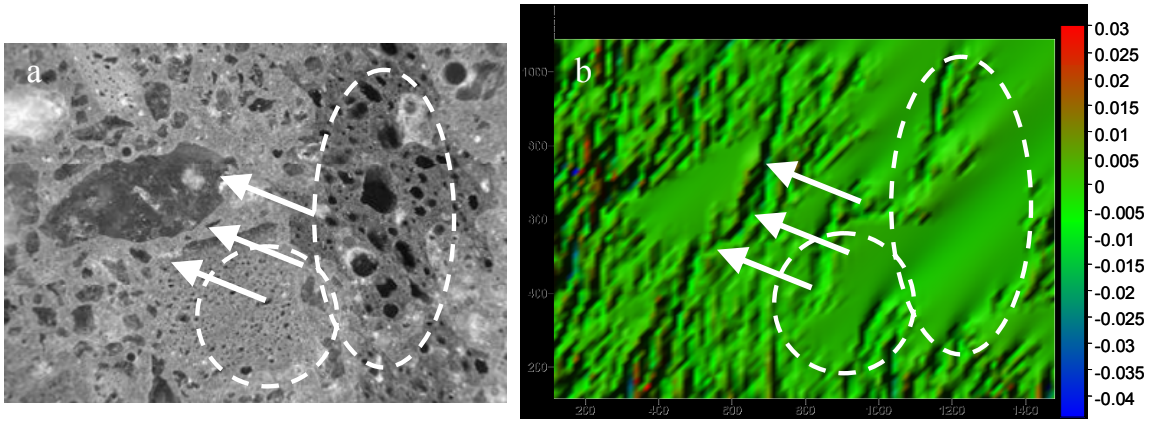

Figure 6.14: Creep plus shrinkage deformation in HPLC after 28 days of loading and drying as seen by DIC in ROI 1 at low magnification, (a) ROI, (b) deformation map

Again creep and shrinkage deformations presented a non-uniform field with differences in deformation between aggregate and paste. The average deformation was -428 με with 69.6% of the values between +2500 and -2500 με.

ROI 1 includes not only lightweight aggregate but also normal weight aggregate (siliceous fine aggregate) as shown by the arrows in Figure 6.14. The deformation map

shown in Figure 6.14b clearly shows the influence of the normal weight fine aggregate in the deformation field. Such particle presented more uniform deformation that the paste surrounding it. Likewise, the lightweight aggregate presented lower deformations than the paste. In fact, the two lightweight particles, highlighted with dashed ovals, seemed to act together as one larger zone of low deformation. Thus both lightweight and normal weight aggregate restrained the cement paste time-dependent deformations [5, 6]. However, ITZ next to the normal weight aggregate presented higher deformations. This high deformation in the ITZ, which was also observed in the HPC specimens (see Figures 6.10 and 6.11), might be due to the large difference in stiffness between the paste and the normal weight aggregate. The lower stiffness of the lightweight aggregate together with the improved bonding [7, 8] might have accommodated the deformation mismatch better than the normal weight aggregate.

There was some deformation redistribution as seen when comparing deformation maps after one and 28 days (Figures 6.13b and 6.14b). The center-top of Figure 6.13b shows lower and more homogenous deformations which virtually disappeared 27 days later (Figure 6.14b). Also, the larger lightweight aggregate particle which presented comparatively large deformations after one day, showed lower values after 28 days.

As observed in the NSC and HPC specimens, not only the average deformation increased between 1 and 28 days of testing but also the standard deviation. The standard deviation after 1 day under loading and drying was 2457 με while after 28 days it increased to 4578 με. This would be a quantitative manifestation of the lower deformations in the aggregate relative to the paste.

6.7.4 Comparison of creep plus deformations in Normal Strength Concrete High Performance Concrete and High Performance Lightweight Concrete

Time-dependent deformation maps obtained for NSC, HPC, and HPLC can be compared to examine the influence of variations in cementitious matrix and coarse aggregate in deformation distribution. As previously described, NSC, HPC, and HPLC specimens were subjected to a compressive stress to at 40% of the compressive strength at the time of loading, but due to their variations in strength, the applied stresses were quite different: 9.7, 28.4, and 21.0 MPa (1410, 4115, and 3040 psi) for NSC, HPC, and HPLC, respectively. In order to meaningfully compare this data, the creep deformations of HPC and HPLC were adjusted to a stress value of 9.7 MPa (1410 psi) which was the applied stress to the NSC specimen. To perform the adjustment, creep and shrinkage must be known separately; thus, the shrinkage portion, which is not stress-related, should be removed from deformation maps that include both creep and shrinkage. By subtracting the shrinkage measured with DEMEC gauge on the small-scale non-loaded companion specimen, from the creep plus shrinkage deformation maps, a measure of creep alone might be obtained. Next, the creep deformation was divided by the applied stress and multiplied by 9.7 MPa (1410 psi) based on the fact the creep is proportional to the applied stress. After that, the adjusted creep was summed with the shrinkage obtained from the non-loaded specimens to obtain creep plus shrinkage deformation under the same conditions for the NSC, HPC and HPLC specimens.

Figures 6.15a, 6.15b, and 6.15c present the adjusted creep plus shrinkage deformation maps of NSC, HPC, and HPLC after 28 days under loading, respectively.

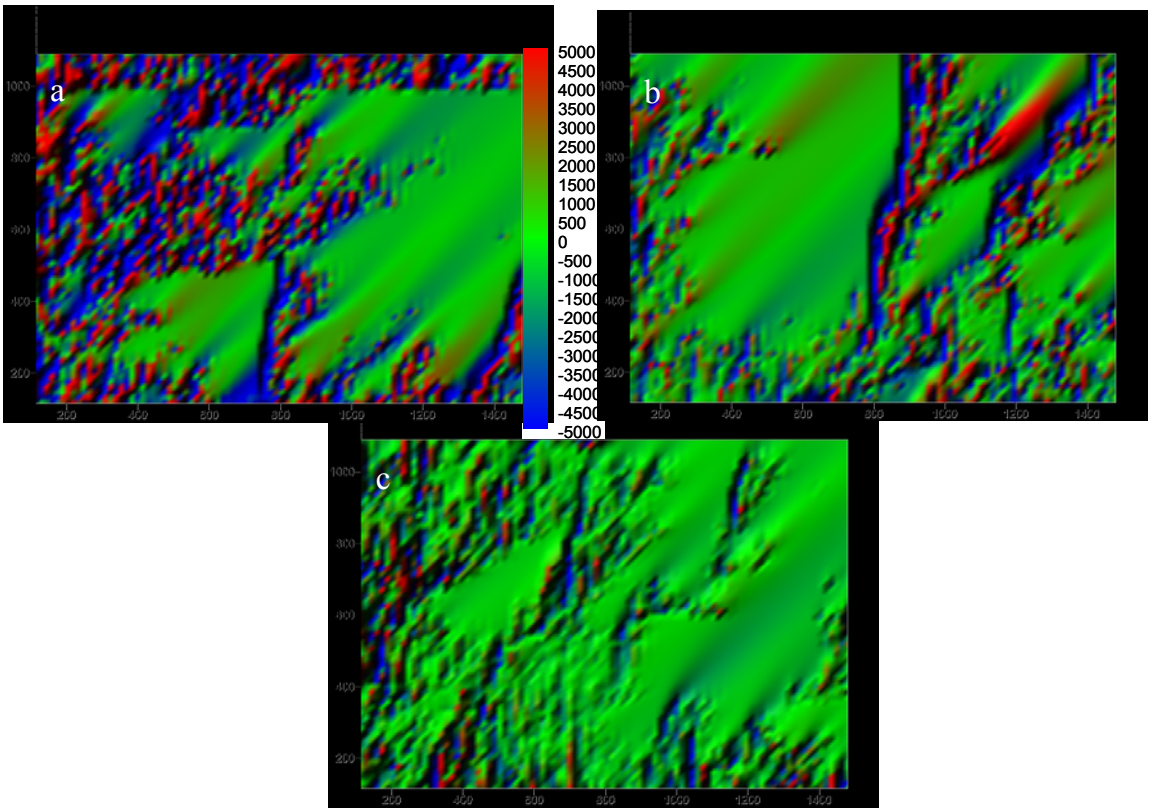

Figure 6.15: Adjusted creep plus shrinkage deformation maps in after 28 days of testing, (a) NSC, (b) HPC, (c) HPLC

As seen previously, the three deformation maps presented non-uniform deformations throughout the ROI with paste-rich regions presented higher deformations. However, creep plus shrinkage deformation map of NSC showed values in a wider range as seen by the large proportion of the deformation map (Figure 6.15a) with extremes values (red or blue). Only 70.1% of pixels in the NSC ROI presented deformation within the range between 5000 and -5000 με given in Figure 6.15, and the standard deviation was 9566 με. On the other hand HPC exhibited 90.6% of its pixels with the mentioned range and only the remaining 9.4% with extreme values and a standard deviation of 5925 με. The average creep plus shrinkage obtained from the maps were -1389 and -555 με for the NSC and HPC, respectively; thus, HPC not only had lower average deformations

but also lower variability within the ROI. This lower and less variable creep plus shrinkage exhibited by HPC with respect to NSC might be a manifestation of the more uniform microstructure of the HPC.

HPLC exhibited even less variability in the deformation map than HPC. The 96.0% of the pixels in Figure 6.15c were within the range between 5000 and -5000 με. In addition the standard deviation and average deformation were 1969 με and -402 με, respectively. Thus, HPLC not only had the lowest creep plus shrinkage but also the lowest variance (only 4% of pixels with extreme values). This further reduction of variability is believed to be a consequence of the improved elastic matching between lightweight aggregate and paste which reduced deformation and possibly cracking at the ITZ. The reduction of highly deformed ITZ decreased overall creep plus shrinkage deformation and reduced the presence of extreme values.

6.8 Deformations from DIC versus Deformations from DEMEC gauge

As described in Section 3.3.3, DEMEC readings were taken every time the ROIs were imaged which allowed for comparison between deformation measured at the surface by DIC and those measured by DEMEC gauge considering the entire specimen. Figure 6.16 presents the elastic, creep and shrinkage deformation as measured by DEMEC gauge versus those obtained from averaging deformation from the maps. The diagonal dashed line in Figure 6.16 represents the equivalence between deformations obtained by the two procedures.

Considering the four ROIs from each of the three types of concrete, it can be seen that the average deformation from the deformation maps was lower than that measured with the DEMEC gauge. On average DIC were lower than DEMEC deformations by

30%. This difference might be due to the fact that DIC was applied to an area equivalent to only 1.4% of the total specimen area in the case of low magnification and 0.04% in the case of high magnification. Thus, important deviations from the bulk measurement might be expected. In addition, as pointed out in Section 6.3.1 (Imaging Procedure) the ROIs were not selected randomly but they were chosen in order to include paste, aggregate and ITZ. The objective with this research approach was to examine variations in the displacement field with structure, and that information can only be gained through this kind of approach.

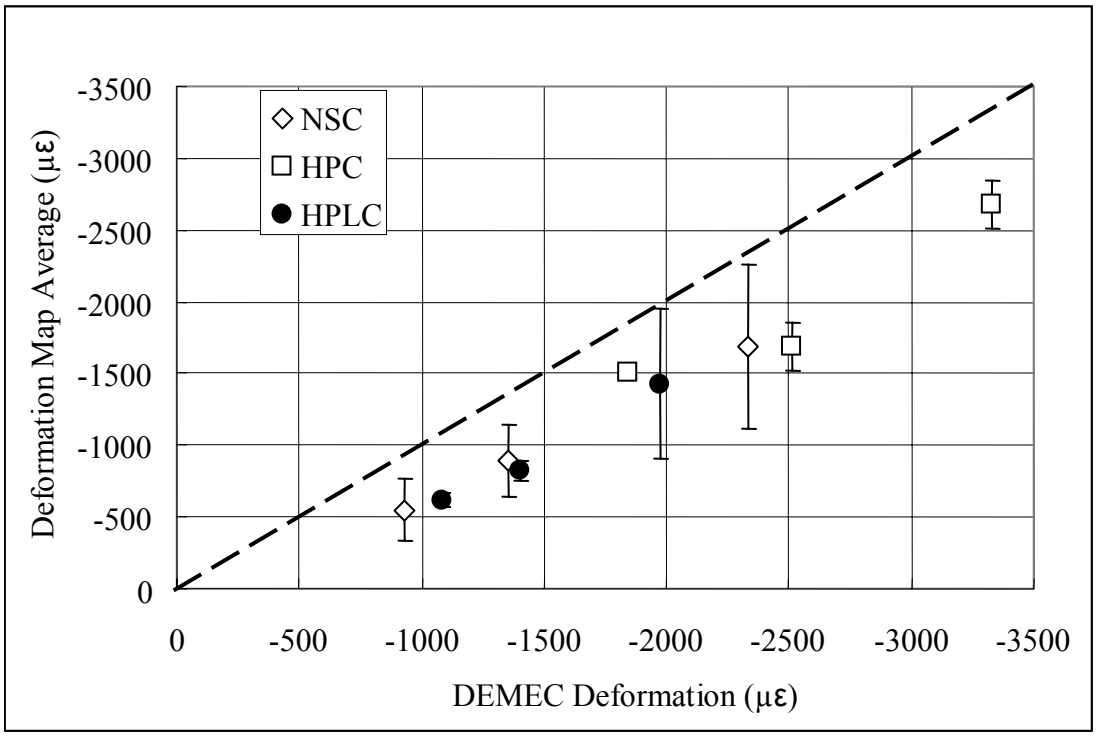

Figure 6.16: Total deformation as measured by DEMEC gauge versus average total deformation from DIC

Another consideration is that DIC measures deformation at the surface while DEMEC gauge included the total volume of the specimen. A previous investigation compared deformations obtained with DIC and x-ray microtomography [9, 10] and found

a strong correspondence between deformations in the surface and in the volume of mortar and concrete specimens under elastic deformations. However, they also suggested that the best results are obtained when using both systems because they provide different information.

Figure 6.16 shows that deformations from DIC and DEMEC followed the same trends and in some cases that were within 5% difference. A regression line showed a coefficient of determination of 0.94. The excellent correlation between deformations using DIC and DEMEC demonstrate the adequate quantitative value of the results presented previously.

6.9 Challenges Using This Technique

As explained in 6.3.2 (Pattern Matching Procedure), the DIC procedure presents some sources of error derived from noise contained in the images. For example, when the pattern matching was tested against rigid body motion (Section 6.5), the matched pixels presented differences in displacement. Variations in lightning and focus, especially at high magnifications, can make the pattern matching challenging.

In addition, changes in the surface produce new features or hide existent features that make difficult the pattern matching process. Carbonation of the sample surface was observed in all samples which affected contrast between different features and phases. As a consequence the percentage of pixels successfully matched declines overtime.

For instance, when the pattern matching was performed between images before and immediately after loading, the percentage of pixels successfully matched was approximately 98%. However, when comparing images taken one day and 28 days apart, the percentage of pixels successfully matched dropped to 95 and 90% respectively. After

120 days, the matching procedure was able to match between 70 and 75% of the pixels. For this reason creep and shrinkage after 120 days was not included here.

Images from the mixture containing steel aggregate yielded, in general, low percentages of matching because of two reasons. First, the steel after being polished did not provide a good contrast for the matching. Secondly, corrosion products appeared and grew at the steel surface overtime. These new features could not be matched because they were not present in the reference image.

In order to successfully perform the pattern matching between two images under different states of deformation, it is essential to have many distinguishable features. Surfaces with poor contrast between phases or surfaces of homogeneous materials might not provide enough details to trace features successfully. This was the case of some of the images obtained from the HP Matrix specimen where the contrast between the siliceous sand and paste was poor especially after carbonation.

6.10 Summary

A new experimental setup was developed to cast, load, and image the surface of concrete specimens under constant stress and drying over time. The specimens are small enough to fit in an optical microscope stage and are maintained under load with an unbonded post-tensioned system.

These initial results showed that the test setup developed combined with DIC could provide new and useful information about the creep plus shrinkage deformations in concrete. Specifically, it allowed for *insitu* measurement of deformation in the specific phases (i.e., bulk paste, aggregate, and ITZ), providing data to complement the global measurements of strain obtained by ASTM C 512.

Creep as measured in small-scale specimens was higher than that measured on 100 x 381-mm (4 x 15-in) cylinders most probably because of the proportionally higher exposed area of the former. It is believed that drying occurred more quickly and was more severe on the small-scale specimens increasing creep and shrinkage.

Elastic deformation was found to be heterogeneously distributed in the cement paste and aggregates. NSC and HPC presented high deformation along the ITZ while HPLC did not show dissimilar elastic deformations between paste and lightweight aggregate.

Nevertheless, HPC showed differences in deformation in the aggregate and in the paste which might have led to microcracking in the ITZ.

Creep plus shrinkage were found to be highly heterogeneous throughout the ROIs examined. As the time under loading and drying increased, both the average and standard deviation of deformations increased in the four ROIs studied from each concrete type. The increase in non-uniformity might prove that creep and shrinkage are phenomena occurring in the cement paste and not in the aggregate. Thus, overtime the difference between deformations located in the cementitious matrix and the aggregate became larger. This corroborates the aggregate restraining effect on creep and shrinkage deformations proposed in the past [5, 6].

The elastic and time-dependent deformation maps showed similarities to the actual ROI indicating higher and more heterogeneous deformation in the paste matrix than in the aggregate particles. In particular, HPC elastic and time-dependent deformation maps showed high deformation at the ITZ probably due to the difference in stiffness between the aggregate and the cementitious paste.

The observed differences between creep plus shrinkage in the aggregate and in the paste constitutes new evidence of a 50-year old hypothesis on the aggregate restraining effect of creep and shrinkage of the paste [5, 6].

Most probably, the time-dependent deformations exhibited by the aggregate are due to delayed elastic deformations rather than creep and shrinkage of the aggregate. As the paste undergoes creep and shrinkage it decreases its relative stiffness with respect to the aggregate which changes the stresses carried by each phase. As the paste stiffness decreases, the stress in the aggregate continuously increases exhibiting a delayed elastic deformation.

When compared with NSC, HPC showed lower creep plus shrinkage deformations and less heterogeneity. This might indicate the better quality achieved by high performance concrete. Likewise, HPLC presented a lower average creep plus shrinkage deformations with also lower heterogeneity than HPC. This is caused by the better strain compatibility between lightweight aggregate and paste than reduces high-deformation areas at the ITZ lowering overall deformations and variability. This is empirical evidence of a 20-year old hypothesis on the improved strain matching between lightweight aggregate and cement matrix [3].

Due to the limited number of ROI explored on each specimen it was not possible to apply statistical tools to assess the possible limitations of the technique. For example, from the experimental data magnification did not seem to play an important role, but further research is needed to verify this observation. Future research should be performed using a large number of ROIs.

In addition this methodology should be applied to standard size creep specimens and full-scale structural elements. This will allow matching the volume-to-surface ratio, and therefore improving the correlation between DIC measurements and real structural behavior. Images should be taken using a high resolution digital camera, such that the size of each pixel is small enough to resolve deformations. The new data obtained from DIC can be used to improve multi-phase models for elastic and time dependent deformations in concrete. Finite element models can also use this data to validate their results.

6.11 References

1. Kennedy, J.B. and A.M. Neville, *Basic statistical methods for engineers and scientists*. 2d ed: Crowell, 1976.
2. Choi, S. and S.P. Shah, "Measurement of Deformations on Concrete Subjected to Compression Using Image Correlation". *Experimental Mechanics*, 37(3): 1997. p. 307-313.
3. Bremner, T.W. and T.A. Holm, "Elastic Compatibility and the Behavior of Concrete". *Journal of the American Concrete Institute*, 83(2): 1986. p. 244-250.
4. Neubauer, C.M., et al., "Drying shrinkage of cement paste as measured in an environmental scanning electron microscope and comparison with microstructural models". *Journal of Materials Science*, 32(24): 1997. p. 6415-6427.
5. Pickett, G., "Effect of aggregate on shrinkage of concrete and hypothesis concerning shrinkage". *American Concrete Institute -- Journal*, 27(5): 1956. p. 581-590.
6. Neville, A.M., "Creep of concrete as function of its cement paste content". *Magazine of Concrete Research*, 16(46): 1964. p. 21-30.
7. Zhang, M.H. and O.E. Gjørv, "Penetration of Cement Paste into Lightweight Aggregate". *Cement and Concrete Research*, 22(1): 1992. p. 47-55.
8. Zhang, M.H. and O.E. Gjørv, "Microstructure of the Interfacial Zone between Lightweight Aggregate and Cement Paste". *Cement and Concrete Research*, 20(4): 1990. p. 610-618.
9. Lawler, J.S., D.T. Keane, and S.P. Shah. "Measuring Three-Dimensional Damage of Mortar in Compression with X-ray Microtomography and Digital Image Correlation". in *High-Performance Concrete: Research to Practice*. Chicago, IL, 1999.p. 187-202.

10. Lawler, J.S., D.T. Keane, and S.P. Shah, "Measuring three-dimensional damage in concrete under compression". *ACI Materials Journal*, 98(6): 2001. p. 465-475.

CHAPTER 7

MULTI-SCALE COMPARISON

7.1 Introduction

7.1.1 Multi-Scale Study

This multi-scale investigation was comprised of large, medium, and small-scale studies. The large-scale study focused on characterizing the short and long-term behavior of six full-scale prestressed concrete girders made from two high performance lightweight concretes (HPLC). The HPLC included pre-soaked expanded slate as coarse aggregate fraction with 56-day compressive strengths of 55.2 and 69.0 MPa (8000 and 10,000 psi) and densities below 1920 kg/m^3 (120 lb/ft^3).

The medium-scale study was focused on understanding the behavior of the 69-MPa (56 day) (10,000 psi) HPLC by isolating the effect of constituents, temperature, age and relative humidity on short and long-term performance. In particular, one mixture with the same mixture proportions as the 69-MPa (10,000 psi) HPLC, but with a smaller maximum size aggregate (MSA), was considered in order to link results between the medium and small-scale studies. This portion of the investigation used standard testing procedures and was meant to facilitate comparisons to previous and future investigation as well as field performance.

The small-scale study was aimed at developing novel testing techniques to further fundamental understanding the interaction among phases of HPLC. The small-scale study used mixtures with MSA of 9.5 mm (0.375 in), and provided new information about elastic and time-dependent deformations.

The objective of this chapter is to compare the data resulting from these three, complementary multi-scale studies to provide further insights into the performance of HPLC.

All test results considered in this chapter were obtained at an age of 24 hours, which was the common testing age for the three scale studies. The only exception was a normal strength concrete (NSC) which was tested at the age of 28 days.

7.1.2 Challenges in a Multi-Scale Research

Even though a carefully designed experimental program was used in this multi-scale study, the three scales used in this investigation presented inherent differences that were expected to influence the results from each scale. Most of the variables such as mixture design, testing procedures, and specimen dimensions remained unchanged among the different scales. Nevertheless, other factors such as size effects, ambient conditions and mixing procedures changed from one scale to the other.

Knowing the possible effect of using different scales helps to analyze and interpret the results accordingly. The following differences were anticipated among the large, medium and small-scale studies.

As explained in Section 5.3, temperature history, and therefore maturity, strongly influenced compressive strength and creep performance of the mixtures tested at 24 hours. The temperature history depended on both the heat of hydration and ambient temperature of the concrete. The former is affected by the amount of cementitious materials and the ambient temperature as well. The concrete of the large-scale portion was batched in a precast plant yard, so the temperature of the constituents and the ambient temperature could not be controlled. Medium and small-scale studies were

carried out in the laboratory with better control of the ambient temperature. Nevertheless, the heat of hydration used during the 24-hour accelerated curing depended on the volume of concrete (i.e., amount of cementitious materials) placed inside the cureboxes. In the medium-scale study, two batches of 50 lit. (1.75 ft^3) each were fabricated each time, so the volume of concrete placed inside the cureboxes was enough to reach temperatures above 50°C (122°F). During the small-scale study, the batch size was about 3 lit. (0.1 ft^3), and, consequently, the maximum temperatures reached during the 24-hour curing period were only around 30°C (86°F).

There were also other differences between field and laboratory. For instance, the field production used a 2.3-m^3 (3-yd^3) capacity auger-type mixer while the medium and small-scale studies considered a 0.056-m^3 (2.0-ft^3) high shear mixer and a 0.004 m^3 (0.15 ft^3) mixer, respectively.

Some of the ambient conditions varied between the large-scale and the medium-scale testing. Particularly, the girders were kept in the precast plant yard for the first two weeks and then moved to the laboratory, but due to their size they could not be stored in the environmentally controlled room. Consequently, the girders were exposed to an average ambient relative humidity higher than that of the creep and shrinkage specimens tested according standards.

Medium and small-scale studies started between two and three and a half years after the large-scale study, so changes in the constituents could have affected the concrete properties. Particularly, the large-scale study used Denopolis Type III cement produced by CEMEX-Southdown corporation and the medium and small-scale studies utilized Type III cement from LaFarge. Although the three studies utilized Class F fly ash from

the same power generating plant, the coal and combustion process were likely to change during the four year period. Oxide analyses of the cements used in the medium-scale and small-scale study are presented in Appendix A.

Size effect was another important factor to be considered. MSA on the small-scale specimens had to be reduced to 9.5 mm (0.375 in) in order to fit in the molds. The smaller MSA provided more surface area and consequently more interfacial transition zone (ITZ). Compressive strength and elastic modulus were likely to be reduced in the mixtures with smaller MSA. At the same time, the intrinsic strength of the lightweight aggregate tends to increase as the MSA decreases. Therefore, compressive strength of the LWW mixtures will be affected by both an increase in both ITZ volume and in intrinsic strength. Additionally, as concluded in Section 5.4, ITZ determined the time-dependent deformations of the mixtures made with granite and steel aggregate.

It was also suggested that for the small-scale specimens the MSA was comparatively large compared to the creep specimen dimensions. Figure 7.1 shows the small-scale creep specimen nominal dimensions. Those specimens had a cross section of 38 x 38 mm (1.5 x 1.5 in) with a center hole of 12.7 mm (0.5 in) in diameter; therefore, the thinnest dimension was 12.7-mm (0.5-in) which was only 33% larger then the nominal 9.5-mm (0.375-in) MSA. In such areas of the specimens the effect of defects in the aggregate, ITZ or matrix would have been amplified. It was concluded that small-scale specimens were likely to present lower mechanical properties and higher time-dependent deformations. In addition, the ROIs used for the image analysis were located where the concrete wall was 9.5-mm (0.375-in) thick which was the thinnest portion as indicated in Figure 7.1.

Another difference derived from the size effects was the comparatively larger exposed area of the specimens as their size decreased. The volume-to-surface ratio, usually used to describe increasing drying exposure of an element as it decreases, was 9.5, 25.4, and 91.4 mm^3/mm^2 (0.375, 1.0, and 3.6 in^3/in^2) for the small-scale prisms, the 100 x 380 mm (4 x 15 in) medium-scale cylinders, and the girders, respectively. The flat surface used in the small-scale specimen further increased the exposed area as compared to a cylinder of the same size.

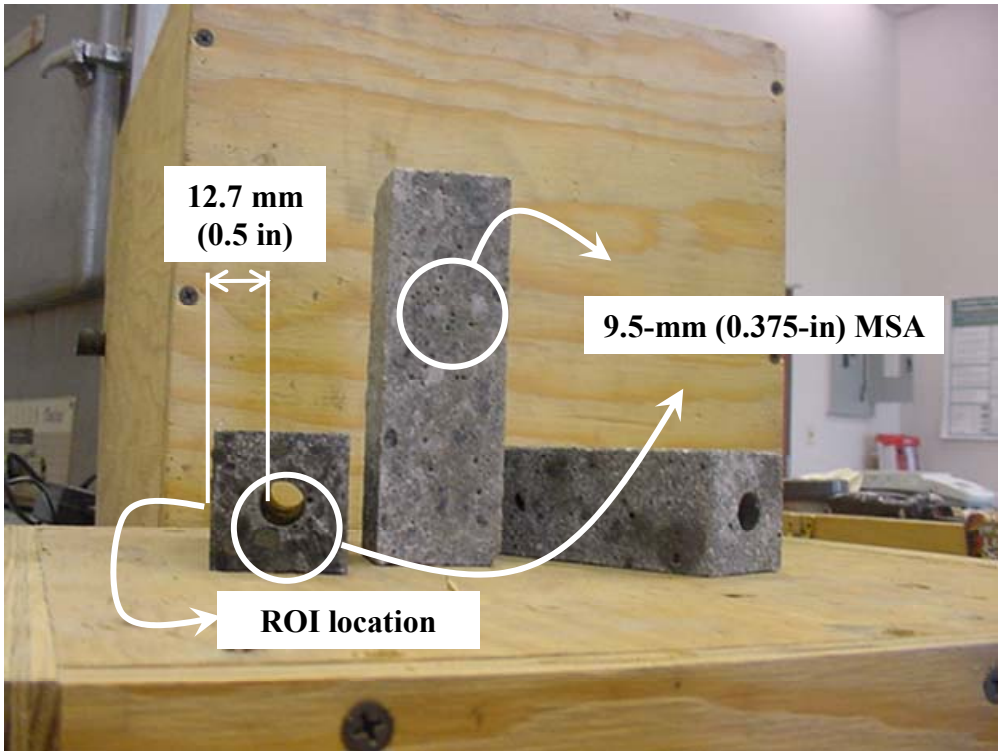

Figure 7.1: Small-scale creep specimen cross section and exposed 9.5-mm (0.375-in) MSA

7.2 Research Significance

No previous research has addressed the short and long-term properties of HPLC at these various scales simultaneously. Important information and conclusions have been obtained from each of the single-scale studies. However, new insights and further

understanding can be extracted from comparing the behavior of similar mixtures under such various scenarios. The information obtained from the small-scale testing can be used to explain the results seen in the large-scale testing and vice versa. In addition, large and small-scale studies can be compared to the work of other investigators by knowing how they related to the standard testing.

The objective of this research was to improve the fundamental understanding of creep and shrinkage of HPLC by characterizing the effect of constituents materials, external conditions and interaction of the different phases of HPLC.

7.3 Experimental Results at Different Scales

The large-scale study was conducted between June 2001 and December 2003. It considered the field construction and testing of six AASHTO Type II prestressed girders made with two HPLC mixtures. The girders, with their composite cast-in-place deck, were 1.2-m (47.5-in) tall and either 11.9 or 13.1-m (39 or 43-ft) long. Three of the girders were produced from a 69-MPa (10,000 psi) 56-day compressive strength HPLC, identified as LWW 69/10 while the three other were made with a 55.5-MPa (8000-psi) 56-day compressive strength HPLC referred as LWW 55/8. In addition to girder testing, compressive strength and elastic modulus, among other properties were measured. Also total creep and total shrinkage were measured for a period of two and a half years.

The medium-scale study was carried out between January 2004 and September 2005. It considered compressive strength, creep and shrinkage testing. Creep and shrinkage were measured in sealed and unsealed specimens for assessing basic, drying, and total creep, in addition to autogenous, drying and total shrinkage. Creep and

shrinkage testing was carried out using either 100 x 380-mm (4 x 15-in) or 150 x 300-mm (6 x 12-in) cylinder specimens.

Three of the ten HPLC mixtures of the medium-scale study were comparable to LWW 69/10 used in the large-scale study. These mixtures were the following:

1. LWW 65-35 which had the same mixture design than LWW 69/10 that included the use of 12.7-mm (0.5-in) pre-soaked (moisture content-MC above 8%) expanded slate lightweight aggregate as coarse aggregate.
2. LWW 65-35-95 which had the same mixture design as LWW 69/10, but with 9.5-mm (0.375-in) MSA pre-soaked lightweight aggregate instead of 12.7-mm (0.5-in) and
3. LWD 65-35 which was the same as LWW 69/10 but with air-dried lightweight aggregate (MC below 1%) instead of pre-soaked.

The small-scale study was carried out between May 2005 and September 2005, and it included compressive strength, total creep and total shrinkage testing in 38 x 38 x 125-mm (1.5 x 1.5 x 5-in) prism specimens. Due to the small dimension of the specimens, the MSA was 9.5 mm (0.375 in), so only two HPLC mixtures were considered in the small-scale study. LWW 65-35-95 and a second mixture with the same MSA but air-dried lightweight aggregate (LWD 65-35-95).

Additionally, medium-scale and small-scale studies considered four other mixtures. Two of them had the same mixture design as LWW 65-35, but the lightweight aggregate was replaced by normal weight granite or A-36 steel cubes. Those mixtures were identified as NWA 65-35 and STL 65-35 when the MSA was 12.7 mm (0.5 in) or NWA 65-35-95 and STL 65-35-95 when the MSA was 9.5 mm (0.375 in). Another mixture with no coarse aggregate with the same relative proportions in all other constituents, named HP Matrix, was also used. The fourth mixture was a NSC of 27.6 MPa (4000 psi) compressive strength. Again, the only difference in the mixtures was the MSA, which was reduced to 9.5 mm (0.375 in) in the small-scale study.

Figure 7.2 present a summary of the comparable mixtures used on each study.

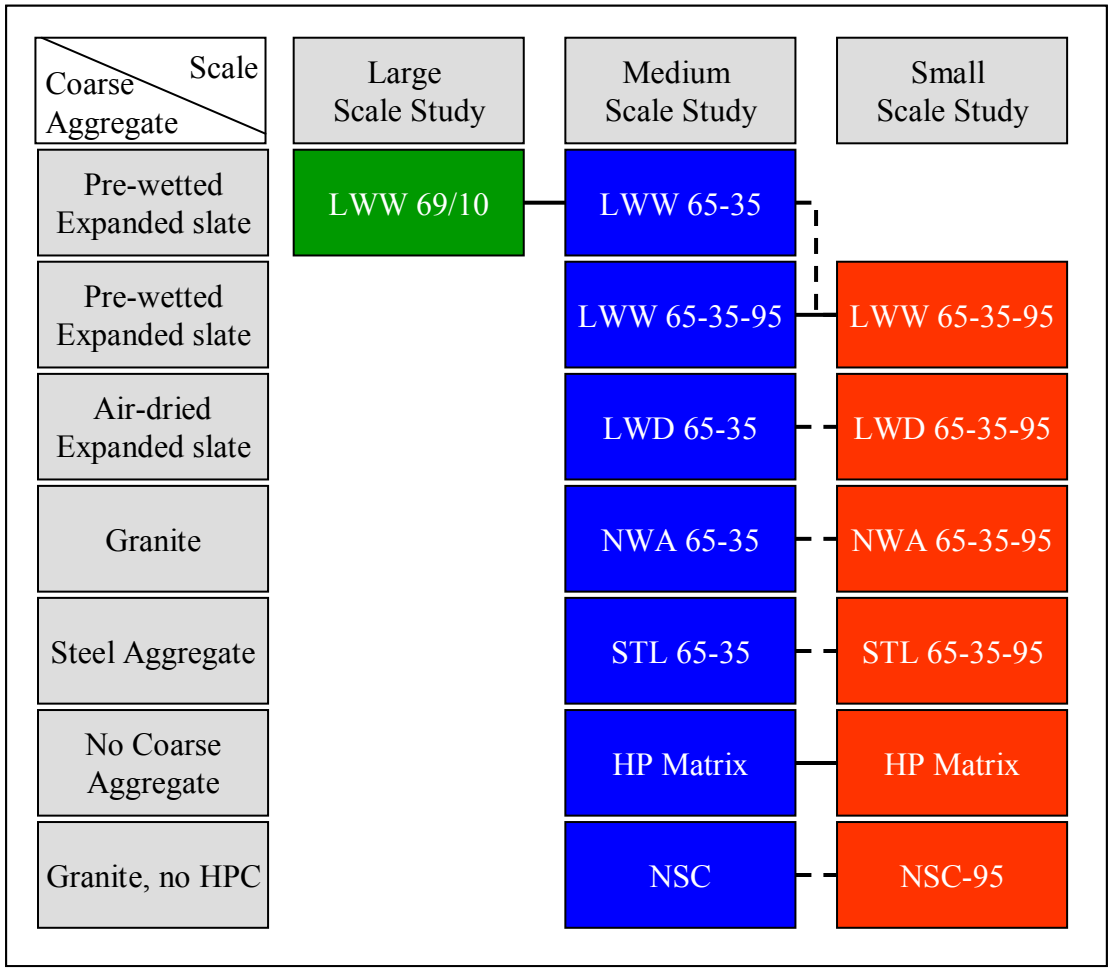

Figure 7.2: Mixtures of the multi-scale study

The columns show the three-scale studies and the rows present the different coarse aggregates considered. The names LWW, LWD, NWA, and STL of the mixtures denote pre-soaked lightweight aggregate, air-dried lightweight aggregate, normal weight aggregate, and steel aggregate, respectively. HP Matrix and NSC stand for the mixtures with no coarse aggregate and normal strength concrete, respectively. The mixtures with MSA of 9.5 mm (0.375-in) instead of 12.7 mm (0.5 in) have a "-95" at the end of it name. Finally, the solid lines denote mixtures that considered the same mixture designs and the

dashed lines designate those mixtures with the same mixtures proportions, but different MSA.

The mixture designs are shown in Tables 3.1 through 3.4 in Chapter 3. When the coarse lightweight aggregate was used in pre-soaked or air-dried condition the weights of the water and coarse aggregate were adjusted accordingly to match the saturated surface dry condition of the mixture designs.

7.3.1 Compressive Strength at Different Scales

Figure 7.3 presents the 24-hour compressive strength of accelerated-cured 100 x 200 mm (4 x 8 in) cylinder specimens tested during the large-scale and the medium-scale studies. It also shows the results obtained on accelerated-cured 50-mm (2-in) cubes tested for the small-scale study. Compressive strengths at the age of 56 days under standard curing are also shown in Figure 7.3 for two of the mixtures. The mixing for the large-scale study was conducted in a precast plant while batching for medium and small-scale studies were carried out in the laboratory.

Unexpectedly, the 24-hour compressive strength with accelerated curing varied significantly between LWW 69/10 and LWW 65-35 even though they had the same mixture design with the identical MSA, and both were tested on 100 x 200-mm (4 x 8-in) cylinders. LWW 69/10 and LWW 65-35 had compressive strength of 62.3 and 73.5 MPa (9025 and 10,655 psi), respectively. This 15% difference might have been caused by three factors: maturity at the time of testing, differences in mixing between laboratory and field, and change in the constituents.

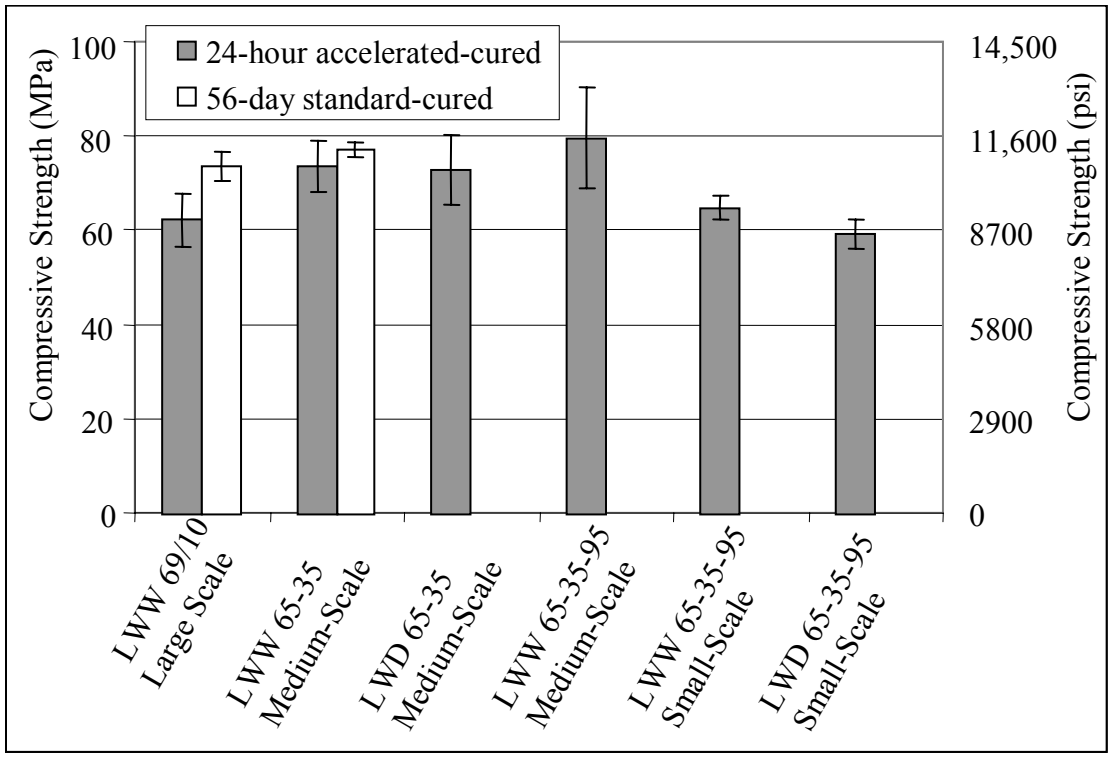

Figure 7.3: Compressive strength of HPLC mixtures used on the large, medium and small-scale studies

As explained previously, differences in temperature history between large-scale and the medium-scale studies at the time of testing could have produced notable differences in compressive strength. It should be pointed out that even though the average compressive strengths were different, some individual results from each study coincided as shown by the standard deviation bars in Figure 7.3. Also differences between laboratory and field mixing could have influenced the compressive strength. For instance, it was difficult to control the amount of water in the large-scale mixtures. This is not likely to be important since comparisons between field and laboratory mixtures made during the large-scale testing revealed no statistically significant differences between them. Finally, the possible differences in constituents might explain the higher

compressive strength measured in the medium-scale study with respect to the large-scale portion.

The compressive strength of standard-cured cylinders tested after 56 days showed only 5% difference between LWW 69/10 and LWW 65-35 which supports the hypothesis of temperature history. Standard-cured specimens from the two studies experienced more similar temperature histories than accelerated-cured cylinders. In addition, the influence of the first 24 hour temperature history decreased when testing was at the age of 56 days.

There were no significant differences between 24-hour compressive strength of LWW 65-35 and LWD 65-35. As discussed in Section 5.5, the use of pre-soaked versus air-dried lightweight aggregate did have an effect on compressive strength measured at ages later than 24 hours.

The reduction in MSA increased the compressive strength of LWW 65-35-95 with respect to LWW 65-35. It was proposed that this is a consequence of an increase in the intrinsic strength of the lightweight aggregate as the aggregate MSA decreased (see Section 5.5). Compressive strength of HPLC was well-described by two-phase models indicating that interface transition zone (ITZ) did not govern the compressive strength (see Section 5.4). Thus, the use of a smaller MSA, which increases the ITZ surface area, did not negatively influence compressive strength.

LWW 65-35-95 from the small-scale study exhibited lower strength than its counterpart from the medium-scale study, even though the specimens in the small-scale study were cubes which are expected to yield higher compressive strength due to their lower height-to-width ratio. The strength differences could be explained by differences in temperature history (i.e., maturity) between the two studies.

In the small-scale study, there was a 9% difference between pre-soaked and air-dried lightweight aggregate 24-hour compressive strength. This might indicate that part of the additional water added to reach SSD condition was not absorbed by the aggregate increasing the water-to-cementitious material ratio.

7.3.2 Elastic Strains at Different Scales

In order to analyze the scale effect on elastic strains, the elastic modulus as obtained from the girders and creep specimens was compared. Elastic modulus was also measured according ASTM C 469 [1], but such standard value did not provide information of the size effect among the different scale studies.

Girders and creep specimens from the different scale studies were subjected to a known stress. In the case of the girders, ten strands were stressed to 202.5 ksi each imposing a stress in their center of gravity equivalent to 16% of the compressive strength at the time of application of load. Creep specimens, regardless of the scale, were loaded to 40% of its compressive strength. Readings were taken before and after loading in each case. The applied stress divided by the elastic strain, calculated as the difference between readings, gave the elastic modulus of the girders and specimens.

Figure 7.4 presents the elastic modulus calculated from the different scale studies. Results are grouped by large-scale girders and large-scale creep specimens made with LWW 69/10 HPLC mixture, medium-scale creep specimens from LWW 65-35 and LWW 65-35-95, and small-scale specimens made with LWW 65-35-95.

Elastic modulus, estimated from girder elastic deformations, was between 19.6 and 22.9 GPa (2840 and 3325 ksi) which was only 75% of the elastic modulus tested according ASTM [1] in 150 x 300 mm (6 x 12 in) specimens. The LWW 69/10 100 x

380 mm (4 x 15 in) creep specimens gave an average elastic modulus of 25.9 GPa (3755 ksi) which was considerably higher than the elastic modulus found from the girders. The differences seen in the large-scale study are likely to be caused by inelastic effects; i.e., the time between the readings taken before and after loading was long enough to include not only concrete elastic deformation, but also creep and possible autogenous shrinkage and thermal shortening. In the case of the girders, strand cut-down took approximately one hour. For the creep testing, the loading process, carried out with a manual hydraulic pump, took around 15 minutes.

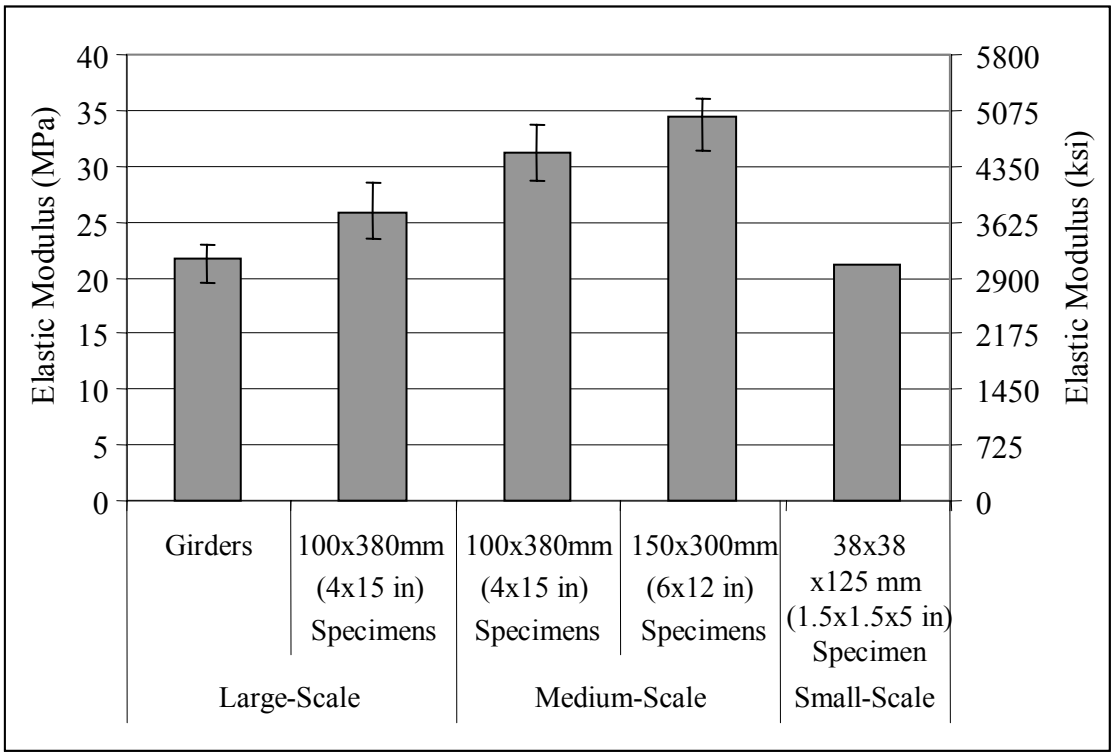

Figure 7.4: Elastic modulus calculated from girders and creep specimens of different sizes

LWW 65-35 creep specimens from the medium-scale study showed consistently higher estimated elastic modulus. The 100 x 380 mm (4 x 15 in) and 150 x 300 mm (6 x 12 in) specimens gave an elastic modulus of 31.1 and 34.6 GPa (4515 and 4980 ksi),

respectively. Those values were more than 40% higher than those from LWW 69/10 of the large-scale study. The same arguments used to explain the difference in compressive strength between those mixtures can be applied to the elastic modulus as well.

Finally, small-scale specimens gave a considerably lower elastic modulus, even though the application of load lasted less than 10 minutes. It was suggested that the presence of defects in the aggregate or in the ITZ could have yielded to this lower elastic modulus given that the small-scale specimens had a relatively thin wall.

7.3.3 Time Dependent Strains at Large and Medium-Scales

Creep and shrinkage deformations measured on the girders and on various creep specimens could not be compared directly because the applied stress was not the same for the girders and for all the specimens. In order to obtain comparable results, the measured creep was adjusted by the applied stress. To do that, creep and shrinkage would be required to be known separately. However, creep and shrinkage were measured together in the large-scale girders, so it was not possible to adjust creep easily.

All laboratory creep testing followed the ASTM C 512 guidelines [2], which required shrinkage measurement in non-loaded companion specimens. Thus, creep and shrinkage strains were in fact known individually for all laboratory creep testing allowing for adjustment of the laboratory specimens to the girder stress conditions.

Regardless of the specimen size or applied load, specific creep was calculated by dividing creep strains by the applied stress. Those specific creep results were then multiplied by 9.6 MPa (1385 psi) which was the effective stress at the center of gravity of the strands in the girders. After that, the adjusted creep was summed with the shrinkage

obtained from the non-loaded specimens to obtain creep plus shrinkage deformation under the same conditions as they were measured in the girders.

Laboratory creep testing from the large-scale study considered unsealed specimens stored at 50 ± 3% of relative humidity. Thus, the laboratory adjusted creep plus shrinkage strains represented less humid environment than that of the girders. Since the girders were exposed to relative humidity between 50 and 95%, the time-dependent deformations under laboratory drying represented an upper bound to those obtained in the girders.

In addition, creep testing from the medium-scale study included both sealed and unsealed specimens. Therefore, the adjusted creep plus shrinkage strains from sealed specimens represented a lower bound to those in the girders, because the sealed specimens had no moisture loss to the environment.

Figure 7.5 presents the time-dependent deformations as measured in the girders compared to those adjusted from creep tests in the large-scale and medium-scale studies. Y-axis presents creep plus shrinkage in με and the X-axis the time after loading in days.

As expected, the creep plus shrinkage of the girders was bound by the time-dependent strains obtained from sealed and unsealed specimens. Creep plus shrinkage of the girders was lower than that measured in the 100 x 380 mm (4 x 15 in) cylinder creep specimens during the large-scale study. This was expected because drying of the girders was not as severe as that experience by the cylinder specimens, with their higher surface area and exposure to lower ambient relative humidity.

Creep plus shrinkage in the girders was higher than that obtained on the sealed specimens, as was expected. However, the difference was not constant and decreased

from of 200 με to 100 με between a few days and 140 days after loading, respectively, as shown in Figure 7.5. In general, creep plus shrinkage in the girders was closer to the lower bound than to the upper bound. This suggested that creep plus shrinkage of the girders was mainly the result of autogenous shrinkage and basic creep; the drying component was of less importance (see Section 5.6).

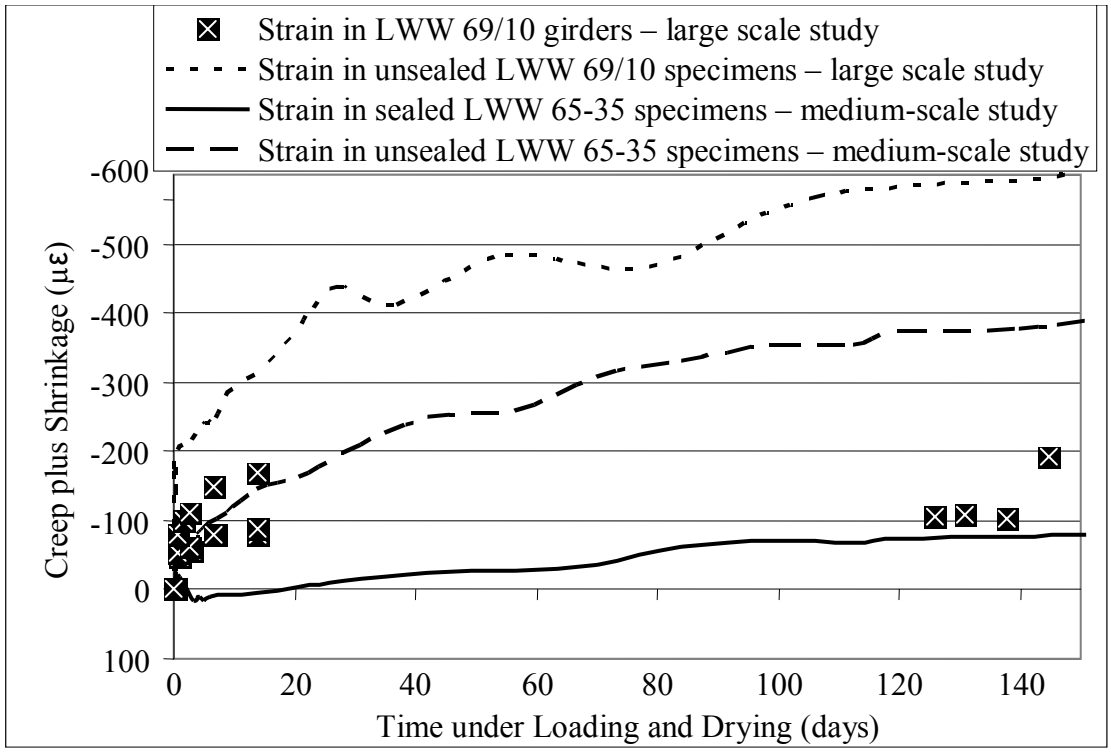

Figure 7.5: Creep plus shrinkage under a compressive stress of 9.6 MPa (1385 psi) in the girders and creep specimens of large and medium-scale studies

After a few days of loading, the creep plus shrinkage of the girders was considerably higher than that of the sealed specimens, as would be expected. The sealed specimens expanded during the first two weeks because the internal cuing afforded by the use of pre-soaked aggregate resulted in some mitigation of autogenous shrinkage which counteracted creep strains from the 9.56-MPa (1385-psi) compressive stress.

It seems, however, that the effect of the pre-soaked lightweight aggregate was not as effective in the LWW 69/10 used in girders as it was in the LWW 65-35 used in the medium-scale study. As shown in Figure 7.5, creep plus shrinkage, calculated for a 9.56-MPa (1385-psi) compressive stress, were close to -400 με after 140 days for the medium-scale study while they reach -600 με in the large-scale study.

7.3.4 Time Dependent Strains at Medium and Small-scales

Comparisons between medium-scale and small-scale studies allowed for comparison of not only HPLC mixtures but also HPC produced with granite and steel aggregate as well as NSC and the HP Matrix (i.e., no coarse aggregate) samples.

Creep testing was performed under a compressive stress equivalent to 40% of the compressive strength at the time of loading. Because each mixture type had a different compressive strength, creep plus shrinkage results were not comparable without a stress adjustment. The same procedure described above was used to make equivalent the creep results, prior to add it to its corresponding shrinkage strains. The stress level used to make the equivalence was 27.6 MPa (4000 psi) for all HPC mixtures, regardless the type of coarse aggregate contained. NSC was not adjusted to such stress level because it had a 28-day compressive strength of 29.0 MPa (4205 psi). Instead, NSC was adjusted to a stress level of 10.7 MPa (1550 psi) which represented an average of the actual stress used in the medium-scale and small-scale testing.

Figure 7.6 summarizes all the creep plus shrinkage data for the five HPLC mixtures. The Y-axes of Figures 7.6a and 7.6b show creep plus shrinkage in με and both X-axes present days under loading and drying. Figure 7.6a compares time-dependent deformations in mixtures where the lightweight aggregate was used in pre-soaked and

air-dried condition for the medium-scale study. Figure 7.6b also compares performance between pre-soaked and air-dried HPLC mixtures, but for the small-scale study which used a smaller MSA. Also in Figure 7.6b, there are data from the smaller MSA mixture tested during the medium-scale study.

As discussed in Section 5.5, the use of pre-soaked lightweight aggregate significantly reduced the creep plus shrinkage of HPLC with respect to the lightweight air-dried aggregate. This was also observed during the small-scale study, as shown in Figure 7.6. This shows that the beneficial effects of pre-soaked lightweight aggregate, for internal curing, were not only limited to standard size specimens or MSA of 12.5 mm (0.5 in) as used in the medium-scale study.

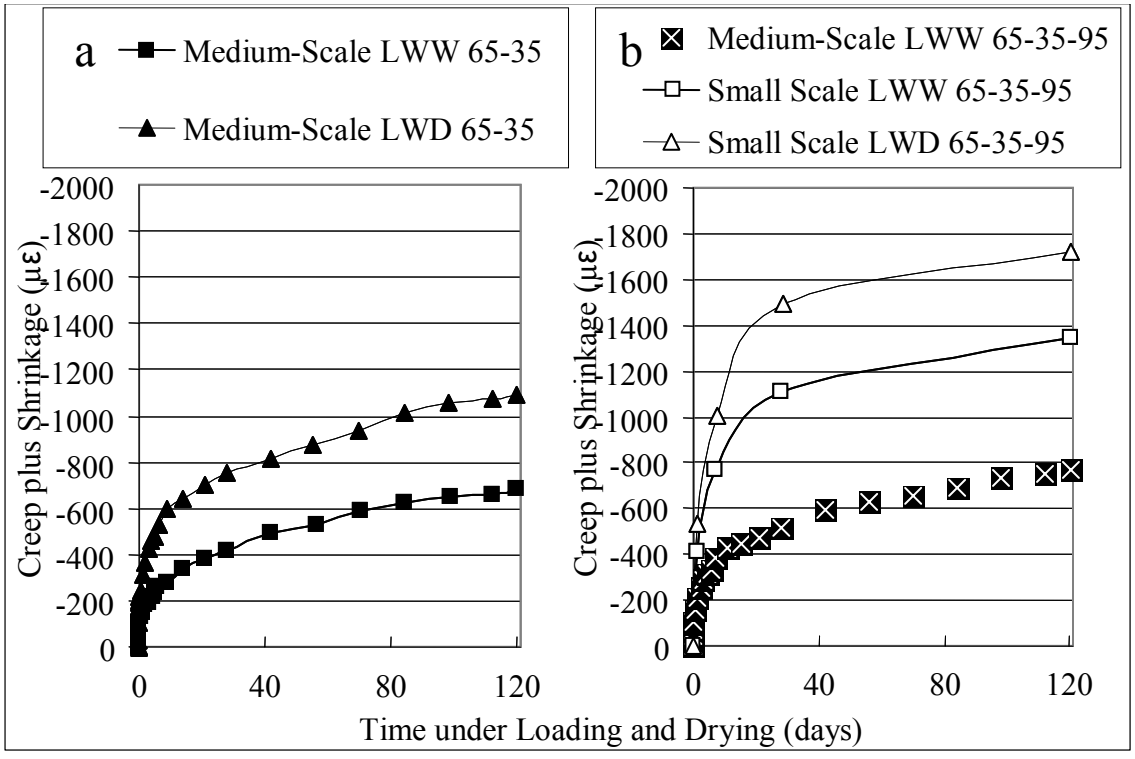

Figure 7.6: Creep plus shrinkage under a compressive stress of 27.6 MPa (4000 psi) in HPLC creep specimens of medium-scale and small-scale studies, (a) mixtures with 12.7-mm (0.5-in) MSA, (b) mixtures with 9.5-mm (0.375-in) MSA

Nevertheless, the larger MSA pre-soaked lightweight aggregate, showed comparatively greater effectiveness in reducing creep plus shrinkage than its 9.5 mm (0.375 in) MWA counterpart. The 120-day creep plus shrinkage of the pre-soaked aggregate (LWW) was 38% less than that of the air-died aggregate (LWD), and the 120-day creep plus shrinkage of the pre-soaked 12.7-mm (0.5-in) MSA mixture (LWW 65-35) was 22% lower than the pre-soaked 9.5-mm (0.375-in) MSA mixture (LWW 65-35-95).

LWW 65-35-95 showed higher creep plus shrinkage for the small-scale study than the medium-scale study. This might be due, as mentioned earlier, to the larger exposed area of the small specimens compared to any of the two sizes of cylinders used in the medium-scale study.

In addition, the aggregate alignment effect, shown in Figure 7.1, could have influenced the time-dependent deformations of the specimen. In such alignment, the properties of the lower stiffness aggregate probably controlled the overall response of the mixture. The larger specimens, on the contrary, provided enough space to randomly accommodate the aggregate and allow matrix and aggregate equally to influence the specimen response.

Creep plus shrinkage measured in the small-scale study were approximately 73% higher than those of the same mixture tested in the medium-scale study. Nevertheless, the same trends, with respect to the effect of pre-soaked lightweight aggregate, were seen at both scales.

Figure 7.7a compares creep plus shrinkage of HPC made with no coarse aggregate, granite and steel aggregate (HP Matrix, NWA and STL) in the medium-scale

and the small-scale studies. The X-axis presents time after loading and under drying in days, and the Y-axis gives creep plus shrinkage strain in με.

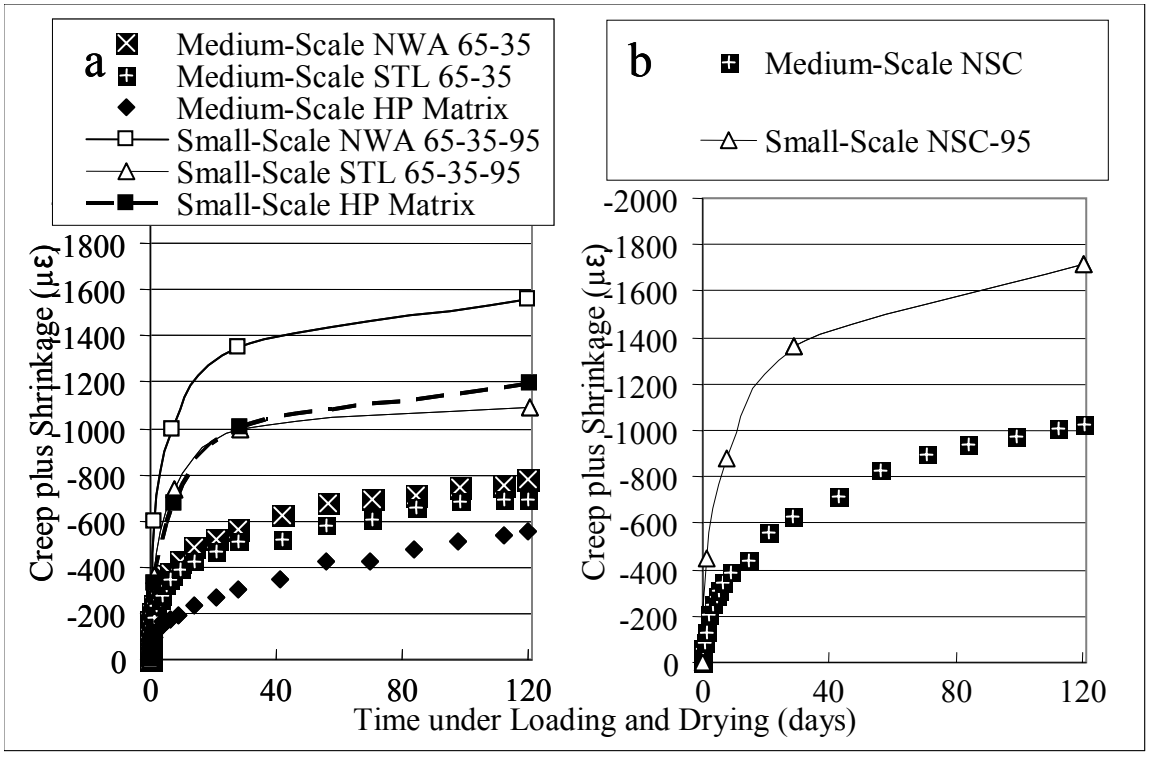

Figure 7.7: Creep plus shrinkage in creep specimens of medium-scale and small-scale studies, (a) granite and steel aggregate HPC's under 27.6-MPa (4000-psi) stress, (b) HP Matrix under 27.6-MPa (4000-psi) stress, and NSC under 10.7-MPa (1550-psi) stress

As seen with the data for the LWW 65-35-95 mixture, the creep plus shrinkage measured in the small-scale specimens was between 57 to 115% larger than the strain in the medium-scale specimens. As before, the different volume-to-surface ratio of the specimens could explain part of the variation, but there was a second fundamental difference that also affected creep plus shrinkage response.

As anticipated, the mixtures with smaller MSA (i.e., the small-scale mixtures) had more interfacial transition zone (ITZ) which could have increased the time-dependent deformations. Moreover, the deformation maps obtained with digital image correlation

given in section 6.7, showed comparatively higher creep plus shrinkage strains in the interface between cementitious matrix and granite. It was believed that the increase in the area of ITZ increased the creep plus shrinkage strain of the small-scale specimens.

Creep plus shrinkage deformation maps obtained for the pre-soaked lightweight aggregate mixtures showed lower or no effect of the ITZ. Thus, a smaller MSA with larger ITZ area would have not affected creep plus shrinkage response of LWW mixtures.

The HPC mixture with steel aggregate showed the least increase (57%) in creep plus shrinkage when decreasing the MSA from 12.7 to 9.5 mm (0.5 to 0.375 in). This was attributed to a comparatively high creep plus shrinkage showed by that mixture in the medium-scale study. ITZ in the HPC with steel was noticeable lower than in any other type of aggregate (see section 5.4). It was concluded that the poor bonding between the steel cubes and the matrix at early ages severely limited the compressive strength, elastic modulus and time-dependent deformations; thus, the worsening effect when decreasing MSA was less noticeable than in the HPC with granite. In the small-scale study some cracks were observed in some of the micrographs of the specimens with steel aggregate.

Since HP Matrix did not include coarse aggregate, the mixture design remained the same between medium ands small-scale studies. This means that ITZ did not play a role in the different creep plus shrinkage observed between the two scales. Creep plus shrinkage of the HP Matrix increased from -556 με, in the medium-scale study, to -1195 με measured in the small-scale specimens. It was concluded that, in addition to the lower volume-to-surface ratio, this 115% increase was caused by differences in maturity of the specimens at the time of loading. The maturity at 24 hour for the small-scale specimens was equivalent to that reached after 3.6 days under standard curing conditions while

maturity at 24 hours of the HP Matrix averaged 5.4 days for the medium-scale study. The maturity at the time of loading was not considerably different between the two scales for the mixtures with lightweight aggregate, granite ,or steel aggregate possibly due to the lower content in cementitious materials compared to HP Matrix. Thus, it was not considered in examining the greater creep plus shrinkage observed in the small-scale specimens of those mixtures.

Figure 7.7b shows the results from the medium-scale and small-scale studied obtained for the NSC mixture. NSC also showed 75% higher creep plus shrinkage in the small-scale study than in the medium-scale study. It was believed that the lesser volume-to-surface ratio was the main factor causing the difference because NSC showed considerably higher pore interconnectivity compared to LWW 65-35 or NWA 65-35. That interconnectivity was believed to be responsible of the higher moisture losses, drying creep and shrinkage of NSC (see Section 5.6). Since NSC was more sensitive to drying than the HPC mixtures, it was expected to be more affected by volume-to-surface ratio than the HPC mixtures.

7.4 Time Dependent Strains of High Performance Lightweight Concrete versus High Performance Concrete

Figure 7.8 presents a comparison of creep plus shrinkage under 27.6-MPa (4000-psi) stress between LWW 65-35 and NWA 65-35 from the medium-scale study and between LWW 65-35-95 and NWA 65-35-95 from the small-scale study. As described previously, the only difference between these mixtures was the type of coarse aggregate (lightweight vs. normal weight). Figure 7.8 presents time under loading and drying in the X-axis and time dependent deformation in the Y-axis.

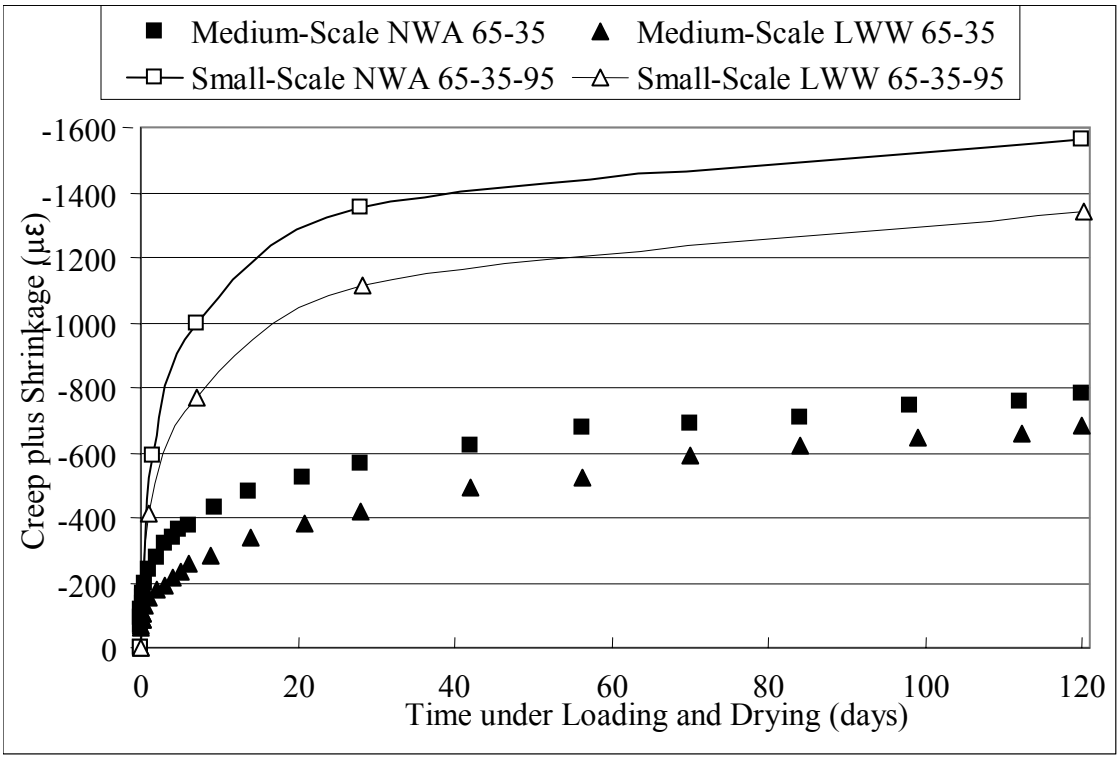

Figure 7.8: Creep plus shrinkage in creep specimens under 27.6-MPa (4000-psi) stress of medium-scale and small-scale studies

The pre-soaked expanded slate HPC showed lower creep plus shrinkage deformations than its granite counterpart in both the medium-scale and small-scale studies. For both scales 120-day creep plus shrinkage of the LWW HPC was approximately 87% of that obtained in the granite HPC. Thus, regardless of the size or volume-to-surface ratio, smaller time-dependent deformations were consistently observed in the pre-soaked lightweight aggregate samples, as concluded by an analysis of variance (ANOVA)

LWW 65-35 exhibited 13% less creep plus shrinkage than NWA 65-35, although the compressive strength of LWW 65-35 was equivalent to 81 and 77% of that observed in NWA 65-35 after 24 hours and 56 days, respectively.

From the analysis of the medium-scale results (see Section 5.5), it was concluded than the smaller deformations observed in LWW 65-35 was due to the water contained on the pre-soaked aggregate which might have promoted hydration, caused expansion, and blocked creep-related water migration through the hydrated cement paste.

The creep plus shrinkage deformation maps obtained from the small-scale study suggested that ITZ in NWA 65-35-95 had higher deformations and possible cracking that might have increased creep plus shrinkage (see Section 6.7). Those maps showed no large deformations in the ITZ of LWW 65-35. This is likely due to better matching between elastic properties of lightweight aggregate and the cementitious matrix. It was also proposed that the enhanced hydration afforded by the pre-soaked aggregate could have improved ITZ strength and resistance to time-dependent deformations.

It was believed that the beneficial effects of the pre-soaked lightweight aggregate observed in the medium-scale and small-scale studies were entirely applicable to the results obtained in the large-scale study. Therefore, the AASHTO Type II prestressed girders produced in the large-scale study would have shown smaller prestress losses due to creep plus shrinkage than some identical hypothetical prestressed girders made with NWA 65-35.

This conclusion was strongly supported by the fact that design methods overestimated creep plus shrinkage prestress losses in expanded slate HPLC by 6 to 8 times. Those same codes overestimated creep plus shrinkage prestress losses in girders made with similar strength normal weight HPC by 2.5 to 4 times. This means that the source of the overestimations was not only due to high strength but also to the use of pre-soaked lightweight aggregate.

7.5 Conclusions

This multi-scale study investigated long-term time-dependent deformations of HPLC at three different scales. The large-scale study considered the construction and testing of six AASHTO Type II prestress girders along with standard ASTM testing of various concrete properties. The medium-scale study was an extensive experimental program to extend the understanding of time-dependent deformations of HPLC. The small-scale study aimed to provide new insights of time-dependent deformations by the use of microscopy and quantitative image analysis.

The results of time-dependent deformations obtained at different scales were influenced by size effects. Drying strains were larger as the size of the specimens, and hence the volume-to-surface area ratio, decreased. Also, the small-scale specimens used a smaller MSA which had greater surface area and increased ITZ. The small-scale specimens had some narrow areas where some defects in the aggregate, ITZ, or matrix could have affected the response of the specimen. Regardless of the scale effects, time-dependent deformations showed similar trends at the three scales.

AASHTO Type II girders made with 69-MPa (10,000-psi) compressive strength HPLC showed creep plus shrinkage strains between those measured on sealed and unsealed creep specimen tested according standard procedures in the laboratory. Time-dependent deformations on sealed specimens were close to those in the girders. This demonstrated that drying was of less importance in the girders.

LWW 65-35 showed lower creep plus shrinkage than NWA 65-35 in both medium-scale and small-scale studies. It was concluded that the smaller time-dependent deformations observed in LWW 65-35 were due to the presence of the absorbed water

contained in the pre-soaked lightweight aggregate through four mechanisms: enhanced hydration, expansion of the microstructure, blockage of load-induced water migration in the hydrated cement paste, and refinement of the ITZ.

7.6 References

1. ASTM C 469, *Standard Test Method for Static Modulus of Elasticity and Poisson's Ratio of Concrete in Compression*. West Conshohocken, PA: American Society for Testing and Materials, 2002.
2. ASTM C 512, *Standard Test Method for Creep of Concrete in Compression*. West Conshohocken, PA: American Society for Testing and Materials, 1992.

CHAPTER 8

CONCLUSIONS AND RECOMMENDATIONS

A multi-scale study that focused on time dependent deformations of high performance lightweight concrete (HPLC) was carried out. This study used a wide range of techniques to assess those deformations. The main conclusions and recommendations are presented below.

8.1 Conclusions

8.1.1 Large-Scale Study

The study using six AASHTO Type girders investigated prestress losses, creep and shrinkage of pretensioned girders made with expanded slate HPLC. LWW 55/8 and LWW 69/10 HPLC had 56-day strengths of 64.5 and 73.0 MPa (9350 and 10,580 psi), and densities of 1855 and 1890 kg/m^3 (116 and 118 lb/ft^3), respectively.

Final prestress losses were estimated using AASHTO refined, AASHTO lump sum, PCI, and ACI-209 methods. All these methods overestimated the total prestress losses in LWW 69/10 AASHTO Type II prestressed girders made with expanded slate HPLC, while the AASHTO refined and ACI-209 also overestimated total prestress losses for the LWW 55/8 HPLC girders; The AASHTO Lump Sum and PCI underestimated total prestress losses of the LWW 55/8 HPLC girders by 1.3% and 1.8%, respectively. This means that these methods are satisfactory for estimating total prestress losses in bridge girders using of expanded slate HPLC.

Long-term performance of the LWW 69/10 mixture was compared to that of a normal weight HPC (called HPC-6) made with comparable constituents and of comparable 24-hour compressive strength. LWW 69/10 had creep plus shrinkage strains equivalent to the 77% of those measured on HPC-6 over a period of 855 days.

Design codes overestimated prestress losses due to creep plus shrinkage by more on girders made with the HPLC than with the normal weight HPC. Thus, the good time-dependent performance exhibit by HPLC was not only due to its low water-to-cementitious material ratio but also to particularities of the pre-soaked expanded slate HPLC.

8.1.2 Medium-Scale Study

8.1.2.1 Maturity Effect

Creep of eight HPC mixtures, including three HPLC mixtures, was studied under three temperature conditions. The maturity of HPC mixtures at the time of loading greatly varied with the ambient conditions which allowed the study of the interaction between creep and maturity.

It was concluded that for the same amount of cementitious materials, mixtures with lightweight aggregate experienced a higher increase in temperature leading to higher maturity at the time of testing than mixtures with other coarse aggregate such as granite or steel aggregate.

The experimental results showed the great influence of maturity on creep, especially when specimens were loaded 24 hours after casting. It was concluded that creep of concrete was inversely proportional to the natural logarithm of maturity at the time of loading.

It also was concluded that replacement of 25% of cement by silica fume and class F fly ash by weight reduced 120-day creep by 15%. The addition of 18.4% and 36.8% of coarse aggregate by volume reduced creep by 28% and 50%, respectively.

8.1.2.2 Phase Interaction

Theory of composite materials estimates properties of a composite based on the properties and relative amount of the constituents. Particularly, two-phase models estimate some concrete properties based on those of aggregate and cement paste assuming that interfacial transition zone (ITZ) does not play an important role. The shortcoming of these simple models is precisely in neglecting ITZ which has been proven by many to have main effect in properties of normal strength concrete (NSC). Therefore, the performance of these two phase models indicated the influence of the ITZ on mechanical properties and creep and shrinkage of mixtures with coarse aggregate of different characteristics.

The good agreement between measured compressive strength and the estimates from some of the two-phase models for the LWW and NWA mixtures indicated that ITZ did not limit the strength of those mixtures. However, STL mixtures presented a strength-limiting ITZ possible due to lack of bonding between steel aggregate and HP Matrix and stress concentrations around the steel aggregate.

Elastic modulus of the expanded slate HPC was in agreement with the estimated values using two-phase models proposed by four different researchers. Granite and steel aggregate mixtures deviated from estimates by 25% and 45%, respectively. ITZ in the steel aggregate mixtures was believed to limit the elastic modulus of the concretes.

The two-phase model proposed for shrinkage of concrete using the aggregate restraining effect concept presented good agreement with experimental data. Nevertheless, the similar model for creep deviated from the experimental values importantly. Creep of expanded slate HPLC was considerably lower than predicted meaning that the restraining effect of expanded slate on creep cannot be modeled based solely on the aggregate mechanical properties. Creep of the steel aggregate mixtures was higher than expected showing a weak ITZ.

8.1.2.3 Internal Curing

The effect of internally stored water in compressive strength, elastic modulus, creep and shrinkage was studied on HPC mixtures, including three HPLC mixtures, containing the same mixture design, but different coarse aggregate. Some of the mixtures considered internally stored water within pre-soaked expanded slate lightweight coarse aggregate (LWW), and other mixture used either air-dried lightweight aggregate (LWD) or normal weight aggregate (NWA).

All expanded slate mixtures presented lower compressive strength than that of NWA due to the lower intrinsic strength of the aggregate. LWW presented practically the same 24-hour compressive strength, but considerably higher 56-day and one-year strengths than that of LWD. It is believed that the water stored in the pre-soaked lightweight aggregate improved the hydration resulting in a higher strength gain.

When tested at the age of 24 hours, statistical analysis revealed that shrinkage and creep of LWD were higher than those of its LWW counterpart with a confidence level of 95%. There was also a significant difference in the deformation rate, so as the time under loading and drying increased the strain difference between those two mixtures also

increased. This difference was believed to be caused by hydration enhancement and expansion in LWW due to curing provided by the internally stored water. It was also proposed that the internally stored water could have inhibited the load-induced water migration from the calcium silicate hydrates (C-S-H) surface by equilibrating the relative humidity through the microstructure.

The statistical comparison also suggested, with 95% confidence, that LWW had lower shrinkage and creep than NWA. Thus, the reduction in creep afforded by the pre-soaked lightweight aggregate could have counteracted the lower stiffness of the lightweight aggregate. This would explain the poor performance of the two-phase models in predicting creep of LWW.

When creep and shrinkage started at the age of 28 days, the same general trends were obtained, but the differences between mixtures were smaller. LWD and NWA mixture showed comparatively higher reduction in creep and shrinkage than that of LWW mixture. It is believed that the external curing between one and 28 days did not change LWW importantly because it already had an adequate moist curing.

8.1.2.4 Drying Effect

The influence of the pore system structure in drying long-term deformations on four concrete mixtures was investigated for one year. One NSC and three HPC mixtures, including one HPLC, were considered. Among the HPC mixtures, one referred to as HP Matrix had only fine aggregate and proportionally more cementitious paste. The other two were LWW and NWA.

Drying as shown by change in weight does not only depend of the pore system of the mixture but also on the initial water content. Thus, mixtures like HP Matrix and

LWW showed more change in weight than NWA, but the same or lower sorptivity. It was believed that sorptivity represented the combined action of interconnectivity and capillary suction of the pore system. The former was found to be dominant in the low water-to-cementitious material ratio mixtures seen herein.

Sorptivity was able to represent well the differences between NSC and HPC mixtures which might be responsible for the reduction in drying shrinkage and drying creep seen on HPC.

Drying shrinkage, which is mainly driven by moisture loss, was mainly affected by the pore system properties, so a reduction in the interconnectivity in the pores produced a proportional decrease in drying shrinkage. Drying creep is affected by both loss of moisture and sustained load, so differences in cement paste content can offset the effect of the pore system structure. When NSC was compared with NWA and LWW (i.e., HP Matrix was not considered), drying creep was decreased in the same proportion than sorptivity suggesting that the interconnectivity of the pore system, reflected by the sorptivity, determined most of drying creep.

8.1.3 Small-Scale Study

Creep and shrinkage of various concrete mixtures were mapped using an optical microscope, a digital camera and image analysis known as digital image correlation (DIC). By locating features of the same region of interest (ROI) in different states of deformation, the deformations, computed as relative displacements, can be known locally. A new experimental setup was developed to cast, load, and image the surface of concrete specimens under loading and drying over time. The specimens were small

enough to fit in an optical microscope stage and were maintained under load with an unbounded post-tensioned system.

This setup allowed for in situ measurement of deformation in the specific phases (i.e., bulk paste and aggregate), providing data to complement the global measurements of strain obtained by standard creep and shrinkage testing.

Creep as measured in small-scale specimens was higher than that measured on the medium-scale study most probably due to the proportionally higher exposed area and the increase in ITZ due to smaller maximum size aggregate (MSA) of the former.

Elastic and time-dependent deformations were mapped on NSC, HPC and HPLC.

Elastic deformation was found to be heterogeneously distributed in the cement paste and aggregates. Nevertheless, HPC showed differences in deformation in the aggregate and in the paste which might have led to microcracking in ITZ. This was not observed in the HPLC specimens.

Creep plus shrinkage of HPC was found to be highly heterogeneous throughout the ROI under study. As the time under loading and drying increased, both the average and standard deviation of deformations increased in all ROI studied. The increase in non-uniformity proved that creep and shrinkage are phenomena occurring in the cement paste and not in the aggregate. Thus, over time the difference between deformations located in the cementitious matrix and the aggregate became larger.

When compared with NSC, HPC showed lower creep plus shrinkage deformations and less heterogeneity. This might indicate the better quality achieved by high performance concrete. Compared with normal weight HPC, HPLC showed less heterogeneity in both elastic and time-dependent deformations. This might indicate the

better elastic matching between lightweight aggregate and cementitious matrix. The deformation maps revealed very high deformations in the ITZ when normal weight aggregate was used. ITZ showed lower peak deformations with expanded slate aggregate.

The elastic and time-dependent deformations maps showed differences among paste and aggregate; particularly there were higher and more heterogeneous deformation in the cement matrix than in the aggregate particles.

Finally, time-dependent deformations mapped using stereomicroscopy followed similar trends as those measured using a conventional DEMEC gauge. Thus, DIC gave not only qualitative but also quantitative information.

8.1.4 General

It was concluded that standard testing of creep and shrinkage adequately represented the difference observed on actual structural elements. More over, results from standard creep and shrinkage testing bounded the strains seen in full-scale prestressed girders.

Basic creep of HPLC was on average 8 times larger than drying creep when creep testing started at the age of 24 hours. That proportion increased to 13 times when testing started at the age of 28 days. It was concluded that the size of the creep specimens was of little importance on creep behavior because the drying creep portion was comparatively low. This was confirmed by comparing total creep obtained in 100 x 380-mm (4 x 15-in) and 150 x 300-mm (6 x 12-in) cylinder specimens. The latter might imply that results from creep testing performed in standard specimens can be used in estimating creep of full-scale concrete members without a large error.

Even though small-scale specimens underwent more creep and shrinkage than that of standard specimens, the interaction among phases was believed to be entirely applicable to larger specimens.

8.2 Recommendations for Future Research

The reduction of creep with increasing maturity found in this study included creep testing started either at very early ages or 28 days after casting. However, it is clear that high temperatures during the first hours might decrease long-term strength, so this detrimental effect might also affect creep meaning that mixtures of comparatively lower maturity might perform better when age of loading is late. It is recommended to extend this study to creep testing starting at later ages such as 56 or 90 days to corroborate if the same trend observed herein is maintained.

Some researchers found that shrinkage of HPLC was initially lower than that of normal weight HPC, but in the long-term the relationship inverted. Consequently, the comparatively good creep performance showed by the HPLC needs to be verified for longer periods under load.

Many of the conclusions about maturity and creep need to be corroborated with studies of the microstructure of the concrete, including cementitious paste, aggregate and ITZ.

Future studies should confirm the hypothesis about water seepage blockage suggested herein. This could be done by tracing water displacement in specimens under loading containing pre-soaked and air-dried lightweight aggregate as previous investigators have traced water movement by means of X-ray absorption.

This limited research study showed that the absorption curves of very low water-to-cementitious material ratio mixtures did not present linearity with the square root of time as previous research in NSC suggested. Further research is needed to verify such deviated behavior. In particular, it is recommended to test intermediate water-to-cement ratio mixtures with and without silica fume. This would allow for understanding of the influence of those variables separately, and it would also define the threshold when absorption curves deviates from linearity observed in NSC.

It is suggested to run absorption tests for longer periods to detect any possible change in absorption rate not observed in the 16-day monitoring period use in this study.

In order to become a fully quantitative technique, the variability of deformation maps needs to be assessed. This can be done by using more ROI's that cover proportionally more area of the specimen. With many ROI's, an analysis of variance along with hypothesis tests can be performed to asses the accuracy of the maps.

Due to the limited number of ROI's explored on each specimen, it was not possible to apply statistical tools to assess the possible limitations of the technique. For example, from the experimental, data magnification did not seem to affect the results, but further research is needed to assure that.

The next step of this research needs to map deformation on standard size creep specimens and full-scale structural elements. This will allow relating insitu measurements with real structural behavior and will eliminate scale effects. Images should be taken using a very high resolution digital camera, so the size of each pixel is small enough to resolve deformations accurately.

Deformation maps can be also used to study the interaction between cement paste and other constituents such as steel, polymeric, or natural fibers.

ITZ has been proposed to be the weakest link in many concrete properties. Many believe that the origin of microcracking of ITZ is due to differential thermal expansion between aggregate and cement paste during the cement hydration. Deformation maps can be used to detect microcracking in the ITZ due to autogenous and drying shrinkage as well as thermal contraction.

The new data obtained from the deformation maps can be used to improve multi-phase models for elastic and time dependent deformations in concrete. Finite element models can also use this data to validate their results.

Curing through internally stored water has proven to improve many properties of concrete; in particular, it is believed that internal curing improved the ITZ between lightweight aggregate and matrix making the concrete more resistant to cracking. The same setup presented herein can be used with higher stress level to induce cracking. Specimens using aggregate with similar stiffness and either with or without internally stored water can provide information about the role of internally stored water on ITZ cracking.

8.3 Recommendations for Design

The use of maturity at the time of loading is preferred over age when using empirical models to predict creep and shrinkage of HPLC girders.

The ACI-209 and PCI methods were adequate for estimating prestress losses of HPLC girders; in most cases those methods gave conservative losses estimates with the

exception of the PCI method that underestimated loses of the LWW 55/8 girders by 1.8%.

The AASHTO-LRFD refined method for estimating prestress losses was conservative for expanded slate HPLC girders. The AASHTO-LRFD lump sum method gave a good estimate of total losses of the LWW 69/10 HPLC and slightly underestimated total losses of LWW 55/8 HPLC girders by 1.3%. Overall, the AASHTO-LRFD refined method may be used conservatively for predicting prestress losses in girders made of high performance lightweight concrete.

APPENDIX A

CONSTITUENT PROPERTIES

A.1 Cement

Tables A.1 and A.2 present the oxide analyses and fineness of the Type III and Type I portland cements from Lafarge used in the medium-scale and small-scale study.

Table A.1: Chemical Composition and fineness of LaFarge Type III Cement

Oxide Analysis	% by weight		**Fineness**	
SiO2	20.5		Blaine Fineness	592 m2/kg
Al2O3	4.7		45 μm sieve, retained	0.1%
Fe2O3	3.0			
CaO	63.6		**Bogue Potential Composition**	%
MgO	2.8		C3S	57.6
SO3	3.4		C2S	15.4
Loss on Ignition	1.4		C3A	7.4
Na2O	0.03		C4AF	9.1
K2O	0.33			
Insoluble Residue	0.09			
Equivalent Alkalis	0.25			

Table A.2: Chemical Composition and fineness of LaFarge Type I Cement

Oxide Analysis	% by weight		**Fineness**	
SiO2	20.6		Blaine Fineness	380 m2/kg
Al2O3	5.7		45 μm sieve, retained	6.2%
Fe2O3	3.0			
CaO	65.0		**Bogue Potential Composition**	%
MgO	2.2		C3S	60.1
SO3	2.8		C2S	14.0
Loss on Ignition	1.0		C3A	9.4
Na2O	0.09		C4AF	9.3
K2O	0.35			
Insoluble Residue	0.24			
Equivalent Alkalis	0.3			

A.2 Supplementary Cementing Materials

Force 10,000 condensed silica fume from grace and Class F fly ash from the Georgia Power Plant in Bowen (provided by Boral Technologies) were use as Supplementary cementing materials. Silica fume was delivered in 25 lb bags and had a relative density of 2.2. The fly ash was obtained in barrels and had a relative density of 2.28.

A.3 Aggregates

Table A.3 present the results of the sieve analyses, the density and absorption of the fine aggregate and the three coarse aggregates used in this investigation. Figure A.1 presents the 19-mm (0.75-in) MSA expanded slate lightweight aggregate particles while Figure A.2 shows the steel aggregate cubes prior to mixing.

Figure A.1: 19-mm (0.75-in) MSA expanded slate lightweight aggregate

Figure A.2: 12-mm (0. 5-in) MSA steel aggregate

Table A.3: Physical Properties of aggregates

		Fine Aggregate	Lightweight aggregate	Normal weight aggregate	Heavy weight aggregate
Description		Siliceous Natural Sand	Rotary Kiln Expanded Slate	Granite	A 36 steel cubes
Maximum size aggregate		2.36 mm (#8 sieve)	12.7 mm (0.5 in)	12.7 mm (0.5 in)	12.7 mm (0.5 in)
Density kg/m^3(lb/ft^3)		2650 (165.2)	1150 (96.8)	2680 (167.4)	7850 (490.1)
24-hour absorption %		0.1	6 to 8	0.1	0.0
Fineness modulus (FM)		3.15	6.93	7.6	8.0
Sieve Analysis					
mm	ASTM	%passing	%passing	%passing	%passing
13.2	1/2"	100.0	90.0	36.8	0.0
9.5	3/8"	100.0	53.0	17.1	0.0
4.75	#4	99.7	12.0	3.2	0.0
2.36	#8	98.1	5.0	0.0	0.0
1.18	#16	89.5	0.0	0.0	0.0
0.600	#30	58.6	0.0	0.0	0.0
0.300	#40	37.0	0.0	0.0	0.0
0.150	#50	16.8	0.0	0.0	0.0
0.075	#100	2.1	0.0	0.0	0.0
Pan	Pan	0.0	0.0	0.0	0.0

In addition mechanical testing was performed in the expanded slate and steel aggregate as described in Section 3.3.4.

Figures A.2 and A.3 show some of the expanded slate prisms used for the mechanical properties tests, and Table A.4 presents the compressive strength and elastic modulus results.

Figure A.3: Expanded slate prisms

Figure A.4: Compressive strength testing of an expanded slate prism

Table A.4: Mechanical Properties of expanded slate aggregate

Specimen ID#	Strength (MPa)	Elastic Modulus (GPa)	Strength (psi)	Elastic Modulus (ksi)
2	12.9	0.7	1868	108.5
3	28.3	1.0	4109	146.9
6	22.8	1.5	3311	212.1
7	17.7	3.6	2571	518.0
8	25.4	2.2	3688	320.1
9	26.3	1.6	3810	239.1
10	27.7		4017	
11	14.1	1.8	2042	255.2
12	14.6	3.1	2117	443.1
13	10.0	0.3	1457	49.9
14	21.6	4.7	3128	685.0
16	37.0	7.2	5367	1041.2
18	9.8	0.8	1426	111.4
20	21.4	5.7	3100	833.4
21	28.2	1.8	4089	264.9
22	21.1	1.6	3054	237.6
23	15.1	2.4	2186	343.6
24	45.0	9.0	6520	1305.5
26	25.6	2.2	3706	319.8
27	11.6	1.2	1680	180.6
28	24.5	2.8	3552	410.5
29	28.6	2.1	4150	302.3
Average	22.2	2.7	3225	397
Max	45.0	9.0	6520	1306
Min	9.8	0.3	1426	50
Standard deviation	8.79	2.22	1275	322
CV	39.5	81.1	39.5	81.1

Compressive and elastic modulus testing were carried out at a loading rate of 14 MPa (2000 psi) per minute. Load and displacement were recording every 0.1 seconds during the elastic modulus testing, and based on the specimen dimensions, stress and strain were calculated. Elastic modulus was calculated as the slope of the stress – strain curve before the first crack assumed to be given by the first drop in stress. A linear curve fitting was performed by minimizing the sum of error square.

Previous to the mechanical testing of the expanded slate specimens, ultrasonic pulse velocity (UPV) tests were performed on each of them for estimating the elastic modulus. Travel times of primary (compression) and secondary (shear) waves was recorded. The results were not used since they presented high variability and in some cases, when primary and secondary waves had similar velocities, gave negative poisons ratios. It is believed that the presence of cracks or large voids could have affected the results. Table A.5 presents the UPV results.

Table A.5: Elastic modulus of steel bars in tension

Sample #	Distance (m)	Time for Vp (s)	Time for Vs (s)	Vp (m/s)	Vt(m/s)	Density DRY (kg/m3)	G (MPa)	u	E (MPa)
1	0.016891	0.00000448	0.00000544	3770.3	3105.0	833.5	8036	-0.55	7172
2	0.021209	0.0000052	0.00001208	4078.7	1755.7	1238.4	3817	0.39	10584
5	0.023368	0.00000624	0.00000616	3744.9	3793.5	1711.4	24628	20.13	1040594
6	0.01778	0.00000416	0.00000488	4274.0	3643.4	1266.8	16816	-0.83	5738
7	0.0315722	0.00001748	0.00001744	1806.2	1810.3	1024.9	3359	109.88	744833
8	0.017526	0.00000472	0.0000088	3713.1	1991.6	1870.5	7419	0.30	19261
9	0.016129	0.00000404	0.00000488	3992.3	3305.1	1428.3	15603	-0.59	12821
10	0.017145	0.00000404	0.00000416	4243.8	4121.4	1259.5	21393	-7.79	-290671
13	0.017272	0.00000456	0.00000436	3787.7	3961.5	1024.5	16077	6.33	235624
14	0.017399		0.00000528		3295.3	1089.9	11835		
15	0.017399	0.000004144	0.00000528	4198.6	3295.3	973.8	10574	-0.30	14761
16	0.011938	0.000004768	0.00000544	2503.8	2194.5	1443.3	6951	-1.16	-2183
17	0.01778	0.000004384	0.00000832	4055.7	2137.0	1138.4	5199	0.31	13598
18	0.01778	0.00000908	0.00000852	1958.1	2086.9	1076.6	4689	4.68	53286
20	0.01651	0.00000384	0.00000436	4299.5	3786.7	1108.8	15900	-1.23	-7285
21	0.016891		0.00000692		2440.9	1648.1	9819		
22	0.016002	0.00000408	0.0000044	3922.1	3636.8	1158.3	15320	-2.57	-48020
23	0.01524		0.00000776		1963.9	1110.3	4282		
24	0.012446	0.00000296	0.00000344	4204.7	3618.0	1314.0	17200	-0.93	2544
25	0.023368	0.00001184	0.00001574	1973.6	1484.6	1170.3	2580	-0.15	4377
26	0.014224	0.00000364	0.00000416	3907.7	3419.2	1183.5	13836	-1.13	-3690
27	0.014224	0.00000352	0.00000372	4040.9	3823.7	1050.1	15353	-3.78	-85314
28	0.017653	0.000004	0.00000468	4413.3	3772.0	1156.0	16448	-0.86	4757
29	0.01016	0.0000029	0.00000492	3503.4	2065.0	1227.1	5233	0.23	12912

Table A.6 present the elastic modulus results of steel bars tested in tension.

Table A.6: Elastic modulus of steel bars in tension

Specimen ID#	12.7-mm (0.5-in) bars		0.25-mm (0.25-in) bars	
	(GPa)	(ksi)	(GPa)	(ksi)
1	201.4	29,209	221.7	32,151
2	200.9	29,132	221.9	32,172
3	216.3	31,367	216.4	31,380
4	220.8	32,022	202.4	29,354
5	224.5	32,553	210.4	30,506
Average	212.8	30,857	214.6	31,113
Max	224.5	32,553	221.9	32,172
Min	200.9	29,132	202.4	29,354
Standard deviation	11.0	1,596	8.3	1,197
CV	0.0	5.2	0.0	3.8

APPENDIX B

PHYSICAL AND MECHANICAL PROPERTIES OF CONCRETE MIXTURES OF LARGE-SCALE STUDY

B.1 Density Study

Set	Mix ID	Curing Type	Wet unit weight	air-dry unit	oven-dry unit	2-year air-dry unit
1	LWW 55/8	Accel	**122.2**	**121.8**	**121.0**	**119.9**
	LWW 55/8	Standard	**125.3**	**125.0**	**123.9**	**123.0**
	LWW 69/10	Accel	**125.7**	**125.3**	**124.4**	**123.7**
	LWW 69/10	Standard	**123.6**	**122.9**	**122.4**	**121.8**
2	LWW 55/8	Accel	**123.6**	**123.2**	**122.5**	**121.5**
	LWW 55/8	Standard	**123.9**	**123.2**	**122.5**	**121.6**
	LWW 69/10	Accel	**125.7**	**125.3**	**124.6**	**123.9**
	LWW 69/10	Standard	**124.6**	**124.3**	**123.6**	**123.0**

B.2 Mechanical Properties

B.2.1. Compressive Strength

HPLC: LWW 55/8

	4" x 8" Cylinders Accelerated Curing				4" x 8" Cylinders ASTM Curing			
Age (Days)	Ultimate Strength (PSI)	Average Strength (PSI)	Ultimate Strength (MPa)	Average Strength (MPa)	Ultimate Strength (PSI)	Average Strength (PSI)	Ultimate Strength (MPa)	Average Strength (MPa)
1	7314	6504	50	45	5620	5568	39	38
1	6753	6504	47	45	5611	5568	39	38
1	7212	6504	50	45	5973	5568	41	38
1	5917	6504	41	45	4516	5568	31	38
1	6004	6504	41	45	7323	5568	51	38
1	5824	6504	40	45	4362	5568	30	38
7	8130	7053	56	49	7324	6606	51	46
7	7717	7053	53	49	7110	6606	49	46
7	7586	7053	52	49	7519	6606	52	46
7	6535	7053	45	49	5824	6606	40	46
7	6148	7053	42	49	5773	6606	40	46
7	6205	7053	43	49	6086	6606	42	46
28	8641	8095	60	56	8827	8215	61	57
28	8743	8095	60	56	8712	8215	60	57
28	8751	8095	60	56	8967	8215	62	57
28	7593	8095	52	56	7575	8215	52	57
28	7429	8095	51	56	7611	8215	52	57
28	7414	8095	51	56	7599	8215	52	57
56	9036	8417	62	58	9329	8708	64	60
56	9039	8417	62	58	9071	8708	63	60
56	9179	8417	63	58	9657	8708	67	60
56	7820	8417	54	58	8132	8708	56	60
56	7815	8417	54	58	8234	8708	57	60
56	7615	8417	53	58	7823	8708	54	60
365	9418	9105	65	63	10229	9674	71	67
365	8792	8792	61	61	9118	9118	63	63

HPLC: LWW 69/10

	4" x 8" Cylinders Accelerated Curing				4" x 8" Cylinders ASTM Curing			
Age (Days)	Ultimate Strength (PSI)	Average Strength (PSI)	Ultimate Strength (MPa)	Average Strength (MPa)	Ultimate Strength (PSI)	Average Strength (PSI)	Ultimate Strength (MPa)	Average Strength (MPa)
1	9872	9060	68	62	9375	7924	65	55
1	10086	9060	70	62	9509	7924	66	55
1	9464	9060	65	62	8999	7924	62	55
1	8541	9060	59	62	6687	7924	46	55
1	7983	9060	55	62	6826	7924	47	55
1	8416	9060	58	62	6148	7924	42	55
7	9764	9305	67	64	9375	8767	65	60
7	9426	9305	65	64	9418	8767	65	60
7	9181	9305	63	64	9592	8767	66	60
7	9472	9305	65	64	8333	8767	57	60
7	8812	9305	61	64	8206	8767	57	60
7	9174	9305	63	64	7676	8767	53	60
28	10299	9755	71	67	10025	9962	69	69
28	10333	9755	71	67	10512	9962	72	69
28	9866	9755	68	67	9812	9962	68	69
28	9193	9755	63	67	9965	9962	69	69
28	9295	9755	64	67	9593	9962	66	69
28	9545	9755	66	67	9862	9962	68	69
56	10506	10334	72	71	10293	10311	71	71
56	10701	10334	74	71	10047	10311	69	71
56	10047	10334	69	71	10793	10311	74	71
56	10372	10334	72	71	10575	10311	73	71
56	10115	10334	70	71	10326	10311	71	71
56	10261	10334	71	71	9833	10311	68	71
365	10965	10710	76	74	11012	10940	76	75
365	10454	10454	72	72	10868	10868	75	75

Normal weight HPC: HPC-6

Batch ID	days	Accelerated Curing	Average Accelerated Curing	ASTM Curing	Average ASTM Curing
1S1	1	10373	8527	7700	6796
2S1	1	6753	8527	5804	6796
2S2	1	8455	8527	6883	6796
1S1	7	11055	10568	10641	10268
2S1	7	9691	10568	9356	10268
2S2	7	10956	10568	10806	10268
1S1	28	12276	12044	12465	12506
2S1	28	11164	12044	11706	12506
2S2	28	12692	12044	13347	12506
1S1	56	12435	12447	13379	13205
2S1	56	11451	12447	12617	13205
2S2	56	13454	12447	13618	13205

B.2.2. Elastic Modulus

HPLC: LWW 55/8 and LWW 69/10

Age	LWW 55/8				LWW 69/10			
	Accelerated Curing		Standard Curing		Accelerated Curing		Standard Curing	
		Average		Average		Average		Average
1	3670	3567			3875	3728		
1	3520	3567			3810	3728		
1	3510	3567			3500	3728		
56	3810	3863	3880	3832	4060	4015	4130	4057
56	3900	3863	3770	3832	4025	4015	3920	4057
56	3880	3863	4100	3832	3960	4015	4130	4057
56			3590	3832			4130	4057
56			3820	3832			3980	4057
stdev	47		185		51		101	
max	3900		4100		4060		4130	
min	3810		3590		3960		3920	

Normal weight HPC: HPC-6

Specimen Number		Age After Cast	Cure Type 0	Concrete Unit Weigh (PCF)	Concrete Unit Weigh (kg/m3)	Ultimate Strength (6 psi	Experimen E-Modulus ksi	Experimen E-Modulus GPa	Poisson's Ratio
1S1-1	1S & 2S	0	Insulated	146.9	2353	11059	3574	24.7	0.17
1S1-2		1	Insulated	146.9	2353	10999	3360	23.2	0.17
1S1-3		1	Insulated	146.9	2353	11350	3375	23.3	0.17
2S1-1		1	Insulated	146.9	2353	8425	3407	23.5	0.17
2S1-2		1	Insulated	146.9	2353	8304	3387	23.4	0.17
2S1-3		1	Insulated	146.9	2353	8393	3407	23.5	0.17
2S2-1		1	Insulated	146.9	2353	9691	3404	23.5	0.17
2S2-2		1	Insulated	146.9	2353	9871	3375	23.3	0.17
2S2-3		1	Insulated	146.9	2353	9362	3405	23.5	0.17
1S1-1	1S & 2S	56	insultated	146.9	2353	12745	5108	35.2	0.15
1S1-2		56	insultated	146.9	2353	12315	4983	34.4	0.15
1S1-3		56	insultated	146.9	2353	12251	5001	34.5	0.15
2S1-1		56	insultated	146.9	2353	11258	4540	31.3	0.15
2S1-2		56	insultated	146.9	2353	11855	4988	34.4	0.15
2S1-3		56	insultated	146.9	2353	11869	4862	33.5	0.16
2S2-1		56	insultated	146.9	2353	12822	5156	35.6	0.15
2S2-2		56	insultated	146.9	2353	12359	5022	34.6	0.16
2S2-3		56	insultated	146.9	2353	12359	5053	34.9	0.15
2S1		56	insultated	146.9	2353	12837	4759	32.8	0.14
1S1-4	1S & 2S	56	ASTM	146.9	2353	13631	5115	35.3	0.14
1S2-5		56	ASTM	146.9	2353	13246	4811	33.2	0.13
1S3-6		56	ASTM	146.9	2353	13602	5052	34.8	0.14
1S4-7		56	ASTM	146.9	2353	12849	5041	34.8	0.14
1S5-8		56	ASTM	146.9	2353	12625	4923	34.0	0.14
1S10-9		56	ASTM	146.9	2353	14140	4955	34.2	0.13
2S2		56	ASTM	146.9	2353	13603	5066	34.9	0.13
2S5		56	ASTM	146.9	2353	11799	4824	33.3	0.15
2S9		56	ASTM	146.9	2353	11452	5013	34.6	0.17
2S17		56	ASTM	146.9	2353	13656	4926	34.0	0.14
2S24		56	ASTM	146.9	2353	13730	4982	34.4	0.14

B.2.3. Rupture Modulus

HPLC: LWW 55/8 and LWW 69/10

Mixture ID		Number of	Curing	Average Strength		Modulus of rupture	
	Age (days)	specimens	Type	psi	MPa	psi	MPa
LWW 55/8	56	3	Standard	9346	64.5	992	6.8
LWW 69/10	56	3	Standard	10664	73.5	981	6.8
LWW 55/8	56	3	Accelerate	9084	62.7	1042	7.2
LWW 69/10	56	3	Accelerate	10333	71.3	1161	8.0

Normal weight HPC: HPC-6

Mixture ID		Number of	Curing	Average Strength		Modulus of rupture	
	Age (days)	specimens	Type	psi	MPa	psi	MPa
HPC-6 1st Cast	56	5	Standard	13379	92.3	1169	8.1
HPC-6 2nd Cast	56	3	Standard	13157	90.7	1272	8.8
HPC-6 1st Cast	56	3	Accelerate	12435	85.8	1184	8.2
HPC-6 2nd Cast	56	13	Accelerate	12453	85.9	1266	8.7

B.3 Rapid Chloride Permeability

HPLC: LWW 55/8 and LWW 69/10

Specimen Identifier	Curing Type	Time of test (days)	Coulombs passed				Permeability
LWA 55/8	Accelerated	56	903	888	767	764	Low
LWA 69/10	Accelerated	56	193	298	230	186	Very Low

Normal weight HPC: HPC-6

Chloride permeability results summary

Specimen	Time of tes	Curing	T	Coulombs	Permeabili
2S	56	ASTM		225	very low
2S	56	ASTM		222	very low
2S	56	ASTM		174	very low
2S	56	ASTM		170	very low
1	28 +	core		200	very low
2	28 +	core		200	very low

This page intentionally left blank

APPENDIX C

PRESTRESS LOSS CALCULATIONS

Prestress loss methods can be classified into two groups: (1) final prestress loss estimate and (2) losses estimated at any time. There are three methods for estimating final prestress losses: Precast Prestressed Concrete Institute Method (PCI, 1998), refined estimate and approximate lump sum estimate, both methods developed by the American Association of State Highway and Transportation Officials (AASHTO-LRFD, 2004). For losses at any time, American Concrete Institute Committee 209 (ACI-209, 1992) proposed a prestress loss estimate method based on creep and shrinkage estimates (Equations C.1 and C.3).

Even though anchorage seating losses and friction losses can be an important portion of the total prestress losses, they are not considered here because such losses are related with the manufacturing process rather than material properties.

C.1. PCI Method

The PCI method gives an estimate of the final prestress losses of a prestressed concrete member based on four equations for each type of losses. Total losses are given by Equation C.1

$$TL = ES + CR + SH + RE \tag{C.1}$$

where

TL: total prestress losses (ksi)

ES: elastic shortening loss (ksi)

CR: creep of concrete loss (ksi)

SH: shrinkage of concrete loss (ksi)

RE: steel relaxation loss (ksi)

Elastic Shortening. Caused by concrete shortening around tendons as the prestressing force is transferred, elastic shortening can be estimated by Equation C.1.

$$ES = \frac{K_{es} \cdot E_{ps} \cdot f_{cir}}{E_{ci}} \qquad \text{(C.2)}$$

where

ES: elastic shortening loss (ksi)

K_{es}: elastic shortening constant, 1.0 for pretensioned members

E_{ps}: elastic modulus of prestressing steel (ksi)

E_{ci}: elastic modulus of concrete at transfer (ksi)

$f_{cir} = K_{cir} \cdot \left(\frac{P_i}{A_g} + \frac{P_i \cdot e^2}{I_g} \right) - \frac{M_g \cdot e}{I_g}$: net compressive stress in the section at the center of gravity of the prestressing force (cgs) immediately after transfer (ksi)

where

K_{cir}: a constant, 0.9 for pretensioned members

P_i: initial prestressing force after anchorage seating loss (kip)

e: eccentricity of the cgs with respect to the center of gravity of the section at the cross section considered. Eccentricity is negative if below concrete section neutral axis (in)

A_g: gross area of the section (in^2)

I_g: gross moment of inertia (in^4)

M_g: the dead load gravity moment applied to the section at time of prestressing (kip-in)

Creep of concrete. The final loss of prestress due to creep is given by Equation C.3.

$$CR = K_{cr} \cdot \left(\frac{E_{ps}}{E_c} \right) \cdot \left(f_{cir} - f_{cds} \right) \qquad \text{(C.3)}$$

where

CR: creep loss (ksi)

$K_{cr} = \begin{cases} 2.0 \text{ for NWC} \\ 1.6 \text{ for SLC} \end{cases}$: creep constant

E_c: elastic modulus at design age (ksi)

E_{ps}: elastic modulus of prestressing steel (ksi)

$f_{cds} = \frac{M_{sd} e}{I_g}$: stress in concrete at the cgs due to all superimposed dead loads (ksi)

M_{sd}: Moment due to all superimposed permanent dead loads and sustained loads after prestressing (kip-inches)

I_g: gross moment of inertia (in^4)

Shrinkage of concrete. The final prestress loss due to drying shrinkage is given by member geometry and relative humidity at which member is exposed. Equation C.4 shows PCI expression to estimate shrinkage loss.

$$SH = \left(8.2 \times 10^{-6} \right) \cdot K_{sh} \cdot E_{ps} \cdot \left(1 - 0.06 \frac{V}{S} \right) \cdot \left(100 - RH \right) \qquad \text{(C.4)}$$

where,

SH: shrinkage loss (ksi)

K_{sh}: 1.0 for pretensioned members

V: specimen volume (in^3)

S: specimen surface area (in^2)

RH: relative humidity (%)

Steel relaxation. defined as the loss of stress over a certain period of time, steel relaxation depends on the type of prestressing steel (stress-relieved or lo relaxation) and the other prestress losses. Equation C.5 gives the loss of prestress due to steel relaxation.

$$RE = \left[K_{re} - J \cdot \left(SH + CR + ES\right) \cdot \left(100 - RH\right)\right] \cdot C \qquad \text{(C.5)}$$

where

RE: steel relaxation loss (ksi)

K_{re}: maximum relaxation stress, 5,000 psi for grade 270, low relaxation strands

J: parameter, 0.04 for grade 270, low relaxation strands,

ES: elastic shortening loss (ksi)

CR: creep of concrete loss (ksi)

SH: shrinkage of concrete loss (ksi)

C: parameter depending on the initial prestress to ultimate strand strength and strand type, 0.70 this case.

C.2. AASHTO-LRFD Refined Estimate of Time-Dependent Losses

According to AASHTO-LRFD (2004), the total loss of prestress, not including anchorage seating loss, is the sum of the elastic shortening, creep, shrinkage, and steel

relaxation losses, given by Equation C.6. Equation C.6 applies to prestressed members with spans no greater than 250 ft., NWC and compressive strength above 3,500 psi.

$$\Delta f_{pT} = \Delta f_{pES} + \Delta f_{pCR} + \Delta f_{pSH} + \Delta f_{pR1} + \Delta f_{pR2} \quad \text{(C.6)}$$

where

Δf_{pT}: total prestress losses (ksi)

Δf_{pES}: elastic shortening loss (ksi)

Δf_{pCR}: creep of concrete loss (ksi)

Δf_{pSR}: shrinkage of concrete loss (ksi)

Δf_{pR1}: initial steel relaxation loss (ksi)

Δf_{pR2}: after transfer steel relaxation loss (ksi)

Elastic Shortening. According to AASHTO-LRFD, the Elastic shortening loss is given by Equation C.7.

$$\Delta f_{pES} = \frac{E_p}{E_{ci}} \cdot f_{cgp} \quad \text{(C.7)}$$

where,

Δf_{pES}: elastic shortening loss (ksi)

$f_{cgp} = \left(\frac{P_i}{A_g} + \frac{P_i \cdot e^2}{I_g} \right) - \frac{M_g \cdot e}{I_g}$: sum of the stresses in the concrete at the cgs due to prestress force at transfer and the maximum dead load moment (ksi)

P_i: initial prestressing force after anchorage seating loss (kip)

e: eccentricity of the cgs. with respect to the center of gravity of the section at the cross section considered. Eccentricity is negative if below concrete section neutral axis (in)

A_g: gross area of the section (in^2)

I_g: gross moment of inertia (in^4)

M_g: the dead load gravity moment applied to the section at time of prestressing (kip-in)

E_p: elastic modulus of prestressing steel (ksi)

E_{ci}: elastic modulus of concrete at transfer (ksi)

Creep of concrete. The final loss of prestress due to creep is given by Equation C.8.

$$\Delta f_{pCR} = 12 \cdot f_{cgp} - 7 \cdot \Delta f_{cdp} \qquad \text{(C.8)}$$

where,

Δf_{pCR}: creep of concrete loss (ksi)

$f_{cgp} = \left(\frac{P_i}{A_g} + \frac{P_i \cdot e^2}{I_g} \right) - \frac{M_g \cdot e}{I_g}$: sum of the stresses in the concrete at the cgs due to prestress force at transfer and the maximum dead load moment (ksi)

P_i: initial prestressing force after anchorage seating loss (kip)

e: eccentricity of the cgs. with respect to the center of gravity of the section at the cross section considered. Eccentricity is negative if below concrete section neutral axis (in)

A_g: gross area of the section (in^2)

I_g: gross moment of inertia (in^4)

M_g: the dead load gravity moment applied to the section at time of prestressing (kip-in)

$\Delta f_{cds} = \frac{M_{sd} e}{I_g}$: change in concrete stress at the center of gravity of prestressing strands due to permanent loads, with the exception of the loads at the time the prestressing force is applied. (ksi)

Shrinkage of concrete. The prestress loss due to drying shrinkage is given in Equation C.9.

$$\Delta f_{pSR} = 17.0 - 0.15 \cdot H \qquad \text{(C.9)}$$

where,

Δf_{pSR}: shrinkage of concrete loss (ksi)

H: relative humidity (%)

Steel relaxation. Steel relaxation loss is considered to be comprised of two components: relaxation at transfer and relaxation over the rest of the life of the girder. For low relaxation strands, the two components are given by Equations C.10 and C.11.

$$\Delta f_{pR1} = \frac{\log(24 \cdot t)}{40} \cdot \left(\frac{f_{pj}}{f_{py}} - 0.55 \right) \cdot f_{pj} \qquad \text{(C.10)}$$

where,

Δf_{pR1}: initial steel relaxation loss (ksi)

t: time since prestressing (days)

f_{pj}: initial prestress (ksi)

f_{py}: yield strength of the prestressing steel (ksi)

$$\Delta f_{pR2} = 6.0 - 0.12 \cdot \Delta f_{pES} - 0.06 \cdot \left(\Delta f_{pSR} + \Delta f_{pCR} \right) \qquad \text{(C.11)}$$

where

Δf_{pR2}: after transfer steel relaxation loss (ksi)

Δf_{pES}: elastic shortening loss (ksi)

Δf_{pCR}: creep of concrete loss (ksi)

Δf_{pSR}: shrinkage of concrete loss (ksi)

C.3. AASHTO-LRFD Approximate Lump Sum Estimate of Time-Dependent Losses

Lump sum method is based on data taken from a large number of prestressed structures, and it gives an estimate of final prestress losses due to concrete creep and shrinkage and steel relaxation. According to AASHTO-LRFD (2004), the lump sum method is applicable to members that are made from NSC. The lump sum method proposes eleven equations depending on the type of beam section and prestressing element (strands, bars). For I-shaped girders prestressed with 235, 250, or 270 ksi wires or strands, the time-dependent losses can be obtained from Equation C.12.

$$\Delta f_{pTD} = 33.0 \cdot \left[1.0 - 0.15 \cdot \frac{f_c' - 6.0}{6.0} \right] + 6.0 \cdot PPR \qquad \text{(C.12)}$$

where

Δf_{pTD}: time-dependent losses (ksi)

f_c': compressive strength of concrete cylinders at 28 days (ksi)

$PPR = \dfrac{A_{ps} \cdot f_{py}}{A_{ps} \cdot f_{py} + A_s \cdot f_y}$: partial prestressing ratio

A_{ps}: area of prestressing steel (in^2)

f_{py}: yield stress of prestressing steel (ksi)

A_s: area of non-prestressing steel (in^2)

f_y: yield stress of non-prestressing steel (ksi)

C.4. ACI-209 Method

Based on creep and shrinkage equations presented in section C.1.1, ACI through its committee 209, proposed a general expression for estimating loss of prestress in prestressed concrete beams as shown in Equation C.13.

$$\lambda_t = \frac{\left[ES + CR + SH + \left(f_{sr}\right)_t\right]}{f_{si}} \times 100 \qquad \text{(C.13)}$$

where

λ_t: prestress losses in percent of the initial tensioning stress

ES: elastic shortening loss (ksi)

CR: creep of concrete loss (ksi)

SH: shrinkage of concrete loss (ksi)

$(f_{sr})_t$: steel relaxation loss (ksi)

f_{si}: initial tensioning stress (ksi)

Elastic Shortening. Elastic shortening can be estimate by Equation C.14

$$ES = n \cdot f_c \qquad \text{(C.14)}$$

where

ES: elastic shortening loss (ksi)

n: modular ratio at the time of prestressing

$f_c = \frac{P_i}{A_g} + \frac{P_i \cdot e^2}{I_g} + \frac{M_g \cdot e}{I_g}$: net compressive stress in the section at the center of gravity of the prestressing force (cgs) immediately after transfer (ksi)

P_i: initial prestressing force after anchorage seating loss (kip)

e: eccentricity of the cgs with respect to the center of gravity of the section at the cross section considered. Eccentricity is negative if below concrete section neutral axis (in)

A_g: gross area of the section (in^2)

I_g: gross moment of inertia (in^4)

M_g: the dead load gravity moment applied to the section at time of prestressing (kip-in)

Creep of concrete. Equation C.15 shows the expression used for creep losses estimate.

$$CR = ES \cdot \phi_t \cdot \left(1 - \frac{F_t}{2 \cdot F_0}\right) \qquad \text{(C.15)}$$

where

CR: creep of concrete loss (ksi)

ES: elastic shortening loss (ksi)

ϕ_t: creep coefficient as defined by ACI-209 (Equation C.1)

$\frac{F_t}{F_0}$: Loss of prestress ratio given in Table C.1

Table C.1. Loss of prestress ratios for different concretes and time under loading conditions

	Type of concrete		
	Normal weight concrete	Sand-lightweight concrete	All-lightweight concrete
For three weeks to one month between prestressing and sustained load application	0.10	0.12	0.14
For two to three months between prestressing and sustained load application	0.14	0.16	0.18
Ultimate	0.18	0.21	0.23

Shrinkage of concrete. Prestress losses due to drying shrinkage are estimated by Equation C.16. The denominator K_{SE} represents the stiffening effect of the steel and the effect of concrete creep. Without K_{SE} the losses due to drying shrinkage are somewhat overestimated.

$$SH = (\varepsilon_{sh})_t \cdot \frac{E_{ps}}{K_{SE}} \qquad \text{(C.16)}$$

where

SH: shrinkage of concrete loss (ksi)

$(\varepsilon_{sh})_t$: shrinkage strain as defined by ACI-209 (Equation C.3)

E_{ps}: Elastic modulus of prestressing steel

$K_{SE} = 1 + n \cdot \rho \cdot \xi_s$ =1.25 (design simplification)

n: modular ratio at the time of prestressing

ρ: non-prestressing reinforcement ratio

ξ_s: cross section shape coefficient

Steel relaxation. Steel relaxation losses depend on the steel of the strands (stress-relieved or low relaxation), and time. For low relaxation strands, the relaxation losses are given by Equation C.17.

$$RE = 0.005 \cdot f_{pj} \cdot \log_{10}[t] \qquad \text{(C.17)}$$

where

RE: steel relaxation loss (ksi)

f_{pj}: initial prestress (ksi)

t: time under load in hours (for $t>10^5$, $RE = 0.025 \cdot f_{pj}$)

C.5. Prestress Loss Computation

C.5.1. Prestress Losses in the Girders

LWW 55/8 HPLC girders

Concrete Strains

Eps= 28,500 ksi From strand spec sheets

	Girder 1			Girder 2		
	Concrete	Strand	Strand	Concrete	Strand	Strand
	Strain (με)	Losses (ksi)	Losses (MPa)	Strain (με)	Losses (ks	Losses (MPa)
ES	-583	-16.63	-114.66	-609	-17.36	-119.69
Long-term	-307	-8.76	-60.39	-307	-8.76	-60.39

Losses

Elastic	DfpES	-16.991	ksi	loss due to ES from experimantal data
Creep and Shrinkage	DfpCR+DfpSH	-8.76	ksi	loss due to creep and shrinkage from experimental data
Relaxation	DfpR2	-3.436	ksi	relaxation after transfer (LOLAX)

LWW 69/10 HPLC girders

Concrete Strains

Eps= 28,500 ksi From strand spec sheets

	Girder 1			Girder 2		
	Concrete	Strand	Strand	Concrete	Strand	Strand
	Strain (με)	Losses (ksi)	Losses (MPa)	Strain (με)	Losses (ks	Losses (MPa)
ES	-426	-12.15	-83.77	-417	-11.87	-81.89
Long-term	-104	-2.96	-20.41	-104	-2.96	-20.41

Losses

Elastic	DfpES	-12.010	ksi	loss due to ES from experimantal data
Creep and Shrinkage	DfpCR+DfpSH	-2.96	ksi	loss due to creep and shrinkage from experimental data
Relaxation	DfpR2	-4.381	ksi	relaxation after transfer

C.5.2. Prestress Losses with AASHTO-LRFD Refined Method

LWW 55/8 HPLC girder			LWW 69/10 HPLC girder			
Steel			**Steel**			
Fpu	59.13	kips	Fpu	59.13	kips	From strand spec sheets
Astrand	0.217	in^2	Astrand	0.217	in^2	area of 0.6-inch strand
fpu	272.5	ksi	fpu	272.5	ksi	Fpu / Astrand
fpy	245.2	ksi	fpy	245.2	ksi	80% fpu
avg F/strd	43.94	kips	avg F/strd	43.94	kips	from load cell data, average force / strand
fpi	202.50	ksi	fpi	202.50	ksi	(avg F/std)/Astrand, init avg stress / strand
# strands	10		# strands	10		Total # of prestressing strands
Eps=	28,500	ksi	Eps=	28,500	ksi	From strand spec sheets
Aps=	2.17	in^2	Aps=	2.17	in^2	# of strands * area per strand
Fsi=	439.43		Fsi=	439.43		fpi * Aps
Fse=	435.24	kips	Fse=	435.24	kips	fpi * Aps - DfpR1 * Aps
Concrete 8,000-psi HPLC			**Concrete 10,000-psi HPLC**			
fc'=	9.350	ksi	fc'=	10.240	ksi	Experimental results
fci=	7.090	ksi	fci=	8.310	ksi	Experimental results
Ec=	3,830	ksi	Ec=	4,050	ksi	Experimental results
Eci=	3,570	ksi	Eci=	3,910	ksi	Experimental results
Unit weight	117	lb/ft^3	Unit weight	119	lb/ft^3	Experimental results
Girder Properties			**Girder Properties**			
h=	36	in	h=	36	in	Given for a Type II girder
yt=	20.17	in	yt=	20.17	in	Given for a Type II girder
yb=	-15.83	in	yb=	-15.83	in	Given for a Type II girder
Ax=	396	in^2	Ax=	396	in^2	Given for a Type II girder
Ix=	50,979	in^4	Ix=	50,979	in^4	Given for a Type II girder
perimeter	109.5	in	perimeter	109.5	in	Given for a Type II girder
e cl	-6.730	in	e cl	-6.730	in	the eccentricity of the cgs at midspan
wsw	0.322	kip/ft	wsw	0.327	kip/ft	selfweight
Length	39.0	ft	Length	42.0	ft	Length of the girder
Msw	734.07	k-in	Msw	865.90	k-in	Moment, self weight of the girder
External Loads			**External Loads**			
wsw	0.225	kip/ft	wsw	0.225	kip/ft	selfweight
Msd	513.34	k-in	Msd	595.35	k-in	Msd = superimposed DL not girder sw
RH=	70	%	RH=	70	%	Atlanta average relative humidity
Losses Parameters						
Elastic Shortening Losses			Elastic Shortening Losses			Midspan
Eci	3570.0	ksi	Eci	3910.0	ksi	(from above)
fcgp	1.389	ksi	fcgp	1.371	ksi	stress in concrete at cgs just before stressing
ΔfpES	-11.088	ksi	ΔfpES	-9.997	ksi	loss due to elastic shortening
f se	191.412	ksi	f se	192.503	ksi	total stress remaining after ES
Fse	415	kips	Fse	418	kips	after ES losses
CR Creep Losses			CR Creep Losses			Midspan
Fse	415.4	kips	Fse	417.7	kips	(from above)
fcgp	1.389	ksi	fcgp	1.371	ksi	stress in concrete at cgs just after stressing
Δfcdp	0.068	ksi	Δfcdp	0.079	ksi	stress in concrete at cgs from superimposed load
ΔfpCR	-16.19	ksi	ΔfpCR	-15.91	ksi	loss due to creep
f se	175.22	ksi	f se	176.60	ksi	total stress remaining after ES and CR
Fse	380	kips	Fse	383	kips	after ES and CR
SH Shrinkage Losses (losses ind			SH Shrinkage Losses (losses independent of load)			
V/S	3.616	in	V/S	3.616	in	Vol / Surface = Area / perimeter
fcgp	1.38889		fcgp	1.37149		axial shortening of concrete due to shrinkage
H	70		H	70		
ΔfpSH	-6.50	ksi	ΔfpSH	-6.50	ksi	loss due to shrinkage
f se mid	168.72	ksi	f se mid	170.10	ksi	total stress remaining after ES, CR, and SH, mid
Fse	366	kips	Fse	369	kips	after ES and CR
RE Relaxation losses (lolax stran			RE Relaxation losses (lolax stran			Midspan
t	1	days	t	1	days	time since prestressing
ΔfpR1	-1.927	ksi	ΔfpR1	-1.927	ksi	loss due to strand relaxation
ΔfpR2	-3.308	ksi	ΔfpR2	-3.456	ksi	
ΔfpRtot	-3.308	ksi	ΔfpRtot	-3.456	ksi	
f se mid	165.41	ksi	f se mid	166.64	ksi	total stress remaining after ES, CR, and SH, mid
Fse	359	kips	Fse	362	kips	after ES and CR
total loss	-37.088	ksi	total loss	-35.860	ksi	total loss from ES, CR, SH, and RE
e total, cgs	-0.0013		e total, cgs	-0.00126		total strain from ES, CR, SH, and RE

C.5.3. Prestress Losses with AASHTO-LRFD Lump Sum Method

LWW 55/8 HPLC girder			LWW 69/10 HPLC girder			
Steel			**Steel**			
Fpu	59.13	kips	Fpu	59.13	kips	From strand spec sheets
Astrand	0.217	in^2	Astrand	0.217	in^2	area of 0.6-inch strand
fpu	272.5	ksi	fpu	272.5	ksi	Fpu / Astrand
fpy	245.2	ksi	fpy	245.2	ksi	80% fpu
avg F/strd	43.94	kips	avg F/strd	43.94	kips	from load cell data, average force / strand
fpi	202.50	ksi	fpi	202.50	ksi	(avg F/std)/Astrand, init avg stress / strand
# strands	10		# strands	10		Total # of prestressing strands
Eps=	28,500	ksi	Eps=	28,500	ksi	From strand spec sheets
Aps=	2.17	in^2	Aps=	2.17	in^2	# of strands * area per strand
Fse=	439.43	kips	Fse=	439.43	kips	fpi * Aps
As	0.00	in^2	As	0.00	in^2	
fy	60.00	ksi	fy	60.00	ksi	
Concrete 8,000-psi HPLC			**Concrete 10,000-psi HPLC**			
fc'=	9.350	ksi	fc'=	10.240	ksi	Experimental results
fci=	7.090	ksi	fci=	8.310	ksi	Experimental results
Ec=	3,830	ksi	Ec=	4,050	ksi	Experimental results
Eci=	3,570	ksi	Eci=	3,910	ksi	Experimental results
Unit weig	117	lb/ft^3	Unit weig	119	lb/ft^3	Experimental results

Girder Properties			**Girder Properties**			
h=	36	in	h=	36	in	Given for a Type II girder
yt=	20.17	in	yt=	20.17	in	Given for a Type II girder
yb=	-15.83	in	yb=	-15.83	in	Given for a Type II girder
Ax=	396	in^2	Ax=	396	in^2	Given for a Type II girder
Ix=	50,979	in^4	Ix=	50,979	in^4	Given for a Type II girder
perimeter	109.5	in	perimeter	109.5	in	Given for a Type II girder
e cl	-6.730	in	e cl	-6.730	in	the eccentricity of the cgs at midspan
wsw	0.322	kip/ft	wsw	0.327	kip/ft	selfweight
Length	39.0	ft	Length	42.0	ft	Length of the girder
Msw	734	k-in	Msw	866	k-in	Moment, self weight of the girder

External Loads			**External Loads**			
wsw	0.225	kip/ft	wsw	0.225	kip/ft	selfweight
Msd	513.34	k-in	Msd	595.35	k-in	Msd = superimposed DL not girder sw
RH=	70	%	RH=	70	%	Atlanta average relative humidity

Losses Parameters			Losses Parameters			
Elastic Shortening Losses			Elastic Shortening Losses			Midspan
Eci	3830.0	ksi	Eci	4050.0	ksi	(from above)
fcgp	1.403	ksi	fcgp	1.386	ksi	stress in concrete at cgs just before stressi
ΔfpES	-10.441	ksi	ΔfpES	-9.752	ksi	loss due to elastic shortening
f se	192.1	ksi	f se	192.7	ksi	total stress remaining after ES
Fse	417	kips	Fse	418	kips	after ES losses

ΔfpR1	-1.927	ksi	ΔfpR1	-1.927	ksi	loss due to strand relaxation

PPR	1.000		PPR	1.000		no nonprestressing steel
fc'=	9.350	ksi	fc'=	10.240	ksi	
ΔfpTD	-22.310	ksi	ΔfpTD	-21.575	ksi	

	LWW 55/8 HPLC girder			LWW 69/10 HPLC girder		
Losses	Fse (kips)	fse (ksi)	fse (%)	Fse (kips)	fse (ksi)	fse (%)
After Jacki	439	202.5	100.0	439	202.5	100.0
ES	-23	-10.4	-5.2	-21	-9.8	-4.8
CR SH RE	-48	-22.3	-11.0	-47	-21.6	-10.7
After Los	368	169.7	83.8	371	171.2	84.5

C.5.4. Prestress Losses with PCI Method

LWW 55/8 HPLC girder

Steel			
Fpu	59.13	kips	From strand spec sheets
Astrand	0.217	in^2	area of 0.6-inch strand
fpu	272.5	ksi	Fpu / Astrand
fpy	245.2	ksi	80% fpu
avg F/strd	43.94	kips	from load cell data, average force / strand
fpi	202.50	ksi	(avg F/std)/Astrand, init avg stress / strand
# strands	10		Total # of prestressing strands
Eps=	28,500	ksi	From strand spec sheets
Aps=	2.17	in^2	# of strands * area per strand
Fse=	439.43	kips	fpi * Aps
Concrete 8,000-psi HPLC			
fc'=	9.350	ksi	Experimental results
fci=	7.090	ksi	Experimental results
Ec=	3,830	ksi	Experimental results
Eci=	3,570	ksi	Experimental results
Unit weight	117	lb/ft^3	Experimental results
Girder Properties			
h=	36	in	Given for a Type II girder
yt=	20.17	in	Given for a Type II girder
yb=	-15.83	in	Given for a Type II girder
Ax=	396	in^2	Given for a Type II girder
Ix=	50,979	in^4	Given for a Type II girder
perimeter	109.5	in	Given for a Type II girder
e cl	-6.730	in	the eccentricity of the cgs at midspan
wsw	0.322	kip/ft	selfweight
Length	39.0	ft	Length of the girder
Msw	734.07	k-in	Moment, self weight of the girder
External Loads			
wsw	0.225	kip/ft	selfweight
Msd	513.34	k-in	Msd = superimposed DL not girder sw
RH=	70	%	Atlanta average relative humidity
Losses Parameters			
kcir=	0.9		for pretensioned members
kes=	1.0		for pretensioned members
kcr=	1.6		for lightweight pretensioned members
ksh=	0.92		for 1 day curing before prestressing
Kre=	5	ksi	for grade 270, low relaxation strands
J=	0.04		for grade 270, low relaxation strands
fpi/fpu	0.74		parameter for determining "C"
C=	1.00		for fpi/fpu= 0.75 low relaxation strand

Elastic Shortening Losses			Midspan
Eci	3397.4	ksi	(from above)
fcir	1.253	ksi	stress in concrete at cgs just before stressing
ε cir	0.00037		strain in concrete at cgs just before stressing
ES (Df)	-10.512	ksi	loss due to elastic shortening
f se	191.988	ksi	total stress remaining after ES
Fse	417	kips	after ES losses
CR Creep Losses			Midspan
Fse	416.6	kips	(from above)
fcir	-1.253	ksi	stress in concrete at cgs just after stressing
f cds	-0.068	ksi	stress in concrete at cgs from superimposed load
CR (Df)	-14.11	ksi	loss due to creep
f se	177.87	ksi	total stress remaining after ES and CR
Fse	386	kips	after ES and CR
SH Shrinkage Losses (losses independent of load)			
V/S	3.616	in	Vol / Surface = Area / perimeter
ε sh	-0.00019		axial shortening of concrete due to shrinkage
SH (Df)	-5.051	ksi	loss due to shrinkage
f se mid	172.82	ksi	total stress remaining after ES, CR, and SH, mid
Fse	375	kips	after ES and CR
RE Relaxation losses (lolax stran			Midspan
RE (Df)	-3.813	ksi	loss due to strand relaxation
f se mid	169.01	ksi	total stress remaining after ES, CR, and SH, mid
Fse	367	kips	after ES and CR
total loss	-33.489	ksi	total loss from ES, CR, SH, and RE
e total, cgs	-0.00118		total strain from ES, CR, SH, and RE
fse	128.2	ksi	
Fse	1571.7	kips	

LWW 69/10 HPLC girder

Steel			
Fpu	59.13	kips	From strand spec sheets
Astrand	0.217	in^2	area of 0.6-inch strand
fpu	272.5	ksi	Fpu / Astrand
fpy	245.2	ksi	80% fpu
avg F/strd	43.94	kips	from load cell data, average force / strand
fpi	202.50	ksi	(avg F/std)/Astrand, init avg stress / strand
# strands	10		Total # of prestressing strands
Eps=	28,500	ksi	From strand spec sheets
Aps=	2.17	in^2	# of strands * area per strand
Fse=	439.43	kips	fpi * Aps
Concrete 10,000-psi HPLC			
fc'=	10.240	ksi	Experimental results
fci=	8.310	ksi	Experimental results
Ec=	4,050	ksi	Experimental results
Eci=	3,910	ksi	Experimental results
Unit weight	119	lb/ft^3	Experimental results
Girder Properties			
h=	36	in	Given for a Type II girder
yt=	20.17	in	Given for a Type II girder
yb=	-15.83	in	Given for a Type II girder
Ax=	396	in^2	Given for a Type II girder
Ix=	50,979	in^4	Given for a Type II girder
perimeter	109.5	in	Given for a Type II girder
e cl	-6.730	in	the eccentricity of the cgs at midspan
wsw	0.327	kip/ft	selfweight
Length	42.0	ft	Length of the girder
Msw	865.90	k-in	Moment, self weight of the girder
External Loads			
wsw	0.225	kip/ft	selfweight
Msd	595.35	k-in	Msd = superimposed DL not girder sw
RH=	70	%	Atlanta average relative humidity
Losses Parameters			
kcir=	0.9		for pretensioned members
kes=	1.0		for pretensioned members
kcr=	1.6		for lightweight pretensioned members
ksh=	0.92		for 1 day curing before prestressing
Kre=	5	ksi	for grade 270, low relaxation strands
J=	0.04		for grade 270, low relaxation strands
fpi/fpu	0.74		parameter for determining "C"
C=	1.00		for fpi/fpu= 0.75 low relaxation strand

Elastic Shortening Losses			Midspan
Eci	3910.0	ksi	(from above)
fcir	1.236	ksi	stress in concrete at cgs just before stressing
ε cir	0.00032		strain in concrete at cgs just before stressing
ES (Df)	-9.007	ksi	loss due to elastic shortening
f se	193.493	ksi	total stress remaining after ES
Fse	420	kips	after ES losses
CR Creep Losses			Midspan
Fse	419.9	kips	(from above)
fcir	-1.236	ksi	stress in concrete at cgs just after stressing
f cds	-0.079	ksi	stress in concrete at cgs from superimposed load
CR (Df)	-13.03	ksi	loss due to creep
f se	180.46	ksi	total stress remaining after ES and CR
Fse	392	kips	after ES and CR
SH Shrinkage Losses (losses independent of load)			
V/S	3.616	in	Vol / Surface = Area / perimeter
ε sh	-0.00019		axial shortening of concrete due to shrinkage
SH (Df)	-5.051	ksi	loss due to shrinkage
f se mid	175.41	ksi	total stress remaining after ES, CR, and SH, mid
Fse	381	kips	after ES and CR
RE Relaxation losses (lolax stran			Midspan
RE (Df)	-3.917	ksi	loss due to strand relaxation
f se mid	171.50	ksi	total stress remaining after ES, CR, and SH, mid
Fse	372	kips	after ES and CR
total loss	-31.003	ksi	total loss from ES, CR, SH, and RE
e total, cgs	-0.00109		total strain from ES, CR, SH, and RE
fse	128.2	ksi	
Fse	1571.7	kips	

C.5.5. Prestress Losses with ACI-209 Method

LWW 55/8 HPLC girder

Steel			
Fpu	59.13	kips	
Astrand	0.217	in^2	
fpu	272.5	ksi	
fpy	245.2	ksi	
avg F/strd	43.94	kips	
fpi	202.50	ksi	
# strands	10		
Eps=	28,500	ksi	From strand spec sheets
Aps=	2.17	in^2	
Fse=	439.43	kips	Applied load in frames
Concrete 8,000-psi HPLC			
fc'=	9.350	ksi	Experimental results
fci=	7.090	ksi	Experimental results
Ec=	3,830	ksi	Experimental results
Eci=	3,570	ksi	Experimental results
Unit weig	117	lb/ft^3	Experimental results
Girder Properties			
h=	36	in	Given for a Type II girder
yt=	20.17	in	Given for a Type II girder
yb=	-15.83	in	Given for a Type II girder
Ax=	396	in^2	Given for a Type II girder
Ix=	50,979	in^4	Given for a Type II girder
perimeter	109.5	in	Given for a Type II girder
e cl	-6.730	in	the eccentricity of the cgs at midspan
wsw	0.322	kip/ft	selfweight
Length	39.0	ft	Length of the girder
Msw	734.07	k-in	Moment, self weight of the girder

External Loads			
wsw	0.225	kip/ft	selfweight
Msd	513.34	k-in	Msd = superimposed DL not girder sw
RH=	70	%	Atlanta average relative humidity

Losses Parameters

kcir=	0.9		for pretensioned members
kes=	1.0		for pretensioned members
kcr=	2.0		for pretensioned members
ksh=	0.92		for 1 day curing before prestressing
Kre=	5	ksi	for grade 270, low relaxation strands
J=	0.04		for grade 270, low relaxation strands
fpi/fpu	0.74		parameter for determining "C"
C=	0.61		for fpi/fpu= 0.69 low relaxation strand

Elastic Shortening Losses — Midspan

ni	8.0		(from above Eps/Eci)
fc	1.500	ksi	stress in concrete at cgs just before stressing
ES (Df)	-11.975	ksi	loss due to elastic shortening
f se	190.525	ksi	total stress remaining after ES
Fse	413	kips	after ES losses

CR Creep Losses — Midspan

ψ	0.6		
d	10		
Øu	1.426		
ES	-12.0	kips	(from above)
t-t'	14600	days	40 years
Øt	0.00	ksi	stress in concrete at cgs just after stressing
Ft/F0	0.21		coefficient at ultimate for sand lightweight
f cds	-0.068	ksi	stress in concrete at cgs from superimposed load
CR (Df)	0.00	ksi	loss due to creep
f se	190.52	ksi	total stress remaining after ES and CR
Fse	413	kips	after ES and CR

SH Shrinkage Losses (losses independent of load)

f	55.0		
(εsh)u	398	με	
t-t0	14600	days	
(εsh)t	0.000397		axial shortening of concrete due to shrinkage
SH (Df)	-11.31	ksi	loss due to shrinkage
f se mid	179.21	ksi	total stress remaining after ES, CR, and SH, mid
Fse	389	kips	after ES and CR

RE Relaxation losses (lolax stra — Midspan

fpj	202.50	ksi	
t-t'	350400	hours	40 years
RE (Df)	-5.614	ksi	loss due to strand relaxation
f se mid	173.60	ksi	total stress remaining after ES, CR, and SH, mid
Fse	377	kips	after ES and CR

total loss	-28.899	ksi	total loss from ES, CR, SH, and RE
e total, cgs	-0.00101		total strain from ES, CR, SH, and RE
fse	128.2	ksi	
Fse	1571.7	kips	

ACI 209 Coeficients

assumption steam cured for 1 day

	Creep			
d	10			
f				
	Øu			
Base	2.35			
Loading Age γ_{la}	1.130			
Differential Shrink	1.000			
Inicial Mois Curing	1.000			
Ambient Relative Hu	0.801	70	@70%	
Volume Surface Rati	0.774	v/s	3.616	in
Temperature other th	1.000			
Slump γ_s	1.122	slump:	4.5	in
Fine Aggregate % γ	0.969	fa%	37.0	%
Cement Content γ_c	1.000	c		
Air Content γ_a	0.7975	air%	3.75	%
Ultimate value	1.426			

$$\phi_t = \frac{t^{0.6}}{d + t^{0.6}} \cdot \phi_u$$

ACI 209 Coeficients

assumpyion steam cured for 1 day

	Shrink			
d				
f	55			
	(εsh)u			
Base	780			
Loading A	1.000			
Differentia	1.000			
Inicial Mo	1.000			
Ambient F	0.700	0.7	@70%	
VS Ratio	0.778	3.616		
Temperatu	1.000			
Slump γ_s	1.075	slump:	4.5	in
Fine Agg '	0.818	fa%	37.0	%
Cement C	1.08984	c	944	lb/yd3
Air Conte	0.98	air%	3.75	%
Ultimate v	398			

$$(\varepsilon_{sh})_t = \frac{t}{f + t} \cdot (\varepsilon_{sh})_u$$

10,000-psi HPLC specimens

Steel			
Fpu	59.13	kips	
Astrand	0.217	in^2	
fpu	272.5	ksi	
fpy	245.2	ksi	
avg F/strd	43.94	kips	
fpi	202.50	ksi	
# strands	10		
Eps=	28,500	ksi	From strand spec sheets
Aps=	2.17	in^2	
Fse=	439.43	kips	Applied load in frames
Concrete1 0,000-psi HPLC			
fc'=	10.240	ksi	Experimental results
fci=	8.310	ksi	Experimental results
Ec=	4,050	ksi	Experimental results
Eci=	3,910	ksi	Experimental results
Unit weigl	119	lb/ft^3	Experimental results
Girder Properties			
h=	36	in	Given for a Type II girder
yt=	20.17	in	Given for a Type II girder
yb=	-15.83	in	Given for a Type II girder
Ax=	396	in^2	Given for a Type II girder
Ix=	50,979	in^4	Given for a Type II girder
perimeter	109.5	in	Given for a Type II girder
e cl	-6.730	in	the eccentricity of the cgs at midspan
wsw	0.327	kip/ft	selfweight
Length	42.0	ft	Length of the girder
Msw	865.90	k-in	Moment, self weight of the girder

External Loads			
wsw	0.225	kip/ft	selfweight
Msd	595.35	k-in	Msd = superimposed DL not girder sw
RH=	70	%	Atlanta average relative humidity

Losses Parameters

kcir=	0.9		for pretensioned members
kes=	1.0		for pretensioned members
kcr=	2.0		for pretensioned members
ksh=	0.92		for 1 day curing before prestressing
Kre=	5	ksi	for grade 270, low relaxation strands
J=	0.04		for grade 270, low relaxation strands
fpi/fpu	0.74		parameter for determining "C"
C=	0.61		for fpi/fpu= 0.69 low relaxation strand

Elastic Shortening Losses — Midspan

ni	7.3		(from above Eps/Eci)
fc	1.500	ksi	stress in concrete at cgs just before stressing
ES (Df)	-10.934	ksi	loss due to elastic shortening
f se	191.566	ksi	total stress remaining after ES
Fse	416	kips	after ES losses

CR Creep Losses — Midspan

ψ	0.6		
d	10		
Øu	1.344		
ES	-10.9	kips	(from above)
t-t'	14600	days	40 years
øt	0.00	ksi	stress in concrete at cgs just after stressing
Ft/F0	0.21		coefficient at ultimate
f cds	-0.079	ksi	stress in concrete at cgs from superimposed load
CR (Df)	0.00	ksi	loss due to creep
f se	191.57	ksi	total stress remaining after ES and CR
Fse	416	kips	after ES and CR

SH Shrinkage Losses (losses independent of load)

f	55.0		
(εsh)u	396	με	
t-t0	14600	days	
(εsh)t	0.000394		axial shortening of concrete due to shrinkage
SH (Df)	-11.24	ksi	loss due to shrinkage
f se mid	180.33	ksi	total stress remaining after ES, CR, and SH, mid
Fse	391	kips	after ES and CR

RE Relaxation losses (lolax stra — Midspan

fpj	202.50	ksi	
t-t'	350400	hours	40 years
RE (Df)	-5.614	ksi	loss due to strand relaxation
f se mid	174.71	ksi	total stress remaining after ES, CR, and SH, mid
Fse	379	kips	after ES and CR

total loss	-27.788	ksi	total loss from ES, CR, SH, and RE
e total, cgs	-0.00098		total strain from ES, CR, SH, and RE
fse	128.2	ksi	
Fse	1571.7	kips	

ACI 209 Coeficients

assumption steam cured for 1 day

	Creep			
d	10			
f		$\phi_t = \frac{t^{0.6}}{d + t^{0.6}} \cdot \phi_u$		
Øu				
Base	2.35			
Loading Age γ_{la}	1.130			
Differential Shrink	1.000			
Inicial Mois Curing	1.000			
Ambient Relative Hu	0.801	70	@70%	
Volume Surface Rati	0.774	v/s	3.616	in
Temperature other th	1.000			
Slump γ_s	1.088	slump:	4	in
Fine Aggregate % γ	0.969	fa%	37.0	%
Cement Content γ_c	1.000	c		
Air Content γ_α	0.775	air%	3.5	%
Ultimate value	1.344			

ACI 209 Coeficients

assumpyion steam cured for 1 day

	Shrink			
d				
f	55			
	(εsh)u			
Base	780			
Loading A	1.000	$(\varepsilon_{sh})_t = \frac{t}{f+t} \cdot (\varepsilon_{sh})_u$		
Differentia	1.000			
Inicial Mo	1.000			
Ambient F	0.700	0.7	@70%	
VS Ratio	0.778	3.616		
Temperatu	1.000			
Slump γ_s	1.054	slump:	4	in
Fine Agg	0.818	fa%	37.0	%
Cement C	1.1064	c	990	lb/yd3
Air Conte	0.978	air%	3.5	%
Ultimate v	396			

APPENDIX D

PHYSICAL AND MECHANICAL PROPERTIES OF CONCRETE MIXTURES OF MEDIUM-SCALE STUDY

D.1. Batching Procedures

D.1.1. Constituents Storage and Conditioning

Cement and fly ash were stored in sealed 200-liter (55-gallon) barrels inside the laboratory were they remained dry and at room temperature. Silica fume was obtained and stored in 11.3-kg (25-lb) bags inside the laboratory.

Aggregates were stored in closed bins outside the laboratory were they stayed at ambient temperature. Normal weight fine aggregate and coarse granite aggregate were air-dried before storing in the bins. Expanded slate lightweight aggregate was preconditioned before batching depending of the HPLC mixture that needed to be batched (LWW or LWD).

For the mixtures made with pre-soaked lightweight aggregate, a sprinkler system was installed on top of the bins. Forty eight hours before mixing the sprinklers were opened, so the running water soaked the lightweight aggregate for a period of 24 hours. Twenty four hours before mixing, the sprinkler system was shut off and the water was allowed to drain until mixing. Two hours before mixing two wheel barrels were filled with the presoaked lightweight aggregate and a wet tarp was placed on top to prevent evaporation.

The preconditioning if the lightweight aggregate for the LWD mixtures started one week before mixing when the aggregate was spread out over polyethylene sheet in the floor of the laboratory. A pedestal fan was placed next to the aggregate to enforce air circulation on top of the aggregate and to accelerate the drying. Two days later the aggregate was placed in a environmentally controlled room at 50% relative humidity where it kept drying for five days.

D.1.2. Moisture Adjustment for Mixture Designs

All mixture designs considered the aggregate in saturated surface dry (SSD) condition, so they needed to be adjusted for actual moisture content before mixing. Moisture content was measured on the fine and coarse aggregate two hours before mixing. 680-gr (1.5-lb) samples were dried using and electrical cook top. The samples were weighted every 10 minutes until constant weight was reached. The moisture content was calculated as the difference between initial and final constant weight divided by the final constant weight. Typical results are shown in Table D.1.

Table D.1. Typical moisture contents in aggregate

	initial weight, gr (lb)	final constant weight, kg (lb)	moisture content (%)	Comment
Pre-soaked expanded slate	680 (1.500)	629 (1.385)	8.8	Above SSD condition
Air-dried expanded slate	680 (1.500)	673 (1.485)	1.0	Below SSD condition
Granite	680 (1.500)	678 (1.495)	0.1	Below SSD condition
Normal weight fine aggregate	680 (1.500)	678 (1.495)	0.1	Below SSD condition

D.1.3. Mixing Procedure

The following batching procedure was followed for all mixtures of the medium and small-scale studies:

1. Add coarse aggregate
2. Add fine aggregate and mix for 1 minute
3. Add cement and mixed for 1 minute
4. Add fly ash and mix for 1 minute
5. Mix the water with the plasticizer and the air entraining agent
6. Add the water with the additives and mix for 1 minute
7. Add the silica fume slowly during 1 minute and mix for an additional minute
8. Add the superplasticizer and mix for 2 minutes

D.2. Fracture Surfaces

Figure D.1: Fracture surface of a STL 65-35 cylinder specimen after testing

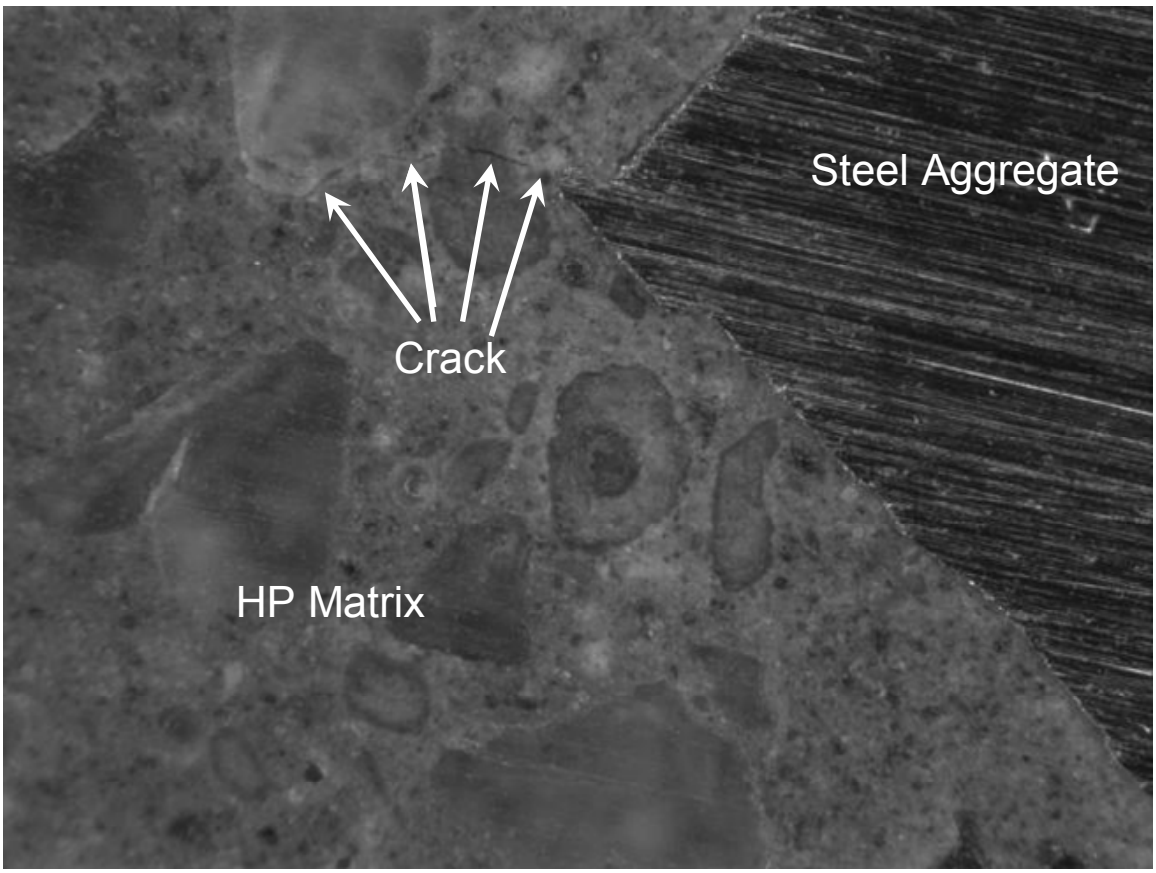

Figure D.2: Stress concentration induced cracking starting at the ITZ in mixture with steel aggregate.

D.3. Compressive Strength

Cement Matrix

Cement Matrix				Strength	Strength	Average			
Stage	Batch	Age	Maturity	MPa	ksi	Unitweight	Strength	Strength	stdev
1	1	1	6.3	108.8	15.8	lb/ft3	MPa	ksi	
1	1	7	13.1	113.1	16.4	146.6	113.2	16.420	6.4
1	1	28	36.9	123.5	17.9	146.4	112.2	16.269	1.9
1	1	56	68.7	112.8	16.4	147.2	125.1	18.144	7.7
1	1	365	419.3	135.1	19.6	147.1	122.3	17.734	7.5
1	1	1	6.3	105.3	15.3	147.7	129.9	18.838	7.2
1	1	7	13.1	109.7	15.9			Average	**6.1**
1	1	28	36.9	115.3	16.7		Strength	Strength	
1	1	56	68.7	120.7	17.5		MPa	ksi	
1	1	365	419.3	125.9	18.3	6.3	106.9	15.5	3.6
1	2	1	6.3	110.8	16.1	8.6	119.6	17.3	2.4
1	2	7	13.1	114.1	16.5	13.1	112.2	16.3	1.9
1	2	28	36.9	125.2	18.2	36.9	120.0	17.4	5.1
1	2	56	68.7	130.3	18.9	39.1	130.3	18.9	0.1
1	2	365	419.3	136.9	19.9	68.7	122.3	17.7	7.5
1	2	1	6.3	102.6	14.9	419.3	129.9	18.8	7.2
1	2	7	13.1	111.9	16.2				**4.0**
1	2	28	36.9	115.8	16.8				
1	2	56	68.7	125.4	18.2				
1	2	365	419.3	121.8	17.7				
2	1	1	8.6	119.5	17.3				
2	1	7	0.0						
2	1	28	39.1	132.9	19.3				
2	1	56	0.0						
2	1	365	0.0						
2	1	1	8.6	116.1	16.8				
2	1	7	0.0						
2	1	28	39.1	132.7	19.2				
2	1	56	0.0						
2	1	365	0.0						

HP Matrix

HP Matrix				Strength	Strength	Average			
Stage	Batch	Age	Maturity	MPa	ksi	Unitweight	Strength	Strength	Std dev
1	1	1	5.1	87.1	12.633	lb/ft3	MPa	ksi	
1	1	7	11.8	104.1	15.091	139.6	95.7	13.876	4.6
1	1	28	35.6	100.6	14.593	139.7	104.2	15.103	8.0
1	1	56	67.4	106.1	15.389	140.6	104.5	15.158	3.8
1	1	365	418.0	125.0	18.123	139.9	109.1	15.826	3.1
1	1	1	5.1	86.9	12.600	140.8	125.1	18.142	3.8
1	1	7	11.8	92.8	13.463			Average	**4.7**
1	1	28	35.6	101.1	14.664		Strength	Strength	
1	1	56	67.4	107.9	15.645		MPa	ksi	
1	1	365	418.0	119.8	17.373	4.6	102.5	14.858	0.3
1	2	1	5.1	95.7	13.870	4.8	97.5	14.141	0.4
1	2	7	11.8	109.8	15.923	5.1	91.8	13.309	5.6
1	2	28	35.6	106.9	15.499	6.9	94.4	13.687	1.5
1	2	56	67.4	112.3	16.286	11.8	104.2	15.103	8.0
1	2	365	418.0	127.3	18.457	35.2	101.1	14.660	6.0
1	2	1	5.1	97.5	14.135	35.4	104.8	15.199	2.1
1	2	7	11.8	109.9	15.934	35.6	104.6	15.172	4.5
1	2	28	35.6	109.9	15.932	37.6	106.0	15.364	3.5
1	2	56	67.4	104.6	15.174	66.9	109.4	15.869	2.7
1	2	365	418.0	128.4	18.616	67.2	110.1	15.971	3.8
2	1	1	6.9	94.8	13.752	67.4	107.7	15.624	3.3
2	1	7				418.0	125.1	18.142	3.8
2	1	28	37.6	101.0	14.652				**3.5**
2	1	56							
2	1	365							
2	1	1	6.9	94.9	13.754				
2	1	7							
2	1	28	37.6	108.1	15.675				
2	1	56							
2	1	365							
2	2	1	6.9	95.7	13.874				
2	2	7							
2	2	28	37.6	105.8	15.337				
2	2	56							
2	2	365							
2	2	1	6.9	92.2	13.369				
2	2	7							
2	2	28	37.6	108.9	15.791				
2	2	56							
2	2	365							
3	1	1	4.6	102.7	14.885				
3	1	7							
3	1	28	35.2	105.3	15.271				
3	1	56	66.9	111.3	16.143				
3	1	365							
3	1	1	4.6	102.3	14.832				
3	1	7							
3	1	28	35.2	96.9	14.049				
3	1	56	66.9	107.6	15.596				
3	1	365							
4	1	1	4.8	97.1	14.080				
4	1	7							
4	1	28	35.4	102.8	14.908				
4	1	56	67.2	113.9	16.519				
4	1	365							
4	1	1	4.8	97.3	14.109				
4	1	7							
4	1	28	35.4						
4	1	56	67.2	113.1	16.403				
4	1	365							
4	1	1							
4	1	7							
4	1	28							
4	1	56	67.2	108.0	15.653				
4	1	365							
4	2	1	4.8	97.6	14.2				
4	2	7							
4	2	28	35.4	104.6	15.2				
4	2	56	67.2	106.4	15.4				
4	2	365							
4	2	1	4.8	98.1	14.2				
4	2	7							
4	2	28	35.4	107.1	15.5				
4	2	56	67.2	109.4	15.9				

LWW 35-65

LWA 35-65				Strength	Strength	Average			
Stage	Batch	Age	Maturity	MPa	ksi	Unitweight	Strength	Strength	stdev
1	1	1	2.7	78.5	11.4	lb/ft3	MPa	ksi	
1	1	7	9.4	71.9	10.4	131.4	80.1	11.613	14.2
1	1	28	33.2	75.4	10.9	131.0	74.7	10.828	7.4
1	1	56	65.0	84.4	12.2	132.0	88.7	12.859	7.7
1	1	365	415.6	93.0	13.5	131.0	85.3	12.364	6.5
1	1	1	2.7	76.5	11.1	131.7	95.0	13.772	1.7
1	1	7	9.4	83.0	12.0	0	0	Average	**7.5**
1	1	28	33.2	89.1	12.9	0	Strength	Strength	
1	1	56	65.0	80.4	11.7	0	MPa	ksi	
1	1	365	415.6	95.1	13.8	2.7	66.6	9.66	13.0
1	2	1	2.7	51.8	7.5	3.98	92.9	13.47	2.0
1	2	7	9.4	65.9	9.6	3.99	85.2	12.36	1.3
1	2	28	33.2	80.7	11.7	9.4	74.7	10.83	7.4
1	2	56	65.0	80.9	11.7	33.2	81.6	11.83	6.9
1	2	365	415.6	94.7	13.7	34.5	97.4	14.12	1.2
1	2	1	2.7	59.7	8.7	34.6	89.5	12.98	4.2
1	2	7	9.4	77.9	11.3	65.0	82.5	11.96	2.2
1	2	28	33.2	81.0	11.8	415.6	95.0	13.77	1.7
1	2	56	65.0	84.4	12.2				**4.4**
1	2	365	415.6	97.1	14.1				
1	3	1	2.7						
1	3	7	9.4						
1	3	28	33.2	96.5	14.0				
1	3	56	65.0						
1	3	365	415.6						
1	3	1	2.7						
1	3	7	9.4						
1	3	28	33.2	82.4	11.9				
1	3	56	65.0						
1	3	365	415.6						
1	3	1	2.7						
1	3	7	9.4						
1	3	28	33.2	82.3	11.9				
1	3	56	65.0						
1	3	365	415.6						
2	1	1	3.99	83.7	12.1				
2	1	7							
2	1	28	34.59	93.3	13.5				
2	1	56							
2	1	365							
2	1	1	3.99	86.2	12.5				
2	1	7							
2	1	28	34.59	90.3	13.1				
2	1	56							
2	1	365							
2	1	1	3.99	85.8	12.4				
2	1	7	0.00						
2	1	28	34.59	85.0	12.3				
2	1	56							
2	1	365							
3	1	1	3.98	93.7	13.6				
3	1	7							
3	1	28	34.53	96.7	14.0				
3	1	56	66.30	96.3	14.0				
3	1	365							
3	1	1	3.98	94.3	13.7				
3	1	7							
3	1	28	34.53	96.6	14.0				
3	1	56							
3	1	365							
3	1	1	3.98	90.6	13.1				
3	1	7							
3	1	28	34.53	98.8	14.3				
3	1	56							
3	1	365							

NWA 35-65

NWA 35-65				Strength	Strength	Average			
Stage	Batch	Age	Maturity	MPa	ksi	Unitweight	Strength	Strength	stdev
1	1	1	3.1	90.6	13.1	lb/ft3	MPa	ksi	
1	1	7	9.8	96.7	14.0	145.9	96.1	13.929	6.5
1	1	28	33.8	105.3	15.3	146.8	94.8	13.741	3.0
1	1	56	65.4	115.7	16.8	146.7	106.8	15.488	5.4
1	1	365	416.0	115.2	16.7	146.4	106.6	15.454	5.9
1	1	1	3.1	92.9	13.5	147.7	120.9	17.537	6.8
1	1	7	9.8	97.4	14.1	0	0	Average	**5.5**
1	1	28	33.8	103.8	15.1	0	Strength	Strength	
1	1	56	65.4	107.4	15.6	0	MPa	ksi	
1	1	365	416.0	126.4	18.3	3.1	91.4	13.3	1.0
1	2	1	3.1	91.5	13.3	4.6	95.3	13.8	1.7
1	2	7	0.0	90.8	13.2	4.9	98.6	14.3	4.3
1	2	28	33.8	104.8	15.2	9.8	94.8	13.7	3.0
1	2	56	0	107.0	15.5	33.8	104.9	15.2	0.7
1	2	365	0	127.1	18.4	35.1	102.2	14.8	2.6
1	2	1	3.1	90.7	13.1	35.6	108.5	15.7	2.3
1	2	7	9.8	94.2	13.7	65.4	109.7	15.9	4.0
1	2	28	33.8	105.5	15.3	68.3	100.3	14.5	2.7
1	2	56	65.4	108.8	15.8	416.0	120.9	17.5	6.8
1	2	365	416.0	115.0	16.7				**2.9**
2	1	1	4.9	103.5	15.0				
2	1	7	0						
2	1	28	35.6	112.7	16.3				
2	1	56	0						
2	1	365	0						
2	1	1	4.9						
2	1	7	0						
2	1	28	35.6	116.6	16.9				
2	1	56	0						
2	1	365	0						
2	1	1	4.9	109.6	15.9				
2	1	7	0						
2	1	28	35.6	112.7	16.3				
2	1	56	0						
2	1	365	0						
3	1	1	4.6	95.4	13.8				
3	1	7	0						
3	1	28	35.1	99.8	14.5				
3	1	56	68.281129	98.4	14.3				
3	1	365	0						
3	1	1	4.6	96.9	14.0				
3	1	7	0						
3	1	28	35.1	105.0	15.2				
3	1	56	68.281129	102.2	14.8				
3	1	365	0						
3	1	1	4.6	93.5	13.6				
3	1	7	0						
3	1	28	35.1	101.9	14.8				
3	1	56	68.281129						
3	1	365	0						

STL 35-65

Steel 35-65				Strength	Strength	Average			
Stage	Batch	Age	Maturity	MPa	ksi	Unitweight	Strength	Strength	stdev
1	1	1	3.4	41.3	5.982	lb/ft3	MPa	ksi	
1	1	7	10.1	62.1	9.005	213.9	58.3	8.447	11.3
1	1	28	33.7	66.9	9.704	213.2	60.1	8.718	2.8
1	1	56	65.7	62.3	9.033	212.1	69.9	10.136	4.8
1	1	365	416.3	74.0	10.726	217.7	65.2	9.452	4.4
1	1	1	3.4	54.5	7.909	206.8	78.5	11.386	4.7
1	1	7	10.1					Average	**5.6**
1	1	28	33.7				Strength	Strength	
1	1	56	65.7	64.4	9.341		MPa	ksi	
1	1	365	416.3	83.6	12.118	3.4	47.7	6.917	6.4
1	2	1	3.4	43.4	6.295	4.8	68.8	9.977	3.4
1	2	7	10.1	58.1	8.431	10.1	60.1	8.718	2.8
1	2	28	33.7	66.7	9.677	33.7	65.7	9.529	1.9
1	2	56	65.7	65.8	9.541	35.4	74.1	10.742	0.9
1	2	365	416.3	75.1	10.889	65.7	65.2	9.452	2.5
1	2	1	3.4	51.6	7.483	416.3	78.5	11.386	4.7
1	2	7	10.1						**3.2**
1	2	28	33.7	63.5	9.208				
1	2	56	65.7	68.2	9.895				
1	2	365	416.3	81.4	11.809				
2	1	1	4.8	66.5	9.650				
2	1	7							
2	1	28	35.4	74.9	10.860				
2	1	56							
2	1	365							
2	1	1	4.8	66.8	9.682				
2	1	7							
2	1	28	35.4	74.3	10.768				
2	1	56							
2	1	365							
2	1	1	4.8	68.1	9.880				
2	1	7							
2	1	28	35.4	73.1	10.597				
2	1	56							
2	1	365							
2	1	1	4.8	73.8	10.696				

LWW 65-35

LWA 65-35				Strength	Strength	Average			
Stage	Batch	Age	Maturity	MPa	ksi	Unitweight	Strength	Strength	Stand Dev
1	1	1	2.2	63.9	9.3	lb/ft3	MPa	ksi	
1	1	7	8.9	76.2	11.0	124.0	73.5	10.657	5.7
1	1	28	32.7	81.6	11.8	125.2	76.0	11.024	1.5
1	1	56	64.5	82.4	12.0	124.5	79.3	11.502	3.9
1	1	365	415.1	88.3	12.8	124.2	80.2	11.633	3.5
1	1	1	2.2	71.7	10.4	124.6	87.5	12.689	4.2
1	1	7	8.9	77.8	11.3			Average	**3.8**
1	1	28	32.7	75.9	11.0		Strength	Strength	
1	1	56	64.5	84.1	12.2		MPa	ksi	
1	1	365	415.1	81.6	11.8	2.2	67.9	9.8	4.3
1	2	1	2.2	71.4	10.4	3.6	74.4	10.8	3.8
1	2	7	8.9	76.1	11.0	4.7	78.2	11.3	3.5
1	2	28	32.7	71.3	10.3	8.9	76.0	11.0	1.5
1	2	56	64.5	81.9	11.9	32.7	77.6	11.3	5.1
1	2	365	415.1	91.4	13.3	34.2	80.9	11.7	4.1
1	2	1	2.2	64.3	9.3	35.4	79.4	11.5	2.3
1	2	7	8.9	74.1	10.7	64.5	81.3	11.8	3.1
1	2	28	32.7	81.7	11.9	65.9	78.8	11.4	4.2
1	2	56	64.5	76.8	11.1	415.1	87.5	12.7	4.2
1	2	365	415.1	88.7	12.9				**3.6**
2	1	1	4.7	77.9	11.3	1	12.0	63.9	82.3
2	1	7	0.0			7		74.1	77.8
2	1	28	35.4	77.7	11.3	28		71.3	85.7
2	1	56	0.0			56		75.0	84.1
2	1	365	0.0			365		81.6	91.4
2	1	1	4.7	78.9	11.4				
2	1	7	0.0						
2	1	28	35.4	82.0	11.9				
2	1	56	0.0						
2	1	365	0.0						
2	2	1	4.7	73.7	10.7				
2	2	7	0.0						
2	2	28	35.4	77.3	11.2				
2	2	56	0.0						
2	2	365	0.0						
2	2	1	4.7	82.3	11.9				
2	2	7	0.0						
2	2	28	35.4	80.6	11.7				
2	2	56	0.0						
2	2	365	0.0						
3	1	1	3.6	71.2	10.3				
3	1	7	0.0						
3	1	28	34.2	82.3	11.9				
3	1	56	65.9						
3	1	365	0.0						
3	1	1	3.6	79.7	11.6				
3	1	7	0.0						
3	1	28	34.2	85.7	12.4				
3	1	56	65.9						
3	1	365	0.0						
3	2	1	3.6	74.3	10.8				
3	2	7	0.0						
3	2	28	34.2	75.9	11.0				
3	2	56	65.9	75.0	10.9				
3	2	365	0.0						
3	2	1	3.6	72.4	10.5				
3	2	7	0.0						
3	2	28	34.2	79.8	11.6				
3	2	56	65.9	83.2	12.1				
3	2	365	0.0						
3	2	1	3.6						
3	2	7	0.0						
3	2	28	34.2						
3	2	56	65.9	78.1	11.3				
3	2	365	0.0						

LWD 65-35

LWA 65-35 dry				Strength	Strength	Average	0	0	
Stage	Batch	Age	Maturity	MPa	ksi	Unitweight	Strength	Strength	Stand Dev
1	1	1	3.2	67.8	9.8	lb/ft3	MPa	ksi	
1	1	7	9.9	75.6	11.0	121.4	72.8	10.550	7.4
1	1	28	33.7	69.3	10.1	119.2	69.4	10.066	5.4
1	1	56	65.5	79.3	11.5	122.7	76.8	11.142	6.6
1	1	365	416.1	75.1	10.9	121.0	79.2	11.489	3.5
1	1	1	3.2	60.9	8.8	120.8	77.5	11.243	8.7
1	1	7	9.9	72.3	10.5	0	0	Average	**6.3**
1	1	28	33.7	74.1	10.7	0	Strength	Strength	
1	1	56	65.5	79.9	11.6	0	MPa	ksi	
1	1	365	416.1	89.3	13.0	3.2	63.8	9.3	
1	2	1	3.223025	67.1	9.7	4.1	76.3	11.1	
1	2	7	9.936213	64.6	9.4	4.5	78.2	11.3	
1	2	28	33.71681	72.9	10.6	9.9	69.4	10.1	
1	2	56	65.53458	72.3	10.5	33.7	69.8	10.1	
1	2	365	416.1447	68.7	10.0	34.7	81.4	11.8	
1	2	1	3.223025	59.4	8.6	35.0	79.4	11.5	
1	2	7	9.936213	65.2	9.5	65.5	77.0	11.2	
1	2	28	33.71681	62.7	9.1	416.1	77.5	11.2	
1	2	56	65.53458	76.5	11.1				
1	2	365	416.1447	77.1	11.2				
2	1	1	4.5	77.9	11.3				
2	1	7	0						
2	1	28	35.0	77.7	11.3		1.010		
2	1	56	0				1.095		
2	1	365	0				1.032		
2	1	1	4.5	78.9	11.4		1.012		
2	1	7	0				1.129		
2	1	28	35.0	82.0	11.9				
2	1	56	0						
2	1	365	0						
2	2	1	4.5	73.7	10.7				
2	2	7	0.0						
2	2	28	35.0	77.3	11.2				
2	2	56	0.0						
2	2	365	0.0						
2	2	1	4.5	82.3	11.9				
2	2	7	0.0						
2	2	28	35.0	80.6	11.7				
2	2	56	0.0						
2	2	365	0.0						
3	1	1	4.1	76.4	11.1				
3	1	7	0						
3	1	28	34.7	84.2	12.2				
3	1	56	0						
3	1	365	0						
3	1	1	4.1	78.4	11.4				
3	1	7	0						
3	1	28	34.7	84.6	12.3				
3	1	56	0						
3	1	365	0						
3	2	1	4.1	73.1	10.6				
3	2	7	0.0						
3	2	28	34.7	82.8	12.0				
3	2	56	0.0						
3	2	365	0.0						
3	2	1	4.1	77.0	11.2				
3	2	7	0.0						
3	2	28	34.7	73.8	10.7				
3	2	56	0.0						
3	2	365	0.0						

NWA 65-35

NWA 65-35				Strength	Strength	Average			
Stage	Batch	Age	Maturity	MPa	ksi	Unitweight	Strength	Strength	Stand Dev
1	1	1	2.0	88.0	12.8	lb/ft3	MPa	ksi	
1	1	7	8.9	90.7	13.1	151.9	90.5	13.129	9.0
1	1	28	32.6	100.1	14.5	153.2	89.5	12.978	4.3
1	1	56	64.4	107.8	15.6	153.6	100.3	14.548	6.4
1	1	365	415.1	121.9	17.7	153.8	104.3	15.129	8.5
1	1	1	2.0	85.1	12.3	154.1	122.2	17.714	2.7
1	1	7	8.9	94.4	13.7			Average	**6.2**
1	1	28	32.6	106.9	15.5		Strength	Strength	
1	1	56	64.4	110.0	16.0		MPa	ksi	
1	1	365	415.1	122.7	17.8	2.0	85.3	12.4	2.0
1	2	1	2.0	85.1	12.3	2.2	79.1	11.5	1.8
1	2	7	8.9	84.1	12.2	3.2	85.1	12.3	5.1
1	2	28	32.6	94.5	13.7	3.5	101.2	14.7	3.5
1	2	56	64.4	111.8	16.2	8.9	89.5	13.0	4.3
1	2	365	415.1	118.8	17.2	32.6	99.7	14.5	5.3
1	2	1	2.0	83.2	12.1	33.7	94.3	13.7	3.9
1	2	7	8.9	88.8	12.9	34.5	107.0	15.5	4.8
1	2	28	32.6	97.5	14.1	64.4	110.8	16.1	2.4
1	2	56	64.4	113.5	16.5	65.5	95.8	13.9	3.9
1	2	365	415.1	125.3	18.2	415.1	122.2	17.7	2.7
1	3	1	2.2	77.2	11.2				**3.6**
1	3	1	2.2	80.8	11.7				
1	3	1	2.2	79.2	11.5				
2	1	1	3.5	102.2	14.8				
2	1	7	0						
2	1	28	34.5	110.3	16.0				
2	1	56	0						
2	1	365	0						
2	1	1	3.5	104.6	15.2				
2	1	7	0						
2	1	28	34.5	111.8	16.2				
2	1	56	0						
2	1	365	0						
2	2	1	3.5	96.2	14.0				
2	2	7	0.0						
2	2	28	34.5	103.6	15.0				
2	2	56	0.0						
2	2	365	0.0						
2	2	1	3.5	101.7	14.8				
2	2	7	0.0						
2	2	28	34.5	102.2	14.8				
2	2	56	0.0						
2	2	365	0.0						
3	1	1	3.2	90.7	13.1				
3	1	7	0.0						
3	1	28	33.7	99.6	14.4				
3	1	56	65.5						
3	1	365	0						
3	1	1	3.2	85.3	12.4				
3	1	7	0						
3	1	28	33.7	94.9	13.8				
3	1	56	65.5						
3	1	365	0						
3	2	1	3.2	86.2	12.5				
3	2	7	0.0						
3	2	28	33.7	91.5	13.3				
3	2	56	65.5	99.5	14.4				
3	2	365	0.0						
3	2	1	3.2	78.2	11.3				
3	2	7	0.0						
3	2	28	33.7	91.3	13.2				
3	2	56	65.5	96.1	13.9				
3	2	365	0.0						
3	2	1	3.2						
3	2	7	0.0						
3	2	28	33.7						
3	2	56	65.5	91.6	13.3				
3	2	365	0.0						

STL 65-35

Steel 65-35				Strength	Strength	Average			
Stage	Batch	Age	Maturity	MPa	ksi	Unitweight	Strength	Strength	Stand Dev
1	1	1	1.8	48.0	7.0	lb/ft3	MPa	ksi	
1	1	28	32.2	56.9	8.3	281.1	56.2	8.148	6.3
1	1	365	414.6	68.1	9.9	280.6	66.3	9.617	7.0
1	1	1	1.8	49.7	7.2	281.5	71.9	10.420	3.0
1	1	28	32.2	60.0	8.7	0	0	Average	**5.4**
1	1	365	414.6	70.7	10.3	0	Strength	Strength	
1	2	1	1.8	49.4	7.2	0	MPa	ksi	
1	2	28	32.2	56.2	8.1	1.8	49.8	7.2	1.7
1	2	365	414.6	74.6	10.8	2.2	55.8	8.1	0.6
1	2	1	1.8	52.1	7.6	3.3	62.9	9.1	4.2
1	2	28	32.2	61.0	8.9	32.18	58.5	8.5	2.3
1	2	365	414.6	74.0	10.7	32.21	71.6	10.4	3.4
2	1	1	3.3	66.7	9.7	33.9	70.2	10.2	4.5
2	1	28	33.9	64.7	9.4	414.6	71.9	10.4	3.0
2	1	365	0.0						**2.8**
2	1	1	3.3	62.8	9.1				
2	1	28	33.9	73.0	10.6				
2	1	365	0.0						
2	1	1	3.3	64.9	9.4				
2	1	28	33.9	68.4	9.9				
2	1	365	0.0						
2	1	1	3.3	57.1	8.3				
2	1	28	33.9	74.6	10.8				
2	1	365	0.0						
3	1	1	2.2	55.2	8.0				
3	1	28	32.2	71.2	10.3				
3	1	365	0.0						
3	1	1	2.2	55.8	8.1				
3	1	28	32.2	68.3	9.9				
3	1	365	0.0						
3	1	1	2.2	56.4	8.2				
3	1	28	32.2	75.2	10.9				
3	1	365	0.0						

LWW 65-35-95

LWA 65-35-95				Strength	Strength	Average	0	0	
Stage	Batch	Age	Maturity	MPa	ksi	Unitweight	Strength	Strength	
1	1	1	2.2	71.8	10.4	lb/ft3	MPa	ksi	
1	1	7	9.0	77.6	11.3	124.8	79.5	11.531	
1	1	28	32.7	90.6	13.1	123.0	75.8	10.994	
1	1	56	64.6	92.0	13.3	125.1	91.3	13.239	
1	1	365	415.2	83.6	12.1	124.2	94.5	13.697	
1	1	1	2.2	65.7	9.5	122.2	90.6	13.137	
1	1	7	9.0	79.2	11.5	0	0	Average	
1	1	28	32.7	91.1	13.2	0	Strength	Strength	
1	1	56	64.6	91.5	13.3	0	MPa	ksi	
1	1	365	415.2	88.9	12.9	2.2	68.7	10.0	
1	2	1	2.2	62.6	9.1	3.3	90.9	13.2	
1	2	7	9.0	69.9	10.1	3.7	82.5	12.0	
1	2	28	32.7	84.9	12.3	9.0	75.8	11.0	
1	2	56	64.6	95.2	13.8	32.7	88.3	12.8	
1	2	365	415.2	94.1	13.6	33.2	94.1	13.6	
1	2	1	2.2	74.9	10.9	34.5	92.5	13.4	
1	2	7	9.0	76.6	11.1	64.6	92.9	13.5	
1	2	28	32.7	86.4	12.5	415.2	90.6	13.1	
1	2	56	64.6	92.8	13.5				
1	2	365	415.2	95.7	13.9		1	62.6	
2	1	1	3.7	81.2	11.8		7	69.9	
2	1	7	0				28	84.9	
2	1	28	34.5	90.7	13.2		56	91.5	
2	1	56	0				365	83.6	
2	1	365	0						
2	1	1	3.7	85.3	12.4				
2	1	7	0						
2	1	28	34.5	94.0	13.6				
2	1	56	0						
2	1	365	0						
2	1	1	3.7	81.2	11.8				
2	1	7	0						
2	1	28	34.5	92.9	13.5				
2	1	56	0						
2	1	365	0						
3	1	1	3.3	85.8	12.4				
3	1	7	0						
3	1	28	33.2	93.4	13.5				
3	1	56	0	97.3	14.1				
3	1	365	0						
3	1	1	3.3	93.5	13.6				
3	1	7	0						
3	1	28	33.2	95.0	13.8				
3	1	56	0	95.9	13.9				
3	1	365	0						
3	1	1	3.3	93.3	13.5				
3	1	7	0						
3	1	28	33.2	94.0	13.6				
3	1	56	0						
3	1	365	0						

NSC

NSC-plain				Strength	Strength	Average			
Stage	Batch	Age	Maturity	MPa	ksi	Unitweight	Strength	Strength	Stand Dev
1	1	1	0.9	8.2	1.2	lb/ft3	MPa	ksi	
1	1	7	7.7	22.3	3.2	146.4	8.9	1.3	1.8
1	1	28	31.4	28.5	4.1	146.5	24.6	3.6	1.7
1	1	56	63.3	32.1	4.7	148.2	29.0	4.2	1.6
1	1	365	413.9	37.1	5.4	147.6	33.8	4.9	2.4
1	1	1	0.9	8.6	1.2	146.2	37.6	5.5	0.7
1	1	7	7.7	24.9	3.6	0	0	Average	
1	1	28	31.4	25.8	3.7	0	Strength	Strength	
1	1	56	63.3	35.4	5.1	0	MPa	ksi	
1	1	365	413.9	37.8	5.5	0.9	7.5	1.1	
1	2	1	0.9	7.1	1.0	1.5	10.3	1.5	
1	2	7	7.7	25.1	3.6	7.7	24.6	3.6	
1	2	28	31.4	29.5	4.3	31.4	28.7	4.2	
1	2	56	63.3	31.4	4.6	32.3	29.2	4.2	
1	2	365	413.9	37.0	5.4	63.3	33.8	4.9	
1	2	1	0.9	6.1	0.9	413.9	37.6	5.5	
1	2	7	7.7	26.3	3.8				
1	2	28	31.4	31.2	4.5				
1	2	56	63.3	36.1	5.2				
1	2	365	413.9	38.5	5.6				
2	1	1	1.5	10.2	1.5				
2	1	7							
2	1	28	32.3	28.9	4.2				
2	1	56							
2	1	365							
2	1	1	1.5	10.0	1.5				
2	1	7							
2	1	28	32.3	29.5	4.3				
2	1	56							
2	1	365							
2	1	1	1.5	9.0	1.3				
2	1	7							
2	1	28	32.3	28.1	4.1				
2	1	56							
2	1	365							
2	1	1	1.5	11.7	1.7				
2	1	7							
2	1	28	32.3	30.4	4.4				
2	1	56							
2	1	365							

D.4. Elastic Modulus

	Density	Elastic Modulus age 1 day	Compressiv Strength age 1 day	Elastic Modulus age 28 day	Compressiv Strength age 28 day	Elastic Modulus age 1 day	Compressiv Strength age 1 day	Elastic Modulus age 28 day	Compressiv Strength age 28 day	fc28
	lb/ft3	psi	psi	psi	psi	kg/m3	GPa	MPa	GPa	MPa
Cement Matrix	141.2	5608527	15500	5693429	17394	2262	38.7	106.9	39.3	120.0
HP Matrix	138.0	5254310	13309	5561827	15172	2212	36.2	91.8	38.4	104.6
LWW 35-65	129.1	4523502	9662	4851396	11826	2068	31.2	66.6	33.5	81.6
LWW 65-35	123.0	4223773	9839	4834286	11255	1970	29.1	67.9	33.3	77.6
HP Matrix	138.0	5254310	13309	5561827	15172	2212	36.2	91.8	38.4	104.6
NWA 35-65	143.8	4630002	13255	5274882	15204	2304	31.9	91.4	36.4	104.9
NWA 65-35	143.8	4528978	12373	5026232	14460	2304	31.2	85.3	34.7	99.7
HP Matrix	138.0	5254310	13309	5561827	15172	2212	36.2	91.8	38.4	104.6
STL 35-65	202.8	4767927	6917	4531060	9573	3249	32.9	47.7	31.2	66.0
STL 65-35	277.4	6571691	7224	7484416	8489	4443	45.3	49.8	51.6	58.5
LWD 65-35	119.9	4074545	9250	4527801	10115	1921	28.1	63.8	31.2	69.8
LWW 65-35-95	123.5	4120810	9968	4618268	12797	1979	28.4	68.7	31.9	88.3

APPENDIX E

TEMPERATURE DEVELOPMENT

This appendix presents the thermocouple readings taken in the medium-scale study during the first 24 hours after casting

E.1 HP Matrix and Cement Matrix

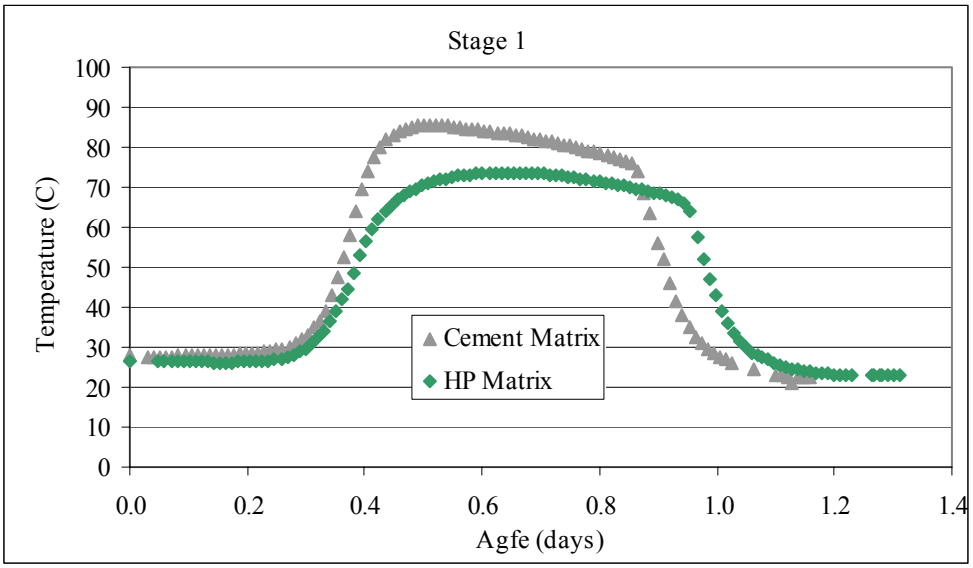

Figure E.1: Temperature history in HP Matrix and Cement Matrix under cold ambient conditions

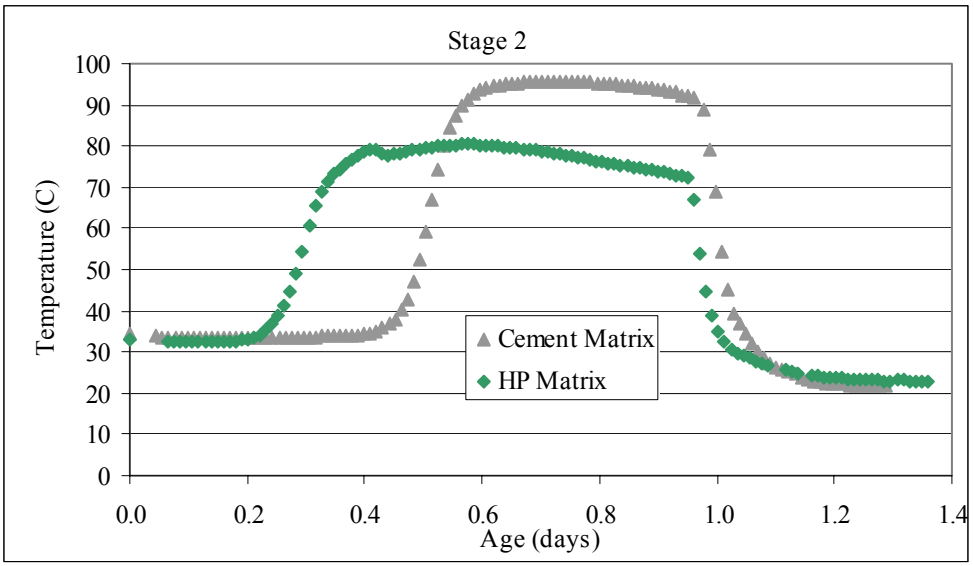

Figure E.2: Temperature history in HP Matrix and Cement Matrix under hot ambient conditions

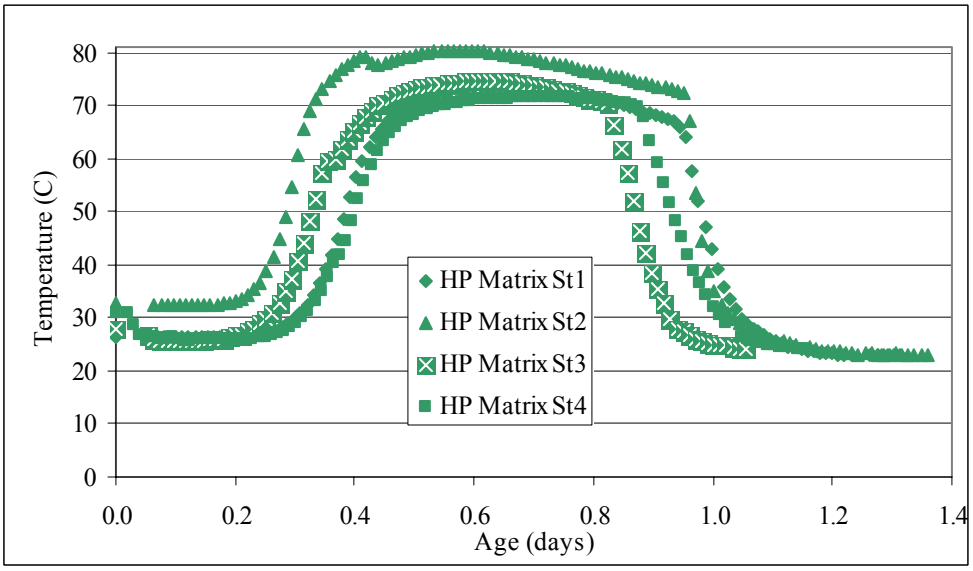

Figure E.3: Temperature history in HP Matrix under intermediate ambient conditions

E.2 LWW 35-65, NWA 35-65, and STL 35-65

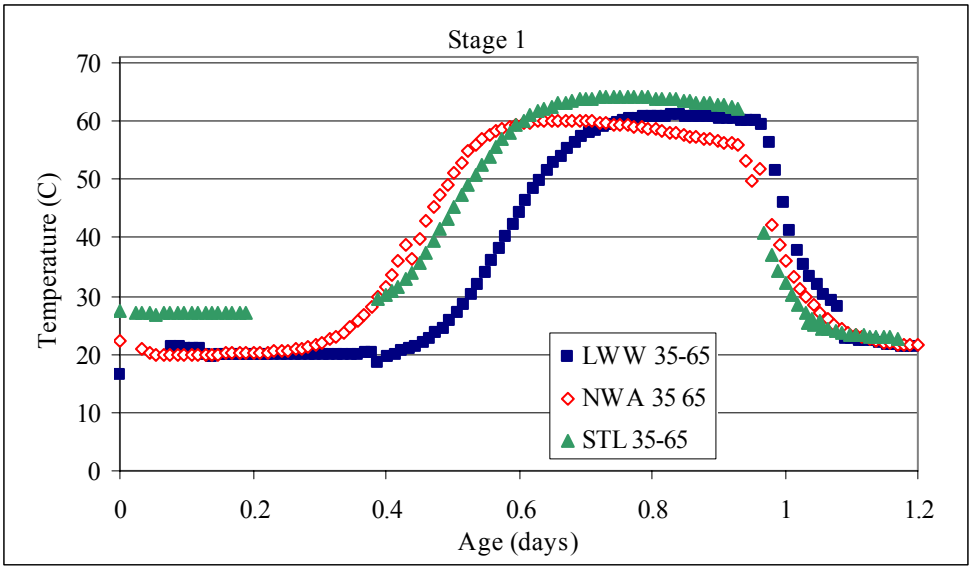

Figure E.4: Temperature history in LWW 35-65, NWA 35-65, and STL 35-65 mixtures under cold ambient conditions

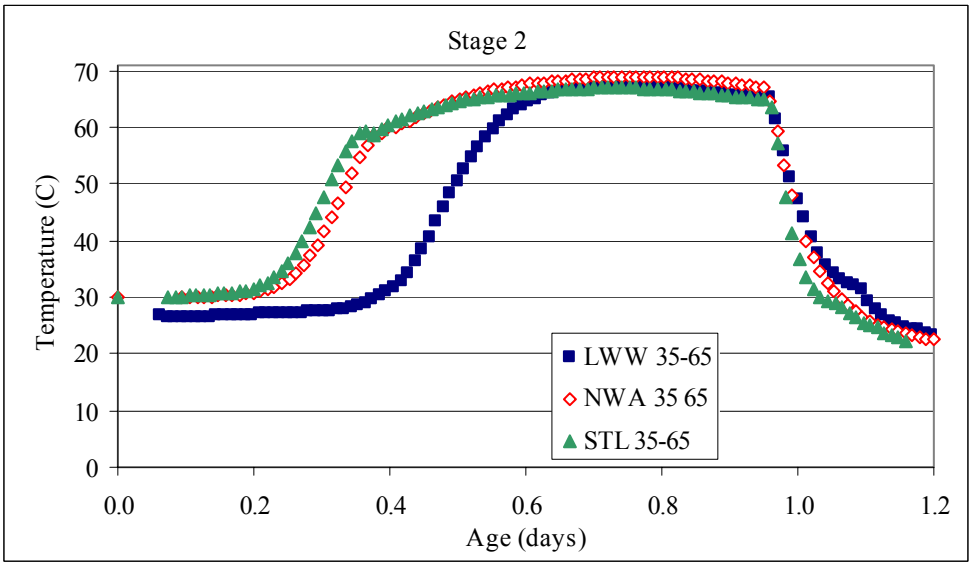

Figure E.5: Temperature history in LWW 35-65, NWA 35-65, and STL 35-65 mixtures under hot ambient conditions

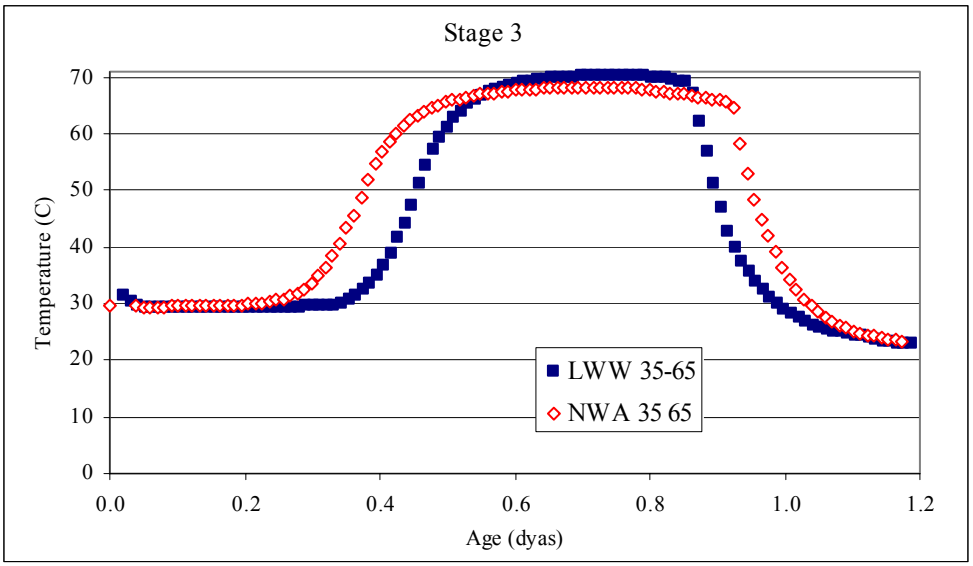

Figure E.6: Temperature history in LWW 35-65, NWA 35-65, and STL 35-65 mixtures under intermediate ambient conditions

E.2 LWW 65-35, NWA 65-35, and STL 65-35

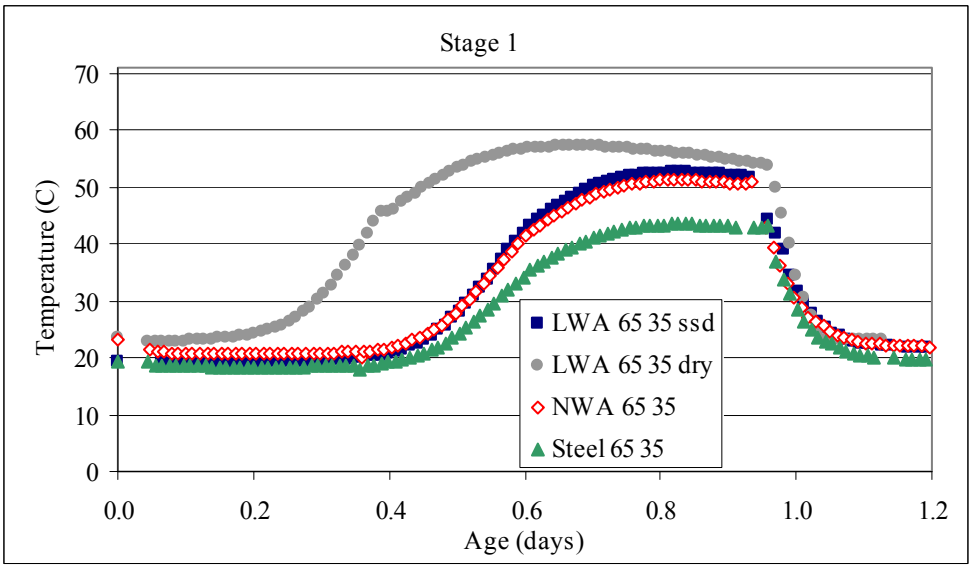

Figure E.7: Temperature history in LWW 65-35, NWA 65-35, and STL 65-35 mixtures under cold ambient conditions

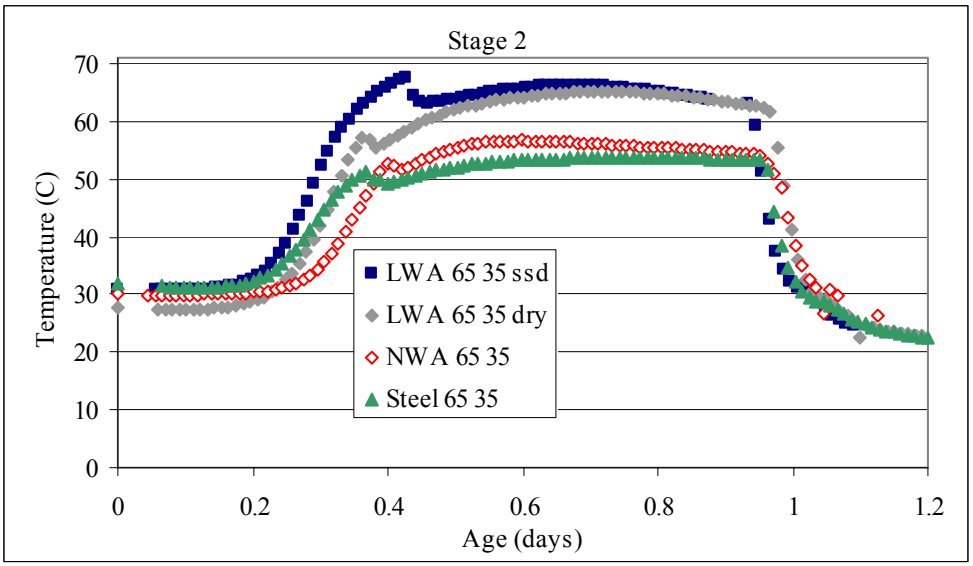

Figure E.8: Temperature history in LWW 65-35, NWA 65-35, and STL 65-35 mixtures under hot ambient conditions

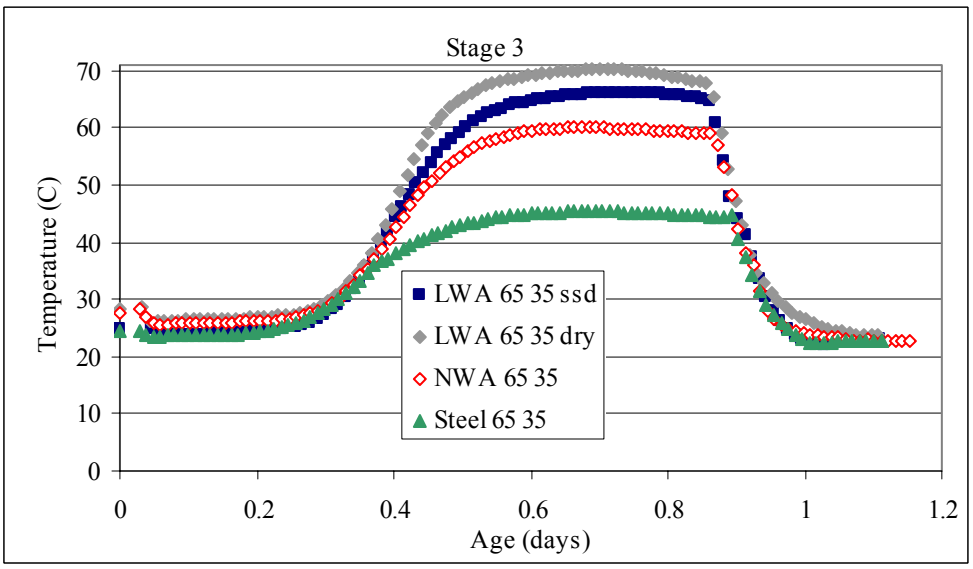

Figure E.9: Temperature history in LWW 65-35, NWA 65-35, and STL 65-35 mixtures under intermediate ambient conditions

This page intentionally left blank

APPENDIX F

CREEP AND SHRINKAGE RESULTS

Table F.1: Creep and shrinkage results for cement matrix in the medium-scale study

Stage 1	24h					Stage 2	24h						Stage1	28d			
	Total SH	Total SH	Spec Tot Cr	Spec Tot Cr	Spec Tot Cr		Total SH	Total SH	Autog SH	Basic Cr&S	Basic Cr&S	Total Cr&Sh		Total SH	Total SH	Autog SH	Autog SH
DAYS	1	2	3	4	5	DAYS	10	11	12	13	14	15	DAYS	6	7	8	9
0.0	0	0	0.000	0.000	0.000	0.0	0	0	0	0.000	0.000	0.000	0.0	0	0	0	0
0.0	-60	-70	0.000	0.001	-0.006	0.0	-25	-15	-20	-0.014	-0.013	-0.007	0.0	-5	23	-8	30
0.1	-80	-88	0.000	-0.005	-0.014	0.1	-28	-33	-62	-0.017	-0.016	-0.016	0.1	15	38	5	28
0.1	-80	-88	0.000	-0.017	-0.022	0.1	-20	-28	-90	-0.015	-0.015	-0.019	0.1	18	20	0	30
0.2	-100	-88	0.000	-0.021	-0.025	0.2	-18	-20	-68	-0.021	-0.021	-0.022	0.2	13	28	-10	28
0.2	-103	-93	0.000	-0.021	-0.023	0.2	-33	-30	-88	-0.017	-0.026	-0.019	0.2	15	30	-20	18
0.2	-105	-95	0.000	-0.022	-0.027	0.3	-58	-38	-83	-0.025	-0.026	-0.022	0.2	14	30	-21	20
0.6	-103	-113	0.000	-0.023	-0.030	0.7	-70	-38	-105	-0.028	-0.026	-0.031	0.5	10	33	-25	33
1.1	-123	-120	0.000	-0.034	-0.043	1.1	-65	-43	-108	-0.030	-0.034	-0.036	1.0	-28	0	-63	-13
2.1	-130	-118	0.000	-0.035	-0.043	2.0	-62	-28	-85	-0.039	-0.040	-0.039	2.4	-55	-30	-93	-33
3.2	-138	-143	0.000	-0.049	-0.055	3.3	-65	-55	-90	-0.042	-0.046	-0.047	3.1	-50	-22	-75	-33
4.3	-138	-135	0.000	-0.059	-0.060	4.1	-87	-65	-115	-0.041	-0.043	-0.046	4.1	-68	-45	-125	-58
5.2	-168	-158	0.000	-0.067	-0.065	5.3	-82	-58	-78	-0.051	-0.055	-0.053	5.4	-80	-38	-115	-48
6.3	-185	-178	0.000	-0.065	-0.065	6.1	-105	-88	-87	-0.049	-0.054	-0.053	6.1	-95	-43	-143	-63
10.4	-233	-218	0.000	-0.077	-0.077	9.1	-95	-60	-77	-0.057	-0.064	-0.062	9.0	-145	-98	-190	-118
14.2	-263	-228	0.000	-0.090	-0.087	14.2	-122	-93	-122	-0.062	-0.067	-0.069	14.5	-168	-145	-233	-158
21.3	-293	-265	0.000	-0.097	-0.093	21.2	-157	-130	-120	-0.074	-0.086	-0.084	21.5	-180	-168	-258	-175
28.1	-315	-290	0.000	-0.110	-0.103	28.1	-175	-130	-120	-0.078	-0.084	-0.087	28.2	-193	-213	-258	-203
41.9	-372	-365	0.000	-0.131	-0.121	42.1	-172	-143	-110	-0.089	-0.095	-0.103	42.5	-275	-288	-375	-263
56.6	-392	-396	0.000	-0.138	-0.126	55.9	-210	-193	-112	-0.108	-0.111	-0.110	56.1	-333	-320	-420	-285
70.3	-427	-428	0.000	-0.151	-0.134	70.4	-260	-235	-152	-0.115	-0.119	-0.123	71.4	-303	-318	-410	-283
83.9	-435	-441	0.000	-0.171	-0.142	84.0	-267	-243	-155	-0.120	-0.121	-0.126	84.2	-328	-348	-428	-305
98.2	-442	-458	0.000	-0.171	-0.150	98.0	-302	-270	-173	-0.125	-0.128	-0.134	98.5	-318	-328	-443	-300
112.1	-465	-511	0.000	-0.174	-0.148	111.9	-307	-275	-173	-0.131	-0.136	-0.139	112.0	-330	-337	-450	-311
120.1	-465	-498	0.000	-0.185	-0.165	120.0	-317	-285	-202	-0.131	-0.135	-0.141	120.2	-338	-343	-455	-318
140.0	-475	-523				140.2	-337	-288	-202	-0.137	-0.140	-0.148	140.0	-345	-368	-458	-333
167.8	-487	-538				168.3	-362	-325	-212	-0.144	-0.150	-0.160	168.2	-370	-383	-468	-345
195.9	-502	-556				197.9	-390	-365	-212	-0.153	-0.159	-0.167	196.1	-408	-433	-503	-388
223.8	-520	-568				225.1	-392	-373	-237	-0.157	-0.155	-0.167	224.4	-420	-448	-535	-403
252.3	-532	-576				255.3	-405	-360	-255	-0.154	-0.161	-0.184	252.0	-420	-463	-538	-410
280.2	-555	-601				280.0	-447	-395	-268	-0.161	-0.174	-0.185	280.1	-435	-458	-538	-415
308.2	-572	-618				308.0	-440	-385	-245	-0.170	-0.181	-0.189	307.7	-438	-472	-548	-429
335.9	-581	-648				335.9	-452	-395	-258	-0.174	-0.185	-0.193	335.7	-453	-496	-555	-446
364.9	-590	-644				365.4	-462	-398	-260	-0.174	-0.184	-0.195	365.1	-460	-500	-570	-455
419.9	-602	-641				418.8	-472	-400	-265	-0.179	-0.191	-0.202	420.2	-520	-515	-600	-478
500.1	-597	-636				500.4	0	0	0	0.000	0.000	0.000	501.1	-518	-528	-628	-498

Table F.2: Creep and shrinkage results for hp matrix in the medium-scale study loading at 24 hours of age

Stage 1	24h					Stage 2	24h					Stage 3	24h				
	Total SH	autog## SH	Spec Tot Cr	Spec Tot Cr	Spec Bas Cr		Total SH	Autog SH	Spec Bas Cr	Spec Bas Cr	Spec Tot Cr		Total SH	Autog SH	Spec Tot Cr	Spec Tot Cr	Spec Bas Cr
DAYS	1	2	3	4	5	DAYS	11	12	13	14	15	DAYS	26	27	28	29	30
0.00	0	0	0.000	0.000	0.000	0.00	0	0	0.000	0.000	0.000	0.00	0	0	0.000	0.000	0.000
0.04	-35	-28	0.004	0.012	-0.002	0.05	-25	20	-0.017	-0.019	-0.009	0.01	-10	-2	-0.018	-0.020	-0.016
0.10	-35	-43	0.017	0.019	0.012	0.09	-38	-10	-0.014	-0.017	-0.014	0.05	-13	-11	-0.020	-0.025	-0.018
0.13	-43	-40	0.024	0.026	0.019	0.13	-73	-10	-0.021	-0.017	-0.008	0.09	-15	-20	-0.022	-0.030	-0.021
0.16	-45	-45	0.021	0.028	0.024	0.19	-78	-30	-0.018	-0.020	-0.014	0.13	-15	-18	-0.025	-0.033	-0.025
0.20	-60	-45	-0.013	-0.011	-0.018	0.25	-50	10	-0.032	-0.029	-0.020	0.17	-15	-17	-0.027	-0.036	-0.028
0.25	-48	-33	0.027	0.022	0.013	0.30	-58	20	-0.031	-0.035	-0.018	0.21	-15	-15	-0.030	-0.038	-0.032
0.50	-60	-34	0.008	0.004	-0.002	0.48	-70	-10	-0.028	-0.034	-0.016	0.47	-28	-15	-0.036	-0.047	-0.037
1.09	-60	-38	0.002	-0.007	-0.010	1.0	-80	-10	-0.030	-0.040	-0.015	0.96	-28	-18	-0.050	-0.065	-0.051
2.01	-80	-55	-0.018	-0.023	-0.023	2.2	-73	-10	-0.039	-0.046	-0.027	2.0	-43	-20	-0.057	-0.080	-0.061
2.92	-85	-60	-0.021	-0.028	-0.026	3.0	-85	-10	-0.047	-0.047	-0.034	3.0	-50	-18	-0.064	-0.085	-0.065
4.25	-110	-58	-0.032	-0.029	-0.035	3.8	-103	-20	-0.050	-0.051	-0.042	4.1	-58	-10	-0.068	-0.093	-0.071
5.31	-110	-63	-0.026	-0.033	-0.035	5.1	-75	20	-0.058	-0.057	-0.038	5.2	-75	-15	-0.071	-0.098	-0.077
6.24	-113	-58	-0.028	-0.031	-0.038	6.2	-90	20	-0.063	-0.062	-0.039	6.1	-78	-15	-0.074	-0.103	-0.079
8.83	-123	-55	-0.036	-0.045	-0.046	9.0	-90	20	-0.060	-0.062	-0.046	9.1	-80	-8	-0.076	-0.108	-0.081
14.19	-143	-62	-0.047	-0.061	-0.064	14.1	-110	30	-0.072	-0.077	-0.061	13.8	-108	-15	-0.095	-0.131	-0.097
20.93	-198	-100	-0.038	-0.064	-0.055	21.0	-120	10	-0.088	-0.093	-0.074	21.3	-118	-15	-0.108	-0.147	-0.106
28.0	-205	-88	-0.051	-0.080	-0.061	28.0	-170	-40	-0.091	-0.094	-0.078	28.1	-123	-15	-0.123	-0.163	-0.120
41.9	-223	-88	-0.061	-0.095	-0.074	41.9	-190	-70	-0.105	-0.106	-0.097	41.0	-128	-10	-0.137	-0.180	-0.131
55.9	-323	-150	-0.064	-0.104	-0.086	56.4	-228	-80	-0.131	-0.132	-0.126	55.8	-140	-13	-0.154	-0.201	-0.143
70.0	-318	-158	-0.067	-0.112	-0.083	70.0	-260	-100	-0.132	-0.138	-0.121	69.7	-170	-10	0.000	0.000	0.000
84.2	-338	-178	-0.103	-0.139	-0.096	83.9	-275	-100	-0.137	-0.140	-0.130	84.1	-201	-3	0.000	0.000	0.000
98.5	-370	-195	-0.106	-0.153	-0.111	97.9	-290	-110	-0.141	-0.150	-0.139	97.7	-233	-5	0.000	0.000	0.000
112.2	-383	-205	-0.105	-0.151	-0.114	111.8	-320	-130	-0.144	-0.148	-0.140	112.1	-250	-11	0.000	0.000	0.000
120.4	-398	-213	-0.102	-0.153	-0.116	120.0	-330	-123	-0.153	-0.154	-0.145	119.8	-273	-14	0.000	0.000	0.000
140.3	-400	-215	0.000	0.000	0.000	138.2	-345	-140	-0.157	-0.158	-0.148	140.2	-288	-23	0.000	0.000	0.000
168.0	-423	-230				168.1	-348	-130				168.1	-278	-20	0.000	0.000	0.000
196.0	-425	-233				196.2	-365	-130				196.1	-283	-18	0.000	0.000	0.000
223.9	-450	-255				223.9	-362	-120				223.8	-290	-10	0.000	0.000	0.000
252.1	-475	-265				251.9	-391	-110				252.2	-298	-13	0.000	0.000	0.000
280.3	-485	-300				280.3	-408	-100				280.2	-293	-5	0.000	0.000	0.000
309.9	-495	-305				308.0	-453	-120				308.1	-300	-18	0.000	0.000	0.000
337.1	-510	-295				336.0	-455	-150				335.3	0	0	0.000	0.000	0.000
364.9	-511	-301				365.0	-453	-140				364.3	0	0	0.000	0.000	0.000
420.2	-513	-288				420.4	-480	-160				419.3	0	0	0.000	0.000	0.000
500.8	-525	-290				499.5	0	0				499.3	0	0	0.000	0.000	0.000

Table F.3: Creep and shrinkage results for hp matrix in the medium-scale study loading at 28 days of age

Stage 3	24h					Stage 4	24h	6x12's				Stage 1	28d				
	Total SH	Autog SH	Spec Tot Cr	Spec Tot Cr	Spec Bas Cr		Total SH	Total SH	Spec Tot Cr	Spec Tot Cr	Spec Tot Cr		Total SH	Autog SH	Spec Tot Cr	Spec Tot Cr	Spec Bas Cr
DAYS	36	37	38	39	40	DAYS	41	42	43	44	45	DAYS	6	7	8	9	u
0.00	0	0	0.000	0.000	0.000	0.00	0	0	0.000	0.000	0.000	0.00	0	0	0.000	0.000	0.000
0.04	2	-17	-0.022	-0.020	-0.018	0.04	-10	-7	-0.037	-0.035	-0.035	0.03	-13	-5	-0.006	-0.010	-0.009
0.08	2	-20	-0.026	-0.025	-0.021	0.08	-10	-15	-0.044	-0.043	-0.046	0.07	-18	-15	-0.022	-0.016	-0.007
0.13	2	-22	-0.029	-0.031	-0.025	0.13	-10	-22	-0.051	-0.051	-0.053	0.11	-2	-18	-0.031	-0.032	-0.008
0.17	0	-28	-0.031	-0.033	-0.026	0.17	-16	-28	-0.056	-0.055	-0.057	0.15	-5	-45	-0.039	-0.028	0.009
0.21	-3	-34	-0.033	-0.035	-0.028	0.21	-22	-34	-0.061	-0.059	-0.060	0.19	-15	-45	-0.037	-0.021	0.002
0.25	-5	-40	-0.035	-0.037	-0.029	0.25	-27	-40	-0.066	-0.063	-0.064	0.23	-18	-44	-0.034	-0.020	0.001
0.50	0	-40	-0.046	-0.046	-0.038	0.50	-27	-47	-0.075	-0.071	-0.072	0.48	-35	-40	-0.018	-0.015	-0.008
1.0	5	-40	-0.056	-0.057	-0.046	1.0	-40	-55	-0.084	-0.082	-0.082	1.09	-35	-35	-0.033	-0.021	-0.010
2.0	7	-37	-0.069	-0.072	-0.059	2.1	-62	-85	-0.093	-0.091	-0.091	2.49	-38	-45	-0.046	-0.032	-0.019
3.2	-8	-45	-0.074	-0.081	-0.064	3.2	-72	-97	-0.112	-0.108	-0.108	3.46	-60	-78	-0.037	-0.037	-0.022
4.2	-15	-40	-0.076	-0.082	-0.067	4.3	-80	-100	-0.124	-0.118	-0.118	4.05	-28	-50	-0.062	-0.048	-0.029
5.2	-28	-40	-0.082	-0.086	-0.072	5.2	-97	-112	-0.130	-0.128	-0.129	5.13	-48	-60	-0.062	-0.062	-0.034
6.2	-25	-45	-0.085	-0.091	-0.074	6.1	-97	-107	-0.133	-0.129	-0.128	6.44	-65	-60	-0.064	-0.061	-0.026
9.0	-45	-47	-0.096	-0.100	-0.083	9.0	-110	-112	-0.147	-0.144	-0.143	9.18	-88	-113	-0.086	-0.076	-0.028
15.0	-70	-45	-0.103	-0.108	-0.091	15.0	-147	-149	-0.169	-0.165	-0.164	14.35	-98	-93	-0.092	-0.077	-0.034
20.1	-80	-39	-0.116	-0.105	-0.087	21.2	-176	-197	-0.191	-0.182	-0.177	20.97	-135	-140	-0.093	-0.091	-0.047
30.9	-90	-32	-0.135	-0.116	-0.103	27.9	-204	-244	-0.211	-0.196	-0.192	28.01	-148	-145	-0.087	-0.084	-0.047
40.8	-165	-35	-0.124	-0.116	-0.118	40.8	-292	-299	-0.207	-0.190	-0.186	42.57	-195	-158	-0.090	-0.101	-0.067
59.2	-178	-77	-0.163	-0.155	-0.126	56.2	-371	-378	-0.248	-0.236	-0.230	56.03	-208	-188	-0.112	-0.119	-0.058
69.9	-190	-102	-0.161	-0.172	-0.145	69.9	-389	-366	-0.247	-0.238	-0.237	70.09	-230	-233	-0.119	-0.135	-0.056
84.3	-195	-92	-0.207	-0.175	-0.149	84.3	-394	-371	-0.258	-0.249	-0.246	84.40	-255	-233	-0.120	-0.133	-0.078
97.9	-205	-100	-0.214	-0.183	-0.153	97.9	-389	-381	-0.273	-0.259	-0.255	98.44	-293	-258	-0.106	-0.117	-0.080
111.9	-220	-107	-0.228	-0.198	-0.167	112.0	-399	-381	-0.279	-0.265	-0.262	112.38	-240	-203	-0.136	-0.148	-0.113
120.2	-228	-100	-0.229	-0.198	-0.169	120.2	-414	-386	-0.287	-0.274	-0.270	120.11	-238	-205	-0.147	-0.171	-0.115
139.9	-243	-110	-0.234	-0.204	-0.172	140.0	-421	-398	-0.291	-0.278	-0.274	140.04	-280	-228			
167.9	-238	-105	-0.246	-0.216	-0.181	167.9	-439	-401	-0.305	-0.291	-0.287	168.02	-298	-228			
196.3	-263	-112	-0.250	-0.224	-0.185	196.3	-456	-416	-0.318	-0.304	-0.300	196.37	-305	-233			
224.3	-270	-115	-0.254	-0.227	-0.185	224.3	-469	-416	-0.333	-0.318	-0.314	224.49	-320	-248			
252.3	-273	-107	-0.259	-0.231	-0.192	252.3	-501	-453	-0.335	-0.322	-0.317	253.41	-343	-273			
279.4	0	0	0.000	0.000	0.000	279.4	0	0	0.000	0.000	0.000	279.32	-348	-283			
307.4	0	0	0.000	0.000	0.000	307.4	0	0	0.000	0.000	0.000	308.04	-363	-295			
335.4	0	0	0.000	0.000	0.000	335.4	0	0	0.000	0.000	0.000	336.06	-385	-325			
364.4	0	0	0.000	0.000	0.000	364.4	0	0	0.000	0.000	0.000	365.14	-390	-325			
419.4	0	0	0.000	0.000	0.000	419.4	0	0	0.000	0.000	0.000	420.03	-408	-348			
499.4	0	0	0.000	0.000	0.000	499.4	0	0	0.000	0.000	0.000	500.03	-410	-368			

Table F.4: Creep and shrinkage results for LWW 65-35-95 in the medium-scale study loaded at 24 hours of age

Stage 1	24h					Stage 2	24h					Stage 3	24h				
	Total SH	Autog** SH	Spec Tot Cr	Spec Tot Cr	Spec Tot Cr		Total SH	Autog SH	Spec Bas Cr	Spec Bas Cr	Spec Tot Cr		Total SH	Autog SH	Spec Tot Cr	Spec Tot Cr	Spec Bas Cr
DAYS	1	2	3	4	5	DAYS	11	12	13	14	15	DAYS	21	22	23	24	25
0.0	0	0	0.000	0.000	0.000	0.0	0	0	0.000	0.000	0.000	0.0	0.000	0.000	0.000	0.000	0.000
0.0	-18	-27	-0.023	-0.022	-0.022	0.0	30	15	-0.010	-0.010	-0.013	0.0	9.990	59.963	-0.007	-0.007	-0.013
0.1	-15	-30	-0.037	-0.036	-0.037	0.1	30	18	-0.012	-0.012	-0.020	0.1	9.990	64.960	-0.009	-0.009	-0.015
0.1	-53	-45	-0.042	-0.037	-0.044	0.1	30	15	-0.021	-0.022	-0.030	0.1	9.990	69.957	-0.011	-0.011	-0.016
0.2	-33	-30	-0.043	-0.045	-0.050	0.2	20	23	-0.026	-0.025	-0.027	0.2	13.320	69.957	-0.011	-0.011	-0.016
0.2	-38	-30	-0.046	-0.044	-0.055	0.2	7	3	-0.024	-0.018	-0.029	0.2	16.650	69.957	-0.011	-0.011	-0.016
0.3	-35	-32	-0.056	-0.056	-0.055	0.3	20	15	-0.025	-0.017	-0.026	0.3	19.980	69.957	-0.011	-0.011	-0.016
1.1	-53	-40	-0.082	-0.086	-0.082	0.5	7	-8	-0.022	-0.017	-0.029	0.5	19.980	69.957	-0.013	-0.013	-0.017
2.2	-80	-57	-0.104	-0.111	-0.108	1.1	12	18	-0.036	-0.030	-0.033	1.0	14.985	69.957	-0.021	-0.022	-0.025
3.0	-95	-65	-0.120	-0.125	-0.119	2.2	5	15	-0.037	-0.026	-0.043	2.1	9.990	69.957	-0.027	-0.026	-0.031
4.3	-108	-62	-0.130	-0.144	-0.137	3.0	-20	-20	-0.037	-0.024	-0.041	2.9	19.980	79.950	-0.030	-0.034	-0.034
5.1	-138	-82	-0.137	-0.145	-0.139	3.9	-10	0	-0.047	-0.031	-0.050	4.0	4.995	59.963	-0.032	-0.035	-0.034
6.0	-128	-70	-0.146	-0.156	-0.149	5.3	-5	8	-0.059	-0.035	-0.059	5.0	0.000	59.963	-0.037	-0.037	-0.035
9.3	-175	-110	-0.171	-0.177	-0.176	6.1	-8	8	-0.054	-0.031	-0.060	6.2	4.995	69.957	-0.039	-0.039	-0.039
14.1	-220	-117	-0.187	-0.198	-0.196	9.3	-3	23	-0.059	-0.039	-0.060	9.0	14.985	69.957	-0.043	-0.044	-0.038
17.4	-220	-117	-0.188	-0.197	-0.192	14.0	-28	23	-0.070	-0.042	-0.064	14.2	9.989	49.969	-0.051	-0.048	-0.040
21.3	-255	-134	-0.179	-0.191	-0.188	20.9	-43	23	-0.057	-0.045	-0.062	20.8	-14.987	49.969	-0.055	-0.058	-0.052
27.9	-275	-144	-0.187	-0.199	-0.192	28.0	-35	35	-0.069	-0.058	-0.083	28.4	-29.972	39.975	-0.061	-0.064	-0.056
41.9	-315	-199	-0.202	-0.211	-0.201	41.9	-75	30	-0.082	-0.071	-0.098	42.1	-39.961	39.975	-0.072	-0.074	-0.063
55.9	-368	-242	-0.204	-0.213	-0.209	55.9	-108	25	-0.095	-0.080	-0.103	56.0	-39.961	69.957	-0.076	-0.077	-0.068
70.3	-348	-224	-0.218	-0.223	-0.219	69.8	-125	25	-0.098	-0.086	-0.110	69.8	-34.965	89.944	-0.080	-0.083	-0.072
84.3	-388	-249	-0.215	-0.236	-0.225	83.8	-125	28	-0.098	-0.091	-0.116	83.6	-41.959	91.943	-0.082	-0.085	-0.073
98.4	-418	-287	-0.230	-0.253	-0.233	97.8	-155	18	-0.099	-0.095	-0.116	97.8	-48.952	93.942	-0.084	-0.087	-0.073
112.4	-440	-289	-0.235	-0.250	-0.231	111.8	-163	18	-0.098	-0.104	-0.125	111.8	-55.946	95.941	-0.086	-0.090	-0.074
120.0	-470	-336	-0.233	-0.253	-0.230	119.9	-185	15	-0.096	-0.105	-0.123	120.2	-59.942	97.083	-0.087	-0.091	-0.075
140.3	-455	-331				140.5	-198	13				139.8	-69.932	99.938	-0.090	-0.095	-0.076
168.1	-465	-329				167.9	-228	8				167.8	-59.942	89.944	-0.099	-0.104	-0.076
195.9	-468	-329				196.1	-253	15				196.0	-79.923	119.926	-0.104	-0.109	-0.090
223.9	-478	-344				223.9	-268	18				223.8	-69.933	139.913	-0.107	-0.113	-0.093
254.5	-485	-351				252.2	-284	14				251.8	-94.907	149.907	-0.107	-0.114	-0.098
279.8	-505	-374				280.0	-300	10				279.8	-99.902	149.907	-0.109	-0.115	-0.098
307.9	-505	-376				307.9	-290	0				307.8	-99.903	159.901	-0.111	-0.117	-0.099
336.0	-515	-391				336.8	-290	5				335.8	-99.903	149.907	-0.113	-0.120	-0.098
365.0	-527	-408				364.8	-298	8				364.4	0.000	0.000	0.000	0.000	0.000
419.2	-538	-416				419.9	-313	13				419.4	0.000	0.000	0.000	0.000	0.000
500.0	-548	-428				499.5	0	0				499.4	0.000	0.000	0.000	0.000	0.000

Table F.5: Creep and shrinkage results for LWW 65-35-95 in the medium-scale study loaded at 28 days of age

Stage 1	28d					Stage 2	28d					
	Total SH	Total SH	Spec Tot Cr	Spec Tot Cr	Spec Bas Cr		Total SH	Autog SH	Spec Bas Cr	Spec Bas Cr	Spec Tot Cr	
DAYS	6	7	8	9	10	DAYS	16	17	18	19	20	
0.0	0	0	0.000	0.000	0.000	0.0	0	0	0.000	0.000	0.000	
0.0	0	5	-0.002	-0.006	-0.003	0.0	-10	-13	-0.010	-0.012	-0.012	
0.1	-2	-25	0.001	-0.005	-0.002	0.1	2	35	-0.024	-0.021	-0.016	
0.1	0	-22	-0.005	-0.008	-0.003	0.1	-10	2	-0.019	-0.014	-0.017	
0.2	3	-5	-0.012	-0.016	-0.008	0.2	-10	15	-0.020	-0.016	-0.014	
0.2	15	5	-0.011	-0.022	-0.011	0.2	5	25	-0.025	-0.021	-0.020	
0.2	11	3	-0.011	-0.022	-0.013	0.3	5	25	-0.025	-0.021	-0.020	
0.5	-15	-7	-0.015	-0.020	-0.011	0.5	8	28	-0.023	-0.022	-0.021	
1.0	-33	-33	-0.017	-0.023	-0.010	1.2	10	50	-0.026	-0.029	-0.025	
2.1	-35	-40	-0.026	-0.028	-0.017	2.1	-8	20	-0.024	-0.022	-0.023	
3.2	-45	-45	-0.028	-0.036	-0.025	2.9	-23	10	-0.026	-0.023	-0.024	
4.2	-47	-60	-0.037	-0.043	-0.028	3.9	-30	13	-0.027	-0.025	-0.029	
5.1	-60	-60	-0.045	-0.049	-0.033	4.9	-15	13	-0.030	-0.026	-0.033	
6.0	-65	-90	-0.042	-0.044	-0.031	5.8	-25	8	-0.030	-0.030	-0.037	
9.1	-50	-68	-0.051	-0.056	-0.042	8.8	-35	8	-0.030	-0.029	-0.033	
14.0	-80	-105	-0.065	-0.071	-0.050	13.9	-33	20	-0.039	-0.040	-0.046	
21.2	-92	-133	-0.068	-0.073	-0.052	20.8	-55	18	-0.054	-0.050	-0.055	
28.0	-102	-150	-0.078	-0.084	-0.058	28.1	-68	23	-0.061	-0.061	-0.064	
42.5	-110	-163	-0.088	-0.088	-0.061	41.8	-105	13	-0.063	-0.061	-0.071	
56.5	-135	-198	-0.102	-0.101	-0.071	56.0	-108	33	-0.070	-0.068	-0.077	
70.1	-157	-220	-0.104	-0.099	-0.070	69.8	-155	13	-0.077	-0.073	-0.077	
84.2	-182	-225	-0.109	-0.110	-0.075	84.1	-170	15	-0.088	-0.083	-0.086	
98.2	-185	-248	-0.112	-0.109	-0.076	97.7	-195	0	-0.087	-0.082	-0.093	
112.2	-175	-278	-0.110	-0.105	-0.074	113.3	-203	3	-0.087	-0.081	-0.090	
120.1	-182	-285	-0.117	-0.109	-0.083	120.0	-205	5	-0.088	-0.083	-0.092	
140.5	-190	-298				139.8	-230	-7	-0.093	-0.083	-0.097	
168.1	-207	-313				167.9	-253	-7	-0.102	-0.095	-0.096	
196.2	-230	-335				196.2	-260	-7	-0.103	-0.090	-0.092	
231.3	-232	-335				223.7	-290	-19	-0.096	-0.090	-0.082	
252.5	-247	-338				252.1	-320	-30	-0.099	-0.088	-0.082	
280.2	-260	-345				280.8	-333	-27	-0.103	-0.093	-0.085	
308.3	-267	-345				307.8	-360	-30	-0.110	-0.099	-0.091	
335.7	-345	-353				335.8	-378	-27	-0.110	-0.098	-0.087	
364.7	-345	-360				364.9	-380	-20	-0.113	-0.099	-0.088	
420.3	-355	-365				419.7	-413	-20	-0.116	-0.105	-0.094	
500.1	-365	-378				499.3	0	0	0.000	0.000	0.000	

Table F.6: Creep and shrinkage results for LWW 65-35 in the medium-scale study loaded at 24 hours of age

Stage 1	24h					Stage 2	24h					Stage 3	24h				
	Total SH	Autog## SH	Spec Tot Cr	Spec Tot Cr	Spec Tot Cr		Total SH	Autog SH	Spec Bas Cr	Spec Bas Cr	Spec Tot Cr		Total SH	Autog SH	Spec Tot Cr	Spec Tot Cr	Spec Bas Cr
DAYS	1	2	3	4	5	DAYS	11	12	13	14	15	DAYS	26	27	28	29	30
0.00	0	0	0.000	0.000	0.000	0.00	0	0	0.000	0.000	0.000	0.00	0	0	0.000	0.000	0.000
0.04	-15	-13	-0.012	-0.014	-0.030	0.05	-13	-8	-0.005	-0.005	-0.005	0.04	-3	5	-0.002	-0.007	-0.006
0.08	0	-7	-0.019	-0.022	-0.039	0.09	-10	-5	-0.008	-0.011	-0.011	0.08	0	6	-0.004	-0.009	-0.008
0.13	-23	-23	-0.026	-0.030	-0.042	0.13	-8	5	-0.012	-0.015	-0.011	0.13	2	8	-0.007	-0.010	-0.010
0.2	-25	-47	-0.029	-0.033	-0.046	0.2	35	22	-0.013	-0.019	-0.019	0.2	3	8	-0.008	-0.012	-0.010
0.2	-30	-37	-0.030	-0.034	-0.049	0.2	-5	-18	-0.010	-0.015	-0.017	0.2	4	9	-0.009	-0.013	-0.010
0.3	-38	-43	-0.032	-0.031	-0.047	0.3	13	-5	-0.009	-0.015	-0.018	0.3	5	10	-0.010	-0.015	-0.010
0.5	-35	-47	-0.041	-0.040	-0.052	0.5	-5	-8	-0.012	-0.019	-0.019	0.5	0	15	-0.012	-0.022	-0.013
1.0	-33	-47	-0.049	-0.052	-0.064	1.1	13	10	-0.019	-0.027	-0.029	1.0	-8	23	-0.018	-0.027	-0.017
2.1	-50	-43	-0.067	-0.060	-0.076	2.1	48	35	-0.017	-0.029	-0.037	2.1	-8	38	-0.028	-0.037	-0.025
3.0	-48	-37	-0.068	-0.059	-0.078	3.2	45	55	-0.019	-0.031	-0.039	3.2	0	65	-0.030	-0.045	-0.032
4.0	-70	-47	-0.072	-0.059	-0.083	4.2	43	57	-0.022	-0.038	-0.045	4.2	0	70	-0.035	-0.048	-0.034
5.1	-75	-40	-0.080	-0.064	-0.090	5.0	50	80	-0.025	-0.042	-0.046	5.2	-5	70	-0.040	-0.054	-0.040
6.0	-80	-30	-0.092	-0.078	-0.104	5.9	60	75	-0.024	-0.041	-0.052	6.0	-20	68	-0.040	-0.054	-0.043
9.0	-93	-57	-0.094	-0.076	-0.105	9.2	48	82	-0.031	-0.053	-0.060	8.8	-25	75	-0.044	-0.061	-0.044
14.2	-153	-53	-0.115	-0.094	-0.128	13.8	60	95	-0.035	-0.060	-0.066	13.8	-33	73	-0.052	-0.073	-0.045
20.3	-173	-73	-0.124	-0.106	-0.137	20.9	48	85	-0.039	-0.062	-0.079	21.1	-25	75	-0.061	-0.083	-0.047
28.4	-168	-83	-0.139	-0.118	-0.143	28.0	18	92	-0.048	-0.075	-0.080	27.9	-88	75	-0.054	-0.078	-0.048
42.1	-213	-87	-0.145	-0.127	-0.155	41.8	-13	95	-0.059	-0.082	-0.087	42.2	-138	75	-0.056	-0.083	-0.051
56.2	-210	-103	-0.157	-0.138	-0.158	55.8	-12	105	-0.064	-0.084	-0.091	56.8	-138	75	-0.069	-0.097	-0.058
69.9	-265	-160	-0.159	-0.148	-0.158	69.8	-30	105	-0.071	-0.088	-0.103	70.2	-180	78	-0.072	-0.101	-0.065
84.7	-293	-170	-0.164	-0.151	-0.169	83.8	-50	57	-0.067	-0.085	-0.112	83.9	-183	60	-0.077	-0.107	-0.059
98.3	-338	-210	-0.145	-0.131	-0.166	98.4	-68	45	-0.064	-0.088	-0.113	99.8	-193	55	-0.082	-0.115	-0.058
111.9	-323	-203	-0.159	-0.132	-0.170	114.3	-58	62	-0.068	-0.091	-0.121	111.8	-200	53	-0.083	-0.118	-0.063
120.0	-333	-220	-0.157	-0.137	-0.170	120.0	-68	65	-0.071	-0.097	-0.124	119.8	-223	55	-0.087	-0.123	-0.066
140.1	-315	-197				139.8	-78	65				139.8	-238	55	-0.086	-0.121	-0.070
168.0	-343	-206				167.8	-90	77				170.8	-255	43	-0.096	-0.126	-0.073
195.9	-355	-223				195.9	-103	85				195.8	-260	50	-0.097	-0.129	-0.076
223.9	-373	-246				224.9	-133	84				223.8	-280	50	-0.101	-0.132	-0.078
251.9	-375	-253				253.3	-150	82				251.8	-303	50	-0.099	-0.132	-0.084
280.3	-383	-263				279.2	-143	82				279.4	0	0	0.000	0.000	0.000
308.3	-400	-280				308.4	-170	75				307.4	0	0	0.000	0.000	0.000
336.3	-400	-296				336.3	-175	92				335.4	0	0	0.000	0.000	0.000
364.5	-396	-298				364.8	-185	97				364.4	0	0	0.000	0.000	0.000
419.9	-408	-306				420.3	-198	85				419.4	0	0	0.000	0.000	0.000
500.9	-430	-316				499.5	0	0				499.4	0	0	0.000	0.000	0.000

Table F.7: Creep and shrinkage results for LWW 65-35 in the medium-scale study loaded at 28 days of age

Stage 1	28d					Stage 2	28d					Stage 2	28d	6x12			
	Total SH	Total SH	Spec Tot Cr	Spec Tot Cr	Spec Tot Cr		Total SH	Autog SH	Spec Bas Cr	Spec Bas Cr	Spec Tot Cr		Total SH	Total SH	Spec Tot Cr	Spec Tot Cr	Spec Tot Cr
DAYS	6	7	8	9	10	DAYS	16	17	18	19	20	DAYS	21	22	23	24	25
0.00	0	0	0.000	0.000	0.000	0.00	0	0	0.000	0.000	0.000	0.0	0	0	0.000	0.000	0.000
0.04	-18	-10	-0.007	-0.005	-0.012	0.04	-5	-5	-0.013	-0.012	-0.009	0.0	3	-5	-0.029	-0.033	-0.004
0.08	-10	-7	-0.015	-0.010	-0.013	0.09	-4	-4	-0.017	-0.015	-0.018	0.1	-2	-15	-0.035	-0.037	-0.012
0.13	-8	-17	-0.016	-0.011	-0.012	0.13	-2	-3	-0.021	-0.018	-0.027	0.1	-7	-25	-0.041	-0.041	-0.021
0.17	-23	-35	-0.018	-0.012	-0.012	0.17	-4	-3	-0.021	-0.017	-0.024	0.2	-7	-17	-0.040	-0.041	-0.017
0.21	-15	-33	-0.015	-0.013	-0.010	0.21	-6	-3	-0.022	-0.017	-0.021	0.2	-6	-8	-0.040	-0.042	-0.013
0.25	-18	-33	-0.016	-0.014	-0.011	0.26	-8	-2	-0.022	-0.016	-0.017	0.3	-5	0	-0.039	-0.042	-0.010
0.50	-33	-38	-0.022	-0.020	-0.018	0.52	-23	-20	-0.025	-0.015	-0.024	0.5	-18	-25	-0.044	-0.048	-0.018
1.51	-25	-33	-0.029	-0.029	-0.028	1.02	-15	-2	-0.032	-0.021	-0.026	1.0	-17	-25	-0.045	-0.054	-0.022
2.56	-48	-53	-0.042	-0.038	-0.034	2.13	-43	-17	-0.034	-0.024	-0.029	2.1	-20	-40	-0.051	-0.060	-0.035
3.40	-25	-40	-0.046	-0.043	-0.041	3.01	-45	-30	-0.032	-0.021	-0.031	3.0	-27	-40	-0.055	-0.062	-0.030
4.45	-35	-48	-0.044	-0.042	-0.049	3.92	-53	-35	-0.037	-0.027	-0.032	3.9	-35	-65	-0.052	-0.057	-0.037
5.42	-7	-25	-0.052	-0.051	-0.049	4.91	-60	-30	-0.041	-0.029	-0.031	4.9	-33	-70	-0.053	-0.060	-0.040
6.48	-17	-53	-0.045	-0.046	-0.042	6.07	-65	-32	-0.038	-0.029	-0.033	6.0	-35	-60	-0.060	-0.066	-0.038
9.16	-53	-80	-0.054	-0.051	-0.050	8.83	-68	-35	-0.044	-0.032	-0.043	8.8	-48	-70	-0.061	-0.074	-0.046
14.20	-50	-73	-0.058	-0.054	-0.051	14.12	-100	-42	-0.052	-0.047	-0.044	14.1	-50	-75	-0.067	-0.082	-0.050
21.47	-53	-90	-0.076	-0.072	-0.066	20.84	-108	-42	-0.054	-0.048	-0.047	20.8	-48	-90	-0.067	-0.083	-0.053
28.08	-65	-78	-0.077	-0.073	-0.067	27.84	-128	-35	-0.057	-0.052	-0.044	27.8	-53	-80	-0.076	-0.091	-0.056
42.55	-108	-120	-0.079	-0.080	-0.074	41.85	-138	-30	-0.064	-0.055	-0.052	41.9	-65	-85	-0.083	-0.097	-0.058
56.20	-125	-123	-0.082	-0.079	-0.070	55.97	-160	-33	-0.071	-0.057	-0.059	56.0	-80	-125	-0.086	-0.105	-0.072
70.48	-163	-155	-0.093	-0.095	-0.084	69.84	-168	-38	-0.069	-0.057	-0.065	69.8	-78	-125	-0.103	-0.120	-0.084
84.09	-178	-180	-0.091	-0.098	-0.080	87.24	-175	-25	-0.078	-0.071	-0.075	87.2	-90	-135	-0.106	-0.118	-0.082
99.32	-188	-185	-0.100	-0.103	-0.091	98.00	-185	-38	-0.076	-0.068	-0.075	98.0	-98	-145	-0.106	-0.120	-0.082
112.19	-185	-163	-0.108	-0.110	-0.101	112.26	-188	-30	-0.079	-0.072	-0.076	112.3	-98	-145	-0.121	-0.132	-0.094
120.10	-178	-173	-0.107	-0.108	-0.098	119.82	-205	-33	-0.084	-0.073	-0.073	119.8	-103	-150	-0.123	-0.134	-0.094
140.41	-180	-180	0.000	0.000	0.000	139.98	-208	-30	-0.086	-0.079	-0.083	140.0	-110	-150			
168.09	-180	-188	0.000	0.000	0.000	168.03	-218	-18	-0.091	-0.084	-0.085	168.0	-100	-140			
196.11	-180	-200	0.000	0.000	0.000	195.84	-253	-20	-0.099	-0.085	-0.088	195.8	-118	-179			
224.09	-188	-210	0.000	0.000	0.000	224.16	-288	-20	-0.107	-0.087	-0.090	223.9	-135	-215			
252.44	-210	-205	0.000	0.000	0.000	252.04	-288	-32	-0.101	-0.084	-0.090	252.0	-145	-219			
280.05	-210	-210	0.000	0.000	0.000	280.08	-283	-33	-0.102	-0.085	-0.093	280.1	-133	-217			
308.07	-218	-220	0.000	0.000	0.000	307.83	-303	-50	-0.101	-0.082	-0.092	307.8	-140	-219			
335.67	-210	-229	0.000	0.000	0.000	335.99	-335	-50	-0.103	-0.082	-0.088	336.0	-155	-219			
364.67	-220	-241	0.000	0.000	0.000	365.12	-333	-50	-0.102	-0.083	-0.094	365.1	-148	-214			
420.10	-240	-253	0.000	0.000	0.000	419.81	-348	-77	-0.099	-0.080	-0.097	419.8	-153	-224			
500.34	-260	-263	0.000	0.000	0.000	499.46	0	0	0.000	0.000	0.000	499.4	0	0			

Table F.8: Creep and shrinkage results for LWD 65-35 in the medium-scale study loaded at 24 hours of age

Stage 1 24h						Stage 2 24h						Stage 3 24h					
	Total SH	Total SH	Spec Tot Cr	Spec Tot Cr	Spec bas Cr		Total SH	Autog SH	Spec Bas Cr	Spec Bas Cr	Spec Tot Cr		Total SH	Autog SH	Spec Tot Cr	Spec Tot Cr	Spec Bas Cr
DAYS	11	12	13	14	15	DAYS	21	22	23	24	25	DAYS	36	37	38	39	40
0.00	0	0	0.000	0.000	0.000	0.00	0	0	0.000	0.000	0.000	0.00	0	0	0.000	0.000	0.000
0.04	-23	-35	0.008	0.007	0.001	0.05	12	-13	-0.028	-0.019	-0.041	0.04	2	-5	-0.027	-0.021	-0.024
0.08	-35	-63	0.006	0.000	0.020	0.09	-17	-20	-0.057	-0.039	-0.051	0.08	0	-8	-0.035	-0.027	-0.033
0.14	-25	-50	-0.006	-0.018	-0.008	0.14	-15	-38	-0.061	-0.037	-0.060	0.13	-3	-10	-0.043	-0.033	-0.041
0.18	-50	-53	0.002	-0.019	-0.015	0.17	-17	-38	-0.065	-0.041	-0.062	0.17	-6	-15	-0.048	-0.038	-0.046
0.21	-53	-53	0.003	-0.017	-0.017	0.22	-17	-43	-0.064	-0.037	-0.068	0.21	-9	-20	-0.053	-0.043	-0.050
0.25	-50	-52	0.002	-0.015	-0.016	0.25	-20	-58	-0.064	-0.042	-0.074	0.26	-13	-25	-0.058	-0.048	-0.055
0.50	-50	-55	-0.014	-0.024	-0.016	0.61	-22	-50	-0.075	-0.048	-0.086	0.50	-18	-23	-0.067	-0.050	-0.066
1.0	-65	-65	-0.033	-0.055	-0.041	1.2	-8	-33	-0.079	-0.055	-0.099	1.0	-10	-15	-0.083	-0.065	-0.078
2.0	-63	-60	-0.066	-0.084	-0.053	2.0	-8	-40	-0.076	-0.060	-0.111	2.1	-13	-18	-0.099	-0.073	-0.088
3.4	-90	-70	-0.076	-0.098	-0.072	3.0	-40	-50	-0.088	-0.069	-0.116	3.0	-18	-15	-0.111	-0.084	-0.098
4.3	-95	-73	-0.090	-0.098	-0.081	4.2	-30	-55	-0.092	-0.062	-0.130	4.0	-35	-15	-0.116	-0.091	-0.108
4.9	-98	-65	-0.089	-0.101	-0.082	5.1	-32	-35	-0.107	-0.080	-0.140	5.2	-38	-20	-0.124	-0.095	-0.113
6.1	-113	-80	-0.111	-0.118	-0.103	6.2	-30	-13	-0.117	-0.093	-0.155	6.2	-35	-20	-0.133	-0.104	-0.120
9.3	-145	-117	-0.122	-0.136	-0.108	9.0	-57	-43	-0.129	-0.089	-0.168	9.2	-40	-18	-0.145	-0.115	-0.130
14.2	-138	-110	-0.142	-0.158	-0.114	14.0	-82	-48	-0.133	-0.101	-0.181	13.8	-55	-20	-0.155	-0.122	-0.140
20.9	-140	-112	-0.166	-0.176	-0.123	21.0	-92	-50	-0.146	-0.116	-0.197	20.6	-80	-24	-0.154	-0.119	-0.138
27.9	-220	-177	-0.158	-0.175	-0.127	28.2	-127	-70	-0.161	-0.123	-0.224	28.2	-89	-24	-0.152	-0.117	-0.138
42.7	-235	-200	-0.188	-0.207	-0.157	41.9	-135	-60	-0.176	-0.140	-0.243	42.2	-98	-24	-0.166	-0.123	-0.134
56.4	-240	-232	-0.197	-0.216	-0.145	56.3	-150	-70	-0.178	-0.147	-0.252	54.8	-112	-20	-0.182	-0.141	-0.144
70.0	-297	-240	-0.200	-0.206	-0.159	70.0	-162	-70	-0.184	-0.152	-0.261	69.9	-121	-28	-0.205	-0.163	-0.170
84.3	-260	-235	-0.230	-0.228	-0.169	83.9	-192	-75	-0.193	-0.163	-0.275	83.8	-133	-30	-0.224	-0.180	-0.184
98.1	-327	-292	-0.213	-0.223	-0.165	98.1	-189	-78	-0.197	-0.165	-0.286	97.8	-128	-30	-0.229	-0.182	-0.190
112.1	-295	-285	-0.220	-0.240	-0.162	109.9	-207	-80	-0.205	-0.171	-0.293	111.8	-130	-30	-0.232	-0.191	-0.190
119.9	-267	-277	-0.240	-0.250	-0.169	119.9	-219	-78	-0.210	-0.174	-0.299	119.8	-125	-20	-0.237	-0.197	-0.193
140.1	-297	-295				140.3	-227	-80				139.8	-130	-20	-0.238	-0.199	-0.194
167.9	-302	-305				168.8	-229	-75				167.8	-138	-15	-0.243	-0.206	-0.202
195.9	-322	-312				196.2	-229	-73				195.8	-138	-18	-0.250	-0.212	-0.203
224.6	-325	-330				223.5	-227	-86				223.8	-158	-15	-0.252	-0.209	-0.206
252.0	-350	-355				251.5	-275	-100				251.7	-165	-15	-0.258	-0.218	-0.212
280.2	-357	-362				279.9	-284	-118				279.4	0	0	0.000	0.000	0.000
308.0	-357	-370				308.3	-272	-110				307.4	0	0	0.000	0.000	0.000
336.3	-400	-375				336.3	-314	-130				335.4	0	0	0.000	0.000	0.000
365.2	-400	-387				364.5	-319	-135				364.4	0	0	0.000	0.000	0.000
420.9	-392	-390				421.3	-316	-125				419.4	0	0	0.000	0.000	0.000
500.1	-382	-392				499.5	0	0				499.4	0	0	0.000	0.000	0.000

Table F.9: Creep and shrinkage results for LWD 65-35 in the medium-scale study loaded at 28 days of age

Stage 1	28d					Stage 2	28d					Stage 2	28d	6x12			
	Total SH	Total	Spec Tot Cr	Spec Tot Cr	Spec Total Cr		Total SH	Autog SH	Spec Bas Cr	Spec Bas Cr	Spec Tot Cr		Total SH	Total SH	Spec Tot Cr	Spec Tot Cr	Spec Tot Cr
DAYS	16	17	18	19	20	DAYS	26	27	28	29	30	DAYS	31	32	33	34	35
0.0	0	0	0.000	0.000	0.000	0.0	0	0	0.000	0.000	0.000	0.00	0	0	0.000	0.000	0.000
0.0	-22	-13	-0.001	0.000	-0.008	0.0	3	-17	0.006	0.001	-0.006	0.04	-7	-5	-0.037	-0.036	-0.043
0.1	-27	-5	-0.006	-0.003	-0.016	0.1	-8	-29	0.000	-0.004	-0.008	0.08	-4	1	-0.041	-0.040	-0.048
0.1	-22	5	-0.012	-0.004	-0.016	0.1	-18	-40	-0.005	-0.009	-0.009	0.13	0	8	-0.045	-0.043	-0.052
0.2	-27	-20	-0.009	-0.009	-0.014	0.2	-20	-43	-0.003	-0.009	-0.010	0.17	-3	2	-0.046	-0.046	-0.055
0.2	-27	-8	-0.011	-0.011	-0.018	0.2	-21	-44	-0.003	-0.009	-0.011	0.21	-7	-4	-0.047	-0.049	-0.058
0.3	-29	-10	-0.012	-0.012	-0.019	0.2	-23	-47	-0.002	-0.009	-0.012	0.25	-10	-10	-0.048	-0.052	-0.060
0.5	-37	-28	-0.017	-0.018	-0.024	0.5	-15	-47	0.000	-0.011	-0.019	0.49	-20	-7	-0.062	-0.061	-0.071
1.0	-100	-55	-0.025	-0.031	-0.045	1.3	-33	-40	-0.008	-0.021	-0.029	1.28	-25	-22	-0.076	-0.069	-0.078
2.1	-99	-70	-0.025	-0.034	-0.040	2.3	-53	-42	-0.015	-0.026	-0.034	2.28	-37	-32	-0.083	-0.081	-0.082
3.0	-124	-115	-0.041	-0.041	-0.046	3.3	-63	-47	-0.015	-0.022	-0.038	3.30	-57	-50	-0.084	-0.081	-0.092
4.5	-122	-95	-0.046	-0.053	-0.065	4.0	-63	-45	-0.020	-0.029	-0.043	4.04	-50	-60	-0.091	-0.087	-0.100
5.5	-169	-133	-0.053	-0.054	-0.062	5.3	-73	-35	-0.023	-0.028	-0.044	5.27	-55	-60	-0.092	-0.088	-0.104
6.6	-152	-113	-0.058	-0.068	-0.075	6.0	-68	-35	-0.022	-0.029	-0.048	6.02	-68	-65	-0.091	-0.092	-0.101
9.6	-152	-115	-0.069	-0.074	-0.079	9.1	-93	-40	-0.033	-0.038	-0.061	9.12	-77	-92	-0.102	-0.101	-0.113
14.6	-132	-108	-0.067	-0.078	-0.087	14.0	-128	-50	-0.038	-0.048	-0.069	13.95	-100	-102	-0.112	-0.119	-0.130
23.6	-162	-173	-0.092	-0.099	-0.088	20.9	-153	-60	-0.043	-0.053	-0.069	20.93	-122	-122	-0.126	-0.132	-0.143
28.5	-167	-183	-0.092	-0.098	-0.091	27.9	-150	-62	-0.046	-0.055	-0.078	27.90	-115	-125	-0.129	-0.134	-0.147
42.1	-209	-195	-0.088	-0.095	-0.097	41.9	-175	-72	-0.055	-0.059	-0.088	41.92	-122	-128	-0.144	-0.145	-0.161
57.3	-214	-215	-0.097	-0.103	-0.104	55.9	-210	-77	-0.061	-0.064	-0.092	55.89	-165	-173	-0.145	-0.150	-0.165
70.2	-224	-255	-0.123	-0.125	-0.111	70.0	-218	-77	-0.071	-0.076	-0.108	69.99	-177	-173	-0.160	-0.171	-0.183
84.4	-234	-260	-0.122	-0.128	-0.121	82.9	-233	-85	-0.076	-0.080	-0.118	82.88	-185	-183	-0.167	-0.174	-0.194
98.3	-244	-265	-0.111	-0.120	-0.115	98.3	-240	-92	-0.073	-0.082	-0.116	98.31	-187	-180	-0.170	-0.176	-0.194
112.0	-254	-270	-0.140	-0.148	-0.143	112.3	-240	-87	-0.078	-0.088	-0.120	112.30	-210	-208	-0.178	-0.183	-0.202
120.1	-264	-275				120.3	-253	-87	-0.078	-0.088	-0.119	120.25	-205	-208	-0.181	-0.187	-0.209
140.3	-274	-280				140.2	-260	-90	-0.083	-0.094	-0.122	140.16	-218	-213	-0.186	-0.192	-0.213
168.4	-284	-285				168.0	-268	-90	-0.093	-0.105	-0.136	167.96	-215	-213			
197.7	-294	-290				195.9	-289	-103	-0.089	-0.103	-0.136	195.49	-243	-215			
224.1	-304	-305				223.9	-304	-117	-0.088	-0.109	-0.138	223.49	-248	-226			
252.2	-294	-323				252.2	-323	-130	-0.081	-0.104	-0.139	252.23	-235	-240			
280.5	-291	-313				279.9	-320	-132	-0.080	-0.105	-0.144	279.91	-250	-260			
307.7	-311	-327				307.9	-328	-127	-0.082	-0.103	-0.142	307.90	-250	-265			
336.4	-331	-348				336.0	-335	-132	-0.084	-0.105	-0.146	335.94	-248	-275			
365.1	-336	-350				365.3	-338	-127	-0.086	-0.106	-0.146	365.26	-265	-288			
420.1	-349	-368				419.9	-358	-130	-0.093	-0.113	-0.152	419.85	-273	-303			
501.6	-366	-383				499.5	0	0	0.000	0.000	0.000	499.49	0	0			

Table F.10: Creep and shrinkage results for NWA 65-35 in the medium-scale study loaded at 24 hours of age

Stage 1	24h					Stage 2	24h					Stage 3	24h				
	Total SH	Autog## SH	Spec Tot Cr	Spec Tot Cr	Spec Bas Cr		Total SH	Autog SH	Spec Bas Cr	Spec Bas Cr	Spec Tot Cr		Total SH	Autog SH	Spec Tot Cr	Spec Tot Cr	Spec Bas Cr
DAYS	11	12	13	14	15	DAYS	16	17	18	19	20	DAYS	31	32	33	34	35
0.0	0	0	0.000	0.000	0.000	0.00	0	0	0.000	0.000	0.000	0.00	0	0	0.000	0.000	0.000
0.0	-23	-20	-0.024	-0.021	-0.023	0.0	17	25	-0.006	-0.006	-0.006	0.0	-8	-10	-0.012	-0.012	-0.012
0.1	-8	-20	-0.032	-0.029	-0.024	0.1	15	5	-0.009	-0.007	-0.015	0.1	-11	-6	-0.015	-0.015	-0.015
0.1	-18	-10	-0.039	-0.034	-0.035	0.1	15	10	-0.011	-0.008	-0.015	0.1	-15	-3	-0.017	-0.018	-0.018
0.2	-25	-10	-0.042	-0.039	-0.036	0.2	18	0	-0.019	-0.015	-0.024	0.2	-15	-1	-0.020	-0.021	-0.021
0.2	-45	-30	-0.039	-0.038	-0.036	0.2	5	10	-0.021	-0.016	-0.023	0.2	-15	1	-0.024	-0.024	-0.024
0.2	-33	10	-0.048	-0.044	-0.046	0.2	-5	15	-0.026	-0.020	-0.024	0.3	-15	2	-0.027	-0.028	-0.028
0.5	-45	0	-0.057	-0.046	-0.056	0.5	-5	-5	-0.022	-0.017	-0.029	0.5	-20	-7	-0.034	-0.037	-0.033
1.0	-50	0	-0.082	-0.064	-0.064	1.1	10	5	-0.034	-0.025	-0.041	1.1	-18	-7	-0.045	-0.046	-0.040
2.1	-75	0	-0.088	-0.080	-0.082	2.0	-20	-10	-0.042	-0.032	-0.045	2.1	-15	-10	-0.054	-0.053	-0.046
3.0	-95	-30	-0.100	-0.091	-0.097	3.0	-20	-10	-0.045	-0.034	-0.049	3.1	-28	-15	-0.060	-0.061	-0.051
4.3	-135	-70	-0.106	-0.096	-0.091	3.9	0	25	-0.053	-0.037	-0.055	4.0	-35	-25	-0.066	-0.064	-0.056
5.1	-143	-90	-0.109	-0.099	-0.088	4.9	-25	-5	-0.048	-0.037	-0.055	4.9	-40	-25	-0.070	-0.066	-0.057
6.0	-143	-80	-0.113	-0.104	-0.095	5.8	-40	5	-0.054	-0.039	-0.052	6.2	-58	-35	-0.068	-0.068	-0.057
9.2	-173	-110	-0.131	-0.122	-0.110	9.0	-27	5	-0.061	-0.041	-0.067	10.0	-73	-42	-0.082	-0.076	-0.068
13.0	-205	-120	-0.136	-0.129	-0.124	13.9	-58	5	-0.066	-0.051	-0.070	14.1	-78	-45	-0.102	-0.088	-0.103
20.4	-243	-170	-0.151	-0.143	-0.130	20.9	-63	15	-0.075	-0.058	-0.082	20.8	-88	-50	-0.104	-0.091	-0.102
28.3	-260	-190	-0.154	-0.147	-0.129	27.9	-83	15	-0.081	-0.060	-0.084	28.1	-97	-55	-0.106	-0.094	-0.100
41.9	-315	-200	-0.169	-0.157	-0.142	41.8	-88	5	-0.084	-0.066	-0.093	42.0	-117	-65	-0.111	-0.100	-0.097
55.9	-338	-200	-0.178	-0.165	-0.155	55.8	-90	5	-0.087	-0.066	-0.094	56.8	-136	-75	-0.116	-0.106	-0.094
70.4	-355	-220	-0.183	-0.172	-0.155	69.8	-108	10	-0.098	-0.073	-0.102	70.1	-155	-85	-0.117	-0.110	-0.090
84.3	-353	-250	-0.188	-0.167	-0.145	83.7	-133	0	-0.103	-0.079	-0.106	84.0	-163	-102	-0.116	-0.113	-0.087
98.3	-398	-290	-0.194	-0.170	-0.148	97.8	-145	5	-0.105	-0.084	-0.107	97.9	-175	-107	-0.119	-0.118	-0.088
112.3	-388	-300	-0.197	-0.175	-0.146	112.4	-148	10	-0.103	-0.084	-0.108	111.8	-195	-90	-0.120	-0.118	-0.098
120.4	-425	-320	-0.188	-0.172	-0.148	119.8	-153	10	-0.104	-0.085	-0.109	119.8	-200	-90	-0.120	-0.118	-0.101
140.0	-403	-280				139.8	-165	0				140.2	-225	-107	-0.124	-0.121	-0.107
170.0	-413	-300				168.1	-183	10				168.8	-230	-100	-0.127	-0.123	-0.108
195.8	-428	-300				195.9	-188	10				195.8	-228	-100	-0.128	-0.124	-0.108
223.8	-430	-310				223.4	-213	2				223.8	-238	-100	-0.133	-0.130	-0.114
251.9	-435	-310				252.0	-215	-5				251.8	-243	-100	-0.134	-0.132	-0.117
280.2	-440	-310				279.9	-238	20				279.4	0	0	0.000	0.000	0.000
308.4	-453	-300				308.8	-240	20				307.4	0	0	0.000	0.000	0.000
336.3	-465	-310				336.3	-238	25				335.4	0	0	0.000	0.000	0.000
364.9	-463	-300				364.8	-245	20				364.4	0	0	0.000	0.000	0.000
420.0	-463	-290				420.3	-248	25				419.4	0	0	0.000	0.000	0.000
500.0	-465	-290				499.4	0	0				499.4	0	0	0.000	0.000	0.000

Table F.11: Creep and shrinkage results for NWA 65-35 in the medium-scale study loaded at 28 days of age

Stage 1	28d					Stage 2	28d					Stage 2	28d	6x12			
	Total SH	Autog## SH	Spec Tot Cr	Spec Tot Cr	Spec bas Cr		Total SH	Autog SH	Spec Bas Cr	Spec Bas Cr	Spec Tot Cr		Total SH	Total SH	Spec Tot Cr	Spec Tot Cr	Spec Tot Cr
DAYS	6	7	8	9	10	DAYS	21	22	23	24	25	DAYS	26	27	28	29	30
0.0	0	0	0.000	0.000	0.000	0.0	0	0	0.000	0.000	0.000	0.0	0	0	0.000	0.000	0.000
0.0	2	3	0.004	0.005	0.005	0.0	-12	-10	-0.018	-0.019	-0.011	0.0	7	15	-0.023	-0.024	-0.020
0.1	-2	-33	-0.003	-0.005	0.005	0.1	-14	-13	-0.019	-0.021	-0.015	0.1	9	12	-0.024	-0.026	-0.023
0.1	-45	-35	0.005	0.003	0.003	0.1	-15	-15	-0.020	-0.024	-0.018	0.1	10	10	-0.024	-0.028	-0.026
0.2	-43	-40	0.002	-0.003	0.004	0.2	-13	-10	-0.022	-0.025	-0.019	0.2	13	11	-0.029	-0.029	-0.028
0.2	-43	-38	-0.001	-0.003	0.001	0.2	-12	-5	-0.025	-0.026	-0.021	0.2	17	12	-0.034	-0.031	-0.030
0.3	-43	-38	-0.002	-0.004	0.001	0.3	-10	0	-0.028	-0.027	-0.022	0.3	20	12	-0.039	-0.032	-0.032
0.5	-45	-38	-0.009	-0.010	-0.004	0.5	-17	-3	-0.028	-0.027	-0.026	0.5	5	0	-0.046	-0.047	-0.043
1.4	-40	-38	-0.014	-0.019	-0.014	1.0	-47	-10	-0.035	-0.034	-0.031	1.0	10	-3	-0.049	-0.049	-0.044
2.5	-48	-35	-0.013	-0.019	-0.012	1.9	-60	-18	-0.038	-0.036	-0.032	1.9	-7	-28	-0.045	-0.047	-0.047
3.2	-73	-50	-0.015	-0.026	-0.018	2.9	-60	-13	-0.039	-0.038	-0.042	2.9	-25	-45	-0.046	-0.046	-0.048
4.4	-78	-78	-0.020	-0.032	-0.018	4.0	-70	-13	-0.041	-0.044	-0.043	4.0	-17	-38	-0.048	-0.051	-0.052
5.4	-103	-93	-0.024	-0.035	-0.023	5.0	-70	-8	-0.048	-0.048	-0.044	5.0	-20	-30	-0.053	-0.053	-0.052
6.5	-120	-93	-0.021	-0.033	-0.022	5.8	-62	5	-0.053	-0.050	-0.047	5.8	-22	-30	-0.053	-0.055	-0.053
9.6	-88	-88	-0.040	-0.048	-0.031	8.8	-77	-23	-0.050	-0.047	-0.047	8.8	-30	-43	-0.061	-0.062	-0.061
14.2	-120	-133	-0.042	-0.051	-0.032	13.8	-107	-35	-0.054	-0.056	-0.053	13.8	-47	-50	-0.067	-0.071	-0.063
21.4	-118	-118	-0.046	-0.059	-0.041	20.8	-129	-18	-0.067	-0.069	-0.061	20.8	-72	-78	-0.066	-0.070	-0.064
28.4	-135	-143	-0.055	-0.060	-0.047	28.1	-107	-3	-0.070	-0.073	-0.066	28.1	-65	-75	-0.069	-0.070	-0.070
42.0	-195	-193	-0.058	-0.060	-0.043	41.9	-149	-28	-0.074	-0.076	-0.072	41.9	-82	-103	-0.070	-0.080	-0.079
56.6	-180	-175	-0.066	-0.071	-0.057	56.1	-172	-43	-0.080	-0.080	-0.079	56.1	-102	-125	-0.076	-0.083	-0.086
70.1	-250	-223	-0.070	-0.073	-0.051	69.8	-177	-45	-0.086	-0.084	-0.085	69.8	-110	-130	-0.082	-0.089	-0.090
84.1	-258	-233	-0.091	-0.076	-0.055	85.4	-189	-35	-0.090	-0.090	-0.085	85.3	-115	-133	-0.085	-0.090	-0.092
98.5	-230	-228	-0.105	-0.082	-0.055	98.2	-207	-35	-0.094	-0.087	-0.087	98.1	-125	-138	-0.087	-0.089	-0.091
112.4	-278	-228	-0.076	-0.082	-0.062	111.8	-222	-43	-0.100	-0.091	-0.094	111.8	-142	-150	-0.090	-0.095	-0.095
120.3	-275	-228	-0.077	-0.082	-0.061	120.2	-219	-43	-0.100	-0.091	-0.096	120.2	-160	-163	-0.091	-0.097	-0.093
140.4	-285	-225				140.0	-241	-58	-0.105	-0.096	-0.096	140.0	-175	-183	-0.090	-0.096	-0.095
168.1	-308	-228				168.2	-249	-50	-0.111	-0.099	-0.100	168.2	-180	-198			
196.1	-313	-225				195.8	-271	-53	-0.113	-0.099	-0.110	195.8	-175	-206			
224.1	-318	-220				224.2	-266	-65	-0.118	-0.105	-0.111	224.2	-170	-215			
253.3	-325	-225				252.8	-261	-68	-0.121	-0.110	-0.117	252.9	-172	-203			
280.4	-325	-245				279.8	-269	-75	-0.123	-0.112	-0.120	279.8	-182	-210			
308.1	-330	-258				307.9	-261	-80	-0.124	-0.110	-0.122	307.8	-180	-210			
336.1	-336	-271				335.8	-264	-80	-0.123	-0.109	-0.121	335.7	-182	-208			
365.1	-342	-280				364.8	-269	-85	-0.121	-0.109	-0.122	364.8	-180	-213			
420.4	-350	-285				420.1	-284	-95	-0.125	-0.113	-0.126	420.1	-195	-213			
500.5	-333	-270				499.4	0	0	0.000	0.000	0.000	499.4	0	0			

Table F.12: Creep and shrinkage results for STL 65-35 in the medium-scale study loaded at 24 hours of age

Stage 1 24h						Stage 2 24h						Stage 3 24h					
	Total SH	Total SH	Spec Tot Cr	Spec Tot Cr	Spec Bas Cr		Total SH	Autog SH	Spec Bas Cr	Spec Bas Cr	Spec Tot Cr		Total SH	Autog SH	Spec Tot Cr	Spec Tot Cr	Spec Bas Cr
DAYS	1	2	3	4	5	DAYS	11	12	13	14	15	DAYS	21	22	23	24	25
0.0	0	0	0.000	0.000	0.000	0.0	0	0	0.000	0.000	0.000	0.00	0.000	0.000	0.000	0.000	0.000
0.0	-10	5	-0.013	-0.011	-0.010	0.0	-3	-15	-0.016	-0.021	-0.012	0.04	2.501	10.029	-0.020	-0.018	-0.016
0.1	-8	15	-0.026	-0.017	-0.016	0.1	-27	-27	-0.025	-0.034	-0.021	0.08	6.250	13.780	-0.024	-0.021	-0.020
0.15	-20	23	-0.033	-0.020	-0.020	0.12	-25	-35	-0.020	-0.028	-0.033	0.13	9.999	17.532	-0.028	-0.024	-0.025
0.18	-24	23	-0.035	-0.026	-0.023	0.16	-32	-45	-0.022	-0.030	-0.038	0.17	9.999	20.029	-0.029	-0.029	-0.029
0.21	-27	23	-0.037	-0.031	-0.026	0.20	-45	-65	-0.033	-0.030	-0.025	0.21	9.998	22.527	-0.031	-0.035	-0.033
0.2	-33	13	-0.041	-0.030	-0.024	0.3	-40	-65	-0.033	-0.029	-0.021	0.25	9.997	25.025	-0.033	-0.040	-0.038
0.5	-43	0	-0.044	-0.039	-0.025	0.5	-37	-70	-0.033	-0.027	-0.023	0.50	-5.015	37.526	-0.043	-0.047	-0.051
1.0	-45	13	-0.049	-0.043	-0.033	1.0	-37	-60	-0.037	-0.035	-0.032	1.11	-7.517	32.534	-0.058	-0.060	-0.059
2.0	-60	3	-0.068	-0.056	-0.046	2.1	-37	-65	-0.040	-0.035	-0.034	2.26	-10.019	30.034	-0.077	-0.078	-0.071
3.2	-83	-20	-0.076	-0.064	-0.048	3.0	-47	-77	-0.040	-0.036	-0.033	3.01	-5.019	35.033	-0.080	-0.082	-0.076
3.8	-100	-20	-0.075	-0.065	-0.054	4.2	-52	-77	-0.045	-0.033	-0.037	4.10	-17.526	25.042	-0.087	-0.088	-0.079
5.1	-110	-35	-0.084	-0.073	-0.054	5.0	-60	-72	-0.056	-0.052	-0.047	5.03	-15.027	25.044	-0.091	-0.094	-0.081
6.3	-118	-38	-0.099	-0.087	-0.069	6.2	-50	-60	-0.058	-0.053	-0.053	6.16	-20.030	25.037	-0.104	-0.096	-0.086
10.2	-125	-38	-0.094	-0.102	-0.075	9.1	-30	-52	-0.062	-0.053	-0.065	9.20	-22.530	25.042	-0.116	-0.112	-0.104
13.9	-140	-58	-0.121	-0.103	-0.074	14.2	-40	-60	-0.056	-0.049	-0.060	13.81	-32.537	27.543	-0.130	-0.125	-0.112
21.1	-155	-83	-0.121	-0.114	-0.081	21.0	-37	-52	-0.070	-0.061	-0.074	20.83	-30.038	27.543	-0.137	-0.133	-0.115
28.2	-143	-88	-0.147	-0.136	-0.106	27.9	-45	-55	-0.069	-0.066	-0.074	27.78	-45.047	25.044	-0.149	-0.143	-0.128
41.9	-158	-88	-0.152	-0.135	-0.108	42.0	-50	-50	-0.073	-0.068	-0.076	41.96	-42.544	35.039	-0.154	-0.144	-0.132
56.3	-178	-148	-0.159	-0.166	-0.128	55.9	-57	-55	-0.081	-0.074	-0.085	55.80	-50.045	37.533	-0.160	-0.153	-0.136
71.3	-180	-158	-0.162	-0.174	-0.128	69.9	-60	-42	-0.091	-0.082	-0.090	70.23	-65.057	40.026	-0.162	-0.153	-0.140
84.8	-205	-163	-0.221	-0.195	-0.140	83.9	-75	-57	-0.090	-0.082	-0.095	83.79	-71.556	25.060	-0.163	-0.152	-0.146
98.2	-205	-173	-0.216	-0.195	-0.127	97.9	-105	-70	-0.099	-0.086	-0.096	97.79	-78.055	27.555	-0.167	-0.162	-0.149
112.2	-198	-170	-0.209	-0.203	-0.144	112.4	-95	-65	-0.104	-0.087	-0.102	111.79	-83.307	30.051	-0.173	-0.170	-0.143
120.0	-193	-159	-0.215	-0.183	-0.143	119.9	-102	-75	-0.105	-0.090	-0.102	119.79	-86.838	32.546	-0.176	-0.174	-0.162
140.2	-205	-148				140.1	-100	-72				139.88	-87.558	32.547	-0.181	-0.165	-0.149
167.9	-225	-215				168.4	-122	-75				167.84	-90.060	20.065	-0.181	-0.167	-0.149
195.8	-215	-213				196.1	-120	-77				195.91	-90.057	22.559	-0.186	-0.171	-0.151
223.8	-215	-215				224.2	-124	-66				223.84	-72.544	62.547	-0.189	-0.174	-0.157
252.2	-218	-218				252.1	-128	-81				251.70	-80.050	42.555	-0.191	-0.174	-0.151
280.3	-220	-230				279.9	-132	-90				279.79	-80.051	45.054	-0.195	-0.178	-0.154
307.8	-233	-240				308.0	-135	-82				307.78	-92.559	35.059	-0.199	-0.178	-0.159
335.4	-232	-243				336.4	-137	-87				335.41	0.000	0.000	0.000	0.000	0.000
364.4	-231	-246				364.9	-142	-92				364.41	0.000	0.000	0.000	0.000	0.000
420.9	-215	-263				420.4	-137	-87				419.41	0.000	0.000	0.000	0.000	0.000
501.3	-220	-255				499.5	0	0				499.41	0.000	0.000	0.000	0.000	0.000

Table F.13: Creep and shrinkage results for STL 65-35 in the medium-scale study loaded at 28 days of age

Stage 1	28d					Stage 2	28d					
	Total SH	Total SH	Spec Tot Cr	Spec Tot Cr	Spec Tot Cr		Total SH	Autog SH	Spec Bas Cr	Spec Bas Cr	Spec Tot Cr	
DAYS	6	7	8	9	10	DAYS	16	17	18	19	20	
0.0	0	0	0.000	0.000	0.000	0.0	0	0	0.000	0.000	0.000	
0.0	3	-7	0.009	0.001	-0.020	0.0	-2	8	-0.017	-0.017	-0.013	
0.1	-3	-15	-0.002	-0.012	-0.026	0.1	3	10	-0.017	-0.008	-0.016	
0.1	-10	-10	-0.008	-0.014	-0.017	0.1	-2	0	-0.010	-0.009	-0.015	
0.2	13	3	-0.003	-0.016	-0.016	0.2	0	3	-0.013	-0.006	-0.016	
0.2	13	-5	-0.006	-0.010	-0.014	0.2	-5	0	-0.012	-0.011	-0.012	
0.2	12	-5	-0.008	-0.011	-0.016	0.2	2	-1	-0.011	-0.011	-0.015	
0.5	7	-2	-0.017	-0.015	-0.031	0.5	-7	-7	-0.009	-0.013	-0.016	
1.0	-20	-20	-0.013	-0.016	-0.022	1.0	-12	-5	-0.015	-0.013	-0.014	
2.4	-20	-5	-0.027	-0.026	-0.018	2.0	-35	-8	-0.016	-0.014	-0.014	
3.4	-50	-10	-0.027	-0.039	-0.043	3.0	-45	-33	-0.013	-0.008	-0.018	
4.2	-50	-28	-0.027	-0.040	-0.046	4.1	-25	-23	-0.018	-0.012	-0.028	
5.0	-60	-40	-0.018	-0.031	-0.043	5.2	-40	-20	-0.025	-0.017	-0.031	
6.1	-47	-33	-0.035	-0.044	-0.051	6.0	-45	-30	-0.023	-0.013	-0.029	
9.3	-37	-23	-0.033	-0.052	-0.048	9.0	-40	-28	-0.023	-0.013	-0.032	
14.1	-47	-30	-0.032	-0.053	-0.056	14.3	-57	-25	-0.033	-0.027	-0.034	
21.5	-80	-70	-0.042	-0.066	-0.055	21.1	-57	-25	-0.032	-0.026	-0.037	
28.5	-87	-85	-0.046	-0.065	-0.065	28.2	-72	-28	-0.038	-0.030	-0.036	
44.6	-93	-93	-0.056	-0.084	-0.081	42.0	-80	-35	-0.039	-0.027	-0.044	
56.4	-90	-105	-0.070	-0.100	-0.090	55.9	-97	-55	-0.037	-0.024	-0.041	
70.4	-100	-123	-0.067	-0.105	-0.080	70.0	-97	-55	-0.043	-0.024	-0.048	
84.2	-113	-153	-0.058	-0.095	-0.074	84.0	-90	-58	-0.040	-0.024	-0.054	
98.5	-113	-153	-0.057	-0.102	-0.090	101.4	-97	-63	-0.047	-0.026	-0.053	
112.3	-97	-150	-0.067	-0.100	-0.087	112.1	-102	-63	-0.048	-0.026	-0.058	
120.0	-93	-155	-0.071	-0.103	-0.089	120.3	-107	-65	-0.049	-0.027	-0.060	
140.1	-107	-175				139.9	-97	-68	-0.051	-0.031	-0.063	
168.0	-103	-183				168.3	-105	-70	-0.050	-0.029	-0.061	
196.3	-100	-185				197.2	-114	-63	-0.054	-0.033	-0.057	
224.3	-103	-188				225.2	-123	-78	-0.048	-0.026	-0.054	
252.1	-113	-190				251.9	-127	-70	-0.052	-0.028	-0.052	
280.1	-110	-193				280.2	-137	-75	-0.053	-0.025	-0.048	
307.7	-112	-196				308.0	-135	-85	-0.051	-0.024	-0.053	
335.7	-123	-215				335.9	-136	-84	-0.051	-0.023	-0.054	
365.4	-110	-210				365.4	-145	-83	-0.052	-0.024	-0.053	
420.5	-120	-200				419.9	-142	-78	-0.057	-0.028	-0.058	
499.0	-113	-195				499.5	0	0	0.000	0.000	0.000	

Table F.14: Creep and shrinkage results for LWW 35-65 in the medium-scale study loaded at 24 hours of age

Stage 1	24h					Stage 2	24h					Stage 3	24h				
	Total SH	Autog SH	Spec Tot Cr	Spec Tot Cr	Spec Bas Cr		Total SH	Autog SH	Spec Bas Cr	Spec Bas Cr	Spec Tot Cr		Total SH	Autog SH	Spec Tot Cr	Spec Tot Cr	Spec Bas Cr
DAYS	1	2	3	4	5	DAYS	16	17	18	19	20	DAYS	21	22	23	24	25
0.0	0	0	0.000	0.000	0.000	0.0	0	0	0.000	0.000	0.000	0.0	0	0	0.000	0.000	0.000
0.0	-78	-40	-0.011	-0.003	-0.023	0.0	-17	5	-0.028	-0.009	-0.011	0.0	-8	-15	-0.004	-0.013	-0.010
0.1	-33	-32	-0.024	-0.025	-0.029	0.1	-7	5	-0.025	-0.011	-0.014	0.1	-13	-16	-0.008	-0.016	-0.012
0.1	-53	-57	-0.016	-0.020	-0.016	0.1	10	10	-0.025	-0.018	-0.021	0.1	-18	-18	-0.011	-0.020	-0.014
0.2	-51	-56	-0.025	-0.022	-0.022	0.2	-20	0	-0.031	-0.016	-0.016	0.2	-15	-17	-0.014	-0.020	-0.014
0.2	-50	-55	-0.026	-0.031	-0.026	0.2	-10	-10	-0.031	-0.018	-0.022	0.2	-13	-16	-0.018	-0.020	-0.015
0.3	-48	-72	-0.027	-0.032	-0.018	0.3	-13	-15	-0.029	-0.020	-0.024	0.3	-10	-15	-0.021	-0.020	-0.015
0.5	-60	-35	-0.029	-0.031	-0.036	0.7	-8	-5	-0.032	-0.024	-0.031	0.5	-7	-10	-0.026	-0.026	-0.017
1.0	-75	-62	-0.043	-0.048	-0.040	1.1	-13	-5	-0.034	-0.033	-0.033	1.0	-12	-17	-0.029	-0.032	-0.021
2.0	-110	-75	-0.060	-0.071	-0.060	2.0	10	0	-0.044	-0.037	-0.046	2.0	-15	-10	-0.033	-0.043	-0.027
3.0	-138	-82	-0.061	-0.070	-0.062	3.0	0	10	-0.049	-0.050	-0.054	3.1	-22	-10	-0.045	-0.049	-0.032
4.0	-125	-77	-0.063	-0.080	-0.065	3.9	-33	15	-0.058	-0.053	-0.051	4.0	-38	-5	-0.049	-0.052	-0.040
5.0	-125	-62	-0.069	-0.080	-0.069	5.3	-30	5	-0.072	-0.059	-0.061	5.0	-28	0	-0.056	-0.060	-0.044
6.0	-153	-87	-0.069	-0.083	-0.063	6.4	-23	15	-0.080	-0.062	-0.061	6.1	-38	3	-0.055	-0.060	-0.044
10.4	-143	-85	-0.094	-0.112	-0.085	9.0	-45	20	-0.073	-0.069	-0.066	9.1	-50	-5	-0.062	-0.069	-0.047
13.0	-165	-82	-0.095	-0.116	-0.089	14.2	-45	25	-0.079	-0.076	-0.072	15.0	-55	-7	-0.071	-0.081	-0.056
20.3	-190	-85	-0.120	-0.137	-0.109	20.9	-40	65	-0.110	-0.098	-0.094	21.2	-58	-5	-0.078	-0.084	-0.058
27.4	-233	-100	-0.130	-0.149	-0.118	27.8	-78	65	-0.117	-0.098	-0.095	27.8	-83	0	-0.087	-0.099	-0.070
41.3	-250	-102	-0.150	-0.168	-0.133	42.1	-83	70	-0.121	-0.107	-0.099	42.1	-108	-12	-0.102	-0.107	-0.080
55.9	-293	-150	-0.167	-0.181	-0.137	55.9	-120	55	-0.125	-0.123	-0.113	55.0	-123	-2	-0.110	-0.118	-0.091
69.8	-335	-192	-0.171	-0.189	-0.143	69.7	-133	60	-0.127	-0.126	-0.122	69.8	-133	-5	-0.116	-0.128	-0.094
84.3	-343	-182	-0.170	-0.191	-0.145	83.7	-163	45	-0.135	-0.132	-0.126	83.8	-150	3	-0.116	-0.126	-0.097
98.3	-398	-200	-0.179	-0.189	-0.155	97.7	-170	35	-0.136	-0.133	-0.128	98.2	-163	-2	-0.120	-0.129	-0.097
112.4	-418	-235	-0.182	-0.192	-0.154	111.7	-185	30	-0.147	-0.147	-0.142	111.8	-176	-7	-0.124	-0.133	-0.096
120.2	-413	-222	-0.187	-0.202	-0.162	119.8	-180	55	-0.153	-0.152	-0.143	119.8	-184	-10	-0.127	-0.135	-0.096
140.1	-415	-240				139.8	-178	45				140.1	-203	-17	-0.132	-0.140	-0.095
167.9	-435	-252				168.2	-185	45				167.8	-210	-10	-0.135	-0.144	-0.102
195.9	-478	-280				195.9	-183	55				195.8	-218	3	-0.142	-0.147	-0.110
223.8	-485	-280				224.1	-200	45				223.8	-228	5	-0.142	-0.148	-0.113
252.4	-498	-305				252.1	-213	33				251.8	-238	0	-0.151	-0.158	-0.118
280.1	-500	-310				279.8	-239	20				279.7	-248	3	-0.155	-0.160	-0.120
308.4	-528	-325				308.0	-270	25				307.8	-258	5	-0.160	-0.162	-0.125
336.1	-535	-335				335.8	-245	25				335.9	-263	10	-0.163	-0.168	-0.129
364.5	0	-341				364.8	-260	20				364.4	0	0	0.000	0.000	0.000
419.8	0	-347				419.8	-268	5				419.4	0	0	0.000	0.000	0.000
499.5	0	-357				499.4	0	0				499.4	0	0	0.000	0.000	0.000

Table F.15: Creep and shrinkage results for LWW 35-65 in the medium-scale study loaded at 28 days of age

Stage 1	28d					Stage 2	28d				
	Total SH	Autog SH	Spec Tot Cr	Spec Tot Cr	Spec Bas Cr		Total SH	Autog SH	Spec Bas Cr	Spec Bas Cr	Spec Tot Cr
DAYS	6	7	8	9	10	DAYS	21	22	23	24	25
0.0	0	0	0.000	0.000	0.000	0.00	0	0	0.000	0.000	0.000
0.0	-30	-20	0.003	-0.001	-0.001	0.0	-5	5	-0.003	-0.006	0.001
0.1	-38	-23	-0.002	-0.003	-0.004	0.1	2	5	-0.005	-0.015	-0.006
0.1	-45	-5	-0.001	-0.008	-0.013	0.1	-5	12	-0.003	-0.013	-0.008
0.2	-50	-8	0.000	-0.008	-0.014	0.2	-1	10	-0.005	-0.015	-0.008
0.2	-55	-8	-0.003	-0.005	-0.012	0.2	2	7	-0.008	-0.018	-0.009
0.3	-56	-8	-0.003	-0.007	-0.013	0.2	2	15	-0.009	-0.018	-0.009
0.5	-63	-10	-0.006	-0.018	-0.019	0.5	-23	22	-0.016	-0.019	-0.008
1.3	-80	-45	-0.013	-0.020	-0.019	1.1	-33	12	-0.008	-0.016	-0.009
2.4	-115	-58	-0.016	-0.027	-0.026	2.2	-58	10	-0.023	-0.022	-0.023
3.5	-100	-80	-0.032	-0.039	-0.021	3.2	-53	10	-0.024	-0.021	-0.028
4.1	-130	-80	-0.026	-0.034	-0.030	4.2	-63	20	-0.029	-0.025	-0.028
5.0	-100	-35	-0.042	-0.052	-0.045	5.0	-50	22	-0.034	-0.028	-0.026
6.6	-110	-48	-0.038	-0.046	-0.038	6.3	-45	27	-0.035	-0.031	-0.035
9.1	-143	-65	-0.051	-0.057	-0.058	9.3	-70	20	-0.028	-0.035	-0.040
14.4	-163	-93	-0.078	-0.085	-0.072	14.1	-48	35	-0.033	-0.043	-0.042
21.0	-193	-108	-0.084	-0.090	-0.079	21.0	-88	22	-0.051	-0.050	-0.061
28.1	-203	-113	-0.086	-0.091	-0.075	27.9	-117	7	-0.052	-0.054	-0.064
42.5	-258	-195	-0.103	-0.111	-0.083	41.9	-150	7	-0.059	-0.071	-0.066
57.4	-243	-135	-0.096	-0.115	-0.094	55.9	-160	2	-0.071	-0.078	-0.073
70.5	-325	-178	-0.103	-0.115	-0.107	69.9	-182	-3	-0.081	-0.088	-0.086
84.6	-368	-233	-0.110	-0.114	-0.094	83.9	-202	0	-0.082	-0.094	-0.085
98.0	-373	-248	-0.107	-0.127	-0.099	98.1	-210	2	-0.087	-0.105	-0.087
113.1	-375	-220	-0.112	-0.123	-0.097	111.9	-235	-5	-0.090	-0.112	-0.091
114.0	-403	-238				120.5	-247	-8	-0.096	-0.116	-0.089
140.1	-425	-238				140.3	-257	-17	-0.090	-0.116	-0.088
168.0	-425	-250				167.9	-260	-8	-0.096	-0.120	-0.092
196.0	-433	-258				195.6	-270	-17	-0.098	-0.125	-0.103
224.0	-435	-268				223.9	-289	-32	-0.104	-0.124	-0.103
252.3	-450	-280				251.9	-307	-37	-0.113	-0.125	-0.102
280.0	-465	-290				279.9	-295	-37	-0.098	-0.125	-0.102
308.3	-473	-288				307.9	-295	-32	-0.106	-0.129	-0.109
336.0	-483	-293				336.2	-312	-42	-0.107	-0.128	-0.109
365.0	-494	-299				365.9	-315	-40	-0.110	-0.128	-0.117
420.2	-563	-305				419.9	-330	-50	-0.112	-0.134	-0.118
500.0	-585	-320				499.5	0	0	0.000	0.000	0.000

Table F.16: Creep and shrinkage results for NWA 35-65 in the medium-scale study loaded at 24 hours of age

Stage 1	24h					Stage 2	24h					Stage 3	24h				
	Total SH	Total SH	Spec Tot Cr	Spec Tot Cr	Spec Tot Cr		Total SH	Autog SH	Spec Bas Cr	Spec Bas Cr	Spec Tot Cr		Total SH	Autog SH	Spec Tot Cr	Spec Tot Cr	Spec Bas Cr
DAYS	1	2	3	4	5	DAYS	11	12	13	14	15	DAYS	21	22	23	24	25
0.0	0	0	0.000	0.000	0.000	0.0	0	0	0.000	0.000	0.000	0.0	0	0	0.000	0.000	0.000
0.0	-38	-30	-0.013	-0.015	-0.011	0.0	-5	-10	-0.004	-0.009	-0.010	0.1	5	0	-0.011	-0.011	-0.009
0.1	-38	-40	-0.014	-0.017	-0.009	0.1	-8	-13	-0.008	-0.009	-0.009	0.1	1	-3	-0.015	-0.015	-0.013
0.1	-50	-30	-0.017	-0.022	-0.018	0.1	-25	-33	-0.023	-0.020	-0.016	0.1	-3	-5	-0.019	-0.020	-0.016
0.2	-48	-20	-0.015	-0.020	-0.020	0.2	-20	-28	-0.023	-0.021	-0.016	0.2	-2	-6	-0.020	-0.020	-0.016
0.2	-43	-10	-0.021	-0.027	-0.024	0.2	-13	-30	-0.021	-0.019	-0.014	0.2	-1	-7	-0.020	-0.021	-0.017
0.3	-48	-20	-0.022	-0.032	-0.026	0.3	-22	-38	-0.020	-0.019	-0.017	0.3	0	-7	-0.020	-0.021	-0.017
0.5	-60	-30	-0.032	-0.046	-0.036	0.5	-27	-43	-0.023	-0.021	-0.018	0.5	2	-13	-0.024	-0.026	-0.022
1.0	-70	-30	-0.039	-0.054	-0.041	1.1	-55	-63	-0.030	-0.027	-0.020	1.0	-2	-15	-0.026	-0.027	-0.025
2.3	-103	-50	-0.056	-0.085	-0.066	2.0	-50	-50	-0.039	-0.033	-0.029	1.9	-2	-18	-0.033	-0.038	-0.027
3.1	-120	-50	-0.052	-0.083	-0.061	3.4	-55	-48	-0.052	-0.037	-0.032	3.0	-17	-30	-0.036	-0.041	-0.033
4.0	-113	-40	-0.055	-0.089	-0.065	4.4	-85	-63	-0.049	-0.034	-0.029	4.0	-22	-30	-0.039	-0.045	-0.035
5.3	-140	-70	-0.093	-0.132	-0.108	5.2	-65	-40	-0.052	-0.043	-0.037	4.9	-27	-25	-0.039	-0.045	-0.037
6.4	-150	-70	-0.117	-0.157	-0.129	6.3	-77	-48	-0.053	-0.042	-0.037	6.0	-25	-25	-0.040	-0.047	-0.037
9.3	-140	-80	-0.131	-0.180	-0.143	8.9	-70	-45	-0.052	-0.041	-0.036	9.2	-45	-23	-0.044	-0.050	-0.043
13.3	-198	-110	-0.147	-0.202	-0.164	14.3	-107	-58	-0.060	-0.049	-0.043	14.2	-45	-25	-0.046	-0.055	-0.045
20.4	-213	-120	-0.165	-0.228	-0.183	21.3	-77	-20	-0.065	-0.058	-0.057	20.8	-82	-50	-0.060	-0.068	-0.056
28.4	-278	-150	-0.170	-0.233	-0.192	28.2	-102	-15	-0.075	-0.063	-0.057	27.8	-95	-40	-0.062	-0.069	-0.061
42.3	-238	-170	-0.201	-0.265	-0.207	42.0	-102	-13	-0.072	-0.069	-0.067	41.8	-120	-43	-0.069	-0.078	-0.068
55.9	-270	-170	-0.206	-0.275	-0.214	56.2	-150	-30	-0.080	-0.081	-0.073	55.8	-135	-43	-0.076	-0.085	-0.073
70.4	-338	-250	-0.218	-0.291	-0.225	69.9	-145	-20	-0.085	-0.083	-0.078	69.8	-137	-38	-0.081	-0.089	-0.075
85.4	-325	-260	-0.229	-0.297	-0.227	84.3	-145	-20	-0.086	-0.086	-0.084	86.1	-151	-43	-0.083	-0.091	-0.077
98.9	-338	-300	-0.227	-0.296	-0.224	98.0	-165	-20	-0.092	-0.091	-0.089	97.8	-164	-48	-0.084	-0.093	-0.079
111.9	-345	-290	-0.229	-0.300	-0.233	111.9	-175	-33	-0.096	-0.097	-0.094	111.8	-178	-53	-0.086	-0.095	-0.082
120.2	-333	-270	-0.237	-0.304	-0.235	119.9	-177	-33	-0.096	-0.097	-0.094	119.8	-186	-55	-0.087	-0.096	-0.083
140.3	-358	-300				137.9	-197	-43				139.8	-205	-63	-0.090	-0.098	-0.086
168.1	-355	-340				168.3	-222	-43				168.8	-230	-73	-0.094	-0.103	-0.088
195.9	-388	-380				198.0	-240	-38				196.2	-232	-60	-0.095	-0.105	-0.092
223.9	-395	-389				224.2	-247	-38				223.8	-257	-68	-0.098	-0.103	-0.091
252.0	-398	-399				251.9	-266	-55				251.8	-262	-68	-0.099	-0.107	-0.092
280.3	-403	-409				279.9	-284	-73				279.9	-260	-58	-0.102	-0.110	-0.096
308.0	-415	-429				308.0	-302	-90				307.8	-267	-48	-0.106	-0.113	-0.100
336.3	-438	-429				336.3	-290	-88				335.7	-275	-48	-0.107	-0.114	-0.101
364.5	-434	-444				364.3	-297	-105				364.4	0	0	0.000	0.000	0.000
420.1	-430	-459				420.2	-310	-105				419.4	0	0	0.000	0.000	0.000
500.0	-430	-469				499.5	0	0				499.4	0	0	0.000	0.000	0.000

Table F.17: Creep and shrinkage results for NWA 35-65 in the medium-scale study loaded at 28 days of age

Stage 1	28d					Stage 2	28d				
	Total SH	Total SH	Spec Tot Cr	Spec Tot Cr	Spec Bas Cr		Total SH	Autog SH	Spec Bas Cr	Spec Bas Cr	Spec Tot Cr
DAYS	6	7	8	9	10	DAYS	16	17	18	19	20
0.0	0	0	0.000	0.000	0.000	0.0	0	0	0.000	0.000	0.000
0.0	-18	-8	-0.004	-0.003	-0.006	0.0	3	-7	-0.010	-0.012	-0.009
0.1	-30	-13	-0.006	-0.006	-0.007	0.1	0	-7	-0.017	-0.019	-0.013
0.1	-33	-18	-0.005	-0.008	-0.005	0.1	3	-10	-0.019	-0.019	-0.018
0.2	-33	-20	-0.008	-0.009	-0.007	0.2	4	-14	-0.019	-0.022	-0.020
0.2	-38	-15	-0.011	-0.011	-0.010	0.2	5	-17	-0.019	-0.024	-0.023
0.3	-39	-19	-0.011	-0.012	-0.011	0.2	5	-12	-0.020	-0.026	-0.023
0.5	-45	-43	-0.014	-0.015	-0.013	0.5	8	12	-0.026	-0.028	-0.026
1.1	-68	-58	-0.026	-0.022	-0.020	1.0	5	7	-0.029	-0.036	-0.030
2.1	-93	-60	-0.026	-0.026	-0.018	2.2	-33	-12	-0.034	-0.038	-0.036
3.0	-113	-75	-0.030	-0.033	-0.025	2.8	-60	-30	-0.037	-0.039	-0.038
4.6	-115	-75	-0.037	-0.040	-0.030	4.2	-48	-17	-0.043	-0.045	-0.044
5.4	-110	-70	-0.040	-0.043	-0.033	5.1	-43	-15	-0.044	-0.046	-0.046
6.0	-125	-73	-0.045	-0.047	-0.037	6.2	-35	-5	-0.045	-0.050	-0.050
9.1	-145	-103	-0.050	-0.053	-0.045	9.0	-63	-15	-0.047	-0.050	-0.050
14.2	-145	-108	-0.062	-0.063	-0.051	13.9	-73	-8	-0.052	-0.054	-0.052
21.0	-168	-130	-0.072	-0.075	-0.061	21.2	-98	-25	-0.063	-0.063	-0.065
28.0	-188	-140	-0.075	-0.079	-0.065	28.1	-113	-22	-0.065	-0.069	-0.066
42.5	-280	-240	-0.075	-0.082	-0.061	41.9	-158	-40	-0.078	-0.080	-0.076
58.6	-273	-203	-0.085	-0.090	-0.075	55.9	-165	-42	-0.080	-0.082	-0.084
70.4	-283	-230	-0.102	-0.091	-0.076	69.9	-183	-42	-0.083	-0.084	-0.090
84.3	-303	-268	-0.100	-0.088	-0.078	83.8	-200	-65	-0.089	-0.091	-0.103
98.2	-313	-275	-0.108	-0.091	-0.079	97.9	-205	-62	-0.092	-0.099	-0.110
112.4	-288	-268	-0.110	-0.094	-0.083	110.8	-210	-62	-0.096	-0.098	-0.115
120.0	-265	-255	-0.117	-0.101	-0.087	120.0	-220	-70	-0.097	-0.099	-0.115
140.1	-255	-270				140.3	-245	-72	-0.097	-0.101	-0.115
168.0	-278	-313				168.1	-275	-82	-0.104	-0.104	-0.117
196.1	-303	-328				195.9	-275	-67	-0.110	-0.112	-0.121
224.1	-315	-333				223.5	-293	-77	-0.117	-0.115	-0.124
252.5	-333	-340				251.5	-310	-87	-0.125	-0.119	-0.126
280.1	-348	-355				280.2	-338	-97	-0.123	-0.121	-0.130
308.0	-358	-368				307.9	-335	-90	-0.125	-0.123	-0.133
336.0	-358	-392				335.9	-345	-97	-0.126	-0.123	-0.135
365.1	-375	-395				365.5	-360	-110	-0.128	-0.129	-0.139
420.0	-365	-403				419.9	-358	-105	-0.133	-0.133	-0.145
500.5	-375	-403				499.5	0	0	0.000	0.000	0.000

Table F.18: Creep and shrinkage results for STL 35-65 in the medium-scale study loaded at 24 hours of age

Stage 1	24h					Stage 2	24h				
	Total SH	Autog SH	Spec Tot Cr	Spec Tot Cr	Spec Bas Cr		Total SH	Autog SH	Spec Bas Cr	Spec Bas Cr	Spec Tot Cr
DAYS	1	2	3	4	5	DAYS	11	12	13	14	15
0.00	0	0	0.000	0.000	0.000	0.00	0	0	0.000	0.000	0.000
0.04	-3	5	-0.011	-0.021	-0.015	0.04	-30	40	-0.031	-0.029	-0.005
0.08	5	-7	-0.024	-0.032	-0.013	0.09	-20	20	-0.040	-0.042	-0.019
0.13	5	2	-0.026	-0.034	-0.025	0.14	-50	20	-0.048	-0.043	-0.015
0.17	2	-11	-0.030	-0.035	-0.020	0.18	-35	70	-0.059	-0.072	-0.023
0.21	1	-13	-0.030	-0.037	-0.020	0.21	-20	80	-0.068	-0.078	-0.026
0.25	2	-3	-0.027	-0.041	-0.027	0.31	-30	90	-0.065	-0.086	-0.026
0.50	-20	-20	-0.039	-0.045	-0.031	0.52	-25	90	-0.076	-0.091	-0.035
1.24	-3	-12	-0.061	-0.058	-0.033	1.05	-30	70	-0.077	-0.094	-0.042
2.06	-25	-15	-0.060	-0.068	-0.043	2.32	-40	60	-0.090	-0.092	-0.057
3.22	-30	-20	-0.074	-0.081	-0.056	3.41	-15	90	-0.090	-0.096	-0.057
4.27	-55	-45	-0.080	-0.087	-0.051	4.02	-40	50	-0.087	-0.091	-0.057
5.35	-65	-55	-0.087	-0.092	-0.050	5.23	-50	70	-0.084	-0.092	-0.055
5.97	-83	-62	-0.084	-0.086	-0.053	5.98	-40	50	-0.082	-0.092	-0.059
9.85	-75	-62	-0.108	-0.113	-0.069	9.22	-50	40	-0.087	-0.096	-0.065
13.97	-78	-60	-0.123	-0.127	-0.071	14.03	-60	80	-0.104	-0.106	-0.072
21.28	-138	-95	-0.130	-0.135	-0.101	21.21	-50	80	-0.109	-0.107	-0.081
27.90	-118	-77	-0.142	-0.142	-0.096	28.18	-45	80	-0.114	-0.106	-0.089
41.93	-193	-135	-0.136	-0.134	-0.092	41.97	-90	70	-0.121	-0.113	-0.090
59.28	-180	-117	-0.162	-0.160	-0.106	55.92	-100	70	-0.130	-0.122	-0.097
70.25	-230	-165	-0.178	-0.164	-0.114	69.84	-125	40	-0.127	-0.119	-0.102
84.45	-250	-165	-0.178	-0.162	-0.117	83.86	-135	40	-0.141	-0.124	-0.101
98.24	-245	-172	-0.182	-0.175	-0.122	97.85	-140	60	-0.142	-0.131	-0.105
112.29	-255	-187	-0.173	-0.167	-0.113	111.86	-145	60	-0.144	-0.130	-0.111
120.21	-268	-205	-0.168	-0.171	-0.111	119.93	-145	50	-0.142	-0.133	-0.120
140.18	-255	-215				140.17	-150	50	-0.147	-0.133	-0.121
168.40	-273	-257				168.31	-165	70	-0.160	-0.143	-0.128
195.92	-290	-270				195.88	-195	60	-0.179	-0.142	-0.136
223.79	-285	-277				224.21	-190	60	-0.179	-0.140	-0.138
252.13	-283	-275				252.13	-185	60	-0.179	-0.138	-0.141
280.10	-293	-280				280.20	-180	60	-0.179	-0.136	-0.143
308.21	-308	-287				307.95	-185	60	-0.184	-0.147	-0.150
335.50	-314	-285				336.01	-195	40	-0.178	-0.146	-0.156
364.50	-321	-283				364.89	-215	80	-0.189	-0.159	-0.152
420.01	-365	-290				419.87	-235	80	-0.196	-0.166	-0.155
500.35	-363	-300				499.50	0	0	0.000	0.000	0.000

Table F.19: Creep and shrinkage results for STL 35-65 in the medium-scale study loaded at 28 days of age

Stage 1	28d					Stage 2	28d				
	Total SH	Total SH	Spec Tot Cr	Spec Tot Cr	Spec Bas Cr		Total SH	Autog SH	Spec Bas Cr	Spec Bas Cr	Spec Tot Cr
DAYS	6	7	8	9	10	DAYS	16	17	18	19	20
0.0	0	0	0.000	0.000	0.000	0.0	0	0	0.000	0.000	0.000
0.0	-15	-18	0.004	0.016	0.005	0.0	-30	-35	-0.007	-0.002	-0.010
0.1	-37	-18	-0.003	0.011	0.008	0.1	-35	-27	-0.016	-0.011	-0.008
0.1	-27	-28	-0.012	0.002	0.010	0.1	-33	-47	-0.018	-0.008	-0.018
0.2	-12	-25	-0.010	-0.001	0.001	0.2	-55	-45	-0.022	-0.008	-0.014
0.2	-22	-38	-0.012	0.002	0.003	0.2	-40	-32	-0.023	-0.011	-0.006
0.3	0	-35	-0.019	-0.005	-0.002	0.3	-42	-35	-0.022	-0.011	-0.007
0.5	-40	-23	-0.022	-0.009	0.004	0.5	-55	-52	-0.019	-0.008	-0.013
1.1	-25	-37	-0.032	-0.012	-0.007	1.1	-65	-45	-0.025	-0.019	-0.007
2.2	-40	-47	-0.035	-0.018	-0.012	1.9	-75	-50	-0.031	-0.022	-0.014
3.2	-45	-60	-0.040	-0.030	-0.016	3.1	-85	-57	-0.035	-0.033	-0.014
4.2	-62	-65	-0.060	-0.033	-0.031	4.1	-93	-60	-0.044	-0.039	-0.012
5.2	-65	-73	-0.067	-0.047	-0.037	4.9	-95	-60	-0.046	-0.042	-0.037
6.3	-65	-75	-0.078	-0.055	-0.053	5.9	-105	-60	-0.051	-0.047	-0.049
9.6	-100	-123	-0.071	-0.053	-0.059	9.2	-115	-55	-0.047	-0.053	-0.059
15.2	-105	-140	-0.108	-0.074	-0.083	14.0	-133	-60	-0.056	-0.056	-0.046
21.8	-133	-147	-0.113	-0.088	-0.080	21.2	-130	-60	-0.058	-0.063	-0.046
28.6	-117	-137	-0.123	-0.094	-0.073	27.9	-153	-80	-0.063	-0.064	-0.054
42.1	-150	-172	-0.136	-0.125	-0.102	42.0	-173	-85	-0.068	-0.072	-0.063
56.2	-188	-177	-0.125	-0.121	-0.106	55.9	-183	-87	-0.074	-0.074	-0.066
70.5	-178	-200	-0.158	-0.139	-0.123	69.9	-183	-92	-0.074	-0.075	-0.077
84.4	-208	-233	-0.131	-0.134	-0.108	84.1	-193	-102	-0.082	-0.082	-0.084
98.4	-188	-225	-0.147	-0.151	-0.125	97.9	-213	-112	-0.080	-0.097	-0.098
112.5	-205	-230	-0.160	-0.173	-0.135	112.3	-208	-107	-0.083	-0.098	-0.103
120.47	-218	-235	-0.170	-0.176	-0.133	120.3	-210	-112	-0.092	-0.093	-0.103
140.19	-233	-247				139.9	-215	-110	-0.098	-0.105	-0.097
168.18	-240	-255				167.9	-235	-110	-0.101	-0.109	-0.096
196.23	-255	-257				196.2	-241	-112	-0.101	-0.111	-0.094
225.38	-258	-262				223.9	-247	-113	-0.101	-0.113	-0.092
252.45	-253	-265				251.9	-253	-115	-0.100	-0.115	-0.090
280.19	-260	-280				280.9	-265	-137	-0.081	-0.111	-0.106
307.75	-273	-317				308.3	-268	-127	-0.089	-0.121	-0.107
335.75	-283	-313				335.9	-270	-135	-0.092	-0.122	-0.106
365.59	-278	-330				364.9	-278	-140	-0.093	-0.121	-0.105
420.51	-288	-335				420.0	-285	-140	-0.100	-0.123	-0.109
500.62	-293	-343				499.5	0	0	0.000	0.000	0.000

Table F.20: Creep and shrinkage results for NSC in the medium-scale study loaded at 28 days of age

Stage 1	28d					Stage 2	28d				
	Total SH	Autog SH	Spec Tot C	Spec Tot C	Spec Bas Cr		Total SH	Total SH	Spec Bas (	Spec Bas (	Spec Tot C
DAYS	1	2	3	4	5	DAYS	6	7	8	9	10
0.0	0	0	0.000	0.000	0.000	0.0	0	0	0.000	0.000	0.000
0.0	-10	-10	-0.013	-0.011	-0.003	0.0	2	-15	-0.014	-0.024	-0.018
0.1	-10	-2	-0.017	-0.018	-0.014	0.1	-5	-7	-0.014	-0.034	-0.018
0.1	-55	-50	-0.022	-0.018	-0.017	0.1	-8	-2	-0.017	-0.029	-0.020
0.2	-25	-25	-0.034	-0.025	-0.031	0.2	-5	-10	-0.027	-0.043	-0.031
0.2	-45	-23	-0.024	-0.021	-0.038	0.2	-10	-15	-0.021	-0.040	-0.027
0.3	-45	-24	-0.027	-0.022	-0.038	0.3	-12	-15	-0.022	-0.041	-0.028
0.5	-48	-35	-0.043	-0.032	-0.039	0.5	-25	-18	-0.026	-0.047	-0.034
1.0	-70	-40	-0.053	-0.046	-0.053	1.0	-47	-52	-0.047	-0.062	-0.050
2.1	-80	-68	-0.091	-0.093	-0.073	2.2	-65	-85	-0.057	-0.072	-0.070
3.4	-110	-70	-0.119	-0.110	-0.085	3.2	-82	-97	-0.069	-0.086	-0.082
4.4	-118	-68	-0.137	-0.142	-0.112	4.0	-90	-102	-0.067	-0.086	-0.087
5.5	-160	-70	-0.137	-0.136	-0.141	5.0	-127	-145	-0.080	-0.096	-0.091
6.2	-163	-100	-0.151	-0.151	-0.127	5.9	-125	-140	-0.083	-0.097	-0.102
9.0	-163	-105	-0.178	-0.172	-0.145	9.1	-152	-165	-0.087	-0.105	-0.124
14.4	-198	-98	-0.189	-0.192	-0.171	14.2	-179	-180	-0.106	-0.120	-0.161
21.0	-255	-158	-0.234	-0.237	-0.197	20.9	-212	-227	-0.138	-0.146	-0.194
28.5	-343	-230	-0.242	-0.243	-0.179	27.9	-247	-257	-0.155	-0.156	-0.217
43.4	-360	-228	-0.291	-0.291	-0.221	42.2	-262	-277	-0.159	-0.165	-0.259
56.5	-425	-285	-0.332	-0.325	-0.253	56.0	-319	-320	-0.198	-0.185	-0.291
70.6	-445	-308	-0.354	-0.340	-0.256	70.2	-351	-367	-0.228	-0.209	-0.321
84.1	-480	-350	-0.367	-0.358	-0.266	83.9	-386	-395	-0.231	-0.216	-0.315
98.4	-493	-375	-0.371	-0.366	-0.287	99.5	-401	-405	-0.245	-0.238	-0.335
112.2	-465	-340	-0.404	-0.391	-0.324	112.1	-426	-435	-0.272	-0.253	-0.346
120.0	-478	-353	-0.409	-0.400	-0.330	120.3	-436	-440	-0.282	-0.259	-0.359
140.3	-490	-358				139.9	-446	-450	-0.298	-0.282	-0.389
169.0	-495	-365				167.9	-453	-455	-0.311	-0.292	-0.407
196.1	-508	-383				196.3	-477	-462	-0.345	-0.311	-0.412
224.4	-528	-410				223.9	-500	-490	-0.347	-0.311	-0.412
252.4	-553	-440				252.0	-523	-517	-0.358	-0.331	-0.411
280.1	-553	-455				279.9	-523	-520	-0.360	-0.341	-0.413
308.0	-555	-468				308.0	-518	-522	-0.361	-0.347	-0.418
336.4	-559	-477				335.9	-516	-520	-0.368	-0.351	-0.422
365.4	-563	-485				364.9	-533	-535	-0.384	-0.371	-0.437
420.6	-568	-525				419.9	-558	-552	-0.411	-0.395	-0.441
500.1	-585	-543				499.5	0	0	0.000	0.000	0.000

Table F.21: Creep and shrinkage results for LWW 55/8 in the large-scale study loaded at 24 hours of age

DAYS	Total 5	Total 6	Total Cr&S 5	Total Cr&S 6	Total SH 1	Total SH 2	Creep @ 40% fci 1	Creep @ 40% fci 2	Creep @ 40% fci 1	Creep @ 40% fci 2
0.00	-1151	-1078	0	0	0	0	0	0	0.000	0.000
0.02	-1238	-1153	-87	-75	-27	23	-85	-73	-0.022	-0.019
0.04	-1243	-1178	-92	-100	65	-7	-121	-129	-0.031	-0.033
0.06	-1576	-1313	-425	-235	-8	-13	-414	-224	-0.106	-0.057
0.10	-1418	-1458	-267	-380	-149	-104	-141	-253	-0.036	-0.065
0.15	-1436	-1535	-285	-457	-170	-7	-196	-369	-0.050	-0.094
0.19	-1458	-1535	-307	-457	-207	-62	-173	-322	-0.044	-0.082
0.40	-1473	-1583	-322	-505	-192	-80	-186	-369	-0.048	-0.094
0.81	-1623	-1655	-472	-577	-115	-102	-364	-469	-0.093	-0.119
2.98	-1643	-1478	-492	-400	-102	-100	-391	-299	-0.100	-0.076
4.98	-1863	-1743	-712	-665	-162	-165	-549	-501	-0.140	-0.128
6.98	-1911	-1758	-760	-680	-199	-212	-554	-474	-0.141	-0.121
8.98	-1966	-1835	-815	-757	-209	-235	-593	-535	-0.151	-0.136
15.98	-2071	-1938	-920	-859	-155	-190	-748	-687	-0.191	-0.175
22.98	-2190	-2015	-1040	-937	-187	-242	-825	-722	-0.210	-0.184
26.98	-2118	-1963	-967	-884	-137	-210	-794	-711	-0.202	-0.181
36.98	-2315	-2140	-1165	-1062	-239	-307	-891	-789	-0.227	-0.201
54.98	-2438	-2247	-1287	-1169	-234	-342	-999	-881	-0.255	-0.225
78.48	-2590	-2382	-1440	-1304	-312	-407	-1080	-945	-0.275	-0.241
106.48	-2823	-2595	-1672	-1517	-457	-569	-1159	-1003	-0.295	-0.256
152.48	-3035	-2782	-1884	-1704	-677	-737	-1178	-997	-0.300	-0.254
166.86	-3180	-2879	-2029	-1801	-679	-767	-1307	-1079	-0.333	-0.275
195.01	-3173	-2862	-2022	-1784	-657	-732	-1327	-1089	-0.338	-0.278
223.31	-3238	-2932	-2087	-1854	-672	-752	-1375	-1142	-0.351	-0.291
251.34	-3310	-3009	-2159	-1931	-666	-759	-1447	-1219	-0.369	-0.311
279.42	-3355	-3054	-2204	-1976	-661	-741	-1503	-1275	-0.383	-0.325
309.23	-3380	-3079	-2229	-2001	-668	-773	-1509	-1281	-0.385	-0.326
335.22	-3388	-3099	-2237	-2021	-668	-748	-1529	-1313	-0.390	-0.335
364.47	-3400	-3117	-2249	-2039	-686	-761	-1526	-1315	-0.389	-0.335
390.46	-3457	-3172	-2307	-2094	-670	-767	-1588	-1375	-0.405	-0.351
419.02	-3485	-3217	-2334	-2139	-693	-778	-1599	-1403	-0.408	-0.358
584.99	-3685	-3402	-2534	-2324	-748	-835	-1743	-1532	-0.444	-0.391
612.91	-3685	-3402	-2534	-2324	-727	-827	-1757	-1547	-0.448	-0.394
679.52	-3727	-3407	-2577	-2329	-750	-827	-1788	-1540	-0.456	-0.393
730.46	-3705	-3414	-2554	-2336	-765	-853	-1745	-1527	-0.445	-0.389
909.34	-3892	-3544	-2742	-2466	-782	-879	-1911	-1635	-0.487	-0.417

DAXS	Total Cr&S 7	Total Cr&S 8	Total Cr&S 9	Total Cr&S 10	Total Cr&S 7	Total Cr&S 8
0.00	-895	-788	-1041	-964	0	0
0.02	-979	-880	-1156	-1094	-83	-92
0.04	-979	-903	-1178	-1116	-83	-115
0.06	-975	-915	-1256	-1204	-80	-127
0.08	-995	-913	-1288	-1199	-100	-125
0.13	-1125	-998	-1226	-1176	-230	-210
0.17	-1105	-980	-1216	-1171	-210	-192
0.24	-1139	-970	-1203	-1119	-243	-182
0.42	-1239	-1050	-1250	-1171	-343	-262
0.83	-1315	-1113	-1343	-1276	-420	-325
1.00	-1359	-1150	-1423	-1376	-464	-362
1.92	-1365	-1210	-1453	-1426	-470	-422
2.92	-1405	-1303	-1571	-1586	-510	-515
4.92	-1412	-1318	-1573	-1629	-517	-530
6.92	-1582	-1433	-1693	-1724	-687	-645
8.92	-1702	-1490	-1733	-1751	-807	-702
15.92	-1649	-1495	-1756	-1759	-754	-707
22.92	-1716	-1613	-1823	-1851	-820	-825
26.92	-1756	-1635	-1846	-1886	-860	-847
36.92	-1902	-1688	-1981	-1966	-1007	-900
54.92	-1929	-1795	-2073	-2046	-1034	-1007
78.92	-2012	-1873	-2143	-2149	-1117	-1085
106.92	-2219	-2073	-2376	-2397	-1324	-1285
147.92	-2346	-2245	-2586	-2612	-1451	-1457
167.03	-2453	-2300	-2633	-2674	-1557	-1512
194.74	-2499	-2330	-2693	-2697	-1604	-1542
223.13	-2566	-2428	-2796	-2772	-1671	-1640
253.00	-2606	-2445	-2831	-2779	-1711	-1657
278.92	-2629	-2460	-2848	-2782	-1734	-1672
306.96	-2643	-2470	-2856	-2784	-1747	-1682
335.71	-2663	-2493	-2876	-2797	-1767	-1705
364.96	-2666	-2490	-2893	-2812	-1771	-1702
418.56	-2673	-2520	-2968	-2899	-1777	-1732
584.70	-2816	-2673	-3076	-3029	-1921	-1885
607.65	-2816	-2695	-3078	-3014	-1921	-1907
678.92	-2869	-2755	-3101	-3087	-1974	-1967
730.40	-2883	-2740	-3126	-3102	-1988	-1952
909.28	-2956	-2808	-3156	-3144	-2061	-2020

Table F.22: Creep and shrinkage results for LWW 69/10 in the large-scale study loaded at 24 hours of age

DAYS	Total 1	Total 2	Total 3	Total 4	Basic Cr&S 1	Basic Cr&Sh 2	3	Total Cr&S 4	Total SH 1	Total SH 2	Total Cree 1	Total Cree 2	Total Cree 3	Total Cree 4	Spec Bas C 1	Spec Bas Cr 2
0.00	-844	-900	-1352	-1429	0	0	0	0	0	0	0	0	0	0	0.000	0.000
0.02	-827	-1343	-1355	-1309	17	-443	-2	120	-30	-30	47	-413	28	150	0.017	-0.146
0.04	-694	-1288	-1352	-1523	150	-388	0	-95	30	30	120	-418	-30	-125	0.042	-0.147
0.08	-877	-1043	-1732	-1863	-32	-143	-380	-435	-50	-20	3	-108	-345	-400	0.001	-0.038
0.13	-1166	-1440	-1492	-1776	-322	-541	-140	-347	-67	-120	-229	-447	-46	-253	-0.081	-0.158
0.17	-1229	-1535	-1570	-1803	-385	-636	-217	-375	-97	-170	-251	-502	-84	-241	-0.088	-0.177
0.38	-1361	-1650	-1615	-1861	-517	-750	-262	-432	-172	-180	-341	-574	-86	-256	-0.120	-0.202
0.58	-1349	-1678	-1712	-1945	-505	-778	-360	-517	-230	-240	-270	-543	-125	-282	-0.095	-0.191
0.79	-1466	-1785	-1780	-2093	-622	-885	-427	-664	-310	-510	-212	-476	-18	-254	-0.075	-0.168
0.96	-1471	-1760	-1905	-2170	-627	-860	-552	-742	-437	-480	-168	-402	-94	-283	-0.059	-0.142
1.96	-1591	-1963	-2027	-2440	-747	-1063	-675	-1011	-435	-500	-280	-595	-207	-544	-0.099	-0.210
2.96	-1661	-1995	-2062	-2385	-817	-1095	-710	-957	-462	-560	-306	-584	-199	-445	-0.108	-0.206
4.96	-1616	-1945	-1979	-2245	-772	-1045	-627	-817	-505	-590	-225	-498	-80	-269	-0.079	-0.176
6.96	-1941	-2090	-2254	-2485	-1097	-1191	-902	-1056	-500	-570	-562	-656	-367	-522	-0.198	-0.231
8.96	-1921	-2110	-2324	-2637	-1077	-1210	-972	-1209	-625	-660	-434	-568	-330	-567	-0.153	-0.200
15.96	-2103	-2353	-2517	-2810	-1259	-1453	-1165	-1381	-637	-690	-595	-789	-501	-718	-0.210	-0.278
22.96	-2143	-2400	-2557	-2867	-1299	-1500	-1205	-1439	-670	-680	-624	-826	-530	-764	-0.220	-0.291
26.96	-2143	-2420	-2607	-2937	-1299	-1520	-1255	-1508	-685	-700	-607	-828	-562	-816	-0.214	-0.292
36.96	-2203	-2488	-2649	-2949	-1359	-1588	-1297	-1521	-745	-650	-662	-891	-600	-824	-0.233	-0.314
54.96	-2305	-2585	-2832	-3147	-1461	-1685	-1480	-1718	-757	-700	-733	-957	-751	-990	-0.258	-0.337
78.96	-2538	-2818	-3094	-3352	-1694	-1918	-1742	-1923	-757	-790	-920	-1144	-969	-1150	-0.324	-0.403
106.96	-2758	-3085	-3342	-3559	-1913	-2185	-1989	-2130	-892	-909	-1013	-1285	-1089	-1230	-0.357	-0.453
148.96	-2967	-3298	-3544	-3779	-2123	-2398	-2192	-2350	-1077	-1099	-1035	-1310	-1104	-1262	-0.365	-0.462
167.10	-3015	-3353	-3624	-3851	-2171	-2453	-2272	-2423	-1087	-1109	-1073	-1355	-1174	-1325	-0.378	-0.477
194.53	-3087	-3403	-3669	-3914	-2243	-2503	-2317	-2485	-1099	-1099	-1144	-1403	-1218	-1386	-0.403	-0.495
223.30	-3140	-3420	-3679	-3941	-2295	-2520	-2327	-2512	-1094	-1099	-1199	-1423	-1230	-1416	-0.422	-0.502
251.32	-3192	-3480	-3722	-4041	-2348	-2580	-2369	-2612	-1097	-1059	-1270	-1502	-1291	-1534	-0.448	-0.529
279.23	-3267	-3543	-3717	-4051	-2423	-2643	-2364	-2622	-1082	-1049	-1357	-1577	-1299	-1557	-0.478	-0.556
307.40	-3305	-3562	-3732	-4063	-2460	-2663	-2379	-2635	-1082	-1049	-1395	-1597	-1314	-1569	-0.492	-0.563
336.41	-3285	-3557	-3722	-4008	-2440	-2658	-2369	-2580	-1007	-989	-1442	-1659	-1371	-1582	-0.508	-0.585
364.18	-3322	-3562	-3761	-4128	-2478	-2663	-2409	-2700	-1012	-989	-1477	-1662	-1409	-1699	-0.521	-0.586
393.43	-3419	-3697	-3831	-4216	-2575	-2798	-2479	-2787	-1102	-1069	-1490	-1712	-1394	-1702	-0.525	-0.603
421.99	-3462	-3717	-3859	-4246	-2618	-2818	-2507	-2817	-1127	-1069	-1520	-1719	-1409	-1719	-0.536	-0.606
587.97	-3594	-3860	-4004	-4338	-2750	-2960	-2652	-2910	-1167	-1139	-1597	-1807	-1499	-1757	-0.563	-0.637
615.89	-3609	-3875	-3964	-4318	-2765	-2975	-2612	-2890	-1172	-1149	-1605	-1815	-1451	-1729	-0.566	-0.640
679.70	-3639	-3882	-4016	-4331	-2795	-2983	-2664	-2902	-1152	-1149	-1645	-1832	-1514	-1752	-0.580	-0.646
728.74	-3632	-3910	-3966	-4348	-2788	-3010	-2614	-2920	-1169	-1119	-1643	-1866	-1470	-1775	-0.579	-0.658
912.68	-3712	-3982	-4026	-4351	-2867	-3082	-2674	-2922	-1167	-1139	-1714	-1929	-1521	-1769	-0.604	-0.680

This page intentionally left blank

APPENDIX G

PHYSICAL AND MECHANICAL PROPERTIES OF CONCRETE MIXTURES OF SMALL-SCALE STUDY

G.1 Compressive Strength

Cement Matrix

Cubes		Specimen 1						Average		
		Weight	Unitweig	Load		Strength		Unitweigh	Strength	
Age		gr	lb/ft3	kip	ksi	MPa	Age	lb/ft3	ksi	MPa
	1	316.200	150.6	61.72	15.430	106.4	1	151.3	15.272	105.3
	28	305.000	145.2	59.18	14.795	102.0	28	145.1	14.291	98.6
		Specimen 2								
		Weight	Unitweig	Load		Strength				
Age		gr	lb/ft3	kip	ksi	MPa				
	1	320.600	152.7	64.19	16.048	110.7				
	28	304.800	145.1	55.52	13.880	95.7				
		Specimen 3								
		Weight	Unitweig	Load		Strength				
Age		gr	lb/ft3	kip	ksi	MPa				
	1	316.700	150.8	57.35	14.338	98.9				
	28	304.600	145.0	56.79	14.198	97.9				

HP Matrix

Cubes		Specimen 1						Average		
		Weight	Unitweig	Load		Strength		Unitweigh	Strength	
Age		gr	lb/ft3	kip	ksi	MPa	Age	lb/ft3	ksi	MPa
	1	303.000	144.3	37.51	9.378	64.7	1	144.6	9.670	66.7
	28	305.000	145.2	50.81	12.703	87.6	28	145.1	12.270	84.6
		Specimen 2								
		Weight	Unitweig	Load		Strength				
Age		gr	lb/ft3	kip	ksi	MPa				
	1	307.500	146.4	40.3	10.075	69.5				
	28	304.800	145.1	47.67	11.918	82.2				
		Specimen 3								
		Weight	Unitweig	Load		Strength				
Age		gr	lb/ft3	kip	ksi	MPa				
	1	300.300	143.0	38.23	9.558	65.9				
	28	304.600	145.0	48.76	12.190	84.1				

LWW 65-35-95

Cubes

Age	Weight gr	Unitweig lb/ft3	Load kip	Strength ksi	Strength MPa
Specimen 1					
1	269.000	128.1	36.01	9.003	62.1
28	273.800	130.4	40.85	10.213	70.4
Specimen 2					
1	277.700	132.2	37.79	9.448	65.2
28	274.400	130.7	47.26	11.815	81.5
Specimen 3					
1	276.600	131.7	39.01	9.753	67.3
28					

Age	**Average Unitweigh lb/ft3**	**Strength ksi**	**Strength MPa**
1	**130.7**	**9.401**	**64.8**
28	**130.5**	**11.014**	**76.0**

LWD 65-35-95

Cubes

Age	Weight gr	Unitweight lb/ft3	Load kip	Strength ksi	Strength MPa
Specimen 1					
1	271.900	129.5	34.38	8.595	59.3
28	267.100	127.2	42.76	10.690	73.7
Specimen 2					
1	268.800	128.0	36.08	9.020	62.2
28	266.400	126.8	43.44	10.860	74.9
Specimen 3					
1	272.200	129.6	32.64	8.160	56.3
28	270.900	129.0	45.62	11.405	78.7

Age	**Average Unitweig lb/ft3**	**Strength ksi**	**Strength MPa**
1	**129.0**	**8.592**	**59.3**
28	**127.7**	**10.985**	**75.8**

NWA 65-35-95

Cubes

Specimen 1						
	Weight	Unitweig	Load		Strength	
Age	gr	lb/ft3	kip	ksi	MPa	
1	328.600	156.5	42.99	10.748	74.1	
28						

Specimen 2						
	Weight	Unitweig	Load		Strength	
Age	gr	lb/ft3	kip	ksi	MPa	
1	330.600	157.4	46.17	11.543	79.6	
28						

Specimen 3						
	Weight	Unitweig	Load		Strength	
Age	gr	lb/ft3	kip	ksi	MPa	
1	332.000	158.1	44.8	11.200	77.2	
28						

Average			
	Unitweigh	**Strength**	
Age	**lb/ft3**	**ksi**	**MPa**
1	**157.3**	**11.163**	**77.0**
28			

STL 65-35-95

Cubes

Specimen 1						
	Weight	Unitweig	Load		Strength	
Age	gr	lb/ft3	kip	ksi	MPa	
1	667.800	318.0	53.67	13.418	92.5	
28						

Specimen 2						
	Weight	Unitweig	Load		Strength	
Age	gr	lb/ft3	kip	ksi	MPa	
1	661.900	315.2	48.76	12.190	84.1	
28						

Specimen 3						
	Weight	Unitweig	Load		Strength	
Age	gr	lb/ft3	kip	ksi	MPa	
1	664.200	316.3	51.14	12.785	88.2	
28						

Average			
	Unitweigh	**Strength**	
Age	**lb/ft3**	**ksi**	**MPa**
1	**316.5**	**12.798**	**88.3**
28			

NSC

Cubes		Specimen 1						Average		
		Weight	Unitweig	Load		Strength		Unitweigh	Strength	
Age		gr	lb/ft3	kip	ksi	MPa	Age	lb/ft3	ksi	MPa
	1									
	28	308.300	146.8	14.86	3.715	25.6	28	146.1	3.551	24.5
		Specimen 2								
		Weight	Unitweig	Load		Strength				
Age		gr	lb/ft3	kip	ksi	MPa				
	1									
	28	307.800	146.6	14.19	3.548	24.5				
		Specimen 3								
		Weight	Unitweig	Load		Strength				
Age		gr	lb/ft3	kip	ksi	MPa				
	1									
	28	304.600	145.0	14.76	3.690	25.4				
		Specimen 4								
		Weight	Unitweig	Load		Strength				
Age		gr	lb/ft3	kip	ksi	MPa				
	1									
	28	307.000	146.2	13.01	3.253	22.4				

G.2 Autogenous Shrinkage

Cement Matrix

Actual Shrinkage (με)												
1A	1B	2A	2B	3A	3B	4A	4B	**1**	**2**	**3**	**4**	**Av**
0	0	0	0	0	0	0	0	**0**	**0**	**0**	**0**	**0**
289	289	293	285	273	285	249	259	**289**	**289**	**279**	**254**	**278**
413	413	497	507	489	504	457	479	**413**	**502**	**497**	**468**	**470**
462	462	573	593	565	583	538	550	**462**	**583**	**574**	**544**	**541**
492	492	598	613	592	600	547	569	**492**	**605**	**596**	**558**	**563**
527	524	627	645	624	632	587	601	**525**	**636**	**628**	**594**	**596**
586	586	667	699	681	683	645	667	**586**	**683**	**682**	**656**	**652**
628	623	718	743	715	735	684	697	**626**	**731**	**725**	**690**	**693**
682	677	768	797	764	787	736	750	**680**	**782**	**775**	**743**	**745**
690	687	785	809	782	794	753	758	**689**	**797**	**788**	**755**	**757**
717	727	812	824	809	809	765	789	**722**	**818**	**809**	**777**	**781**
739	744	821	844	816	817	786	804	**741**	**832**	**816**	**795**	**796**
742	747	822	846	817	818	789	807	**744**	**834**	**818**	**798**	**798**

HP Matrix

Actual Shrinkage (με)									
1A	1B	2A	2B	3A	3B	**1**	**2**	**3**	**Av**
0	0	0	0	0	0	**0**	**0**	**0**	**0**
73	78	54	64	74	72	**75**	**59**	**73**	**69**
90	92	78	78	67	82	**91**	**78**	**74**	**81**
109	107	105	108	89	103	**108**	**107**	**96**	**104**
141	141	147	142	135	142	**141**	**144**	**138**	**141**
214	207	203	208	159	204	**210**	**206**	**181**	**199**
289	277	291	277	262	269	**283**	**284**	**266**	**278**
328	321	328	323	315	317	**324**	**326**	**316**	**322**
374	362	367	360	346	351	**368**	**364**	**348**	**360**
386	386	389	380	375	377	**386**	**384**	**376**	**382**
391	391	397	397	380	382	**391**	**397**	**381**	**390**
440	416	419	431	416	423	**428**	**425**	**419**	**424**
442	435	433	436	425	428	**439**	**435**	**426**	**433**

LWW 65-35-95

Actual Shrinkage (με)									
1A	1B	2A	2B	3A	3B	**1**	**2**	**3**	**Av**
0	0	0	0	0	0	**0**	**0**	**0**	**0**
0	5	-17	22	0	0	**2**	**2**	**0**	**2**
0	10	19	71	39	49	**5**	**45**	**44**	**31**
12	27	24	71	46	51	**19**	**47**	**49**	**38**
36	29	24	68	44	49	**33**	**46**	**46**	**42**
17	10	15	56	29	34	**13**	**35**	**32**	**27**
-5	-17	-27	22	2	2	**-11**	**-2**	**2**	**-4**
-17	-31	-46	2	-29	-29	**-24**	**-22**	**-29**	**-25**
-46	-60	-85	-24	-63	-66	**-53**	**-55**	**-65**	**-57**
-55	-68	-105	-39	-73	-78	**-62**	**-72**	**-76**	**-70**
-118	-128	-173	-112	-73	-80	**-123**	**-142**	**-77**	**-114**
-178	-205	-246	-175	-141	-124	**-192**	**-210**	**-133**	**-178**
-174	-191	-243	-173	-136	-107	**-182**	**-208**	**-122**	**-171**

LWD 65-35-95

Actual Shrinkage (με)									
1A	1B	2A	2B	3A	3B	**1**	**2**	**3**	**Av**
0	0	0	0	0	0	**0**	**0**	**0**	**0**
5	0	10	10	7	2	**2**	**10**	**5**	**6**
-27	-32	-12	-7	-19	-19	**-29**	**-10**	**-19**	**-19**
-61	-49	-44	-42	-53	-58	**-55**	**-43**	**-56**	**-51**
-68	-70	-51	-54	-61	-68	**-69**	**-53**	**-64**	**-62**
-102	-107	-95	-86	-107	-109	**-104**	**-91**	**-108**	**-101**
-129	-146	-120	-125	-138	-145	**-137**	**-122**	**-142**	**-134**
-165	-170	-159	-157	-167	-184	**-168**	**-158**	**-176**	**-167**
-182	-199	-154	-174	-184	-153	**-191**	**-164**	**-168**	**-174**
-221	-238	-188	-203	-225	-199	**-229**	**-196**	**-212**	**-212**
-262	-270	-225	-237	-252	-225	**-266**	**-231**	**-239**	**-245**
-284	-313	-257	-257	-291	-274	**-299**	**-257**	**-282**	**-279**
-294	-318	-269	-272	-296	-284	**-306**	**-270**	**-290**	**-289**

NWA 65-35-95

Actual Shrinkage									
1A	1B	2A	2B	3A	3B	**1**	**2**	**3**	**Av**
		0	0	0	0		**0**	**0**	**0**
		-29	-41	7	2		**-35**	**5**	**-15**
		-148	-167	-89	-92		**-157**	**-91**	**-124**
		-199	-218	-111	-111		**-208**	**-111**	**-160**
		-225	-237	-131	-121		**-231**	**-126**	**-178**
		-257	-271	-152	-160		**-264**	**-156**	**-210**
		-322	-324	-215	-230		**-323**	**-222**	**-273**
		-337	-344	-232	-239		**-340**	**-236**	**-288**
		-397	-404	-268	-280		**-401**	**-274**	**-338**
		-419	-443	-295	-305		**-431**	**-300**	**-365**
		-414	-448	-290	-309		**-431**	**-300**	**-365**
		-453	-504				**-478**		
		-470	-504				**-487**		

STL 65-35-95

Actual Shrinkage (με)									
1A	1B	2A	2B	3A	3B	**1**	**2**	**3**	**Av**
0	0	0	0	0	0	**0**			**0**
34	27	0	0	0	0	**30**			**30**
56	49	0	0	0	0	**52**			**52**
56	49	0	0	0	0	**52**			**52**
66	66					**66**			**66**
90	100					**95**			**95**
139	132					**135**			**135**
170	163					**167**			**167**
156	146					**151**			**151**
153	156					**155**			**155**
166	180					**173**			**173**
188	180					**184**			**184**
188	175					**181**			**181**

G.3 Creep and Shrinkage

HP Matrix

Actual Shortenning				Applied Stress (psi)		3068
Shrinkage		Creep plus Shrinkage				Specific
1A	1B	2A	2B	**1**	**2**	Creep
0.000000	0.000000	0.000000	0.000000	**0.000000**	**0.000000**	
0.000000	0.000000	-0.001342	-0.000917	**0.000000**	**-0.001129**	0.00
-0.000186	-0.000130	-0.001801	-0.001460	**-0.000158**	**-0.001630**	-0.11
-0.000410	-0.000242	-0.002297	-0.001984	**-0.000326**	**-0.002140**	-0.22
-0.000633	-0.000372	-0.002793	-0.002470	**-0.000503**	**-0.002632**	-0.33
-0.000708	-0.000372	-0.003087	-0.002845	**-0.000540**	**-0.002966**	-0.42

LWW 65-35-95

Actual Shortenning				Applied Stress (psi)		3041
Shrinkage		Creep plus Shrinkage				Specific
1A	1B	2A	2B	**1**	**2**	Creep
0.000000	0.000000	0.000000	0.000000	**0.000000**	**0.000000**	
0.000000	0.000000	-0.001176	-0.000803	**0.000000**	**-0.000989**	0.00
-0.000162	-0.000091	-0.001465	-0.001204	**-0.000127**	**-0.001335**	-0.07
-0.000343	-0.000236	-0.001755	-0.001533	**-0.000290**	**-0.001644**	-0.12
-0.000451	-0.000309	-0.002026	-0.001824	**-0.000380**	**-0.001925**	-0.18
-0.000506	-0.000382	-0.002189	-0.002043	**-0.000444**	**-0.002116**	-0.22

LWD 65-35-95

Actual Shortenning				Applied Stress (psi)		3699
Shrinkage		Creep plus Shrinkage				Specific
1A	1B	2A	2B	**1**	**2**	Creep
0	0	0	0	**0**	**0**	
0	0	-1040	-1226	**0**	**-1133**	0.00
-90	-108	-1551	-1721	**-99**	**-1636**	-0.11
-287	-252	-2080	-2087	**-269**	**-2083**	-0.18
-395	-323	-2555	-2526	**-359**	**-2540**	-0.28
-413	-341	-2792	-2709	**-377**	**-2750**	-0.34

NWA 65-35-95

Actual Shortenning				Applied Stress (psi)		4114
Shrinkage		Creep plus Shrinkage				Specific
1A	1B	2A	2B	**1**	**2**	Creep
0	0	0	0	**0**	**0**	
0	0	-2167	-880	**0**	**-1523**	0.00
-193	18	-2896	-1366	**-88**	**-2131**	-0.13
-439	106	-3344	-1740	**-166**	**-2542**	-0.21
-667	159	-3755	-2058	**-254**	**-2907**	-0.27
-702	123	-3979	-2264	**-289**	**-3122**	-0.32

STL 65-35-95

Actual Shortenning				Applied Stress (psi)		2685
Shrinkage		Creep plus Shrinkage				Specific
1A	1B	2A	2B	**1**	**2**	Creep
0	0	0	0	**0**	**0**	
0	0	-761	-196	**0**	**-478**	0.00
-18	-54	-1097	-374	**-36**	**-735**	-0.08
-144	-126	-1468	-570	**-135**	**-1019**	-0.15
-234	-234	-1716	-730	**-234**	**-1223**	-0.19
-234	-216	-1822	-748	**-225**	**-1285**	-0.22

NSC

Actual Shortenning				Applied Stress (psi)		1411
Shrinkage		Creep plus Shrinkage				Specific
1A	1B	2A	2B	**1**	**2**	Creep
0	0	0	0	**0**	**0**	
0	0	-823	-1257	**0**	**-1040**	0.00
-90	-55	-1263	-1646	**-73**	**-1454**	-0.24
-199	-128	-1793	-1923	**-163**	**-1858**	-0.46
-361	-220	-2360	-2256	**-290**	**-2308**	-0.69
-397	-257	-2745	-2515	**-327**	**-2630**	-0.89

G.4 Setting time

Table G.1: Final setting time

Mixture	Final Set (hours)
Cement Matrix	8.75
HP Matrix	10.0
LWW 65-35-95	7.25
LWD 65-35-95	10.3
NWA 65-35-95	8.5
STL 65-35-95	12.0

APPENDIX H

CREEP AND DRYING SHRINKAGE MODELS (US CUSTOMARY UNITS)

Among the variety of methods proposed for creep and shrinkage in concrete, seven of them are presented in this section: American Concrete Institute committee 209 (ACI-209, 1992), American Association of State Highway and Transportation Officials (AASHTO-LRFD, 2004), Comite Euro-Internacional du Beton and Federation Internationale de la Precontrainte (CEB-FIP, 1990), Bažant and Panula's (BP, 1978a, 1978b, 1978c, 1978d), Bažant and Baweja's (B3, 1995a, 1995b, 1995c), Gardner and Lockman's (GL, 2001), and Sakata's model (SAK, 1993). Finally, five methods aimed to be used for high strength high performance concrete are presented: CEB-FIP as modified by Yue and Taerwe (1993), BP as modified by Bažant and Panula (1984), SAK as modified by Sakata et al. (2001), Association Française de Recherches et d'Essais sur les Matériaux de Construction (AFREM, Le Roy, de Larrard, and Pons, 1996), and AASHTO-LRFD as modified by Shams and Kahn (2000). Most of the expressions presented here are empirical, so they have different versions depending on the unit system. US customary unit version is presented in this section while S.I. unit version is presented in Appendix D.

H.1 Models for Normal Strength Concrete

The variables considered by the creep and shrinkage models for normal strength concrete can be grouped in three types: ambient conditions, mix design, and concrete element geometric properties.

Among the ambient variables, there are: type of curing, age or maturity of concrete at loading, age of concrete at starting of drying, relative humidity, and temperature. Slump, fine aggregate content, coarse aggregate content, air content, water content, cement content, type of cement, cementitious materials content, and concrete strength are the variables related with the mix design. Finally, within the member variables, there are: shape of the member and volume-to- surface ratio.

H.1.1. ACI-209 Method

American Concrete Institute through its committee 209 "Prediction of Creep, Shrinkage and Temperature Effects in Concrete Structures" proposes an empirical model for predicting creep and shrinkage strain as a function of time. The two models have the same principle: a hyperbolic curve that tends to an asymptotic value called the ultimate value. The shape of the curve and ultimate value depend on several factors such as curing conditions, age at application of load, mix design, ambient temperature and humidity.

Creep Model. Creep model proposed by ACI-209 has three constants that determine the asymptotic value, creep rate and change in creep rate. The predicted parameter is not creep strain, but creep coefficient (creep strain-to-initial strain ratio). The latter allows for the calculation of a creep value independent from the applied load. Equation H.1 presents the general model.

$$\phi_t = \frac{(t-t')^{\psi}}{d+(t-t')^{\psi}} \cdot \phi_u \qquad \text{(H.1)}$$

where

ϕ_t: creep coefficient at age "t" loaded at t′

t: age of concrete (days)

t′: age of concrete at loading (days)

ψ: constant depending on member shape and size

d: constant depending on member shape and size

ϕ_u: ultimate creep coefficient

ACI-209 recommended a value of 0.6 and 10 for ψ and *d,* respectively. Ultimate creep coefficient value depends on the factors described in Section H.2. ACI proposed an average creep coefficient value of 2.35 which is multiplied by six factors depending on particular conditions, as shown in Equation H.2

$$\phi_u = 2.35 \cdot \gamma_{la} \cdot \gamma_{\lambda} \cdot \gamma_{vs} \cdot \gamma_s \cdot \gamma_{\psi} \cdot \gamma_{\alpha} \qquad \text{(H.2)}$$

where

ϕ_u: ultimate creep coefficient

$\gamma_{la} = \begin{cases} 1.25 \cdot t'^{-0.118} & \textit{for moist curing} \\ 1.13 \cdot t'^{-0.094} & \textit{for steam curing} \end{cases}$; age of loading factor

t′: age of concrete at loading (days)

$\gamma_{\lambda} = \begin{cases} 1.27 - 0.67 \cdot h \ \textit{for } h \geq 0.40 \\ 1.00 \ \textit{otherwise} \end{cases}$; ambient relative humidity factor

h: relative humidity in decimals

$\gamma_{VS} = \frac{2}{3}\left(1 + 1.13 \cdot \exp\left\{-0.54 \cdot V/S\right\}\right)$; volume-to-surface ratio factor

V: specimen volume (in^3)

S: specimen surface area (in^2)

$\gamma_s = 0.82 + 0.067 \cdot s$; slump factor

s: slump (in)

$\lambda_\psi = 0.88 + 0.24 \cdot \psi$; fine aggregate content factor

ψ: fine aggregate-to-total aggregate ratio in decimals

$\gamma_\alpha = 0.46 + 0.09 \cdot \alpha$; air content factor

α: air content (%)

After applying the factors above, ultimate creep coefficient value is usually between 1.3 and 4.15, which means that creep strain is between 1.3 and 4.15 times the initial elastic strain.

Drying Shrinkage Model. Similar to creep, ACI-209 shrinkage model has constants that determine the shrinkage asymptotic value, shrinkage rate and rate change. Equation H.3 shows such a model.

$$(\varepsilon_{sh})_t = \frac{(t - t_0)^\alpha}{f + (t - t_0)^\alpha} \cdot (\varepsilon_{sh})_u \qquad \text{(H.3)}$$

where

t: age of concrete (days)

t_0: age at the beginning of drying (days)

$(\varepsilon_{sh})_t$: shrinkage strain after "t-t_0" days under drying (in/in)

α: constant depending on member shape and size

f: constant depending on member shape and size

$(\varepsilon_{sh})_u$: ultimate shrinkage strain (in/in)

ACI-209 recommends a value for *f* of 35 and 55, for seven days moist curing and 1 to 3 days steam curing, respectively, while a value of 1.0 is suggested for α. Ultimate shrinkage value depends on the factors described in Section H.3. As shown in Equation H.4, ACI-209 proposes an average value of 780 με for shrinkage which is multiplied by seven factors depending on particular conditions.

$$(\varepsilon_{sh})_u = 780 \cdot \gamma_\lambda \cdot \gamma_{vs} \cdot \gamma_s \cdot \gamma_\psi \cdot \gamma_c \cdot \gamma_\alpha \qquad \text{(H.4)}$$

where

$(\varepsilon_{sh})_u$: ultimate shrinkage strain

$\gamma_\lambda = \begin{cases} 1.40 - 1.0 \cdot h \ \ for\ 0.40 \le h \le 0.80 \\ 3.00 - 3.0 \cdot h \ \ for\ h > 0.80 \end{cases}$; ambient relative humidity factor

h: relative humidity in decimals

$\gamma_{VS} = 1.2 \cdot \exp\left\{-0.12 \cdot V/S\right\}$; volume-to-surface ratio factor

V: specimen volume (in^3)

S: specimen surface area (in^2)

$\gamma_s = 0.89 + 0.041 \cdot s$; slump factor

s: slump (in)

$\gamma_\psi = \begin{cases} 0.30 - 1.4 \cdot \psi \ \ for\ \psi \le 0.50 \\ 0.90 - 0.2 \cdot \psi \ \ for\ \psi > 0.50 \end{cases}$; fine aggregate content factor

ψ: fine aggregate-to-total aggregate ratio in decimals

$\gamma_c = 0.75 + 0.00036 \cdot c$; cementitious materials content factor

c: cementitious materials content (lb/yd^3)

$\gamma_\alpha = 0.95 + 0.08 \cdot \alpha$; air content factor

α: air content (%)

After applying the factors above, ultimate shrinkage value is usually between 415 and 1,070 με.

H.1.2. AASHTO-LRFD Method

AASHTO-LRFD method (2004) is very similar to ACI-209 method, but it incorporates more recent data. AASHTO-LRFD method proposes slightly different correction factors.

Creep Model. The general equation for creep coefficient is the same as ACI-209 (Equation H.1). However the expression for calculating ultimate creep coefficient differs from ACI expression (Equation H.2). Equation H.5 presents AASHTO-LRFD expression for ultimate creep coefficient.

$$\phi_u = 3.50 \cdot k_{la} \cdot k_h \cdot k_c \cdot k_f \qquad \text{(H.5)}$$

where

ϕ_u: ultimate creep coefficient

$k_{la} = 1.00 \cdot t'^{-0.118}$ *for moist curing* ; age of loading factor

$$t' = \sum_{\text{loading}}^{\text{until}} \Delta t_i \cdot \exp\left\{-\left[\frac{4{,}000}{273 + T(\Delta t_i)/T_0} - 13.65\right]\right\}$$; maturity of concrete at loading (days)

Δt_i: period of time (days) at temperature $T(\Delta t_i)$ (^oC) ($^oC = 0.556 \times {}^oF - 17.778$)

T_0: 1 ^oC

$k_h = 1.58 - 0.83 \cdot h$; ambient relative humidity factor

h: relative humidity in decimals

$$k_c = \left[\frac{t}{\frac{26 \cdot \exp\left\{0.36 \cdot V/S\right\} + t}{\frac{t}{45+t}}} \right] \cdot \left[\frac{1.80 + 1.77 \cdot \exp\left\{-0.54 \cdot V/S\right\}}{2.587} \right]$$; size factor

$$t = \sum_{day\ n}^{until} \Delta t_i \cdot \exp\left\{ -\left[\frac{4{,}000}{273 + T(\Delta t_i)/T_0} - 13.65 \right] \right\}$$; maturity of concrete (days) after "n" days

V: specimen volume (in^3)

S: specimen surface area (in^2)

$$k_f = \frac{1}{0.67 + \frac{f_c'}{9}}$$; concrete strength factor

f_c': compressive strength of concrete cylinders at 28 days (ksi)

Drying Shrinkage Model. ASSHTO-LRFD general expression for shrinkage is the same as ACI expression (Equation H.3) including the values for *f* of 35 and 55 for moist and steam curing, respectively. The expression for calculating ultimate shrinkage is different from ACI expression, and it is presented in Equation H.6.

$$(\varepsilon_{sh})_u = K \cdot k_s \cdot k_h \qquad \text{(H.6)}$$

where

$(\varepsilon_{sh})_u$: ultimate shrinkage strain (in/in)

$$K = \begin{cases} 510\ \mu\varepsilon\ for\ moist\ curing \\ 560\ \mu\varepsilon\ for\ steam\ curing \end{cases}$$; ultimate shrinkage base value

$$k_s = \left[\frac{(t-t_0)}{\frac{26 \cdot \exp\left\{0.36 \cdot V/S\right\} + (t-t_0)}{(t-t_0)}} \right] \cdot \left[\frac{1064 - 0.94 \cdot V/S}{923} \right]$$; size factor

t: age of concrete (days)

t_0: age at the beginning of drying (days)

V: specimen volume (in^3)

S: specimen surface area (in^2)

$$k_h = \begin{cases} 2.00 - 1.43 \cdot h \ \ for \ h < 0.80 \\ 4.29 - 4.29 \cdot h \ \ for \ h \geq 0.80 \end{cases}$$; ambient relative humidity factor

h: relative humidity in decimals

H.1.3. CEB-FIP Method

CEB-FIP method has a similar concept that ACI-209 in the sense that it gives a hyperbolic change with time for creep and shrinkage, and it also uses an ultimate value corrected according to mix design and environment conditions. One difference of CEB-FIP method with respect to the methods above is that it predicts creep strain rather than creep coefficient.

Creep Model. CEB-FIP general model is presented in Equation H.7. This model predicts creep strain by multiplying creep coefficient by elastic strain. Creep coefficient has its own equation based on two parameters, as shown in Equation H.8

$$\varepsilon_{cr}(t,t') = \frac{\sigma_c(t')}{E_{28}} \phi(t,t') \qquad \text{(H.7)}$$

$$\phi = \phi_0 \cdot \left[\frac{(t - t')}{\beta_H + (t - t')} \right]^{0.3} \qquad \text{(H.8)}$$

where

t: age of concrete (days)

t′: age of concrete at loading (days)

ε_{cr}: creep strain in με

$\sigma_c(t')$: applied stress (ksi)

E_{28}: 28-day elastic modulus (ksi)

ø: creep coefficient at age "t" loaded at t′

$$\phi_0 = \left[1 + \frac{(1 - h)}{0.367 \cdot \left(A_c / u \right)^{1/3}} \right] \cdot \frac{5.3}{\sqrt{\frac{f_c'}{1.45}}} \cdot \frac{1}{0.1 + t'^{0.2}}$$; notional creep coefficient

h: relative humidity in decimals

A_c: cross sectional area (in^2)

u: exposed perimeter (in)

f_c': compressive strength of concrete cylinders at 28 days (ksi)

$\beta_H = 150 \cdot \left[1 + (1.2 \cdot h)^{18} \right] \cdot 0.508 \cdot A_c / u + 250 \le 1{,}500$; constant depending on member size and relative humidity

Equations H.9 and H.10 are used when strength gaining different from normal is expected.

$$t' = t'_T \left[\frac{9}{2 + (t'_T)^{1.2}} + 1 \right]^{\alpha} \ge 0.5 \; days \qquad \text{(H.9)}$$

$$t'_T = \sum \Delta t_i \cdot \exp\left\{-\left[\frac{4{,}000}{273 + T(\Delta t_i)/T_0} - 13.65\right]\right\} \qquad \text{(H.10)}$$

where

t′: age of concrete at loading (days)

t'_T: adjusted age of concrete at loading

$$\alpha = \begin{cases} -1 \textit{ for slowly hardening cement} \\ 0 \textit{ for normal / rapid hardening cement} \\ +1 \textit{ for rapid hardening high early strength cement} \end{cases} \quad \text{; cement type parameter}$$

Δt_i: period of time (days) at temperature $T(\Delta t_i)$ (^oC) ($^oC = 0.556 \times {}^oF - 17.778$)

T_0: 1 ^oC

When stresses between 40 and 60 percent of compressive strength are applied, CEB-FIP recommends using a high stress correction to the notional creep "ϕ_0" as shown in Equation H.11.

$$\phi_{0,k} = \phi_0 \cdot \exp\{1.5 \cdot (k_\sigma - 0.4)\} \qquad \text{(H.11)}$$

where

$\phi_{0,k}$: notional creep coefficient corrected by stress level

ϕ_0: notional creep coefficient

k_σ: stress-to-strength ratio at time of application of load.

Drying Shrinkage Model. Equation H.12 presents CEB-FIP expression for predicting shrinkage.

$$\varepsilon_s(t,t_0) = \varepsilon_{so} \cdot \beta_s \cdot (t - t_0) \qquad \text{(H.12)}$$

where

t: age of concrete (days)

t_0: age of concrete at the beginning of drying (days)

$\varepsilon_{s0} = \left[160 + 10 \cdot \beta_{sc} \cdot \left(9 - \frac{f_c'}{1{,}450}\right)\right] \cdot \beta_{RH}$; notional shrinkage coefficient

$$\beta_{sc} = \begin{cases} 4 \text{ for slowly hardening cement} \\ 5 \text{ for normal / rapid hardening cement} \\ 8 \text{ for rapid hardening high early strength cement} \end{cases}$$; cement type parameter

$$\beta_{RH} : \begin{cases} -1.55 \cdot \left[1 - h^3\right] & \text{for} \quad 0.40 \le h \le 0.99 \\ 0.25 & \text{for} \quad h \ge 0.99 \end{cases}$$; relative humidity factor

h: relative humidity in decimals

f_c': compressive strength of concrete cylinders at 28 days (ksi)

$\beta_s(t,t_0) = \left[\frac{(t - t_0)}{\beta_{sH} + (t - t_0)}\right]^{0.5}$; shrinkage-time function

$\beta_{sH} = 350 \cdot \left(5.08 \cdot {}^{A_c}\!/_{u}\right)^2$; geometric factor

A_c: cross sectional area (in^2)

u: exposed perimeter (in)

When temperatures above 30°C (86°F) are applied, CEB-FIP recommends using an elevated temperature correction for β_{sH} and β_{RH} as shown below.

$$\beta_{sH,T} = \beta_{sH} \cdot \exp\{-0.06 \cdot (T - 20)\} \qquad \beta_{RH,T} = \beta_{RH} \cdot \left[1 + \left(\frac{0.08}{1.03 - h}\right) \cdot \left(\frac{T - 20}{40}\right)\right]$$

where

$\beta_{sH,T}$: geometric factor corrected by temperature

$\beta_{sH} = 350 \cdot \left(5.08 \cdot {}^{A_c}\!/_{u}\right)^2$; geometric factor

$\beta_{RH,T}$; relative humidity factor corrected by temperature

$$\beta_{RH} : \begin{cases} -1.55 \cdot \left[1 - h^3\right] & for \quad 0.40 \le h \le 0.99 \\ 0.25 & for \quad h \ge 0.99 \end{cases}$$; relative humidity factor

T: ambient temperature (^{o}C) (${}^{o}C = 0.556 \times {}^{o}F - 17.778$)

h: relative humidity in decimals

H.1.4. Bažant and Panula's - BP Method

First proposed in the late 1970's (Bažant and Panula, 1978a, 1978b, 1979a), the BP model suggested some computations quite different from ACI and CEB models. Among those are the modeling of creep using three portions (basic, drying, and after drying creep) based on a double power law in time and drying shrinkage based on a square-root hyperbolic law in time (Bažant and Panula 1978b, 1978d).

Creep Model. The BP model proposed that creep of concrete is comprised of three portions: Basic creep modeled by a double power law in time; drying creep modeled by a hyperbolic law multiplied by drying shrinkage; and creep decrease after drying which is modeled by a hyperbolic law multiplied by double power law in time. Equation H.13 presents the BP model general compliance function.

$$J(t,t') = \frac{1}{E_0} + C_0(t,t') + C_d(t,t',t_0) - C_p(t,t',t_0) \qquad \text{(H.13)}$$

where

J: compliance function

E_0: Modulus of elasticity at the age of loading (ksi)

C_0: basic creep portion [specific creep - (in/in)/ksi]

C_d: drying creep portion [specific creep - (in/in)/ksi]

C_p: creep decrease after drying [specific creep - (in/in)/ksi]

Basic Creep Model. Basic creep can be best approximated by a double power law (Bažant and Panula, 1978a, 1978b), in the form:

$$C_0(t,t') = \frac{\phi_1}{E_0} \cdot \left(t'^{-m} + \alpha\right) \cdot \left(t - t'\right)^n \qquad \text{(H.14)}$$

where

C_0: basic creep portion [specific creep - (in/in)/ksi]

E_0: Modulus of elasticity at the age of loading (ksi)

t: age of concrete (days)

t′: age of concrete at loading (days)

$\phi_1 = \dfrac{10^{3 \cdot n}}{2 \cdot \left(28^{-m} + \alpha\right)}$ material parameter

$$n = \begin{cases} 0.12 + \dfrac{0.07 \cdot x^6}{5130 + x^6} \; for \; x > 4 \\ \\ 0.12 \; for \; x \le 4 \end{cases} \qquad x = \left[2.1 \cdot \frac{\left(a/c\right)}{\left(s/c\right)} + 0.1 \cdot \left(f_c'\right)^{1.5} \cdot \left(\frac{w}{c}\right)^{1/3} \cdot \left(\frac{a}{g}\right)^{2.2} \right] \cdot a_1 - 4$$

c: cementitious materials content (lb/yd^3)

w: water content (lb/yd^3)

a: total aggregate content (lb/yd^3)

s: fine aggregate content (lb/yd^3)

g: coarse aggregate content (lb/yd^3)

f_c': compressive strength of concrete cylinders at 28 days (ksi)

$m = 0.28 + \frac{1}{(f_c')^2}$; $\alpha = \frac{1}{40 \cdot \left(w/c\right)}$; material parameters

a_1: cement type coefficient $\begin{cases} 1.00 \text{ for Type I and II cements} \\ 0.93 \text{ for Type III cement} \\ 1.05 \text{ for Type IV cement} \end{cases}$

Drying Creep Model:

According to Bažant and Panula (1978c and 1984) drying creep can be modeled by Equation H.15:

$$C_d(t,t',t_0) = \frac{\phi_d'}{E_0} \cdot t'^{-m/2} \cdot k_h' \cdot \varepsilon_{sh\infty} \cdot \left(1 + \frac{10 \cdot \tau_{sh}}{t - t'}\right)^{-c_d \cdot n} \qquad \text{(H.15)}$$

where

C_d: drying creep portion [specific creep - (in/in)/ksi]

E_0: Modulus of elasticity at the age of loading (ksi)

t: age of concrete (days)

t′: age of loading (days)

t_0: age of concrete at the beginning of drying (days)

$$\phi_d' = \left(1 + \frac{t' - t_0}{10 \cdot \tau_{sh}}\right)^{-1/2} \cdot \phi_d$$

$$\phi_d = \begin{cases} 0.008 + 0.027 \cdot \dfrac{1}{1 + 0.7 \cdot r^{-1.4}} \ for\ r > 0 \\ 0.008 \ for\ r \le 0 \end{cases} \qquad r = 56{,}000 \cdot \left(\frac{s}{a} \cdot f_c' \right)^{0.3} \cdot \left(\frac{g}{s} \right)^{1.3} \cdot \left(\frac{w/c}{\varepsilon_{s\infty}} \right)^{1.5} - 0.85$$

c: cementitious materials content (lb/yd^3)

w: water content (lb/yd^3)

a: total aggregate content (lb/yd^3)

s: fine aggregate content (lb/yd^3)

g: coarse aggregate content (lb/yd^3)

f_c': compressive strength of concrete cylinders at 28 days (ksi)

$$\tau_{sh} = 600 \cdot \left(\frac{k_s}{150} \cdot 50.8 \cdot V/S \right)^2 \cdot \frac{C_1^{ref}}{C_1(t_0)} \text{ ; size-dependent factor}$$

$$k_s = \begin{cases} 1.0 \text{ for infinite slab} \\ 1.15 \text{ for infinite cylinder} \\ 1.25 \text{ for infinite squared prism} \\ 1.30 \text{ for a sphere} \\ 1.55 \text{ for a cube} \end{cases} \text{ ; shape factor}$$

V: specimen volume (in^3)

S: specimen surface area (in^2)

$$C_1^{ref} = 10\ mm^2 / day$$

$$C_1(t_0) = C_7 \cdot k_T' \cdot \left(0.05 + \sqrt{\frac{6.3}{t_0}} \right)$$

$$C_7 = \frac{1}{8} \cdot \frac{w}{c} \cdot (0.593 \cdot c) - 12 \qquad 7 \le C_7 \le 21$$

$$k_T' = \frac{T}{T_0}\exp\left\{\frac{5{,}000}{T_0} - \frac{5{,}000}{T}\right\}$$

T: ambient temperature ^{o}K ($^{o}K = 0.556 \times {}^{o}F + 255.372$)

T_0: 296.15 ^{o}K (reference temperature)

$$n = \begin{cases} 0.12 + \dfrac{0.07 \cdot x^6}{5130 + x^6} \; for \; x > 4 \\ \\ 0.12 \; for \; x \le 4 \end{cases} \qquad x = \left[2.1 \cdot \frac{\left(a/c\right)}{\left(s/c\right)} + 0.1 \cdot \left(f_c'\right)^{1.5} \cdot \left(\frac{w}{c}\right)^{1/3} \cdot \left(\frac{a}{g}\right)^{2.2} \right] \cdot a_1 - 4$$

$m = 0.28 + \dfrac{1}{\left(f_c'\right)^2}$; $\alpha = \dfrac{1}{40 \cdot \left(w/c\right)}$; material parameters

a_1: cement type coefficient $\begin{cases} 1.00 \; for \; Type \; I \; and \; II \; cements \\ 0.93 \; for \; Type \; III \; cement \\ 1.05 \; for \; Type \; IV \; cement \end{cases}$

$k_h' = \left| h_0^{1.5} - h^{1.5} \right|$; humidity dependent parameter

h: relative humidity in decimals

h_0: 0.98 to 1.0

$\varepsilon_{s\infty}$: final shrinkage in με as in Equation H.17

$c_d = 2.8 - 7.5 \cdot n$

Creep Decrease after Drying

Creep decrease after drying follows a function of time similar to drying creep as shows Equation H.16:

$$C_p(t, t', t_0) = c_p \cdot k_h'' \cdot \left(1 + \frac{100 \cdot \tau_{sh}}{t - t_0}\right) \cdot C_0\left(t, t'\right) \qquad \text{(H.16)}$$

where

C_p: creep decrease after drying portion [specific creep - (in/in)/ksi]

t: age of concrete (days)

t′: age of concrete at loading (days)

t_0: age of concrete at the beginning of drying (days)

$c_p = 0.83$

$k_h'' = h_0^2 - h^2$ humidity dependent parameter

h: relative humidity in decimals

h_0: 0.98 to 1.0

$\tau_{sh} = 600 \cdot \left(\frac{k_s}{150} \cdot 50.8 \cdot V/S \right)^2 \cdot \frac{C_1^{ref}}{C_1(t_0)}$; size-dependent factor

$$k_s = \begin{cases} 1.0 \text{ for infinite slab} \\ 1.15 \text{ for infinite cylinder} \\ 1.25 \text{ for infinite squared prism} \\ 1.30 \text{ for a sphere} \\ 1.55 \text{ for a cube} \end{cases} \text{ ; shape factor}$$

V: specimen volume (in^3)

S: specimen surface area (in^2)

$C_1^{ref} = 10\ mm^2 / day$

$C_1(t_0) = C_7 \cdot k_T' \cdot \left(0.05 + \sqrt{\frac{6.3}{t_0}} \right)$

$C_7 = \frac{1}{8} \cdot \frac{w}{c} \cdot (0.593 \cdot c) - 12 \qquad 7 \le C_7 \le 21$

c: cementitious materials content (lb/yd^3)

w: water content (lb/yd^3)

$$k_T' = \frac{T}{T_0}\exp\left\{\frac{5{,}000}{T_0} - \frac{5{,}000}{T}\right\}$$

T: ambient temperature ^{o}K ($^{o}K = 0.556 \times {}^{o}F + 255.372$)

T_0: 296.15 ^{o}K (reference temperature)

C_0: basic creep portion [specific creep - (in/in)/ksi]

Drying Shrinkage Model. Drying shrinkage can be approximate by square-root hyperbolic law in time, as shown in Equation H.17

$$\varepsilon_{sh}(t,t_0) = \varepsilon_{sh\infty} \cdot k_h \cdot \sqrt{\frac{t-t_0}{\tau_{sh}+t-t_0}} \qquad \text{(H.17)}$$

where

$\varepsilon_{sh\infty}$: ultimate shrinkage stain με

$$k_h = \begin{cases} 1-h^3 \ \ for\ h \le 0.98 \\ -0.2 \ \ for\ h = 1.00 \\ linear\ \text{int}erpolation\ \ for\ 0.98 \le h \le 1.00 \end{cases} \quad \text{; humidity-dependent factor}$$

h: relative humidity in decimals

t: age of concrete (days)

t_0: age of concrete at the beginning of drying (days)

$$\tau_{sh} = 600 \cdot \left(\frac{k_s}{150} \cdot 50.8 \cdot V/S\right)^2 \cdot \frac{C_1^{ref}}{C_1(t_0)} \ \text{; size-dependent factor}$$

$$k_s = \begin{cases} 1.0 \text{ for infinite slab} \\ 1.15 \text{ for infinite cylinder} \\ 1.25 \text{ for infinite squared prism} \\ 1.30 \text{ for a sphere} \\ 1.55 \text{ for a cube} \end{cases} \quad \text{; shape factor}$$

V: specimen volume (in^3)

S: specimen surface area (in^2)

$C_1^{ref} = 10\ mm^2 / day$

$$C_1(t_0) = C_7 \cdot k_T' \cdot \left(0.05 + \sqrt{\frac{6.3}{t_0}}\right)$$

$$C_7 = \frac{1}{8} \cdot \frac{w}{c} \cdot (0.593 \cdot c) - 12 \qquad 7 \le C_7 \le 21$$

$$k_T' = \frac{T}{T_0} \exp\left\{\frac{5{,}000}{T_0} - \frac{5{,}000}{T}\right\}$$

T: ambient temperature ^oK ($^oK = 0.556 \times {}^oF + 255.372$)

T_0: 296.15 ^oK (reference temperature)

$$\varepsilon_{s\infty} = 1210 - \frac{880}{\frac{390}{z} + 1} \quad ; \quad z = \left[\left[1.25 \cdot \sqrt{\frac{a}{c}} + 0.5 \cdot \left(\frac{g}{s}\right)^2\right] \cdot \left(\frac{1 + s/c}{w/c}\right)^{1/3} \cdot \sqrt{f_c'}\right] - 12 \ge 0$$

c: cementitious materials content (lb/yd^3)

w: water content (lb/yd^3)

a: total aggregate content (lb/yd^3)

s: fine aggregate content (lb/yd^3)

g: coarse aggregate content (lb/yd^3)

f_c': compressive strength of concrete cylinders at 28 days (ksi)

H.1.5. Bažant and Baweja's - B3 Method

B3 model was proposed by Bažant and Baweja (1995a, 1995b, 1995c) as a new improvement and an update of previous models such as BP (Bažant and Panula, 1978a, 1978b, 1978c, 1978d) and BP-KX (Bažant, Panula, Kim, Koo, and Xi, 1992). According to the Bažant and Baweja (1995a, 1995b, 1995c), B3 model is simpler, better

theoretically supported and more exact than the previous ones. The main difference with the BP model is that the B3 model only takes into account basic and drying creep portions.

Creep Model. The average compliance function incorporating instantaneous deformation, basic and drying creep, is expressed in Equation H.18:

$$J(t,t') = q_1 + C_0(t,t') + C_d(t,t',t_o) \qquad \text{(H.18)}$$

where

$q_1 = \dfrac{0.6\times10^6}{E_0}$ instantaneous strain due to unit stress (1/ksi)

C_0: basic creep portion [specific creep - (in/in)/ksi]

C_d: drying creep portion [specific creep - (in/in)/ksi]

t: age of concrete (days)

t′: age of concrete at loading (days)

E_0: asymptotic modulus elastic modulus (ksi) (age independent)

Basic Creep Model. Basic creep is given by Equation H.19, as follows:

$$C_0(t,t') = q_2 \cdot Q(t,t') + q_3 \cdot \ln\left[1 + (t-t')^n\right] + q_4 \ln\left[\frac{t}{t'}\right] \qquad \text{(H.19)}$$

where

C_0: basic creep portion [specific creep - (in/in)/ksi]

$q_2 = 451.1\sqrt{c}\cdot {f_c}'^{-0.9}$; ageing viscoelastic compliance

f_c': compressive strength of concrete cylinders at 28 days (psi)

$$Q(t,t') = Q_f(t')\cdot\left[1+\left(\frac{Q_f(t')}{Z(t,t')}\right)^{r(t')}\right]^{-1/r(t')} \quad ; \quad Q_f(t') = \left[0.086\cdot(t')^{2/9} + 1.21\cdot(t')^{4/9}\right]^{-1}$$

$$Z(t,t') = (t')^{-m}\cdot\ln\left[1+(t-t')^n\right]$$

$$r(t') = 1.7\cdot(t')^{0.12} + 8$$

m = 0.5; n = 0.1

t: age of concrete (days)

t′: age of concrete at loading (days)

$q_3 = 0.29 \cdot \left(\frac{w}{c}\right)^4 \cdot q_2$; non-ageing viscoelastic compliance

$q_4 = 0.14 \cdot \left(\frac{a}{c}\right)^{-0.7}$; flow compliance

c: cementitious materials content (lb/yd^3)

w: water content (lb/yd^3)

a: total aggregate content (lb/yd^3)

Drying Creep Model. Additional creep due to drying is given by Equation H.20

$$C_d(t,t',t_0) = q_5 \cdot \left[\exp\{-8 \cdot H(t)\} - \exp\{-8 \cdot H(t_0')\}\right]^{1/2} \qquad \text{(H.20)}$$

where

$$q_5 = \frac{757{,}000}{f'_c} \cdot \left|\varepsilon_{sh\infty}\right|^{-0.6}$$

f_c': compressive strength of concrete cylinders at 28 days (psi)

$$H(t) = 1 - (1-h) \cdot \tanh\sqrt{\frac{t-t_0}{\tau_{sh}}}$$

h: relative humidity in decimals

t: age of concrete (days)

t′: age of concrete at loading (days)

t_0: age of concrete at the beginning of drying (days)

t_0': max(t′,t_0) (days)

τ_{sh}: size factor as shown in Equation H.21

Drying Shrinkage Model. Drying shrinkage expression is given by Equation H.21, as follows:

$$\varepsilon_{sh}(t,t_0) = -\varepsilon_{sh\infty} \cdot k_h \cdot \tanh\sqrt{\frac{t-t_0}{\tau_{sh}}} \qquad \text{(H.21)}$$

where

ε_{sh}: shrinkage strain

$$\varepsilon_{sh\infty} = -\alpha_1 \cdot \alpha_2 \cdot \left[0.02565 \cdot w^{2.1} \cdot (f_c')^{-0.28} + 270\right] \cdot \frac{\left(\frac{607}{4+0.85\cdot 607}\right)^{1/2}}{\left(\frac{(t_0+\tau_{sh})}{4+0.85\cdot(t_0+\tau_{sh})}\right)^{1/2}}$$

$$\alpha_1 = \begin{cases} 1.00, \textit{ for type I cement} \\ 0.85, \textit{ for type II cement} \\ 1.10, \textit{ for type III cement} \end{cases} \text{; cement type factor}$$

$$\alpha_2 = \begin{cases} 0.75, \textit{ for steam} - \textit{cured specimens} \\ 1.00, \textit{ for water or } h = 1.00 - \textit{cured specimens} \\ 1.20, \textit{ for sealed specimens} \end{cases} \text{; curing factor}$$

w: water content (lb/yd^3)

f_c': compressive strength of concrete cylinders at 28 days (psi)

$$k_h = \begin{cases} 1-h^3 \ \textit{ for } h \le 0.98 \\ -0.2 \ \textit{ for } h = 1.00 \\ \text{linear interpolation for } 0.98 \le h \le 1.00 \end{cases} \text{; humidity-dependent factor}$$

h: relative humidity in decimals

t: age of concrete (days)

t_0: age of concrete at the beginning of drying (days)

$$\tau_{sh} = 190.8 \cdot t_0^{-0.008} \cdot f_c'^{-0.25} \cdot \left(k_s \cdot 2 \cdot V/S\right)^2 \text{ ; size-dependent factor}$$

$$k_s = \begin{cases} 1.0 \text{ for infinite slab} \\ 1.15 \text{ for infinite cylinder} \\ 1.25 \text{ for infinite squared prism} \\ 1.30 \text{ for a sphere} \\ 1.55 \text{ for a cube} \end{cases} \text{ ; shape factor}$$

V: specimen volume (in^3)

S: specimen surface area (in^2)

H.1.6. Gardner and Lockman's - GL Method

Gardner and Lockman (2001) proposed a more compact model for creep coefficient depending only on relative humidity and member geometry. Equations H.22 and H.23 present GL model equations for creep and shrinkage.

Creep Model:

$$c_{cr}(t,t') = \left[\frac{2 \cdot (t-t')^{0.3}}{(t-t')^{0.3} + 14} + \left(\frac{7}{t_o} \right)^{1/2} \cdot \left(\frac{(t-t')}{(t-t') + 7} \right)^{1/2} + \right.$$

$$\left. 2.5 \cdot \left(1 - 1.086 \cdot h^2\right) \cdot \left(\frac{(t-t')}{(t-t') + 0.15 \cdot \left(25.4 \cdot V/S\right)^2} \right)^{1/2} \right] \cdot \frac{1}{E_{c28}} \quad \text{(H.22)}$$

where

c_{cr}: specific creep at age t loaded at t′ (με/ksi)

t: age of concrete (days)

t′: age of concrete at loading (days)

t_0: age of concrete at the beginning of drying (days)

h: relative humidity in decimals

V: specimen volume (in^3)

S: specimen surface area (in^2)

E_{c28}: 28-day elastic modulus (ksi)

Drying Shrinkage Model:

$$\varepsilon_{sh}(t,t_0) = \varepsilon_{shu} \cdot \left(1 - 1.18 \cdot h^4\right) \cdot \left(\frac{(t-t_0)}{(t-t_0) + 0.15 \cdot \left(25.4 \cdot V/S\right)^2} \right)^{1/2} \qquad \text{(H.23)}$$

where

ε_{sh}: shrinkage strain

$\varepsilon_{shu} = 1{,}000 \cdot K \cdot \left(\frac{4.35}{f_c'} \right)^{1/2} \cdot 10^{-6}$; ultimate shrinkage strain

$$K = \begin{cases} 1.00 \text{ for Type I cement} \\ 0.70 \text{ for Type II cement} \\ 1.15 \text{ for Type III cement} \end{cases} \text{; cement factor}$$

f_c': compressive strength of concrete cylinders at 28 days (ksi)

h: relative humidity in decimals

t: age of concrete (days)

t_0: age of concrete at the beginning of drying (days)

V: specimen volume (in^3)

S: specimen surface area (in^2)

H.1.7. Sakata's - SAK 93 Method

Sakata (1993) developed an exponential model for specific creep and drying shrinkage. The models presented in Equations H.24 through H.26 are based on relative humidity, member geometry, and water and cement content.

Creep Model. SAK method models specific creep based on two portions: basic creep and drying creep. Equation H.24 proposes that both portions progress following an exponential curve.

$$\varepsilon_{cr}(t,t') = \left(\varepsilon'_{bc} + \varepsilon'_{dc}\right) \cdot \left(1 - \exp\left\{-0.09 \cdot (t - t')^{0.6}\right\}\right) \quad \text{(H.24)}$$

where

ε_{cr}: specific creep at age "t" loaded at t′ (με/ksi)

t: age of concrete (days)

t′: age of concrete at loading (days)

ε'_{bc}: basic creep portion, parameter depending on water and cement content, water-to-cement ratio, and age of loading

ε'_{dc}: drying creep portion, parameter depending on water and cement content, water-to-cement ratio, member volume-to-surface ratio, and relative humidity

Basic Creep Model. Basic creep is given by Equation H.25, as follows:

$$\varepsilon'_{bc} = 3.641 \cdot (c + w)^2 \cdot \left(w/c\right)^{2.4} \cdot \left(\ln[t']\right)^{-0.67} \quad \text{(H.25)}$$

where

ε'_{bc}: basic specific creep portion (με/ksi)

c: cement content (lb/yd^3)

w: water content (lb/yd^3)

t′: age of concrete at loading (days)

Drying Creep Model. Drying creep is given by Equation H.26

$$\varepsilon'_{dc} = 0.015 \cdot (c + w)^{1.4} \cdot \left(w/c\right)^{4.2} \cdot \left(\ln\left[25.4 \cdot \left(V/S\right)\right]\right)^{-2.2} \cdot (1 - h)^{0.36} \cdot (t_0)^{-0.3} \quad \text{(H.26)}$$

where

ε'_{dc}: drying specific creep portion (με/ksi)

c: cement content (lb/yd^3)

w: water content (lb/yd^3)

V: specimen volume (in^3)

S: specimen surface area (in^2)

h: relative humidity in decimals

t_0: age of concrete at the beginning of drying (days)

Drying Shrinkage Model

$$\varepsilon_{sh}(t,t_0) = \varepsilon_{sh\infty} \cdot \left(1 - \exp\left\{-0.108 \cdot (t - t_0)^{0.56}\right\}\right) \times 10^{-5} \qquad \text{(H.27)}$$

where

ε_{sh}: shrinkage strain

t: age of concrete (days)

t_0: age of concrete at the beginning of drying (days)

$\varepsilon_{sh\infty} = -600 + 780 \cdot (1 - \exp\{h\}) + 380 \cdot \ln[0.593 \cdot w] - 50 \cdot \left(\ln\left[25.4 \cdot \left(V/S\right)\right]\right)^2 + 44 \cdot \ln[t_0]$;

ultimate shrinkage strain

h: relative humidity in decimals

w: water content (lb/yd^3)

V: specimen volume (in^3)

S: specimen surface area (in^2)

H.2 Models for High Strength High Performance Concrete

The creep and shrinkage models for high strength high performance concrete consider variables than can be grouped in ambient condition variables, mix design variables, and concrete element geometric properties.

Among the ambient variables, there are: type of curing, length of curing, age or maturity of concrete at loading, stress-to-strength ration at loading, age of concrete at starting of drying, relative humidity, and temperature. fine aggregate content, coarse aggregate content, water content, cement content, type of cement, cementitious materials content, use of silica fume, and concrete strength are the variables related with the mix design. Finally, within the member variables, there are: shape of the member and volume-to- surface ratio.

H.2.1 CEB-FIP Method as modified by Yue and Taerwe (1993)

Han (1996) reported the changes suggested by Yue and Taerwe (1993) to CEB-FIP creep equations in order to predict creep of high strength concrete. β_H and $ø_0$ from Equation H.8 can be modified as shown in Equations H.28 and H.29

$$\beta_H = \frac{18.85}{f_c'} \cdot \left[1 + (0.012 \cdot h)^{18}\right] \cdot \left(50.8 \cdot {}^{A_c}\!/_{u}\right) + 250 \le 1500 \qquad \text{(H.28)}$$

where

β_H: constant depending on member size and relative humidity

f_c': compressive strength of concrete cylinders at 28 days (ksi)

h: relative humidity in decimals

A_c: cross sectional area (in^2)

u: exposed perimeter (in)

$$\phi_0 = \left[1 + \frac{(1-h)}{0.367 \cdot \left(A_c / u\right)^{1/3}}\right] \cdot \frac{2.6}{\sqrt{\frac{f_c'}{1.45}} - 1} \cdot \frac{1}{0.1 + t'^{0.2}} \qquad \text{(H.29)}$$

where

ϕ_0: ; notional creep coefficient

h: relative humidity in decimals

A_c: cross sectional area (in^2)

u: exposed perimeter (in)

f_c': compressive strength of concrete cylinders at 28 days (ksi)

t′: age of concrete at loading (days)

H.2.2. Bažant and Panula's - BP Method

Bažant and Panula (1984) proposed some modifications to drying creep portion of the BP model to take into account high strength concrete. They found that the rest of the expressions were still valid for HSH. Equation H.30 presents the new version of Equation H.15 where the new parameters b_d and a_d are introduced.

$$C_d(t,t',t_0) = \frac{\phi_d'}{E_0} \cdot t'^{-m/2} \cdot k_h' \cdot \varepsilon_{sh\infty} \cdot \left(1 + \frac{b_d \cdot \tau_{sh}}{t - t'}\right)^{-c_d \cdot n} \qquad \text{(H.30)}$$

where

C_d: drying creep portion [specific creep - (με)/ksi]

t: age of concrete (days)

t′: age of loading (days)

t_0: age of concrete at the beginning of drying (days)

$$\phi_d' = \left(1 + \frac{t' - t_0}{a_d \cdot \tau_{sh}}\right)^{-1/2} \cdot \phi_d$$

$$a_d = \begin{cases} 10 \ for f_c' \le 6{,}000 \ psi \\ \qquad\qquad\qquad\qquad\qquad \text{; linear interpolation between 6,000 and 10,000 psi} \\ 1 \ for f_c' \ge 10{,}000 \ psi \end{cases}$$

$$\tau_{sh} = 600 \cdot \left(\frac{k_s}{150} \cdot 50.8 \cdot V/S\right)^2 \cdot \frac{C_1^{ref}}{C_1(t_0)} \text{ ; size-dependent factor}$$

$$k_s = \begin{cases} 1.0 \text{ for infinite slab} \\ 1.15 \text{ for infinite cylinder} \\ 1.25 \text{ for infinite squared prism ; shape factor} \\ 1.30 \text{ for a sphere} \\ 1.55 \text{ for a cube} \end{cases}$$

V: specimen volume (in^3)

S: specimen surface area (in^2)

$$C_1^{ref} = 10 \ mm^2 / day$$

$$C_1(t_0) = C_7 \cdot k_T' \cdot \left(0.05 + \sqrt{\frac{6.3}{t_0}}\right)$$

$$C_7 = \frac{1}{8} \cdot \frac{w}{c} \cdot (0.593 \cdot c) - 12 \qquad 7 \le C_7 \le 21$$

$$k_T' = \frac{T}{T_0} \exp\left\{\frac{5{,}000}{T_0} - \frac{5{,}000}{T}\right\}$$

T: ambient temperature ^oK ($^oK = 0.556 \times {}^oF + 255.372$)

T_0: 296.15 ^oK (reference temperature)

$$\phi_d = \begin{cases} 0.008 + 0.027 \cdot \dfrac{1}{1 + 0.7 \cdot r^{-1.4}} \ \ for\ r > 0 \\ 0.008 \ \ for\ r \le 0 \end{cases} \qquad r = 56000 \cdot \left(\frac{s}{a} \cdot f_c'\right)^{0.3} \cdot \left(\frac{g}{s}\right)^{1.3} \cdot \left(\frac{w/c}{\varepsilon_{s\infty}}\right)^{1.5} - 0.85$$

c: cementitious materials content (lb/yd^3)

w: water content (lb/yd^3)

a: total aggregate content (lb/yd^3)

s: fine aggregate content (lb/yd^3)

g: coarse aggregate content (lb/yd^3)

f'_c: compressive strength (ksi)

$$\varepsilon_{s\infty} = 1{,}210 - \frac{880}{\frac{390}{z} + 1} \quad ; \quad z = \left[\left[1.25 \cdot \sqrt{\frac{a}{c}} + 0.5 \cdot \left(\frac{g}{s}\right)^2\right] \cdot \left(\frac{1 + s/c}{w/c}\right)^{1/3} \cdot \sqrt{f_c'}\right] - 12 \ge 0$$

E_0: Modulus of elasticity at the age of loading (ksi)

$m = 0.28 + \dfrac{1}{(f_c')^2}$; material parameter

$k_h' = \left|h_0^{1.5} - h^{1.5}\right|$ humidity dependent parameter

h: relative humidity in decimals

$$b_d = \begin{cases} 10 \ \ for f_c' \le 6{,}000\ psi \\ \\ 100 \ \ for f_c' \ge 10{,}000\ psi \end{cases}$$; linear interpolation between 6,000 and 10,000 psi

$c_d = 2.8 - 7.5 \cdot n$

$$n = \begin{cases} 0.12 + \dfrac{0.07 \cdot x^6}{5130 + x^6} \; for \; x > 4 \\ \\ 0.12 \; for \; x \le 4 \end{cases} \qquad x = \left[2.1 \cdot \dfrac{\left(a/c\right)}{\left(s/c\right)} + 0.1 \cdot \left(f_c'\right)^{1.5} \cdot \left(\dfrac{w}{c}\right)^{1/3} \cdot \left(\dfrac{a}{g}\right)^{2.2} \right] \cdot a_1 - 4$$

H.2.3. Sakata's - SAK 01 Method

Sakata et al. (2001) derived new Equations for predicting creep and drying shrinkage for a wide range of concrete strength. Equations H.31 and H.32 show the new specific creep and drying shrinkage expressions:

$$\varepsilon_{cr}(t,t') = \left(\frac{2.373 \cdot w \cdot (1-h) + 350 \cdot}{12 + 6.8966 \cdot \left(f_c'(t')\right)} \cdot \ln\left[t - t' + 1\right] \right) \times 6.8966 \qquad \text{(H.31)}$$

where

ε_{cr}: specific creep at age "t" loaded at t′ (με/ksi)

t: age of concrete (days)

t′: age of concrete at loading (days)

w: water content (lb/yd^3)

h: relative humidity in decimals

$f_c'(t')$: compressive strength at the age of t′(psi)

Drying Shrinkage Model

$$\varepsilon_{sh}(t,t_0) = \frac{\varepsilon_{sh\infty} \cdot (t - t_0)}{\beta + (t - t_0)} \qquad \text{(H.32)}$$

where

ε_{sh}: shrinkage strain

t: age of concrete (days)

t_0: age of concrete at the beginning of drying (days)

$$\varepsilon_{sh\infty} = \frac{\alpha(1-h)\cdot 0.5933\cdot w}{1+150\exp\left\{-\frac{72.5}{f_c'}\right\}}\cdot\frac{1}{1+\eta\cdot t_0}$$; ultimate shrinkage strain

$$\alpha = \begin{cases} 10 \text{ for normal portland cement} \\ 8 \text{ for slow hardening cement} \end{cases}$$; cement factor

h: relative humidity in decimals

w: water content (lb/yd^3)

f_c': compressive strength of concrete cylinders at 28 days (ksi)

$$\eta = \left(15\cdot\exp\{0.0483\cdot f_c'\}+0.1483\cdot w\right)\times 10^{-4}$$

$$\beta = \frac{19.8\cdot w\sqrt{V/S}}{100+0.7\cdot t_0}$$

V: specimen volume (in^3)

S: specimen surface area (in^2)

H.2.4. AFREM Method

le Roy, de Larrard, and Pons (1996) described the AFREM model for modeling long-term deformations of high strength concrete. AFREM method main expressions for modeling creep and drying shrinkage are presented in Equations H.33 through H.36.

Creep Model. Equation H.33 presents AFREM creep prediction Equation which is comprised of basic creep portion and drying creep portion.

$$\varepsilon_{cr}(t,t') = \frac{\sigma(t')}{E_{28}}\left(\phi_b(t,t')+\phi_d(t,t')\right) \qquad \text{(H.33)}$$

where

ε_{cr}: creep strain in με

$\sigma(t')$: applied stress at t′ (ksi)

E_{28}: 28-day elastic modulus (ksi)

t: age of concrete (days)

t′: age of concrete at loading (days)

$ø_b$: basic creep coefficient at age "t" loaded at t′

$ø_d$: drying creep coefficient at age "t" loaded at t′

Basic Creep Model. Basic creep coefficient can be expressed as shown in Equation H.34, as follows:

$$\phi_b(t,t') = \phi_{b0} \cdot \frac{\sqrt{t-t'}}{\beta_{bc} + \sqrt{t-t'}} \qquad \text{(H.34)}$$

where

$$\phi_{b0} = \begin{cases} \dfrac{1.762}{f_c'(t')^{0.37}} \text{ for silica fume concrete} \\ 1.4 \text{ for non silica fume concrete} \end{cases}$$

$f'_c(t')$: compressive strength at the age of t′ (ksi)

$$\beta_{bc} = \begin{cases} 0.37 \cdot \exp\left\{2.8 \cdot \dfrac{f_c'(t')}{f_c'}\right\} \text{ for silica fume concrete} \\ 0.40 \cdot \exp\left\{3.1 \cdot \dfrac{f_c'(t')}{f_c'}\right\} \text{ for non silica fume concrete} \end{cases}$$

f'_c: compressive strength of concrete cylinders at 28 days (ksi)

Drying Creep Model.

Drying creep coefficient is given by Equation H.35

$$\phi_d(t,t',t_0) = \phi_{d0} \cdot (\varepsilon_{sh}(t,t_0) - \varepsilon_{sh}(t',t_0)) \quad \text{(H.35)}$$

where

$$\phi_{d0} = \begin{cases} 1{,}000 \text{ for silica fume concrete} \\ 3{,}200 \text{ for non silica fume concrete} \end{cases}$$

ε_{sh}: drying shrinkage as shown in Equation H.36

Drying Shrinkage Model. Drying creep expression is shown in Equation H.36, as follows:

$$\varepsilon_{sh}(t,t_0) = \frac{K(f_c') \cdot (72 \cdot \exp\{-0.3172 \cdot f_c'\} + 75 - 100 \cdot h)}{\beta_{ds0} \cdot \left(50.8 \cdot A_c/u\right)^2 + (t - t_0)} \cdot (t - t_0) \times 10^{-6} \quad \text{(H.36)}$$

where

ε_{sh}: shrinkage strain

t: age of concrete (days)

t_0: age of concrete at the beginning of drying (days)

$$K(f_c') = \begin{cases} 18 \text{ for } f_c' \le 8.25 \text{ ksi} \\ 30 - 1.448 \cdot f_c' \text{ for } f_c' \ge 8.25 \text{ ksi} \end{cases} \text{; strength-dependent factor}$$

f_c': compressive strength of concrete cylinders at 28 days (ksi)

h: relative humidity in decimals

$$\beta_{ds0} = \begin{cases} 0.007 \text{ for silica fume concrete} \\ 0.021 \text{ for non silica fume concrete} \end{cases}$$

A_c: cross sectional area (in^2)

u: exposed perimeter (in)

H.2.5. AASHTO-LRFD as modified by Shams and Kahn (2000)

Shams and Kahn (2000), proposed some changes to AASHTO-LRFD creep and shrinkage expression (see Section H.1.2) in order to better predict long-term strains of HPH.

Creep Model. Shams and Kahn method for estimating creep is presented in Equation H.37.

$$\phi_t = \phi_\infty \cdot k_{vs} \cdot k_{f_c} \cdot k_H \cdot k_{t'} \cdot k_\sigma \cdot k_m \cdot \frac{(t-t')^{0.6}}{d+(t-t')^{0.6}} \qquad \text{(H.37)}$$

where

ϕ_t: creep coefficient at "t" loaded at t′

$t = \sum_{\text{day } n}^{\text{until}} \Delta t_i \cdot \exp\left\{-\left[\frac{4{,}000}{273 + T(\Delta t_i)/T_0} - 13.65\right]\right\}$; maturity of concrete (days) after "n" days

$t' = \sum_{\text{loading}}^{\text{until}} \Delta t_i \cdot \exp\left\{-\left[\frac{4{,}000}{273 + T(\Delta t_i)/T_0} - 13.65\right]\right\}$; maturity of concrete at loading (days)

Δt_i: period of time (days) at temperature $T(\Delta t_i)$ (^oC) ($^oC = 0.556 \times {}^oF - 17.778$)

T_0: 1 ^oC

$\phi_\infty = 2.73$: ultimate creep coefficient

$$k_{vs} = \left[\frac{t}{26 \cdot \exp\left\{0.36 \cdot V/S\right\} + t}{\frac{t}{45+t}}\right] \cdot \left[\frac{1.80 + 1.77 \cdot \exp\left\{-0.54 \cdot V/S\right\}}{2.587}\right]$$; size factor

V: specimen volume (in^3)

S: specimen surface area (in^2)

$k_{f_c} = \frac{4.8}{1.645 + f_c'}$; concrete strength factor

f_c': compressive strength of concrete cylinders at 28 days (ksi)

$k_H = 1.58 - 0.83 \cdot h$; ambient relative humidity factor

h: relative humidity in decimals

$k_{t'} = 0.65 \cdot \exp\left\{\frac{0.7}{t'+0.57}\right\}$; maturity at loading factor

$$k_\sigma = \begin{cases} \exp\{1.5 \cdot (\Gamma - 0.4)\} \; for \; 0.4 \le \Gamma \le 0.6 \\ 1.0 \; for \; \Gamma \le 0.4 \end{cases}$$; stress-to-strength ratio factor

Γ: stress-to-strength ratio at loading

$k_m = 1 + 0.65 \cdot (1 - \exp\{-0.59 \cdot m\})^{5.73}$: moist curing period factor

m: moist curing period (days)

$d = \frac{t'}{0.356 + 0.09 \cdot t'}$: maturity for 50 percent of ultimate creep coefficient

Drying Shrinkage Model. Equation H.38 shows Shams and Kahn drying shrinkage expression.

$$\varepsilon_{sh}(t, t_o) = \varepsilon_{sh\infty} \cdot k_{vs}' \cdot k_H' \cdot k_{t_o} \cdot \left[\frac{t - t_o}{f + (t - t_o)}\right]^{0.5} \qquad \text{(H.38)}$$

where

$$\varepsilon_{sh\infty} = \begin{cases} 510 \; \mu\varepsilon \text{ for steam - cured concrete} \\ 560 \; \mu\varepsilon \text{ for moist - cured concrete} \end{cases}$$; ultimate shrinkage strain

$$t = \sum_{\substack{until\\ day\ n}}^{} \Delta t_i \cdot \exp\left\{-\left[\frac{4{,}000}{273 + T(\Delta t_i)/T_0} - 13.65\right]\right\}$$; maturity of concrete (days) after "n" days

$$t_0 = \sum_{\substack{until\\ beginning\\ drying}}^{} \Delta t_i \cdot \exp\left\{-\left[\frac{4{,}000}{273 + T(\Delta t_i)/T_0} - 13.65\right]\right\}$$; maturity of concrete at the beginning of drying (days)

Δt_i: period of time (days) at temperature $T(\Delta t_i)$ (^oC) ($^oC = 0.556 \times {}^oF - 17.778$)

T_0: 1 ^oC

$$k_{vs} = \left[\frac{(t - t_0)}{26 \cdot \exp\left\{0.36 \cdot V/S\right\} + (t - t_0)}{(t - t_0)}{45 + (t - t_0)}\right] \cdot \left[\frac{1064 - 0.94 \cdot V/S}{923}\right]$$; size factor

$$k_H = \begin{cases} 2.00 - 1.43 \cdot h \ \ for\ h < 0.80 \\ 4.29 - 4.29 \cdot h \ \ for\ h \geq 0.80 \end{cases}$$; ambient relative humidity factor

h: relative humidity in decimals

$$k_{t_0} = 0.67 \cdot \exp\left\{\frac{4.2}{9.45 + t_o}\right\}$$; factor for maturity at the beginning of drying

f: 23 (days)

This page intentionally left blank

APPENDIX I

CREEP AND DRYING SHRINKAGE MODELS (S. I. UNITS)

I.1 Models for Normal Strength Concrete

I.1.1. ACI-209 Method

Creep Model:

$$\phi_t = \frac{(t-t')^{\psi}}{d+(t-t')^{\psi}} \cdot \phi_u \qquad \text{(I.1)}$$

where

ϕ_t: creep coefficient at age "t" loaded at t′

t: age of concrete (days)

t′: age of concrete at loading (days)

ψ: constant depending on member shape and size

d: constant depending on member shape and size

ϕ_u: ultimate creep coefficient

$$\phi_u = 2.35 \cdot \gamma_{la} \cdot \gamma_{\lambda} \cdot \gamma_{vs} \cdot \gamma_{s} \cdot \gamma_{\psi} \cdot \gamma_{\alpha} \qquad \text{(I.2)}$$

where

ϕ_u: ultimate creep coefficient

$\gamma_{la} = \begin{cases} 1.25 \cdot t'^{-0.118} & \textit{for moist curing} \\ 1.13 \cdot t'^{-0.094} & \textit{for steam curing} \end{cases}$; age of loading factor

t′: age of concrete at loading (days)

$\gamma_\lambda = \begin{cases} 1.27 - 0.67 \cdot h \ \ for\ h \geq 0.40 \\ 1.00 \ otherwise \end{cases}$; ambient relative humidity factor

h: relative humidity in decimals

$\gamma_{VS} = \frac{2}{3}\left(1 + 1.13 \cdot \exp\left\{-0.0213 \cdot V/S\right\}\right)$; volume-to-surface ratio factor

V: specimen volume (mm^3)

S: specimen surface area (mm^2)

$\gamma_s = 0.82 + 0.00264 \cdot s$; slump factor

s: slump (mm)

$\lambda_\psi = 0.88 + 0.24 \cdot \psi$; fine aggregate content factor

ψ: fine aggregate-to-total aggregate ratio in decimals

$\gamma_\alpha = 0.46 + 0.09 \cdot \alpha$; air content factor

α: air content (%)

Drying Shrinkage Model:

$$(\varepsilon_{sh})_t = \frac{(t - t_0)^\alpha}{f + (t - t_0)^\alpha} \cdot (\varepsilon_{sh})_u \qquad \text{(I.3)}$$

where

t: age of concrete (days)

t_0: age at the beginning of drying (days)

$(\varepsilon_{sh})_t$: shrinkage strain after "$t-t_0$" days under drying (mm/mm)

α: constant depending on member shape and size

f: constant depending on member shape and size

$(\varepsilon_{sh})_u$: ultimate shrinkage strain (mm/mm)

$$(\varepsilon_{sh})_u = 780 \cdot \gamma_\lambda \cdot \gamma_{vs} \cdot \gamma_s \cdot \gamma_\psi \cdot \gamma_c \cdot \gamma_\alpha \qquad \text{(I.4)}$$

where

$(\varepsilon_{sh})_u$: ultimate shrinkage strain

$\gamma_\lambda = \begin{cases} 1.40 - 1.0 \cdot h \ \ for\ 0.40 \le h \le 0.80 \\ 3.00 - 3.0 \cdot h \ \ for\ h > 0.80 \end{cases}$; ambient relative humidity factor

h: relative humidity in decimals

$\gamma_{VS} = 1.2 \cdot \exp\left\{-0.00472 \cdot V/S\right\}$; volume-to-surface ratio factor

V: specimen volume (mm^3)

S: specimen surface area (mm^2)

$\gamma_s = 0.89 + 0.00161 \cdot s$; slump factor

s: slump (mm)

$\gamma_\psi = \begin{cases} 0.30 - 1.4 \cdot \psi \ \ for\ \psi \le 0.50 \\ 0.90 - 0.2 \cdot \psi \ \ for\ \psi > 0.50 \end{cases}$; fine aggregate content factor

ψ: fine aggregate-to-total aggregate ratio in decimals

$\gamma_c = 0.75 + 0.00061 \cdot c$; cement content factor

c: cement content (kg/m^3)

$\gamma_\alpha = 0.95 + 0.08 \cdot \alpha$; air content factor

α: air content (%)

I.1.2. AASHTO-LRFD Method

Creep Model:

$$\phi_u = 3.50 \cdot k_{la} \cdot k_h \cdot k_c \cdot k_f \qquad \text{(I.5)}$$

where

$ø_u$: ultimate creep coefficient

$k_{la} = 1.00 \cdot t'^{-0.118}$ *for moist curing* ; age of loading factor

$$t = \sum_{\text{day } n}^{\text{until}} \Delta t_i \cdot \exp\left\{-\left[\frac{4000}{273 + T(\Delta t_i)/T_0} - 13.65\right]\right\}$$; maturity of concrete (days) after "n" days

$$t' = \sum_{\text{loading}}^{\text{until}} \Delta t_i \cdot \exp\left\{-\left[\frac{4000}{273 + T(\Delta t_i)/T_0} - 13.65\right]\right\}$$; maturity of concrete at loading (days)

Δt_i: period of time (days) at temperature $T(\Delta t_i)$ (^oC)

T_0: 1 ^oC

$k_h = 1.58 - 0.83 \cdot h$; ambient relative humidity factor

h: relative humidity in decimals

$$k_c = \left[\frac{t}{26 \cdot \exp\left\{0.0142 \cdot V/S\right\} + t}{\frac{t}{45 + t}}\right] \cdot \left[\frac{1.80 + 1.77 \cdot \exp\left\{-0.0216 \cdot V/S\right\}}{2.587}\right]$$; size factor

V: specimen volume (mm^3)

S: specimen surface area (mm^2)

$$k_f = \frac{1}{0.67 + \frac{f_c'}{9}}$$; concrete strength factor

f_c': compressive strength at 28 days (ksi)

Shrinkage Model:

$$(\varepsilon_{sh})_u = K \cdot k_s \cdot k_h \qquad \text{(I.6)}$$

where

$(\varepsilon_{sh})_u$: ultimate shrinkage strain

$$K = \begin{cases} 510\ \mu\varepsilon\ for\ moist\ curing \\ 560\ \mu\varepsilon\ for\ steam\ curing \end{cases}$$; ultimate shrinkage base value

$$k_s = \left[\frac{(t - t_0)}{\frac{26 \cdot \exp\left\{0.0142 \cdot V/S\right\} + (t - t_0)}{45 + (t - t_0)}} \right] \cdot \left[\frac{1064 - 0.037 \cdot V/S}{923} \right]$$; size factor

t: age of concrete (days)

t_0: age at the beginning of drying (days)

V: specimen volume (mm^3)

S: specimen surface area (mm^2)

$$k_h = \begin{cases} 2.00 - 1.43 \cdot h\ for\ h < 0.80 \\ 4.29 - 4.29 \cdot h\ for\ h \geq 0.80 \end{cases}$$; ambient relative humidity factor

h: relative humidity in decimals

I.1.3. CEB-FIP Method

Creep Model:

$$\varepsilon_{cr}(t,t') = \frac{\sigma_c(t')}{E_{28}}\phi_{28}(t,t') \tag{I.7}$$

$$\phi_{28} = \phi_0 \cdot \left[\frac{(t-t')}{\beta_H + (t-t')}\right]^{0.3} \tag{I.8}$$

where

t: age of concrete (days)

t′: age of concrete at loading (days)

ε_{cr}: creep strain in με

$\sigma_c(t')$: applied stress (MPa)

E_{28}: 28-day elastic modulus (MPa)

$ø_{28}$: creep coefficient at age "t" loaded at t′

$$\phi_0 = \left[1 + \frac{(1-h)}{0.46 \cdot \left(\frac{2 \cdot A_c/u}{100}\right)^{1/3}}\right] \cdot \frac{5.3}{\sqrt{\frac{f_c'}{10}}} \cdot \frac{1}{0.1 + t'^{0.2}}$$; notional creep coefficient

h: relative humidity in decimals

A_c: cross sectional area (mm^2)

u: exposed perimeter (mm)

f_c': compressive strength at 28 days (MPa)

$\beta_H = 150 \cdot \left[1 + (1.2 \cdot h)^{18}\right] \cdot \frac{2 \cdot A_c / u}{100} + 250 \le 1500$; constant depending on member size and relative humidity

When cement different from normal hardening is used and/or special curing regime is followed, t′ is modified following Equations I.9 and I.10 which incorporate the maturity concept.

$$t' = t'_T \left[\frac{9}{2 + (t'_T)^{1.2}} + 1\right]^{\alpha} \ge 0.5 \; days \qquad \text{(I.9)}$$

$$t'_T = \sum \Delta t_i \cdot \exp\left\{-\left[\frac{4000}{273 + T(\Delta t_i)/To} - 13.65\right]\right\} \qquad \text{(I.10)}$$

where

$$\alpha = \begin{cases} -1 \; for \; slowly \; hardening \; cement \\ 0 \; for \; normal / rapid \; hardening \; cement \\ +1 \; for \; rapid \; hardening \; high \; early \; strength \; cement \end{cases}$$; cement type parameter

t'_T: adjusted age of concrete at loading

Δt_i: period of time (days) at temperature $T(\Delta t_i)$ (^oC)

T_0: 1 ^oC

When stresses between 40 and 60% of compressive strength are applied, CEB-FIP recommends using a high stress correction to the notional creep "ϕ_0" as shown in Equation I.11.

$$\phi_{0,k} = \phi_0 \cdot \exp\{1.5 \cdot (k_\sigma - 0.4)\} \qquad \text{(I.11)}$$

where

k_σ: stress-to-strength ratio at time of application of loaI.

Drying Shrinkage Model:

$$\varepsilon_s(t,t_0) = \varepsilon_{so} \cdot \beta_s \cdot (t - t_0) \qquad \text{(I.12)}$$

where

t: age of concrete (days)

t_0: age of concrete at the beginning of drying (days)

$\varepsilon_{s0} = \left[160 + 10 \cdot \beta_{sc} \cdot \left(9 - \frac{f_c'}{10}\right)\right] \cdot \beta_{RH}$; notional shrinkage coefficient

$$\beta_{sc} = \begin{cases} 4 \ for\ slowly\ hardening\ cement \\ 5 \ for\ normal\,/\,rapid\ hardening\ cement \\ 8 \ for\ rapid\ hardening\ high\ early\ strength\ cement \end{cases}$$; cement type parameter

$$\beta_{RH} : \begin{cases} -1.55 \cdot \left[1 - h^3\right] & for \quad 0.40 \le h \le 0.99 \\ 0.25 & for \quad h \ge 0.99 \end{cases}$$

h: relative humidity in decimals

f_c': compressive strength of concrete cylinders at 28 days (MPa)

$\beta_s(t,t_0) = \left[\frac{(t - t_0)}{\beta_{sH} + (t - t_0)}\right]^{0.5}$; shrinkage function

$$\beta_{sH} = 350 \cdot \left(\frac{2 \cdot A_c / u}{100}\right)^2$$

A_c: cross sectional area (mm^2)

u: exposed perimeter (mm)

When temperatures above 30°C (86°F) are applied, CEB-FIP recommends using an elevated temperature correction for β_{sH} and β_{RH} as shown below.

$$\beta_{sH,T} = \beta_{sH} \cdot \exp\{-0.06 \cdot (T - 20)\} \qquad \beta_{RH,T} = \beta_{RH} \cdot \left[1 + \left(\frac{0.08}{1.03 - h}\right) \cdot \left(\frac{T - 20}{40}\right)\right]$$

$\beta_{sH,T}$: geometric factor corrected by temperature

$\beta_{RH,T}$; relative humidity factor corrected by temperature

T: ambient temperature (°C)

h: relative humidity in decimals

I.1.4. Bažant and Panula's - BP Method

Creep Model:

$$J(t,t') = \frac{1}{E_0} + C_0(t,t') + C_d(t,t',t_0) - C_p(t,t',t_0) \qquad \text{(I.13)}$$

where

J: compliance function

E_0: Modulus of elasticity at the age of loading (MPa)

C_0: basic creep portion [specific creep - (mm/mm)/MPa]

C_d: drying creep portion [specific creep - (mm/mm)/MPa]

C_p: creep decrease after drying [specific creep - (mm/mm)/MPa]

t: age of concrete (days)

t′: age of loading (days)

t_0: age of concrete at the beginning of drying (days)

Basic Creep Model:

$$C_0(t,t') = \frac{\phi_1}{E_0} \cdot \left(t'^{-m} + \alpha\right) \cdot (t - t')^n \qquad \text{(I.14)}$$

where

C_0: basic creep portion [specific creep - (mm/mm)/MPa]

E_0: Modulus of elasticity at the age of loading (MPa)

$\phi_1 = \dfrac{10^{3 \cdot n}}{2 \cdot \left(28^{-m} + \alpha\right)}$ material parameter

t: age of concrete (days)

t′: age of concrete at loading (days)

$$n = \begin{cases} 0.12 + \dfrac{0.07 \cdot x^6}{5130 + x^6} \; for \; x > 4 \\ 0.12 \; for \; x \le 4 \end{cases} \qquad x = \left[2.1 \cdot \frac{a/c}{s/c} + 0.1 \cdot \left(0.145 \cdot f_c'\right)^{1.5} \cdot \left(\frac{w}{c}\right)^{1/3} \cdot \left(\frac{a}{g}\right)^{2.2} \right] \cdot a_1 - 4$$

c: cement content (kg/m^3)

w: water content (kg/m^3)

a: aggregate content (kg/m^3)

s: sand content (kg/m^3)

g: coarse aggregate content (kg/m^3)

f_c': compressive strength at 28 days (MPa)

a_1: cement type coefficient $\begin{cases} 1.00 \; for \; Type \; I \; and \; II \; cements \\ 0.93 \; for \; Type \; III \; cement \\ 1.05 \; for \; Type \; IV \; cement \end{cases}$

$m = 0.28 + \frac{1}{(0.145 \cdot f_c')^2}$; $\alpha = \frac{1}{40 \cdot \left(w/c\right)}$; material parameters

Drying Creep Model:

According to Bažant and Panula (1978c and 1984) drying creep can be modeled by Equation I.15:

$$C_d(t,t',t_0) = \frac{\phi_d'}{E_0} \cdot t'^{-m/2} \cdot k_h' \cdot \varepsilon_{sh\infty} \cdot \left(1 + \frac{10 \cdot \tau_{sh}}{t - t'}\right)^{-c_d \cdot n} \qquad \text{(I.15)}$$

where

C_d: drying creep portion [specific creep - (mm/mm)/MPa]

E_0: Modulus of elasticity at the age of loading (MPa)

$$\phi_d' = \left(1 + \frac{t' - t_0}{10 \cdot \tau_{sh}}\right)^{-1/2} \cdot \phi_d$$

$$\phi_d = \begin{cases} 0.008 + 0.027 \cdot \dfrac{1}{1 + 0.7 \cdot r^{-1.4}} \ \textit{for } r > 0 \\ 0.008 \ \textit{for } r \le 0 \end{cases} \qquad r = 56000 \cdot \left(\frac{s}{a} \cdot 0.145 \cdot f_c'\right)^{0.3} \cdot \left(\frac{g}{s}\right)^{1.3} \cdot \left(\frac{w/c}{\varepsilon_{s\infty}}\right)^{1.5} - 0.85$$

c: cement content (kg/m^3)

w: water content (kg/m^3)

a: aggregate content (kg/m^3)

s: sand content (kg/m^3)

g: coarse aggregate content (kg/m^3)

f_c': compressive strength at 28 days (MPa)

$\tau_{sh} = 600 \cdot \left(\frac{k_s}{150} \cdot 2 \cdot V/S \right)^2 \cdot \frac{C_1^{ref}}{C_1(t_0)}$ size-dependent parameter

$$k_s = \begin{cases} 1.0 \ for \ \ infinite \ slab \\ 1.15 \ for \ \ infinite \ cylinder \\ 1.25 \ for \ \ infinite \ squared \ \ prism \\ 1.30 \ for \ a \ sphere \\ 1.55 \ for \ a \ cube \end{cases}$$; shape factor

V: specimen volume (mm^3)

S: specimen surface area (mm^2)

$C_1^{ref} = 6451 \ mm^2 / day$

$$C_1(t_0) = C_7 \cdot k_T' \cdot \left(0.05 + \sqrt{\frac{6.3}{t_0}} \right)$$

$$C_7 = \frac{1}{8} \cdot \frac{w}{c} \cdot c - 12 \quad 7 \le C_7 \le 21$$

$$k_T' = \frac{T}{T_0} \exp\left\{ \frac{5000}{T_0} - \frac{5000}{T} \right\}$$

T_0: 296.15 K (reference temperature)

T: ambient temperature K

$m = 0.28 + \frac{1}{(0.145 \cdot f_c')^2}$; material parameters

$$n = \begin{cases} 0.12 + \frac{0.07 \cdot x^6}{5130 + x^6} \ for \ x > 4 \\ 0.12 \ for \ x \le 4 \end{cases} \qquad x = \left[2.1 \cdot \frac{a/c}{s/c} + 0.1 \cdot (0.145 \cdot f_c')^{1.5} \cdot \left(\frac{w}{c} \right)^{1/3} \cdot \left(\frac{a}{g} \right)^{2.2} \right] \cdot a_1 - 4$$

a_1: cement type coefficient $\begin{cases} 1.00 \ for \ Type \ I \ and \ II \ cements \\ 0.93 \ for \ Type \ III \ cement \\ 1.05 \ for \ Type \ IV \ cement \end{cases}$

$k_h' = \left| h_0^{1.5} - h^{1.5} \right|$ humidity dependent parameter

h: relative humidity in decimals

h_0: 0.98 to 1.0

$c_d = 2.8 - 7.5 \cdot n$

$\varepsilon_{s\infty}$: final shrinkage in με as in Equation I.17

Creep Decrease after Drying

$$C_p(t,t',t_0) = c_p \cdot k_h'' \cdot \left(1 + \frac{100 \cdot \tau_{sh}}{t - t_0}\right)^{-n} \cdot C_0(t,t') \qquad \text{(I.16)}$$

where

C_p: creep decrease after drying portion (specific creep)

t: age of concrete (days)

t′: age of concrete at loading (days)

t_0: age of concrete at the beginning of drying (days)

$c_p = 0.83$

$k_h'' = h_0^2 - h^2$ humidity dependent parameter

h: relative humidity in decimals

h_0: 0.98 to 1.0

$\tau_{sh} = 600 \cdot \left(\frac{k_s}{150} \cdot 2 \cdot V/S\right)^2 \cdot \frac{C_1^{ref}}{C_1(t_0)}$ size-dependent parameter

$$k_s = \begin{cases} 1.0 \ for \ \ infinite \ slab \\ 1.15 \ for \ \ infinite \ cylinder \\ 1.25 \ for \ \ infinite \ squared \ \ prism \\ 1.30 \ for \ a \ sphere \\ 1.55 \ for \ a \ cube \end{cases} ; \text{shape factor}$$

V: specimen volume (mm^3)

S: specimen surface area (mm^2)

$$C_1^{ref} = 6451 \ mm^2 / day$$

$$C_1(t_0) = C_7 \cdot k_T' \cdot \left(0.05 + \sqrt{\frac{6.3}{t_0}} \right)$$

$$C_7 = \frac{1}{8} \cdot \frac{w}{c} \cdot c - 12 \qquad 7 \le C_7 \le 21$$

$$n = \begin{cases} 0.12 + \dfrac{0.07 \cdot x^6}{5130 + x^6} \ for \ x > 4 \\ 0.12 \ for \ x \le 4 \end{cases} \qquad x = \left[2.1 \cdot \frac{a/c}{s/c} + 0.1 \cdot (0.145 \cdot f_c')^{1.5} \cdot \left(\frac{w}{c} \right)^{1/3} \cdot \left(\frac{a}{g} \right)^{2.2} \right] \cdot a_1 - 4$$

a_1: cement type coefficient $\begin{cases} 1.00 \ for \ Type \ I \ and \ II \ cements \\ 0.93 \ for \ Type \ III \ cement \\ 1.05 \ for \ Type \ IV \ cement \end{cases}$

c: cement content (kg/m^3)

w: water content (kg/m^3)

a: aggregate content (kg/m^3)

s: sand content (kg/m^3)

g: coarse aggregate content (kg/m^3)

f_c': compressive strength at 28 days (MPa)

Drying Shrinkage Model:

$$\varepsilon_{sh}(t,t_0) = \varepsilon_{sh\infty} \cdot k_h \cdot \sqrt{\frac{t-t_0}{\tau_{sh}+t-t_0}} \tag{I.17}$$

where

$\varepsilon_{sh\infty}$: ultimate shrinkage stain με

$$k_h = \begin{cases} 1-h^3 \ \ for\ h \le 0.98 \\ -0.2 \ \ for\ h = 1.00 \\ linear\ \text{int}erpolation\ \ for\ 0.98 \le h \le 1.00 \end{cases} \quad ; \text{humidity-dependent factor}$$

h: relative humidity in decimals

t: age of concrete (days)

t_0: age of concrete at the beginning of drying (days)

$$\tau_{sh} = 600 \cdot \left(\frac{k_s}{150} \cdot 2 \cdot V/S \right)^2 \cdot \frac{C_1^{ref}}{C_1(t_0)} \ ; \text{size-dependent factor}$$

$$k_s = \begin{cases} 1.0 \ \ for\ \ infinite\ slab \\ 1.15 \ \ for\ \ infinite\ cylinder \\ 1.25 \ \ for\ \ infinite\ squared\ \ prism \\ 1.30 \ \ for\ a\ sphere \\ 1.55 \ \ for\ a\ cube \end{cases} \ ; \text{shape factor}$$

V: specimen volume (mm^3)

S: specimen surface area (mm^2)

$$C_1^{ref} = 6451\ mm^2 / day$$

$$C_1(t_0) = C_7 \cdot k_T' \cdot \left(0.05 + \sqrt{\frac{6.3}{t_0}} \right) ; \ C_7 = \frac{1}{8} \cdot \frac{w}{c} \cdot c - 12 \quad 7 \le C_7 \le 21$$

$$k_T' = \frac{T}{T_0} \exp\left\{ \frac{5000}{T_0} - \frac{5000}{T} \right\}$$

T_0: 296.15 K (reference temperature)

T: ambient temperature K

$$\varepsilon_{s\infty} = 1210 - \frac{880}{\frac{390}{z}+1} \quad ; \quad z = \left[\left[1.25 \cdot \sqrt{\frac{a}{c}} + 0.5 \cdot \left(\frac{g}{s}\right)^2\right] \cdot \left(\frac{1+s/c}{w/c}\right)^{1/3} \cdot \sqrt{0.145 \cdot f_c'}\right] - 12 \geq 0$$

c: cement content (kg/m^3)

w: water content (kg/m^3)

a: aggregate content (kg/m^3)

s: sand content (kg/m^3)

g: coarse aggregate content (kg/m^3)

f_c': compressive strength at 28 days (MPa)

I.1.5. Bažant and Baweja's - B3 Method

Creep Model:

$$J(t,t') = q_1 + C_0(t,t') + C_d(t,t',t_o) \qquad \text{(I.18)}$$

where

J: compliance function

$q_1 = \frac{0.6 \times 10^6}{E_0}$ instantaneous strain due to unit stress

C_0: basic creep portion [specific creep - (mm/mm)/MPa]

C_d: drying creep portion [specific creep - (mm/mm)/MPa]

t: age of concrete (days)

t′: age of concrete at loading (days)

t_0: age of concrete at the beginning of drying (days)

E_0: asymptotic modulus elastic modulus (MPa) (age independent)

Basic Creep Model

Basic creep is given by Equation I.19, as follows:

$$C_0(t,t') = q_2 \cdot Q(t,t') + q_3 \cdot \ln\left[1 + (t-t')^n\right] + q_4 \ln\left[\frac{t}{t'}\right] \qquad \text{(I.19)}$$

where

$q_2 = 451.1\sqrt{1.6856 \cdot c} \cdot (145 \cdot f_c')^{-0.9}$; ageing viscoelastic compliance

c: cement content (kg/m^3)

f_c': compressive strength at 28 days (MPa)

$$Q(t,t') = Q_f(t') \cdot \left[1 + \left(\frac{Q_f(t')}{Z(t,t')}\right)^{r(t')}\right]^{-1/r(t')} \quad ; \quad \begin{array}{l} Q_f(t') = \left[0.086 \cdot (t')^{2/9} + 1.21 \cdot (t')^{4/9}\right]^{-1} \\ Z(t,t') = (t')^{-m} \cdot \ln\left[1 + (t-t')^n\right] \\ r(t') = 1.7 \cdot (t')^{0.12} + 8 \end{array}$$

m = 0.5; n = 0.1

t: age of concrete (days)

t′: age of concrete at loading (days)

$q_3 = 0.29 \cdot \left(\frac{w}{c}\right)^4 \cdot q_2$; non-ageing viscoelastic compliance

$q_4 = 0.14 \cdot \left(\frac{a}{c}\right)^{-0.7}$; flow compliance

c: cement content (kg/m^3)

w: water content (kg/m^3)

a: aggregate content (kg/m^3)

Drying Creep Model

Additional creep due to drying is given by Equation I.20

$$C_d(t,t',t_0) = q_5 \cdot \left[\exp\{-8 \cdot H(t)\} - \exp\{-8 \cdot H(t_0')\}\right]^{1/2} \qquad \text{(I.20)}$$

where

$$q_5 = \frac{5220.7}{f'_c} \cdot \left|\varepsilon_{sh\infty}\right|^{-0.6}$$

f_c': compressive strength at 28 days (MPa)

$\varepsilon_{sh\infty}$: ultimate shrinkage as shown in Equation I.21

$$H(t) = 1 - (1-h) \cdot \tanh\sqrt{\frac{t-t_0}{\tau_{sh}}}$$

h: relative humidity in decimals

t: age of concrete (days)

t′: age of concrete at loading (days)

t_0: age of concrete at the beginning of drying (days)

t_0': max(t′,t_0) (days)

τ_{sh}: size factor as shown in Equation I.21

<u>Drying Shrinkage Model:</u>

$$\varepsilon_{sh}(t,t_0) = -\varepsilon_{sh\infty} \cdot k_h \cdot \tanh\sqrt{\frac{t-t_0}{\tau_{sh}}} \qquad \text{(I.21)}$$

where

ε_{sh}: shrinkage strain

t: age of concrete (days)

t_0: age of concrete at the beginning of drying (days)

$$\varepsilon_{sh\infty} = -\alpha_1 \cdot \alpha_2 \cdot \left[0.00856 \cdot w^{2.1} \cdot \left(145 \cdot f_c'\right)^{-0.28} + 270\right] \cdot \frac{\left(\frac{607}{4 + 0.85 \cdot 607}\right)^{1/2}}{\left(\frac{\left(t_0 + \tau_{sh}\right)}{4 + 0.85 \cdot \left(t_0 + \tau_{sh}\right)}\right)^{1/2}}$$

$$\alpha_1 = \begin{cases} 1.00, \textit{ for type I cement} \\ 0.85, \textit{ for type II cement} \\ 1.10, \textit{ for type III cement} \end{cases} ; \text{cement type factor}$$

$$\alpha_2 = \begin{cases} 0.75, \textit{ for steam} - \textit{cured specimens} \\ 1.00, \textit{ for water or } h = 1.00 - \textit{cured specimens} \\ 1.20, \textit{ for sealed specimens} \end{cases} ; \text{curing factor}$$

w: water content (kg/m^3)

f_c': compressive strength at 28 days (MPa)

$$k_h = \begin{cases} 1 - h^3 \textit{ for } h \le 0.98 \\ -0.2 \textit{ for } h = 1.00 \\ \textit{linear interpolation for } 0.98 \le h \le 1.00 \end{cases} ; \text{humidity-dependent factor}$$

h: relative humidity in decimals

$$\tau_{sh} = 190.8 \cdot t_0^{-0.008} \cdot \left(145 \cdot f_c'\right)^{-0.25} \cdot \left(k_s \cdot 0.0787 \cdot V/S\right)^2 ; \text{size-dependent factor}$$

$$k_s = \begin{cases} 1.0 \textit{ for infinite slab} \\ 1.15 \textit{ for infinite cylinder} \\ 1.25 \textit{ for infinite squared prism} \\ 1.30 \textit{ for a sphere} \\ 1.55 \textit{ for a cube} \end{cases} ; \text{shape factor}$$

V: specimen volume (mm^3)

S: specimen surface area (mm^2)

I.1.6. Gardner and Lockman's - GL Method

Creep Model:

$$c_{cr}(t,t') = \left[\frac{2\cdot(t-t')^{0.3}}{(t-t')^{0.3}+14} + \left(\frac{7}{t_o}\right)^{1/2} \cdot \left(\frac{(t-t')}{(t-t')+7}\right)^{1/2} + \right.$$

$$\left. + 2.5\cdot\left(1-1.086\cdot h^2\right)\cdot\left(\frac{(t-t')}{(t-t')+0.15\cdot\left(V/S\right)^2}\right)^{1/2}\right] \cdot \frac{1}{E_{c28}} \qquad \text{(I.22)}$$

where

c_{cr}: creep coefficient at age "t" loaded at t′ (με/MPa)

t: age of concrete (days)

t′: age of concrete at loading (days)

t_0: age of concrete at the beginning of drying (days)

h: relative humidity in decimals

V: specimen volume (mm^3)

S: specimen surface area (mm^2)

E_{c28}: 28-day elastic modulus (MPa)

Drying Shrinkage Model:

$$\varepsilon_{sh}(t,t_0) = \varepsilon_{shu}\cdot\left(1-1.18\cdot h^4\right)\cdot\left(\frac{(t-t_0)}{(t-t_0)+0.15\cdot\left(V/S\right)^2}\right)^{1/2} \qquad \text{(I.23)}$$

where

ε_{sh}: shrinkage strain

$$\varepsilon_{shu} = 1000 \cdot K \cdot \left(\frac{30}{f_c'}\right)^{1/2} \cdot 10^{-6}$$; ultimate shrinkage strain

$$K = \begin{cases} 1.00 \ \textit{for Type I cement} \\ 0.70 \ \textit{for Type II cement} \\ 1.15 \ \textit{for Type III cement} \end{cases}$$; cement factor

f_c': compressive strength at 28 days (MPa)

h: relative humidity in decimals

t: age of concrete (days)

t_0: age of concrete at the beginning of drying (days)

V: specimen volume (mm^3)

S: specimen surface area (mm^2)

I.1.7. Sakata's - SAK Method

Creep Model:

$$\varepsilon_{cr}(t,t') = \left(\varepsilon'_{bc} + \varepsilon'_{dc}\right) \cdot \left(1 - \exp\left\{-0.09 \cdot (t - t')^{0.6}\right\}\right) \qquad \text{(I.24)}$$

where

ε_{cr}: specific creep at age "t" loaded at t′ (με/MPa)

t: age of concrete (days)

t′: age of concrete at loading (days)

ε'_{bc}: basic creep portion, parameter depending on water and cement content, water-to-cement ratio, and age of loading

ε'_{dc}: drying creep portion, parameter depending on water and cement content, water-to-cement ratio, member volume-to-surface ratio, and relative humidity

Basic Creep Model

Basic creep is given by Equation I.25, as follows:

$$\varepsilon'_{bc} = 1.5 \cdot (c + w)^2 \cdot \left(w/c\right)^{2.4} \cdot (\ln[t'])^{-0.67} \qquad \text{(I.25)}$$

where

ε'_{bc}: basic specific creep portion (με/MPa)

c: cement content (kg/m^3)

w: water content (kg/m^3)

t′: age of concrete at loading (days)

Drying Creep Model

Drying creep is given by Equation I.26

$$\varepsilon'_{dc} = 0.0045 \cdot (c + w)^{1.4} \cdot \left(w/c\right)^{4.2} \cdot \left(\ln\left[V/S\right]\right)^{-2.2} \cdot (1 - h)^{0.36} \cdot (t_0)^{-0.3} \qquad \text{(I.26)}$$

where

ε'_{dc}: drying specific creep portion (με/MPa)

h: relative humidity in decimals

t_0: age of concrete at the beginning of drying (days)

V: specimen volume (mm^3)

S: specimen surface area (mm^2)

Drying Shrinkage Model

$$\varepsilon_{sh}(t, t_0) = \varepsilon_{sh\infty} \cdot \left(1 - \exp\left\{-0.108 \cdot (t - t_0)^{0.56}\right\}\right) \times 10^{-5} \qquad \text{(I.27)}$$

where

ε_{sh}: shrinkage strain

t: age of concrete (days)

t_0: age of concrete at the beginning of drying (days)

$\varepsilon_{sh\infty} = -600 + 780 \cdot (1 - \exp\{h\}) + 380 \cdot \ln[w] - 50 \cdot \left(\ln\left[V/S\right]\right)^2 + 44 \cdot \ln[t_0]$; ultimate shrinkage strain

h: relative humidity in decimals

w: water content (kg/m^3)

V: specimen volume (mm^3)

S: specimen surface area (mm^2)

I.2 Models for High Strength Concrete

I.2.1. CEB-FIP Method as modified by Yue and Taerwe (1993)

$$\beta_H = \frac{130}{f_c'} \cdot \left[1 + (0.012 \cdot h)^{18}\right] \cdot \left(2 \cdot A_c/u\right) + 250 \le 1500 \qquad \text{(I.28)}$$

where

β_H: constant depending on member size and relative humidity

h: relative humidity in decimals

A_c: cross sectional area (mm^2)

u: exposed perimeter (mm)

$$\phi_0 = \left[1 + \frac{(1-h)}{0.46 \cdot \left(\frac{2 \cdot A_c/u}{100}\right)^{1/3}}\right] \cdot \frac{2.6}{\sqrt{\frac{f_c'}{10} - 1}} \cdot \frac{1}{0.1 + t'^{0.2}} \qquad \text{(I.29)}$$

where

ϕ_0: ; notional creep coefficient

h: relative humidity in decimals

A_c: cross sectional area (mm^2)

u: exposed perimeter (mm)

f_c': compressive strength at 28 days (MPa)

t′: age of concrete at loading (days)

I.2.2. Bažant and Panula's - BP Method

$$C_d(t,t',t_0) = \frac{\phi_d'}{E_0} \cdot t'^{-m/2} \cdot k_h' \cdot \varepsilon_{sh\infty} \cdot \left(1 + \frac{b_d \cdot \tau_{sh}}{t - t'}\right)^{-c_d \cdot n} \qquad \text{(I.30)}$$

where

C_d: drying creep portion [specific creep - (με)/MPa]

E_0: Modulus of elasticity at the age of loading (MPa)

$$\phi_d' = \left(1 + \frac{t' - t_0}{a_d \cdot \tau_{sh}}\right)^{-1/2} \cdot \phi_d$$

$$a_d = \begin{cases} 10 \ for f_c' \le 41.4 \ MPa \\ \\ 1 \ for f_c' \ge 69.0 \ MPa \end{cases} \text{; linear interpolation between 41.4 and 69.0 MPa}$$

$$\tau_{sh} = 600 \cdot \left(\frac{k_s}{150} \cdot 2 \cdot V/S\right)^2 \cdot \frac{C_1^{ref}}{C_1(t_0)} \text{ size-dependent parameter}$$

$$k_s = \begin{cases} 1.0 \ for \ \ infinite \ slab \\ 1.15 \ for \ \ infinite \ cylinder \\ 1.25 \ for \ \ infinite \ squared \ \ prism \\ 1.30 \ for \ a \ sphere \\ 1.55 \ for \ a \ cube \end{cases} \text{; shape factor}$$

V: specimen volume (mm^3)

S: specimen surface area (mm^2)

$C_1^{ref} = 6451\ mm^2 / day$

$$C_1(t_0) = C_7 \cdot k_T' \cdot \left(0.05 + \sqrt{\frac{6.3}{t_0}}\right)$$

$$C_7 = \frac{1}{8} \cdot \frac{w}{c} \cdot c - 12 \qquad 7 \le C_7 \le 21$$

$$k_T' = \frac{T}{T_0} \exp\left\{\frac{5000}{T_0} - \frac{5000}{T}\right\}$$

T: ambient temperature ^oK

T_0: 296.15 ^oK (reference temperature)

$$\phi_d = \begin{cases} 0.008 + 0.027 \cdot \dfrac{1}{1 + 0.7 \cdot r^{-1.4}} \ \ for\ r > 0 \\ 0.008 \ \ for\ r \le 0 \end{cases} \qquad r = 56000 \cdot \left(\frac{s}{a} \cdot f_c'\right)^{0.3} \cdot \left(\frac{g}{s}\right)^{1.3} \cdot \left(\frac{w/c}{\varepsilon_{s\infty}}\right)^{1.5} - 0.85$$

c: cement content (kg/m^3)

w: water content (kg/m^3)

a: aggregate content (kg/m^3)

s: sand content (kg/m^3)

g: coarse aggregate content (kg/m^3)

f_c': compressive strength at 28 days (MPa)

$$\varepsilon_{s\infty} = 1210 - \frac{880}{\frac{390}{z} + 1} \quad ; \quad z = \left[\left[1.25 \cdot \sqrt{\frac{a}{c}} + 0.5 \cdot \left(\frac{g}{s}\right)^2\right] \cdot \left(\frac{1 + s/c}{w/c}\right)^{1/3} \cdot \sqrt{0.145 \cdot f_c'}\right] - 12 \ge 0 :$$

final shrinkage in με

$$m = 0.28 + \frac{1}{(0.145 \cdot f_c')^2}$$

$k_h' = \left| h_0^{1.5} - h^{1.5} \right|$ humidity dependent parameter

h: relative humidity in decimals

h_0: 0.98 to 1.0

$$b_d = \begin{cases} 10 \ for f_c' \le 41.4 \ MPa \\ \\ 100 \ for f_c' \ge 69.0 \ MPa \end{cases}$$; linear interpolation between 41.4 and 69.0 MPa

$$c_d = 2.8 - 7.5 \cdot n$$

$$n = \begin{cases} 0.12 + \dfrac{0.07 \cdot x^6}{5130 + x^6} \ for \ x > 4 \\ \\ 0.12 \ for \ x \le 4 \end{cases} \qquad x = \left[2.1 \cdot \frac{a/c}{s/c} + 0.1 \cdot (0.145 \cdot f_c')^{1.5} \cdot \left(\frac{w}{c} \right)^{1/3} \cdot \left(\frac{a}{g} \right)^{2.2} \right] \cdot a_1 - 4$$

a_1: cement type coefficient $\begin{cases} 1.00 \ for \ Type \ I \ and \ II \ cements \\ 0.93 \ for \ Type \ III \ cement \\ 1.05 \ for \ Type \ IV \ cement \end{cases}$

I.2.3. Sakata's - SAK Method

$$\varepsilon_{cr}(t,t') = \frac{4 \cdot w \cdot (1-h) + 350 \cdot}{12 + f_c'(t')} \cdot \ln[t - t' + 1] \qquad \text{(I.31)}$$

where

ε_{cr}: specific creep at age "t" loaded at t′ (με/MPa)

t: age of concrete (days)

t′: age of concrete at loading (days)

$f_c'(t')$: compressive strength at the age of t′(MPa)

w: water content (kg/m^3)

h: relative humidity in decimals

Drying Shrinkage Model

$$\varepsilon_{sh}(t,t_0)=\frac{\varepsilon_{sh\infty}\cdot(t-t_0)}{\beta+(t-t_0)} \tag{I.32}$$

where

ε_{sh}: shrinkage strain

t: age of concrete (days)

t_0: age of concrete at the beginning of drying (days)

$\varepsilon_{sh\infty}=\dfrac{\alpha(1-h)\cdot w}{1+150\exp\left\{-\dfrac{500}{f_c'}\right\}}\cdot\dfrac{1}{1+\eta\cdot t_0}$; ultimate shrinkage strain

$\alpha=\begin{cases}10 \text{ for normal portland cement}\\ 8 \text{ for slow hardening cement}\end{cases}$; cement factor

h: relative humidity in decimals

w: water content (kg/m^3)

f_c': compressive strength at 28 days (MPa)

$\eta=(15\cdot\exp(0.007\cdot f_c')+0.25\cdot w)\times10^{-4}$

$\beta=\dfrac{4\cdot w\sqrt{V/S}}{100+0.7\cdot t_0}$

V: specimen volume (mm^3)

S: specimen surface area (mm^2)

I.2.4. AFREM Method

Creep Model:

$$\varepsilon_{cr}(t,t') = \frac{\sigma(t')}{E_{28}}\left(\phi_b(t,t') + \phi_d(t,t')\right) \tag{I.33}$$

where

ε_{cr}: creep strain in με

$\sigma(t')$: applied stress at t′ (MPa)

E_{28}: 28-day elastic modulus (MPa)

t: age of concrete (days)

t′: age of concrete at loading (days)

$ø_b$: basic creep coefficient at age "t" loaded at t′

$ø_d$: drying creep coefficient at age "t" loaded at t′

Basic Creep Model

$$\phi_b(t,t') = \phi_{b0} \cdot \frac{\sqrt{t-t'}}{\beta_{bc} + \sqrt{t-t'}} \tag{I.34}$$

where

$$\phi_{b0} = \begin{cases} \dfrac{3.6}{f_c'(t')^{0.37}} \; for\ silica-fume\ concrete \\ 1.4 \; for\ non\ silica-fume\ concrete \end{cases}$$

$$\beta_{bc} = \begin{cases} 0.37 \cdot \exp\left\{2.8 \cdot \dfrac{f_c'(t')}{f_c'}\right\} \; for\ silica-fume\ concrete \\ 0.40 \cdot \exp\left\{3.1 \cdot \dfrac{f_c'(t')}{f_c'}\right\} \; for\ non\ silica-fume\ concrete \end{cases}$$

$f'_c(t')$: compressive strength at the age of t′ (MPa)

f'_c: compressive strength at 28 days (MPa)

Drying Creep Model

$$\phi_d(t,t',t_0) = \phi_{d0} \cdot (\varepsilon_{sh}(t,t_0) - \varepsilon_{sh}(t',t_0)) \quad \text{(I.35)}$$

where

$$\phi_{d0} = \begin{cases} 1000 \ for\ silica-fume\ concrete \\ 3200 \ for\ non\ silica-fume\ concrete \end{cases}$$

ε_{sh}: drying shrinkage as shown in Equation I.36

Drying Shrinkage Model:

$$\varepsilon_{sh}(t,t_0) = \frac{K(f_c') \cdot (72 \cdot \exp\{-0.046 \cdot f_c'\} + 75 - 100 \cdot h)}{\beta_{ds0} \cdot \left(2 \cdot A_c / u\right)^2 + (t - t_0)} \cdot (t - t_0) \times 10^{-6} \quad \text{(I.36)}$$

where

ε_{sh}: shrinkage strain

$$K(f_c') = \begin{cases} 18 \ for\ f_c' \le 57\ MPa \\ 30 - 0.21 \cdot f_c' \ for\ f_c' \ge 57\ MPa \end{cases} \text{; strength-dependent factor}$$

h: relative humidity in decimals

t: age of concrete (days)

t_0: age of concrete at the beginning of drying (days)

f_c': compressive strength at 28 days (MPa)

$$\beta_{ds0} = \begin{cases} 0.007 \ for\ silica-fume\ concrete \\ 0.021 \ for\ non\ silica-fume\ concrete \end{cases}$$

A_c: cross sectional area (mm^2)

u: exposed perimeter (mm)

I.2.5. AASHTO-LRFD method as modified by Shams and Kahn (2000)

Shams and Kahn (2000), proposed some changes to AASHTO-LRFD creep expression (see Section I.1.2) in order to better predict creep of HPC. Shams and Kahn method for estimating creep is presented in Equation I.37.

$$\phi_t = \phi_\infty \cdot k_{vs} \cdot k_{f_c} \cdot k_H \cdot k_{t'} \cdot k_\sigma \cdot k_m \cdot \frac{(t-t')^{0.6}}{d+(t-t')^{0.6}} \qquad \text{(I.37)}$$

where

ϕ_t: creep coefficient at "t" loaded at t′

$$t = \sum_{\text{day } n}^{\text{until}} \Delta t_i \cdot \exp\left\{-\left[\frac{4000}{273 + T(\Delta t_i)/T_0} - 13.65\right]\right\}$$; maturity of concrete (days) after "n" days

$$t' = \sum_{\text{loading}}^{\text{until}} \Delta t_i \cdot \exp\left\{-\left[\frac{4000}{273 + T(\Delta t_i)/T_0} - 13.65\right]\right\}$$; maturity of concrete at loading (days)

Δt_i: period of time (days) at temperature $T(\Delta t_i)$ (^oC)

T_0: 1 ^oC

$\phi_\infty = 2.73$: ultimate creep coefficient

$$k_{vs} = \left[\frac{t}{26 \cdot \exp\{0.0142 \cdot V/S\} + t}{\frac{t}{45+t}}\right] \cdot \left[\frac{1.80 + 1.77 \cdot \exp\{-0.0216 \cdot V/S\}}{2.587}\right]$$; size factor

V: specimen volume (mm^3)

S: specimen surface area (mm^2)

$k_{f_c} = \frac{4.8}{1.645 + 145 \cdot f_c'}$; concrete strength factor

f_c': compressive strength of concrete cylinders at 28 days (MPa)

$k_H = 1.58 - 0.83 \cdot h$; ambient relative humidity factor

h: relative humidity in decimals

$k_{t'} = 0.65 \cdot \exp\left\{\frac{0.7}{t'+0.57}\right\}$; maturity at loading factor

$k_\sigma = \begin{cases} \exp\{1.5 \cdot (\Gamma - 0.4)\} \; for \; 0.4 \le \Gamma \le 0.6 \\ 1.0 \; for \; \Gamma \le 0.4 \end{cases}$; stress-to-strength ratio factor

Γ: stress-to-strength ratio at loading

$k_m = 1 + 0.65 \cdot (1 - \exp\{-0.59 \cdot m\})^{5.73}$: moist curing period factor

m: moist curing period (days)

$d = \frac{t'}{0.356 + 0.09 \cdot t'}$: maturity for 50% of ultimate creep coefficient

Drying Shrinkage Model: Equation I.37 shows Shams and Kahn drying shrinkage expression.

$$\varepsilon_{sh}(t, t_o) = \varepsilon_{sh\infty} \cdot k_{vs}' \cdot k_H' \cdot k_{t_o} \cdot \left[\frac{t - t_o}{f + (t - t_o)}\right]^{0.5} \qquad \text{(I.38)}$$

where

$\varepsilon_{sh\infty} = \begin{cases} 510 \; \mu\varepsilon \text{ for } steam\text{-cured concrete} \\ 560 \; \mu\varepsilon \text{ for moist-cured concrete} \end{cases}$; ultimate shrinkage strain

$$t = \sum_{\substack{until\\ day\ n}} \Delta t_i \cdot \exp\left\{-\left[\frac{4000}{273 + T(\Delta t_i)/T_0} - 13.65\right]\right\}$$; maturity of concrete (days) after "n" days

$$t_0 = \sum_{\substack{until\\ beginning\\ drying}} \Delta t_i \cdot \exp\left\{-\left[\frac{4000}{273 + T(\Delta t_i)/T_0} - 13.65\right]\right\}$$; maturity of concrete at the beginning of drying (days)

Δt_i: period of time (days) at temperature $T(\Delta t_i)$ (^oC) ($^oC = 0.556 \times {}^oF - 17.778$)

T_0: 1 ^oC

$$k_{vs} = \left[\frac{t}{\frac{26 \cdot \exp\{0.0142 \cdot V/S\} + t}{t/(45+t)}}\right] \cdot \left[\frac{1.80 + 1.77 \cdot \exp\{-0.0216 \cdot V/S\}}{2.587}\right]$$; size factor

V: specimen volume (mm^3)

S: specimen surface area (mm^2)

$$k_H = \begin{cases} 2.00 - 1.43 \cdot h \ \ for\ h < 0.80 \\ 4.29 - 4.29 \cdot h \ \ for\ h \geq 0.80 \end{cases}$$; ambient relative humidity factor

h: relative humidity in decimals

$$k_{t_0} = 0.67 \cdot \exp\left\{\frac{4.2}{9.45 + t_o}\right\}$$; factor for maturity at the beginning of drying

f: 23 (days)

VITA

Mauricio Lopez was born in Santiago, Chile on March 10th, 1972. He obtained his Bachelor's degree from the School of Engineering of the Pontificia Universidad Católica de Chile in 1997. In 1999, he earned the title of Civil Engineer and his Masters in Science from the same University. In the same year he joined the Department of Construction Engineering and Management of the School of Engineering of the Pontificia Universidad Católica de Chile where he worked for two and a half years before starting his Ph.D. studies.

He earned his Masters in Civil Engineering from the Georgia Institute of Technology in May 2005 and he was awarded a Doctor of Philosophy in Civil Engineering in December 2005.

He currently participates actively in the American Concrete Institute and he joined back the Department of Construction Engineering and Management at the Pontificia Universidad Católica de Chile.